INNATE IMMUNITY PROGRAMMING AND MEMORY IN RESOLVING AND NON-RESOLVING INFLAMMATION

EDITED BY: Liwu Li, Charles E. McCall and Xiaoyu Hu
PUBLISHED IN: Frontiers in Immunology

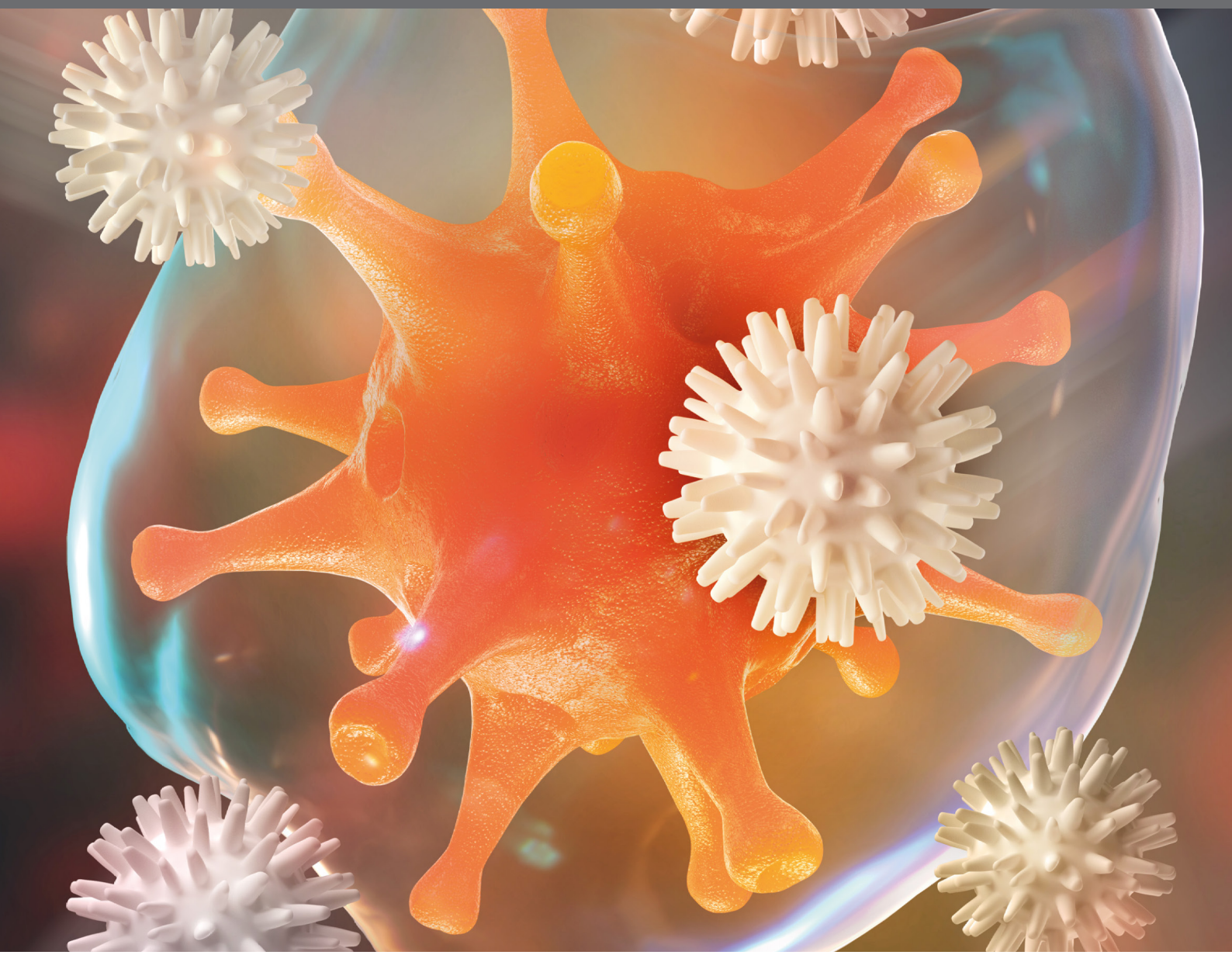

frontiers Research Topics

frontiers

ISSN 1664-8714
ISBN 978-2-88963-582-5
DOI 10.3389/978-2-88963-582-5

About Frontiers

Frontiers is more than just an open-access publisher of scholarly articles: it is a pioneering approach to the world of academia, radically improving the way scholarly research is managed. The grand vision of Frontiers is a world where all people have an equal opportunity to seek, share and generate knowledge. Frontiers provides immediate and permanent online open access to all its publications, but this alone is not enough to realize our grand goals.

Frontiers Journal Series

The Frontiers Journal Series is a multi-tier and interdisciplinary set of open-access, online journals, promising a paradigm shift from the current review, selection and dissemination processes in academic publishing. All Frontiers journals are driven by researchers for researchers; therefore, they constitute a service to the scholarly community. At the same time, the Frontiers Journal Series operates on a revolutionary invention, the tiered publishing system, initially addressing specific communities of scholars, and gradually climbing up to broader public understanding, thus serving the interests of the lay society, too.

Dedication to Quality

Each Frontiers article is a landmark of the highest quality, thanks to genuinely collaborative interactions between authors and review editors, who include some of the world's best academicians. Research must be certified by peers before entering a stream of knowledge that may eventually reach the public - and shape society; therefore, Frontiers only applies the most rigorous and unbiased reviews.
Frontiers revolutionizes research publishing by freely delivering the most outstanding research, evaluated with no bias from both the academic and social point of view. By applying the most advanced information technologies, Frontiers is catapulting scholarly publishing into a new generation.

What are Frontiers Research Topics?

Frontiers Research Topics are very popular trademarks of the Frontiers Journals Series: they are collections of at least ten articles, all centered on a particular subject. With their unique mix of varied contributions from Original Research to Review Articles, Frontiers Research Topics unify the most influential researchers, the latest key findings and historical advances in a hot research area! Find out more on how to host your own Frontiers Research Topic or contribute to one as an author by contacting the Frontiers Editorial Office: researchtopics@frontiersin.org

INNATE IMMUNITY PROGRAMMING AND MEMORY IN RESOLVING AND NON-RESOLVING INFLAMMATION

Topic Editors:
Liwu Li, Virginia Tech, United States
Charles E. McCall, Wake Forest Baptist Medical Center, United States
Xiaoyu Hu, Tsinghua University, China

Cover image: Yurchanka Siarhei/Shutterstock.com

Citation: Li, L., McCall, C. E., Hu, X., eds. (2020). Innate Immunity Programming and Memory in Resolving and Non-Resolving Inflammation. Lausanne: Frontiers Media SA. doi: 10.3389/978-2-88963-582-5

Table of Contents

frontiers in Immunology

EDITORIAL
published: 11 February 2020
doi: 10.3389/fimmu.2020.00177

Editorial: Innate Immunity Programming and Memory in Resolving and Non-Resolving Inflammation

Liwu Li[1]*, *Charles McCall*[2]* and *Xiaoyu Hu*[3]*

[1] Department of Biological Sciences, Virginia Tech, Blacksburg, VA, United States, [2] Department of Medicine, Wake Forest University School of Medicine, Winston-Salem, NC, United States, [3] Institute for Immunology and School of Medicine, Tsinghua University, Beijing, China

Keywords: innate immune memory, inflammation dynamics, resolving and non-resolving inflammation, acute disease, chronic disease

Editorial on the Research Topic

Innate Immunity Programming and Memory in Resolving and Non-Resolving Inflammation

Emerging studies reveal that "memory" responses of innate leukocytes generate adaptive reprogramming following challenges with signals of varying strength and durations. As a result, there are dynamic memory states such as priming, tolerance and exhaustion, as previously published by the Li research group in the *Frontiers of Immunology* (1). Diverse signals including microbial cues, cytokines, and metabolic products induce the varied reprogramming of inflammation and immunity, leading to distinct nature of the memory states of innate leukocytes. Innate memory dynamics profoundly impact, not only on our fundamental understanding of the immune system's cohesive functions, but may translate to interventions for infectious and inflammatory diseases, ranging from acute sepsis to chronic atherosclerosis (2–4).

To heed the emerging challenge of further defining the novel memory dynamics of innate immunity, we assembled research articles that represent various aspects of innate immune memory and are relevant to inflammatory diseases within this Research Topic. In addition to bacterial endotoxin, Walachowski et al. demonstrated that β-Glucan (BG) primes a short-term murine macrophage memory state coupled to enhanced inflammatory response to LPS, potentially by inducing Dectin-1. Dectin-1 increased expression of GM-CSF as an amplifying signal for macrophage priming induced by β-Glucan (Walachowski et al.). Shi et al. showed that myeloid cell innate immune training responses not only occur at the mature cellular stage, but during hematopoiesis. Acting at the translational level, trained immunity through BG or Bacillus Calmette-Guérin (BCG) signaling could potentially enhance host anti-microbial defenses, as reviewed by Arts et al. On a precautionary note, BG or BCG mediated immune modulation may also exacerbate inflammatory diseases, and de Bree et al. reported that the protective effects of BCG training may be limited and do not apply to protection against influenza infection. In addition to microbial products, host secondary metabolites may similarly imprint innate immune memory, such as S100A9, which Dai et al. identified as a potentiator of myeloid derived suppressive cells (MDSC) during late stage sepsis.

Molecular mechanisms dynamically reprogram innate immunity using complex and multi-layered signaling networks that are dose dependent and coupled with transient signals as well as prolonged epigenetic modifications. Intra-cellular organelle communications among

OPEN ACCESS

Edited and reviewed by:
Francesca Granucci,
University of Milano Bicocca, Italy

***Correspondence:**
Liwu Li
lwli@vt.edu
Charles McCall
chmccall@wakehealth.edu
Xiaoyu Hu
xiaoyuhu@tsinghua.edu.cn

Specialty section:
This article was submitted to Molecular Innate Immunity, a section of the journal Frontiers in Immunology

Received: *17 January 2020*
Accepted: *23 January 2020*
Published: *11 February 2020*

Citation:
Li L, McCall C and Hu X (2020) Editorial: Innate Immunity Programming and Memory in Resolving and Non-Resolving Inflammation. Front. Immunol. 11:177. doi: 10.3389/fimmu.2020.00177

mitochondria, autophagosomes, and lysosomes modulate innate immune cell decision-making (5, 6). Mitochondria controls over energy, anabolism and catabolism and cell redox state, and new evidence supports Krebs cycle metabolites as signaling molecules during the training of innate immunity and inflammation (Williams and O'Neill.). Tao et al. reported that mitochondria-localized Sirtuin 4 can resolve monocyte tolerance through rebalancing glycolysis and restoring glucose oxidation. This homeostasis promoting response suggests promise for a novel molecular targeting route to treating sepsis-associated immunoparalysis. Babaev et al. demonstrated that depletion of a mTOR complex component Rictor improves inflammation resolution in monocytes and macrophages, another possible route for chronic inflammatory reprogramming in atherosclerosis.

This collection of publications clarifies some of the mechanisms and provide a more comprehensive understanding of innate immune memory dynamics. They emphasize that future inter-disciplinary studies with integrated experimental and computational approaches at single cell level are needed. Single cell analyses during early, the post-acute, and chronic innate immune cell reprogramming among distinct tissue niches will clarify "real-life" dynamics of innate immune non-autonomous and autonomous signals, and hopefully hasten translational research of infectious and inflammatory diseases in the near future.

AUTHOR CONTRIBUTIONS

LL wrote the manuscript. CM and XH provided critical revision.

ACKNOWLEDGMENTS

We appreciate all contributing authors and research groups who contributed to this Research Topic, diligent reviewers/editors for the submitted manuscripts, as well as the Frontiers Editorial Office for the assistance.

REFERENCES

1. Yuan R, Geng S, Li L. Molecular mechanisms that underlie the dynamic adaptation of innate monocyte memory to varying stimulant strength of TLR ligands. *Front Immunol*. (2016) 7:497. doi: 10.3389/fimmu.2016.00497
2. Morris MC, Gilliam EA, Li L. Innate immune programing by endotoxin and its pathological consequences. *Front Immunol*. (2014) 5:680. doi: 10.3389/fimmu.2014.00680
3. Chen K, Geng S, Yuan R, Diao N, Upchurch Z, Li L. Super-low dose endotoxin pre-conditioning exacerbates sepsis mortality. *EBioMedicine*. (2015) 2:324–33. doi: 10.1016/j.ebiom.2015.03.001
4. Geng S, Chen K, Yuan R, Peng L, Maitra U, Diao N, et al. The persistence of low-grade inflammatory monocytes contributes to aggravated atherosclerosis. *Nat Commun*. (2016) 7:13436. doi: 10.1038/ncomms13436
5. Geng S, Zhang Y, Lee C, Li L. Novel reprogramming of neutrophils modulates inflammation resolution during atherosclerosis. *Sci Adv*. (2019) 5:eaav2309. doi: 10.1126/sciadv.aav2309
6. Baker B, Geng S, Chen K, Diao N, Yuan R, Xu X, et al. Alteration of lysosome fusion and low-grade inflammation mediated by super-low-dose endotoxin. *J Biol Chem*. (2015) 290:6670–8. doi: 10.1074/jbc.M114.611442

Conflict of Interest: The authors declare that the research was conducted in the absence of any commercial or financial relationships that could be construed as a potential conflict of interest.

frontiers in Immunology

ORIGINAL RESEARCH
published: 11 September 2017
doi: 10.3389/fimmu.2017.01089

Molecular Analysis of a Short-term Model of β-Glucans-Trained Immunity Highlights the Accessory Contribution of GM-CSF in Priming Mouse Macrophages Response

Sarah Walachowski†, Guillaume Tabouret†, Marion Fabre and Gilles Foucras*

Université de Toulouse, INRA, INP, ENVT, IHAP, Toulouse, France

β-Glucans (BGs) are glucose polymers present in the fungal cell wall (CW) and, as such, are recognized by innate immune cells as microbial-associated pattern through Dectin-1 receptor. Recent studies have highlighted the ability of the pathogenic yeast *Candida albicans* or its CW-derived β(1,3) (1,6)-glucans to increase human monocytes cytokine secretion upon secondary stimulation, a phenomenon now referred as immune training. This ability of monocytes programming confers BGs an undeniable immunotherapeutic potential. Our objective was to determine whether BGs from *Saccharomyces cerevisiae*, a non-pathogenic yeast, are endowed with such a property. For this purpose, we have developed a short-term training model based on lipopolysaccharide re-stimulation of mouse bone marrow-derived macrophages primed with *S. cerevisiae* BGs. Through a transcriptome analysis, we demonstrated that BGs induced a specific gene expression signature involving the PI3K/AKT signaling pathway as in human monocytes. Moreover, we showed that over-expression of *Csf2* (that encodes for GM-CSF) was a Dectin-1-dependent feature of BG-induced priming of macrophages. Further experiments confirmed that GM-CSF up-regulated Dectin-1 cell surface expression and amplified macrophages response along BG-mediated training. However, the blockade of GM-CSFR demonstrated that GM-CSF was not primarily required for BG-induced training of macrophages although it can substantially improve it. In addition, we found that mouse macrophages trained with BGs upregulated their expression of the four and a half LIM-only protein 2 (*Fhl2*) in a Dectin-1-dependent manner. Consistently, we observed that intracellular levels of FHL2 increased after stimulation of macrophages with BGs. In conclusion, our experiments provide new insights on GM-CSF contribution to the training of cells from the monocytic lineage and highlights FHL2 as a possible regulator of BG-associated signaling.

Keywords: β-glucans, macrophage, trained immunity, Dectin-1, GM-CSF

OPEN ACCESS

Edited by:
Liwu Li,
Virginia Tech, United States

Reviewed by:
Maximiliano Gutierrez,
Francis Crick Institute, United Kingdom
Isabelle Vergne,
Centre national de la recherche scientifique (CNRS), France

***Correspondence:**
Guillaume Tabouret
g.tabouret@envt.fr

†These authors have contributed equally to this work.

Specialty section:
This article was submitted to Molecular Innate Immunity, a section of the journal Frontiers in Immunology

Received: *09 May 2017*
Accepted: *21 August 2017*
Published: *11 September 2017*

Citation:
Walachowski S, Tabouret G, Fabre M and Foucras G (2017) Molecular Analysis of a Short-term Model of β-Glucans-Trained Immunity Highlights the Accessory Contribution of GM-CSF in Priming Mouse Macrophages Response. Front. Immunol. 8:1089. doi: 10.3389/fimmu.2017.01089

Abbreviations: BG, β-glucan; Curd, curdlan; CW, cell wall; DEG, differentially expressed genes; NEAA, non-essential amino acids; Pam3, Pam3CSK4; PAMP, pathogen-associated molecular pattern; Pen–Strep, penicillin–streptomycin; PRR, pattern recognition receptor; SEAP, secreted embryonic alkaline phosphatase; *Sc*, *Saccharomyces cerevisiae*; TEPM, thioglycollate-elicited peritoneal macrophages; WGPd, dispersible whole glucan particle; WGPs, soluble whole glucan particle; WT, wild type; Zym, Zymosan.

INTRODUCTION

The immune system has the complex task of detecting invading pathogens, a critical step in mounting efficient mechanisms of defense. For that, innate immunity has evolved an elaborated system of pathogen surveillance with a wide variety of receptors also referred as pathogen recognition receptors (PRRs) encompassing toll-like and C-type lectin receptors (TLRs and CLRs) (1, 2). These receptors are highly expressed by innate immune cells from the monocytic lineage and are able to recognize a broad spectrum of highly conserved micro-organisms-associated molecular patterns (MAMPs). The nature of MAMPs shapes the immune response orchestrated by macrophages and dendritic cells (3). Among CLRs, Dectin-1 is essential for mounting an effective innate immune response to fungal pathogens, as demonstrated *in vivo* by several authors using *Clec7a*-deficient mice (4–6). The recognition of β-glucans (BGs) from the cell wall (CW) of various fungi, including yeasts, by Dectin-1 induces a Syk/CARD9 signaling cascade (7–11). Soluble BGs from *Grifola frondosa* have also been shown to stimulate the production of GM-CSF, a hematopoietic growth factor that could mediate part of their immunostimulant activity (12, 13). Indeed, in collaboration with Dectin-1 engagement, GM-CSF was shown to synergistically and robustly initiate a BG-specific inflammatory response in macrophages as well as in dendritic cells (12–15).

Moreover, it was demonstrated that TLR and Dectin-1-associated signaling pathways could synergize to enhance macrophages response against pathogenic fungi as *Candida albicans*, *Aspergillus fumigatus*, and *Pneumocystis carinii* (6, 16–19). Indeed, the combination of TLR2/4 and Dectin-1-dependent stimuli, such as those constituting yeasts CW, including mannans, phospholipomannans, and BG, triggers a strong activation of macrophages secreting high levels of inflammatory cytokines (17, 20–22). However, we recently demonstrated that preferentially targeting Dectin-1 through BG enrichment from *Saccharomyces cerevisiae* (*Sc*) CW only elicit low or no relevant cytokine or chemokine production in mouse macrophages (23). And yet, several studies have brought pieces of major evidence that pre-exposure to *C. albicans* or *C. albicans*-derived BG could enhance the response of human monocytes to a secondary stimulation with TLR ligands, while respecting a 6-day resting period between pretreatment and re-stimulation (24, 25). This effect is now referred as BG-mediated immune training of monocytes (26, 27). Recent findings highlighted some molecular mechanisms involved in this long-term trained immunity model, including a metabolic shift toward aerobic glycolysis (a feature of cell activation and proliferation) *via* PI3K/AKT/mTOR pathway (28) and epigenetic modifications (29) in BG-trained human monocytes. Although GM-CSF priming was very recently shown to increase responsiveness to lipopolysaccharide (LPS) in a short-term model of training (30), less is known regarding its role in BG-related trained immunity.

If producible to a large scale, *C. albicans* BG could be highly promising molecules to develop immunotherapeutic strategies where reprogramming of monocytes is required. Thus, we thought that *Sc* BG, presenting a quite analogous structure to those from *C. albicans* and industrially obtainable, could be used as surrogates, provided they share a similar ability to prime mononuclear phagocytes. In the perspective of deciphering the mechanisms underlying this effect and more convenient *in vivo* investigations, we attempted to establish a short-term model of trained immunity (devoid of resting period between both stimulations) with mouse macrophages.

By combining cellular and molecular approaches, we confirmed that pre-exposure of mouse macrophages with *Sc* BG promoted intense cytokine production upon secondary stimulation with TLR agonists. Through microarray analysis, we highlighted significant transcriptional modifications specific from BG pretreatment. Among these, *Csf2* and *Fhl2* over-expression was further investigated to evaluate their potential contribution to BG-induced priming of mouse macrophages.

MATERIALS AND METHODS

Reagents

Cell culture media RPMI 1640 GlutaMAX™ and DMEM GlutaMAX™, PBS, non-essential amino acids (NEAA), sodium pyruvate and antibiotics [Penicillin–Streptomycin (Pen–Strep™), Gentamicin™, Normocin™, and Zeocin™] were purchased from GIBCO (Life Technologies). Fetal bovine serum (FBS) was provided by Eurobio, France. Zymosan (Zym), particulate and dispersible whole glucan particle (WGPd, Biothera) and soluble whole glucan particle compounds (WGPs, Biothera) and curdlan (Curd), a linear β1,3-glucan extracted from *Alcaligenes faecalis*, synthetic triacylated lipoprotein Pam3CSK4 (Pam3) and ultraPure LPS from *Escherichia coli* O111:B4 were purchased from InvivoGen (France). BG compounds of interest were extracted from the same strain of *S. cerevisiae* owned by Phileo-Lesaffre Animal Care. Their composition was already described in a recent study (23). The previous name given to the crude compounds BG15 was replaced in this study by ScCW for better understanding and more convenience.

Animals

Wild type (WT) C57Bl/6 mice were purchased from Janvier Labs (St Berthevin, France) and *Clec7a*$^{-/-}$ mice (5) were originally provided by Pr. Gordon Brown (University of Aberdeen, Scotland) and were bred in-house. Eight- to 12-week-old C57Bl/6 *Clec7a*$^{-/-}$ mice and their strain-matched WT controls from both sexes were housed under pathogen-free conditions in an accredited research animal facility of the National Veterinary College (UMR IHAP, Toulouse, France). This study was carried out in strict accordance with the Federation of European Laboratory Animal Science Association guidelines (FELASA). Experiments were performed by FELASA accredited investigators (no. 311155580) and approved by the local ethics committee, "Science et Santé Animale" (SSA). All efforts were made to minimize animal pain and distress.

Cells and Bacteria

NFκB/AP-1 Activity Using Reporter Cell Line

The NFκB/AP-1 reporter RAW-Blue™ Cells (InvivoGen™) were cultured and propagated according to the manufacturer's recommendations. The NFκB/AP-1 activity was assessed as described

in *Walachowski* et al. (23). RAW-Blue™ macrophages (1×10^5 cells/well) were stimulated with 100 µg/mL of BG-containing preparations (ScCW, BG65, and BG75) for 8 h. Supernatants were then removed and 100 ng/mL of ultraPure LPS was added in each well for the rest of the stimulation period. Supernatants were collected and stored at −20°C or processed immediately. Secreted embryonic alkaline phosphatase was measured using a colorimetric enzymatic assay. Supernatants were incubated with Quanti-Blue™ (InvivoGen) 25% v/v. for 2 h at 37°C, and optical density (OD 650 nm) was measured (VERSAmax plate reader, Molecular Devices).

Bacteria

Staphylococcus aureus N305 and *E. coli* P4 strains were prepared as described previously by Accarias et al. (31) using growth medium adapted to each strain of bacteria [tryptic soy broth for N305 and Lysogeny broth (LB) for P4]. Briefly, a 100-fold dilution of the overnight bacteria culture was grown in medium to mid log phase to obtain an OD600 nm of around 1. After cautious washing and homogenization, the concentration of bacteria was estimated by measuring the absorbance at 600 nm (considering that 1 D.O. unit corresponds to 5×10^8 CFU/mL) and was adjusted to the desired concentration. CFUs were further determined in serially diluted inoculum after 24 h of culture on agar plates.

Primary Cell Culture and Functional Assays

Murine wild type or *Clec7a*$^{-/-}$ bone marrow-derived macrophages (BMDM) were obtained as described previously (31). Inflammatory peritoneal macrophages were elicited and handled as previously described (23). BMDM and thioglycollate-elicited peritoneal macrophages (TEPM) (1×10^5 cells/well) were seeded in 96-well tissue culture plates for 16 h in complete RPMI until complete adherence (37°C, 5% CO_2). Non-adherent contaminating peritoneal cells were eliminated by repeating three gentle washings of wells with pre-warmed culture medium or PBS. After stimulation with *Sc* BG compounds or Dectin-1 ligands controls (WGPd, WGPs or Zym) for 8 h, supernatants were removed and cells were then stimulated with 100 ng/mL of ultraPure LPS or Pam3, or with live bacteria (*S. aureus* N305 or *E. coli* P4 strains, MOI = 10) for 1 h followed by 16 h incubation with cell culture medium supplemented with Gentamicin™. Supernatants were then collected, complete protease inhibitor cocktail (Roche, France) was added in infected conditions, and supernatants were finally stored at −20°C or −80°C until further use.

For the dose-dependent experiments, BMDM were pre-incubated with 1:10 serial dilution of BG75 from 0.1 to 100 µg/mL before another 16 h LPS stimulation. For the two kinds of kinetics assays, several time points were used for BG incubation (1, 4, 8, or 16 h) before 16 h of LPS stimulation as well as for LPS stimulation (1, 4, 8, or 16 h) after 8 h of BG incubation.

For short-term model of immune training, cells were pre-treated with BG75 or complete RPMI as above. After the first incubation, BMDM were washed with warm PBS and maintained in complete RPMI for 24 or 72 h. Thereafter, cells were submitted to a secondary stimulus using 100 ng/mL of ultraPure LPS for 16 h. For GM-CSF and M-CSF influence analyses, BMDM were first pre-incubated for 2 h with recombinant GM-CSF (rGM-CSF, 5 ng/mL, PeproTech, Rocky Hill, NJ, USA) or M-CSF (rM-CSF, 5 ng/mL, PeproTech, Rocky Hill, NJ, USA), or using serial 10-fold dilutions as described in corresponding figure legends. Cells were then stimulated with 100 or 10 µg/mL of BG75 for 8 h followed, where applicable, by 16-h LPS stimulation.

For blocking antibody assays, macrophages were pre-incubated with blocking anti-GM-CSFR antibodies or their isotype control (Novus Biologicals, CO, USA) for 1 h, followed by incubation with rGM-CSF (100 pg/mL) for 2 h. Then BMDM were treated with BG75 (100 µg/mL) for 8 h and further stimulated with 100 ng/mL of LPS for 16 h. All triplicate supernatants were harvested and handled as previously described before cytokine measurement.

Quantification of Cytokines and Chemokines by ELISA

TNFα, IL-6, and IL-1β (Biolegend, Ozyme-France) and GM-CSF (R&D Systems, France) levels in culture supernatants were assayed using individual cytokine detection kits according to the manufacturer's recommendations. Data are expressed as the mean ± SD and are representative of three individual experiments performed in triplicate.

Dectin-1 and CD11b Surface Expression Analysis by Flow Cytometry

Wild-type BMDM were incubated with rGM-CSF (5 ng/mL) or rM-CSF (5 ng/mL) or medium for 2 h. Supernatants were discarded and cells were collected using cold PBS supplemented with 5 mM EDTA. After harvest, cells were centrifuged (300 g, 5 min) and absolute macrophages number was determined by flow cytometry (MACSQuant, Miltenyi Biotech, Germany). BMDM were pre-incubated with anti-CD16/CD32 (Biolegend, Ozyme-France) to block FcγRII/III receptors and then incubated with the following fluorochrome-conjugated mAbs: anti-Dectin-1 (2A11; AbD serotec) or its isotype control IgG1 (A110-1, BD biosciences Pharmingen) and anti-CD11b (M1/70, Biolegend) or its isotype control. A 7-AAD staining (Biolegend, Ozyme-France) was used to discriminate death cells and doublets of cells were excluded with a gating on FSC-H/FSC-A. The acquisition was performed on 1×10^5 cells using MACSQuantify software (Miltenyi Biotech, Germany). Data were analyzed with FlowJo software (FlowJo LLC, USA).

Microarray Analysis

After stimulation with *Sc* BG compounds and then with ultraPure LPS, BMDM were lysed in Buffer RLT (Qiagen, Hilden, Germany) and was subjected to RNA extraction using the RNeasy Mini Kit (Qiagen, Hilden, Germany) according to the manufacturer's instructions. RNA was quantified with a NanoDrop®1000 spectrophotometer and NanoDrop 1000.3.7 software.

RNA quality assessment and microarray experiment were performed at the GeT-TRiX platform (INRA, Toulouse, France). RNA quality was assessed using the Agilent RNA 6000 Nano Kit on BioAnalyzer and 2100 Expert Software (Agilent Technologies, Santa Clara, CA, USA). RNA samples with RNA integrity number more than 8.5 were chosen to be prepped for further analysis. A

total RNA material of 100 ng was amplified and labeled using a Low Input QuickAmp Labeling kit (Agilent Technologies, Santa Clara, CA, USA). RNA were hybridized to Agilent Sure Print G3 Mouse GE 8 × 60K microarrays, washed, stained, and scanned on an Agilent G2505C instrument following the manufacturers' protocols. Agilent Feature Extraction software was used to analyze signal intensity values of the spots generated from the scans. Post-hybridization quality controls were done to eliminate outliers and irrelevant data from the expression data set. Background was subtracted and data were normalized using Agilent procedure. All validated and normalized transcripts expression data were processed using the Agilent GeneSpring GX software.

All entities with flag values present in at least 1 out of the eight conditions were considered. Statistical analysis (two-way ANOVA) was used to generate a unique list of up- or down-regulated entities with associated Benjamini–Hochberg false discovery rate corrected *p*-value and fold change (FC) and for hierarchical clustering. Transcripts with detection *p*-value of less than or equal to 0.001 in at least one sample were selected for further analysis. A filter was set to include only transcripts that had at least 1.5-FC compared to the LPS-stimulated cells without BG treatment control.

Using Ingenuity Pathway Analysis (IPA) software, a final list of unique identified genes (*p*-value <0.001 and absolute FC ≥2) was generated after selection of mapped entities and deduplication exercise on them, and which was then used to perform IPA bio-function analysis. IPA categorized modulated genes according to *p*-values (calculated by the Fisher exact test) and *z*-scores. The *z*-score predicts the direction of change of a function: a function is increased when *z*-score is ≥2 and decreased when *z*-score ≤2. IPA also calculated a bias-corrected *z*-score to correct dataset bias (i.e., when there are more up- than downregulated genes in a bio-function or vice-versa). Lists of modulated genes (FC ≥1.5) were also processed using InnateDB online tool to identify the biological functions associated with the primary BG compounds treatment (*p*-value <0.001). All data files have been deposited in NCBI's Gene Expression Omnibus and are accessible through GEO series accession number GSE101959 (https://www.ncbi.nlm.nih.gov/geo/query/acc.cgi?acc=GSE101959).

Gene Expression by Quantitative Polymerase Chain Reaction Analysis

Total RNA (300 ng) was reverse transcribed using the SuperScript III First-Strand Synthesis Super Mix Kit (Invitrogen) as per the manufacturer's protocol. Quantitative PCR was performed individually with Power SYBR Green PCR Master Mix (Applied Biosystems) and LightCycler™ 480 (Roche, France) for *Csf2* and *Fhl2*; or with the Biomark HD System (Fluidigm, France) at the GeT-PlaGe genotyping service platform (INRA, Toulouse, France) according to the manufacturer's recommendations. For individual quantification, dissociation curves analysis was performed at 40 cycles to verify the identity of PCR product. Primer3plus software was used to design the primers (Table S1 in Supplementary Material) and housekeeping genes were selected with GeNorm Software. The abundance of mRNA of interest was normalized to that of *Sdha, Rpl9*, and *Hprt1* and relative expression was calculated using the $2^{-\Delta\Delta Ct}$ method. The comparative threshold cycle values are expressed as arbitrary unit.

Western Blot

After 8 h of *Sc* CW extracts stimulation, WT BMDM were exposed to 100 ng/mL of ultraPure LPS for 16 h. Supernatants were removed and cells were then lysed in RIPA lysis buffer supplemented with 5 mM EDTA and protease inhibitor (Pierce™, USA). Lysates were centrifuged (14000 rpm, 10 min), pellets were discarded and proteins concentrations were determined using BCA kit (Pierce™, USA). Following a 1:1 dilution in Laemmli buffer (Biorad, CA, USA), 10 µg of total protein were separated on NuPAGE® 4–12% Bis-Tris Mini gels (1.0 mm, 12 wells, Invitrogen™) and blotted onto nitrocellulose membrane (0.2 µm, Invitrogen™) using the XCell *Sure*Lock™ Mini gel system (Invitrogen™, USA). After blocking with 1% BSA and 0.05% Tween 20 (Sigma-Aldrich®, USA) in Tris-Buffer Saline (TBS, Euromedex, France), the membrane was stained with primary anti-FHL2 (F4B2-B11) and anti-β-actin (C4) as loading control mAbs (Santa Cruz Biotechnologies, Germany) at 4°C, overnight. The membrane was then washed in TBS with 0.05% Tween 20 and incubated with goat anti-mouse antibodies conjugated with horseradish peroxidase (Jackson ImmunoResearch, PA, USA) for 1 h at room temperature. Signals were detected with Clarity™ Western ECL substrate and the ChemiDoc™ MP instrument according to the manufacturer's instructions (Biorad, CA, USA). Image Lab software was used for minor linear adjustments in contrast, if needed and the quantitative tool was used to determine the relative quantity of FHL2 protein in each sample as compared to the reference value (fixed to 1) corresponding to the untouched macrophages condition.

Statistical Analysis

All experiments were performed three times unless otherwise specified and data are expressed as the mean ± SD of the values from all experiments. Each condition was performed in triplicate. Statistical significance was assessed using a two-tailed unpaired Student's *t*-test or a two-way ANOVA analysis (as stated in the figure legends) with a threshold set at $p < 0.05$. Mean values shown with different letters on plots are significantly different. For these analyses, we used XLStat (Addinsoft, France) and GraphPad Prism 5 (San Diego, CA, USA) softwares.

RESULTS

Priming with *S. cerevisiae* BGs Enhances the Macrophage Response to Secondary Stimulation with TLR Ligands in a Dectin-1-Dependent Manner

In vitro, pre-incubation of TEPM with various yeast CW-derived products resulted in different degrees of cytokine production. As previously published (23), unpurified or poorly purified products such as Zym or crude CW induced strong cytokine secretion as measured in the culture supernatants (**Figure 1A**). In comparison, the secretion induced by particulate BG-enriched products was lower but still significant if compared to mock or soluble BG

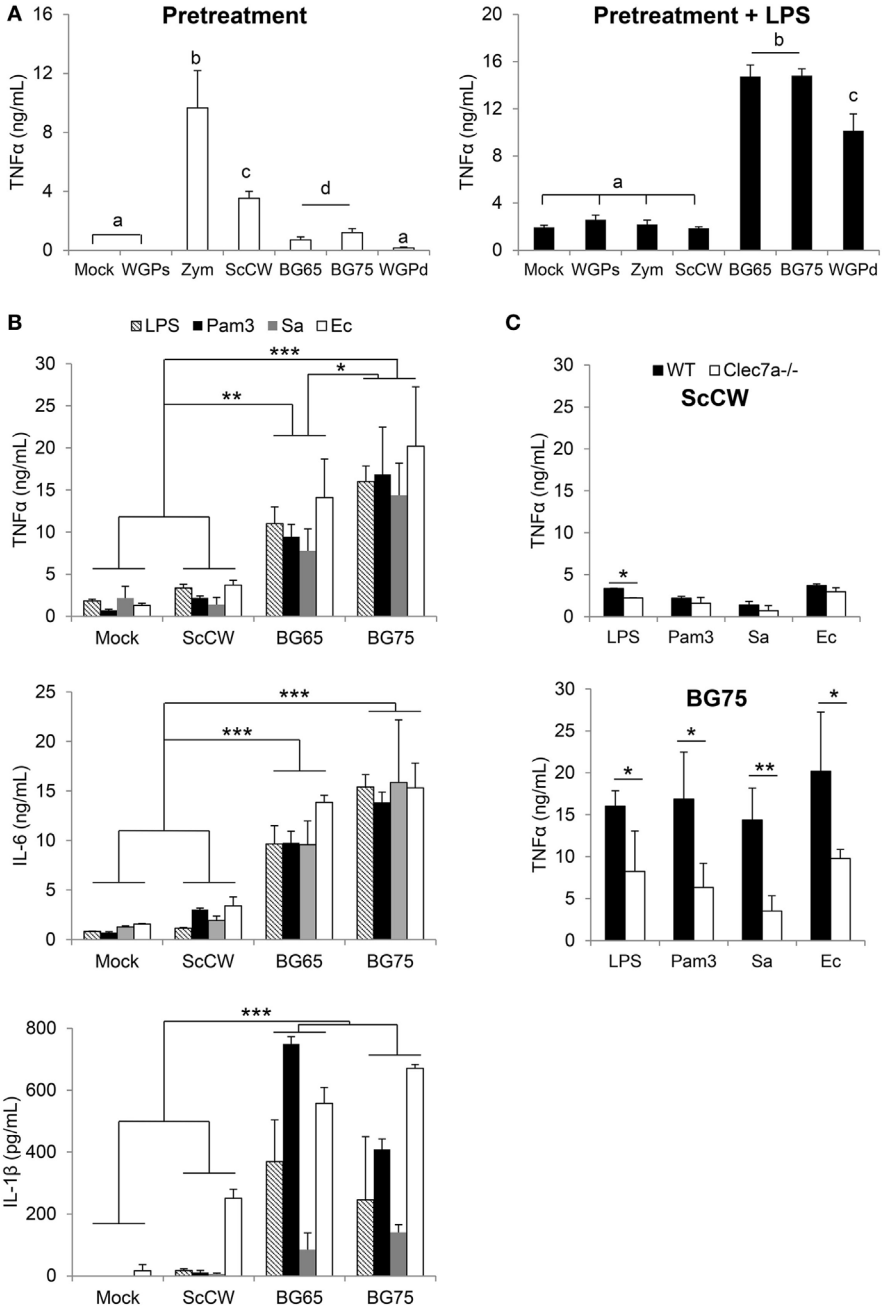

FIGURE 1 | BG-enriched preparations of *Saccharomyces cerevisiae* cell wall (ScCW) prime the macrophage response predominantly *via* Dectin-1 upon toll-like lectin receptor (TLR) ligands or whole bacteria exposure. Wild-type (WT) thioglycollate-elicited peritoneal macrophages **(A)** and WT or *Clec7a*$^{-/-}$ bone marrow-derived macrophages from C57BL/6 mice **(B,C)** were stimulated with 100 µg/mL of crude (ScCW) or BG-enriched (BG65, BG75) compounds for 8 h. After incubation, cell culture supernatants were collected [panel **(A)** on the left, white bars] and stored at −20°C. Cells were then stimulated with 100 ng/mL of ultraPure lipopolysaccharide (LPS) for 16 h [panel **(A)** on the right: dark bars, **(B)** and **(C)**] or Pam3CSK4 (Pam3) [**(B)** and **(C)**]. For the stimulation with live bacteria, *Staphylococcus aureus* N305 or *Escherichia coli* P4 strains were used at MOI = 10 for 1 h, followed by 16 h incubation with cell culture medium supplemented with Gentamicin™ **(B)** and **(C)**. At the end of the incubation, supernatants were collected and immediately stored at −20°C. TNFα, IL-6, and IL1β were quantified by ELISA. Data are expressed as the mean ± SD from three independent experiments performed in triplicate. In **(A,C)**, a Student's *t*-test was used to assess significance between conditions (*$p < 0.05$; **$p < 0.01$) and mean values not sharing the same letter in **(A)** are significantly different. In **(B)**, a two-way ANOVA with Bonferroni post-tests was used to compare pretreatment conditions (*$p < 0.05$; **$p < 0.01$, ***$p < 0.001$).

(WGPs) which seemed devoid of activity. The results appeared strikingly different when pre-incubated macrophages were further stimulated with LPS. Indeed, pre-treating TEPM with BG (BG65, BG75, and WGPd) enhanced their response to LPS by at least a factor of 10 compared to untreated cells or cells pretreated with WGPs. Surprisingly, ScCW or Zym preparations, despite

the presence of low concentrations of BG, did not amplify TEPM response to LPS. We next confirmed these observations by using BMDM pre-incubated with crude CW (ScCW) or purified BG (BG65/BG75) and further stimulated with various TLR agonists (**Figure 1B**). As with TEPM, pretreating BMDM with BG dramatically enhanced their response to TLR agonists whether these were presented to macrophages as purified molecules (TLR4: LPS, TLR2: Pam3) or in the context of living Gram-positive or Gram-negative bacteria (*S. aureus* and *E. Coli,* respectively). This effect was observed for the three inflammatory cytokines TNFα, IL-6, or IL-1β, and again, pretreatment with ScCW (or Zym, data not shown) did not allow significant priming of the macrophage response. Given significant levels of IL-1β measured in BG-enriched pretreatment conditions, we evaluated the viability of BMDM using Propidium Iodide labeling assay. Any difference of fluorescence between mock and BG75-pretreated experimental conditions was detected before or after LPS stimulation, meaning that cells were perfectly viable in our short-term training model (Figure S1 in Supplementary Material).

Bone marrow-derived macrophages from *Clec7a*$^{-/-}$ mice, which do not express Dectin-1, the main surface receptor of BG, were then used to evaluate the influence of the Dectin-1 pathway in the ability of BG to prime macrophages. Whereas the absence of Dectin-1 had no effect on the ScCW-mediated response, it significantly inhibited the ability of BG to prime BMDM response against TLR agonists (**Figure 1C**). Nevertheless, this inhibition was only partial and led to a reduction by 60% on average of cytokine production. Moreover, the surface expression of TLR4 on BMDM was evaluated after BG pretreatment, and we showed that the BG-induced exacerbated cytokine response observed following a secondary LPS stimulation is not explained by an upregulation of TLR4 levels at the surface of BMDM (Figure S2 in Supplementary Material). Of interest, priming of macrophages was perfectly correlated with the dose of BG used during pretreatment (**Figure 2A**). We determined that 1 µg/mL was enough to prime macrophages although concentrations higher than 10 µg/mL were significantly more efficient. Next, we evaluated the incubation time needed for BG to exert their priming effect on the macrophage response to secondary stimuli. First, the simultaneous addition of BG or ScCW and LPS (co-stimulation) or short pre-incubation times (up to 4 h) only resulted in a slight increase of the macrophage response reflecting the previously described synergism between TLR and Dectin-1 pathways (6, 17, 19). By contrast, longer pre-incubation times allowed a significant priming of macrophages but exclusively when using BG-enriched preparations (**Figure 2B**). In parallel, we also assessed importance of the time for the secondary stimulation to maximize cytokine production. By doing so, we observed that, as expected, TNFα levels produced in response to LPS stimulation rose with the incubation time (**Figure 2C**). However, for shorter LPS incubation times (from 1 up to 8 h), no difference was noticed between TNFα levels produced by untreated or BG-pretreated macrophages. Thus, at least 16 h of incubation with LPS were needed to observe significant differences between pretreatment conditions. A good correlation was identified between NFκB/AP-1 activity and incubation times after LPS stimulation. However, after 16 h of incubation, the levels of TNFα secretion and NFκB/AP-1 activity did not match (**Figure 2D**), suggesting that the increased secretion of cytokine induced by BG pretreatment did not rely on NFκB/AP-1 activity. Finally, we evaluated how long the priming effect of BG on macrophages lasted. As shown in **Figure 2E**, enhancement of the macrophages response to LPS could be observed at least up to 72 h after BG pretreatment. This was also observed for longer latency times and up to 5 days (data not shown). Taken together, these results indicate that BG priming is a slow process that probably involves *de novo* protein synthesis and induces profound and long-lasting changes in macrophage biology and phenotype.

Transcriptome Analysis Reveals Specific Hallmarks of BG-Primed Macrophages

To get further insight on how BG altered macrophages responsiveness, we performed a gene expression analysis by microarray. Gene expression profiling was performed in BMDM pretreated with ScCW, BG65, and BG75, or mock controls for 8 h, and then stimulated with LPS for 4 and 8 h. Using a two-way ANOVA with a false discovery rate of 0.001 and a fold expression difference of at least 1.5, we determined differentially expressed genes (DEG) between conditions of priming: BG65, BG75, or ScCW versus mock (**Figure 3A**). A total of 787/670 (4 h) and 935/664 (8 h) DEG were found when comparing BG65/BG75 versus mock. Comparatively, ScCW pretreatment modified the expression of a greater number of genes (2,268 and 1,627 at 4 and 8 h, respectively). Microarray results were confirmed using RT-qPCR on a different set of samples. qPCR results were strongly correlated with the microarray results for all the genes that were evaluated ($n = 26$ genes), with a Pearson's correlation coefficient of 0.57 (p-value <0.001), and confirmed most of the microarray results (Figure S3A in Supplementary Material).

Based on a fold difference above 5, DEG were organized by hierarchical clustering (Euclidian distance) according to similarities in the expression profiles. Conditions with BG65 and BG75 clustered together in contrast to ScCW and mock conditions that remained separated, and so whatever the time point analyzed (**Figure 3B**). The discrimination was also confirmed by principal component analysis (data not shown). Two gene clusters (1 and 3) were associated with pretreatment of macrophages with BG. Cluster 1 was composed of only three differentially up-regulated genes by BG65/75: *Csf2*, *Fhl2*, *and Cish* that presented the highest FC compared to mock (**Table 1**, A). Interestingly, these genes were poorly modulated in ScCW pretreatment condition. Consequently, genes from cluster 1 could be considered as hallmarks of BG-enriched pretreatment of macrophages. Cluster 3 was also associated with BG pretreatment and comprised 40 DEG. However, these genes were also modified in ScCW condition but with a lower FC compared to BG pretreatment. The comparison between BG75 and ScCW pretreatments confirmed that, although ScCW contains very limited BG (15%), stimulation with BG-enriched preparations triggered specific pathways in macrophages (**Table 1**, B). Clusters 2 and 4 comprised genes specifically modulated by ScCW pretreatment. Cluster 2 comprised 35 genes that were downregulated in ScCW condition but precociously (after 4 h of LPS stimulation) over-expressed in mock and BG conditions. Cluster 4 comprised 47 genes

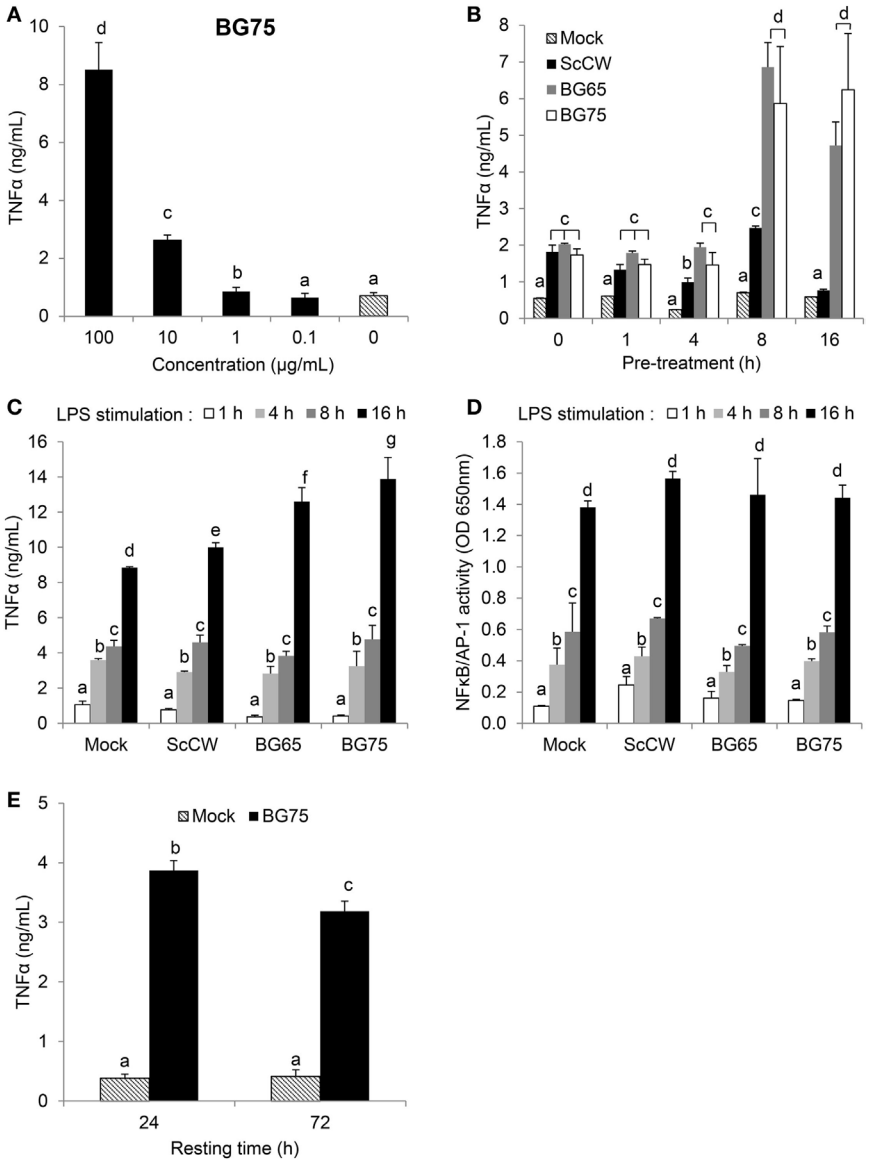

FIGURE 2 | β-glucans (BGs) prime the production of TNFα in macrophages *via* a late and dose-dependent mechanism lasting beyond BG incubation. **(A,B,E)** bone marrow-derived macrophages (BMDM) were subcultured in 96-well plates. **(A)** Cells were incubated for 8 h with a 10-fold serial dilution from 100 to 0.1 µg/mL of BG75. After supernatant removal, BMDM were then stimulated with 100 ng/mL of ultraPure lipopolysaccharide (LPS) for 16 h. Supernatants were collected at the end of the incubation for further analysis. **(B)** Cells were stimulated for 1, 4, 8, 16, and 24 h with 100 µg/mL of BG-containing products (ScCW, BG65, and BG75). Supernatants were discarded and 100 ng/mL of ultraPure LPS was added in each well for 16 h incubation. Supernatants were immediately collected and stored at −20°C. TNFα was measured using ELISA and data are expressed as the mean ± SD from two independent experiments performed in triplicate. **(C,D)** NFκB/AP-1 reporter RAW-Blue™ macrophages were treated with 100 µg/mL of BG-containing compounds for 8 h before stimulation with 100 ng/mL of ultraPure LPS for 1, 4, 8, or 16 h. At the end of the incubation, supernatants were harvested and stored at −20°C until further use. NFκB/AP-1 activity was determined by a colorimetric enzyme assay where cell culture supernatants were incubated with Quanti-Blue™ reagent before reading OD at 650 nm. TNFα was quantified by ELISA. Data are expressed as the mean ± SD from three independent experiments performed in triplicate. **(E)** BMDM were incubated for 8 h with 100 µg/mL of BG75 or control. After supernatant removal, fresh medium was added for further 24 or 72 h (resting time) and cells were stimulated with 100 ng/mL of ultraPure LPS for 16 h. Supernatants were collected and stored at −20°C. TNFα was measured using ELISA and data are expressed as the mean ± SD from three independent experiments performed in triplicate. Mean values not sharing the same letter are significantly different according to the Student's *t*-test ($p < 0.05$). For **(B–D)**, results of statistical analyses are displayed for comparisons between each compound according to the incubation time.

significantly upregulated after 8 h of LPS exposure (and to a lesser extent at 4 h) but exclusively in ScCW-pretreated macrophages. By contrast, these genes were down-modulated in mock or BG pretreatment conditions (Table S2 in Supplementary Material). These results demonstrate that pretreatment of macrophages with BG-enriched preparations induced the modulation of a specific array of genes that were distinct from those modulated by ScCW pretreatment.

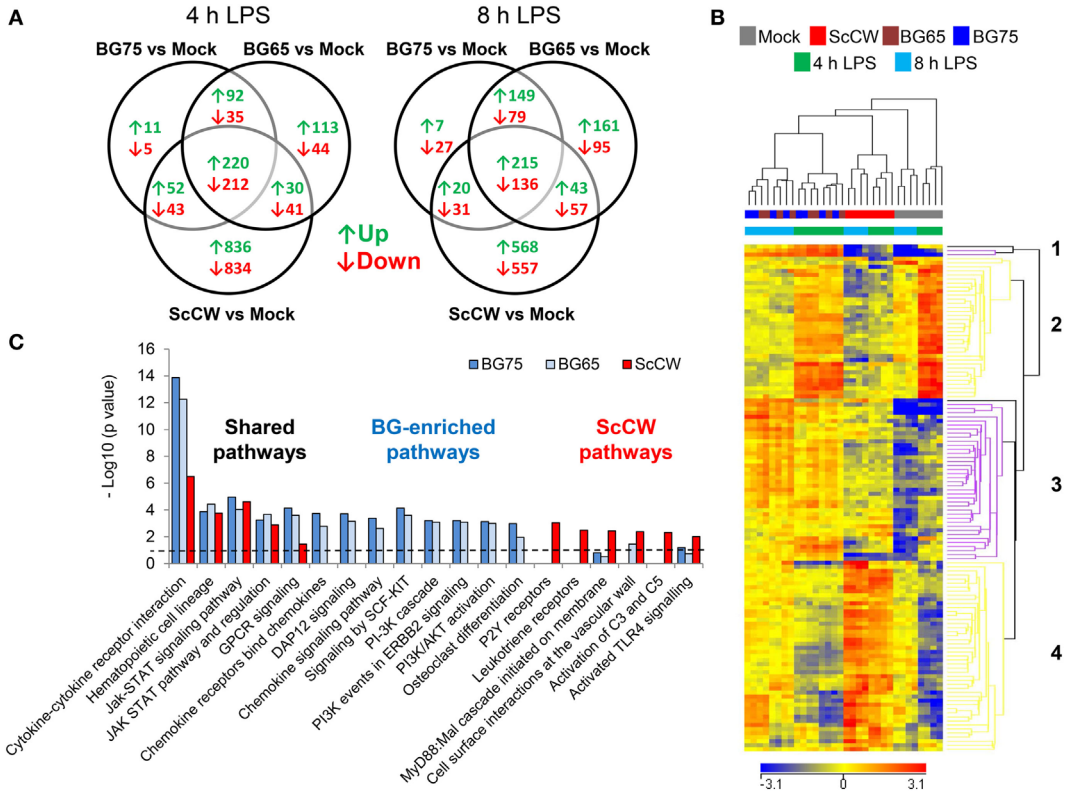

FIGURE 3 | Gene expression profiling reveals specific hallmarks of β-glucan (BG)-pretreated macrophages after lipopolysaccharide (LPS) exposure. Wild-type bone marrow-derived macrophages (BMDM) were cultured in 24-well plates and treated with 100 µg/mL of the set of three BG extracts for 8 h in triplicate. After incubation, supernatants were removed and cells were stimulated with 100 ng/mL of ultraPure LPS for 4 or 8 h. A microarray analysis was performed using Agilent mRNA transcriptomic analysis. After quality control and normalization, data were analyzed using Agilent GeneSpring GX software by two-way ANOVA and Benjamini–Hochberg *post hoc* correction. Transcripts with a *p*-value of less than or equal to 0.001 and a fold change (FC) value of at least 1.5 between conditions in at least one sample were selected for further analysis. **(A)** Venn diagrams showing the overlap of upregulated (↑) and downregulated (↓) genes in each condition were obtained using VENNY 2.0. **(B)** Unsupervised hierarchical clustering (Euclidian distance) of transcriptional profiles, displayed as a heatmap of FC expression values, from BG-treated BMDM compared to non-treated BMDM upon LPS exposure. Each row represents a transcript and each column an individual sample. The heatmap shows 4 clusters constituted by entities with a *p*-value of 0.001 for which FC were greater than 5 compared to mock plus 8 h LPS-stimulated cells. Red indicates over-expressed and blue indicated under-expressed transcripts. **(C)** Based on a comparison of FC expression values between BG pretreatments and the non-pretreated condition upon 8 h of LPS exposure obtained from GeneSpring software (FC >1.5), we performed a pathway over-representation analysis using Innate DB. Significant pathways which *p*-values (calculated by the hypergeometric algorithm) were lower than 0.05 are displayed for each BG pretreatment condition (threshold value–log *p*-value = 1.30).

Based on these panels of DEG, we performed a functional analysis using InnateDB online tool to uncover macrophage pathways that were significantly influenced by each pretreatment. Among the pathways identified (with a corrected *p*-value <0.05), some were clearly specific to each pretreatment whereas some were shared (**Figure 3C**; Figure S3B in Supplementary Material). JAK–STAT signaling and regulation and hematopoietic cell lineage pathways were targeted by BG and ScCW pretreatments in a similar extent. By contrast, although commonly targeted, cytokine–cytokine receptor interactions and G-protein-coupled receptors (GPCRs) signaling (strongly associated with *Csf2* overexpression) appeared much more induced by BG65/75 pretreatments and this was compatible with the enhanced cytokine response observed (**Figure 1**). Compared to BG-enriched conditions, ScCW showed a significant enrichment for TLR signaling pathways associated with MyD88 cascade, complement activation, and also functions linked to leukotriene and P2Y (Purinergic GPCRs) receptors (GPCRs signaling). This result confirmed that ScCW pretreatment significantly stimulated TLR cascade in macrophages (**Figure 1A**). By contrast, we identified functions specifically triggered by BG pretreatment mainly related to PI3K/AKT pathway (cascade, activation, and events in ERBB2, SCF-KIT, and DAP12 signaling). In line with this result, we observed a significant increase of NAD^+/NADH ratio in macrophages following BG75 exposure, a biological feature linked to aerobic glycolysis (Warburg effect) and activation of cell metabolism through PI3K/AKT signaling (Figure S4 in Supplementary Material). Moreover, several genes coding for chemokines and chemokines receptors (*Cxcl1*, *Cxcl2*, *Cxcl5*, *Ccl17*, or *Cxcr6*, etc.) were upregulated by BG pretreatment leading to enrichment of this pathway in our analysis. Finally, osteoclasts differentiation pathway appeared significantly and

TABLE 1 | Top-10 list of the most differentially expressed genes after BG75 treatment upon lipopolysaccharide (LPS) exposure.

(A) ↑Up-regulated, Pretreated versus mock (fold change)			4 h LPS			8 h LPS		
Rank	**Gene**	**Gene title**	***Saccharomyces cerevisiae* cell wall (ScCW)**	**BG65**	**BG75**	**ScCW**	**BG65**	**BG75**
1	*Csf2*	Colony stimulating factor 2 (granulocyte-macrophage)	1.8	20.3	14.0	4.2	64.9	43.1
2	*Fhl2*	Four and a half LIM domains 2	2.4	43.3	31.1	1.7	41.0	35.7
3	*Hbegf*	Heparin-binding EGF-like growth factor	2.8	11.3	8.3	6.0	46.0	32.6
4	*Inhba*	Inhibin beta-A	16.3	20.1	15.3	20.9	41.0	29.9
5	*Car2*	Carbonic anhydrase II	10.9	29.2	19.6	9.8	36.9	27.2
6	*Dok7*	Docking protein 7	9.4	19.6	13.1	11.8	34.0	22.9
7	*Csf3*	Colony stimulating factor 3 (granulocyte)	32.1	11.4	12.7	15.2	21.2	19.2
8	*Cish*	Cytokine inducible SH2-containing protein	-2.9	3.0	2.1	1.5	19.8	13.0
9	*F3*	Coagulation factor III	1.8	5.6	4.8	2.1	13.1	11.4
10	*Vasn*	Vasorin	1.6	4.5	3.3	3.2	13.3	10.8

(B) ↑Up-regulated, β-glucan (BG)- versus *Saccharomyces cerevisiae* cell wall-pretreated (fold change)			4 h LPS		8 h LPS	
Rank	**Gene**	**Gene title**	**BG65**	**BG75**	**BG65**	**BG75**
1	*Fhl2*	Four and a half LIM domains 2	18.0	13.0	24.1	20.9
2	*Csf2*	Colony stimulating factor 2 (granulocyte-macrophage)	11.3	7.8	15.5	10.3
3	*Cish*	Cytokine inducible SH2-containing protein	8.7	5.9	13.1	8.6
4	*Lrrc32*	Leucine rich repeat containing 32	8.2	6.0	11.0	8.0
5	*Ccl17*	C-C motif chemokine ligand 17	6.4	4.3	10.3	6.6
6	*F3*	Coagulation factor III (thromboplastin, tissue factor)	3.2	2.7	6.4	5.5
7	*Hbegf*	Heparin-binding EGF-like growth factor	4.0	2.9	7.6	5.4
8	*Tnfsf18*	Tumor necrosis factor superfamily member 18	1.7	1.8	4.9	4.8
9	*Spry1*	Sprouty RTK signaling antagonist 1	1.8	1.5	5.1	4.7
10	*Egr2*	Early growth response 2	4.3	3.4	5.4	4.7

specifically associated with BG condition as a result of the overexpression of *Fhl2*.

GM-CSF Enhances BG Signaling but Is Not Primarily Involved in the Improvement of BG-Primed Macrophage Response to a Secondary TLR Stimulus

We first confirmed by RT-qPCR that, as observed in the microarray analysis, *Csf2* expression was dramatically upregulated in macrophages pretreated with BG and further stimulated by LPS (**Figure 4A**). This induction appeared highly associated with BG signaling in macrophages, as a huge difference of expression could be observed with BG-enriched preparations and ScCW or mock. At the protein levels, the quantification of GM-CSF (*Csf2* expression product) by ELISA confirmed data from the gene expression analysis and showed an increased production of GM-CSF that correlated with the degree of BG enrichment after a secondary LPS stimulation (**Figure 4B**). Taken together, these data strongly suggested that GM-CSF production by macrophages was highly associated with BG recognition by macrophages. The use of Dectin-1-deficient macrophages in this model of pretreatment/stimulation induced a strong inhibition of GM-CSF secretion and confirmed that Dectin-1 signaling is essential in this process (**Figure 4B**). In a previously published study, we demonstrated that *Csf2* expression was readily induced in macrophages stimulated by BG only (23). We also reported that macrophages stimulation with BG resulted in a very marginal secretion of inflammatory cytokines. It has been previously demonstrated that Curd, a linear β(1,3)-glucan from *A. faecalis,* a gram negative bacterium, could synergize with GM-CSF and confer a strong inflammatory signature to dendritic cells (14). Thus, we examined the influence of recombinant GM-CSF on macrophage activation by BG. As previously observed, BG stimulation on its own induced a very low cytokine production (<50 pg/mL) by macrophages cultured in the absence of growth factors (**Figure 4C**). However, pre-incubating macrophages with rGM-CSF (5 ng/mL) for 2 h before BG stimulation dramatically increased the resulting levels of cytokine secretion. This effect appeared highly associated with rGM-CSF as pre-incubation with rM-CSF (*Csf1* expression product), another major hematopoietic factor influencing macrophages growth, differentiation, and phenotype, did not allow increase of cytokine secretion levels. Using flow cytometry, we confirmed that, as previously described (15), rGM-CSF significantly upregulated the expression of Dectin-1 at the macrophage cell surface (**Figure 4D**). This effect was not reproduced by pre-incubating cells with rM-CSF. Furthermore, rGM-CSF had no effect on the expression of CR3 (CD11b), another BG receptor. These results suggested that GM-CSF could significantly amplify BG signaling by increasing Dectin-1 expression and consequently be strongly involved in the improved response of BG-primed macrophages to secondary TLR stimuli. And, indeed, pre-incubation of macrophages with rGM-CSF (5 ng/mL) significantly improved this priming and resulted in levels of TNFα secretion higher than the secretion by macrophages pre-incubated with rM-CSF or cultured in the absence of stimulating factors (**Figure 4E**). Of note, rGM-CSF alone induced a moderate increase of cytokine production upon LPS secondary stimulation.

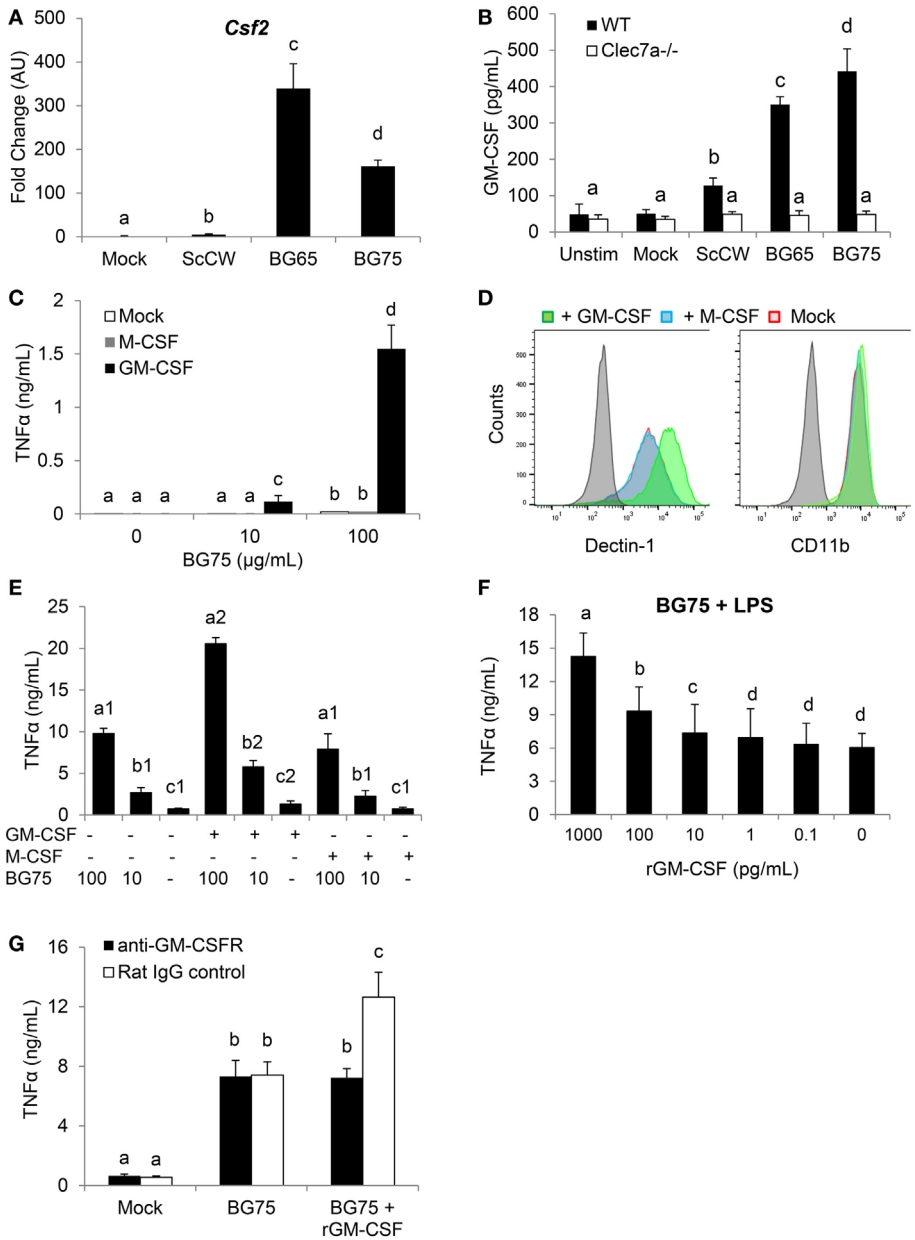

FIGURE 4 | *Csf2* upregulation induced by BG-enriched compounds treatment and lipopolysaccharide (LPS) exposure is mainly Dectin-1-dependent. Wild-type or *Clec7a*$^{-/-}$ bone marrow-derived macrophages (BMDM) were stimulated with 100 μg/mL of the various BG-containing compounds for 8 h. After incubation, cell culture supernatants were removed and 100 ng/mL of ultraPure LPS or medium was added in each well for 8 h **(A)** or 48 h **(B)**. **(A)** Supernatants were discarded and BMDM were lysed in RLT lysis buffer. Total RNA was extracted as described before and retro-transcribed. *Csf2* expression was determined by quantitative PCR after normalization with three housekeeping genes (*Sdha, Rpl9*, and *Hprt1*). Fold change (FC) data are expressed as the mean ± SD as compared to the mock condition in three independent experiments. Mean values not sharing the same letter are significantly different according to the Student's *t*-test ($p < 0.05$). **(B)** After incubation, cell culture supernatants were harvested and stored at −20°C. GM-CSF was measured by ELISA. **(C–E)** WT BMDM were pre-incubated 2 h with rGM-CSF (5 ng/mL) or rM-CSF (5 ng/mL) or medium. **(C)** Cells were further stimulated with 100 μg/mL or 10 μg/mL of BG75 for 8 h. Cell culture supernatants were then removed and TNFα was quantified by ELISA. **(D)** After incubation, cells were harvested to assess surface expression of Dectin-1 and CD11b by flow cytometry. Expression data of Dectin-1 or CD11b are presented as overlaid histograms for each condition. **(E)** After pre-incubation with rGM-CSF, rM-CSF, or medium, BMDM were treated with 100 or 10 μg/mL of BG75 for 8 h before further stimulation with 100 ng/mL of ultraPure LPS or medium for 16 h. Supernatants were collected and TNFα was measured by ELISA. **(F)** BMDM were pre-incubated for 2 h with 10-fold serial dilutions of rGM-CSF from 0.1 to 1000 pg/mL, before assessment as in **(E)**. **(G)** In this experiment, BMDM were first incubated with an anti-GM-CSFR monoclonal antibody or its isotype control for 2 h. rGM-CSF (100 pg/mL) was added to cells for 2 h as a positive control for neutralization. Cells were then stimulated as in **(E)**. Data are expressed as the mean ± SD from two independent experiments performed in triplicate. Mean values not sharing the same letter are significantly different according to the Student's *t*-test ($p < 0.05$).

At this step, we could not exclude an endogenous production of GM-CSF during the priming step of macrophages with BG. In a previous study, we showed that macrophage stimulation with BG led to the detection of low levels of GM-CSF secretion (from 1 to 5 pg/mL) (23). Thus, we evaluated the effect of rGM-CSF in a dose-dependent manner using our stimulation model and observed that 10 pg/mL of rGM-CSF were sufficient to improve the priming of macrophages by BG (**Figure 4F**). As this dose was not very far from the endogenous levels of production previously measured in BG-treated macrophages, we blocked the GM-CSF activity by using a GM-CSFR blocking antibody. For these experiments, we used rGM-CSF (100 pg/mL) to validate blocking conditions. As expected, in the absence of blocking antibody, the pretreatment of macrophages with BG enhanced the response to LPS stimulation and addition of rGM-CSF significantly improved the priming of macrophages by BG (**Figure 4G**). The addition of anti-GM-CSFR completely abolished this gain of response and confirmed that our experimental conditions allowed blocking the activity of at least 100 pg/mL of GM-CSF. However, the intrinsic ability of BG to prime macrophages response was not affected by the addition of anti-GM-CSFR antibody. This, finally, demonstrated that GM-CSF could improve macrophages priming by BG but was not primarily involved in this mechanism.

Specific Induction of FHL2 by BG-Enriched Pretreatment Is Dectin-1-Dependent

Significant *Fhl2* upregulation in BG-enriched conditions upon a secondary LPS stimulation was confirmed by qPCR (**Figure 5A**). As *Fhl2* expression seems to be highly correlated with the degree of purity of BG in the preparations we used, we next investigated the influence of Dectin-1 on *Fhl2* transcription following incubation with BG compounds. WT and *Clec7a*$^{-/-}$ BMDM from C57Bl/6 were incubated 8 h with BG65/75 and ScCW to examine *Fhl2* expression. In WT or *Clec7a*$^{-/-}$ cells, the gene was basically poorly expressed and even following treatment with ScCW (**Figure 5B**). However, induction of *Fhl2* was triggered by BG65 or BG75 pretreatments (around 5-fold upregulations) in WT cells. Interestingly, Dectin-1-deficiency entailed a severe loss of *Fhl2* induction following BG65 treatment and almost abolished it after BG75 incubation. Western Blotting on BMDM lysates confirmed that FHL2 protein was more abundant after pretreatment with BG65 and BG75 (at least 2-fold more as compared to mock) than with ScCW following a secondary LPS stimulation and was poorly detectable in mock condition, with or without LPS stimulation (**Figure 5C**). Therefore, BG-enriched compounds induce *Fhl2* expression, essentially *via* the Dectin-1 pathway.

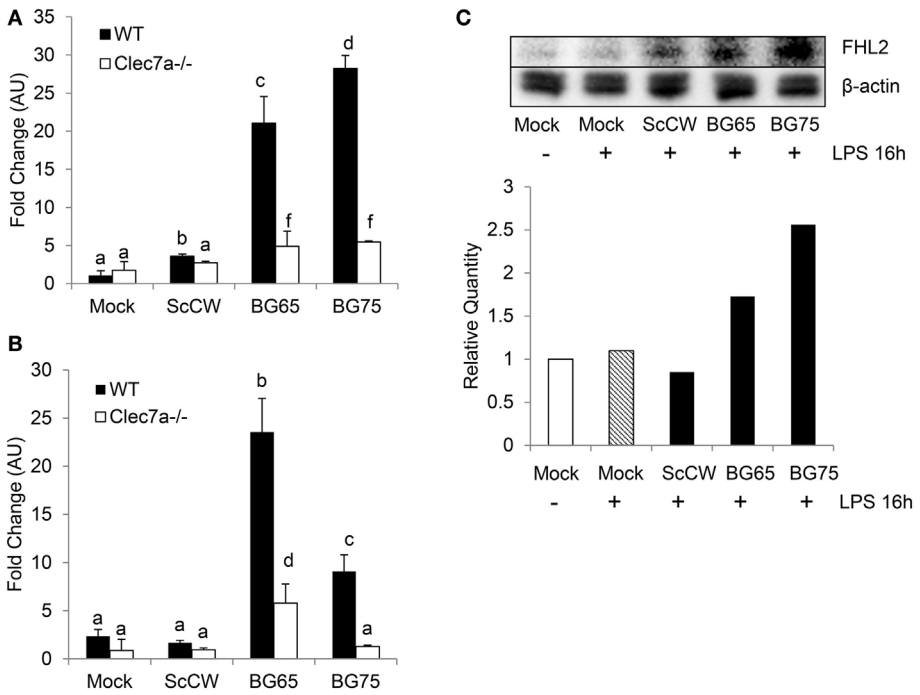

FIGURE 5 | *Fhl2* upregulation induced by BG-enriched compounds is under the control of Dectin-1. **(A)** Wild-type WT or *Clec7a*$^{-/-}$ bone marrow-derived macrophages (BMDM) were pre-treated as described in **Figure 4A**. *Fhl2* expression was determined by RT-qPCR as described for *Csf2*. **(B)** WT or *Clec7a*$^{-/-}$ BMDM were stimulated with BG-containing compounds for 8 h. At the end of the incubation, BMDM were lysed in RLT lysis buffer. After RNA extraction, cDNA synthesis and RT-qPCR were performed. Data are expressed as the fold change (FC) related to the mock condition value and are representative of two experiments performed in triplicate. **(C)** WT BMDM were stimulated following the same protocol as in **(A)**. After incubation, BMDM were lysed in RIPA buffer supplemented with 5 mM EDTA and protease inhibitor (Pierce™). After clarification and protein quantitation, 10 mg of total lysates were separated on a polyacrylamide gel. After transfer, nitrocellulose membrane was subjected to Western blotting with anti-FHL2 (F4B2-B11) and anti-β-actin (C4) mAbs (Santa Cruz Biotechnologies). Blotting was revealed using chemiluminescence. Results are also presented as the relative quantity of FHL2 protein detected in each condition as compared to the reference corresponding to the unstimulated cells. The data are representative of three independent experiments.

DISCUSSION

As previously described, the stimulation with ScCW or Zym led to a strong inflammatory response by macrophages resulting from a synergy between TLR (mainly TLR2) and Dectin-1-associated signaling (17, 20, 21, 32). By contrast, and as observed in our former study (23), BG-enriched parietal fractions failed to do so. And yet, the experiments presented here suggest that BG exposure profoundly imprints macrophage, phenotype, and functions. Indeed, we demonstrated that, when pretreated with BG-enriched preparations (BG65, BG75, or WGPd), TEPM or BMDM showed an exacerbated cytokine production in response to a secondary TLR-associated stimulus. This priming effect could be revealed through various secondary stimulations, including TLR2 or TLR4 ligands but also live *S. aureus* or *E. coli*. However, whether other ligands or pathogens have the same potential should be further tested.

The pretreatment with soluble BG (WGPs) did not improve macrophage response to LPS stimulation, suggesting that Dectin-1 clustering (33) by particulate BG and subsequent downstream signaling events are prerequisites for macrophage priming. The significant inhibition of priming observed in Dectin-1-deficient macrophages was consistent with this hypothesis. However, this inhibition was only partial and raised the question about the possible involvement of other BG receptors, at least in this experimental model.

Interestingly, the pretreatment with crude ScCW or Zym failed to prime macrophages although both of these yeast-derived preparations do contain BG (15 and 50%, respectively) (23, 34, 35). In a previous study, using TLR pathway reporter cell lines HEK293, we showed that BG enrichment process from ScCW to BG65 and BG75 removed the majority of TLR agonists including mannans (23). Taken together, these observations suggest that the simultaneous targeting of multiple PRRs, leading to a strong inflammatory response of macrophages, prevents the BG-induced priming.

Such a priming effect of BG was previously observed with the pretreatment of human PBMC with the pathogenic yeast *C. albicans* that results in an enhanced response to TLR-associated secondary stimulus (36). The engineering of *C. albicans* strains demonstrated that BG were central in this effect (36). Similarly, pretreating human monocytes with whole *C. albicans* or purified BG not only led to an enhanced cytokine response but also modified the cell shape, granulosity, and expression of surface markers. This "immune training" was observable in short term (24 h) (36) or long-term conditions (6 days) (37). Here, we unambiguously demonstrated that BG could train fully differentiated mouse macrophages in a short-term model. We also evaluated this training for longer resting periods between pretreatment and LPS re-stimulation. For up to 6 days, we observed increased cytokine production by BG-pretreated cells compared to non-pretreated cells (data not shown). However, these experiments were done in the absence of exogenous M-CSF. Under these conditions, non-pretreated macrophages started to present evident signs of cell suffering after 4 days of culture unlike BG-pretreated macrophages that appeared unaffected by growth factor deprivation. At days 5 and 6, cell numbers were clearly decreased in control wells creating an obvious bias in the measurement of cytokine production after LPS re-stimulation. Consequently, we decided to present data up to 3 days after pretreatment, as we did not observe differences in cell numbers that could explain a 5-fold increase in cytokine levels.

Taken together, these results fully demonstrate that exposure to fungal BGs profoundly modifies monocyte/macrophage physiology, and functions. Through a microarray analysis, we showed that BG pretreatment induced a specific set of genes in mouse macrophages. This was highlighted by comparing BG-pretreated cells versus non-pretreated cells or cells pretreated with ScCW that was shown unable to perform training of macrophages. By doing so, we identified molecular pathways preferentially triggered by BG. These pathways were highly related to PI3K cascade upstream of AKT. Consistently, we also found that GPCR signaling, known to activate PI3K cascade, was involved in BG-induced priming of macrophages. These findings were in agreement with previous studies, indicating that BGs induce a metabolic shift toward aerobic glycolysis mediated by an AKT–mTOR–HIF1α pathway in human monocytes (28, 37). Furthermore, BG-trained monocytes revealed higher intracellular ratio of nicotinamide adenine dinucleotide (NAD^+) to its reduced form (NADH) (28). We showed higher fluorescence of resofurin in BG75-treated BMDM using a Biotool Vita-Blue Cell Viability reagent. This assay is based on a redox reaction that transforms weakly fluorescent resazurin to highly fluorescent resofurin by oxidation of NADH in NAD^+ in metabolically active cells, meaning that BG-treated BMDM displayed higher NAD^+/NADH ratio, in line with results reported by *Cheng* et al.

By contrast, ScCW pretreatment mainly induced TLR-associated pathways signaling that is in line with our previous observations, showing a robust inflammatory response of macrophages through NFκB activation mediated by MyD88-dependent pathways after exposure with crude yeast CW or Zym (23). The leukotriene pathway was also triggered by ScCW pretreatment which is consistent with findings concerning Zym activity on human monocytes (38).

The microarray analysis consistently identified *Csf2* (that encodes for GM-CSF), the keystone of the gene network, and *Fhl2* as the two main upregulated genes by BG65 and BG75 priming conditions. IPA analysis revealed their enrichment for inflammatory response, proliferation and differentiation of bone marrow progenitors, migration and binding of cells, in antigen presentation and cell survival, immune cell trafficking, and development of hematological system. These two genes further targeted pathways highlighting the crucial role of cytokines as mediators of the communication between innate and adaptive responses.

GM-CSF is a highly pleiotropic cytokine and a growth factor involved in the differentiation of hematopoietic progenitors from bone marrow but GM-CSF is also recognized as a key mediator during inflammation (39–41).

In this study, we demonstrated that *Csf2* expression and GM-CSF production were highly specific of BG pretreatment as ScCW pretreatment failed to do so. Moreover, this dramatic enhancement was totally abrogated in Dectin-1-deficient macrophages, confirming the strong association between Dectin-1

and GM-CSF production. In agreement with this result, it was demonstrated that pre-incubating dendritic cells with GM-CSF substantially enhances the cytokine secretion upon Curd, a linear BG from *A. faecalis* stimulation (14). By using flow cytometry, we showed that GM-CSF treatment increased Dectin-1 expression on BMDM as previously observed with dendritic cells or with resident and thioglycollate-elicited macrophages treated with GM-CSF or IL-4 or a combination of both cytokines (12, 14, 15). It was, thus, suggested that such an upregulation of Dectin-1 expression consequently to GM-CSF allows Dectin-1-mediated TNFα induction (12). In line with this, GM-CSF was shown to be required to trigger a robust production of TNFα, IL-6, and IL-1β in Curd-stimulated dendritic cells (14).

In a previous study, we evidenced a late Dectin-1-dependent overexpression of *Csf2* following stimulation with BG65 or BG75 but unexpectedly, we found very low amounts (<5 pg/mL) of GM-CSF in culture supernatants even after 24 h of incubation (23). By contrast, the stimulation of peritoneal macrophages with soluble BG from *Grifola frondosa* mushroom results in a significant expression of *Csf2* with subsequent production of GM-CSF (100 pg/mL) after 6 h of incubation (12). However and again in contrast with our results, the induction of GM-CSF production by soluble BG appeared to be Dectin-1-independent confirming that particulate and soluble BG do not trigger similar pathways. In agreement with this, we showed here that, compared to *Sc* particulate BG, soluble BGs (WGPs) were unable to induce macrophages priming.

Our data seem to target GM-CSF as a pivotal actor of the BG-induced priming of macrophages. Consistently with this hypothesis, GM-CSF-treated macrophages/monocytes exposed to TLR2 or TLR4 ligands were shown to produce significantly more IL-1β, IL-6, and TNFα (30, 40–42). Furthermore, GM-CSF was also able to prevent endotoxin tolerance in macrophages by restoring TNFα production on LPS-tolerized human monocytes (43).

Similarly, it was very recently shown that GM-CSF, and IL-3, on its own, was sufficient to train human monocytes in a p38- and SIRT2-dependent manner (30). In this study, we also observed that GM-CSF pretreatment of mouse macrophages induced a moderate but significant increase of cytokine secretion upon LPS re-stimulation. Yet, this training effect remained much lower than the one mediated by BG or GM-CSF plus BG.

As GM-CSF appears to be strongly related to the priming of macrophages by particulate BG, we further investigated the influence of GM-CSF on BG-induced TNFα production.

Using decreasing concentrations of rGM-CSF during BG pretreatment, we showed that 10 pg/mL were enough to improve the priming of macrophages. Taken together with our previous observations, this result suggests that the endogenous production of GM-CSF induced by BG along the pretreatment step could be responsible for macrophage training. To rule out this hypothesis, we inhibited GM-CSF-associated signaling in macrophages by using a GM-CSFR blocking antibody. The amount of blocking antibody used was sufficient to completely inhibit the activity of 100 pg/mL rGM-CSF, a far greater concentration than the one supposed to be produced endogenously following BG pretreatment. Under these conditions, we showed that blockade of GM-CSF pathway did not affect the levels of training induced by BG, highlighting that endogenous GM-CSF is not required for the BG-induced training of macrophages, which clearly argues against results from previous studies in favor of a strong reduction of BG-induced TNFα in macrophages neutralized with anti-GM-CSF antibodies (12, 44).

Taken together, our results demonstrate that GM-CSF, which is endowed with low immune training properties on its own, is not intrinsically involved in the BG-induced training of macrophages although it can substantially improve it. However, we cannot exclude a contribution of GM-CSF in the long-term training model, as it favors cell survival and adherence (39–41, 45). This later hypothesis should be accurately investigated.

Intriguingly, we identified *Fhl2* (four-and-a-half LIM-only protein 2) as the second most upregulated gene in macrophages pretreated with BG and further stimulated with LPS. We demonstrated that *Fhl2* expression was specifically induced by BG in a Dectin-1-dependent manner. At the protein level, we showed that production of FHL2 was significantly increased after BG pretreatment and was not influenced by the secondary LPS stimulation. Here, we revealed for the first time the involvement of *Fhl2* in Dectin-1-mediated pathway. Again, ScCW was not able to modulate FHL2 expression and production, confirming the predominant role of Dectin-1- as compared to TLR-associated pathways.

Fhl2 is expressed in a cell-and tissue-specific manner and molecular mechanisms by which this protein exerts its roles remain incompletely understood, especially in cells where its expression is limited or absent. Moreover, according to its cytoplasmic or nuclear localization within the cell, FHL2 seems to have highly variable molecular partners as reviewed in Ref. (46) and to play important role as mediator in many signaling pathways, including NFκB signaling pathways (47, 48) or TGF-β signaling (49, 50).

Interestingly, FHL2 was reported to interact with NFκB but in a cell type-dependent manner. Indeed, FHL2 has been shown to inhibit NFκB activity during osteoclastogenesis by displacing TRAF6 from RANK (51). By contrast, FHL2 was shown to mediate IL-6 production through NFκB and p38 MAPK signaling pathway in muscle cells (48). Similarly, FHL2-deficiency in macrophages significantly reduced TNFα and IL-6 production following LPS exposure, suggesting that FHL2 acts as a positive regulator of NFκB through TRAF6 in liver macrophages (47) but also in FHL2-transfected HEK cells (52). Although our study does not bring definitive proofs of FHL2 involvement in short-term training of macrophages, its NFκB activating capacity is not consistent with the high levels of cytokine secretion recorded by BG-primed macrophages upon a secondary TLR-associated stimulation. Indeed, NFκB activity recorded in BG-trained BMDM was similar in ScCW-incubated cells, meaning that BG immune training is poorly correlated with NFκB-related signaling. Consequently, it remains highly plausible that FHL2 interacts with other nuclear transcription factors or cell signaling molecules.

However, there is no evidence that FHL2 activity directly result from Dectin-1 triggering and downstream signaling.

Indeed, we observed that at least 8 h of BG pretreatment were needed to induce macrophage priming and that 16 h of incubation with LPS were required to reveal macrophage training. These incubation times are sufficient to allow *de novo* synthesis of molecules that could link Dectin-1 and FHL2 activity. Undeniably, further investigations will be needed to decipher FHL2 regulation by Dectin-1 pathway and the associated molecular mechanisms.

Altogether, we established for the first time a short-term model of trained immunity with mouse macrophages using BG from *S. cerevisiae* and evidenced GM-CSF and FHL2 as potential co-actors of this priming effect. Considering the availability of industrial byproducts of *S. cerevisiae*, reprogramming monocytes/macrophages becomes possible using BG from this source to improve their response against invading pathogens.

ETHICS STATEMENT

WT C57Bl/6 mice were purchased from Janvier Labs (St Berthevin, France) and Clec7a$^{-/-}$ mice (5) were originally provided by Pr. Gordon Brown (University of Aberdeen, Scotland) and were bred in-house. Eight- to 12-week-old C57Bl/6 Clec7a$^{-/-}$ mice and their strain-matched WT controls from both sexes were housed under pathogen-free conditions in an accredited research animal facility of the National Veterinary College (UMR IHAP, Toulouse, France). This study was carried out in strict accordance with the Federation of European Laboratory Animal Science Association guidelines (FELASA). Experiments were performed by FELASA accredited investigators (no. 311155580) and approved by the local ethics committee, "Science et Santé Animale" (SSA). All efforts were made to minimize animal pain and distress.

AUTHOR CONTRIBUTIONS

Participated in research design: SW, GF, and GT; conducted experiments: SW, GT, and MF; performed data analysis: SW, GF, and GT; wrote or contributed to the writing of the manuscript: SW, GF, and GT.

ACKNOWLEDGMENTS

The authors would like to thank Dr. A. Roulet from the GeT-PlaGe platform (INRA, Toulouse) for analyzing gene expression using Biomark HD system (Fluidigm). We also thank Dr. Y. Lippi and C. Naylies from the GeT-TRiX platform (Toxalim, INRA, Toulouse) for helping in the microarray analysis. Finally, we thank Pr. GD. Brown (University of Aberdeen) for supplying us with C57Bl/6 *Clec7a*$^{-/-}$ mice. This manuscript includes for part Dr. Walachowski PhD thesis dataset (53).

FUNDING

This work was partly financed by Phileo-Lesaffre Animal Care. This work has received support from an "Investissements d'avenir" grant managed by Agence Nationale de la Recherche under the reference ANR-11-EQPX-0003 and from a joint call between "Institut Carnot en Santé Animale" and "Institut Carnot Pasteur Maladies Infectieuses" under the reference Glucastimmune.

SUPPLEMENTARY MATERIAL

The Supplementary Material for this article can be found online at http://journal.frontiersin.org/article/10.3389/fimmu.2017.01089/full#supplementary-material.

REFERENCES

1. Taylor PR, Martinez-Pomares L, Stacey M, Lin H-H, Brown GD, Gordon S. Macrophage receptors and immune recognition. *Annu Rev Immunol* (2005) 23:901–44. doi:10.1146/annurev.immunol.23.021704.115816
2. Creagh EM, O'Neill LAJ. TLRs, NLRs and RLRs: a trinity of pathogen sensors that co-operate in innate immunity. *Trends Immunol* (2006) 27:352–7. doi:10.1016/j.it.2006.06.003
3. Goodridge HS, Underhill DM. Fungal recognition by TLR2 and dectin-1. *Handb Exp Pharmacol* (2008) 183:87–109. doi:10.1007/978-3-540-72167-3_5
4. LeibundGut-Landmann S, Groß O, Robinson MJ, Osorio F, Slack EC, Tsoni SV, et al. Syk- and CARD9-dependent coupling of innate immunity to the induction of T helper cells that produce interleukin 17. *Nat Immunol* (2007) 8:630–8. doi:10.1038/ni1460
5. Taylor PR, Tsoni SV, Willment JA, Dennehy KM, Rosas M, Findon H, et al. Dectin-1 is required for β-glucan recognition and control of fungal infection. *Nat Immunol* (2007) 8:31–8. doi:10.1038/ni1408
6. Netea MG, Gow NA, Munro CA, Bates S, Collins C, Ferwerda G, et al. Immune sensing of *Candida albicans* requires cooperative recognition of mannans and glucans by lectin and toll-like receptors. *J Clin Invest* (2006) 116:1642–50. doi:10.1172/JCI27114
7. Underhill DM, Rossnagle E, Lowell CA, Simmons RM. Dectin-1 activates Syk tyrosine kinase in a dynamic subset of macrophages for reactive oxygen production. *Blood* (2005) 106:2543–50. doi:10.1182/blood-2005-03-1239
8. Goodridge HS, Shimada T, Wolf AJ, Hsu Y-MS, Becker CA, Lin X, et al. Differential use of CARD9 by dectin-1 in macrophages and dendritic cells. *J Immunol* (2009) 182:1146–54. doi:10.4049/jimmunol.182.2.1146
9. Brown GD, Taylor PR, Reid DM, Willment JA, Williams DL, Martinez-Pomares L, et al. Dectin-1 is a major β-glucan receptor on macrophages. *J Exp Med* (2002) 196:407–12. doi:10.1084/jem.20020470
10. Rogers NC, Slack EC, Edwards AD, Nolte MA, Schulz O, Schweighoffer E, et al. Syk-dependent cytokine induction by dectin-1 reveals a novel pattern recognition pathway for C type lectins. *Immunity* (2005) 22:507–17. doi:10.1016/j.immuni.2005.03.004
11. Gross O, Gewies A, Finger K, Schäfer M, Sparwasser T, Peschel C, et al. Card9 controls a non-TLR signalling pathway for innate anti-fungal immunity. *Nature* (2006) 442:651–6. doi:10.1038/nature04926
12. Masuda Y, Togo T, Mizuno S, Konishi M, Nanba H. Soluble β-glucan from *Grifola frondosa* induces proliferation and dectin-1/Syk signaling in resident macrophages via the GM-CSF autocrine pathway. *J Leukoc Biol* (2012) 91:547–56. doi:10.1189/jlb.0711386
13. Harada T, Ohno N. Contribution of dectin-1 and granulocyte macrophage–colony stimulating factor (GM-CSF) to immunomodulating actions of β-glucan. *Int Immunopharmacol* (2008) 8:556–66. doi:10.1016/j.intimp.2007.12.011
14. Min L, Isa SABM, Fam WN, Sze SK, Beretta O, Mortellaro A, et al. Synergism between curdlan and GM-CSF confers a strong inflammatory signature to dendritic cells. *J Immunol* (2012) 188:1789–98. doi:10.4049/jimmunol.1101755
15. Willment JA, Lin H-H, Reid DM, Taylor PR, Williams DL, Wong SYC, et al. Dectin-1 expression and function are enhanced on alternatively activated and GM-CSF-treated macrophages and are negatively regulated by IL-10, dexamethasone, and lipopolysaccharide. *J Immunol* (2003) 171:4569–73. doi:10.4049/jimmunol.171.9.4569
16. Saijo S, Fujikado N, Furuta T, Chung S, Kotaki H, Seki K, et al. Dectin-1 is required for host defense against *Pneumocystis carinii* but not against *Candida albicans*. *Nat Immunol* (2007) 8:39–46. doi:10.1038/ni1425

17. Ferwerda G, Meyer-Wentrup F, Kullberg B-J, Netea MG, Adema GJ. Dectin-1 synergizes with TLR2 and TLR4 for cytokine production in human primary monocytes and macrophages. *Cell Microbiol* (2008) 10:2058–66. doi:10.1111/j.1462-5822.2008.01188.x
18. Lebron F, Vassallo R, Puri V, Limper AH. *Pneumocystis carinii* cell wall β-glucans initiate macrophage inflammatory responses through NF-κB activation. *J Biol Chem* (2003) 278:25001–8. doi:10.1074/jbc.M301426200
19. Underhill DM. Collaboration between the innate immune receptors dectin-1, TLRs, and Nods. *Immunol Rev* (2007) 219:75–87. doi:10.1111/j.1600-065X.2007.00548.x
20. Gantner BN, Simmons RM, Canavera SJ, Akira S, Underhill DM. Collaborative induction of inflammatory responses by dectin-1 and toll-like receptor 2. *J Exp Med* (2003) 197:1107–17. doi:10.1084/jem.20021787
21. Dennehy KM, Ferwerda G, Faro-Trindade I, Pyż E, Willment JA, Taylor PR, et al. Syk kinase is required for collaborative cytokine production induced through dectin-1 and toll-like receptors. *Eur J Immunol* (2008) 38:500–6. doi:10.1002/eji.200737741
22. Yadav M, Schorey JS. The β-glucan receptor dectin-1 functions together with TLR2 to mediate macrophage activation by mycobacteria. *Blood* (2006) 108:3168–75. doi:10.1182/blood-2006-05-024406
23. Walachowski S, Tabouret G, Foucras G. Triggering dectin-1-pathway alone is not sufficient to induce cytokine production by murine macrophages. *PLoS One* (2016) 11:e0148464. doi:10.1371/journal.pone.0148464
24. Quintin J, Saeed S, Martens JHA, Giamarellos-Bourboulis EJ, Ifrim DC, Logie C, et al. *Candida albicans* infection affords protection against reinfection via functional reprogramming of monocytes. *Cell Host Microbe* (2012) 12:223–32. doi:10.1016/j.chom.2012.06.006
25. Bistoni F, Vecchiarelli A, Cenci E, Puccetti P, Marconi P, Cassone A. Evidence for macrophage-mediated protection against lethal *Candida albicans* infection. *Infect Immun* (1986) 51:668–74.
26. Netea MG, Quintin J, van der Meer JWM. Trained immunity: a memory for innate host defense. *Cell Host Microbe* (2011) 9:355–61. doi:10.1016/j.chom.2011.04.006
27. van der Meer JWM, Joosten LAB, Riksen N, Netea MG. Trained immunity: a smart way to enhance innate immune defence. *Mol Immunol* (2015) 68:40–4. doi:10.1016/j.molimm.2015.06.019
28. Cheng S-C, Quintin J, Cramer RA, Shepardson KM, Saeed S, Kumar V, et al. mTOR- and HIF-1α-mediated aerobic glycolysis as metabolic basis for trained immunity. *Science* (2014) 345:1250684. doi:10.1126/science.1250684
29. Saeed S, Quintin J, Kerstens HHD, Rao NA, Aghajanirefah A, Matarese F, et al. Epigenetic programming of monocyte-to-macrophage differentiation and trained innate immunity. *Science* (2014) 345:1251086. doi:10.1126/science.1251086
30. Borriello F, Iannone R, Di Somma S, Loffredo S, Scamardella E, Galdiero MR, et al. GM-CSF and IL-3 modulate human monocyte TNF-α production and renewal in in vitro models of trained immunity. *Front Immunol* (2017) 7:680. doi:10.3389/fimmu.2016.00680
31. Accarias S, Lugo-Villarino G, Foucras G, Neyrolles O, Boullier S, Tabouret G. Pyroptosis of resident macrophages differentially orchestrates inflammatory responses to *Staphylococcus aureus* in resistant and susceptible mice. *Eur J Immunol* (2015) 45:794–806. doi:10.1002/eji.201445098
32. Brown GD, Herre J, Williams DL, Willment JA, Marshall ASJ, Gordon S. Dectin-1 mediates the biological effects of β-glucans. *J Exp Med* (2003) 197:1119–24. doi:10.1084/jem.20021890
33. Goodridge HS, Reyes CN, Becker CA, Katsumoto TR, Ma J, Wolf AJ, et al. Activation of the innate immune receptor dectin-1 upon formation of a "phagocytic synapse". *Nature* (2011) 472:471–5. doi:10.1038/nature10071
34. Carlo FJD, Fiore JV. On the composition of zymosan. *Science* (1958) 127:756–7. doi:10.1126/science.127.3301.756-a
35. Riggi SJ, Di Luzio NR. Identification of a reticuloendothelial stimulating agent in zymosan. *Am J Physiol* (1961) 200:297–300.
36. Ifrim DC, Joosten LAB, Kullberg B-J, Jacobs L, Jansen T, Williams DL, et al. *Candida albicans* primes TLR cytokine responses through a dectin-1/Raf-1-mediated pathway. *J Immunol* (2013) 190:4129–35. doi:10.4049/jimmunol.1202611
37. Ifrim DC, Quintin J, Joosten LAB, Jacobs C, Jansen T, Jacobs L, et al. Trained immunity or tolerance: opposing functional programs induced in human monocytes after engagement of various pattern recognition receptors. *Clin Vaccine Immunol* (2014) 21:534–45. doi:10.1128/CVI.00688-13
38. Czop JK, Austen KF. Generation of leukotrienes by human monocytes upon stimulation of their beta-glucan receptor during phagocytosis. *Proc Natl Acad Sci U S A* (1985) 82:2751–5. doi:10.1073/pnas.82.9.2751
39. Hamilton JA, Anderson GP. GM-CSF biology. *Growth Factors* (2004) 22:225–31. doi:10.1080/08977190412331279881
40. Sorgi CA, Rose S, Court N, Carlos D, Paula-Silva FWG, Assis PA, et al. GM-CSF priming drives bone marrow-derived macrophages to a pro-inflammatory pattern and downmodulates PGE2 in response to TLR2 ligands. *PLoS One* (2012) 7:e40523. doi:10.1371/journal.pone.0040523
41. Däbritz J, Weinhage T, Varga G, Wirth T, Walscheid K, Brockhausen A, et al. Reprogramming of monocytes by GM-CSF contributes to regulatory immune functions during intestinal inflammation. *J Immunol* (2015) 194:2424–38. doi:10.4049/jimmunol.1401482
42. Rosas M, Liddiard K, Kimberg M, Faro-Trindade I, McDonald JU, Williams DL, et al. The induction of inflammation by dectin-1 in vivo is dependent on myeloid cell programming and the progression of phagocytosis. *J Immunol* (2008) 181:3549–57. doi:10.4049/jimmunol.181.5.3549
43. Adib-Conquy M, Cavaillon J-M. Gamma interferon and granulocyte/monocyte colony-stimulating factor prevent endotoxin tolerance in human monocytes by promoting interleukin-1 receptor-associated kinase expression and its association to MyD88 and not by modulating TLR4 expression. *J Biol Chem* (2002) 277:27927–34. doi:10.1074/jbc.M200705200
44. Harada T, Miura NN, Adachi Y, Nakajima M, Yadomae T, Ohno N. Granulocyte-macrophage colony-stimulating factor (GM-CSF) regulates cytokine induction by 1,3-β-D-glucan SCG in DBA/2 mice in vitro. *J Interferon Cytokine Res* (2004) 24:478–89. doi:10.1089/1079990041689656
45. Lacey DC, Achuthan A, Fleetwood AJ, Dinh H, Roiniotis J, Scholz GM, et al. Defining GM-CSF- and macrophage-CSF-dependent macrophage responses by in vitro models. *J Immunol* (2012) 188:5752–65. doi:10.4049/jimmunol.1103426
46. Johannessen M, Møller S, Hansen T, Moens U, Ghelue MV. The multifunctional roles of the four-and-a-half-LIM only protein FHL2. *Cell Mol Life Sci* (2006) 63:268–84. doi:10.1007/s00018-005-5438-z
47. Dahan J, Nouët Y, Jouvion G, Levillayer F, Adib-Conquy M, Cassard-Doulcier A-M, et al. LIM-only protein FHL2 activates NF-κB signaling in the control of liver regeneration and hepatocarcinogenesis. *Mol Cell Biol* (2013) 33:3299–308. doi:10.1128/MCB.00105-13
48. Wong C-H, Mak GW-Y, Li M-S, Tsui SK-W. The LIM-only protein FHL2 regulates interleukin-6 expression through p38 MAPK mediated NF-κB pathway in muscle cells. *Cytokine* (2012) 59:286–93. doi:10.1016/j.cyto.2012.04.044
49. Ding L, Wang Z, Yan J, Yang X, Liu A, Qiu W, et al. Human four-and-a-half LIM family members suppress tumor cell growth through a TGF-β-like signaling pathway. *J Clin Invest* (2009) 119:349–61. doi:10.1172/JCI35930
50. Xia T, Lévy L, Levillayer F, Jia B, Li G, Neuveut C, et al. The four and a half LIM-only protein 2 (FHL2) activates transforming growth factor β (TGF-β) signaling by regulating ubiquitination of the E3 ligase Arkadia. *J Biol Chem* (2013) 288:1785–94. doi:10.1074/jbc.M112.439760
51. Bai S, Kitaura H, Zhao H, Chen J, Müller JM, Schüle R, et al. FHL2 inhibits the activated osteoclast in a TRAF6-dependent manner. *J Clin Invest* (2005) 115:2742–51. doi:10.1172/JCI24921
52. Stilo R, Leonardi A, Formisano L, Di Jeso B, Vito P, Liguoro D. TUCAN/CARDINAL and DRAL participate in a common pathway for modulation of NF-κB activation. *FEBS Lett* (2002) 521:165–9. doi:10.1016/S0014-5793(02)02869-7
53. Walachowski S. *Etude des propriétés immunostimulantes de composés pariétaux de levure sur les macrophages murins et évaluation dans des modèles infectieux*. (2016). Available from: https://tel.archives-ouvertes.fr/tel-01477575/document

Conflict of Interest Statement: The authors declare that the research was conducted in the absence of any commercial or financial relationships that could be construed as a potential conflict of interest.

frontiers in Immunology

ORIGINAL RESEARCH
published: 17 November 2017
doi: 10.3389/fimmu.2017.01565

Intracellular S100A9 Promotes Myeloid-Derived Suppressor Cells during Late Sepsis

*Jun Dai[1], Ajinkya Kumbhare[1], Dima Youssef[1], Charles E. McCall[2] and Mohamed El Gazzar[1]**

[1] Department of Internal Medicine, East Tennessee State University College of Medicine, Johnson City, TN, United States, [2] Section of Molecular Medicine, Department of Internal Medicine, Wake Forest University School of Medicine, Winston-Salem, NC, United States

Myeloid precursor cell reprogramming into a myeloid-derived suppressor cell (MDSC) contributes to high mortality rates in mouse and human sepsis. S100A9 mRNA and intracellular protein levels increase during early sepsis and remain elevated in Gr1$^+$CD11b$^+$ MDSCs after pro-inflammatory sepsis transitions to the later chronic anti-inflammatory and immunosuppressive phenotype. The purpose of this study was to determine whether intracellular S100A9 protein might sustain Gr1$^+$CD11b$^+$ MDSC repressor cell reprogramming during sepsis. We used a chronic model of sepsis in mice to show that S100A9 release from MDSCs and circulating phagocytes decreases after early sepsis and that targeting the *S100a9* gene improves survival. Surprisingly, we find that intracellular S100A9 protein translocates from the cytosol to nucleus in Gr1$^+$CD11b$^+$ MDSCs during late sepsis and promotes expression of miR-21 and miR-181b immune repressor mediators. We further provide support of this immunosuppression pathway in human sepsis. This study may inform a new therapeutic target for improving sepsis outcome.

Keywords: sepsis, myeloid-derived suppressor cells, immune suppression, S100A9, myeloid cell reprogramming

OPEN ACCESS

Edited by:
Janos G. Filep, Université de Montréal, Canada

Reviewed by:
Daniel Remick, Boston University School of Medicine, United States
Amiram Ariel, University of Haifa, Israel

***Correspondence:**
Mohamed El Gazzar
elgazzar@etsu.edu

Specialty section:
This article was submitted to Molecular Innate Immunity, a section of the journal Frontiers in Immunology

Received: *09 August 2017*
Accepted: *01 November 2017*
Published: *17 November 2017*

Citation:
Dai J, Kumbhare A, Youssef D, McCall CE and El Gazzar M (2017) Intracellular S100A9 Promotes Myeloid-Derived Suppressor Cells during Late Sepsis. Front. Immunol. 8:1565. doi: 10.3389/fimmu.2017.01565

INTRODUCTION

Sepsis is the leading cause of death among critically ill patients (1, 2). The initial/acute phase of sepsis, which may cause cardiovascular collapse and rapid death, more commonly progresses to chronic sepsis, which is clinically characterized by innate and adaptive immune incompetence and organ failure (3–5). This chronic sepsis state has been named the persistent inflammation-immunosuppression and catabolism syndrome (PICS) (6). Although well recognized and characterized, the molecular events that promote this unresolving state of sepsis are unclear, but sustained presence of a cell phenotype called myeloid-derived suppressor cells (MDSCs) likely contributes to PICS (7). This broad-based immune-suppressor state with organ failure is typified by repressed effector phenotypes of CD4$^+$ and CD8$^+$ T-cells, circulating, splenic, and myeloid- dendritic, NK cells and other heterogeneous innate and adaptive immune cells (4, 8). PICS clinical phenotype is reflected by persistent bacterial infection and reactivation of latent viruses (4, 6). Importantly, the immune-suppressor phenotype typifies endotoxin tolerance and develops within hours of the early hyper-inflammatory cytokine-mediated "cytokine storm" (9, 10). Other characteristics are increased apoptosis of different cell types (4) and repressed mitochondrial fueling by glucose and fatty acids (11, 12).

Calcium-binding proteins S100A8 and S100A9 are markedly increased during sepsis (13), and their elevated levels in circulating innate immune phagocytes during sepsis may contribute to acute

and chronic inflammation (14, 15). S100A8 and S100A9 are mainly expressed in the myeloid lineage cells (16), including monocytes and granulocytes, but not resident tissue macrophages (15) and are dominant in the systemic circulation. The two proteins are also expressed in early stages of myeloid differentiation and decline during maturation, but remain elevated in neutrophils (17). S100A8/A9 protein complexes are mostly cytosolic, where they are recruited to the plasma membrane and secreted after protein kinase C (PKC) activation and cytoskeletal rearrangement following phagocytosis (14).

Most studies of S100A8/A9 proteins emphasize them as pro-inflammatory mediators, which amplify acute and chronic inflammatory processes during phagocyte activation (14, 18, 19). S100A8/A9 heterodimers released at sites of inflammation induce more S100A8/A9 in phagocytes, thereby acting as a feedforward loop to amplify the local inflammatory reaction (15, 20). Heterodimeric S100A8/A9 binds to and activates toll-like receptor 4 (TLR4), a master "alarmin" sensor (21). S100A8/A9 heterodimers are secreted readily from bone marrow cells and blood monocytes following bacterial lipopolysaccharide (LPS)-mediated activation of TLR4 (14). Further supporting pro-inflammatory functions is the finding that S100A9$^{-/-}$ mice exhibit blunted LPS-induced endotoxemia (21). In contrast, there are reports of anti-inflammatory properties of S100A8/A9 showing that intraperitoneal injections of S100A8/A9 heterodimers into rat after LPS administration reduces serum levels of pro-inflammatory IL-6 and nitrite (22). In addition, because S100A8/A9 supports phagocyte migration, inhibiting S100A8/A9 would have anti-inflammatory potential (14). An important finding suggesting a repressor function is that immune repressor mediator IL-10 induces S100A8 in human macrophages (23).

Here, we report a new function for S100A9 that further supports the repressor concept of S100A8/A9. We find that mice genetically deficient for S100A9 are protected from late sepsis deaths by preventing MDSC repressor activity. We further find that S100A8/A9 proteins are released from phagocytes during early, but not late sepsis, and that cytosolic S100A9 translocates from cytosol to the nucleus of MDSCs. Mechanistically, our data support that nuclear S100A9 promotes the expression of known immunosuppressive miR-21 and miR-181b (24). The findings of this study support therapeutic targeting of S100A9 for chronic sepsis.

MATERIALS AND METHODS

Mice

The S100a9 mutant mouse strain [S100a9tm1$^{(KOMP)/VLcg}$] used for this study was created from ES cell clone 12158a-E1, generated by Regeneron Pharmaceuticals (Eastview, NY, USA), and made into live mice by the KOMP Repository[1] and the Mouse Biology Program[2] at the University of California Davis. Methods used to create the Velocigene targeted alleles have been published (25). Cryopreserved sperm from the KOMP repository was used for *in vitro* fertilization of C57BL/6NJ oocytes to reconstitute the strain (work performed by TransViragen, Chapel Hill, NC, USA). Heterozygous animals were intercrossed to generate homozygous (−/−) mutant animals for study. The mice were bred and housed in a pathogen-free facility in the Division of Laboratory Animal Resources. Wild-type male C57BL/6J mice, 8–10 weeks were purchased from Jackson Laboratory (Bar Harbor, ME, USA) and used as controls, and were acclimated to the new environment for a week before surgery. All experiments were conducted in accordance with National Institutes of Health guidelines and were approved by the East Tennessee State University Animal Care and Use Committee.

Polymicrobial Sepsis

Polymicrobial sepsis was induced in male wild-type and S100A9 knockout mice, 8–10 week old, by cecal ligation and puncture (CLP) as described previously (26). Briefly, mice were anesthetized *via* inhalation with 2.5% isoflurane (Abbott Laboratories, Abbott Park, IL, USA). A midline abdominal incision was made and the cecum was exteriorized, ligated distal to the ileocecal valve, and then punctured twice with a 23-gauge needle. A small amount of feces was extruded into the abdominal cavity. The abdominal wall and skin were sutured in layers with 3-0 silk. Sham-operated mice were treated identically except that the cecum was neither ligated nor punctured. Mice received (i.p.) 1 ml lactated Ringers plus 5% dextrose for fluid resuscitation. To induce sepsis that develops into early and late phases, mice were subcutaneously administered antibiotic (Imipenem; 25 mg/kg body weight) or an equivalent volume of 0.9% saline. To establish intra-abdominal infection and approximate the clinical condition of early human sepsis where there is a delay between the onset of sepsis and the delivery of therapy (27), injections of Imipenem were given at 8 and 16 h after CLP. Based on our experience, these levels of injury and manipulation create prolonged infections with high mortality (~60–70%) during the late/chronic phase (26).

The presence of early sepsis was confirmed by transient systemic bacteremia and elevated cytokine levels in the first 5 days after CLP. Late/chronic sepsis (after day 5) was confirmed by enhanced peritoneal bacterial overgrowth and reduced circulating pro-inflammatory cytokines. Table S1 in Supplementary Material includes the CLP mice that were used in the study.

Sepsis Patients

Patients 18 years of age or older who were admitted to Johnson City Medical Center and Franklin Woods Hospital in Johnson City, Tennessee, and who were diagnosed with sepsis or septic shock were included in the study. Sepsis was defined as the presence of suspected or documented infection with at least two of the following criteria: core temperature >38°C or <36°C; heart rate >90 beats/min; respiratory rate >20 breaths/min or arterial blood partial pressure of carbon dioxide <32 mmHg; or white blood cell count >12,000 cells/mm^3 or <4,000/mm^3. Septic shock was defined as sepsis with persisting hypotension requiring vasopressors to maintain MAP ≥65 mmHg and having a serum lactate >2 mmol/L despite adequate volume resuscitation (28). Patients presented with infections related to Gram-negative or Gram-positive bacteria. The primary infection included urinary

[1] http://www.komp.org.
[2] http://www.mousebiology.org.

tract infection, blood stream infection, and respiratory tract infection. Patients had at least 1 comorbid condition, including nephropathy, psoriasis, splenectomy, colon cancer, or pulmonary aspergillosis. Patients with leukopenia due to chemotherapy or glucocorticoid therapy or HIV infection were excluded from the study. Patients were divided into two categories: early sepsis and late sepsis, relative to the day of sepsis diagnosis. The early septic group included patients within 1–5 days of sepsis diagnosis. Those who have been septic for more than 6 days were considered late septic. For this latter group, blood was drawn at days 6–68 after sepsis diagnosis. Blood samples obtained from healthy control subjects were supplied by Physicians Plasma Alliance (Gray, TN, USA). The study was approved by the Institutional Review Board (IRB) of the East Tennessee State University (IRB#: 0714.6s). Signed informed consent was obtained from all subjects.

Immunoblotting

Whole cell lysate, cytoplasmic, and nuclear proteins were prepared as described previously (29). Equal amounts of protein extracts were mixed with 5× Laemmeli sample buffer, separated by SDS-10% polyacrylamide gel (Bio-Rad, Hercules, CA, USA) and subsequently transferred to nitrocellulose membranes (Thermo Fisher Scientific, Waltham, MA, USA). After blocking with 5% milk in Tris-buffered saline/Tween-20 for 1 h at room temperature, membranes were probed overnight at 4°C with the following primary antibodies: anti-goat S100A8 (sc-8112; Santa Cruz Biotechnology, Santa Cruz, CA, USA); anti-Rabbit S100A9 (ab75478) and anti-mouse S100A8/A9 heterodimer (ab17050), both from Abcam (Cambridge, MA, USA); anti-Rabbit phospho-threonine113 S100A9 (12782; Signalway Antibody LLC., College Park, MD, USA); anti-Rabbit p38 (sc-7149) and p-p38 (sc-17852-R), anti-mouse phospho-serine 657 PKC (sc-377565), anti-Rabbit phospho-serine 660 PKC (sc-11760-R) (Santa Cruz Biotechnology). The S100A8/9 heterodimer was detected under non-denaturing conditions. After washing, blots were incubated with the appropriate HRP-conjugated secondary antibody (Life Technologies, Grand Island, NY) for 2 h at room temperature. Proteins were detected with the enhanced chemiluminescence detection system (Thermo Fisher Scientific, Waltham, MA, USA), the bands were visualized using the ChemiDoc XRS System (Bio-Rad), and the images were captured with the Image Lab Software V3.0. Membranes were stripped and re-probed with actin (Sigma-Aldrich, Saint Louis, MO, USA) antibody as a loading control.

Blood Phagocytes and Plasma

Mice were subjected to deep anesthesia with isoflurane and blood was collected *via* cardiac puncture using EDTA-rinsed syringes. Blood was diluted fivefold (up to 2.5 ml) in phosphate-buffered saline containing 0.3 mM EDTA. To obtain phagocytes (mainly monocytes and polymorphonuclear neutrophils), we first isolated peripheral blood mononuclear cells (PBMCs) and granulocytes by gradients of Histopage-1077 and Histopaque-1119 following the manufacturer's instructions (Sigma-Aldrich, Saint Louis, MO, USA). Briefly, diluted blood (2.5 ml) was layered in a 15-ml conical tube containing 2.5 ml Histopague-1119 (bottom layer) and 2.5 ml Histopaque-1077. Samples were centrifuged at 700*g* for 30 min at room temperature. Plasma was collected and stored at −20°C for later analysis. The upper cell layer containing PBMCs was removed and washed with PBS. The lower cell layer containing granulocytes was washed with PBS three times by centrifugation at 200*g* for 10 min. With this method, erythrocytes and platelets are removed by the low speed centrifugation during the washing steps. Monocytes were then isolated from the PBMCs by positive selection with anti-Ly6C antibody and combined with the granulocytes (mainly neutrophils), to represent the phagocyte population used in the study. In some experiments, granulocytes were used separately.

Peritoneal Bacterial Quantification

Immediately after mice were euthanized, the peritoneal cavity was lavaged with 5 ml PBS. The lavage was cleared by centrifugation and plated on trypticase soy agar base (BD Biosciences, Sparks, MD, USA). The plates were incubated for 24 h at 37°C under aerobic conditions. The plates were read by a microbiologist and the colony-forming units (CFUs) were enumerated.

Isolation of Gr1$^+$CD11b$^+$ Cells

Gr1$^+$CD11b$^+$ cells were isolated from the bone marrow or spleens by use of magnetically assisted cell sorting according to the manufacturer's protocol (Miltenyi Biotech, Auburn, CA, USA). The bone marrow was flushed out of the femurs with RPMI-1640 medium (without serum) under aseptic conditions (26). The spleens were dissociated in RPMI-1640 medium. A single cell suspension of the bone marrow or spleens was made by pipetting up and down and filtering through a 70-μm nylon strainer, followed by incubation with erythrocyte lysis buffer and washing. To purify total Gr1$^+$CD11b$^+$ cells, the single cell suspension was subjected to positive selection of the Gr1$^+$ cells by incubating with biotin-coupled mouse anti-Gr1 antibody (Clone RB6-8C5; eBioscience, San Diego, CA, USA) for 15 min at 4°C. Cells were then incubated with anti-biotin magnetic beads for 20 min at 4°C and subsequently passed over a MS column. Purified Gr1$^+$CD11b$^+$ cells were then washed and resuspended in sterile saline. The cell purity was more than 90% as determined by flow cytometry.

Flow Cytometry

Gr1$^+$CD11b$^+$ cells were stained by incubation for 30 min on ice in staining buffer (PBS plus 2% FBS) with the following mouse antibodies: fluorescein isothiocyanate (FITC)-conjugated anti-Gr1, phycoerythrin (PE)-conjugated anti-CD11b, allophycocyanin-conjugated anti-F4/80, PE-conjugated anti-CD11c, FITC-conjugated anti-MHC II. CD4$^+$ T cells were stained with PE-conjugated anti-CD4 antibody (all antibodies were from eBioscience, San Diego, CA, USA). An appropriate isotype-matched control was used for each antibody. After washing, the samples were analyzed by an Accuri C6 flow cytometer (BD, Franklin Lakes, NJ, USA).

Cell Proliferation Assay

Spleen CD4$^+$ T cells were isolated from normal (naive) mice by positive selection using magnetic beads (Miltenyi). Cells were

fluorescently labeled with carboxy-fluorosceindiacetate, succinimidyl ester (CFSE) dye using the Vybrant CFDA SE Cell Tracer Kit (Invitrogen Molecular Probes, Eugene, OR, USA). Cells were incubated for 10 min at room temperature with 10 μM CFSE dye and then cocultured (at 1:1 ratio) with the $Gr1^+$ $CD11b^+$ cells, which were isolated from the bone marrow of sham or late septic mice. T cell proliferation was induced by the stimulation with an anti-CD3 plus anti-CD28 antibody (1 μg/ml/each). After 3 days, cells were harvested and $CD4^+$ T cell proliferation was determined by the step-wise dilution of CFSE dye in dividing $CD4^+$ T cells, using flow cytometry.

Real-time PCR

Quantitative real-time qPCR was used to determine the expression levels of S100A8, S100A9, miR-21, and miR-181b in $Gr1^+CD11b^+$ cells. For S100A8 and S100A9, total RNA was isolated using TRIzol reagent (Invitrogen, Carlsbad, CA, USA) and amplified using QuantiNova SYBR Green RT-PCR kit and QuantiTect Primer Assays specific to S100A8 and S100A9 (Qiagen, Germantown, MD). The target RNA: 18S rRNA ratio was calculated using the $2^{-\Delta\Delta Ct}$ cycle threshold.

For miR-21 and miR-181b measurements, miRNA-enriched RNA was isolated and measured using miScript SYBR Green PCR kit and miScript Primer Assays specific to miR-21 and miR-181b (Qiagen). The expression level was calculated using the $2^{-\Delta\Delta Ct}$ cycle threshold method after normalization to the endogenous U6 RNA as an internal control.

Ca^{2+} Assay

Intracellular calcium levels in phagocytes were measured using the cell-based Fluo-4 NW Calcium Assay kit according to the manufacturer's protocol (Molecular Probes, Eugene, OR, USA).

ELISA

Specific ELISA kits were used to measure the levels of S100A8, S100A9 (MyBioSource, San Diego, CA, USA) and S100A8/A9 heterodimer (R&D Systems, Minneapolis, MN, USA). Levels of TNFα and IL-10 were determined using specific ELISA kits (eBioscience) according to the manufacturer's instructions. Each sample was run in duplicate.

Statistical Analysis

The Kaplan–Meier survival curve was plotted by use of a GraphPad Prism 5 (GraphPad Software, La Jolla, CA, USA) and survival significance was determined by a log-rank test. Other data were analyzed by Microsoft Excel, V3.0. Data are expressed as mean ± SD. Differences among groups were analyzed by a two-tailed Student's *t*-test for two groups and by ANOVA for multiple groups. P values < 0.05 were considered statistically significant.

RESULTS

S100A8/9 Play a Major Role in Sepsis Mortality

To examine the physiologic contribution of S100A8/A9 to sepsis, we created an S100A9 knockout mouse on a C57BL/6 background. A diagram showing the *S100a9* knockout allele and location of the PCR genotyping primers is presented in **Figure 1**.

Our model of polymicrobial sepsis with fluid resuscitation and limited antibiotic treatment develops into early and late sepsis phases (26). We previously showed that mortality is higher during the late/chronic phase and is mainly due to immunosuppression (30). Sepsis was induced by CLP, and survival was reported for a 4-week period. Mice moribund during early sepsis (defined as the first 5 days after CLP) or late sepsis (the time after day 6) were sacrificed and analyzed. Because most of the S100A9 knockout mice survived late sepsis, for each moribund and sacrificed mouse from the wild-type group, a healthy appearing mouse from the S100A9 knockout group was also sacrificed at the same time, but is reported as "survivor."

As shown in **Figure 2A**, 100% of the wild-type mice died before the end of the 4-week period. Lack of S100A8/A9 proteins slightly improved survival during early sepsis at days 3–5, with 14.7 and 15.2% increases in survival, respectively, at days 3 and 5 compared to the wild-type mice. Of note, survival in the late sepsis phase was improved by 80% in the S100A9 knockout ($S100A9^{-/-}$) vs. wild-type mice (**Figure 2A**). As expected, S100A8 mRNA, but not protein, was detected in phagocytes from septic wild-type and S100A9 knockout mice (**Figures 2B,C**).

S100A9 Knockout Attenuates Late Sepsis Immunosuppression

Early/acute septic mice display elevated levels of pro-inflammatory cytokines such as TNFα, whereas late/chronic septic mice are known to progress to an anti-inflammatory/immunosuppressive phenotype characterized by elevated levels of IL-10 and increased peritoneal bacterial growth (30). We

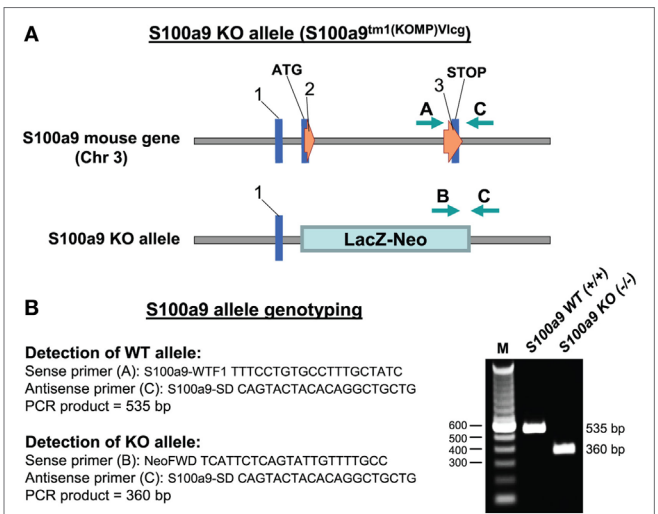

FIGURE 1 | Targeted deletion of the *S100a9* gene. **(A)** The *S100a9* gene was inactivated by insertion of the lacZ-neo cassette into exon 2 immediately next to the transcription start site (ATG). **(B)** Nucleotide sequences of the genotyping primers used for detection of the WT and KO alleles and agarose gel electrophoresis of the PCR products generated from $Gr1^+CD11b^+$ cells (right). M, size marker; WT, wild-type; KO, knockout.

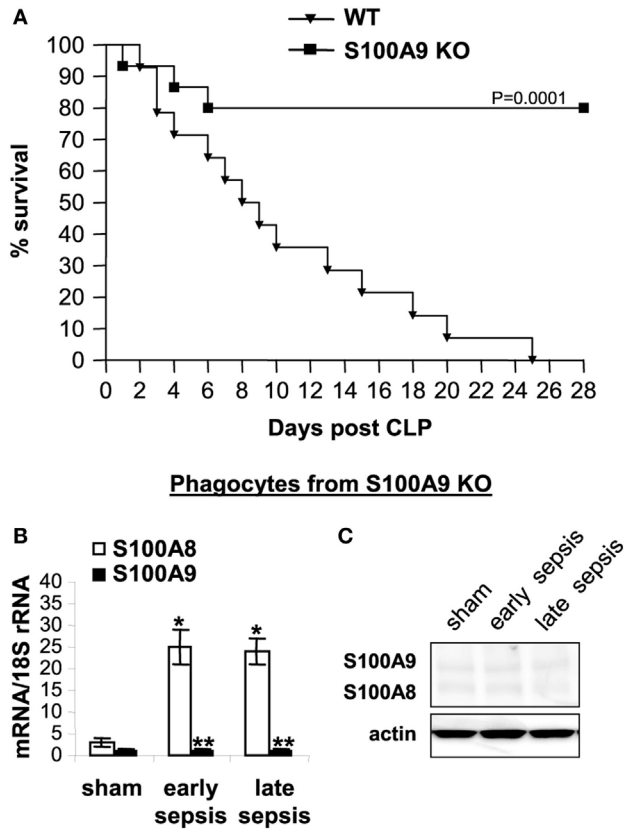

FIGURE 2 | The S100A9 knockout improves late sepsis survival. Sepsis was induced by cecal ligation and puncture (CLP) using a 23-gauge needle, and mice were given antibiotics with fluid resuscitation. With this injury and treatment, sepsis develops into an early phase (defined as days 1–5 after CLP) and a late phase (day 6 thereafter). **(A)** Kaplan–Meier survival curve ($n = 22$ mice per group). Mortality was monitored for 28 days and the deaths were separated into two categories: early deaths (those occurring on days 1–5) and late deaths (those occurring on days 6–28). All moribund mice suffered significant weight loss (>30%), hypothermia (<34°C) and loss of righting reflex. Each group included 30 mice. Mice that died spontaneously (i.e., did not meet the criteria for morbundity) were excluded. The results are representative of three experiments. Mice used in all subsequent experiments were pooled from three experiments. **(B)** S100A8 and S100A9 mRNA levels. Blood was collected from moribund mice that were killed at days 1–5 (representing early sepsis) or days 6–25 post CLP (representing late sepsis). During late sepsis, a corresponding number of surviving, healthy appearing S100A9 KO mice were also sacrificed and analyzed at the same time, but are reported as "survivors." Phagocytes were isolated from peripheral blood by gradients of Histopage-1077 and Histopaque-1119. Total RNA was extracted and analyzed by real-time PCR. The S100A8 and S100A9 expression levels were normalized to 18S rRNA. Data are means ± SD ($n = 6$–8 mice per group), and are representative of three experiments (*$p < 0.001$ vs. sham; **$p < 0.001$ vs. S100A8). **(C)** Levels of S100A8 and S100A9 proteins in phagocyte lysate were determined by immunoblotting. The membranes were first incubated with anti-S100A8 antibody, followed by anti-S100A9 antibody. Cells were pooled from 2–3 mice per group, and the results are representative of two immunoblots. WT, wild-type; KO, knockout.

measured levels of IL-10 and the pro-inflammatory cytokine TNFα in the plasma, as well as levels of peritoneal bacteria. As shown in **Figure 3A**, TNFα levels increased in both wild-type and S100A9 knockout mice during early sepsis, but were significantly higher in wild-type mice. During late sepsis, however, TNFα significantly decreased in both wild-type and knockout mice. In contrast, wild-type and S100A9 knockout mice produced small amounts of the immunosuppressive IL-10 during early sepsis, but significantly increased during late sepsis in the wild-type mice and not in knockout mice (**Figure 3A**). Peritoneal bacteria significantly increased in wild-type mice during late sepsis, but diminished in the S100A9 knockout mice (**Figure 3B**). These results support that improved sepsis survival in the S100A9 knockout mice parallels reduced immunosuppressive cytokine production and increased local bacterial clearance. These findings suggest that S100A9 expression may promote late sepsis immunosuppression and predicts that its genetic reduction would limit MDSC repressor cells.

S100A9 Deficiency Prevents MDSC Development during Sepsis

Because S100A9 knockout prevented late sepsis deaths, we first tested whether S100A9 deficiency affects MDSC generation during sepsis response. We determined MDSC numbers in sham and septic mice. Numbers of $Gr1^+CD11b^+$ cells significantly increased in the bone marrow in wild-type and S100A9 knockout mice in early sepsis (**Figure 4A**), as we reported previously (30), but were significantly decreased in the S100A9 knockout mice in late sepsis (**Figure 4A**). We observed similar patterns of $Gr1^+CD11b^+$ cell expansion in the spleens, but the numbers were far less compared with the bone marrow (**Figure 4B**).

It is known that $Gr1^+CD11b^+$ MDSCs from late, but not early, septic mice suppress T cell activation and proliferation (31). Accordingly, we investigated effects of $Gr1^+CD11b^+$ cells on T cell proliferation and activation in wild-type and S100A9 knockout mice, as assessed by IFNγ production. Spleen $CD4^+$ T cells from naive, wild-type mice were cocultured with $Gr1^+CD11b^+$ cells from sham (as a control) and septic mice, and then stimulated with anti-CD3 and anti-CD28 antibodies in order to activate the antigen receptor and assess immune competence. $Gr1^+CD11b^+$ cells from early septic wild-type or S100A9 knockout mice could not suppress $CD4^+$ T cell proliferation but exhibited slightly reduced IFNγ production (**Figures 4C,D**). In contrast, $Gr1^+CD11b^+$ cells from late septic wild-type mice significantly decreased $CD4^+$ T cell proliferation and IFNγ production compared with $Gr1^+CD11b^+$ cells from sham or early septic mice. Moreover, $Gr1^+CD11b^+$ cells from late septic knockout mice could not inhibit T cell proliferation, nor could they reduce IFNγ production after antigen stimulation by anti-CD3 and anti-CD28 (**Figures 4C,D**). These results suggest that S100A9 promotes MDSC repressor function during chronic sepsis. Next, we investigated the S100A8/9 biology in septic mice.

S100A8/A9 Secretion from Phagocytes Decreases in Late Septic Mice

Having linked gene expression to sepsis outcome, we more closely assessed these proteins during sepsis. First, we tested whether S100A8/A9 proteins accumulate in plasma obtained from sham and septic mice during early and late sepsis. Both S100A8/

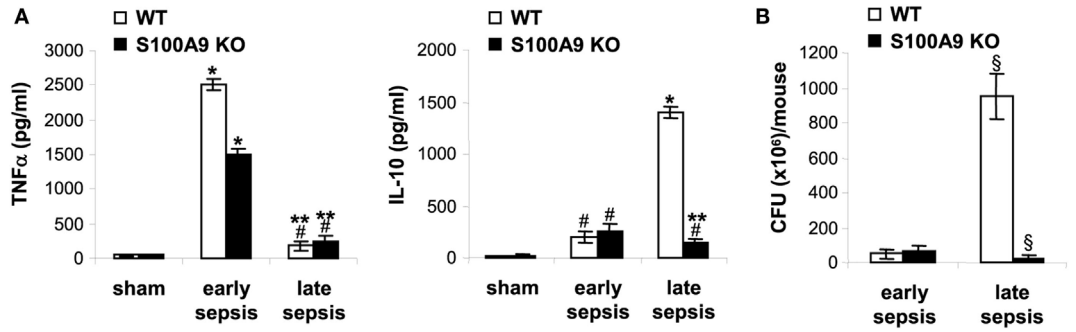

FIGURE 3 | The S100A9 knockout mice do not develop immunosuppressive phenotypes during late sepsis. **(A)** Decreased production of the immunosuppressive cytokine IL-10 in S100A9 knockout mice during late sepsis. Blood was collected from moribund mice undergoing early and late sepsis. The early and late sepsis groups, respectively, included mice that were killed between days 1–5 and 6–28 after cecal ligation and puncture. During late sepsis, a corresponding number of surviving, healthy appearing S100A9 KO mice were also killed and analyzed at the same time. Plasma was collected and levels of TNFα and IL-10 were measured by ELISA. **(B)** Diminished peritoneal bacterial growth in the S100A9 knockout mice during late sepsis. Mice were subjected to peritoneal lavaging immediately after sacrifice. Lavage bacteria were cultured on tryptase soy agar plates and the colony-forming units (CFUs) were enumerated 24 h later. Data are means ± SD (n = 5–7 mice per group), and are representative of three experiments. $^{*}p < 0.0001$ vs. sham; $^{\#}p < 0.05$ vs. sham; $^{**}p < 0.0002$ vs. early sepsis (TNFα) or late sepsis WT (IL-10); $^{\S}p < 0.001$ vs. early sepsis or late sepsis WT **(B)**. WT, wild type; KO, knockout.

A9 protein levels increased in plasma during early sepsis, but decreased during late sepsis (**Figure 5A**). Similar patterns of S100A8/A9 heterodimer secretion occurred (data not shown). We then determined whether S100A8 and S100A9 gene expressions paralleled plasma levels during early and late sepsis by measuring mRNA and protein in circulating phagocytes (mainly monocytes and neutrophils), the primary source of S100A8/A9 (14). S100A8/A9 mRNA and protein levels, in contrast to plasma levels, were similar in circulating phagocytes during early and late septic mice (**Figures 5B,C**). These results support that S100A8/A9 expression increases in mature phagocytes during early and late sepsis, while protein secretion decreases or extracellular clearance increases.

S100A9 Secretion from Gr1^{+}CD11b^{+} MDSC Decreases during Late Sepsis

The results presented above suggested that secreted or intracellular S100A8/A9 protein may be needed to generate the MDSC repressor phenotype. To examine this question, we first measured mRNA and protein levels in Gr1^{+}CD11b^{+} cells isolated from the bone marrow of wild-type mice with or without sepsis. S100A8/A9 mRNAs similarly increased during early and late sepsis (**Figure 6A**). Immunoblotting revealed that S100A8/A9 protein levels also increased during early sepsis and accumulated in late sepsis Gr1^{+}CD11b^{+} cells (**Figure 6B**). We next studied release of S100A8/A9 from MDSCs.

Stimulation of bone marrow myeloid cells with bacterial endotoxin LPS induces release of S100A8/A9 proteins from the cytosol (21). We found that Gr1^{+}CD11b^{+} cells from early septic mice released large amounts of S100A8/A9 proteins after stimulation with LPS (**Figure 6C**). In contrast, S100A8/A9 protein release from late sepsis Gr1^{+}CD11b^{+} MDSCs diminished after LPS stimulation. This unexpected finding suggests a dichotomous regulation of S100A8/A9 release with intracellular accumulation during late vs. early sepsis.

S100A9 Protein Phosphorylation and Dimerization Is Inhibited, and the Protein Is Translocated to the Nucleus in Late Sepsis Gr1^{+}CD11b^{+} MDSCs

To probe what prevents S100A8/A9 release from late sepsis Gr1^{+}CD11b^{+} cells, we examined S100A9 protein phosphorylation and subcellular localization. S100A9 protein is phosphorylated by p38 MAPK (32, 33) on threonine113 at the C-terminal domain in a Ca^{2+}-dependent manner (34), a modification that facilitates translocating S100A8/A9 complex from the cytosol to plasma membrane for secretion (35). Immunoblotting showed that S100A9 protein was phosphorylated on threonine 113 and formed heterodimers with S100A8 in early, but not late sepsis Gr1^{+}CD11b^{+} cells (**Figure 7A**), despite activation of p38 MAPK (**Figure 7B**).

Secretion of S100A8/A9 complexes is also an energy-dependent process, requires activation of PKC and Ca^{2+}-dependent signaling to support S100A8/A9 interactions with microtubules and translocation to plasma membrane and subsequent release (16). We detected similar phosphorylation (activation) of PKC in early and late sepsis Gr1^{+}CD11b^{+} cells (**Figure 7C**). In addition, Ca^{2+} binding increases the stability of the S100A8/A9 protein complexes (36). An assay of intracellular calcium did not reveal significant differences in the Ca^{2+} levels between early and late sepsis Gr1^{+}CD11b^{+} cells (**Figure 7D**). We also examined subcellular localization of S100A8/A9 proteins. S100A8/A9 proteins are mainly localized in the cytosol (35). As shown in **Figure 7E**, S100A9 protein was mainly detected in the cytosol in Gr1^{+}CD11b^{+} cells in early sepsis, but was mainly localized in the nucleus in late sepsis. We did not detect phospho-S100A9 protein in the nucleus by western blot in early or late sepsis Gr1^{+}CD11b^{+} cells (**Figure 7E**), suggesting that S100A9 protein accumulates in the nucleus in an unphosphorylated form. In addition, we detected S100A8 protein mainly in the cytosol

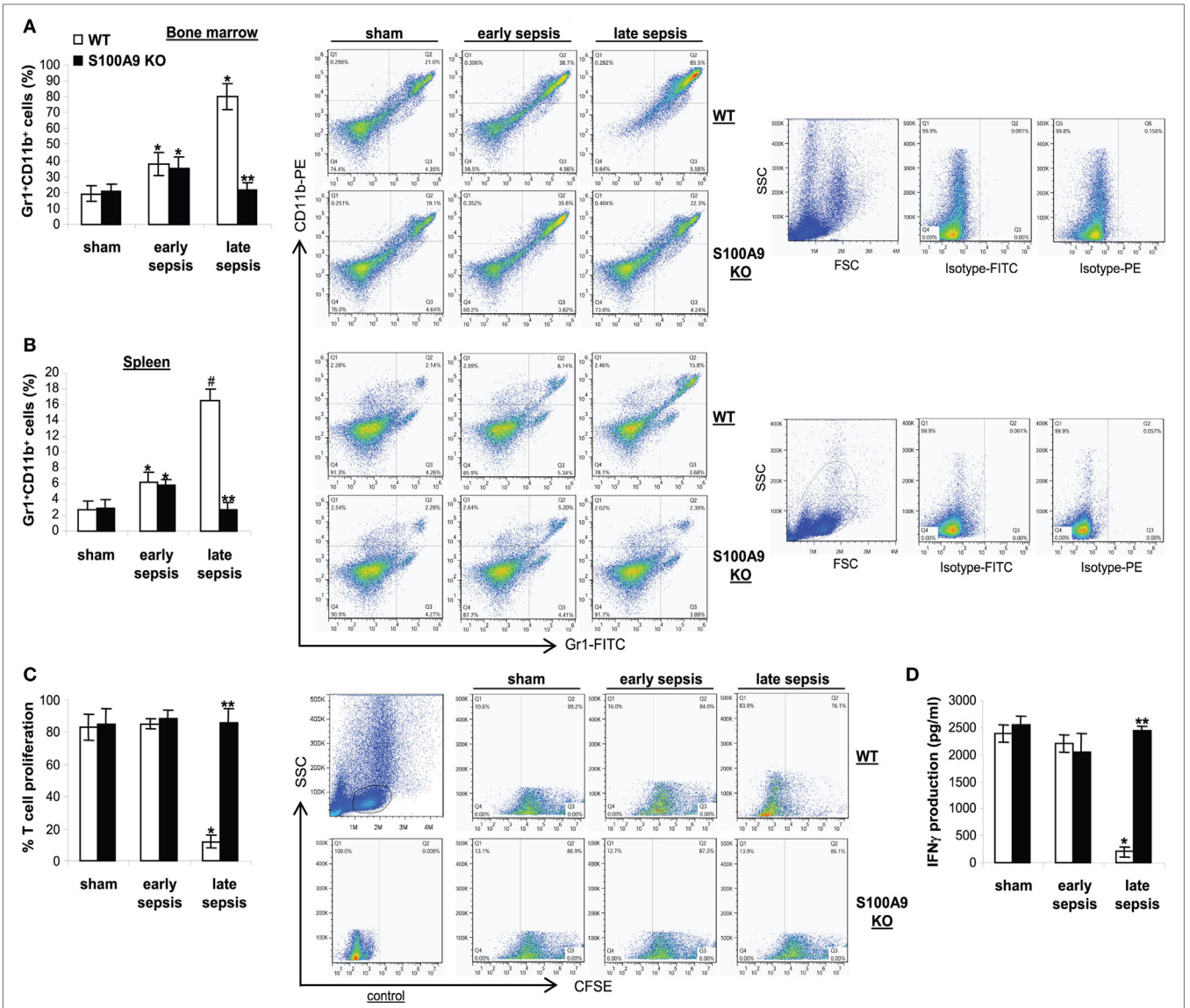

FIGURE 4 | The S100A9 knockout mice do not generate immunosuppressive Gr1$^+$CD11b$^+$ myeloid-derived suppressor cells (MDSCs). Sepsis was induced by cecal ligation and puncture (CLP), and mice were treated and sampled as described in **Figure 2**. The early and late sepsis groups, respectively, included mice that were killed between days 1–5 and 6–28 after CLP. **(A,B)** Inhibition of MDSC expansion in the S100A9 knockout mice during late sepsis. Bone marrow **(A)** and spleen cells **(B)** cells were harvested, stained with anti-Gr1 and anti-CD11b antibodies and analyzed by flow cytometry. Representative dot plots (right) and percentages of cells gated on Gr1 and CD11b staining are shown. *$p < 0.05$ vs. sham; #$p < 0.001$ vs. sham; **$p < 0.001$ vs. WT. **(C)** Effect of MDSCs on T cell proliferation. To determine the immunosuppressive effect of sepsis Gr1$^+$ CD11b$^+$ MDSCs, spleen CD4$^+$ T cells were isolated from normal (naive) mice and labeled with the fluorescent dye carboxy-fluorosceindiacetate, succinimidyl ester (CFSE) for 10 min at room temperature. Gr1$^+$ CD11b$^+$ cells were then cocultured (at 1:1 ratio) with CD4$^+$ T cells. The culture was stimulated with anti-CD3 plus anti-CD28 antibodies (1 μg/ml/each). After 3 days, CD4$^+$ T cell proliferation was determined by the step-wise dilution of CFSE dye in dividing CD4$^+$ T cells by flow cytometry. Percentages of cell proliferation were calculated as follow: % cell proliferation = 100 × (count from T cell + Gr1$^+$CD11b$^+$ cell culture/count from T cell culture). *$p < 0.001$ vs. sham or early sepsis; **$p < 0.001$ vs. late sepsis WT. **(D)** The culture supernatants were analyzed for IFNγ levels by ELISA. *$p < 0.001$ vs. sham or early sepsis; **$p < 0.0001$ vs. late sepsis WT. Data are means ± SD (n = 4–6 mice per group) and are representative of three experiments. WT, wild type; KO, knockout.

in early and late sepsis Gr1$^+$CD11b$^+$ cells, but its levels were markedly reduced in late sepsis cells (data not shown), likely due to lack of S100A9 in the cytosol. Together, these results suggest that nuclear translocation of S100A9 in Gr1$^+$CD11b$^+$ MDSCs during late sepsis prevents its secretion and pro-inflammatory effects.

MDSCs Lacking S100A9 Do Not Express miR-21 and miR-181b during Late Sepsis

Expression of miR-21 and miR-181b is induced in Gr1$^+$CD11b$^+$ cells during sepsis and promotes Gr1$^+$CD11b$^+$ cell expansion (24). We reported that blocking miR-21 and miR-181b in septic mice by administration of miRNA antagomiRs diminishes Gr1$^+$CD11b$^+$

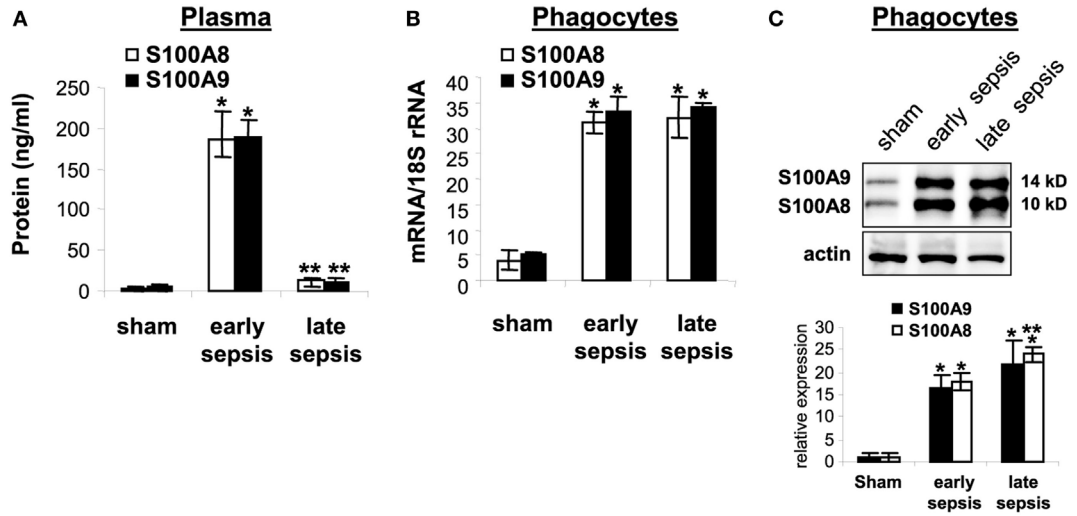

FIGURE 5 | The S100A8 and S100A9 protein secretion is inhibited during late sepsis despite normal expression levels. **(A)** Secreted S100A8 and S100A9 proteins was determined by measuring their plasma levels using ELISA. **(B)** Levels of S100A8 and S100A9 mRNAs. Phagocytes were isolated from peripheral blood by gradients of Histopage-1077 and Histopaque-1119, and mRNA levels were determined by real-time PCR. The S100A8 and S100A9 expression levels were normalized to 18S rRNA. Data are means ± SD (n = 5–9 mice per group), and are representative of three experiments (*$p < 0.001$ vs. sham; **$p < 0.001$ vs. early sepsis). **(C)** Levels of S100A8 and S100A9 proteins in phagocyte lysate were determined by immunoblotting. The membranes were first incubated with anti-S100A8 antibody. After washing (without stripping), the membranes were incubated with anti-S100A9 antibody. Cells were pooled from 2–3 mice per group. The early and late sepsis groups, respectively, included mice that were killed between days 1–5 and 6–28 after cecal ligation and puncture. Representative blot (upper) and densitometric analysis of blots from three experiments (lower) are shown. Values were normalized to β-actin, and are presented relative to sham (*$p < 0.001$ vs. sham; **$p < 0.05$ vs. early sepsis).

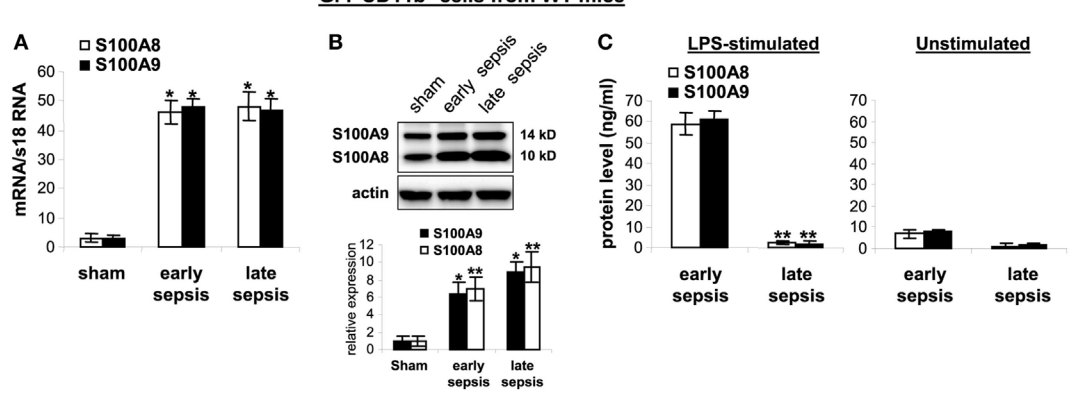

FIGURE 6 | The S100A8 and S100A9 proteins are retained in Gr1+CD11b+ cells during late sepsis. Gr1+CD11b+ cells were isolated from the bone marrow cells by positive selection. The early and late sepsis groups, respectively, included mice that were killed between days 1–5 and 6–28 after cecal ligation and puncture. **(A)** Levels of S100A8 and S100A9 mRNAs. Total RNA was extracted from Gr1+CD11b+ cells, and mRNA levels were determined by real-time PCR. The S100A8 and S100A9 expression levels were normalized to 18S rRNA (*$p < 0.001$ vs. sham). **(B)** Levels of S100A8 and S100A9 proteins in Gr1+CD11b+ whole cell lysates were determined by immunoblotting. Cells were pooled from 2–3 mice per group. Representative blot (upper) and densitometric analysis of blots from three experiments (lower) are shown. Values were normalized to β-actin and are presented relative to sham (*$p < 0.01$ vs. sham; **$p < 0.05$ vs. sham). **(C)** Protein secretion after stimulation with lipopolysaccharide (LPS). Gr1+CD11b+ cells were isolated from the bone marrow of septic mice and stimulated for 24 h with 1 μg/ml LPS (*E. coli* serotype 0111:B4). Levels of S100A8 and S100A9 in the culture supernatants were determined by ELISA. Data in *A* and *C* are means ± SD (n = 5–6 mice per group), and are representative of three experiments (**$p < 0.0003$ vs. early sepsis).

MDSC expansion during late sepsis response (24). Accordingly, we measured miR-21 and miR-181b levels by RT-PCR in early and late sepsis. Levels of miR-21 and miR-181b in Gr1+CD11b+ cells were increased during early sepsis in both wild-type and knockout mice (**Figure 8A**). In late sepsis Gr1+CD11b+ cells, both miRNAs further increased in wild-type mice, but diminished in S100A9 knockout mice.

We previously reported that miR-21 and miR-181b induction during sepsis is dependent on both C/EBPβ expression and Stat3 phosphorylation, which synergize to activate miR-21 and

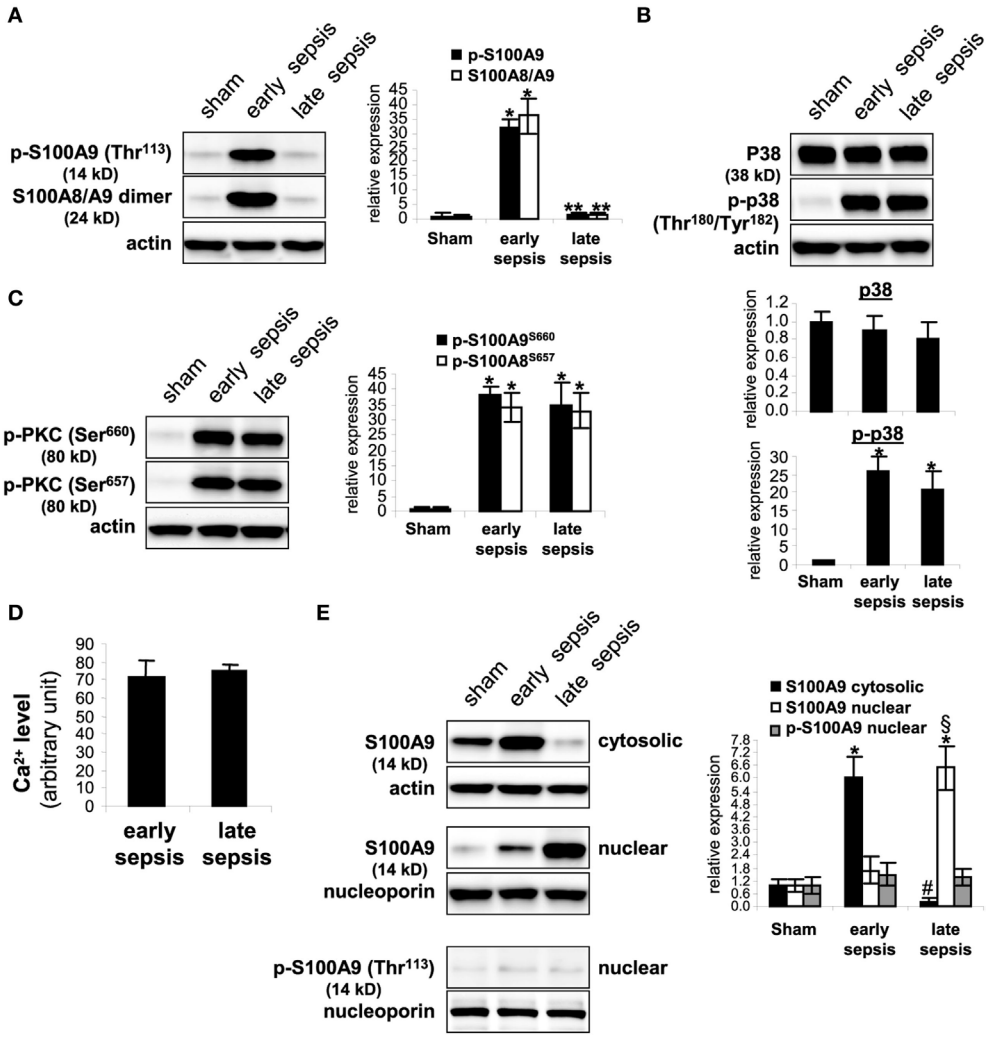

FIGURE 7 | The S100A9 protein phosphorylation and dimerization with S100A8 is inhibited and translocated to the nucleus in Gr1$^+$CD11b$^+$ cells during late sepsis. Gr1$^+$CD11b$^+$ cells were isolated from the bone marrow cells by positive selection. The early and late sepsis groups, respectively, included mice that were killed between days 1–5 and 6–28 after cecal ligation and puncture. Cell lysates were prepared, and expression of the indicated proteins was determined by immunoblotting. **(A)** S100A9 phosphorylation was probed with anti-phospho threonine 113 antibody. To detect the S100A8/A9 heterodimer, the lysate was resolved under non-denaturing conditions which produced a protein band of ~24 kDa. **(B)** Levels of p38 MAPK phosphorylation were determined using anti-phospho tyrosine antibody that recognizes tyrosine number 180 and 182. **(C)** Levels of phosphorylated protein kinase C were determined using anti-phospho serines 643 and 660 antibodies. **(D)** Intracellular calcium levels were measured using a cell-based Fluo-4 NW calcium assay. Data are means ± SD of four mice per group and are representative of two experiments. **(E)** Localization of the S100A9 protein. Nuclear and cytosolic proteins were extracted from Gr1$^+$CD11b$^+$ cells and immunoblotted with the S100A9 antibody. Nuclear extracts were probed for p-S100A9. Membranes were re-probed with actin or nucleoporin antibody as a loading control. In **(A–C,E)**, cells were pooled from 2–3 mice per group. Representative blots [left; **(A,C,E)**; upper, **(B)**] and densitometric analysis of blots from three experiments are shown. Values were normalized to β-actin or nucleoporin, and are presented relative to sham [$^*p < 0.001$ vs. sham; $^{**}p < 0.001$ vs. early sepsis; $^{\#}p < 0.001$ vs. early sepsis S100A9 cytosolic; $^{\S}p < 0.02$ vs. early sepsis S100A9 nuclear **(E)**].

miR-181b promoters (37). To determine whether decreased miR-21 and miR-181b expression in S100A9 knockout mice during late sepsis is due to lack of C/EBPβ expression and/or Stat3 phosphorylation, we examined C/EBPβ and phosphorylated Stat3 protein levels in the Gr1$^+$CD11b$^+$ cell lysates. C/EBPβ expression and Stat3 phosphorylation were similarly induced in wild-type and S100A9 knockout mice (**Figure 8B**). We also reported that NFI-A expression is induced downstream of miR-21 and miR-181b and promotes Gr1$^+$CD11b$^+$ cell expansion during sepsis by attenuating myeloid cell differentiation and maturation (31). Here, we detected NFI-A in Gr1$^+$CD11b$^+$ cells from early, but not late septic S100A9 knockout mice (**Figure 8B**). These results strongly support that S100A9 sustains both NFI-A and miR-21 and miR-181b levels during late sepsis immunosuppression.

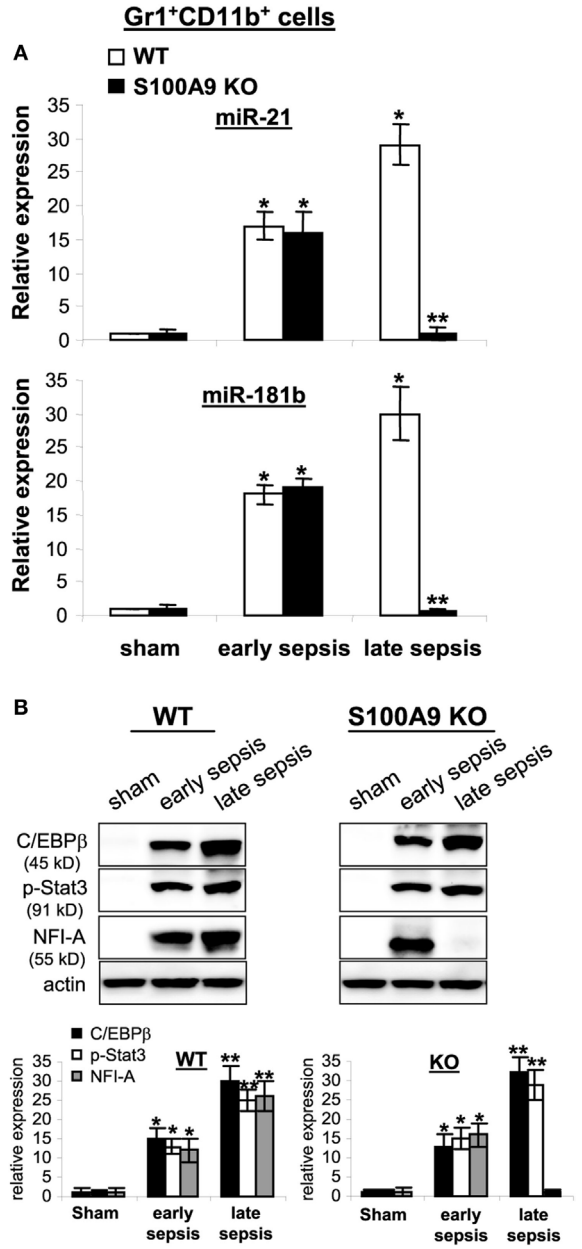

FIGURE 8 | The expression of miR-21 and miR-181b in Gr1+CD11b+ cells is inhibited during late sepsis. The Gr1+CD11b+ cells were isolated from the bone marrow of sham and septic mice using magnetic beads. The early and late sepsis groups, respectively, included mice that were killed between days 1–5 and 6–28 after cecal ligation and puncture. **(A)** Measurements of miR-21 and miR-181b expression. MiRNA-enriched RNA was isolated, and levels of miR-21 and miR-181b were determined by quantitative real-time qPCR using miR-21 and miR-181b specific assay primers. Sample values were normalized to U6 RNA as an internal control. Data are means ± SD (n = 3–5 mice per group), presented relative to values from sham mice (set at onefold). Results are representative of three experiments (*$p < 0.001$ vs. sham; **$p < 0.001$ vs. late sepsis WT). **(B)** Protein levels C/EBPβ, p-Stat3 and NFI-A. Gr1+CD11b+ cell lysates were prepared and immunoblotted with antibodies against the indicated proteins. Representative blots (upper) and densitometric analysis of blots (lower) from three experiments is shown. Values were normalized to β-actin, and are presented relative to sham (*$p < 0.01$ vs. sham; **$p < 0.05$ vs. early sepsis).

Administration of S100A8/A9 to S100A9 Knockout Mice Has No Impact on Sepsis Response

S100A9 integrates two signaling pathways that facilitate S100A8/9 release and may functionally dominate complex function (35). Other studies suggested that S100A8 may be dominant in the S100A8/A9 complex (21). Because S100A8 protein is diminished in the S100A9 knockout mice (**Figure 2C**), we examined whether reconstitution of the S100A9 knockout mice with S100A8 and/or S100A9 affects late sepsis responses. We injected (i.p.) the wild-type and S100A9 knockout mice with recombinant mouse S100A8 and/or S100A9 at day 5 after CLP (i.e., at the end of early sepsis phase). Administration of S100A8 alone or in combination with S100A9 did not affect survival of the S100A9 knockout mice (**Figure 9A**). In the wild-type mice, only injection of S100A8/A9 increased mortality by ~24–16% between days 6 and 11 compared with mice injected with saline (**Figure 9B**). In addition, we did not detect significant changes in plasma levels of immunosuppressive cytokine IL-10 in mice treated with S100A8 or S100A8/A9, but levels of pro-inflammatory TNFα slightly increased in mice treated with S100A8/A9 compared with S100A8 alone (**Figure 9C**). In the wild-type mice, S100A8/A9 injection slightly, but significantly, increased TNFα production. Of note, levels of IL-10 were significantly higher compared with the S100A9 knockout mice, and were further elevated after S100A8/A9 injection. These results suggest that S100A8 absence in the S100A9 knockout mice does not affect the inflammatory response to sepsis. These results also suggest that administration of S100A8/A9 into wild-type mice undergoing late sepsis can further enhance immunosuppression.

S100A8/A9 Plasma Levels Decrease in Chronic Septic Patients, but Remain Elevated within Phagocytes

Secreted S100A8/A9 may promote acute and/or chronic inflammation (18). To determine whether S100A8/A9 expression in sepsis patients correlates with sepsis inflammation, we first measured plasma S100A8/A9 during human sepsis. Patients were divided into two groups: the early septic group included patients within 1–5 days of clinically detected sepsis and the chronic sepsis group had been septic at least 6 days and up to 31 days. **Figure 10A** shows significant increases in S100A8/A9 plasma levels in the early septic group compared with healthy controls. Notably, circulating S100A8/A9 levels decreased in late septic patients. We then determined whether the decrease in plasma levels of S100A8/A9 proteins correlated with reduced protein expression by phagocytes. Using western blotting, we observed marked increases in S100A8/A9 proteins in blood phagocytes from early and late septic patients compared with healthy controls (**Figure 10B**). We further examined whether S100A9 expression correlates with sepsis prognosis for the late septic group. Both mRNA and protein levels of S100A9 markedly decreased in phagocytes from patients who later recovered from chronic sepsis but remained elevated in those who eventually died

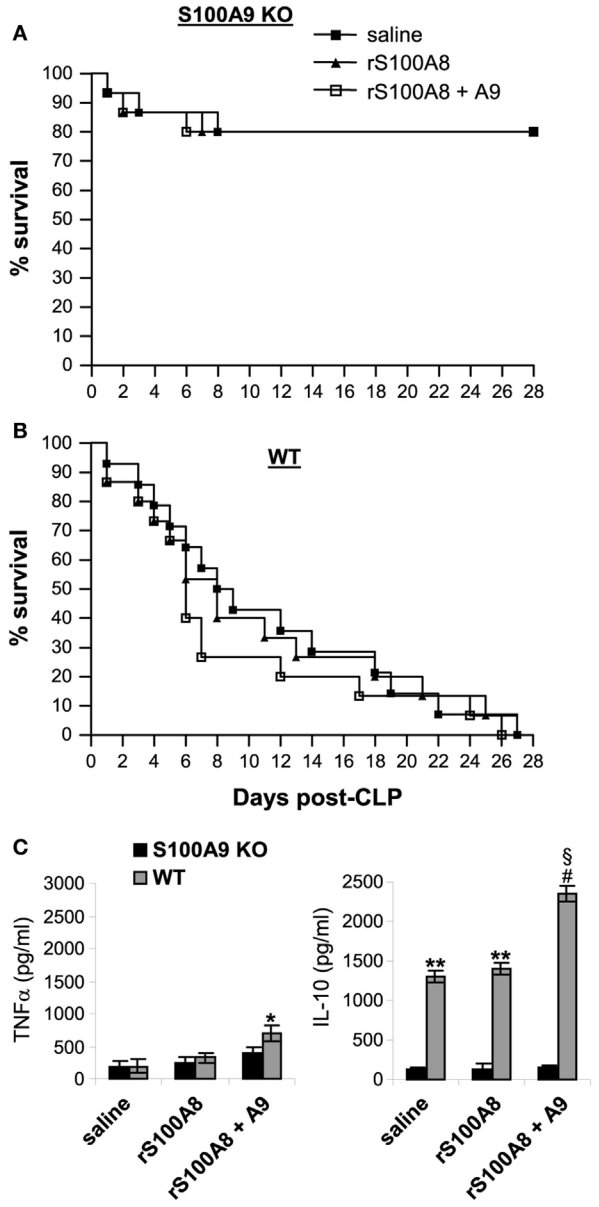

FIGURE 9 | Administration of rS100A8/9 into the S100A9 knockout mice undergoing sepsis has no effect on sepsis survival or inflammatory cytokine production. Sepsis was induced by cecal ligation and puncture (CLP), and mice were treated as described in **Figure 2**. On day 5 and day 6 after CLP, mice were injected (i.p.) with 50 µg each of recombinant mouse S100A8 and/or S100A9 protein or 100 µl saline. **(A,B)** Kaplan–Meier survival curves showing deaths during the early and late sepsis phases in KO and WT mice ($n = 15$ per group). **(C)** Plasma levels of TNFα and IL-10. Blood was collected at day 15 after CLP from the KO mice ($n = 6$ mice per group) and at days 7–18 from the WT mice ($n = 4$–6 mice per group). Plasma was collected, and levels of TNFα and IL-10 were determined by ELISA. Data are means ± SD. $^{*}p < 0.05$ vs. KO; $^{**}p < 0.001$ vs. KO; $^{\#}p < 0.0001$ vs. KO; $^{\S}p < 0.01$ vs. saline or rS100A8 WT. r, recombinant.

(**Figures 10C,D**). Together, these results suggest that sustained intracellular S100A9 in phagocytes and perhaps MDSCs promote chronic sepsis by sustaining immunosuppression.

DISCUSSION

It is increasingly evident that MDSCs promote sepsis-induced immunosuppression in mice (30, 38) and their counterparts may contribute to the profound and sustained immunosuppression in human sepsis (7). Despite decades of studies on sepsis pathobiology and multiple therapeutic failures, sepsis is still a health-care crisis without available targeted treatment options (8, 39). Importantly, the mediators that sustain MDSC generation and immunosuppression in chronic sepsis remain a mystery. This study, for the first time, introduces the concept that S100A9 protein contributes to late sepsis mortality in mice by its sustained expression and nuclear retention. Tantamount to molecular targeting therapeutics, genetic deletion of S100A9 in mice improves chronic sepsis mortality. That this new paradigm may translate to human sepsis, we show that S100A8/A9 intracellular mRNA and protein levels in phagocytes are elevated in patients with more chronic sepsis, and that a correlation may exist between this repressor like phenotype and human sepsis mortality. However, more research in humans is needed to test this new theory before targeted therapy is developed. The emerging use of immune checkpoint, as well as metabolic checkpoint, drugs (40, 41) may allow translation of our concept into both a better understanding and treatment of human sepsis—a major gap and health-care need.

We detected significantly elevated levels of S100A8/A9 proteins in the plasma of early septic mice, a known feature of S100 proteins as pro-inflammatory, acute phase proteins (15, 16). However, we showed that S100A8/A9 proteins in septic mice decreased in the late sepsis phase, despite elevated levels of mRNAs and proteins in circulating phagocytes and $Gr1^{+}CD11b^{+}$ MDSCs in the bone marrow and spleens. Another important observation supporting our paradigm was decreases in immunosuppressive IL-10 cytokine and increased microbial clearance from peritoneum in S100A9 knockout mice during late sepsis. This supports that S100A9 directs immune suppression in phagocytes and MDSCs. However, the mechanistic link between miR-21 and miR-181b expression, as well as the signaling regulatory path involving C/EBPβ and NFI-A, supports that S100A9 acts as a transcription co-factor or an indirect epigenetic mediator. Epigenetic pathways like those regulated by NAD^{+} Sirtuins 1 and 6 (12) are candidates, as well as direct cooperativity with transcription repressor complexes like RelB (42, 43).

Our study does not refute the substantive reports showing S100A8/A9 proteins function mainly as extracellular pro-inflammatory mediators (14–16). A recent study showed that S100A8/A9 proteins promote septic shock in mice *via* activating TLR4 on innate immunity cells (21). Other findings support that S100A8/A9 proteins also exert anti-inflammatory effects (22), and our data suggest a dual role for S100A9 protein. Intracellular S100A9 may act as an anti-inflammatory/immunosuppressive mediator through reprogramming the $Gr1^{+}CD11b^{+}$ myeloid cells into MDSCs, whereas extracellular S100A9 may promote inflammation in the plasma and when secreted by phagocytes. This interpretation of dual functioning proteins is not without precedent. For example, we previously discovered that HMGB1 histone binding protein, which like S100A9 induces

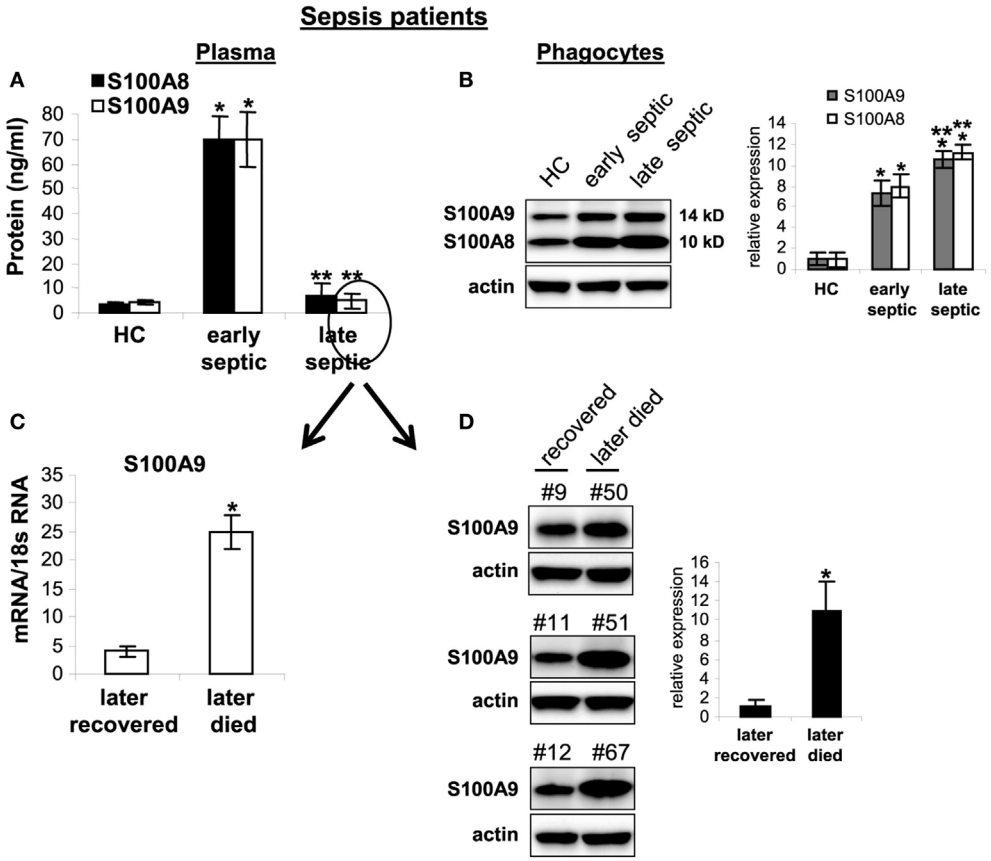

FIGURE 10 | Release of S100A8/A9 proteins is blocked in late septic patients. Blood phagocytes and plasma were isolated by gradients of Histopage-1077 and Histopaque-1119 (Sigma). **(A)** Levels of S100A8/A9 proteins in plasma were determined by ELISA (run in duplicate). Data are means ± SD ($n = 8$ subjects/group) (*$p < 0.001$ vs. HC; **$p < 0.001$ vs. early septic). **(B)** levels of S100A8/A9 proteins in phagocytes lysates were determined by western blot. Representative blot (left) and densitometric analysis of blots (right) are shown. Results are representative of three immunoblots (*$p < 0.01$ vs. HC; *$p < 0.05$ vs. early septic). **(C,D)** The late septic patient group shown in panel **(A)** was divided into two sub-groups: those who later recovered ($n = 5$) from sepsis or died ($n = 3$). Their frozen phagocytes were divided. A portion of the cells was used for RNA extraction and determination of S100A8/A9 mRNA levels by real-time PCR, and expression levels were normalized to 18S rRNA **(C)** (*$p < 0.001$). The remainder of the cells were lysed and S100A9 protein levels were determined by western blot **(D)**. Representative blots (left) and densitometric analysis of blots (right) are shown. Results are representative of three immunoblots (*$p < 0.01$). Patient numbers are shown on top of the blots. Early septic included patients who were within 1–5 days after diagnosis. Late septic included patients who have been septic for 6–31 days. HC, health control.

inflammation after release and through stimulation of TLR4, is also an epigenetic repressor during endotoxin tolerance in human monocytes, a biomarker of immunosuppression (44). Of note, administration of recombinant S100A8 and/or S100A9 at the onset of the late sepsis phase did not impact sepsis outcomes in the S100A9 knockout mice. However, S100A8/A9 enhanced mortality in the wild-type mice for the first few days after the injection, and this response was accompanied by increases in the levels of immunosuppressive IL-10 production.

Many MDSCs accumulate during late sepsis in mice (30, 38). Our finding that S100A9 knockout mice did not generate immunosuppressive $Gr1^+CD11b^+$ cells (i.e., MDSCs) during late sepsis response is physiologically significant, and supports that S100A9 is necessary for chronic MDSC repressor function. Moreover, S100A9 knockout mice in early sepsis response were still able to generate normal (immune competent) $Gr1^+CD11b^+$ cells, similar to wild-type mice. While these functionally competent myeloid cells were phenotypically similar to the MDSCs generated in late sepsis, they did not suppress T cell activation or proliferation. Thus, S100A9 protein reprograms immature $Gr1^+CD11b^+$ myeloid cells into MDSCs in late sepsis, but has no impact on myeloid cell phenotype or functions under normal conditions or during the early phase of sepsis.

S100A9 protein phosphorylation and dimerization with S100A8 and subsequent secretion require phosphorylation on S100A9 by p38 MAPK (32, 33) and activation of PKC in a Ca^{2+}-dependent manner (16). Our results showed that S100A9 protein phosphorylation and dimerization were inhibited in the $Gr1^+CD11b^+$ cells from late, but not early, septic mice despite normal activation of p38 and PKC throughout the sepsis course. In addition, we did not observe changes in the intracellular Ca^{+2} levels. Most importantly, we found that S100A9 protein was mainly localized in the nuclear compartment in late sepsis $Gr1^+CD11b^+$ cells (i.e., MDSCs). S100A8/A9 proteins

are known to have diverse functional properties based on location and posttranslational phosphorylation/dephosphorization mechanisms (16). It is unclear from the current study how S100A9 protein is translocated into the nucleus in late sepsis cells, since a nuclear localization signal has not been reported, to the best of our knowledge. Since S100A9 phosphorylation promotes its translocation from the cytosol to the plasma membrane for secretion and increases its Ca^{2+} binding property (16, 45), it is possible that nuclear translocation only occurs in the dephosphorylated state in which calcium is unbound. Testing that possible mechanism will require genetic and therapeutic targeting.

In summary, this study for the first time identifies a novel chronic immune repressor mechanism in MDSCs, which may have untoward consequences on sepsis resolution during the PICS syndrome (46). Unanswered important questions include what controls S100A9 translocation to the nucleus, what disrupts its secretion? and whether this novel path can be a therapeutic target?

ETHICS STATEMENT

All animal experiments were conducted in accordance with National Institutes of Health guidelines and were approved by the East Tennessee State University Animal Care and Use Committee (Protocol #: 160704). The human study was approved by the Institutional Review Board (IRB) of the East Tennessee State University (IRB#: 0714.6s). Signed informed consent was obtained from all subjects.

AUTHOR CONTRIBUTIONS

JD and AK conducted and analyzed the experiments; DY recruited patients and collected blood samples; CM edited the manuscript; ME designed the project, supervised research, and wrote the manuscript.

ACKNOWLEDGMENTS

We thank Dr. Dale Cowley and colleagues (TransViragen, Chapel Hill, NC, USA) for generating the S100a9 knockout strain. We also thank Dr. Michelle Duffourc and Rhesa Dykes (ETSU Molecular Biology Core) for assisting with the mouse genotyping and Dr. Christopher Pritchett and Danielle Williams (ETSU College of Public Health) for assisting with the bacterial cultures.

FUNDING

This work was supported by National Institutes of Health Grants R01GM103887 (to ME) and C06RR0306551 (to College of Medicine).

SUPPLEMENTARY MATERIAL

The Supplementary Material for this article can be found online at http://www.frontiersin.org/article/10.3389/fimmu.2017.01565/full#supplementary-material.

REFERENCES

1. Angus DC, Linde-Zwirble WT, Lidicker J, Clermont G, Carcillo J, Pinsky MR. Epidemiology of severe sepsis in the United States: analysis of incidence, outcome, and associated costs of care. *Crit Care Med* (2001) 29:1303–10. doi:10.1097/00003246-200107000-00002
2. Gaieski DF, Edwards JM, Kallan MJ, Carr BG. Benchmarking the incidence and mortality of severe sepsis in the United States. *Crit Care Med* (2013) 41:1167–74. doi:10.1097/CCM.0b013e31827c09f8
3. Boomer JS, To K, Chang KC, Takasu O, Osborne DF, Walton AH, et al. Immunosuppression in patients who die of sepsis and multiple organ failure. *JAMA* (2011) 306:2594–605. doi:10.1001/jama.2011.1829
4. Hotchkiss RS, Monneret G, Payen D. Sepsis-induced immunosuppression: from cellular dysfunctions to immunotherapy. *Nat Rev Immunol* (2013) 13:862–74. doi:10.1038/nri3552
5. Ward PA. Immunosuppression in sepsis. *JAMA* (2011) 306:2618–9. doi:10.1001/jama.2011.1831
6. Gentile LF, Cuenca AG, Efron PA, Ang D, Bihorac A, McKinley BA, et al. Persistent inflammation and immunosuppression: a common syndrome and new horizon for surgical intensive care. *J Trauma Acute Care Surg* (2012) 72:1491–501. doi:10.1097/TA.0b013e318256e000
7. Mathias B, Delmas AL, Ozrazgat-Baslanti T, Vanzant EL, Szpila BE, Mohr AM, et al. Human myeloid-derived suppressor cells are associated with chronic immune suppression after severe sepsis/septic shock. *Ann Surg* (2017) 265:827–34. doi:10.1097/SLA.0000000000001783
8. Delano MJ, Ward PA. Sepsis-induced immune dysfunction: can immune therapies reduce mortality? *J Clin Invest* (2016) 126:23–31. doi:10.1172/JCI82224
9. Hutchins NA, Unsinger J, Hotchkiss RS, Ayala A. The new normal: immunomodulatory agents against sepsis immune suppression. *Trends Mol Med* (2014) 20:224–33. doi:10.1016/j.molmed.2014.01.002
10. McCall CE, Yoza B, Liu T, El Gazzar M. Gene-specific epigenetic regulation in serious infections with systemic inflammation. *J Innate Immun* (2010) 2:395–405. doi:10.1159/000314077
11. Arts RJ, Gresnigt MS, Joosten LA, Netea MG. Cellular metabolism of myeloid cells in sepsis. *J Leukoc Biol* (2017) 101:151–64. doi:10.1189/jlb.4MR0216-066R
12. Liu TF, Vachharajani VT, Yoza BK, McCall CE. NAD+-dependent sirtuin 1 and 6 proteins coordinate a switch from glucose to fatty acid oxidation during the acute inflammatory response. *J Biol Chem* (2012) 287:25758–69. doi:10.1074/jbc.M112.362343
13. van Zoelen MA, Vogl T, Foell D, Van Veen SQ, van Till JW, Florquin S, et al. Expression and role of myeloid-related protein-14 in clinical and experimental sepsis. *Am J Respir Crit Care Med* (2009) 180:1098–106. doi:10.1164/rccm.200810-1552OC
14. Ehrchen JM, Sunderkotter C, Foell D, Vogl T, Roth J. The endogenous toll-like receptor 4 agonist S100A8/S100A9 (calprotectin) as innate amplifier of infection, autoimmunity, and cancer. *J Leukoc Biol* (2009) 86:557–66. doi:10.1189/jlb.1008647
15. Foell D, Roth J. Proinflammatory S100 proteins in arthritis and autoimmune disease. *Arthritis Rheum* (2004) 50:3762–71. doi:10.1002/art.20631
16. Vogl T, Gharibyan AL, Morozova-Roche LA. Pro-inflammatory S100A8 and S100A9 proteins: self-assembly into multifunctional native and amyloid complexes. *Int J Mol Sci* (2012) 13:2893–917. doi:10.3390/ijms13032893
17. Roth J, Goebeler M, van den Bos C, Sorg C. Expression of calcium-binding proteins MRP8 and MRP14 is associated with distinct monocytic differentiation pathways in HL-60 cells. *Biochem Biophys Res Commun* (1993) 191:565–70. doi:10.1006/bbrc.1993.1255
18. Foell D, Frosch M, Sorg C, Roth J. Phagocyte-specific calcium-binding S100 proteins as clinical laboratory markers of inflammation. *Clin Chim Acta* (2004) 344:37–51. doi:10.1016/j.cccn.2004.02.023

19. Goyette J, Geczy CL. Inflammation-associated S100 proteins: new mechanisms that regulate function. *Amino Acids* (2011) 41:821–42. doi:10.1007/s00726-010-0528-0
20. Hiratsuka S, Watanabe A, Aburatani H, Maru Y. Tumour-mediated upregulation of chemoattractants and recruitment of myeloid cells predetermines lung metastasis. *Nat Cell Biol* (2006) 8:1369–75. doi:10.1038/ncb1507
21. Vogl T, Tenbrock K, Ludwig S, Leukert N, Ehrhardt C, van Zoelen MA, et al. Mrp8 and Mrp14 are endogenous activators of toll-like receptor 4, promoting lethal, endotoxin-induced shock. *Nat Med* (2007) 13:1042–9. doi:10.1038/nm1638
22. Ikemoto M, Murayama H, Itoh H, Totani M, Fujita M. Intrinsic function of S100A8/A9 complex as an anti-inflammatory protein in liver injury induced by lipopolysaccharide in rats. *Clin Chim Acta* (2007) 376:197–204. doi:10.1016/j.cca.2006.08.018
23. Hsu K, Passey RJ, Endoh Y, Rahimi F, Youssef P, Yen T, et al. Regulation of S100A8 by glucocorticoids. *J Immunol* (2005) 174:2318–26. doi:10.4049/jimmunol.174.4.2318
24. McClure C, Brudecki L, Ferguson DA, Yao ZQ, Moorman JP, McCall CE, et al. MicroRNA 21 (miR-21) and miR-181b couple with NFI-A to generate myeloid-derived suppressor cells and promote immunosuppression in late sepsis. *Infect Immun* (2014) 82:3816–25. doi:10.1128/IAI.01495-14
25. Valenzuela DM, Murphy AJ, Frendewey D, Gale NW, Economides AN, Auerbach W, et al. High-throughput engineering of the mouse genome coupled with high-resolution expression analysis. *Nat Biotechnol* (2003) 21:652–9. doi:10.1038/nbt822
26. Brudecki L, Ferguson DA, Yin D, Lesage GD, McCall CE, El Gazzar M. Hematopoietic stem-progenitor cells restore immunoreactivity and improve survival in late sepsis. *Infect Immun* (2012) 80:602–11. doi:10.1128/IAI.05480-11
27. Mazuski JE, Sawyer RG, Nathens AB, DiPiro JT, Schein M, Kudsk KA, et al. The surgical infection society guidelines on antimicrobial therapy for intra-abdominal infections: an executive summary. *Surg Infect (Larchmt)* (2002) 3:161–73. doi:10.1089/109629602761624171
28. Singer M, Deutschman CS, Seymour CW, Shankar-Hari M, Annane D, Bauer M, et al. The third international consensus definitions for sepsis and septic shock (sepsis-3). *JAMA* (2016) 315:801–10. doi:10.1001/jama.2016.0287
29. Brudecki L, Ferguson DA, McCall CE, El Gazzar M. MicroRNA-146a and RBM4 form a negative feed-forward loop that disrupts cytokine mRNA translation following TLR4 responses in human THP-1 monocytes. *Immunol Cell Biol* (2013) 91:532–40. doi:10.1038/icb.2013.37
30. Brudecki L, Ferguson DA, McCall CE, El Gazzar M. Myeloid-derived suppressor cells evolve during sepsis and can enhance or attenuate the systemic inflammatory response. *Infect Immun* (2012) 80:2026–34. doi:10.1128/IAI.00239-12
31. McClure C, Ali E, Youssef D, Yao ZQ, McCall CE, El Gazzar M. NFI-A disrupts myeloid cell differentiation and maturation in septic mice. *J Leukoc Biol* (2016) 99:201–11. doi:10.1189/jlb.4A0415-171RR
32. Lominadze G, Rane MJ, Merchant M, Cai J, Ward RA, McLeish KR. Myeloid-related protein-14 is a p38 MAPK substrate in human neutrophils. *J Immunol* (2005) 174:7257–67. doi:10.4049/jimmunol.174.11.7257
33. Vogl T, Ludwig S, Goebeler M, Strey A, Thorey IS, Reichelt R, et al. MRP8 and MRP14 control microtubule reorganization during transendothelial migration of phagocytes. *Blood* (2004) 104:4260–8. doi:10.1182/blood-2004-02-0446
34. Edgeworth J, Freemont P, Hogg N. Ionomycin-regulated phosphorylation of the myeloid calcium-binding protein p14. *Nature* (1989) 342:189–92. doi:10.1038/342189a0
35. van den Bos C, Roth J, Koch HG, Hartmann M, Sorg C. Phosphorylation of MRP14, an S100 protein expressed during monocytic differentiation, modulates Ca(2+)-dependent translocation from cytoplasm to membranes and cytoskeleton. *J Immunol* (1996) 156:1247–54.
36. Vogl T, Leukert N, Barczyk K, Strupat K, Roth J. Biophysical characterization of S100A8 and S100A9 in the absence and presence of bivalent cations. *Biochim Biophys Acta* (2006) 1763:1298–306. doi:10.1016/j.bbamcr.2006.08.028
37. McClure C, McPeak MB, Youssef D, Yao ZQ, McCall CE, El Gazzar M. Stat3 and C/EBPbeta synergize to induce miR-21 and miR-181b expression during sepsis. *Immunol Cell Biol* (2017) 95:42–55. doi:10.1038/icb.2016.63
38. Delano MJ, Scumpia PO, Weinstein JS, Coco D, Nagaraj S, Kelly-Scumpia KM, et al. MyD88-dependent expansion of an immature GR-1(+) CD11b(+) population induces T cell suppression and Th2 polarization in sepsis. *J Exp Med* (2007) 204:1463–74. doi:10.1084/jem.20062602
39. Hotchkiss RS, Monneret G, Payen D. Immunosuppression in sepsis: a novel understanding of the disorder and a new therapeutic approach. *Lancet Infect Dis* (2013) 13:260–8. doi:10.1016/S1473-3099(13)70001-X
40. Renner K, Singer K, Koehl GE, Geissler EK, Peter K, Siska PJ, et al. Metabolic hallmarks of tumor and immune cells in the tumor microenvironment. *Front Immunol* (2017) 8:248. doi:10.3389/fimmu.2017.00248
41. Sharma P, Allison JP. The future of immune checkpoint therapy. *Science* (2015) 348:56–61. doi:10.1126/science.aaa8172
42. Chen X, El GM, Yoza BK, McCall CE. The NF-kappaB factor RelB and histone H3 lysine methyltransferase G9a directly interact to generate epigenetic silencing in endotoxin tolerance. *J Biol Chem* (2009) 284:27857–65. doi:10.1074/jbc.M109.000950
43. El Gazzar M, Liu T, Yoza BK, McCall CE. Dynamic and selective nucleosome repositioning during endotoxin tolerance. *J Biol Chem* (2010) 285:1259–71. doi:10.1074/jbc.M109.067330
44. El Gazzar M, Yoza BK, Chen X, Garcia BA, Young NL, McCall CE. Chromatin-specific remodeling by HMGB1 and linker histone H1 silences proinflammatory genes during endotoxin tolerance. *Mol Cell Biol* (2009) 29:1959–71. doi:10.1128/MCB.01862-08
45. Roth J, Burwinkel F, van den Bos C, Goebeler M, Vollmer E, Sorg C. MRP8 and MRP14, S-100-like proteins associated with myeloid differentiation, are translocated to plasma membrane and intermediate filaments in a calcium-dependent manner. *Blood* (1993) 82:1875–83.
46. Mira JC, Gentile LF, Mathias BJ, Efron PA, Brakenridge SC, Mohr AM, et al. Sepsis pathophysiology, chronic critical illness, and persistent inflammation-immunosuppression and catabolism syndrome. *Crit Care Med* (2017) 45:253–62. doi:10.1097/CCM.0000000000002074

Conflict of Interest Statement: The authors declare that the research was conducted in the absence of any commercial or financial relationships that could be construed as a potential conflict of interest.

frontiers in Immunology

ORIGINAL RESEARCH
published: 20 November 2017
doi: 10.3389/fimmu.2017.01469

Program Cell Death Receptor-1-Mediated Invariant Natural Killer T-Cell Control of Peritoneal Macrophage Modulates Survival in Neonatal Sepsis

Eleanor A. Fallon, Tristen T. Chun, Whitney A. Young, Chyna Gray, Alfred Ayala† and Daithi S. Heffernan†*

Division of Surgical Research, Department of Surgery, Brown University and Rhode Island Hospital, Providence, RI, United States

We have shown that invariant natural killer T (*i*NKT) cells mediate sepsis-induced end-organ changes and immune responses, including macrophage bacterial phagocytosis, a finding regulated by the check point protein program cell death receptor-1 (PD-1). Furthermore, PD-1 mediates mortality in both adult and neonatal murine sepsis as well as in surgical patients. Given our previous findings, we hypothesize that *i*NKT cells will also modulate neonatal sepsis survival, and that this effect is regulated in part through PD-1. We utilized a polymicrobial intra-peritoneal cecal slurry (CS) sepsis model in wild type (WT), *i*NKT$^{-/-}$ or PD-1$^{-/-}$ 5–7 day old neonatal pups. Typically, tissues were harvested at 24 h for various bio-assays/histology and, in some cases, survival was assessed for up to 7 days. Interestingly, similar to what we recently reported for PD-1$^{-/-}$ mice following CS, *i*NKT$^{-/-}$-deficient animals exhibit a markedly improved survival vs. WT. Histologically, minor alterations in liver architectural, which were noted in WT pups, were attenuated in both *i*NKT$^{-/-}$ and PD-1$^{-/-}$ pups. Following CS, PECAM-1 expression was unchanged in the WT pups but increased in both *i*NKT$^{-/-}$ and PD-1$^{-/-}$ pups. In WT, following CS the emergence of a Ly6C^{low} subpopulation was noted among the influxed peritoneal macrophage population. Conversely, within *i*NKT$^{-/-}$ pups, there were fewer peritoneal macrophages and a greater percentage of Ly6C^{high} macrophages. We show not only a key role for *i*NKT cells in affecting end-organ damage as well as alterations in phagocytes phenotypes in neonatal sepsis but that this *i*NKT cell mediated effect is driven by the central checkpoint protein PD-1.

Keywords: invariant natural killer T cells, programmed cell death receptor-1, neonatal, sepsis, peritoneal macrophage

OPEN ACCESS

Edited by:
Charles E. McCall, Wake Forest University Medical Center, United States

Reviewed by:
Nina Ivanovska, Institute of Microbiology (BAS), Bulgaria
Robert Adam Harris, Karolinska Institute (KI), Sweden

***Correspondence:**
Daithi S. Heffernan
dheffernan@brown.edu

†These authors were co-senior authors on this work.

Specialty section:
This article was submitted to Molecular Innate Immunity, a section of the journal Frontiers in Immunology

Received: *14 July 2017*
Accepted: *19 October 2017*
Published: *20 November 2017*

Citation:
Fallon EA, Chun TT, Young WA, Gray C, Ayala A and Heffernan DS (2017) Program Cell Death Receptor-1-Mediated Invariant Natural Killer T-Cell Control of Peritoneal Macrophage Modulates Survival in Neonatal Sepsis. Front. Immunol. 8:1469. doi: 10.3389/fimmu.2017.01469

INTRODUCTION

Sepsis in neonates remains a devastating illness. Despite significant advances in medical and surgical ICU care, both sepsis-related mortality and long-term morbidity from residual multi-organ dysfunction remain dismally high (1, 2). Intra-abdominal sepsis, from a variety of causes, remains a leading etiology of neonatal sepsis. Several investigators aim to mimic a specific surgical

Abbreviations: WT, wild type; *i*NKT, invariant natural killer T; PD-1, program cell death receptor-1; Sh, sham; CS, cecal slurry; PECAM-1, platelet endothelial cell adhesion molecule; GAPDH, glyceraldehyde 3-phosphate dehydrogenase; α-GalCer, alpha-galactosylceramide; CD, cluster of differentiation; FITC, fluorescein isothiocyanate; PE, phycoerythrin; APC, allophycocyanin; H&E, hematoxylin and eosin; kDa, KiloDalton; ANOVA, analysis of variance.

disease such as necrotizing enterocolitis by including a variety of components to the models (3). However, there is a paucity of data pertaining to the isolated effect of the abdominal bacterial burden without a significant tissue damage component. Using a neonatal model, we demonstrated a role for the check point protein program cell death receptor-1 (PD-1) in modulating the mortality seen with isolated peritoneal polymicrobial sepsis (4). PD-1 is a check point protein involved in both co-stimulatory and co-inhibitory regulation of a variety of acute and chronic immune responses (4–7).

Immune dysfunction induced by sepsis is a major driver of the noted mortality and the morbidity from distant organ failure/dysfunction (8). Following sepsis patients manifest immunosuppression (9). However, the predominance of our understanding of the immune dysfunction seen in sepsis is derived from adult data, both murine models and critically ill patients. It is well recognized that considerable differences exist between the neonatal and adult immune systems. Compared to the adult immune system, it is noted that the neonatal system exhibits a predominance of the innate arm and a poorly developing cellular immunity component (10). Despite these well-described differences in naive baseline immune systems, it is critical to identify key clinical and immunological manifestations of immune suppression that are present across all ages. It will be key to understand whether pathways described in adult sepsis, for which therapeutic agents are currently available, also exist in neonatal sepsis.

We and others have previously demonstrated that several key regulators of the immune response exist. Specifically, this includes a central role for invariant natural killer T (*i*NKT) cells (11–14). *i*NKT cells are innate regulatory cells, which may modulate the immune response to polymicrobial sepsis in both adult mice and humans. This involves regulating peritoneal macrophages (11) and liver kupffer cells (15). *i*NKT cells regulate clearance of the peritoneal bacterial septic burden and affect influx of key immune cells. Specifically, within adults, we have noted that this *i*NKT cell regulation of the immune response to sepsis is controlled by the regulatory checkpoint protein PD-1 (16), a finding not previously observed in neonates.

Invariant natural killer T cells appear to be well developed early in the neonatal immune system and display a considerable non-thymic component to their development and mobilization and functioning. Furthermore, they play key roles in response to non-infectious allergic responses in the early immune system. Given this and the key role for iNKT cells in adult polymicrobial sepsis, we hypothesize that iNKT cells will play a key role in regulating neonatal response to peritoneal sepsis, a finding regulated by the checkpoint protein PD-1.

MATERIALS AND METHODS

Mice

Wild-type (WT) mouse pups were bred from C57BL/6J parents. Mice deficient in either *i*NKT cells (to the deletion of the Vα14Jα18 T-cell receptor gene; Jα18$^{-/-}$) or gene for PD-1 (PD-1$^{-/-}$) breed on a C57BL/6 background were used to breed the knock-out strains. All mice were bred at Rhode Island Hospital and maintained at our institution's rodent facility receiving standard care and standard diet. All pups used were aged 5–7 days old at the start of any experimental procedure. Research objectives and all animal protocols were approved by the Institutional Animal Care and Use Committee of Rhode Island Hospital (ACUP# 0040-16) and conducted in accordance with the Animal Welfare Act and National Institutes of Health guidelines for animal care and use.

Cecal Slurry (CS) Model

The CS model at our institution is modification (16) of the model previously described by Wynn et al. (17). In brief, a naive WT adult donor mouse (C57BL/6J) was euthanized and cecal contents were harvested. These cecal contents were mixed with 5% dextrose solution to create a CS with a concentration of 80 mg/mL. Pups from each litter used were randomly assigned to Sham (Sh) or CS groups. This was repeated across several litters. For the CS group, pups aged 5–7 days old underwent intra-peritoneal (IP) injection of CS at an LD_{70} (1.3 mg/g BW) as a septic challenge (17). Matched pups from the same litter underwent IP injection of 0.9% saline served as the Sh control.

Survival Study

Survival studies were undertaken comparing survival of the pups up with 7 days following either Sh or CS injection. Survival checks were undertaken four times per day for the first 3 days and then twice daily up to 7 days. Given that a striking difference in mortality (50% mortality in the WT) was evident by 24 h both in this study as well as our previous work (4), the 24 h time point was chosen for the rest of the experiments.

Tissue Collection

Pups were euthanized at 24 h following Sh or CS *via* decapitation. They underwent peritoneal lavage for the collection of cells, which were freshly prepared for flow cytometric analysis. Liver was then harvested and stored either in formalin or at −80°C for later western blot analysis.

Flow Cytometry

Peritoneal cells were collected by lavage, centrifuged, and analyzed fresh by flow cytometry. Cell counts were also undertaken to calculate absolute numbers of cells within each population. To identify *i*NKT cells, we used α-GalCer pre-loaded CD1d tetramers conjugated to allophycocyanin (APC) (specific for the Vα14Jα18-TCR). The control was unloaded tetramer, both of which have been obtained from the NIAID Tetramer Facility (Germantown, MD). Monoclonal antibodies were used for most analyses. These included fluorescein isothiocyanate-conjugated F4/80 (peritoneal macrophages), phycoerythrin (PE)-conjugated anti-CD69 (activation), APC-conjugated anti-Ly6C (maker of activation and transmigration ability), and APC-conjugated CD11b (macrophage activation and mobilization factor). All antibodies used were in accordance with both manufacturer's recommendation and our previous publications and analyzed *via* FloJo software.

Histology

Liver samples were placed in formalin and subsequently embedded in paraffin for later sectioning. Sections were stained with hematoxylin and eosin and reviewed for architecture, including ballooning and apoptosis. All H&E samples were analyzed in a fashion blinded to the strain or experiment of origin.

Western Blot

Protein lysates of mouse hepatocytes were run on 10% Tris-glycine gels (Invitrogen, Carlsbad, CA, USA). Blotting procedures, chemiluminescent detection, and densitometric analysis were performed as previously described by our laboratory (18). Membranes were probed with PECAM-1 polyclonal antibody (cat# ab28364; Abcam, USA) and bands detected at 130 kDa. Glyceraldehyde 3-phosphate dehydrogenase was used for loading control.

Statistical Analysis

SigmaPlot 12.5 (Systat Software, San Jose, CA, USA) was used for all analyses. Data are expressed as mean and standard error of the mean. Categorical data were assessed using chi-squared or Fisher's exact test. Mann–Whitney *U* test was used to assess continuous data across two groups. One-way analysis of variance with Holm–Sidak *post hoc* analysis was used for continuous data across multiple groups. Alpha was set to 0.05.

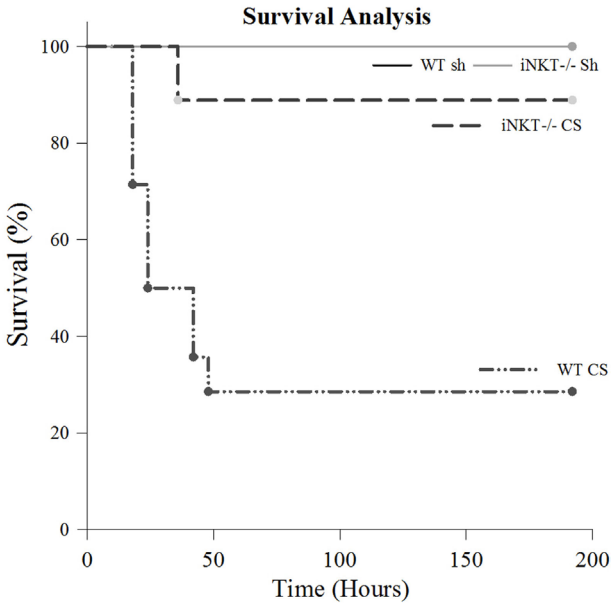

FIGURE 1 | Survival study. There was no mortality among either wild type (WT) or *i*NKT$^{-/-}$ pups subjected to sham ($N = 7$). Compared to sham, sepsis induced approximately 70% mortality among WT pups ($p < 0.001$) ($N = 14$). However, compared to WT, this mortality was considerably abrogated among *i*NKT$^{-/-}$ pups mortality, noted to be only approximately 10% ($N = 21$) ($p < 0.001$ compared to WT).

RESULTS

Given our finding that *i*NKT cells play a role in modulating mortality from sepsis in adult mice (11, 13), we first undertook a survival analysis to assess for a potential role for *i*NKT cells in neonatal sepsis. Akin to previous observations in both adult as well as in neonatal sepsis (4), no mortality was noted in either WT or *i*NKT$^{-/-}$ pups following Sh injection ($N = 7$). CS injection induced an early mortality of approximately 70% in WT pups ($N = 14$) ($p < 0.001$ compared to both Sh groups). The mortality difference was evident as early as 24 h. However, it was abrogated in *i*NKT$^{-/-}$ pups wherein a mortality of only approximately 10% was noted ($N = 21$) ($p < 0.05$ – compared to WT CS) (**Figure 1**). Given the fact that mortality effects occurred as early as 24 h following CS in WT, we opted for 24 h as the time point for all further work. Specifically, we reviewed the role for *i*NKT cells in affecting both the local (peritoneal cavity) as well as remote organ (liver) responses to polymicrobial sepsis.

We have previously demonstrated a role for *i*NKT cells in regulating the peritoneal macrophage phenotype and function in response to sepsis in adults (11), we determined whether *i*NKT cells would affect changes in the neonatal peritoneal macrophage response which may begin to explain the role of *i*NKT cells in affecting mortality following neonatal sepsis. Twenty-four hours following induction of sepsis, the peritoneal cavity underwent lavage with aspiration of peritoneal cells, which were then assessed using flow cytometry. Initially, we noted that in WT pups, CS induced an influx of *i*NKT cells into the peritoneal cavity, both as a percentage of $CD3^+$ cells as well as absolute numbers (**Figure 2**).

Among the WT pups, compared to Sh, CS induced a marked influx of macrophages into the peritoneal cavity at 24 h both as a percentage of total peritoneal cells (3% vs. 49%; $p < 0.01$), as well as absolute numbers of cells. However, in *i*NKT$^{-/-}$ pups, although there was a small increase in peritoneal macrophage influx, there was a marked reduction of peritoneal macrophages when compared with WT pups (**Figure 3**). To assess for PD-1's role in this finding, we repeated the study among PD-1$^{-/-}$ pups and observed a similar finding wherein CS within PD-1$^{-/-}$ pups was not associated with a significant peritoneal macrophage influx.

To further determine whether *i*NKT cells played a role in altering the phenotype of these infiltrated macrophages, we undertook flow cytometric analysis for $CD11b^{high}$ versus $CD11b^{low}$ expression among the peritoneal macrophages. In WT, CS was noted to induce an expansion of the $CD11b^{low}$ subpopulation (9.5% vs. 40%; $p < 0.05$) and a decline in the $CD11^{high}$ (58% vs. 40%; $p < 0.05$) population within the peritoneal cavity. Conversely, in *i*NKT$^{-/-}$ pups, the opposite effect was noted, wherein there was a decline in the $CD11b^{low}$ (49% vs. 29%; $p < 0.05$) and an expansion of the $CD11b^{high}$ subpopulation (**Figure 4A**). A similar effect was noted when assessing for Ly6C expression, wherein sepsis in WT induced an expansion of $Ly6C^{low}$ peritoneal macrophages, but in *i*NKT$^{-/-}$pups, this was reversed with an expansion of the $Ly6C^{high}$ peritoneal macrophage subpopulation. To address a potential role of PD-1 in this observation, we also assessed a similar peritoneal macrophage phenotype in PD-1$^{-/-}$ pups. In pups lacking PD-1, the peritoneal macrophage phenotype mimicked that found

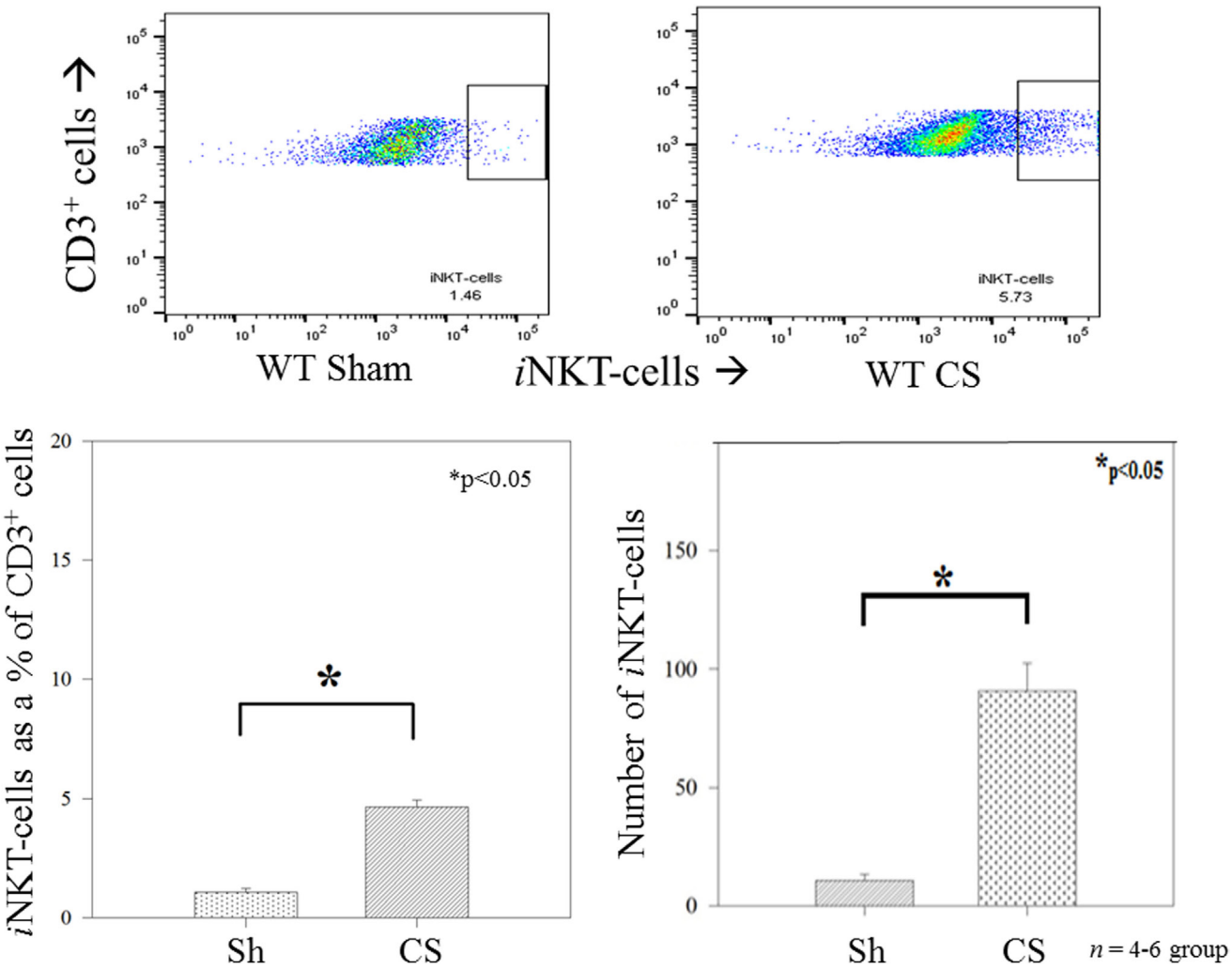

FIGURE 2 | Invariant natural killer T cells were noted to appear in the peritoneal cavity following sepsis, both as a percentage of CD3+ cells as well as absolute numbers of cells. $N = 4–6$ per group. $^*p < 0.05$ comparing sham to CS groups.

in the *i*NKT$^{-/-}$ pups for both CD11b and Ly6C populations (**Figure 4B**).

We next assessed whether *i*NKT cells may affect distant organ response to sepsis. Given the fact that a large contribution to the morbidity and mortality of neonatal sepsis has previously been shown to be derived from distal organ failure (19), and specifically liver dysfunction (20), coupled with the central role of hepatic *i*NKT cells in responding to both local and distal sterile and infectious insults, we next focused on whether *i*NKT cells may also contribute to potential liver damage as a contributing aspect to the noted sepsis related mortality differences. On H&E staining, it was evident that CS did not lead to any gross architectural damage or any evidence of fulminant liver architectural changes in either the WT pups or *i*NKT$^{-/-}$ or PD-1$^{-/-}$ pups. We next reviewed minor liver derangements that may contribute to mortality. We have previously noted within adult models that sepsis induces apoptosis, thus, we looked for apoptotic cells, per 5 high power fields, in liver specimens. Compared to Sh, CS sepsis was associated with an induction of apoptosis in the WT pups (0.5 vs. 3.8; $p = 0.002$). *i*NKT cells appeared to play a role in sepsis induced apoptosis, given that no difference in hepatic apoptosis was evident between Sh and CS in *i*NKT$^{-/-}$ pups. To assess whether the check point protein PD-1 may play a role in this finding, we undertook a similar analysis in PD-1$^{-/-}$ pups. There were two interesting findings within this group. First, it was noted that levels of apoptosis within Sh PD-1$^{-/-}$ were markedly higher than had been noted within WT Sh pups. Sepsis was noted to induce comparable levels of apoptosis within the liver in both *i*NKT$^{-/-}$ and PD-1$^{-/-}$ pups. However, relative to Sh levels, counter to the findings in *i*NKT$^{-/-}$ pups, we noted that when compared to Sh, rather than being increased, we note decreased apoptosis in PD-1$^{-/-}$ pups (4.3 vs. 2; $p = 0.01$) (**Figure 5**).

Given the central role for PECAM-1 in a combination of both gap junction integrity as well as a role in mediating leukocyte

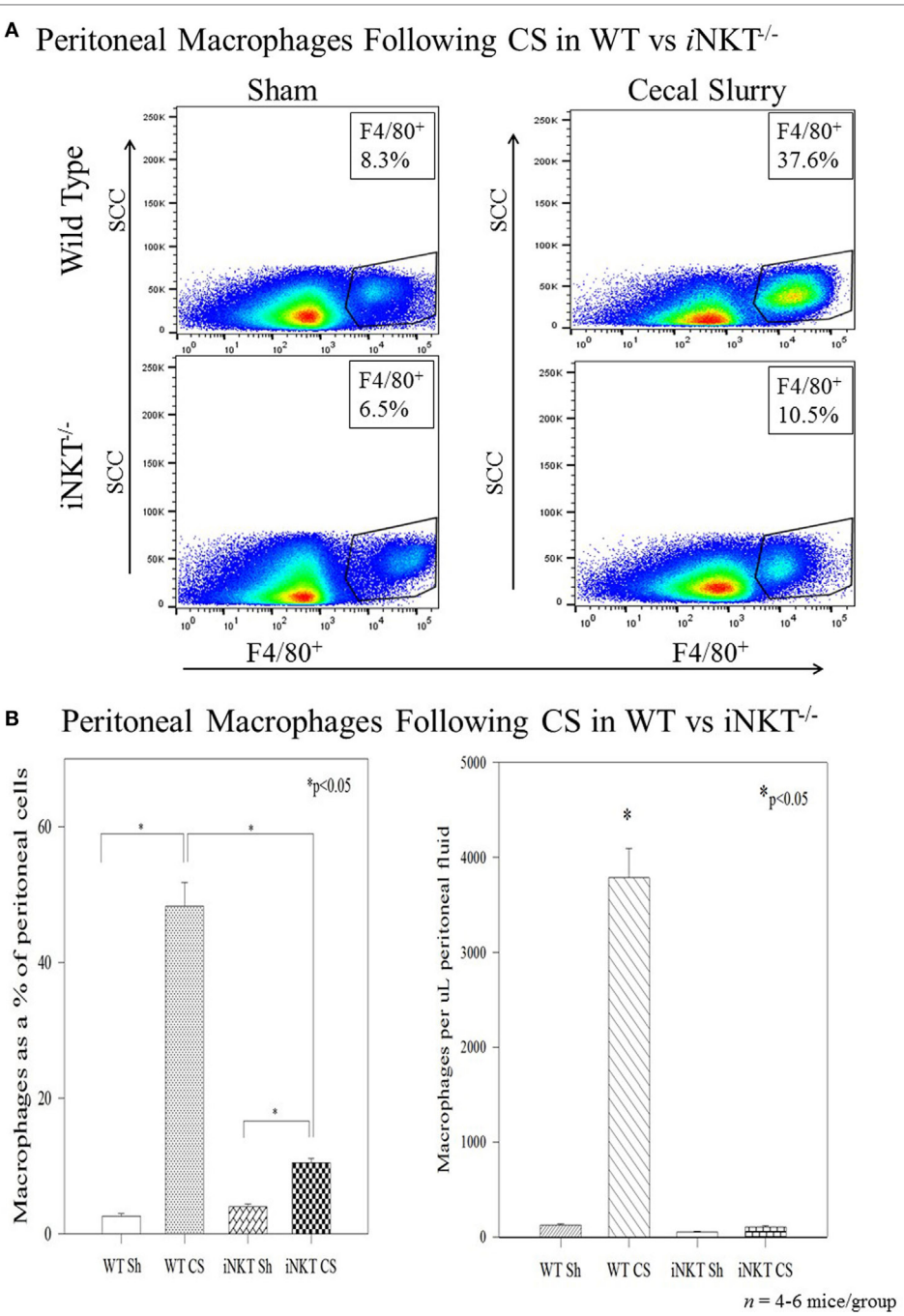

FIGURE 3 | **(A,B)** Sepsis induced an influx of macrophages into the peritoneal cavity in wild-type pups but not in *i*NKT$^{-/-}$ pups. Analysis of variance with $^*p < 0.05$ to detect differences between each group.

transendothelial migration in response to inflammation in distant organs, we assessed PECAM-1 expression in the liver. Within WT pups, CS did not induce any alteration in PECAM-1 expression. This was also noted within PD-1$^{-/-}$ pups following sepsis. However, within *i*NKT$^{-/-}$ pups, it was notable that the baseline level of PECAM-1 was markedly elevated compared across the other strains as well as compared with the other disease states. Furthermore, within *i*NKT$^{-/-}$ pups, CS was noted to induce a marked decline, compared to Sh in PECAM-1 expression. However, this was still elevated when compared to the either WT or PD-1$^{-/-}$ pups (**Figure 6**).

DISCUSSION

Sepsis from a peritoneal source in the neonate remains a devastating illness with high mortality rates and, among those

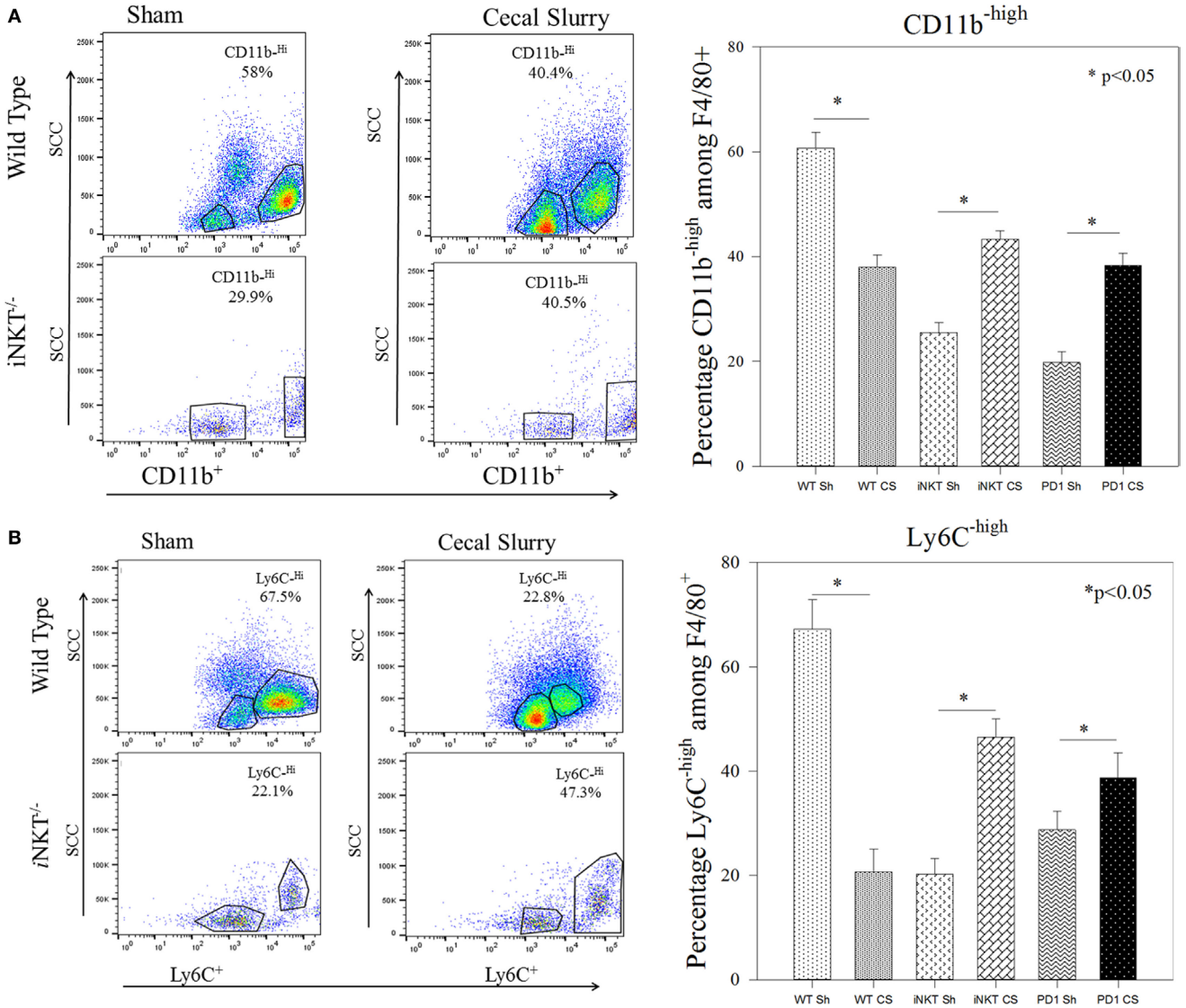

FIGURE 4 | **(A,B)** Representative flow cytometry of CD11b^{high} and Ly6C^{high} phenotyping of the peritoneal F4/80^{+} macrophages. Sepsis in wild-type sepsis induced a decline of the CD11b^{high} and Ly6C^{high} sub-populations, a finding reversed in both *i*NKT$^{-/-}$ and PD-1$^{-/-}$ pups. *N* = 4–6 per group. Analysis of variance with $^{*}p < 0.05$ to detect differences between each group.

who survive, high rates of long-term morbidity and residual end-organ dysfunction (2). Factors controlling the neonate's immune response to sepsis have begun to be elucidated. Despite the marked differences that exist between the neonatal and adult immune systems, understanding which similarities will offer insights into controlling mechanism of the sepsis response across the ages. Specifically, within the neonate, it is emerging that innate regulatory cells appear to be more abundantly present. Specifically, a distinct and active population of *i*NKT cells exists in neonatal cord blood (21, 22). We have previously demonstrated a significant role for *i*NKT cells in controlling the immune response to sepsis in adults (11, 13). In this study, we echo some of those findings. We note a role for *i*NKT cells in affecting both the local peritoneal macrophage response and a distal organ (liver) response to polymicrobial abdominal sepsis. Previous authors have demonstrated some functional differences between naive neonate and adult *i*NKT cells, wherein both specific stimuli and local environment dictate type of *i*NKT cell as well as response from the *i*NKT cells from neonates compared to adults (23). However, this prior work is almost exclusively undertaken in cord blood and following stimulation of isolated naive *i*NKT cells and does not reflect a potential role for these unique regulatory cells in response to polymicrobial neonatal sepsis. Furthermore, our current work echoes a previously noted role for the check point protein PD-1 in modulating mortality from sepsis in both humans and mice as well as a role for PD-1 in modulating the adult iNKT cell response to sepsis (16). Furthermore, we recently demonstrated a role for PD-1 in survival in neonatal sepsis (16). The current work using a model of neonatal peritoneal bacterial sepsis distinct from the additive

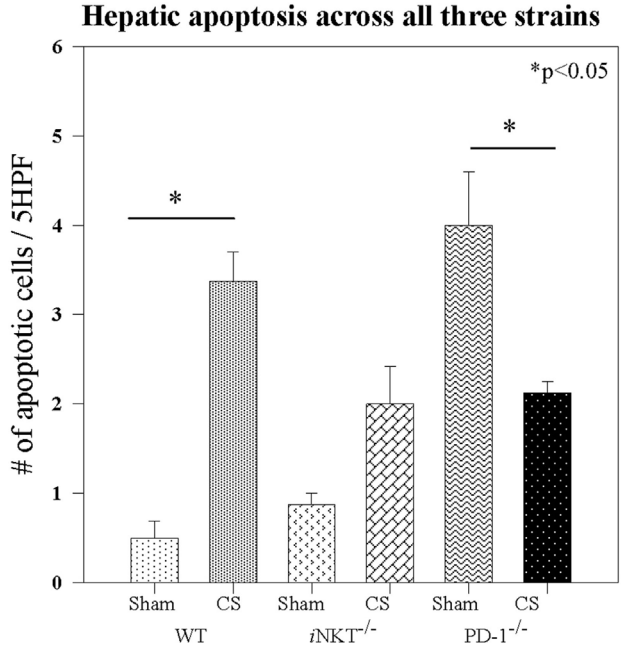

FIGURE 5 | Sepsis induced apoptosis in wild-type pups, but sepsis did not increase apoptosis in either *i*NKT$^{-/-}$ pups or PD-1$^{-/-}$ pups. $N = 4–6$ per group. Analysis of variance with $^*p < 0.05$ to detect differences between each group.

effects of tissue destruction demonstrates a role for *i*NKT cells in affecting both the local peritoneal and distant organ response to neonatal sepsis and focused on PD-1 as a possible driver of these *i*NKT-cell-mediated effects. These results offer exciting potential therapeutic targets given the clinical availability, for adults as well as pediatric patients, of both specific modulators of *i*NKT cells (24, 25) and PD-1 antagonists.

We have previously demonstrated in adult mice, following initiation of sepsis, that hepatic *i*NKT cells leave the liver and migrate to the peritoneal cavity, wherein, they have a regulatory role in controlling the peritoneal macrophage response to sepsis. As a mechanism, we demonstrated that this *i*NKT-cell migration and *i*NKT cell control of the peritoneal macrophage response was under the regulation of the checkpoint protein PD-1 (16). Within the neonate, it is known that innate regulatory immune cells, such as *i*NKT cells, play major roles in responding a variety of antigens, including the fact that *i*NKT cells are noted to accumulate in the small intestine in the second trimester (26). This supports our current observation that *i*NKT cells emigrate into the peritoneal cavity in response to sepsis and that these *i*NKT cells played a significant role in altering the peritoneal macrophage population.

Neonates are known to display an attenuated and down-regulated inflammatory response to many stimuli (8, 10, 27). Despite this dampened inflammatory response, it has been postulated that neonatal mortality may be driven from end organs being more susceptible to the immune response to an infection (8). Although we did not find any gross histologic hepatic damage following sepsis, we did detect minor alterations within the liver following sepsis. Any degree of organ dysfunction among vulnerable neonates may display marked effects; however, further work will be needed to assess whether these observed minor effects indeed play a role in altering sepsis related mortality. *i*NKT cells appear to play a role in the sepsis induced apoptosis, wherein apoptosis was diminished in Jα18$^{-/-}$ pups following sepsis. CS induced an alteration in PECAM-1 expression in WT pups. PECAM-1 (CD31) is expressed at the lateral borders of endothelial cells. Within the fetal and neonatal liver, PECAM-1 is expressed upon endothelial cells of all blood vessels and is involved in many of the developmental and pathologic changes seen in response to disease processes (28, 29). Alterations in PECAM-1 affect vascular responses and leukocyte trafficking in response to a septic challenge (30). We herein noted that *i*NKT cells potentially maintain gap junction integrity by regulating PECAM-1, wherein *i*NKT$^{-/-}$ pups displayed lowered hepatic PECAM-1 expression compared with the WT. This is in keeping with the observations of Clement et al who demonstrated key interactions between innate regulatory lymphocytes and cell adhesion molecules (31).

Here, we have demonstrated that several features of the peritoneal macrophage response to peritoneal polymicrobial septic challenge are controlled by *i*NKT cells in the neonate. Within WT pups, sepsis induced an influx of *i*NKT cells into the peritoneal cavity. This peritoneal influx of *i*NKT cells is in keeping with our adult murine data, in which the liver is the major source of *i*NKT cells in the mouse, and that when a septic source is detected, hepatic *i*NKT cells become activated, enter the circulation, and localize to the peritoneal cavity to affect the immune response to sepsis (11, 16). Most importantly, there was a marked decline in the influx of macrophages in the absence of *i*NKT cells; this speaks to a central role for *i*NKT cells in mobilizing macrophages to the source of the sepsis. Furthermore, we noted *i*NKT-cell-dependent alteration in the activation status of the peritoneal macrophages in response to sepsis. We chose to assess CD11b and Ly6C$^{high/low}$ level expression among these cells. CD11b is often seen as a marker of activation of macrophages and is also involved in facilitating transendothelial migration (32, 33). The emergence of CD11b^{low} subpopulation following sepsis in the WT is in keeping with the generalized immunosuppression seen in sepsis. However, the reversal of this effect with the lack of CD11b^{low} and the expansion of CD11b^{high} among *i*NKT-cell-deficient mice is in keeping with the known role for *i*NKT cells as suppressive or anti-inflammatory immune cell. Many have described the *i*NKT-cell as the brake on the immune system to control and prevent an over-exuberant inflammatory and immune response (34, 35). Ly6C was chosen as both a marker of activation and surface receptor involved in aiding mobilization of macrophages in anticipation of possible migration (36). Again given the emergence of Ly6C^{low} in WT, but not in *i*NKT cell-deficient mice, would suggest a role for *i*NKT cells in modulating and preventing too many macrophages getting to the site of injury or sepsis and, thus, preventing an excessive response.

We believe that our data are in keeping with the known dual abilities of *i*NKT cells (14, 35, 37, 38). It has been well-described that *i*NKT cells are capable of both a Th1 response and a Th2

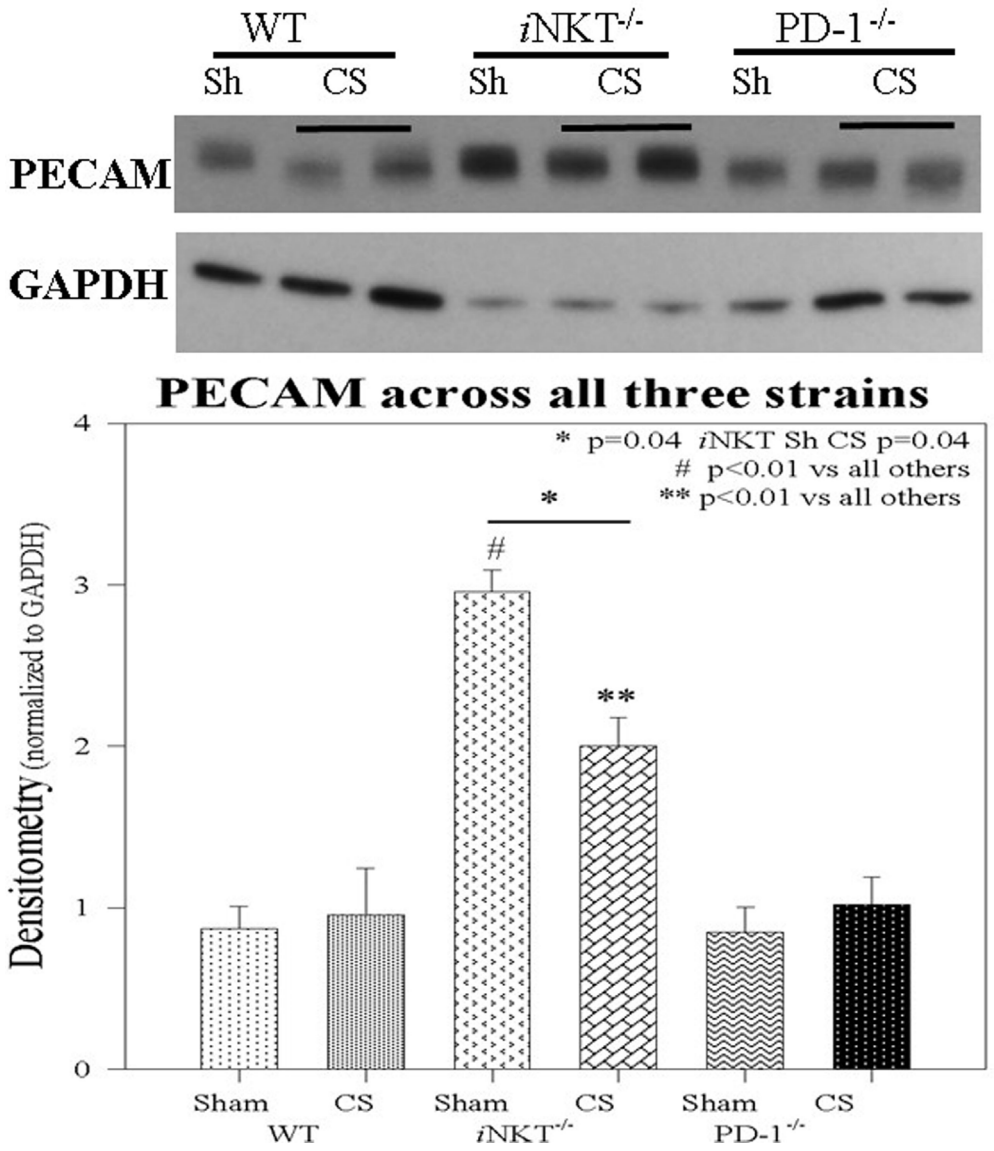

FIGURE 6 | PECAM-1 expression was unchanged in either wild-type or PD-1$^{-/-}$ pups following cecal slurry (CS). However, within *i*NKT$^{-/-}$ pups, PECAM-1 expression was noted to be significantly elevated at baseline following sham compared to all others. Following CS sepsis, levels of PECAM were noted to significantly decrease. $N = 4$–6 per group. $^{*}p = 0.04$ comparing *i*NKT$^{-/-}$ sham versus CS; $^{\#}p < 0.01$ comparing *i*NKT$^{-/-}$ sham versus all others; $^{**}p < 0.01$ comparing *i*NKT$^{-/-}$ CS versus all others; by analysis of variance.

response to a variety of insults as well as affecting the local or distal Th1/Th2 response in adult animal models. Our data supports a model of *i*NKT cells acting as co-stimulator cells licensing macrophages to respond to a stimulus (the bacterial burden) and then mobilize and migrate to the peritoneal cavity (the source of the sepsis) as reflected by the lack of peritoneal macrophages in CS in *i*NKT cell deficient mice. However, once these macrophages are activated and arrive at the peritoneal cavity, then *i*NKT cells appear to be responsible for controlling and preventing an over-exuberant immune response and, thus, preventing tissue destruction and by-stander tissue injury.

Our findings also support the concept that the *i*NKT-cell migration and their actions directed at macrophages were under the influence of PD-1. Among immune regulators, PD-1 has arisen to play an integral role in a variety of physiologic derangements, including sepsis and malignancy (39). PD-1 is a transmembrane receptor that is recognized to serve as a check-point protein in both pro- and anti-inflammatory cascades. It has been demonstrated to alter cell-trafficking in response to intra-abdominal sepsis in the adult mouse model *via* release of the immunoparalysis (40, 41) induced by severe sepsis (42, 43). This includes affecting the trafficking of *i*NKT cells to the source of sepsis in adult mice (16). When PD-1 is activated *via* binding to one of its two ligands, it acts to prevent the activation of immune cells. This causes downregulation of the function of T and pro-B cells among other effects (6, 41). Although

as it name suggests the molecule promotes apoptosis among antigen-specific T cells in lymph nodes, it reduces apoptosis among regulatory suppressor T cells. It also contributes to inhibition of macrophage function in the setting of sepsis (44). Conversely, when PD-1 is blocked, it cannot exert its inhibitory effects on most T cells (6). PD-1 inactivation neutralizes the pathway thought to be critical in T-cell co-stimulatory signal regulation.

This work, expanding upon an aspect of *i*NKT-cell biology, offers intriguing future potential targets for currently available therapeutic agents. *i*NKT cells are activated *via* α-galactosylceramide (αGalCer), which is a potent and very specific glycolipid. Although much of the clinical work on *i*NKT-cell and PD-1 modulation has been undertaken among cancer patients, modified αGalCer glycolipids have been used to modulate *i*NKT cells in phase I/II clinical studies involving patients with chronic hepatitis B (45) and chronic hepatitis C infections (24). Interestingly, Yang et al. demonstrated that the effectiveness of *i*NKT cells in affecting control of chronic hepatitis B was, in part, driven through PD-1 expression upon *i*NKT cells. Tefit et al. demonstrated the safety of ABX196, another αGalCer analog, as a vaccine against hepatitis B (46). Given the safety and effectiveness of these early cancer and hepatitis trials involving αGalCer glycolipid analogs, future work will be aimed at sicker and more vulnerable septic patient population, specifically as it relates to the need for higher and repeat dosing to overcome profound immunosuppression. Furthermore, an ability to direct a Th1 versus a Th2 response has been demonstrated based on specific structural analogs of αGalCer (47).

Several authors have begun to explore the ability to harness the power of donor *i*NKT cells. Specifically relating to our findings, De Lalla et al. noted that, among pediatric patients with hematological malignancies receiving hematopoietic stem cell transplantation, the successful reconstitution of *i*NKT cells was key to maintaining cancer remission (48). This work is also in keeping with our prior data among septic adult/geriatric patients wherein we noted that loss of an adequate circulating *i*NKT population following sepsis was associated with an increased risk of death (12). With the expanded abilities to grow and maintain transplantable *i*NKT cells, one can foresee septic patients receiving transplanted *i*NKT cells followed by either modified αGalCer glycolipids or CD1d blocking agents to modulate the function of these transplanted *i*NKT cells.

CONCLUSION

Here, we demonstrate a key role for *i*NKT cells in affecting both peritoneal macrophages as well as end-organ damage in neonatal sepsis. This *i*NKT-cell-mediated effect is, in part, driven by the central checkpoint protein PD-1, a ligand for which therapeutic agents are currently clinically available. Given the currently available agents either in clinical use or undergoing clinical trials for the modulation of both *i*NKT cells as well as PD-1, ongoing elucidation of this mechanism will allow further refinement of potential therapeutic targets in this vulnerable population with neonatal sepsis.

ETHICS STATEMENT

The study was carried out in accordance with the recommendations of the Rhode Island Hospital IACUC (Institutional Animal Care and Use Committee). The protocol was approved by the Rhode Island Hospital IACUC.

AUTHOR CONTRIBUTIONS

Design and concept: EF, TC, WY, CG, AA, and DH. Conduct of experiments: EF, TC, WY, CG, and DH. Results analysis and interpretation: EF, TC, WY, AA, and DH. Manuscript preparation, revisions, and approval: EF, TC, WY, AA, and DH.

FUNDING

This project was supported by NIH grant K08-GM110495 (DH), NIH grant R35-GM118097 (AA), NIH grant T35-HL67704 (CG), a Surgical Infections Society Foundation-Basic & Clinical Translational Research Fellowship (EF), and "Armand D. Versaci" Research Scholar in Surgical Sciences Fellowship awards (to EF, TC, and WY).

REFERENCES

1. Singer M, Deutschman C, Seymour C, Shankar-Hari M, Annane D, Bauer M, et al. The third international consensus definitions for sepsis and septic shock (Sepsis-3). *JAMA* (2016) 315(8):801–10. doi:10.1001/jama.2016.0287
2. Wynn J. Defining neonatal sepsis. *Curr Opin Pediatr* (2016) 28(2):135–40. doi:10.1097/MOP.0000000000000315
3. Nino D, Sodhi C, Hackam D. Necrotizing enterocolitis: new insights into pathogenesis and mechanisms. *Nat Rev Gastroenterol Hepatol* (2016) 13(10): 590–600. doi:10.1038/nrgastro.2016.119
4. Young W, Fallon E, Heffernan D, Efron P, Cioffi W, Ayala A. Improved survival after induction of sepsis by cecal slurry in PD-1 knockout murine neonates. *Surgery* (2017) 161(5):1387–93. doi:10.1016/j.surg.2016.11.008
5. Rao M, Valentini D, Dodoo E, Zumla A, Maeurer M. Anti-PD-1/PD-L1 therapy for infectious diseases: learning from the cancer paradigm. *Int J Infect Dis* (2017) 56:221–8. doi:10.1016/j.ijid.2017.01.028
6. Tumeh P, Harview C, Yearley J, Shintaku I, Taylor E, Robert L, et al. PD-1 blockade induces responses by inhibiting adaptive immune resistance. *Nature* (2014) 515(7528):568–71. doi:10.1038/nature13954
7. Bardhan K, Anagnostou T, Boussiotis V. The PD1: PD-L1/2 pathway from discovery to clinical implementation. *Front Immunol* (2016) 7:550. doi:10.3389/fimmu.2016.00550
8. Raymond S, Stortz J, Mira J, Larson S, Wynn J, Moldawer L. Immunological defects in neonatal sepsis and potential therapeutic approaches. *Front Pediatr* (2017) 5:14. doi:10.3389/fped.2017.00014
9. Thakkar R, Huang X, Lomas-Neira J, Heffernan D, Ayala A. Sepsis and the immune response. In: Eremin O, Sewell H, editors. *Essential Immunology for Surgeons*. Oxford: Oxford University Press (2011). p. 303–42.
10. Kan B, Razzaghian H, Lavoie P. An immunological perspective on neonatal sepsis. *Trends Mol Med* (2016) 22(4):290–302. doi:10.1016/j.molmed.2016.02.001
11. Heffernan D, Monaghan S, Thakkar R, Tran M, Chung C, Gregory S, et al. Inflammatory mechanisms in sepsis: elevated invariant natural killer T-cell

numbers in mouse and their modulatory effect on macrophage function. *Shock* (2013) 40(2):122–8. doi:10.1097/SHK.0b013e31829ca519
12. Heffernan D, Monaghan S, Chung C, Cioffi W, Gravenstein S, Ayala A. A divergent response of innate regulatory T-cells to sepsis in humans: circulating invariant natural killer T-cells are preserved. *Hum Immunol* (2014) 75(3):277–82. doi:10.1016/j.humimm.2013.11.004
13. Hu C, Venet F, Heffernan D, Wang Y, Horner B, Huang X, et al. The role of hepatic invariant NKT cells in systemic/local inflammation and mortality during polymicrobial septic shock. *J Immunol* (2009) 182(4):2467–75. doi:10.4049/jimmunol.0801463
14. Szabo P, Anantha R, Shaler C, McCormick J, Haeryfar S. CD1d- and MR1- restricted T cells in sepsis. *Front Immunol* (2015) 6:401. doi:10.3389/fimmu.2015.00401
15. Lee W, Moriarty T, Wong C, Zhou H, Strieter R, van Rooijen N, et al. An intravascular immune response to *Borrelia burgdorferi* involves Kupffer cells and iNKT cells. *Nat Immunol* (2010) 11(4):295–302. doi:10.1038/ni.1855
16. Young J, Heffernan D, Chung C, Kettenmann M, Young W, Guillen V, et al. Effect of PD-1: PD-L1 in invariant natural killer T-cell emigration and chemotaxis following sepsis. *Shock* (2016) 45(5):534–9. doi:10.1097/SHK.0000000000000553
17. Wynn J, Scumpia P, Delano M, O'Malley K, Ungaro R, Abouhamze A, et al. Increased mortality and altered immunity in neonatal sepsis produced by generalized peritonitis. *Shock* (2007) 28(6):675–83. doi:10.1097/SHK.0b013e3180556d09
18. Thakkar R, Chung C, Chen Y, Monaghan S, Lomas-Neira J, Heffernan D, et al. Local tissue expression of the cell death ligand, fas ligand, plays a central role in the development of extrapulmonary acute lung injury. *Shock* (2011) 36(2):138–43. doi:10.1097/SHK.0b013e31821c236d
19. Wynn J, Wong H. Pathophysiology and treatment of septic shock in neonates. *Clin Perinatol* (2010) 37(2):439–79. doi:10.1016/j.clp.2010.04.002
20. Smith S, Tagge E, Hannakan C, Rowe M. Characterization of neonatal multisystem organ failure in the surgical newborn. *J Pediatr Surg* (1991) 26(4):494–7. doi:10.1016/0022-3468(91)91002-G
21. Lopez M, Palmer B, Lawrence D. Naive T cells, unconventional NK and NKT cells and highly responsive monocyte-derived macrophages characterize human cord blood. *Immunobiology* (2014) 219(10):756–65. doi:10.1016/j.imbio.2014.06.001
22. Ladd M, Sharma A, Huang Q, Wang A, Xu L, Genowati I, et al. Natural killer T cells constitutively expressing the interleukin-2 receptor alpha chain early in life are primed to respond to lower antigenic stimulation. *Immunology* (2010) 131(2):289–99. doi:10.1111/j.1365-2567.2010.03304.x
23. Moreira-Teixeira L, Resende M, Coffre M, Devergne O, Herbeuval J, Hermine O, et al. Proinflammatory environment dictates the IL-17 producing capacity of human invariant NKT cells. *J Immunol* (2011) 186(10):5758–65. doi:10.4049/jimmunol.1003043
24. Schneiders F, Scheper R, von Blomberg B, Woltman A, Janssen H, van den Eertwegh A, et al. Clinical experience with alpha-galactosylceraminde (KRN7000) in patients with advanced cancer and chronic hepatitis B/C infection. *Clin Immunol* (2011) 140(2):130–41. doi:10.1016/j.clim.2010.11.010
25. Exley M, Nakayama T. NKT-cell-based immunotherapies in clinical trials. *Clin Immunol* (2011) 140(2):117–8. doi:10.1016/j.clim.2011.04.015
26. Loh L, Ivarsson M, Michaelsson J, Sandberg J, Nixon D. Invariant natural killer T cells developing in the human fetus accumulate and mature in the small intestine. *Mucosal Immunol* (2014) 7(5):1233–43. doi:10.1038/mi.2014.13
27. Valiathan R, Ashman M, Asthana D. Effects of ageing on the immune system: infants to elderly. *Scand J Immunol* (2016) 83(4):255–66. doi:10.1111/sji.12413
28. Shiojiri N, Sugiyama Y. Immunolocalization of extracellular matrix components and integrins during mouse liver development. *Hepatology* (2004) 40(2):346–55. doi:10.1002/hep.20303
29. Sugiyama Y, Koike T, Shiojiri N. Developmental changes of cell adhesion molecule expression in the fetal mouse liver. *Anat Rec* (2010) 293(10):1698–710. doi:10.1002/ar.21204
30. Privratsky J, Tilkens S, Newman D, Newman P. PECAM-1 dampens cytokine levels during LPS-induced endotoxemia by regulating leykocyte trafficking. *Life Sci* (2012) 90(5–6):177–84. doi:10.1016/j.lfs.2011.11.002
31. Clement M, Fornasa G, Guedj K, Mkaddem S, Gaston A, Khallow-Laschet J, et al. CD31 is a key coinhibitory receptor in the development of immunogenic dendritic cells. *Proc Natl Acad Sci U S A* (2014) 111(12):E1101–10. doi:10.1073/pnas.1314505111
32. Maiguel D, Faridi M, Wei C, Kuwano Y, Balla K, Hernandez D, et al. Small molecule-mediated activation of the integrin CD11b/CD18 reduces inflammatory disease. *Sci Signal* (2011) 4(189):ra57. doi:10.1126/scisignal.2001811
33. Rougerie P, Miskolci V, Cox D. Generation of membrane stuctures during phagocytosis and chemotaxis of macrophages: role and regulation of the actin cytoskeleton. *Immunol Rev* (2013) 256(1):222–39. doi:10.1111/imr.12118
34. Bendelac A, Savage P, Teyton L. The biology of NKT cells. *Annu Rev Immunol* (2007) 25:297–336. doi:10.1146/annurev.immunol.25.022106.141711
35. Van Kaer L, Parekh V, Wu L. The response of CD1d-restricted invariant NKT cells to microbial pathogens and their products. *Front Immunol* (2015) 6:226. doi:10.3389/fimmu.2015.00226
36. Epelman S, Lavine K, Randolph G. Origin and functions of tissue macrophages. *Immunity* (2014) 41(1):21–35. doi:10.1016/j.immuni.2014.06.013
37. Liew P, Kubes P. Intravital imaging – dynamic insights into natural killer T cell biology. *Front Immunol* (2015) 6:240. doi:10.3389/fimmu.2015.00240
38. Brennan P, Brigl M, Brenner M. Invariant natural killer T-cells: an innate activation scheme linked to diverse effector functions. *Nat Rev Immunol* (2013) 13(2):101–17. doi:10.1038/nri3369
39. Chen L, Han X. Anti-PD-1/PD-L1 therapy of human cancer: past, present and future. *J Clin Invest* (2015) 125(9):3384–91. doi:10.1172/JCI80011
40. Freeman G, Long A, Iwai Y, Bourque K, Chernova T, Nishimura H, et al. Engagement of the PD-1 immunoinhibitory receptor by a novel B7 family member leads to negative regulation of lymphocyte activation. *J Exp Med* (2000) 192(7):1027–34. doi:10.1084/jem.192.7.1027
41. Tarrio M, Grabie N, Bu D, Sharpe A, Lichtman A. PD-1 protects against inflammation and myocyte damage in T cell mediated myocarditis. *J Immunol* (2012) 188(10):4876–84. doi:10.4049/jimmunol.1200389
42. Huang X, Venet F, Wang Y, Lepape A, Yuan Z, Chen Y, et al. PD-1 expression by macrophages plays a pathologic role in alterting microbial clearance and the innate inflammatory response to sepsis. *Proc Natl Acad Sci U S A* (2009) 106(15):6303–8. doi:10.1073/pnas.0809422106
43. Brahmamdam P, Inoue S, Unsinger J, Chang KC, McDunn JE, Hotchkiss RS. Delayed administration of anti-PD-1 antibody reverses immune dysfunction and improves survival during sepsis. *J Leukoc Biol* (2010) 88(2):233–40. doi:10.1189/jlb.0110037
44. Brown K, Freeman G, Wherry E, Sharpe A. Role of PD-1 in regulating acute infections. *Curr Opin Immunol* (2010) 22(3):397–401. doi:10.1016/j.coi.2010.03.007
45. Woltman A, Ter Borg M, Blinda R, Sprengers D, Von Blomberg B, Scheper R, et al. Alpha-galactosylceramide in chronic hepatitis B infection: results from a randomized placebo controlled phase I/II trial. *Antivir Ther* (2009) 14(6):809–18. doi:10.3851/IMP1295
46. Tefit J, Crabe S, Orlandini B, Nell H, Bendelac A, Deng S, et al. Efficacy of ABX196, a new NKT agonist, in prophylactic human vaccination. *Vaccine* (2014) 32(46):6138–45. doi:10.1016/j.vaccine.2014.08.070
47. Goff R, Gao Y, Mattner J, Zhou D, Yin N, Cantu C, et al. Effects if lipid chain lengths in alpha-galactosylceramides on cytokine release by natural killer T cells. *J Am Chem Soc* (2004) 126(42):13602–3. doi:10.1021/ja045385q
48. de Lalla C, Rinaldi A, Montagna D, Azzimonti L, Bernardo M, Sangalli L, et al. Invariant NKT cell reconstitution in pediatric leukemia patients given HLA-haploidentical stem cell transplantation defines distinct CD4+ and CD4- subset dynamics and correlates with remission state. *J Immunol* (2011) 186(7):4490–9. doi:10.4049/jimmunol.1003748

Conflict of Interest Statement: The authors declare that the research was conducted in the absence of any commercial or financial relationships that could be construed as a potential conflict of interest.

frontiers in Immunology

REVIEW
published: 05 February 2018
doi: 10.3389/fimmu.2018.00141

A Role for the Krebs Cycle Intermediate Citrate in Metabolic Reprogramming in Innate Immunity and Inflammation

*Niamh C. Williams and Luke A. J. O'Neill**

School of Biochemistry and Immunology, Trinity Biomedical Sciences Institute, Trinity College Dublin, Dublin, Ireland

Metabolism in immune cells is no longer thought of as merely a process for adenosine triphosphate (ATP) production, biosynthesis, and catabolism. The reprogramming of metabolic pathways upon activation is also for the production of metabolites that can act as immune signaling molecules. Activated dendritic cells (DCs) and macrophages have an altered Krebs cycle, one consequence of which is the accumulation of both citrate and succinate. Citrate is exported from the mitochondria *via* the mitochondrial citrate carrier. Cytosolic metabolism of citrate to acetyl-coenzyme A (acetyl-CoA) is important for both fatty-acid synthesis and protein acetylation, both of which have been linked to macrophage and DC activation. Citrate-derived itaconate has a direct antibacterial effect and also has been shown to act as an anti-inflammatory agent, inhibiting succinate dehydrogenase. These findings identify citrate as an important metabolite for macrophage and DC effector function.

Keywords: immunometabolism, citrate, ATP-citrate lyase, itaconate, acetylation, metabolism, macrophages, Krebs cycle

OPEN ACCESS

Edited by:
Charles E. McCall, Wake Forest Baptist Medical Center, United States

Reviewed by:
Markus Munder, Johannes Gutenberg-Universität Mainz, Germany
Xiaoyu Hu, Tsinghua University, China
Geanncarlo Lugo-Villarino, UMR5089 Institut de Pharmacologie et de Biologie Structurale (IPBS), France

****Correspondence:***
Luke A. J. O'Neill
laoneill@tcd.ie

Specialty section:
This article was submitted to Molecular Innate Immunity, a section of the journal Frontiers in Immunology

Received: *06 October 2017*
Accepted: *16 January 2018*
Published: *05 February 2018*

Citation:
Williams NC and O'Neill LAJ (2018) A Role for the Krebs Cycle Intermediate Citrate in Metabolic Reprogramming in Innate Immunity and Inflammation. Front. Immunol. 9:141. doi: 10.3389/fimmu.2018.00141

METABOLIC REPROGRAMMING IN MACROPHAGES AND DENDRITIC CELLS (DCs)

The innate immune system is the first line of defense against infection. Cells of the innate immune system have a range of germline encoded receptors, pathogen recognition receptors that allow for the recognition of pathogen-associated molecular patterns, and danger-associated molecular patterns from damaged cells or tissues (1, 2). Macrophages and DCs play an important role in the

Abbreviations: ACC, acetyl-CoA carboxylase; ACLY, ATP-citrate lyase; ACO2, aconitase 2; ACSS, acetyl-CoA synthase; aKG, α-ketoglutarate; AMPK, AMP-activated protein kinase; ATP, adenosine triphosphate; BMDM, bone marrow-derived macrophage; CIC, citrate carrier; CPT1, carnitine palmitoyltransferase 1; CS, citrate synthase; DC, dendritic cell; DMI, dimethyl itaconate; ETC, electron transport chain; FAO, fatty acid oxidation; FASN, fatty acid synthase; FIH, factor inhibiting HIF; GAPDH, glyceraldehyde 3-phosphate dehydrogenase; HIF, hypoxia-inducible factor; HK2, hexokinase 2; ICL, isocitrate lyase; IDH, isocitrate dehydrogenase; IFN-γ, interferon-γ; IKKε, IκB kinase ε; iNOS, inducible nitric oxide synthase; IRF, interferon regulatory factor; IRG1, immune-responsive gene 1; LDHA, lactate dehydrogenase A; LPS, lipopolysaccharide; MDH, malate dehydrogenase; MPC, mitochondrial pyruvate carrier; MTB, *Mycobacterium tuberculosis*; mTOR, mammalian target of rapamycin; NAA, N-acetylaspartic acid; NF-κB, nuclear factor-κB; NK cell, natural killer cell; NO, nitric oxide; OCR, oxygen consumption rate; OXPHOS, oxidative phosphorylation; PDH, pyruvate dehydrogenase; PDK1, pyruvate dehydrogenase kinase 1; PFK, phosphofructokinase; PGE_2, prostaglandin E_2; PI3K, phosphatidylinositide-3-kinase; PK, pyruvate kinase; PPP, pentose phosphate pathway; RET, reverse electron transport; ROS, reactive oxygen species; SDH, succinate dehydrogenase; SREBP, sterol regulatory element-binding protein; TBK1, TANK-binding kinase 1; TLR, toll-like receptor; TNFα, tumour necrosis factor α.

initiation and resolution of the immune response. Both can produce inflammatory mediators, phagocytose pathogens and release chemokines to recruit other immune cells to the site of infection (3). DCs are also important in the activation of naive T cells as they can present antigen to the T cell initiating an adaptive immune response (4).

The dual role played by macrophages in initiation and resolution of inflammation requires cells to adopt different processes. In macrophages, this can be broadly described in terms of M1, lipopolysaccharide (LPS)- or classically activated macrophages, and M2, IL-4-activated macrophages. M1 macrophages are more pro-inflammatory and will produce inflammatory mediators, such as nitric oxide (NO) and reactive oxygen species (ROS) (3, 5). M2 macrophages are important in helminth infection and the resolution of inflammation, secreting growth factors to aid in tissue repair and regeneration and cytokines such as IL-10 that can dampen the immune response (3, 6).

Both macrophages and DCs must be able to switch rapidly from a resting to an activated state. A hallmark of immune cell activation is a change in their metabolism. M1 macrophages upregulate glycolysis and the pentose phosphate pathway (PPP) while the Krebs cycle is broken at two points and the fatty acid oxidation (FAO) and oxidative phosphorylation (OXPHOS) are downregulated (5). Toll-like receptor (TLR)-activated DCs also have increased aerobic glycolysis and decreased OXPHOS and FAO (7). This inhibition of mitochondrial respiration in murine DCs is due to NO and long-term activation of glycolysis in activated DCs serves to produce adenosine triphosphate (ATP) to compensate for the collapse in mitochondrial function, maintain the mitochondrial membrane potential ($\Delta\psi_M$) and prevent cell death (8). The high rate of glycolysis is similar to that seen in tumor cells (3). Murine M2 macrophages also upregulate glycolysis, but the Krebs cycle is intact and OXPHOS is functioning (5). A general theme exists among immune cells where a reliance on aerobic glycolysis is important for cells, such as M1 macrophages and DCs, whereas immunomodulatory cells, such as M2 macrophages and regulatory T cells (Tregs), make use of OXPHOS (9).

Recent work has shed light on several of the key determinants of metabolic reprogramming in M1 macrophages and DCs. The upregulation of inducible nitric oxide synthase (iNOS) and resulting generation of NO causes inhibition of mitochondrial respiration in murine cells (10–12). Hypoxia-inducible factor-1α (HIF1α) can be induced under normoxic conditions in immune cells and this is crucial for upregulation of glycolysis (13). HIF-target genes included those encoding for glycolytic enzymes, the glucose transporter GLUT1, and lactate dehydrogenase (LDH), as well as inflammatory factors such as interleukin-1β (IL1β) (14–16). LPS-treatment of macrophages or DCs activates the mammalian target of rapamycin (mTOR), a central regulator of metabolism, which in turn boosts expression and activity of HIF1α (17). Finally AMP-activated protein kinase (AMPK) is inhibited by LPS treatment (18). AMPK senses the energy status of a cell, and when that is low this inhibits anabolic pathways and drives catabolic ones such as FAO, while also inhibiting mTOR and nuclear factor-κB (NF-κB) signaling. Its inhibition by LPS allows changes necessary for a pro-inflammatory response to occur. Several processes that are upregulated in M1 macrophages are downregulated in M2 macrophages. In mouse macrophages, iNOS expression is decreased and arginase-1 (ARG1) is highly upregulated, and so arginine is preferentially metabolized to proline and polyamines (19). mTOR is inhibited by activation of upstream repressors TSC1 and TSC2 while AMPK activity is high (18, 20).

It is possible that the upregulation and reliance on aerobic glycolysis is in part due to the rate of response required of these cells for an effective immune system. Glycolysis, though less efficient at producing ATP, is able to do so more rapidly than OXPHOS. However, there is evidence that upregulation of metabolic pathways is more nuanced than that. Metabolic changes are important not only in terms of generating biosynthetic precursors and for ATP production, but it also has emerged that metabolites themselves can act as signaling molecules and affect important inflammatory pathways (21, 22). Of particular interest are metabolites of the Krebs cycle. The oxidation of succinate by succinate dehydrogenase (SDH) has been shown to be of importance in the classical activation of macrophages (23). This leads to reverse electron transport (RET) in complex I of the electron transport chain (ETC) driving the production of ROS, which in turn leads to activation of HIF1α. Increased levels of cytosolic succinate can inhibit the prolyl hydroxylase domain enzymes *via* product inhibition, also potentiating HIF1α stabilization (24). This prevents the hydroxylation of proline residues on HIF1α, and so it is not ubquitinated and targeted for proteasomal degradation (25–28). Instead, it can heterodimerize with its binding partner the aryl hydrocarbon nuclear translocator (ARNT/HIF-1β). The HIF-1 complex can translocate to the nucleus and bind hypoxia response elements in the promoters of HIF target genes (29). HIF also represses mitochondrial function through upregulation of pyruvate dehydrogenase kinase 1 (PDK1) (30). PDK1 phosphorylates and inhibits pyruvate dehydrogenase (PDH) and so pyruvate cannot be converted into acetyl-CoA in order to enter the mitochondria and feed the Krebs cycle (31).

The fragmented Krebs cycle in macrophages is not only due to the break after succinate. A second breakpoint, at isocitrate dehydrogenase (IDH), allows for the withdrawal of citrate from the cycle. This proves not only to be important for lipid biosynthesis in macrophages and DCs, but also for the production of both pro- and anti-inflammatory mediators (32, 33). Glycolysis is rapidly upregulated in LPS-activated DCs for the production of citrate. This is necessary for the upregulation of fatty acid synthesis to allow for membrane expansion which is crucial for antigen presentation (34). Once exported to the cytosol citrate can be broken down to provide a source of acetyl-CoA for acetylation of both histone and non-histone proteins (35). Citrate metabolism provides a connection between carbohydrate metabolism, fatty acid metabolism, and epigenetic reprogramming and so changes in flux through this pathway may have wide ranging effects. This review will describe the role of citrate in innate immune cell function.

CITRATE PROVIDES A BRIDGE BETWEEN CARBOHYDRATE AND FATTY ACID METABOLISM

Citrate is produced in the Krebs cycle (also known as the citric acid cycle or TCA cycle) from the aldol condensation of oxaloacetate, the end product of a previous turn of the cycle, and acetyl-CoA (**Figure 1**) (36). Acetyl-CoA may be derived from glucose *via* the glycolytic pathway, entering the mitochondria as pyruvate or from fatty acids that have undergone β-oxidation (36). In the Krebs cycle, citrate is converted into isocitrate *via* cis-aconitate by aconitase (36). IDH will then convert isocitrate to α-ketogluterate (αKG) in a decarboxylation reaction (36). The Krebs cycle continues and provides a major source of cellular ATP and also reducing equivalents that feed the electron transfer chain (36).

The mitochondrial citrate carrier (CIC), also known as solute carrier family 25 member 1 (Slc25a1), can export citrate from the mitochondria in exchange for malate (37). Once in the cytosol citrate is broken down by ATP-Citrate lyase (ACLY) into acetyl-CoA and oxaloacetate (37). Oxaloacetate can be converted to malate by malate dehydrogenase (MDH) which can re-enter the mitochondria through CIC (37). Acetyl-CoA is further processed into malonyl-coenzyme A (malonyl-CoA) by acetyl-coA carboxylase (ACC) (38). Malonyl-CoA can be incorporated into cholesterol or fatty acids (38). The fatty acids are incorporated into phospholipids. Malonyl-CoA can also limit the β-oxidation of fatty acids as high levels can inhibit carnitine palmitoyltransferase 1 (CPT1) (39). Two isoforms of ACC exist, ACC1 and ACC2 (40). ACC2 is associated with the outer mitochondrial membrane and so can control the concentration of malonyl-CoA near CPT1 and

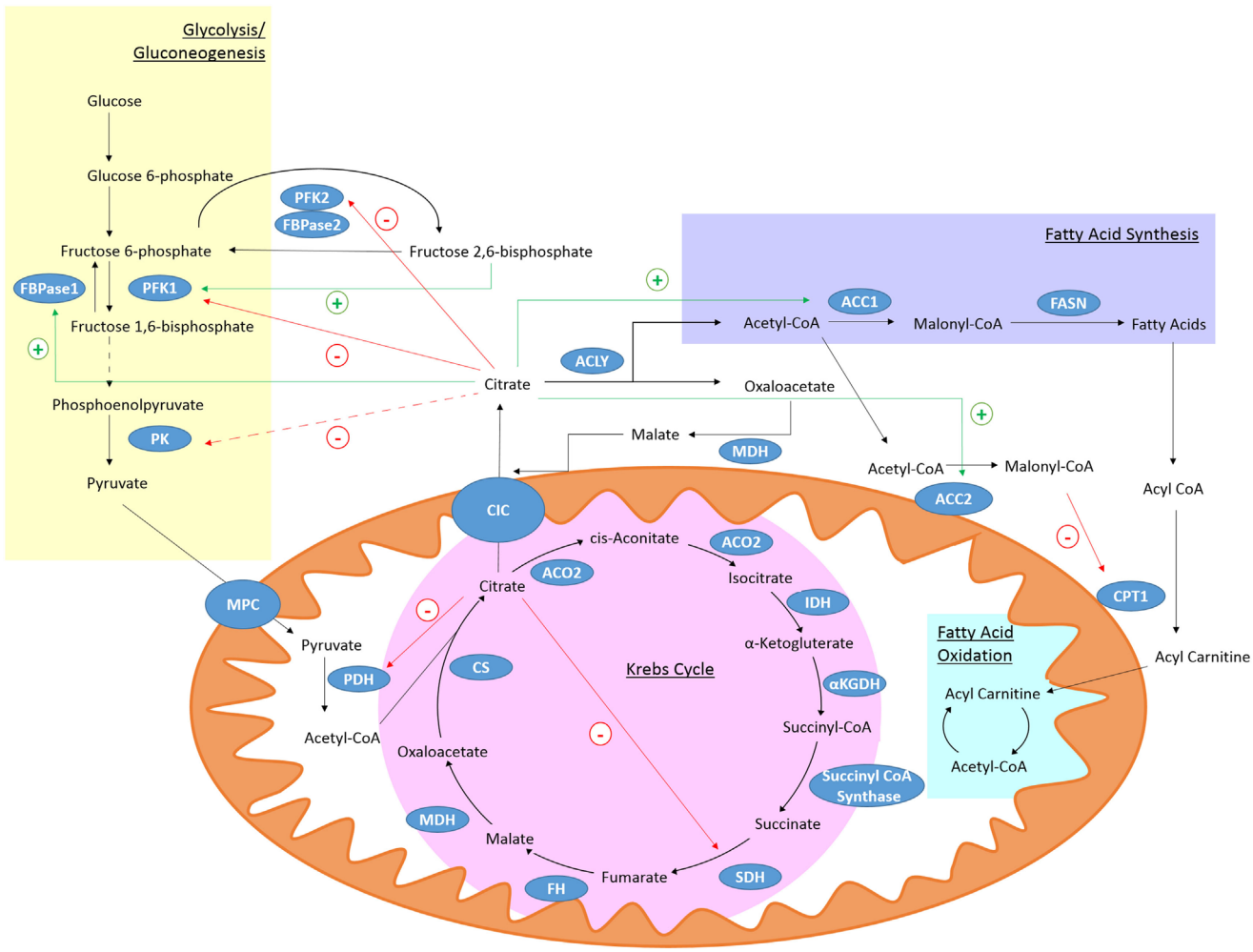

FIGURE 1 | Citrate metabolism. Citrate is produced in the Krebs cycle from oxaloacetate and acetyl-CoA by citrate synthase (CS). It can be exported from the mitochondria through citrate carrier (CIC). Cytosolic citrate is broken down by ACLY to oxaloacetate and acetyl-CoA. Acetyl-CoA can be used as a substrate for fatty acid synthesis. High levels of cytosolic citrate can directly inhibit the glycolytic enzymes PFK1 and PFK2. PFK1 is also indirectly inhibited by decreased levels of fructose 2,6-bisphosphate and pyruvate kinase (PK) is indirectly inhibited (broken line) due to reduced levels of its activator, fructose-1,6-bisphosphate. Mitochondrial citrate can inhibit pyruvate dehydrogenase (PDH) and succinate dehydrogenase (SDH). Citrate-derived malonyl-CoA can block fatty acid oxidation (FAO) by inhibiting carnitine palmitoyltransferase 1 (CPT1). Citrate can activate the gluconeogenic enzyme fructose 1,6-bisphosphatase (FBPase1) and ACC, and so stimulate fatty acid synthesis.

regulate its activity (38). Acetyl-CoA can also be a substrate for protein and histone acetylation and so can have a wide ranging role in many cellular processes (41).

Citrate itself is known to inhibit several key glycolytic enzymes as part of a negative feedback loop. Phosphofructokinase (PFK) 1 and 2 are directly inhibited by citrate while pyruvate kinase (PK) is indirectly inhibited as citrate decreases levels of fructose-1,6-bisphosphate, which is a PK activator (42). PDH (43) and SDH (44), and therefore the Krebs cycle, can also be inhibited by high citrate levels. While citrate inhibits pathways producing ATP, it stimulates those that consume it. Citrate can allosterically activate ACC (45) and the gluconeogenic enzyme fructose-1,6-bisphosphatase (46). With citrate occupying a position that links many metabolic and cellular processes, it is not surprising that the metabolism of citrate may be of importance in the immune response.

CITRATE AS AN INFLAMMATORY SIGNAL

While the role of other metabolites as inflammatory signals has been well discussed (21, 22) citrate also plays a role in key inflammatory pathways (**Figure 2**). In M1 macrophages, there is an increased isocitrate:αKG ratio and transcriptional downregulation of *Idh1* (47). This break was also seen in DCs (34). With increased glycolytic flux in both activated DCs and macrophages and a break in the Krebs cycle, pyruvate derived from glucose feeds into Krebs cycle but cannot continue past citrate/isocitrate. An increase in the levels of citrate is detected in both mouse (LPS-stimulated) and human [tumour necrosis factor α (TNFα)- or interferon-γ (IFNγ)-stimulated] macrophages (24, 48). This coincides with upregulation of CIC and ACLY, both of which occur in an NF-κB-dependent manner where LPS or TNFα is used to activate the cells, or IFNγ can also induce CIC and ACLY *via* STAT1 (32, 49). The export and breakdown of mitochondrial citrate has been linked to the production of several important pro-inflammatory mediators in macrophages, namely NO, ROS, and prostaglandin E_2 (PGE_2) production in human macrophages (32, 48, 49). Inhibition of CIC activity or its genetic silencing with siRNA leads to a marked reduction in NO, ROS, and PGE_2 production in LPS and cytokine-stimulated macrophages. Infantino et al. suggest that the decrease in PGE_2 production is due to a decreased availability of precursors for PGE_2 synthesis as adding exogenous acetate rescues the effect of CIC inhibition on PGE_2 productions. Acetate can be converted to acetyl-CoA by acetyl-CoA synthase (ACSS) (50). Inhibition of fatty acid synthase (FASN) with C75 in DCs also reduced LPS-induced PGE_2 (34). Endogenous PGE_2 is essential for the production of LPS-induced pro-IL1β (51). This implies that citrate may be critical to IL1β production.

While Infantino et al. speculated that the effect of CIC inhibition on the production of NO and ROS was due to decreased production of NADPH by the breakdown of citrate-derived oxaloacetate to pyruvate by malic enzyme, a follow-up study reports that the $NADP^+$/NAPDH ratio is unchanged in cytokine-activated macrophages treated with the CIC inhibitor 4-chloro-3-[(3-nitrophenyl)amino]sulfonyl benzoic acid (CNSB) versus

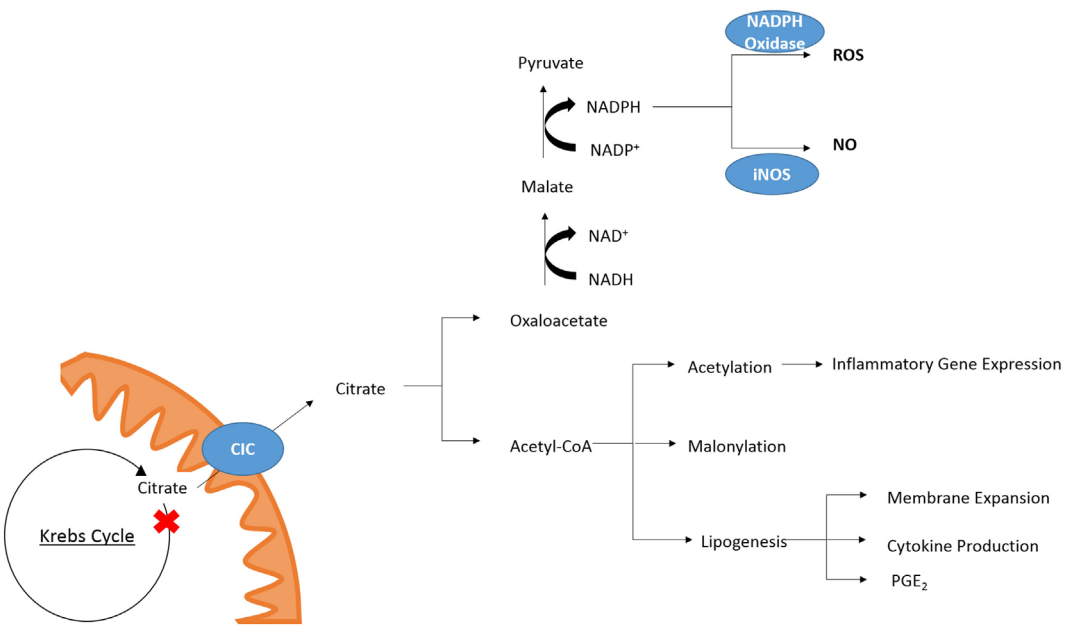

FIGURE 2 | Citrate in inflammation. Cytosolic citrate is broken down into acetyl-CoA and oxaloacetate. Further processing of oxaloacetate can provide a source of NADPH which is required by NAPDH oxidase and iNOS for the production of ROS and NO, respectively. Acetyl-CoA is required for acetylation of proteins and can be converted to malonyl-CoA for lysine-malonylation. Citrate-derived lipid synthesis has been linked to membrane expansion necessary for DC activation and cytokine production. In macrophages, the production of PGE_2 has been linked to citrate metabolism.

untreated when they are in a glucose rich environment (52). When the same experiment was carried out in glucose-deprived conditions, there was a marked increase in the $NADP^+$/NADPH ratio in activated, CNSB-treated macrophages compared to control cells. Citrate export from the mitochondria can provide a source of NADPH *via* two routes. The first is from oxaloacetate as mentioned, and the second is *via* the cytosolic, $NADP^+$-dependent IDH (IDH1). IDH1 is known to be suppressed in cells activated by a pro-inflammatory stimuli (53), however, in glucose-deprived conditions the authors show *IDH1* mRNA expression is increased in activated macrophages (52). While this could provide a mechanism for the decreased production of NO and ROS in glucose-deprived cells other processes such as the PPP may be compensating for decreased production of NADPH in macrophages treated with a CIC inhibitor but grown in a glucose-rich environment.

The processing of citrate by ACLY has also been suggested as an anti-cancer target as ACLY has been found to be overexpressed in several cancer types (54). Inhibition of ACLY with siRNA or pharmacologically induces cell death (55–58). One study has suggested that the anti-cancer effect of ACLY inhibition is directly due to its role in lipid synthesis (55). In several cancer cell lines, depletion of ACLY was observed to induce apoptosis, accompanied by increased levels of ROS. This increase in ROS was suggested to initiate cell death by activating AMPK (59). Another study has suggested that enzymatic activity alone is not enough to explain the initiation of growth arrest in tumor cells, and has shown that ACLY may be able to directly interact with AMPK (60). While ACLY has not been linked to the production of ROS in immune cells, an exact mechanism for the role of citrate metabolism in macrophages has not been defined and it would be an interesting avenue of investigation.

Similarly, citrate has been shown to be important for DC activation. Mitochondrial respiration in blood monocyte-derived DCs will begin to collapse in TLR-activated DCs 6 h after treatment, and by 24 h, there will be no detectable consumption of oxygen by the mitochondria (8). However, before 6 h the mitochondria are still functioning. Up until this time, the increase in glycolysis is important for DC activation but the increase does not fuel a greater rate of OXPHOS, inhibiting ATP synthase with oligomycin has no effect on early DC activation. Instead citrate is withdrawn from the Krebs cycle and used to support *de novo* fatty acid synthesis (34). Inhibition of ACC or FASN, with TOFA and C75, respectively, or blocking expression of *Slc25a1* by retroviral introduction of shRNA diminished the early activation of DCs differentiated from bone marrow in the presence of the growth factor GM-CSF (GM-DCs). Production of fatty acids is required for membrane synthesis for the expansion of both the endoplasmic reticulum and Golgi. Their expansion allows for increased synthesis and secretion of various proteins important following TLR-activation. The PPP is also an important process in early DC activation, as it creates the reducing equivalent, NADPH, required not only for nucleotide synthesis and redox balance but also as a cofactor for lipogenesis. While the long-term commitment to glycolysis and collapse in mitochondrial respiration seen in activated DCs is dependent on a phosphatidylinositide-3-kinase (PI3K)/Akt pathway, the rapid upregulation of glycolysis was due to TANK-binding kinase 1 (TBK1)- and IκB Kinase ε (IKKε)-dependent activation of Akt. The PI3K/Akt pathway lead to production of NO, and inhibition of OXPHOS, forcing the cells to rely on increased glycolysis for activation and survival but the early TBK1-IKKε/Akt pathway increased glycolysis by promoting the association of hexokinase 2 (HK2) with voltage-dependant anion channels on the outer mitochondrial membrane.

While the same breakpoints in the Krebs cycle have not been described in activated natural killer cells (NK cells), the citrate–malate shuttle has recently been shown to be of importance in the metabolic reprogramming that occurs following NK cell activation (61). The citrate–malate shuttle refers to the export of citrate into the cytosol *via* CIC, and its breakdown by ACLY and malate dehydrogenase 1 (MDH1) yielding cytosolic malate which CIC exchanges for citrate. Assmann et al. show that increased expression of *Slc25a1* and *ACLY* mRNA in activated NK cells is dependent on sterol regulatory element-binding protein (SREBP) activity, which is consistent with reports in other cell types including macrophages (62–66). Activated NK cells have increased glycolysis and OXPHOS which is crucial for their activation and growth. Pharmacological inhibition of SREBP activation or ACLY activity (therefore, inhibiting the citrate–malate shuttle) reduced cytokine-induced granzyme B expression and IFN-γ production. Similar results were seen with genetic inhibition of SREBP using $SCAP^{-/-}$ mice. This effect is independent of lipid and cholesterol synthesis downstream of ACLY as inhibition of ACC or FASN with TOFA or C75, respectively, does not affect NK cell activation. The authors speculate that the citrate–malate shuttle serves to convert cytosolic NADH to mitochondrial NADH, therefore, fueling OXPHOS and mitochondrial ATP synthesis while also replenishing the cytosolic pool of NAD^+, which is an important cofactor for glyceraldehyde 3-phosphate dehydrogenase (GAPDH). Inhibition of the malate–aspartate shuttle, which would be more commonly thought of as a means of replenishing mitochondrial NADH, did not affect OXPHOS in activated NK cells and neither did inhibition of the Krebs cycle enzyme SDH with dimethyl-malonate. This suggests that in NK cells elevated OXPHOS is maintained by the citrate–malate shuttle. While these studies show the cytosolic processing of citrate to be generally a pro-inflammatory event, citrate itself has been shown to inhibit the HIF asparaginyl hydroxylase [factor inhibiting HIF (FIH)] (67). FIH hydroxylates asparagine residues on HIF1α, preventing it from interacting with transcriptional coactivators such as CRE binding protein/p300 (67, 68). Increased flux through CIC and the cytosolic processing of citrate has, therefore, been shown to be of importance in the activation of macrophages, DCs, and NK cells.

HISTONE AND POST-TRANSLATIONAL MODIFICATIONS BY CITRATE-DERIVED ACETYLATION

Acetyl-CoA is not only a substrate for *de novo* lipogenesis, it also is an important cofactor for the acetylation of histones and non-histone proteins (69). Acetylation can be co-translational, effecting the α-amino group of a protein's N-terminal residue, or

post-translational which concerns the ε-amino group of lysine residues (69, 70). Lysine acetylation is reversible and so provides a very useful mechanism for the regulation of gene expression and general protein function (69). Acetyl-CoA cannot travel across cell membranes, and so to exert its effects it must be generated in different cellular compartments (70). In the mitochondria, acetyl-CoA is present due to the β-oxidation of fatty acids or is generated from pyruvate by the PDH complex (41). In the cytosol, acetyl-CoA can be derived from citrate as previously discussed or from acetate by ACSS (71) or the degradation or N-acetylaspartate (NAA) by aspartoacylase (72). The generation of acetyl-CoA from NAA is more commonly associated with processes in the brain and it has also been shown to be a source of nuclear and cytosolic acetyl-CoA in brown adipose tissue (73).

ATP-citrate lyase links metabolism to histone acetylation as it converts glucose-derived citrate to acetyl-CoA and it has been found to localize to both nucleus and cytoplasm (35). Citrate is small enough to diffuse across nuclear pores allowing for acetyl-CoA to be produced in either cellular compartment, and siRNA-mediated knockdown of ACLY reduced global histone acetylation (35). In adipocytes mRNA expression of HK2, PFK1, and lactate dehydrogenase A (LDHA) were all reduced when ACLY was silenced (35). Since ACLY is upregulated in lipopolysaccharide (LPS)-stimulated macrophages (49), it would be interesting to see where ACLY localized to and if there was a direct effect on the expression of glycolytic genes due to changes in histone acetylation. ACLY has been shown to control glucose to acetate switch. ACLY-deficient cells upregulate ACSS2 allowing for the production of acetyl-CoA from acetate, ensuring cell viability and providing substrates for both fatty acid synthesis and histone acetylation (74).

As previously discussed, in glucose-deprived conditions, increased flux through CIC can sustain NADPH levels in glucose-deprived activated macrophages (52). Acetylation of CIC increases in glucose-deprived growth conditions compared to media containing glucose. By reconstituting liposomes with mitochondrial extracts, it was shown that the acetylation of CIC causes an increase in V_{max} for citrate (52). In memory, $CD8^+$ T cells GAPDH has been shown to be acetylated in an ACLY-dependent manner which increased its activity (75). Acetate is taken up and processed *via* the Krebs cycle to produce citrate. Citrate-derived acetyl-CoA was then used to acetylate GAPDH which may prevent it from binding IFNγ mRNA, and allowing its translation (76). Acetylated GAPDH had increased catalytic activity. While acetate can be used directly to generate acetyl-CoA, knockdown of the cytosolic ACSS (ACSS1) had no effect on IFNγ production, knockdown of ACLY, however, did decrease IFNγ production. It has also been shown that LDHA in T cells promotes the expression of IFNγ, independent of GAPDH regulation, as it ensures a high acetyl-CoA concentration produced *via* ACLY for histone acetylation (77). Though metabolic reprogramming differs in activated T cells compared to macrophages and DCs, this highlights the importance of the citrate pathway in control of both the metabolism of immune cells and their production of pro-inflammatory mediators, unlike in T cells. No work has yet been carried out to directly link citrate-derived acetylation in M1 macrophages or DCs, however, histone acetylation is important in macrophage activation and DC differentiation. IL-6 and IL-10 production are both regulated on histone and non-histone protein acetylation, respectively (78, 79). NF-κB activation is also dependent on acetylation of its RelA/p65 subunit (80) and a large number of enzymes involved in metabolic processes have been found to be acetylated in non-immune cells (78, 81). Therefore, it is likely that acetylation plays a role in the regulation of immune cell metabolism. Histone acetylation downstream of ACLY has been shown to be of importance in M2 macrophage activation (82). While STAT6 is the major regulator of IL4 induced genes a subset of genes important in the regulation of cellular proliferation and the production of chemokines are under additional control of an Akt–mTORC1 signaling pathway. Covarrubias et al. suggest a mechanism in which Akt regulates both protein levels and activity of ACLY to increase the acetyl-CoA pool for histone acetylation. They suggest that certain transcription factors and histone acetyltransferases, e.g., P300, are regulated by acetyl-CoA levels and that may link AKT/ACLY-dependent acetyl-CoA levels to specific gene induction.

Lysine-malonylation causes a net change in charge of the lysine residue from +1 to −1 and cause a change in mass of approximately 86 Da (83). Malonyl-CoA is the cofactor required (84). Malonyl-CoA can be produced in the cytosol from citrate-derived acetyl-CoA by ACC1/2 (38). The cytosolic pool of malonyl-CoA is regulated by both ACC and malonyl-CoA decarboxylase which catalyzes the reverse reaction from malonyl-CoA to acetyl-CoA (38). A malonyl-CoA pool also exists in the mitochondria, produced from acetyl-CoA by propionyl-CoA carboxylase or from malonate by acyl-CoA synthase family member 3 (ACSF3) (85). Lysine-malonylation has been shown to play a role in the regulation of mitochondrial function, FAO and glycolysis (86, 87). Notably histone malonylation does not occur at the N-terminal tail as happens with acetylation, suggesting that the regulatory role these two modification carry out may be very functionally different to acetylation (86). A large number of proteins involved in fatty acid metabolism are malonylated, including ACLY. However, no studies have yet been carried out regarding the functional consequence of lysine-malonylation in immune cells.

ITACONATE

While the accumulation of citrate caused by the IDH1 breakpoint in the TCA cycle can be used to fuel fatty acid synthesis and histone acetylation, another fate of this citrate is the production of itaconate (**Figure 3**). First identified in 1836 as a product of the distillation of citric acid, itaconate has recently become a focus of the field of immunometabolism due to its potential role as an anti-inflammatory modulator. Itaconate is derived from citrate produced in the Krebs cycle and, in M1 macrophages, is one of the most highly induced metabolites following LPS treatment (33). Itaconate has also been shown to accumulate in LPS-treated DCs (34). Citrate is acted on by the mitochondrial aconitase 2 (ACO2) to produce cis-aconitate. Cis-aconitate is decarboxylated by cis-aconitate decarboxylase, also known as immune-responsive gene 1 (IRG1), to produce itaconate. Itaconate has long been used in an industrial setting and is produced on an industrial scale as a

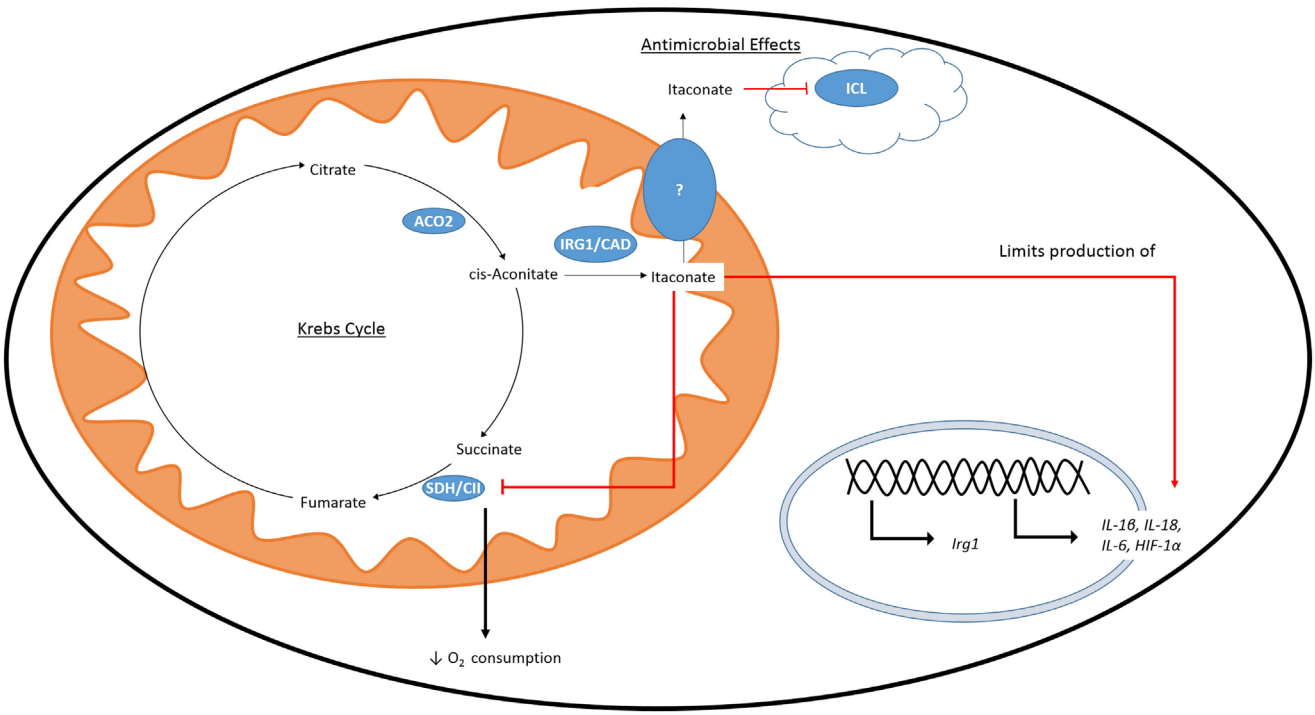

FIGURE 3 | Citrate-derived itaconate. Citrate is converted to cis-aconitate by the Krebs cycle enzyme ACO2. Activation of macrophages with LPS causes induction of IRG1 which can produce itaconate by the decarboxylation of cis-aconitate. LPS also initiates the production of other pro-inflammatory mediators, such as HIF1 α, NO, and IL1β. Itaconate is toxic to microorganisms expressing ICL, a key component of the glycoxylate shunt in bacteria. Itaconate is also able to inhibit SDH and cause decreased production of NO, IL1β, IL18, and HIF1α.

fermentation product of *Aspergillus terreus* for use in the creation of polymer formation (88).

In 1995, it was found that *immunoresponsive gene 1 (Irg1)* is highly upregulated in peritoneal macrophages following LPS stimulation (89), and has since been seen to be upregulated in the blood of human sepsis patients (90) and in the time during embryo implantation (91, 92). Despite lacking a sequence targeting it, there IRG1 has been found to associate with the mitochondria (93, 94). It was only in 2011 that itaconate was identified in multiple studies in an immune context and in 2013 that IRG1 and itaconate were connected (95). Itaconate was seen in the lungs of mice infected with *Mycobacterium tuberculosis* (MTB) and was not present in the lungs of control mice (96). In a separate study, itaconate was shown to be secreted by the macrophage cell line RAW264.7 following treatment with LPS (97). Michelucci et al. identified the role of IRG1 by siRNA-mediated silencing of *Irg1* (officially renamed *Acod1* after its function was discovered) and performing a metabolic screen to elucidate which metabolites were affected. They further showed by isotope-labeling that itaconate was derived from citrate. Genetic silencing of *Irg1* causes macrophages to lose their bactericidal activity, which was due to decreased amounts of itaconate and the loss of its inhibitory effect on isocitrate lyase (ICL), a crucial enzyme of the glycoxylate shunt in bacteria (98). The glycoxylate shunt is a means for bacteria to survive in conditions of low glucose availability where acetate is the primary fuel source. Instead of the normal sequence of reaction in the Krebs cycle, the steps from αKG to fumarate are bypassed, and isocitrate is instead cleaved by ICL to glycoxylate and succinate in bacteria. Succinate enters the Krebs cycle and glycoxylate is then converted to malate by malate synthase. Malate can be processed to oxaloacetate by MDH as in the normal reactions of the Krebs cycle. Itaconate has been shown to inhibit growth of a number of ICL expressing microorganisms, including MTB, *S. enterica* and multidrug-resistant *Staphylococcus aureus* (MRSA) (95, 96, 99). Some bacteria are able to degrade itaconate, producing acetyl-CoA and pyruvate, due to the expression of genes that encode for itaconate-CoA transferase, itaconyl-CoA hydratase, and (S)-citramalyl-CoA ligase. Possession of these genes allows *Pseudomonas aeruginosa* and *Yersinia pestis* to survive in activated macrophages (100). There is a discussion as to the relevance of these studies due to differences in concentrations of itaconate used both in terms of the variety of concentrations used exogenously to inhibit bacterial growth and the range in reported intracellular concentrations (101, 102). It may be that intracellular itaconate is concentrated in vacuoles, and whole cell analysis will not adequately represent this, and that measuring the

concentration of secreted itaconate in cell culture media does not determine what the local concentration would be.

While the effect of itaconate on bacterial survival has been well documented, more recent work has sought to elucidate the effect that a high intracellular concentration of itaconate has on the immune cells that produce it. Dimethyl itaconate (DMI) has been used in several studies as a cell permeable itaconate analog to boost the intracellular levels of itaconate. Pre-treatment of murine bone marrow-derived macrophages (BMDMs) with DMI prior to LPS stimulation reduced the reduced the expression of many pro-inflammatory genes including iNOS (33). DMI also impaired production of ROS, NO, IL1β, IL18, and IL6. While IL1β and IL18 mRNA expression was reduced by DMI it also caused a reduction in protein levels of both NLRP3 and ASC, indicating that inflammasome priming was also impaired. *Irg1*$^{-/-}$ BMDMs do not produce itaconate and have increased production of NO, IL1β, IL18, and IL6 when compared to WT BMDMs. HIF1α protein levels were also increased in LPS-activated *Irg1*$^{-/-}$ BMDMs while treatment with DMI inhibited its protein levels. Interestingly, *Irg1*$^{-/-}$ BMDMs show an altered profile of Krebs cycle metabolites than WT cells. WT BMDMs have increased levels of succinate, fumarate, and malate following LPS stimulation (47). LPS-stimulated *Irg1*$^{-/-}$ BMDMs have significantly higher levels of fumarate and malate than WT controls, while succinate levels are almost that of unstimulated cells. The authors suggest that this is due to the ability of itaconate to inhibit SDH, and they showed itaconate to inhibit a purified form of SDH. In contrast to the decrease in oxygen consumption rate (OCR) seen in WT BMDMs upon treatment with LPS, in *Irg1*$^{-/-}$ BMDMs OCR increases. As SDH also acts as complex II of the ETC, this highlights the ability of endogenous itaconate to regulate mitochondrial metabolism and is consistent with other reports of itaconate competitively inhibiting SDH, albeit weakly, the first of which was in 1949 (103–105). This led Lampropoulou et al. to suggest that LPS-induced *Irg1* expression and corresponding increase in intracellular itaconate is responsible for the second break in the Krebs cycle at SDH. By inhibiting SDH itaconate would also prevent the generation of ROS through RET (106). When succinate accumulates and is oxidized by SDH, it will produce a large amount of coenzyme Q. Electrons are then forced back through complex I of the ETC-generating ROS. ROS is able to activate the inflammasome and, therefore, drive the production of IL1β and IL18 (107).

IRG1 has also been shown to play a role in the establishment of endotoxin tolerance in LPS-tolerized macrophages. siRNA-mediated knockdown of IRG1 in these macrophages was able to increase NF-κB and IRF3 activation, while the production of ROS and subsequent expression of the zinc-finger protein A20 were reduced (90). Heme oxygenase 1 and carbon monoxide were able to induce IRG1 and through IRG1 downregulated pro-inflammatory gene expression in LPS-treated RAW264.7 cells and in a LPS mouse sepsis model (108). Several other elements regulating IRG1 expression and, therefore, itaconate production have also recently been identified. Computational modeling coupled with siRNA knockdown identified interferon regulatory factor 1 as a regulator of IRG1 transcription in RAW264.7 macrophages and human PBMCs (94). Inhibition of branched-chain aminotransferase 1 in human monocyte-derived macrophages decreased levels of glycolysis and oxygen consumption while also reduced IRG1 mRNA and protein levels as well as itaconate production (109).

A major issue with the study of the functional effect of itaconate in macrophages to date has been the use of DMI. DMI was utilized as it is cell permeable, however, it has been shown that while DMI boosts the level of itaconate in the cell it is not itself metabolized to itaconate (110). This suggests that DMI somehow promotes LPS-driven synthesis of itaconate. El Azzouny et al. also confirm that LPS-stimulated macrophages have increased succinate levels and that this is not the result of itaconate being metabolized to succinate. The authors speculate that the effects of DMI on macrophage metabolism may be due to an ability to act as a cysteine alkylating agent or to alter redox homeostasis. They further suggest that, though one has not been identified, it is possible a cell surface receptor for itaconate exists that DMI would be able to bind. Other metabolites have been shown to signal through G-protein-coupled receptors, such as succinate through GPR91, which has been renamed SUCNR1 (111). While the effects of studies carried out utilizing DMI have been drawn into question, the body of work carried out using genetic inhibition or deletion of *Irg1* and the striking amount by which *Irg1* mRNA and itaconate synthesis are upregulated in activated immune cells still leaves it worthy of further investigation.

CONCLUSION

Our understanding of immune cell metabolism has come far since the early observations that activated macrophages were highly glycolytic (112, 113). It is now well accepted that these pathways play a part outside of their traditional energetic and biosynthetic roles. The discovery that the Krebs cycle is not complete in activated M1 macrophages and DCs highlights the importance of the withdrawal of citrate from the cycle for DC activation, the production of pro-inflammatory mediators and for the generation of itaconate. Citrate links many important cellular processes, bridging carbohydrate and fatty acid metabolism and protein modification. Its role in producing acetyl-CoA for the acetylation of histones may turn out to be its most striking role in regulating immune cell function. There is still much to be discovered regarding the regulation and consequences of metabolic reprogramming in immune cells, however, it is clear that a "citrate pathway" plays an important role in these processes and may be amenable to therapeutic targeting.

AUTHOR CONTRIBUTIONS

NW wrote the manuscript. LO'N supervised and edited the manuscript.

FUNDING

This work was funded by Wellcome Trust UK and Science Foundation Ireland. Wellcome Trust (Award number(s): 205455/14107); Science Foundation Ireland (Award number(s): 12/IA/1531).

REFERENCES

1. Takeuchi O, Akira S. Pattern recognition receptors and inflammation. *Cell* (2010) 140(6):805–20. doi:10.1016/j.cell.2010.01.022
2. Barton GM. A calculated response: control of inflammation by the innate immune system. *J Clin Invest* (2008) 118(2):413–20. doi:10.1172/JCI34431
3. Kelly B, O'Neill LAJ. Metabolic reprogramming in macrophages and dendritic cells in innate immunity. *Cell Res* (2015) 25(7):771–84. doi:10.1038/cr.2015.68
4. Pearce EJ, Everts B. Dendritic cell metabolism. *Nat Rev Immunol* (2015) 15(1):18–29. doi:10.1038/nri3771
5. Galván-Peña S, O'Neill LAJ. Metabolic reprograming in macrophage polarization. *Front Immunol* (2014) 5:420. doi:10.3389/fimmu.2014.00420
6. Reece JJ, Siracusa MC, Scott AL. Innate immune responses to lung-stage helminth infection induce alternatively activated alveolar macrophages. *Infect Immun* (2006) 74(9):4970–81. doi:10.1128/IAI.00687-06
7. Krawczyk CM, Holowka T, Sun J, Blagih J, Amiel E, DeBerardinis RJ, et al. Toll-like receptor-induced changes in glycolytic metabolism regulate dendritic cell activation. *Blood* (2010) 115(23):4742–9. doi:10.1182/blood-2009-10-249540
8. Everts B, Amiel E, van der Windt GJW, Freitas TC, Chott R, Yarasheski KE, et al. Commitment to glycolysis sustains survival of NO-producing inflammatory dendritic cells. *Blood* (2012) 120(7):1422–31. doi:10.1182/blood-2012-03-419747
9. O'Neill LAJ. Glycolytic reprogramming by TLRs in dendritic cells. *Nat Immunol* (2014) 15(4):314–5. doi:10.1038/ni.2852
10. Lorsbach RB, Murphy WJ, Lowenstein CJ, Snyder SH, Russell SW. Expression of the nitric oxide synthase gene in mouse macrophages activated for tumor cell killing. Molecular basis for the synergy between interferon-gamma and lipopolysaccharide. *J Biol Chem* (1993) 268(3):1908–13.
11. Lu L, Bonham CA, Chambers FG, Watkins SC, Hoffman RA, Simmons RL, et al. Induction of nitric oxide synthase in mouse dendritic cells by IFN-gamma, endotoxin, and interaction with allogeneic T cells: nitric oxide production is associated with dendritic cell apoptosis. *J Immunol* (1996) 157(8):3577–86.
12. Clementi E, Brown GC, Feelisch M, Moncada S. Persistent inhibition of cell respiration by nitric oxide: crucial role of S-nitrosylation of mitochondrial complex I and protective action of glutathione. *Proc Natl Acad Sci U S A* (1998) 95(13):7631–6. doi:10.1073/pnas.95.13.7631
13. Blouin CC, Pagé EL, Soucy GM, Richard DE. Hypoxic gene activation by lipopolysaccharide in macrophages: implication of hypoxia-inducible factor 1α. *Blood* (2004) 103(3):1124–30. doi:10.1182/blood-2003-07-2427
14. Chen C, Pore N, Behrooz A, Ismail-Beigi F, Maity A. Regulation of glut1 mRNA by hypoxia-inducible factor-1. Interaction between H-ras and hypoxia. *J Biol Chem* (2001) 276(12):9519–25. doi:10.1074/jbc.M010144200
15. Semenza GL, Jiang BH, Leung SW, Passantino R, Concordet JP, Maire P, et al. Hypoxia response elements in the aldolase A, enolase 1, and lactate dehydrogenase A gene promoters contain essential binding sites for hypoxia-inducible factor 1. *J Biol Chem* (1996) 271(51):32529–37. doi:10.1074/jbc.271.51.32529
16. Palsson-McDermott EM, Curtis AM, Goel G, Lauterbach MAR, Sheedy FJ, Gleeson LE, et al. Pyruvate kinase M2 regulates Hif-1α activity and IL-1β induction, and is a critical determinant of the Warburg effect in LPS-activated macrophages. *Cell Metab* (2015) 21(1):65–80. doi:10.1016/j.cmet.2015.01.017
17. Byles V, Covarrubias AJ, Ben-Sahra I, Lamming DW, Sabatini DM, Manning BD, et al. The TSC-mTOR pathway regulates macrophage polarization. *Nat Commun* (2013) 4:2834. doi:10.1038/ncomms3834
18. Sag D, Carling D, Stout RD, Suttles J. Adenosine 5'-monophosphate-activated protein kinase promotes macrophage polarization to an anti-inflammatory functional phenotype. *J Immunol* (2008) 181(12):8633–41. doi:10.4049/jimmunol.181.12.8633
19. Hesse M, Modolell M, La Flamme AC, Schito M, Fuentes JM, Cheever AW, et al. Differential regulation of nitric oxide synthase-2 and arginase-1 by type 1/type 2 cytokines in vivo: granulomatous pathology is shaped by the pattern of L-arginine metabolism. *J Immunol* (2001) 167(11):6533–44. doi:10.4049/jimmunol.167.11.6533
20. Inoki K, Zhu T, Guan KL. TSC2 mediates cellular energy response to control cell growth and survival. *Cell* (2003) 115(5):577–90. doi:10.1016/S0092-8674(03)00929-2
21. McGettrick AF, O'Neill LAJ. How metabolism generates signals during innate immunity and inflammation. *J Biol Chem* (2013) 288(32):22893–8. doi:10.1074/jbc.R113.486464
22. Mills E, O'Neill LAJ. Succinate: a metabolic signal in inflammation. *Trends Cell Biol* (2014) 24(5):313–20. doi:10.1016/j.tcb.2013.11.008
23. Mills EL, Kelly B, Logan A, Costa ASH, Varma M, Bryant CE, et al. Succinate dehydrogenase supports metabolic repurposing of mitochondria to drive inflammatory macrophages. *Cell* (2016) 167(2):457–70.e13. doi:10.1016/j.cell.2016.08.064
24. Tannahill GM, Curtis AM, Adamik J, Palsson-McDermott EM, McGettrick AF, Goel G, et al. Succinate is an inflammatory signal that induces IL-1[bgr] through HIF-1[agr]. *Nature* (2013) 496(7444):238–42. doi:10.1038/nature11986
25. Huang LE, Arany Z, Livingston DM, Bunn HF. Activation of hypoxia-inducible transcription factor depends primarily upon redox-sensitive stabilization of its α subunit. *J Biol Chem* (1996) 271(50):32253–9. doi:10.1074/jbc.271.50.32253
26. Epstein ACR, Gleadle JM, McNeill LA, Hewitson KS, O'Rourke J, Mole DR, et al. *C. elegans* EGL-9 and mammalian homologs define a family of dioxygenases that regulate HIF by Prolyl hydroxylation. *Cell* (2001) 107(1):43–54. doi:10.1016/S0092-8674(01)00507-4
27. Bruick RK, McKnight SL. A conserved family of Prolyl-4-hydroxylases that modify HIF. *Science* (2001) 294(5545):1337–40. doi:10.1126/science.1066373
28. Maxwell PH, Wiesener MS, Chang G-W, Clifford SC, Vaux EC, Cockman ME, et al. The tumour suppressor protein VHL targets hypoxia-inducible factors for oxygen-dependent proteolysis. *Nature* (1999) 399(6733):271–5. doi:10.1038/20459
29. Corcoran SE, O'Neill LAJ. HIF1α and metabolic reprogramming in inflammation. *J Clin Invest* (2016) 126(10):3699–707. doi:10.1172/JCI84431
30. Kim J-W, Tchernyshyov I, Semenza GL, Dang CV. HIF-1-mediated expression of pyruvate dehydrogenase kinase: a metabolic switch required for cellular adaptation to hypoxia. *Cell Metab* (2006) 3(3):177–85. doi:10.1016/j.cmet.2006.02.002
31. Patel MS, Korotchkina LG. Regulation of mammalian pyruvate dehydrogenase complex by phosphorylation: complexity of multiple phosphorylation sites and kinases. *Exp Mol Med* (2001) 33:191–7. doi:10.1038/emm.2001.32
32. Infantino V, Convertini P, Cucci L, Panaro Maria A, Di Noia Maria A, Calvello R, et al. The mitochondrial citrate carrier: a new player in inflammation. *Biochem J* (2011) 438(3):433–6. doi:10.1042/BJ20111275
33. Lampropoulou V, Sergushichev A, Bambouskova M, Nair S, Vincent EE, Loginicheva E, et al. Itaconate links inhibition of succinate dehydrogenase with macrophage metabolic remodeling and regulation of inflammation. *Cell Metab* (2016) 24(1):158–66. doi:10.1016/j.cmet.2016.06.004
34. Everts B, Amiel E, Huang SC-C, Smith AM, Chang C-H, Lam WY, et al. TLR-driven early glycolytic reprogramming via the kinases TBK1-IKK[epsiv] supports the anabolic demands of dendritic cell activation. *Nat Immunol* (2014) 15(4):323–32. doi:10.1038/ni.2833
35. Wellen KE, Hatzivassiliou G, Sachdeva UM, Bui TV, Cross JR, Thompson CB. ATP-citrate lyase links cellular metabolism to histone acetylation. *Science* (2009) 324(5930):1076–80. doi:10.1126/science.1164097
36. Akram M. Citric acid cycle and role of its intermediates in metabolism. *Cell Biochem Biophys* (2014) 68(3):475–8. doi:10.1007/s12013-013-9750-1
37. Palmieri F. The mitochondrial transporter family (SLC25): physiological and pathological implications. *Pflugers Arch* (2004) 447(5):689–709. doi:10.1007/s00424-003-1099-7
38. Saggerson D. Malonyl-CoA, a key signaling molecule in mammalian cells. *Annu Rev Nutr* (2008) 28(1):253–72. doi:10.1146/annurev.nutr.28.061807.155434
39. Paumen MB, Ishida Y, Muramatsu M, Yamamoto M, Honjo T. Inhibition of carnitine palmitoyltransferase I augments sphingolipid synthesis and palmitate-induced apoptosis. *J Biol Chem* (1997) 272(6):3324–9. doi:10.1074/jbc.272.6.3324
40. Brownsey RW, Zhande R, Boone AN. Isoforms of acetyl-CoA carboxylase: structures, regulatory properties and metabolic functions. *Biochem Soc Trans* (1997) 25(4):1232–8. doi:10.1042/bst0251232

41. Pietrocola F, Galluzzi L, Bravo-San Pedro JM, Madeo F, Kroemer G. Acetyl coenzyme A: a central metabolite and second messenger. *Cell Metab* (2015) 21(6):805–21. doi:10.1016/j.cmet.2015.05.014
42. Yalcin A, Telang S, Clem B, Chesney J. Regulation of glucose metabolism by 6-phosphofructo-2-kinase/fructose-2,6-bisphosphatases in cancer. *Exp Mol Pathol* (2009) 86(3):174–9. doi:10.1016/j.yexmp.2009.01.003
43. Taylor WM, Halperin ML. Regulation of pyruvate dehydrogenase in muscle. Inhibition by citrate. *J Biol Chem* (1973) 248(17):6080–3.
44. Hillar M, Lott V, Lennox B. Correlation of the effects of citric acid cycle metabolites on succinate oxidation by rat liver mitochondria and submitochondrial particles. *J Bioenerg* (1975) 7(1):1–16. doi:10.1007/BF01558459
45. Martin DB, Vagelos PR. The mechanism of tricarboxylic acid cycle regulation of fatty acid synthesis. *J Biol Chem* (1962) 237(6):1787–92.
46. Iacobazzi V, Infantino V. Citrate – new functions for an old metabolite. *Biol Chem* (2014) 395(4):387–99. doi:10.1515/hsz-2013-0271
47. Jha Abhishek K, Huang Stanley C-C, Sergushichev A, Lampropoulou V, Ivanova Y, Loginicheva E, et al. Network integration of parallel metabolic and transcriptional data reveals metabolic modules that regulate macrophage polarization. *Immunity* (2015) 42(3):419–30. doi:10.1016/j.immuni.2015.02.005
48. Infantino V, Iacobazzi V, Menga A, Avantaggiati ML, Palmieri F. A key role of the mitochondrial citrate carrier (SLC25A1) in TNFα- and IFNγ-triggered inflammation. *Biochim Biophys Acta* (2014) 1839(11):1217–25. doi:10.1016/j.bbagrm.2014.07.013
49. Infantino V, Iacobazzi V, Palmieri F, Menga A. ATP-citrate lyase is essential for macrophage inflammatory response. *Biochem Biophys Res Commun* (2013) 440(1):105–11. doi:10.1016/j.bbrc.2013.09.037
50. Starai VJ, Escalante-Semerena JC. Acetyl-coenzyme A synthetase (AMP forming). *Cell Mol Life Sci* (2004) 61(16):2020–30. doi:10.1007/s00018-004-3448-x
51. Zasłona Z, Pålsson-McDermott EM, Menon D, Haneklaus M, Flis E, Prendeville H, et al. The induction of pro-IL-1β by lipopolysaccharide requires endogenous prostaglandin E2 production. *J Immunol* (2017) 198(9):3558–64. doi:10.4049/jimmunol.1602072
52. Palmieri EM, Spera I, Menga A, Infantino V, Porcelli V, Iacobazzi V, et al. Acetylation of human mitochondrial citrate carrier modulates mitochondrial citrate/malate exchange activity to sustain NADPH production during macrophage activation. *Biochim Biophys Acta* (2015) 1847(8):729–38. doi:10.1016/j.bbabio.2015.04.009
53. Haseeb A, Makki MS, Haqqi TM. Modulation of ten-eleven translocation 1 (TET1), isocitrate dehydrogenase (IDH) expression, α-ketoglutarate (α-KG), and DNA hydroxymethylation levels by interleukin-1β in primary human chondrocytes. *J Biol Chem* (2014) 289(10):6877–85. doi:10.1074/jbc.M113.512269
54. Wang Y, Wang Y, Shen L, Pang Y, Qiao Z, Liu P. Prognostic and therapeutic implications of increased ATP citrate lyase expression in human epithelial ovarian cancer. *Oncol Rep* (2012) 27(4):1156–62. doi:10.3892/or.2012.1638
55. Zaidi N, Royaux I, Swinnen JV, Smans K. ATP citrate lyase knockdown induces growth arrest and apoptosis through different cell- and environment-dependent mechanisms. *Mol Cancer Ther* (2012) 11(9):1925. doi:10.1158/1535-7163.MCT-12-0095
56. Migita T, Narita T, Nomura K, Miyagi E, Inazuka F, Matsuura M, et al. ATP citrate lyase: activation and therapeutic implications in non-small cell lung cancer. *Cancer Res* (2008) 68(20):8547–54. doi:10.1158/0008-5472.CAN-08-1235
57. Wang D, Yin L, Wei J, Yang Z, Jiang G. ATP citrate lyase is increased in human breast cancer, depletion of which promotes apoptosis. *Tumor Biol* (2017) 39(4):1010428317698338. doi:10.1177/1010428317698338
58. Zaidi N, Swinnen JV, Smans K. ATP-citrate lyase: a key player in cancer metabolism. *Cancer Res* (2012) 72(15):3709–14. doi:10.1158/0008-5472.CAN-11-4112
59. Migita T, Okabe S, Ikeda K, Igarashi S, Sugawara S, Tomida A, et al. Inhibition of ATP citrate lyase induces an anticancer effect via reactive oxygen species: AMPK as a predictive biomarker for therapeutic impact. *Am J Pathol* (2013) 182(5):1800–10. doi:10.1016/j.ajpath.2013.01.048
60. Lee J-H, Jang H, Lee S-M, Lee J-E, Choi J, Kim TW, et al. ATP-citrate lyase regulates cellular senescence via an AMPK- and p53-dependent pathway. *FEBS J* (2015) 282(2):361–71. doi:10.1111/febs.13139
61. Assmann N, O'Brien KL, Donnelly RP, Dyck L, Zaiatz-Bittencourt V, Loftus RM, et al. Srebp-controlled glucose metabolism is essential for NK cell functional responses. *Nat Immunol* (2017) 18(11):1197–206. doi:10.1038/ni.3838
62. Infantino V, Iacobazzi V, Santis FD, Mastrapasqua M, Palmieri F. Transcription of the mitochondrial citrate carrier gene: role of SREBP-1, upregulation by insulin and downregulation by PUFA. *Biochem Biophys Res Commun* (2007) 356(1):249–54. doi:10.1016/j.bbrc.2007.02.114
63. Shimano H, Yahagi N, Amemiya-Kudo M, Hasty AH, Osuga J-I, Tamura Y, et al. Sterol regulatory element-binding protein-1 as a key transcription factor for nutritional induction of lipogenic enzyme genes. *J Biol Chem* (1999) 274(50):35832–9. doi:10.1074/jbc.274.50.35832
64. Gnoni GV, Priore P, Geelen MJH, Siculella L. The mitochondrial citrate carrier: metabolic role and regulation of its activity and expression. *IUBMB Life* (2009) 61(10):987–94. doi:10.1002/iub.249
65. Shimomura I, Shimano H, Korn BS, Bashmakov Y, Horton JD. Nuclear sterol regulatory element-binding proteins activate genes responsible for the entire program of unsaturated fatty acid biosynthesis in transgenic mouse liver. *J Biol Chem* (1998) 273(52):35299–306. doi:10.1074/jbc.273.52.35299
66. Moon Y-A, Lee J-J, Park S-W, Ahn Y-H, Kim K-S. The roles of sterol regulatory element-binding proteins in the transactivation of the rat ATP citrate-lyase promoter. *J Biol Chem* (2000) 275(39):30280–6. doi:10.1074/jbc.M001066200
67. Koivunen P, Hirsilä M, Remes AM, Hassinen IE, Kivirikko KI, Myllyharju J. Inhibition of hypoxia-inducible factor (HIF) hydroxylases by citric acid cycle intermediates: possible links between cell metabolism and stabilization of HIF. *J Biol Chem* (2007) 282(7):4524–32. doi:10.1074/jbc.M610415200
68. Zhang N, Fu Z, Linke S, Chicher J, Gorman JJ, Visk D, et al. The asparaginyl hydroxylase factor inhibiting HIF-1alpha is an essential regulator of metabolism. *Cell Metab* (2010) 11(5):364–78. doi:10.1016/j.cmet.2010.03.001
69. Choudhary C, Weinert BT, Nishida Y, Verdin E, Mann M. The growing landscape of lysine acetylation links metabolism and cell signalling. *Nat Rev Mol Cell Biol* (2014) 15(8):536–50. doi:10.1038/nrm3841
70. Shi L, Tu BP. Acetyl-CoA and the regulation of metabolism: mechanisms and consequences. *Curr Opin Cell Biol* (2015) 33:125–31. doi:10.1016/j.ceb.2015.02.003
71. Schug ZT, Peck B, Jones DT, Zhang Q, Grosskurth S, Alam IS, et al. Acetyl-CoA synthetase 2 promotes acetate utilization and maintains cancer cell growth under metabolic stress. *Cancer Cell* (2015) 27(1):57–71. doi:10.1016/j.ccell.2014.12.002
72. Mehta V, Namboodiri MA. N-acetylaspartate as an acetyl source in the nervous system. *Brain Res Mol Brain Res* (1995) 31(1–2):151–7. doi:10.1016/0169-328X(95)00044-S
73. Prokesch A, Pelzmann HJ, Pessentheiner AR, Huber K, Madreiter-Sokolowski CT, Drougard A, et al. N-acetylaspartate catabolism determines cytosolic acetyl-CoA levels and histone acetylation in brown adipocytes. *Sci Rep* (2016) 6:23723. doi:10.1038/srep23723
74. Zhao S, Torres A, Henry RA, Trefely S, Wallace M, Lee JV, et al. ATP-citrate lyase controls a glucose-to-acetate metabolic switch. *Cell Rep* (2016) 17(4):1037–52. doi:10.1016/j.celrep.2016.09.069
75. Balmer Maria L, Ma Eric H, Bantug Glenn R, Grählert J, Pfister S, Glatter T, et al. Memory CD8(+) T cells require increased concentrations of acetate induced by stress for optimal function. *Immunity* (2016) 44(6):1312–24. doi:10.1016/j.immuni.2016.03.016
76. Chang CH, Curtis JD, Maggi LB Jr, Faubert B, Villarino AV, O'Sullivan D, et al. Posttranscriptional control of T cell effector function by aerobic glycolysis. *Cell* (2013) 153(6):1239–51. doi:10.1016/j.cell.2013.05.016
77. Peng M, Yin N, Chhangawala S, Xu K, Leslie CS, Li MO. Aerobic glycolysis promotes T helper 1 cell differentiation through an epigenetic mechanism. *Science* (2016) 354(6311):481–4. doi:10.1126/science.aaf6284
78. Wang B, Rao YH, Inoue M, Hao R, Lai CH, Chen D, et al. Microtubule acetylation amplifies p38 kinase signalling and anti-inflammatory IL-10 production. *Nat Commun* (2014) 5:3479. doi:10.1038/ncomms4479
79. Hu L, Yu Y, Huang H, Fan H, Hu L, Yin C, et al. Epigenetic regulation of interleukin 6 by histone acetylation in macrophages and its role in paraquat-induced pulmonary fibrosis. *Front Immunol* (2017) 7:696. doi:10.3389/fimmu.2016.00696
80. Greene WC, Chen LF. Regulation of NF-kappaB action by reversible acetylation. *Novartis Found Symp* (2004) 259:208–17; discussion 18–25. doi:10.1002/0470862637.ch15

81. Zhao S, Xu W, Jiang W, Yu W, Lin Y, Zhang T, et al. Regulation of cellular metabolism by protein lysine acetylation. *Science* (2010) 327(5968):1000. doi:10.1126/science.1179689
82. Covarrubias AJ, Aksoylar HI, Yu J, Snyder NW, Worth AJ, Iyer SS, et al. Akt-mTORC1 signaling regulates Acly to integrate metabolic input to control of macrophage activation. *Elife* (2016) 5:e11612. doi:10.7554/eLife.11612
83. Peng C, Lu Z, Xie Z, Cheng Z, Chen Y, Tan M, et al. The first identification of lysine malonylation substrates and its regulatory enzyme. *Mol Cell Proteomics* (2011) 10(12):M111.012658. doi:10.1074/mcp.M111.012658
84. Du J, Zhou Y, Su X, Yu JJ, Khan S, Jiang H, et al. Sirt5 is a NAD-dependent protein lysine demalonylase and desuccinylase. *Science* (2011) 334(6057):806–9. doi:10.1126/science.1207861
85. Witkowski A, Thweatt J, Smith S. Mammalian ACSF3 protein is a malonyl-CoA synthetase that supplies the chain extender units for mitochondrial fatty acid synthesis. *J Biol Chem* (2011) 286(39):33729–36. doi:10.1074/jbc.M111.291591
86. Colak G, Pougovkina O, Dai L, Tan M, Te Brinke H, Huang H, et al. Proteomic and biochemical studies of lysine malonylation suggest its malonic aciduria-associated regulatory role in mitochondrial function and fatty acid oxidation. *Mol Cell Proteomics* (2015) 14(11):3056–71. doi:10.1074/mcp.M115.048850
87. Nishida Y, Rardin MJ, Carrico C, He W, Sahu AK, Gut P, et al. SIRT5 regulates both cytosolic and mitochondrial protein malonylation with glycolysis as a major target. *Mol Cell* (2015) 59(2):321–32. doi:10.1016/j.molcel.2015.05.022
88. Willke T, Vorlop KD. Biotechnological production of itaconic acid. *Appl Microbiol Biotechnol* (2001) 56(3–4):289–95. doi:10.1007/s002530100685
89. Lee CG, Jenkins NA, Gilbert DJ, Copeland NG, O'Brien WE. Cloning and analysis of gene regulation of a novel LPS-inducible cDNA. *Immunogenetics* (1995) 41(5):263–70. doi:10.1007/BF00172150
90. Li Y, Zhang P, Wang C, Han C, Meng J, Liu X, et al. Immune responsive gene 1 (IRG1) promotes endotoxin tolerance by increasing A20 expression in macrophages through reactive oxygen species. *J Biol Chem* (2013) 288(23):16225–34. doi:10.1074/jbc.M113.454538
91. Cheon Y-P, Xu X, Bagchi MK, Bagchi IC. Immune-responsive gene 1 is a novel target of progesterone receptor and plays a critical role during implantation in the mouse. *Endocrinology* (2003) 144(12):5623–30. doi:10.1210/en.2003-0585
92. Chen B, Zhang D, Pollard JW. Progesterone regulation of the mammalian ortholog of methylcitrate dehydratase (immune response gene 1) in the uterine epithelium during implantation through the protein kinase C pathway. *Mol Endocrinol* (2003) 17(11):2340–54. doi:10.1210/me.2003-0207
93. Degrandi D, Hoffmann R, Beuter-Gunia C, Pfeffer K. The proinflammatory cytokine-induced IRG1 protein associates with mitochondria. *J Interferon Cytokine Res* (2009) 29(1):55–67. doi:10.1089/jir.2008.0013
94. Tallam A, Perumal TM, Antony PM, Jager C, Fritz JV, Vallar L, et al. Gene regulatory network inference of immunoresponsive gene 1 (IRG1) identifies interferon regulatory factor 1 (IRF1) as its transcriptional regulator in mammalian macrophages. *PLoS One* (2016) 11(2):e0149050. doi:10.1371/journal.pone.0149050
95. Michelucci A, Cordes T, Ghelfi J, Pailot A, Reiling N, Goldmann O, et al. Immune-responsive gene 1 protein links metabolism to immunity by catalyzing itaconic acid production. *Proc Natl Acad Sci U S A* (2013) 110(19):7820–5. doi:10.1073/pnas.1218599110
96. Shin J-H, Yang J-Y, Jeon B-Y, Yoon YJ, Cho S-N, Kang Y-H, et al. 1H NMR-based metabolomic profiling in mice infected with *Mycobacterium tuberculosis*. *J Proteome Res* (2011) 10(5):2238–47. doi:10.1021/pr101054m
97. Sugimoto M, Sakagami H, Yokote Y, Onuma H, Kaneko M, Mori M, et al. Non-targeted metabolite profiling in activated macrophage secretion. *Metabolomics* (2012) 8(4):624–33. doi:10.1007/s11306-011-0353-9
98. Berg IA, Filatova LV, Ivanovsky RN. Inhibition of acetate and propionate assimilation by itaconate via propionyl-CoA carboxylase in isocitrate lyase-negative purple bacterium *Rhodospirillum rubrum*. *FEMS Microbiol Lett* (2002) 216(1):49–54. doi:10.1111/j.1574-6968.2002.tb11413.x
99. Naujoks J, Tabeling C, Dill BD, Hoffmann C, Brown AS, Kunze M, et al. IFNs modify the proteome of *Legionella*-containing vacuoles and restrict infection via IRG1-derived itaconic acid. *PLoS Pathog* (2016) 12(2):e1005408. doi:10.1371/journal.ppat.1005408
100. Sasikaran J, Ziemski M, Zadora PK, Fleig A, Berg IA. Bacterial itaconate degradation promotes pathogenicity. *Nat Chem Biol* (2014) 10(5):371–7. doi:10.1038/nchembio.1482
101. Luan Harding H, Medzhitov R. Food fight: role of itaconate and other metabolites in antimicrobial defense. *Cell Metab* (2016) 24(3):379–87. doi:10.1016/j.cmet.2016.08.013
102. Ryan DG, O'Neill LAJ. Krebs cycle rewired for macrophage and dendritic cell effector functions. *FEBS Lett* (2017) 591(19):2992–3006. doi:10.1002/1873-3468.12744
103. Cordes T, Wallace M, Michelucci A, Divakaruni AS, Sapcariu SC, Sousa C, et al. Immunoresponsive gene 1 and itaconate inhibit succinate dehydrogenase to modulate intracellular succinate levels. *J Biol Chem* (2016) 291(27):14274–84. doi:10.1074/jbc.M115.685792
104. Ackermann WW, Potter VR. Enzyme inhibition in relation to chemotherapy. *Proc Soc Exp Biol Med* (1949) 72(1):1–9. doi:10.3181/00379727-72-17313
105. Nemeth B, Doczi J, Csete D, Kacso G, Ravasz D, Adams D, et al. Abolition of mitochondrial substrate-level phosphorylation by itaconic acid produced by LPS-induced Irg1 expression in cells of murine macrophage lineage. *FASEB J* (2016) 30(1):286–300. doi:10.1096/fj.15-279398
106. Murphy Michael P. How mitochondria produce reactive oxygen species. *Biochem J* (2009) 417(Pt 1):1–13. doi:10.1042/BJ20081386
107. Bauernfeind F, Bartok E, Rieger A, Franchi L, Núñez G, Hornung V. Cutting edge: reactive oxygen species inhibitors block priming, but not activation, of the NLRP3 inflammasome. *J Immunol* (2011) 187(2):613–7. doi:10.4049/jimmunol.1100613
108. Jamal Uddin M, Joe Y, Kim S-K, Oh Jeong S, Ryter SW, Pae H-O, et al. IRG1 induced by heme oxygenase-1/carbon monoxide inhibits LPS-mediated sepsis and pro-inflammatory cytokine production. *Cell Mol Immunol* (2016) 13(2):170–9. doi:10.1038/cmi.2015.02
109. Papathanassiu AE, Ko J-H, Imprialou M, Bagnati M, Srivastava PK, Vu HA, et al. BCAT1 controls metabolic reprogramming in activated human macrophages and is associated with inflammatory diseases. *Nat Commun* (2017) 8:16040. doi:10.1038/ncomms16040
110. ElAzzouny M, Tom CTMB, Evans CR, Olson LL, Tanga MJ, Gallagher KA, et al. Dimethyl itaconate is not metabolized into itaconate intracellularly. *J Biol Chem* (2017) 292(12):4766–9. doi:10.1074/jbc.C117.775270
111. Sundstrom L, Greasley PJ, Engberg S, Wallander M, Ryberg E. Succinate receptor GPR91, a Galpha(i) coupled receptor that increases intracellular calcium concentrations through PLCbeta. *FEBS Lett* (2013) 587(15):2399–404. doi:10.1016/j.febslet.2013.05.067
112. Newsholme P, Curi R, Gordon S, Newsholme EA. Metabolism of glucose, glutamine, long-chain fatty acids and ketone bodies by murine macrophages. *Biochem J* (1986) 239(1):121–5. doi:10.1042/bj2390121
113. Hard GC. Some biochemical aspects of the immune macrophage. *Br J Exp Pathol* (1970) 51(1):97–105.

Conflict of Interest Statement: The authors declare that the research was conducted in the absence of any commercial or financial relationships that could be construed as a potential conflict of interest.

frontiers in Immunology

ORIGINAL RESEARCH
published: 13 February 2018
doi: 10.3389/fimmu.2018.00215

Loss of *Rictor* in Monocyte/Macrophages Suppresses Their Proliferation and Viability Reducing Atherosclerosis in LDLR Null Mice

Vladimir R. Babaev[1], Jiansheng Huang[1], Lei Ding[1], Youmin Zhang[1], James M. May[1] and MacRae F. Linton[1]**

[1] Atherosclerosis Research Unit, Division of Cardiovascular Medicine, Department of Medicine, Vanderbilt University School of Medicine, Nashville, TN, United States, [2] Department of Pharmacology, Vanderbilt University School of Medicine, Nashville, TN, United States

Background: Rictor is an essential component of mammalian target of rapamycin (mTOR) complex 2 (mTORC2), a conserved serine/threonine kinase that may play a role in cell proliferation, survival and innate or adaptive immune responses. Genetic loss of *Rictor* inactivates mTORC2, which directly activates Akt S^{473} phosphorylation and promotes pro-survival cell signaling and proliferation.

Methods and results: To study the role of mTORC2 signaling in monocytes and macrophages, we generated mice with myeloid lineage-specific *Rictor* deletion (M*Rictor*$^{-/-}$). These M*Rictor*$^{-/-}$ mice exhibited dramatic reductions of white blood cells, B-cells, T-cells, and monocytes but had similar levels of neutrophils compared to control *Rictor* flox-flox (*Rictor*$^{fl/fl}$) mice. M*Rictor*$^{-/-}$ bone marrow monocytes and peritoneal macrophages expressed reduced levels of mTORC2 signaling and decreased Akt S^{473} phosphorylation, and they displayed significantly less proliferation than control *Rictor*$^{fl/fl}$ cells. In addition, blood monocytes and peritoneal macrophages isolated from M*Rictor*$^{-/-}$ mice were significantly more sensitive to pro-apoptotic stimuli. In response to LPS, M*Rictor*$^{-/-}$ macrophages exhibited the M1 phenotype with higher levels of pro-inflammatory gene expression and lower levels of *Il10* gene expression than control *Rictor*$^{fl/fl}$ cells. Further suppression of LPS-stimulated Akt signaling with a low dose of an Akt inhibitor, increased inflammatory gene expression in macrophages, but genetic inactivation of *Raptor* reversed this rise, indicating that mTORC1 mediates this increase of inflammatory gene expression. Next, to elucidate whether mTORC2 has an impact on atherosclerosis *in vivo*, female and male *Ldlr* null mice were reconstituted with bone marrow from M*Rictor*$^{-/-}$ or *Rictor*$^{fl/fl}$ mice. After 10 weeks of the Western diet, there were no differences between the recipients of the same gender in body weight, blood glucose or plasma lipid levels. However, both female and male M*Rictor*$^{-/-}$ → *Ldlr*$^{-/-}$ mice developed smaller atherosclerotic lesions in the distal and proximal aorta. These lesions contained less macrophage area and more apoptosis than lesions of control *Rictor*$^{fl/fl}$ → *Ldlr*$^{-/-}$ mice. Thus, loss of *Rictor* and, consequently, mTORC2 significantly compromised monocyte/macrophage survival, and this markedly diminished early atherosclerosis in *Ldlr*$^{-/-}$ mice.

OPEN ACCESS

Edited by:
Liwu Li,
Virginia Tech, United States

Reviewed by:
Paola Italiani,
Consiglio Nazionale Delle Ricerche (CNR), Italy
Alessandro Arduini,
Broad Institute, United States

***Correspondence:**
Vladimir R. Babaev
vladimir.babaev@vanderbilt.edu;
MacRae F. Linton
macrae.linton@vanderbilt.edu

Specialty section:
This article was submitted to Molecular Innate Immunity, a section of the journal Frontiers in Immunology

Received: *02 November 2017*
Accepted: *25 January 2018*
Published: *13 February 2018*

Citation:
Babaev VR, Huang J, Ding L, Zhang Y, May JM and Linton MF (2018) Loss of Rictor in Monocyte/Macrophages Suppresses Their Proliferation and Viability Reducing Atherosclerosis in LDLR Null Mice. Front. Immunol. 9:215. doi: 10.3389/fimmu.2018.00215

Conclusion: Our results demonstrate that mTORC2 is a key signaling regulator of macrophage survival and its depletion suppresses early atherosclerosis.

Keywords: atherosclerosis, monocytes, macrophages, proliferation, apoptosis, Akt signaling, mammalian target of rapamycin complex 2

INTRODUCTION

Atherosclerosis, the underlying cause of myocardial infarction and stroke, is an inflammatory disease process, and both the innate and adaptive immune responses play important roles in its pathogenesis (1). Monocytes and macrophages play key roles in the pathogenesis of atherosclerosis. Furthermore, alterations in macrophage phenotypes and survival play crucial roles in the development of atherosclerosis. Current studies of immunotherapy have focused on immune checkpoint therapy targeting regulatory pathways in T-cells (2). However, there are also multiple ways to modulate the immune response by changing the activation of myeloid cells, which belong to the innate immune system, performing essential roles in tissue homeostasis by initiating, sustaining, or inhibiting adaptive immunity (3, 4). Therefore, identification of mechanisms that control macrophage metabolism and survival should provide insights into the regulation of immune responses and identify novel approaches to treat disease (5).

Recent studies suggest that interplay between protein kinase B (or Akt) and mammalian target of rapamycin (mTOR) pathways is crucial for myeloid cell activation (4). Akt is a serine/threonine-specific kinase that regulates multiple cellular processes, including cell viability, proliferation, transcription, and migration (6, 7). mTOR is an evolutionarily conserved serine/threonine kinase that is constitutively expressed and plays a central role in integrating environmental cues in the form of growth factors, amino acids, and energy (8). mTOR also controls and shapes the effector responses of innate immune cells. Therefore, knowledge of how Akt/mTOR signaling coordinates the responses of myeloid cells may provide important insights into immunity in health and disease (3, 4).

There are two distinct types of mTOR complexes, termed mTORC1 and mTOR complex 2 (mTORC2), the first contains regulatory associated protein of mTOR (Raptor) and the second involves rapamycin-insensitive companion of mTOR (Rictor) (9). Inhibition of mTORC1 with a class of macrolide immunosuppressive drugs, called rapalogs, reduces atherosclerosis in a variety of animal models, and rapalog eluting stents are widely used to treat atherosclerotic coronary artery disease in humans (10). By contrast, relatively little is known about the role of mTOR2 in atherosclerosis.

Genetic loss of *Rictor* inactivates mTORC2, and, since total *Rictor* deficiency in mice causes embryonic lethality (11, 12), generation of mice with tissue-specific knockouts of *Rictor* has been instrumental in delineating the specific roles of mTORC2 in different cell types. For example, liver-specific disruption of *Rictor* induces glucose intolerance, hepatic insulin resistance, and decreased hepatic lipogenesis (13, 14). Remarkably, the liver-specific knockout or an inducible total body loss of *Rictor* in adult mice specifically reduces male lifespan (15). In contrast, *Rictor* knockout in muscle tissue contributes to glucose homeostasis by positively regulating insulin-stimulated glucose uptake and negatively regulating basal glycogen synthase activity (16). mTORC2 regulates cardiomyocyte growth and survival, and loss of *Rictor* in mouse heart results in progressive cardiac dysfunction (17). Adipose-specific knockout of *Rictor* in mice increases whole-body size (18) but leads to hepatic steatosis and insulin resistance (19). Loss of *Rictor* in pancreatic beta cells reduces beta cell mass and insulin secretion resulting in hyperglycemia and glucose intolerance (20). These data indicate that mTORC2 may play varied roles depending on the cell type and conditions.

Notably, mTORC2 initiates the phosphorylation of Akt S^{473} (21), which accelerates Akt signaling promoting cell survival and proliferation. Despite the predominant role of mTORC2 as a regulator of pro-survival Akt signaling, the impact of mTORC2 on cell viability remains unclear (22). For example, several studies showed no indication that loss of *Rictor* and consequently mTORC2 increased apoptosis, at least under otherwise normal physiological conditions (16, 18, 20, 23). Moreover, a recent report indicates that *Rictor*-deficient keratinocytes display increased lifespan, protection from senescence, and enhanced tolerance of cellular stressors such as growth factor deprivation (24). These findings appear to contradict several other reports indicating that *Rictor* deficiency increases apoptosis in pulmonary arterial vascular smooth muscle cells (25), endothelial cells (26) and skin tumor cells (27). Rictor plays an important role in regulating cellular survival after ischemic cardiac damage (28) and in B-cells acting via a c-Myc-dependent pathway (29). In addition, we recently demonstrated that loss of IκB kinase alpha (IKKα) in macrophages suppresses Akt S^{473} phosphorylation and this compromises cell survival and decreases early atherosclerosis (30). This suppression of p-Akt S^{473} was mediated *via* mTORC2 suggesting the hypothesis that mTORC2 initiates important pro-survival signaling in monocytes and macrophages that impacts the pathogenesis of atherosclerosis. However, IKKα is located upstream of the NF-κB signal transduction cascade and loss of *IKK*α-enhanced macrophage activation (31), limiting the ability to draw conclusions regarding the role of mTORC2 in macrophage function and atherogenesis.

Therefore, we used myeloid lineage-specific *Rictor* deletion in mice to examine directly whether loss of mTORC2 in myeloid cells impacts monocyte and macrophage viability and proliferation and the development of atherosclerosis. We found that mTORC2 signaling is crucial for monocyte and macrophage proliferation and survival, and loss of mTORC2 signaling in myeloid cells results in decreased early atherosclerosis.

MATERIALS AND METHODS

Animal Procedures, Mice

Rictor$^{flox/flox}$ (32), *LysM-Cre* (33), *Raptor*$^{flox/flox}$ (34), and the recipient LDLR$^{-/-}$ mice were all on the C57BL/6 background, and they were purchased from the Jackson Laboratories together with C57BL/6 mice. Mice with myeloid lineage-specific *Raptor* deletion (M*Raptor*$^{-/-}$) were generated by crossing *Raptor* floxed mice (*Raptor*$^{flox/flox}$) with LysM-Cre mice. Mice were maintained in microisolator cages on a rodent chow diet containing 4.5% fat (PMI 5010, St. Louis, MO, USA) or a Western-type diet containing 21% milk fat and 0.15% cholesterol (Teklad, Madison, WI, USA).

Ethics Statement

All animal experiments were approved by the Institutional Animal Care and Use Committee at Vanderbilt University Medical Center. Vanderbilt University Medical Center Animal Care and Use Program is registered with the USDA (USDA Registration #63-R-0129) and operates under a PHS Animal Welfare Assurance Statement (PHS Assurance #A3227-01).

Bone Marrow Transplantation, Blood Monocyte, and Peritoneal Macrophage Isolation

Bone marrow cells were isolated from mouse tibias and fibulas. Recipient *Ldlr*$^{-/-}$ or C57BL6 mice were lethally irradiated (9 Gy) and transplanted with (5×10^6) bone marrow cells as described (35). Blood was collected by retro-orbital bleeding under anesthesia, and peripheral blood mononuclear cells were isolated by centrifugation in Histopaque-1077 (Sigma). Cells that attached to the plastic dish within 2–3 h of incubation were cultured in DMEM media containing 10% FBS and macrophage colony-stimulating factor (M-CSF; 10 ng/ml). Thioglycollate-elicited peritoneal macrophages were isolated and treated with insulin from bovine pancreas, or fatty acid free bovine serum albumin (BSA) (both from Sigma), or with palmitic acid complexed to BSA (PA-BSA), human oxidized LDL, or an Akt inhibitor IV (EMD Millipore).

Western Blotting

Cells were lysed in a lysis buffer (Cell Signaling Technology, Danvers, MA, USA) containing protease and phosphatase inhibitors. Proteins were measured with the DC Protein assay reagents (Bio-Rad Laboratories) and resolved by NuPAGE Bis-Tris electrophoresis and transferred onto nitrocellulose membranes (Amersham Bioscience). Blots were probed with rabbit antibodies to Akt, p-Akt (both S^{473} and T^{308}), Rictor, p-mTOR S^{2448}, p-70S6K T^{389}, p-4E-BP1 $T^{37/46}$ (all from Cell signaling Technology), p-SGK S^{422}R and p-PKCα S^{657}-R, p-NDRG1 T^{346} and β-actin antibodies (Santa Cruz Biotechnology), and goat anti-rabbit horseradish peroxidase-conjugated secondary antibodies (Sigma). Proteins were visualized with ECL western blotting detection reagents (GE Healthcare) and quantified by densitometry using ImageJ software (NIH).

Flow Cytometry

Blood cells were stained with a cocktail of antibodies against lineage markers, including CD3 (clone 17A2), CD45RB220 (clone RA3-6B2), Ly-6G (clone 1A8), CD11b (clone M1/70), and Ly-6C (clone AL-21) (all from BioLegend). Blood or bone marrow cells were treated with lysing buffer (BD Pharm, cat#555899), washed and analyzed using FACS DiVa v6.1 software (BD Biosciences) in the Research Flow Cytometry Core Laboratory, Veterans Administration Medical Center. Akt phosphorylation levels were evaluated in bone marrow cells using a methanol-based permeabilization protocol (36).

BrdU-Labeled Cell Proliferation Assay

For the *in vivo* experiments, BrdU labeling reagent (Invitrogen, catalog#000103) was injected intraperitoneal [10 ml/kg body weight (BW)], and, 24 h later, cells were isolated, fixed, permeabilized, treated with DNAse and then analyzed by flow cytometry using a FITC BrdU flow kit (cat#51-2354AK). For *in vitro* studies, cells were treated with or without human recombinant platelet-derived growth factor (PDGF-BB, eBisoscience; 20 ng/m) together with BrdU, diluted 1:100, for 24 h. Then cells were fixed with 2% paraformaldehyde for 20 min, permeabilized with 0.1% Triton X-100, DNA was denatured by incubation with 2 N HCl for 60 min at 37°C, followed by five rinses in 0.1 Borate buffer, pH8.5 and PBS. Cells were blocked for 30 min by using 3% BSA in PBS, probed with a fluorochrome-conjugated anti-BrdU antibody and analyzed under a microscope (Olympus AX70, camera DP72).

Apoptosis Assessment

Apoptotic cells were analyzed by flow cytometry and in cultured cells seeded in Laboratory-Tek chambers (Nalge Nunc International) using an Alexa Fluor488 Annexin V/Dead Cell Apoptosis kit (Life Technologies, catalog number V13241). To detect apoptosis in the vascular wall, 5-μm cryostat sections of the proximal aorta were fixed in 2% paraformaldehyde in PBS, treated with 3% citric acid and stained using an *in situ* cell death detection kit (Roche Applied Science). TUNEL-positive (TUNEL+) cells were counted in four different sections of each aorta as described (37). The numbers of TUNEL+ cells were counted as a percentage of the total number of cells in at least four separate fields (containing ≈1,000 cells) from duplicate chambers.

RNA Isolation and Real-Time PCR

Total RNA was isolated and relative quantitation of the target mRNA was analyzed using gene expression assays (Applied Biosystems, Foster City, CA, UK) as described (37).

Analysis of Serum Lipids and Aortic Lesions

Serum total cholesterol and triglyceride (TG) levels were determined after overnight fasting by the enzyme-based technique. Aortas were flushed through the left ventricle and the entire aorta was dissected *en face* and stained with Sudan IV as described (37). Cryostat sections of aortic sinus were stained with Oil-red-O, images of the proximal and distal aortas were analyzed using an Imaging system KS 300 (Kontron Electronik GmbH.).

Statistical Analysis

All analyses were performed using GraphPad Prizm v 7 (GraphPad Software, Inc., USA) or a SPSS Statistics Premium v22 (IBM, USA) software. Data were assessed for normality of distribution. Statistical analyses of data were performed using Student's *t*-test, a Mann–Whitney *U*-test or 1- to 2-way ANOVAs. Data are provided as means ± SEM. A difference was considered to be statistically significant at a *P*-value less than 0.05 by Mann–Whitney Rank Sum Test.

RESULTS

Loss of Rictor Reduces Akt and mTORC2 Signaling in Blood Monocytes and Macrophages

The stability and integrity of mTORC2 depends on the presence of Rictor, which is an essential component of the complex. Deficiency in Rictor disrupts mTORC2 assembly and this significantly diminishes cell AktS^{473} phosphorylation (11). However, total Rictor deficiency in mice causes embryonic lethality (11, 12). Therefore, tissue-specific Rictor knockout mice represent an approach for investigating the role of mTORC2 in cell-specific functions (38).

To elucidate the role of mTORC2 signaling in monocytes and macrophages, we generated mice with myeloid lineage-specific *Rictor* deletion by crossing *Rictor* floxed mice (*Rictor*$^{fl/fl}$) with lysozyme M Cre (*LysM-Cre*)–recombinase mice. These myeloid-specific *Rictor* knockout *(*M*Rictor*$^{-/-}$) mice were born at the expected Mendelian ratio and were viable and fertile with no differences in BW or plasma lipid levels compared to control *Rictor*$^{fl/fl}$ mice. Analysis of peritoneal macrophages isolated from M*Rictor*$^{-/-}$mice demonstrated that these cells had significantly less Rictor protein than control *Rictor*$^{fl/fl}$ cells (**Figure 1A**). In response to insulin treatment, Akt S^{473} and Akt T^{308} phosphorylation were significantly suppressed in M*Rictor*$^{-/-}$ macrophages compared to *Rictor*$^{fl/fl}$ cells (**Figures 1A–C**). In addition, M*Rictor*$^{-/-}$ macrophages had diminished levels of proteins known to be downstream targets of mTORC2. The levels of protein kinase C alpha and the serum and glucocorticoid-induced kinase 1 substrate, N-myc downstream regulated gene 1 (NDRG1), were only slightly detectable in M*Rictor*$^{-/-}$ macrophages compared to *Rictor*$^{fl/fl}$ cells (**Figure 1A**). Together, these results are consistent with our expectation that loss of *Rictor* prevents mTORC2 formation and this significantly suppresses p-Akt S^{473} and Akt signaling.

In order to evaluate whether *Rictor* deficiency suppresses Akt signaling *in vivo*, we analyzed Akt S^{473} phosphorylation in mouse bone marrow cells by flow cytometry using antibodies to CD11b and Ly-6G to separate monocytes and neutrophils (**Figures 1D,E**). As we anticipated, M*Rictor*$^{-/-}$ granulocytes and monocytes expressed decreased levels of Akt Ser^{473} phosphorylation compared to control *Rictor*$^{fl/fl}$ cells (**Figures 1F,G**). These results confirm that *Rictor* deletion in myeloid cells significantly suppresses Akt signaling *in vivo*.

Next, to examine the impact of myeloid *Rictor* deficiency on bone marrow and blood cells, we used multicolor flow cytometry analysis. Interestingly, we isolated similar total numbers of bone marrow cells from *Rictor*$^{fl/fl}$ and M*Rictor*$^{-/-}$ mice (n = 18/group; 47.1 ± 2.1 vs. 45.8 ± 2.8 × 10^6 cells, respectively; p = 0.71). However, bone marrow cells from M*Rictor*$^{-/-}$ mice showed increased numbers of T-cells and neutrophils, but no changes in B-cells or monocytes compared to bone marrow of *Rictor*$^{fl/fl}$ mice (**Figure 1H**). By contrast, blood cells from M*Rictor*$^{-/-}$ mice had significantly lower numbers of total white blood cell counts, decreased B-cells, T-cells, and monocytes, but not neutrophils, than *Rictor*$^{fl/fl}$ mice (**Figure 1I**). These data indicate that mTORC2 is an important determinant of blood cell numbers including monocytes. These findings also suggest the loss of mTORC2 may influence hematopoietic cell proliferation and viability.

Rictor Is Necessary for Proliferation of Myeloid Cells

Since one of the distinct characteristic of macrophages is self-renewal via proliferation (39), we examined whether elimination of mTORC2 disturbs the proliferation of monocytes and macrophages. The BrdU incorporation rate was analyzed in bone marrow and blood cells of *Rictor*$^{fl/fl}$ and M*Rictor*$^{-/-}$ mice. There were no differences between these groups of mice in total bone marrow cells, total number of BrdU-positive (BrdU+) marrow cells and BrdU+ monocytes (**Figures 2A–C**). In contrast, blood cells of M*Rictor*$^{-/-}$ mice had lower levels of white blood cell counts, total number of BrdU+ cells and BrdU+monocytes compared to control *Rictor*$^{fl/fl}$ mice (**Figures 2D–F**). Thus, loss of *Rictor* diminishes numbers of proliferative monocytes in the blood but not in the bone marrow.

To test whether M*Rictor*$^{-/-}$ blood monocytes respond appropriately to a proliferative stimulus, we isolated blood monocytes from *Rictor*$^{fl/fl}$ and M*Rictor*$^{-/-}$ mice and 2 days later treated them with PDGF. The treatment increased numbers of BrdU+ cells in both groups although to a significantly greater degree in *Rictor*$^{fl/fl}$ monocytes than in M*Rictor*$^{-/-}$ cells (**Figures 2G,H**). Similarly, peritoneal macrophages isolated from M*Rictor*$^{-/-}$ mice and treated with PDGF also exhibited diminished numbers of BrdU+ cells compared to M*Rictor*$^{fl/fl}$ cells (**Figures 2I,J**). Correspondingly, a simple cell count after treatment with PDGF revealed a greater increase of *Rictor*$^{fl/fl}$ macrophages compared to M*Rictor*$^{-/-}$ cells (**Figure 2K**). Collectively, these results indicate that mTORC2 is required for proliferation of monocytes and macrophages.

M*Rictor*$^{-/-}$ Macrophages Are Less Viable and Express High Levels of Inflammatory Genes in Response to LPS

Since loss of *Rictor* disrupts assembly of mTORC2, thus significantly diminishing Akt signaling, which is the major pro-survival pathway that suppresses apoptosis (6), we hypothesized that *Rictor* deficiency may compromise monocyte and macrophage survival. To test this hypothesis, we analyzed blood cells isolated from *Rictor*$^{fl/fl}$ *and* M*Rictor*$^{-/-}$ mice by flow cytometry using the Alexa Fluor488 Annexin V antibody. The analysis of the representative flow cytometry plots revealed that M*Rictor*$^{-/-}$ mice had an increase of apoptosis in blood neutrophils and monocytes but not in B- or T-cells compared to *Rictor*$^{fl/fl}$ mice (**Figure 3A**). Indeed, M*Rictor*$^{-/-}$ mice had increased apoptotic neutrophils and monocytes but not B- and T-cells compared to *Rictor*$^{fl/fl}$

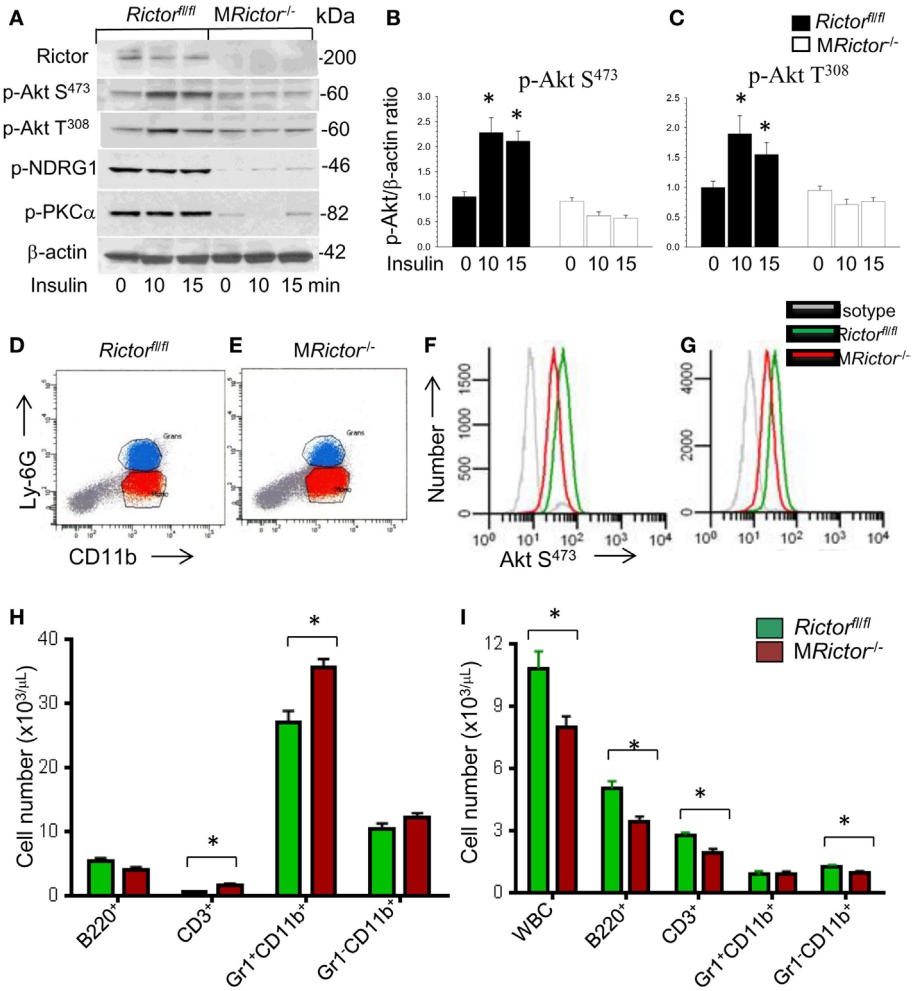

FIGURE 1 | Loss of *Rictor* significantly suppresses Akt and mammalian target of rapamycin complex 2 (mTORC2) signaling in peritoneal macrophages, reduces p-Akt S^{473} in monocytes and neutrophils *in vivo*, and decreases blood leukocyte numbers. **(A–C)** Peritoneal macrophages were isolated from *Rictor*$^{fl/fl}$ and M*Rictor*$^{-/-}$ mice (n = 3/group), incubated overnight in serum-free media then untreated or treated with insulin (100 nM) for 10 and 15 min. Proteins were extracted, resolved (60 μg/well) and analyzed by western blot using the antibodies as indicated. Note the reduction of p-Akt S^{473}, p-Akt^{308} and mTORC2 downstream signaling, p-NDRG1 and p-PKCα in M*Rictor*$^{-/-}$ macrophages compared to control *Rictor*$^{fl/fl}$ cells. Graphs represent data (mean ± SEM; $^*p < 0.05$ compared to control untreated *Rictor*$^{fl/fl}$ cells). **(D–G)** Representative plots of gaiting strategy to analyze Akt S^{473} phosphorylation levels in bone marrow cells of *Rictor*$^{fl/fl}$ and M*Rictor*$^{-/-}$ mice *in vivo* **(D,E)**. Note M*Rictor*$^{-/-}$ bone marrow neutrophils **(F)** and monocytes **(G)** expressed significantly less p-Akt S^{473} (red) than control *Rictor*$^{fl/fl}$ cells (green) but were higher than the isotype control antibodies (gray). **(H,I)** Multicolor flow cytometry analysis of bone marrow **(H)** and blood cells **(I)** isolated from *Rictor*$^{fl/fl}$ (green) and *MRictor*$^{-/-}$ (red) mice. Note the increase of T-cells and neutrophils in bone marrow and decrease of white blood cells, B- and T-cells and monocytes but not granulocytes in blood (mean ± SEM; $^*p < 0.05$ compared to control sample). These experiments were repeated three times.

mice (**Figure 3B**). Thus, loss of mTORC2 significantly increases apoptosis in blood neutrophils and monocytes.

To further investigate this phenomenon, we isolated blood monocytes and treated them overnight with BSA or BSA complexed with palmitic acid (PA), a lipotoxic factor that induces ER stress and triggers apoptosis (40). Analysis of apoptosis by the Annexin V labeling kit demonstrated that PA treatment dramatically increased apoptosis in both groups of cells although more notably in M*Rictor*$^{-/-}$ monocytes (91%) than *Rictor*$^{fl/fl}$ cells (**Figures 3C,D**). Thus, M*Rictor*$^{-/-}$ monocytes exhibit compromised resistance to ER stress-induced apoptosis. Similar results were obtained when peritoneal macrophages were treated with PA or human oxidized LDL, which may be more relevant to atherosclerosis, M*Rictor*$^{-/-}$ macrophages had significantly higher levels of apoptosis than *Rictor*$^{fl/fl}$ cells (**Figures 3E–G**). Together these data indicate that loss of *Rictor* and consequently mTORC2 significantly compromises the ability of monocytes and macrophages to survive under conditions of ER stress.

Recently, several reports (41–43) have shown that mTORC2 signaling is crucial in promoting the M2 phenotype. To verify these findings, M*Rictor*$^{-/-}$ *Rictor*$^{fl/fl}$ peritoneal macrophages were treated with lipopolysaccharides (LPS) and analyzed by real-time PCR. Accordingly, M*Rictor*$^{-/-}$ macrophages expressed significantly higher levels of inflammatory genes including *TNFα*,

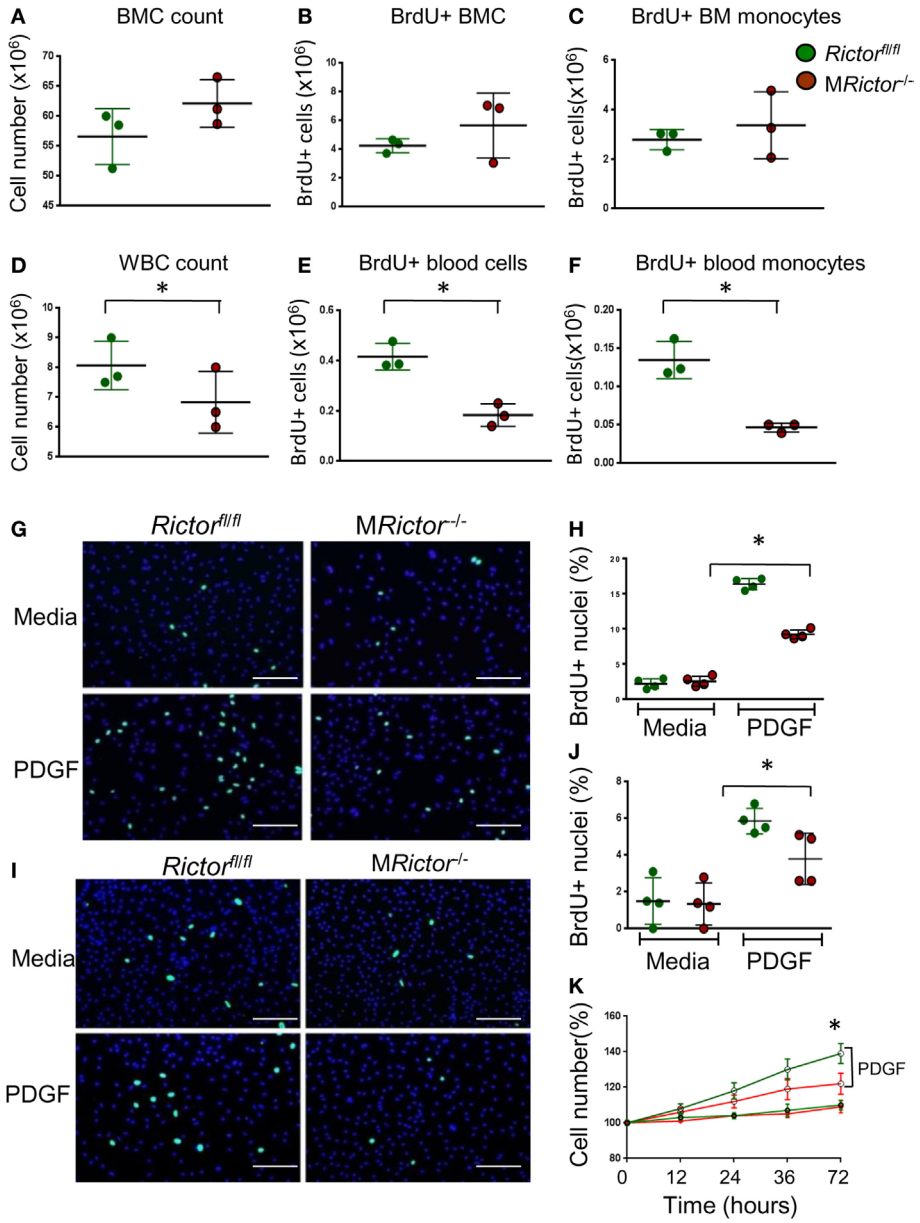

FIGURE 2 | Loss of *Rictor* suppresses proliferation of blood monocytes and macrophages. **(A–F)** BrdU (10 ml/kg) was I/P injected into *Rictor*$^{fl/fl}$ and M*Rictor*$^{-/-}$ mice, 24 h later bone marrow and blood cells were isolated and analyzed by flow cytometry. Note there were no differences in bone marrow cell count, total BrdU+ cells and BrdU+ monocytes **(A–C)**; however, white blood cell count, total BrdU+ blood cells and BrdU+ monocytes were reduced in M*Rictor*$^{-/-}$ compared to *Rictor*$^{fl/fl}$ mice. Graphs represent data (mean ± SEM) of the experiment with three mice per group (*$p < 0.05$ compared to control untreated group). **(G–J)** Blood monocytes **(G,H)** and peritoneal macrophages **(I,J)** were isolated from *Rictor*$^{fl/fl}$ and M*Rictor*$^{-/-}$ mice, and two days incubation in DMEM media containing 10% FBS (and M-CSF for monocytes) treated with or without PDGF (20 ng/ml) and BrdU overnight. The incorporation of BrdU was analyzed under a fluorescent microscopy. Note PDGF treatment significantly increased proliferation but less prominent in M*Rictor*$^{-/-}$ than in *Rictor*$^{fl/fl}$ cells. Graphs represent data (mean ± SEM) obtained from different mice ($n = 4$/group; *$p < 0.05$ *t*-test analysis compared to *Rictor*$^{fl/fl}$ cells); Scale bar is 50 mm. **(K)** WT and M*Rictor*$^{-/-}$ peritoneal macrophages were seeded in triplicate on a 48-well plate and then treated with DMEM media alone or together with PDGF (20 ng/ml) for the indicated times. The cells were counted using an EVOS FL Auto imaging System (Life Technology). Note, top two lines of the graph represent cells treated with PDGF, as indicated.

Il6, and *Il12a* than *Rictor*$^{fl/fl}$ cells (**Figures 4A–C**). At the same time, the level of *Il10 g*ene expression was significantly lower in M*Rictor*$^{-/-}$ than in *Rictor*$^{fl/fl}$ macrophages (**Figure 4D**). In addition, we demonstrated that suppression of Akt signaling with a low dose of an Akt inhibitor further increased expression of these inflammatory cytokines (**Figures 4E–J**). Importantly, genetic loss of *Raptor*, which is an essential member of mTORC1, eliminated this increase, indicating that mTORC1 is responsible for the increase of expression of inflammatory genes (**Figures 4E–J**). Thus, our results demonstrate that deletion of mTORC2 inhibits

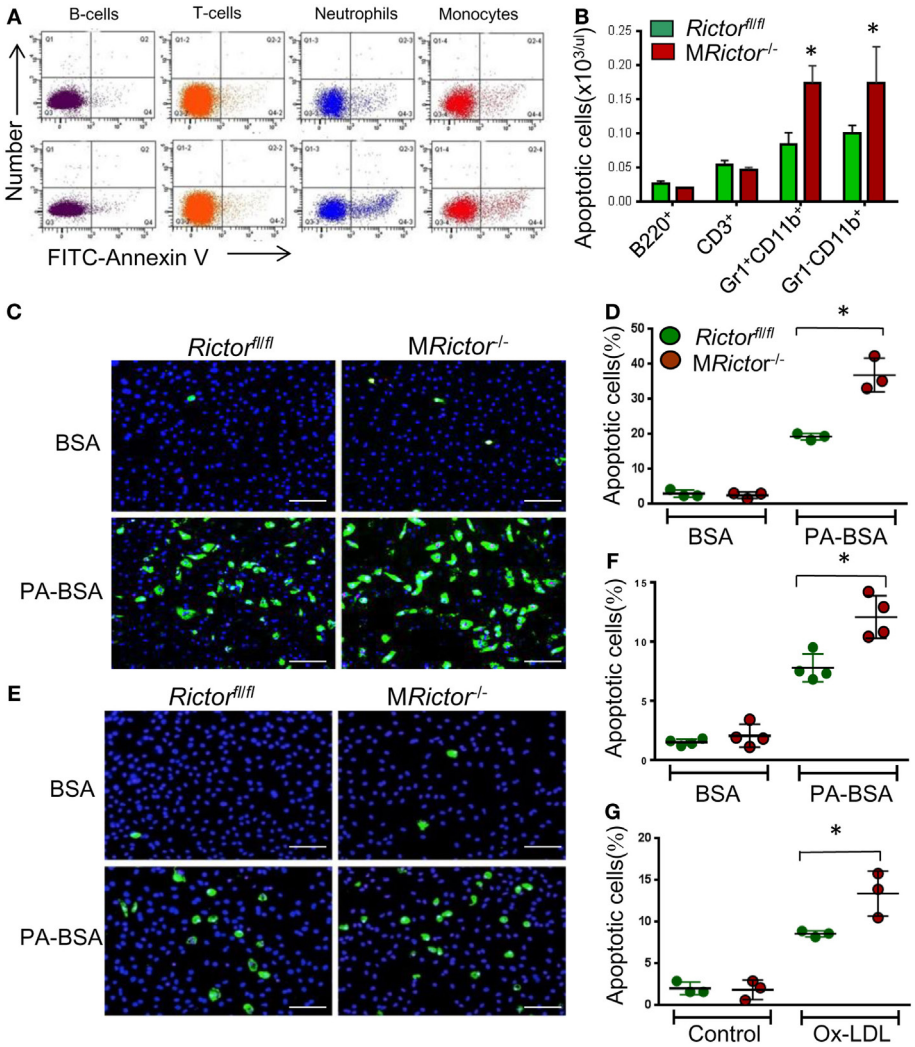

FIGURE 3 | M*Rictor*$^{-/-}$ macrophages are less resistant to different pro-apoptotic stimuli than *Rictor*$^{fl/fl}$ cells. **(A,B)** Representative flow cytometry plots of apoptotic blood cells isolated from *Rictor*$^{fl/fl}$ (top panel) and M*Rictor*$^{-/-}$ mice (bottom panel) and stained with the Alexa Fluor 488 Annexin V. Note increase of apoptosis in blood monocytes and neutrophils of M*Rictor*$^{-/-}$ mice compared to *Rictor*$^{fl/fl}$ mice. Graphs represent data (mean ± SEM) of the experiment (n = 3/group, *$p < 0.05$ t-test analysis compared to *Rictor*$^{fl/fl}$ mice). **(C,D)** Blood monocytes were isolated from *Rictor*$^{fl/fl}$ and M*Rictor*$^{-/-}$ mice (n = 3/group), incubated in DMEM media containing 10% FBS, M-CSF for 2 days, and then treated overnight with 0.3 M palmitic acid complexed to bovine serum albumin (PA-BSA) in the presence of 1% FBS and M-CSF. The Alexa Flour 488 Nalge Nunc International/dead cell apoptosis kit was used to detect apoptotic cells. Note PA-BSA treatment significantly increased apoptosis in both group of cells, more prominently in M*Rictor*$^{-/-}$ than *Rictor*$^{fl/fl}$ cells; scale bars, 50 μm. Graphs represent data (mean ± SEM; *$p < 0.05$ by Mann–Whitney rank sum test). **(E,G)** Peritoneal macrophages were isolated from *Rictor*$^{fl/fl}$ and M*Rictor*$^{-/-}$ mice (n = 4/group), and 2 days later treated with 0.5 M PA-BSA overnight **(E,F)** or human oxidized LDL (100 μg/ml) for 24 h **(G)**. Annexin V/dead cell apoptosis kit was used to detect apoptotic cells; Note PA-BSA increases apoptosis more obviously in M*Rictor*$^{-/-}$ than *Rictor*$^{fl/fl}$ macrophages; scale bars, 50 μm. Graphs represent data (mean ± SEM) of four mice/group; *$p < 0.05$ by Mann–Whitney rank sum test.

M2 polarization, and the levels of Akt signaling are important in this process.

Loss of Rictor in Hematopoietic Cells Reduces Early Atherosclerosis in Female and Male *Ldlr*$^{-/-}$ Mice

To evaluate whether loss of mTORC2 signaling in macrophages has an impact on atherosclerosis *in vivo*, we generated female and male chimeric *Ldlr*$^{-/-}$ mice with M*Rictor*$^{-/-}$ or *Rictor*$^{fl/fl}$ hematopoietic cells using bone marrow transplantation (35). In the first experiment, 19-week-old female *Ldlr*$^{-/-}$ mice were lethally irradiated and transplanted with female *Rictor*$^{fl/fl}$ ($n = 10$) or M*Rictor*$^{-/-}$($n = 9$) bone marrow cells. After 4 weeks, the recipient mice were fed with the Western-type diet for 10 weeks. There were no statistically significant differences in BW, serum total cholesterol or TG levels between the groups (**Table 1**). However, the recipients of M*Rictor*$^{-/-}$ bone marrow cells had 32% smaller atherosclerotic lesions in the *en face* analysis compared to mice reconstituted with *Rictor*$^{fl/fl}$ marrow cells (**Figures 5A,C**).

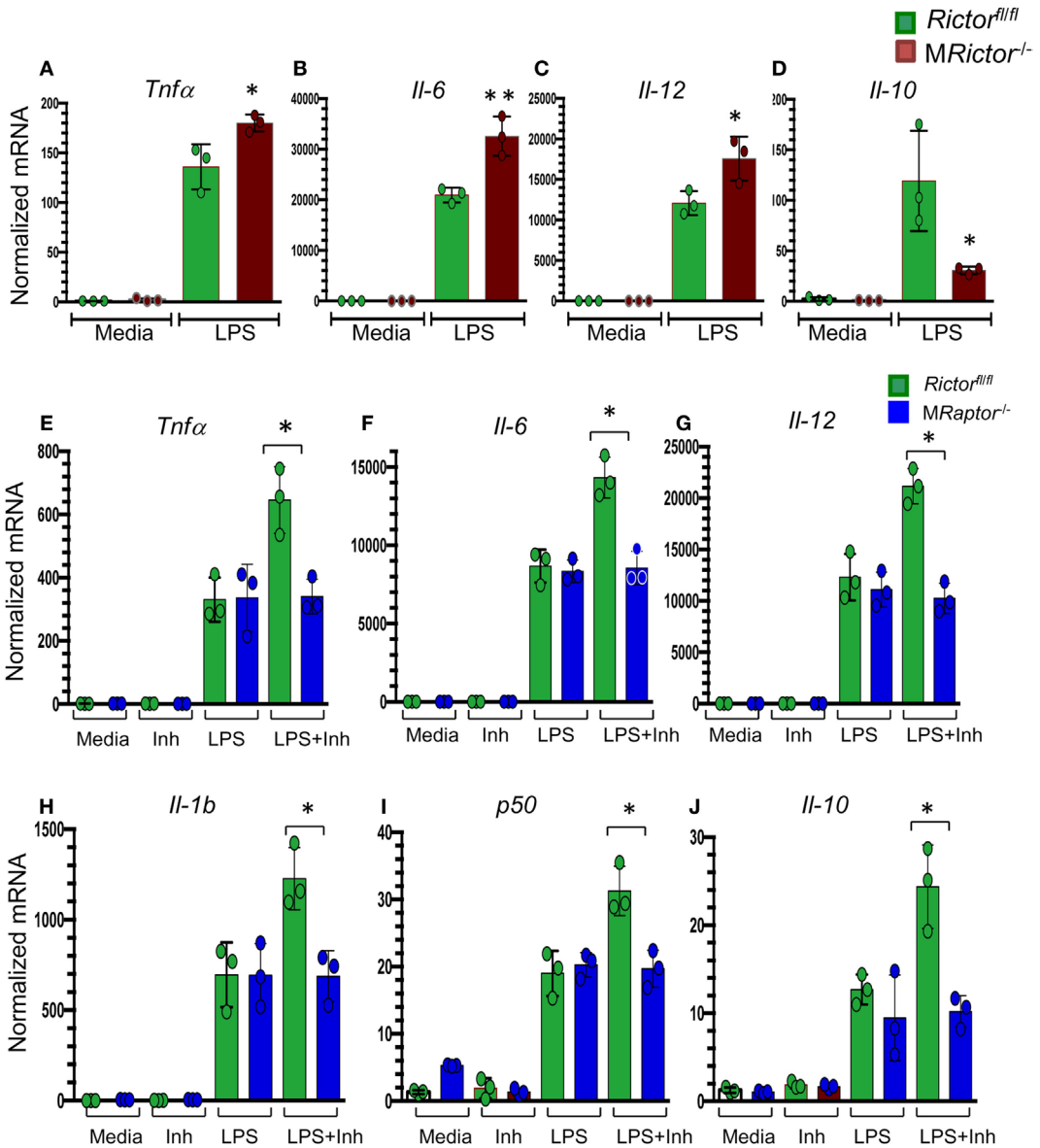

FIGURE 4 | M*Rictor*$^{-/-}$ macrophages have increased levels of inflammatory gene expression in response to lipopolysaccharide (LPS) and a low dose of Akt inhibitor increases the LPS-induced expression of inflammatory genes in *Rictor*$^{fl/fl}$ but not in M*Raptor*$^{-/-}$ macrophages. **(A–D)** Peritoneal macrophages were incubated with media alone (control) or together with LPS (20 ng/ml) for 5 h and the gene-expression levels were measured by real-time polymerase chain reaction. Note M*Rictor*$^{-/-}$ macrophages have increased pro-inflammatory and decreased of interleukin-10 gene expression. Graphs represent data (mean ± SEM) obtained from the same numbers ($n = 3$ per group) of mice (*$p < 0.05$ and **$p < 0.001$ compared to *Rictor*$^{fl/fl}$ cells treated with LPS by *t*-test). **(E–J)** Peritoneal macrophages were isolated from *Rictor*$^{fl/fl}$ and M*Raptor*$^{-/-}$ mice and 2 days later were treated with media (Control), with the Akt inhibitor IV (31 μM, Inh) or LPS (20 ng/ml) alone or together with the inhibitor (LPS + Inh) for 5 h at 37°C and the gene-expression levels were measured by real-time polymerase chain reaction. Note a low dose of the Akt inhibitor increases LPS-mediated inflammatory gene expression but loss of Raptor reverses the increase. Graphs represent data (mean ± SEM) obtained from the same numbers ($n = 3$ per group) of mice (*$p < 0.05$ and **$p < 0.001$ compared to WT cells treated with LPS by *t*-test test).

Similarly, M*Rictor*$^{-/-}$ → *Ldlr*$^{-/-}$ mice had 28% smaller atherosclerotic lesions in the cross sections of aortic sinus compared to control mice with *Rictor*$^{fl/fl}$ marrow (**Figures 5B,D**). The lesions of M*Rictor*$^{-/-}$ → *Ldlr*$^{-/-}$ mice had a smaller macrophage area stained with antibody to CD68 than lesions of *Rictor*$^{fl/fl}$ → *Ldlr*$^{-/-}$ mice (**Figure 5E**). Remarkably, M*Rictor*$^{-/-}$ → *Ldlr*$^{-/-}$ mice had significantly more TUNEL-positive cells in atherosclerotic lesions than control *Rictor*$^{fl/fl}$ → *Ldlr*$^{-/-}$ mice (**Figure 5F**). Thus, loss of mTORC2 signaling in hematopoietic cells significantly increases macrophage apoptosis in atherosclerotic lesions and this reduces the extent of atherosclerosis in *Rictor*$^{fl/fl}$ → *Ldlr*$^{-/-}$ mice.

In a second experiment, 12-week-old male *Ldlr*$^{-/-}$ mice were lethally irradiated and transplanted with male *Rictor*$^{fl/fl}$ (control group; $n = 10$) or M*Rictor*$^{-/-}$($n = 10$) bone marrow

TABLE 1 | Body weight (BW), blood glucose (BG), total serum cholesterol (TC), and triglyceride (TG) levels in *Ldlr*$^{-/-}$ mice reconstituted with female (A) and male (B) *Rictor*$^{fl/fl}$ and M*Rictor*$^{-/-}$ bone marrow cells after 10 weeks of the Western diet.

Recipient mice	BW (g)	BG (mg/dL)	TC (mg/dL)	TG (mg/dL)
(A) Females				
Rictor$^{fl/fl}$ (n = 10)	22.7 ± 0.7	163.5 ± 4.4	935 ± 33	203 ± 17
M*Rictor*$^{-/-}$ (n = 10)	22.2 ± 0.9	156.2 ± 5.0	949 ± 52	187 ± 18
p	0.91	0.21	0.87	0.90
(B) Males				
Rictor$^{fl/fl}$ (n = 10)	23.4 ± 0.2	139.7 ± 4.7	750 ± 38	158 ± 28
M*Rictor*$^{-/-}$ (n = 9)	22.6 ± 0.6	151.1 ± 9.9	714 ± 22	131 ± 19
p	0.73	0.58	0.41	0.59

Values are (Mean ± SEM). The number of recipient mice in each group is indicated by n. p = the differences are not statistically significant between the groups.

cells. Again, after 10 weeks on the Western diet, there were no statistically significant differences in BW, blood glucose and serum lipids between these two groups of recipients (**Table 1**). In contrast, M*Rictor*$^{-/-}$ → *Ldlr*$^{-/-}$ male recipients had 40% smaller atherosclerotic lesions in pinned out aortas en face than control male *Rictor*$^{fl/fl}$ → *Ldlr*$^{-/-}$ mice (**Figures 6A–C**). Furthermore, M*Rictor*$^{-/-}$ → *Ldlr*$^{-/-}$ mice also had significantly decreased atherosclerosis in the aortic sinus (42%), a smaller CD68 + macrophage area and more TUNEL-positive cells in the atherosclerotic lesions than lesions of control male *Rictor*$^{fl/fl}$ → *Ldlr*$^{-/-}$ recipients (**Figures 6D–F**). These results demonstrate that loss of mTORC2 in hematopoietic cells of both female and male recipients significantly increases macrophage apoptosis and diminishes atherosclerosis.

DISCUSSION

The mTOR pathway plays a central role in sensing environmental cues and regulating cell growth, metabolism (8) and immune responses (3, 4). However, the roles of mTORC2 signaling in monocyte/macrophage proliferation and survival, and in atherogenesis remain unclear. Here we generated myeloid lineage-specific *Rictor* deletion in mice to demonstrate for the first time that mTORC2 signaling is crucial for proliferation and survival of monocytes and macrophages. Rictor deficiency prevents mTORC2 assembly and this causes a dramatic reduction of insulin-mediated Akt S^{473} phosphorylation in macrophages. In addition, suppression of Akt signaling was observed in monocytes and neutrophils of M*Rictor*$^{-/-}$ mice *in vivo*. Ablation of mTORC2 signaling inhibited monocyte and macrophage proliferation. Furthermore, *Rictor* deficiency compromised monocyte and macrophage viability, and these dramatic changes in monocyte/macrophage survival were associated with dramatic reductions of atherosclerosis in male and female *Ldlr*$^{-/-}$ mice *in vivo*.

Mammalian target of rapamycin complex 2 regulates cellular metabolism and previous studies have shown that cell-specific *Rictor* ablation significantly suppresses proliferation of endothelial cells (26), helper T-cells (44) and pancreatic β-cells (20). Our results are consistent with these data and indicate that loss of *Rictor* in monocytes and macrophages suppresses their proliferation causing a diminished response to a proliferative factor, PDGF. Surprisingly, Oh and co-workers (45) recently reported that mTORC2 ablation increased proliferation in peritoneal resident macrophages compared to wild-type cells. This discrepancy with our results may be explained by the fact that we analyzed peritoneal macrophages originating predominantly from monocytes, whereas they focused on tissue-resident peritoneal macrophages. The tissue-resident peritoneal macrophages express F4/80 and GATA6 transcription factor, and they presumably originated from the yolk sac (46). In our experiment, only a small fraction (5%) of peritoneal macrophages expressed F4/80 after two days in culture. Moreover, the same group also showed that *Rictor* null monocyte-derived peritoneal macrophages have less proliferation than wild-type cells (45) and this finding is consistent with our results.

Although loss of Rictor in macrophages appears to only modestly affect basal Akt activity, a fact that has been noted previously in several different types of cells (16, 18, 20, 23), the response to insulin was significantly suppressed in M*Rictor*$^{-/-}$ compared to *Rictor*$^{fl/fl}$ macrophages (**Figures 1A–C**). Moreover, there was an increase in apoptotic monocytes and neutrophils in blood of M*Rictor*$^{-/-}$ mice (**Figures 3A,B**). More importantly, our *in vitro* experiments convincingly demonstrated that M*Rictor*$^{-/-}$ monocytes and macrophages exhibit compromised viability and generate more apoptosis under conditions of ER stress than *Rictor*$^{fl/fl}$ cells (**Figures 3C–F**). These data support the idea that mTORC2 with Akt S^{473} phosphorylation are essential for pro-survival signaling (6) and that the failure of this response under conditions of ER stress leads to early apoptosis. Previously we have shown that *IKK*α$^{-/-}$ macrophages exhibited a similar defect in Akt S^{473} phosphorylation and a related increase of apoptosis (30). It is known that IKKα interacts with Rictor and that chemical inhibition or genetic suppression of IKK significantly diminishes mTORC2 activity and Akt signaling (47). Low levels of white blood cells and reduced proliferation of macrophages have been associated with reduced atherosclerosis. Interestingly, proliferation of macrophages in the artery wall has been reported to be an important determinant of atherogenesis (48). Our current findings establish that M*Rictor*$^{-/-}$ mice exhibited relatively low levels of white blood cells, and this is due, at least in part, to decreased proliferation and compromised viability of both monocytes and neutrophils. Furthermore, we cannot exclude the possibility that MRictor$^{-/-}$ neutrophils or monocytes may have an inefficient or delayed response for mobilization from the bone marrow. It remains unclear whether the reduced numbers of T- and B-cells in the blood of M*Rictor*$^{-/-}$ mice are causally related to the reduced numbers or functions of myeloid cells.

Macrophages may be polarized into two distinct subtypes including classically activated M1 and alternatively stimulated M2 macrophages (49, 50). A recent concept of the immune response proposes that Akt-mTORC1 signaling controls polarization by changing metabolism of macrophages (5, 51, 52). For example, LPS treatment induces a switch to high aerobic glycolysis, fatty acid synthesis and a truncated citric acid cycle (the Krebs cycle) to form the M1 pro-inflammatory phenotype. In contrast, IL-4 induces oxidative phosphorylation to generate M2 macrophages for tissue remodeling, immunosuppression and phagocytosis. Both of these shifts generate many metabolites that are acting as signaling molecules with

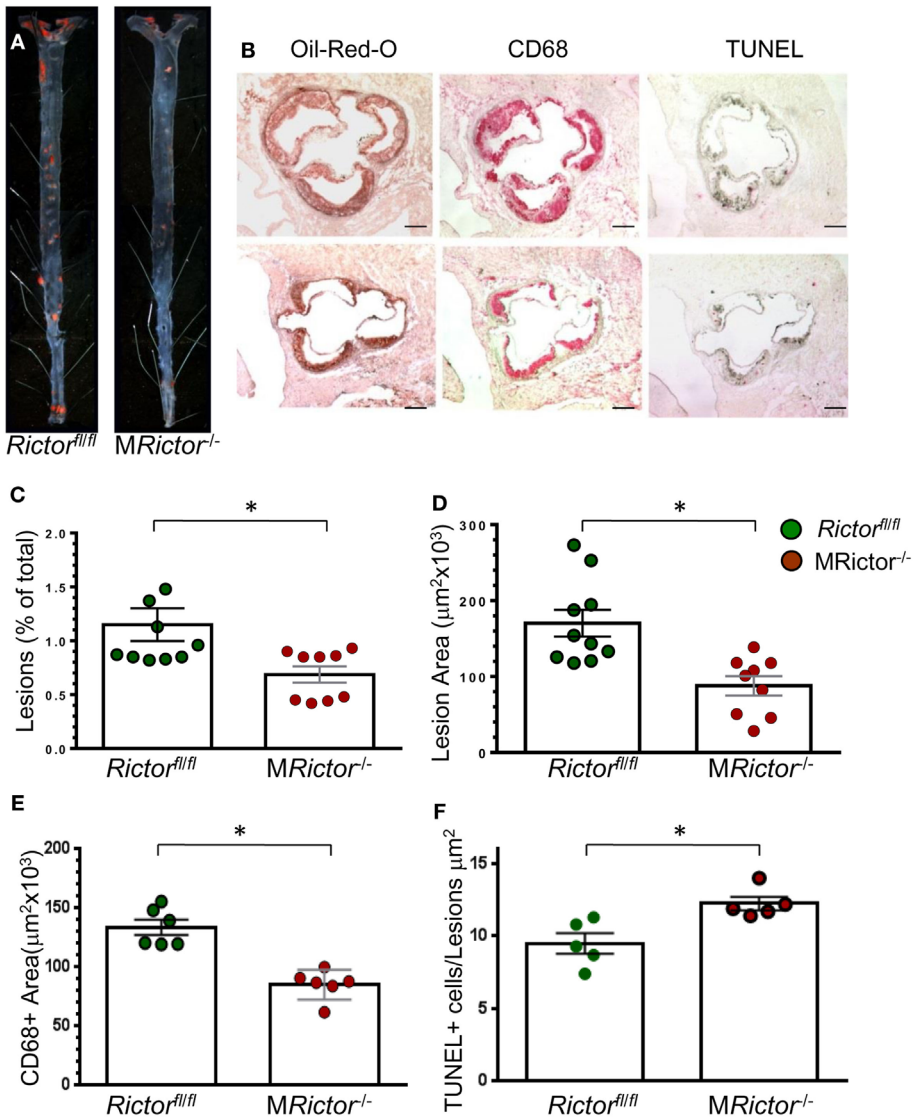

FIGURE 5 | Female M*Rictor*$^{-/-}$ → *Ldlr*$^{-/-}$ mice had smaller atherosclerotic lesions, less macrophage area and more apoptotic cells in the lesions than control *Rictor*$^{fl/fl}$ → *Ldlr*$^{-/-}$ mice. **(A)** Representative images of and Sudan IV-stained en face preparation of aortas and **(B)** and serial cross sections of aortic sinus stained with Oil-Red-O/hematoxylin, CD68 and TUNEL AP from *Rictor*$^{fl/fl}$ → *Ldlr*$^{-/-}$ mice (B, top panel) and M*Rictor*$^{-/-}$ → *Ldlr*$^{-/-}$ mice (B, bottom panel) mice. Scale bars, 200 μm. **(C,D)** Quantitation of atherosclerotic lesions in aortas en face and cross sections of aortic sinus of *Rictor*$^{fl/fl}$ → *Ldlr*$^{-/-}$ and M*Rictor*$^{-/-}$ → *Ldlr*$^{-/-}$ bone marrow cells; *$p < 0.05$ by Mann–Whitney rank sum test. **(E,F)** Macrophage area stained with CD68 and number of TUNEL + cells in atherosclerotic lesions of mice reconstituted with WT or M*Rictor*$^{-/-}$ bone marrow cells; *$p < 0.05$ by *t*-test.

consequent alteration of the downstream immune response. In this context, mTORC1 is considered as a major mediator of the cellular response to stress (53). Loss of tuberous sclerosis 1 leads to constitutive mTORC1 activation in macrophages making them resistant to M2 polarization and producing an increased inflammatory response (54). Accordingly, *Raptor* deficiency in macrophages reduced chemokine gene expression (55) and loss of mTORC1 in hematopoietic cells impaired myelopoiesis at steady state with dampening of some innate immune responses (56). Thus, Akt-mTORC1 signaling is coupled to metabolic input to regulate a key enzyme of Acetyl-CoA synthesis, leading to increased histone acetylation and induction of a subset of M2 genes in macrophages (57).

Compared to mTORC1, our understanding of the role of mTORC2 in macrophage polarization is less well defined. Brown and co-workers (58) were the first to demonstrate that mTORC2 negatively regulates the Toll-like receptor 4-mediated inflammatory response acting via Forkhead box protein O1, a transcription factor regulating glucose metabolism. Festuccia and co-authors later reported that *Rictor* deletion induces M1 macrophage polarization potentiating pro-inflammatory responses (41). More recent studies revealed that loss of *Rictor* inhibits the generation

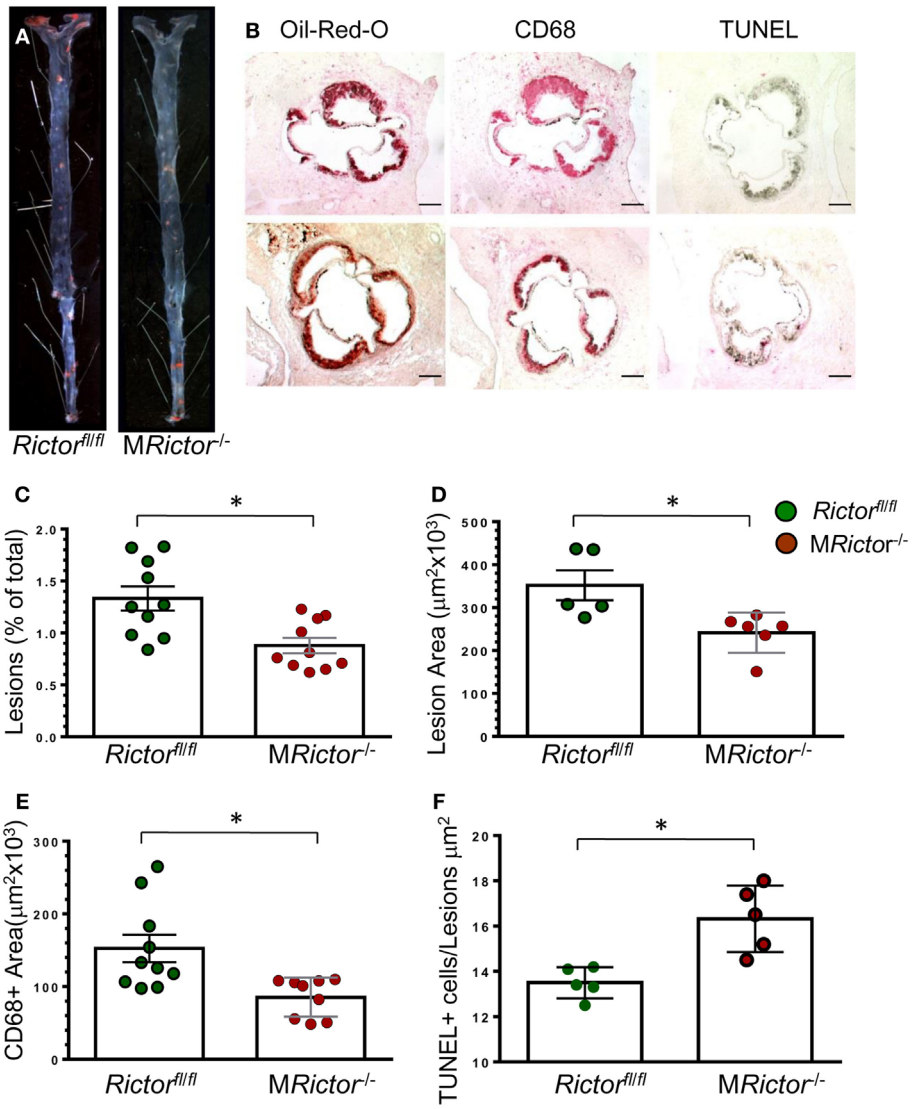

FIGURE 6 | Male M*Rictor*$^{-/-}$ → *Ldlr*$^{-/-}$ mice had less atherosclerosis, smaller macrophage area and more apoptotic cells in the lesion area than control *Rictor*$^{fl/fl}$ → *Ldlr*$^{-/-}$ mice. **(A)** Representative images of and Sudan IV-stained en face preparation of aortas and **(B)** serial cross sections of aortic sinus stained with Oil-Red-O/hematoxylin, CD68 and TUNEL AP from *Rictor*$^{fl/fl}$ → *Ldlr*$^{-/-}$ [**(B)** top panel] and M*Rictor*$^{-/-}$ → *Ldlr*$^{-/-}$ [**(B)** bottom panel] mice. Scale bars, 200 μm. **(C,D)** Quantitation of atherosclerotic lesions in aortas en face and cross sections of aortic sinus of *Rictor*$^{fl/fl}$ → *Ldlr*$^{-/-}$ and M*Rictor*$^{-/-}$ → *Ldlr*$^{-/-}$ mice; *$p < 0.05$ by Mann–Whitney rank sum test. **(E,F)** Macrophage area stained with MOMA-2 and number of TUNEL + cells in atherosclerotic lesions of mice reconstituted with *Rictor*$^{fl/fl}$ or M*Rictor*$^{-/-}$ bone marrow cells; *$p < 0.05$ by *t*-test.

of M2 macrophages while preserving the production of classically activated M1 cells (42). Furthermore, mTORC2 operates in parallel with the STAT6 pathway to facilitate increased glycolysis during M2 activation (43).

Depending on the degree of activation, PI3K-Akt signaling crucially contributes to macrophage polarization with subsequent activation or dampening the immune response (59). The individual Akt isoforms promote distinct polarization phenotypes in macrophages. For example, macrophage *Akt1* ablation induces M1, whereas *Akt2* deficiency promotes the M2 phenotype (60). Recently we have shown that *Akt2*$^{-/-}$ macrophages express significantly lower levels of inflammatory genes and display the M2 phenotype with a suppressed ability for M1 polarization and CCR2 induction (61). In addition to the ratio of Akt1/Akt2 isoforms, the levels of Akt signaling are also crucial for macrophage polarization. For example, overexpression of the PI3K-Akt pathway caused by myeloid cell-specific deficiency of SH2-containing inositol phosphatase or phosphatase and tensin homolog (PTEN), which are negative regulators of PI3K signaling, significantly promote M2 macrophage differentiation decreasing inflammatory cytokine production in macrophages (62–64). In contrast, genetic deficiency of *IKK*α as well as pharmacologic inhibition of IKK, significantly reduces Akt S^{473} phosphorylation via suppression of mTORC2 signaling, and

this is accompanied by an M1-related increase in the expression of inflammatory genes (30). Our current results are consistent with these data and indicate that suppression of Akt signaling increases of inflammatory gene expression in M*Rictor*$^{-/-}$ macrophages. Moreover, further suppression of signaling with a low dose of Akt inhibitor IV additionally increased cytokine gene expression levels. Importantly, the genetic loss of Raptor, the main component of mTORC1, eliminated this increase, indicating that mTORC1 mediates the increased expression of these pro-inflammatory genes. Together these data support the concept that the PI3K-Akt-mTOR pathway is critical for restriction of the inflammatory reaction and that overexpression of this signaling pathway reduces macrophage activation by LPS, whereas the inhibition of Akt signaling significantly augments NF-κB activity (65). Furthermore our results suggest an opportunity to pharmacologically control Akt signaling activity and polarization of macrophages in order to modulate innate or adaptive immune responses.

Atherosclerosis remains the number one cause of death and disability in modern societies. Surprisingly, relatively little is known about the role of mTORC2 in atherosclerosis. One can propose mechanisms by which loss of mTORC2 might promote atherosclerosis, including increased inflammatory cytokines in response to LPS or increased production of damage-associated molecular patterns; whereas reduced proliferation and increased apoptosis of macrophages would be predicted to reduce the extent of early atherosclerosis. Therefore, we examined the impact of mTORC2 elimination in hematopoietic myeloid cells on atherosclerosis *in vivo*. M*Rictor*$^{-/-}$ → *Ldlr*$^{-/-}$ recipients had smaller atherosclerotic lesions enriched in apoptotic cells compared to *Rictor*$^{fl/fl}$ → *Ldlr*$^{-/-}$ mice. Thus, loss of *Rictor* in hematopoietic myeloid cells significantly suppressed atherosclerosis in *Ldlr*$^{-/-}$ mice, and these results demonstrate for the first time that macrophage mTORC2 plays a critical role of in atherogenesis. The reduction of atherosclerotic lesions was likely mediated through several inter-related mechanisms such as the inhibition of proliferation and suppression of viability of monocytes that cause monocytopenia in M*Rictor*$^{-/-}$ → *Ldlr*$^{-/-}$ mice. In addition, we found decreased proliferation and viability of M*Rictor*$^{-/-}$ macrophages, which are the major type of cells atherosclerotic lesions. These results are consistent with the current concepts that low numbers of circulating monocytes and high sensitivity of macrophages to pro-apoptotic stimuli are key drivers that suppress atherogenesis (66, 67). Our study also suggests a potential role of targeted inhibition of mTORC2 in monocytes and macrophages as a novel approach for the treatment of atherosclerotic cardiovascular disease.

AUTHOR CONTRIBUTIONS

VB. designed and performed experiments, analyzed data, and wrote the manuscript; JH, LD, and YZ performed experiments and analyzed data; JM critically revised the manuscript; and ML supervised the project, designed the studies, analyzed data, and revised the manuscript.

ACKNOWLEDGMENTS

The authors are grateful to Catherine E. Alford (Veterans Administration Medical Center, Nashville TN, USA) for help with flow cytometry.

FUNDING

This work was supported by National Institutes of Health grants HL105375, HL116263, DK50435, DK59637 (Lipid, Lipoprotein, and Atherosclerosis Core of the Vanderbilt Mouse Metabolic Phenotype Centers).

REFERENCES

1. Linton MF, Yancey PG, Davies SS, Jerome WGJ, Linton EF, Vickers KC. The role of lipids and lipoproteins in atherosclerosis. In: De Groot LJ, Chrousos G, Dungan K, Feingold KR, Grossman A, Hershman JM, et al., editors. *Endotext* [Internet]. South Dartmouth (MA): MDTextcom, Inc. (2000). p. 1–92. Available from: https://www.ncbi.nlm.nih.gov/books/NBK343489/
2. Sharma P, Allison JP. The future of immune checkpoint therapy. *Science* (2015) 348:56–61. doi:10.1126/science.aaa8172
3. Powell JD, Pollizzi KN, Heikamp EB, Horton MR. Regulation of immune responses by mTOR. *Annu Rev Immunol* (2012) 30:39–68. doi:10.1146/annurev-immunol-020711-075024
4. Weichhart T, Hengstschlager M, Linke M. Regulation of innate immune cell function by mTOR. *Nat Rev Immunol* (2015) 15:599–614. doi:10.1038/nri3901
5. Bettencourt IA, Powell JD. Targeting metabolism as a novel therapeutic approach to autoimmunity, inflammation, and transplantation. *J Immunol* (2017) 198:999–1005. doi:10.4049/jimmunol.1601318
6. Duronio V. The life of a cell: apoptosis regulation by the PI3K/PKB pathway. *Biochem J* (2008) 415:333–44. doi:10.1042/BJ20081056
7. Manning BD, Toker A. AKT/PKB signaling: navigating the network. *Cell* (2017) 169:381–405. doi:10.1016/j.cell.2017.04.001
8. Saxton RA, Sabatini DM. mTOR signaling in growth, metabolism, and disease. *Cell* (2017) 169:361–71. doi:10.1016/j.cell.2017.03.035
9. Laplante M, Sabatini David M. mTOR signaling in growth control and disease. *Cell* (2012) 149:274–93. doi:10.1016/j.cell.2012.03.017
10. Kurdi A, De Meyer GRY, Martinet W. Potential therapeutic effects of mTOR inhibition in atherosclerosis. *Br J Clin Pharmacol* (2016) 82:1267–79. doi:10.1111/bcp.12820
11. Guertin DA, Stevens DM, Thoreen CC, Burds AA, Kalaany NY, Moffat J, et al. Ablation in mice of the mTORC components raptor, Rictor, or mLST8 reveals that mTORC2 is required for signaling to Akt-FOXO and PKCα, but Not S6K1. *Dev Cell* (2006) 11:859–71. doi:10.1016/j.devcel.2006.10.007
12. Shiota C, Woo J-T, Lindner J, Shelton KD, Magnuson MA. Multiallelic disruption of the Rictor gene in mice reveals that mTOR complex 2 is essential for fetal growth and viability. *Dev Cell* (2006) 11:583–9. doi:10.1016/j.devcel.2006.08.013
13. Hagiwara A, Cornu M, Cybulski N, Polak P, Betz C, Trapani F, et al. Hepatic mTORC2 activates glycolysis and lipogenesis through Akt, Glucokinase, and SREBP1c. *Cell Metab* (2012) 15:725–38. doi:10.1016/j.cmet.2012.03.015
14. Yuan M, Pino E, Wu L, Kacergis M, Soukas AA. Identification of Akt-independent regulation of hepatic lipogenesis by mammalian target of rapamycin (mTOR) complex 2. *J Biol Chem* (2012) 287:29579–88. doi:10.1074/jbc.M112.386854
15. Lamming DW, Mihaylova MM, Katajisto P, Baar EL, Yilmaz OH, Hutchins AG, et al. Depletion of Rictor, an essential protein component of mTORC2, decreases male lifespan. *Aging Cell* (2014) 13:911–7. doi:10.1111/acel.12256
16. Kumar A, Harris TE, Keller SR, Choi KM, Magnuson MA, Lawrence JC. Muscle-specific deletion of Rictor impairs insulin-stimulated glucose transport and enhances basal glycogen synthase activity. *Mol Cell Biol* (2008) 28:61–70. doi:10.1128/MCB.01405-07

17. Sciarretta S, Zhai P, Maejima Y, Del Re Dominic P, Nagarajan N, Yee D, et al. mTORC2 regulates cardiac response to stress by inhibiting MST1. *Cell Rep* (2015) 11:125–36. doi:10.1016/j.celrep.2015.03.010
18. Cybulski N, Polak P, Auwerx J, Rüegg MA, Hall MN. mTOR complex 2 in adipose tissue negatively controls whole-body growth. *Proc Natl Acad Sci U S A* (2009) 106:9902–7. doi:10.1073/pnas.0811321106
19. Kumar A, Lawrence JC, Jung DY, Ko HJ, Keller SR, Kim JK, et al. E: fat cell–specific ablation of Rictor in mice impairs insulin-regulated fat cell and whole-body glucose and lipid metabolism. *Diabetes* (2010) 59:1397–406. doi:10.2337/db09-1061
20. Gu Y, Lindner J, Kumar A, Yuan W, Magnuson MA. Rictor/mTORC2 is essential for maintaining a balance between β-cell proliferation and cell size. *Diabetes* (2011) 60:827–37. doi:10.2337/db10-1194
21. Sarbassov DD, Guertin DA, Ali SM, Sabatini DM. Phosphorylation and regulation of Akt/PKB by the Rictor-mTOR complex. *Science* (2005) 307:1098–101. doi:10.1126/science.1106148
22. Hung C-M, Calejman CM, Sanchez-Gurmaches J, Li H, Clish CB, Hettmer S, et al. Rictor/mTORC2 loss in the Myf5 lineage reprograms brown fat metabolism and protects mice against obesity and metabolic disease. *Cell Rep* (2014) 8:256–71. doi:10.1016/j.celrep.2014.06.007
23. Bentzinger CF, Romanino K, Cloëtta D, Lin S, Mascarenhas JB, Oliveri F, et al. Skeletal muscle-specific ablation of raptor, but not of Rictor, causes metabolic changes and results in muscle dystrophy. *Cell Metab* (2008) 8:411–24. doi:10.1016/j.cmet.2008.10.002
24. Tassone B, Saoncella S, Neri F, Ala U, Brusa D, Magnuson MA, et al. Rictor/mTORC2 deficiency enhances keratinocyte stress tolerance via mitohormesis. *Cell Death Differ* (2017) 24:731–46. doi:10.1038/cdd.2017.8
25. Goncharov DA, Kudryashova TV, Ziai H, Ihida-Stansbury K, DeLisser H, Krymskaya VP, et al. mTORC2 coordinates pulmonary artery smooth muscle cell metabolism, proliferation and survival in pulmonary arterial hypertension. *Circulation* (2014) 129:864–74. doi:10.1161/CIRCULATIONAHA.113.004581
26. Wang S, Amato KR, Song W, Youngblood V, Lee K, Boothby M, et al. Regulation of endothelial cell proliferation and vascular assembly through distinct mTORC2 signaling pathways. *Mol Cell Biol* (2015) 35:1299–313. doi:10.1128/MCB.00306-14
27. Carr TD, Feehan RP, Hall MN, Rüegg MA, Shantz LM. Conditional disruption of Rictor demonstrates a direct requirement for mTORC2 in skin tumor development and continued growth of established tumors. *Carcinogenesis* (2015) 36:487–97. doi:10.1093/carcin/bgv012
28. Völkers M, Konstandin MH, Doroudgar S, Toko H, Quijada P, Din S, et al. Mechanistic target of rapamycin complex 2 protects the heart from ischemic damage. *Circulation* (2013) 128:2132–44. doi:10.1161/CIRCULATIONAHA.113.003638
29. Zou Z, Chen J, Liu A, Zhou X, Song Q, Jia C, et al. mTORC2 promotes cell survival through c-Myc-dependent up-regulation of E2F1. *J Cell Biol* (2015) 211:105–22. doi:10.1083/jcb.201411128
30. Babaev VR, Ding L, Zhang Y, May JM, Lin PC, Fazio S, et al. Macrophage IKKα deficiency suppresses Akt phosphorylation, reduces cell survival, and decreases early atherosclerosis. *Arterioscler Thromb Vasc Biol* (2016) 36:598–607. doi:10.1161/ATVBAHA.115.306931
31. Lawrence T, Bebien M, Liu GY, Nizet V, Karin M. IKK[alpha] limits macrophage NF-[kappa]B activation and contributes to the resolution of inflammation. *Nature* (2005) 434:1138–43. doi:10.1038/nature03491
32. Magee JA, Ikenoue T, Nakada D, Lee JY, Guan K-L, Morrison SJ. Temporal changes in PTEN and mTORC2 regulation of hematopoietic stem cell self-renewal and leukemia suppression. *Cell Stem Cell* (2012) 11:415–28. doi:10.1016/j.stem.2012.05.026
33. Clausen BE, Burkhardt C, Reith W, Renkawitz R, Forster I. Conditional gene targeting in macrophages and granulocytes using LysMcre mice. *Transgenic Res* (1999) 8:265–77. doi:10.1023/A:1008942828960
34. Peterson T, Sengupta S, Harris T, Carmack A, Kang S, Balderas E, et al. mTOR complex 1 regulates lipin 1 localization to control the SREBP pathway. *Cell* (2011) 146:408–20. doi:10.1016/j.cell.2011.06.034
35. Linton MF, Atkinson JB, Fazio S. Prevention of atherosclerosis in apolipoprotein E-deficient mice by bone marrow transplantation. *Science* (1995) 267:1034–7. doi:10.1126/science.7863332
36. Krutzik PO, Trejo A, Schulz KR, Nolan GP. Phospho flow cytometry methods for the analysis of kinase signaling in Cell lines and primary human blood samples. In: Hawley TS, Hawley RG, editors. *Flow Cytometry Protocols*. Totowa, NJ: Humana Press (2011). p. 179–202.
37. Babaev VR, Chew JD, Ding L, Davis S, Breyer MD, Breyer RM, et al. Macrophage EP4 deficiency increases apoptosis and suppresses early atherosclerosis. *Cell Metab* (2008) 8:492–501. doi:10.1016/j.cmet.2008.09.005
38. Oh WJ, Jacinto E. mTOR complex 2 signaling and functions. *Cell Cycle* (2011) 10:2305–16. doi:10.4161/cc.10.14.16586
39. Sieweke MH, Allen JE. Beyond stem cells: self-renewal of differentiated macrophages. *Science* (2013) 342:1242974. doi:10.1126/science.1242974
40. Borradaile NM, Han X, Harp JD, Gale SE, Ory DS, Schaffer JE. Disruption of endoplasmic reticulum structure and integrity in lipotoxic cell death. *J Lipid Res* (2006) 47:2726–37. doi:10.1194/jlr.M600299-JLR200
41. Festuccia WT, Pouliot P, Bakan I, Sabatini DM, Laplante M. Myeloid-specific Rictor deletion induces M1 macrophage polarization and potentiates in vivo pro-inflammatory response to lipopolysaccharide. *PLoS One* (2014) 9:e95432. doi:10.1371/journal.pone.0095432
42. Hallowell RW, Collins SL, Craig JM, Zhang Y, Oh M, Illei PB, et al. mTORC2 signalling regulates M2 macrophage differentiation in response to helminth infection and adaptive thermogenesis. *Nat Commun* (2017) 8:14208. doi:10.1038/ncomms14208
43. Huang Stanley C-C, Smith Amber M, Everts B, Colonna M, Pearce Erika L, Schilling Joel D, et al. Metabolic reprogramming mediated by the mTORC2-IRF4 signaling axis is essential for macrophage alternative activation. *Immunity* (2016) 45:817–30. doi:10.1016/j.immuni.2016.09.016
44. Van de Velde L-A, Murray PJ. Proliferating helper T cells require Rictor/mTORC2 complex to integrate signals from limiting environmental amino acids. *J Biol Chem* (2016) 291:25815–22. doi:10.1074/jbc.C116.763623
45. Oh M-H, Collins SL, Sun I-H, Tam AJ, Patel CH, Arwood ML, et al. mTORC2 signaling selectively regulates the generation and function of tissue-resident peritoneal macrophages. *Cell Rep* (2017) 20:2439–54. doi:10.1016/j.celrep.2017.08.046
46. Rosas M, Davies LC, Giles PJ, Liao C-T, Kharfan B, Stone TC, et al. The transcription factor Gata6 links tissue macrophage phenotype and proliferative renewal. *Science* (2014) 344:645–8. doi:10.1126/science.1251414
47. Xu Y, Lai E, Liu J, Lin J, Yang C, Jia C, et al. IKK interacts with Rictor and regulates mTORC2. *Cell Signal* (2013) 25:2239–45. doi:10.1016/j.cellsig.2013.07.008
48. Robbins CS, Hilgendorf I, Weber GF, Theurl I, Iwamoto Y, Figueiredo J-L, et al. Local proliferation dominates lesional macrophage accumulation in atherosclerosis. *Nat Med* (2013) 19:1166–72. doi:10.1038/nm.3258
49. Gordon S, Martinez FO. Alternative activation of macrophages: mechanism and functions. *Immunity* (2010) 32:593–604. doi:10.1016/j.immuni.2010.05.007
50. Mantovani A, Garlanda C, Locati M. Macrophage diversity and polarization in atherosclerosis. *Arterioscler Thromb Vasc Biol* (2009) 29:1419–23. doi:10.1161/ATVBAHA.108.180497
51. O'Neill LAJ, Pearce EJ. Immunometabolism governs dendritic cell and macrophage function. *J Exp Med* (2016) 213:15–23. doi:10.1084/jem.20151570
52. Geeraerts X, Bolli E, Fendt S-M, Van Ginderachter JA. Macrophage metabolism as therapeutic target for cancer, atherosclerosis, and obesity. *Front Immunol* (2017) 8:289. doi:10.3389/fimmu.2017.00289
53. Sengupta S, Peterson TR, Sabatini DM. Regulation of the mTOR complex 1 pathway by nutrients, growth factors, and stress. *Mol Cell* (2010) 40:310–22. doi:10.1016/j.molcel.2010.09.026
54. Byles V, Covarrubias AJ, Ben-Sahra I, Lamming DW, Sabatini DM, Manning BD, et al. The TSC-mTOR pathway regulates macrophage polarization. *Nat Commun* (2013) 4:2834. doi:10.1038/ncomms3834
55. Ai D, Jiang H, Westerterp M, Murphy AJ, Wang M, Ganda A, et al. Disruption of mammalian target of rapamycin complex 1 in macrophages decreases chemokine gene expression and atherosclerosis. *Circ Res* (2014) 114:1576–84. doi:10.1161/CIRCRESAHA.114.302313
56. Karmaus PWF, Herrada AA, Guy C, Neale G, Dhungana Y, Long L, et al. Critical roles of mTORC1 signaling and metabolic reprogramming for M-CSF–mediated myelopoiesis. *J Exp Med* (2017) 214:2629–47. doi:10.1084/jem.20161855
57. Covarrubias AJ, Aksoylar HI, Yu J, Snyder NW, Worth AJ, Iyer SS, et al. Akt-mTORC1 signaling regulates Acly to integrate metabolic input to control of macrophage activation. *eLife* (2016) 5:e11612.

58. Brown J, Wang H, Suttles J, Graves DT, Martin M. Mammalian target of rapamycin complex 2 (mTORC2) negatively regulates toll-like receptor 4-mediated inflammatory response via FoxO1. *J Biol Chem* (2011) 286:44295–305. doi:10.1074/jbc.M111.258053
59. Fruman DA, Chiu H, Hopkins BD, Bagrodia S, Cantley LC, Abraham RT. The PI3K pathway in human disease. *Cell* (2017) 170:605–35. doi:10.1016/j.cell.2017.07.029
60. Arranz A, Doxaki C, Vergadi E, Martinez de la Torre Y, Vaporidi K, Lagoudaki ED, et al. Akt1 and Akt2 protein kinases differentially contribute to macrophage polarization. *Proc Natl Acad Sci U S A* (2012) 109:9517–22. doi:10.1073/pnas.1119038109
61. Babaev VR, Hebron KE, Wiese CB, Toth CL, Ding L, Zhang Y, et al. Macrophage deficiency of Akt2 reduces atherosclerosis in Ldlr null mice. *J Lipid Res* (2014) 55:2296–308. doi:10.1194/jlr.M050633
62. Sahin E, Haubenwallner S, Kuttke M, Kollmann I, Halfmann A, Dohnal AB, et al. Macrophage PTEN regulates expression and secretion of arginase I modulating innate and adaptive immune responses. *J Immunol* (2014) 193:1717–27. doi:10.4049/jimmunol.1302167
63. Weisser SB, McLarren KW, Voglmaier N, van Netten-Thomas CJ, Antov A, Flavell RA, et al. Alternative activation of macrophages by IL-4 requires SHIP degradation. *Eur J Immunol* (2011) 41:1742–53. doi:10.1002/eji.201041105
64. Yue S, Rao J, Zhu J, Busuttil RW, Kupiec-Weglinski JW, Lu L, et al. Myeloid PTEN deficiency protects livers from ischemia reperfusion injury by facilitating M2 macrophage differentiation. *J Immunol* (2014) 192:5343–53. doi:10.4049/jimmunol.1400280
65. Vergadi E, Ieronymaki E, Lyroni K, Vaporidi K, Tsatsanis C. Akt signaling pathway in macrophage activation and M1/M2 polarization. *J Immunol* (2017) 198:1006–14. doi:10.4049/jimmunol.1601515
66. Tabas I, García-Cardeña G, Owens GK. Recent insights into the cellular biology of atherosclerosis. *J Cell Biol* (2015) 209:13–22. doi:10.1083/jcb.201412052
67. Jaiswal S, Natarajan P, Silver AJ, Gibson CJ, Bick AG, Shvartz E, et al. Clonal hematopoiesis and risk of atherosclerotic cardiovascular disease. *N Engl J Med* (2017) 377:111–21. doi:10.1056/NEJMoal1701719

Conflict of Interest Statement: The authors declare that our research was conducted and performed in the absence of any commercial or financial relationships that could be construed as a potential conflict of interest.

frontiers in Immunology

REVIEW
published: 20 February 2018
doi: 10.3389/fimmu.2018.00298

The Potential Role of Trained Immunity in Autoimmune and Autoinflammatory Disorders

Rob J. W. Arts[1], Leo A. B. Joosten[1,2] and Mihai G. Netea[1,3]*

[1] Department of Internal Medicine, Radboud Center for Infectious Diseases, Radboud University Medical Center, Nijmegen, Netherlands, [2] Department of Medical Genetics, Iuliu Haţieganu University of Medicine and Pharmacy, Cluj-Napoca, Romania, [3] Department for Genomics and Immunoregulation, Life and Medical Sciences Institute (LIMES), University of Bonn, Bonn, Germany

During induction of trained immunity, monocytes and macrophages undergo a functional and transcriptional reprogramming toward increased activation. Important rewiring of cellular metabolism of the myeloid cells takes place during induction of trained immunity, including a shift toward glycolysis induced through the mTOR pathway, as well as glutaminolysis and cholesterol synthesis. Subsequently, this leads to modulation of the function of epigenetic enzymes, resulting in important changes in chromatin architecture that enables increased gene transcription. However, in addition to the beneficial effects of trained immunity as a host defense mechanism, we hypothesize that trained immunity also plays a deleterious role in the induction and/or maintenance of autoimmune and autoinflammatory diseases if inappropriately activated.

Keywords: epigenetics, monocytes, immunometabolism, innate immune memory, rheumatoid arthritis, systemic lupus erythematosus, Wegener's granulomatosis, hyper Ig-D syndroom

OPEN ACCESS

Edited by:
Liwu Li,
Virginia Tech, United States

Reviewed by:
Min Wu,
University of North Dakota, United States
Paola Italiani,
Consiglio Nazionale Delle Ricerche (CNR), Italy

****Correspondence:***
Rob J. W. Arts
rob.jw.arts@radboudumc.nl

Specialty section:
This article was submitted to Molecular Innate Immunity, a section of the journal Frontiers in Immunology

Received: *11 December 2017*
Accepted: *02 February 2018*
Published: *20 February 2018*

Citation:
Arts RJW, Joosten LAB and Netea MG (2018) The Potential Role of Trained Immunity in Autoimmune and Autoinflammatory Disorders. Front. Immunol. 9:298. doi: 10.3389/fimmu.2018.00298

INTRODUCTION

Since the introduction of the term trained immunity for the non-specific memory of the innate immune system in 2011 (1), an increasing number of studies have investigated its role in homeostasis and disease. Innate immune memory has been described in plants and non-vertebrates for a relatively long time, representing the immune adaptation in these species that lack an adaptive immune system (2). In vertebrates, it was firstly shown that NK cells possess a non-specific memory that contributes in the innate host defense (3, 4). Later also monocytes and macrophages were shown to have a non-specific memory (5, 6). When human monocytes were exposed *in vitro* with microbial components such as β-glucan of the *Candida albicans* cell wall or the Bacillus Calmette-Guérin (BCG) vaccine, and a week later restimulated with non-related stimuli, the capacity of cells to produce cytokines was increased compared with non-trained (naive) cells (3, 5). Moreover, when mice were challenged (or "trained") with β-glucan or BCG *in vivo*, they showed lower mortality after lethal *C. albicans* or *Staphyococcus aureus* infections, a process that was largely dependent on the innate immune system (3, 5, 6). Moreover, in humans, BCG vaccination results in trained monocytes with increased responsiveness against microorganisms, which probably explains at least partly the lower mortality from a variety of infections in vaccinated children (3, 6–9).

There are a set of important characteristics that distinguish innate and adaptive immune memory processes. In case of the classical adaptive immune memory, a specific antigen is recognized and

specific T- and/or B-lymphocytes expand that specifically respond to that antigen. The breadth of needed responses is insured by gene recombination of V-D-J system. Upon reinfection, long-term memory cells will respond very specifically to the same antigen: thus, adaptive memory is both specific and enhanced, compared to the primary response. In contrast, the molecular substrate of trained immunity is epigenetically mediated, with genome-wide changes in histone marks and thus chromatin architecture playing a major role in the change of the phenotype of monocytes and macrophages (6, 10). By stimulation of an innate immune cell (or its precursors) an enhanced non-specific immunological reaction will be evoked due to differences in which gene transcription takes place due to changes in chromatin configuration (11). Innate immune memory (trained immunity) will thus evoke an increased response, but which is non-specific.

Also changes in cellular metabolism of trained monocytes and macrophages were shown to be a major important component of the trained immunity phenotype. Induction of glycolysis in an mTOR/HIF-1α-dependent manner is indispensible for the induction of trained immunity (12, 13), just as induction of glutamine metabolism that results in fumarate accumulation (14, 15). Interestingly, there is a tight link between metabolic and epigenetic changes that occur in cells (16). We have for example recently shown, that induction of glycolysis is essential for the induction of epigenetic changes seen in trained immunity. When glycolysis was inhibited also the induction of trained immunity by its epigenetic changes was inhibited (12, 13). How induction of glycolysis exactly leads to epigenetic changes is still unclear, but accumulation of acetyl-CoA has been suggested as a mechanism, inducing histone acetylation (11). Moreover, also accumulation of fumarate (one of the intermediates of the TCA cycle) was shown to induce trained immunity by inhibiting histone demethylases and therefore inducing epigenetic changes in human monocytes (14). Recently, we have shown that induction of the cholesterol synthesis pathway, which results in mevalonate accumulation, is also one of the contributors to the induction of epigenetic changes in trained immunity (17). However, this remains a rather new topic of research and more research has to be performed to better understand the exact link between metabolism en epigenetics and its role in trained immunity.

Induction of trained immunity may be important for diseases characterized by defective function of innate immune responses. We have recently shown that the induction of trained immunity by β-glucan is able to counteract the epigenetic changes induced in monocytes in postsepsis immunoparalysis (18): this may represent a potential new therapy. However, trained immunity could also be the cause or play a role in maintaining disease activity in diseases characterized by excessive inflammation, although this needs to be investigated in future studies. In this review, we give an overview of literature that provides indications for the potential role of trained immunity in autoimmune and autoinflammatory diseases. We focus on the possibility that increased function of the myeloid cells in these conditions may be mediated by epigenetic rewiring, and thus possibly a trained immunity phenotype. Another possible mechanism how monocytes of patients with autoimmune and autoinflammatory diseases are more responsive is by specific genetic variations: this hypothesis has been extensively discussed in other reviews, and it will therefore be not presented here. Importantly, adaptive memory responses are also very well known to play a crucial part in autoimmune diseases. However, the role of the adaptive immune system in these diseases has been discussed elsewhere in very good recent review articles (19–21) and was therefore not included in this review.

RHEUMATOID ARTHRITIS

Rheumatoid arthritis (RA) is one of the most common inflammatory arthritis. The pathogenesis of this autoimmune disease is complex and remains partially elusive; it is partly genetically regulated, but environmental factors also play a role, finally leading to synovial inflammation and destruction of bone and cartilage (22). Initially, the role of the adaptive immune system was mainly studied, as the loss of self tolerance of $CD4^+$ T lymphocytes was considered the main defect in RA (23). However, this paradigm is changing and nowadays the focus has also shifted to the role of the innate immune system in RA (24–26). Innate immune cells have been defined as being the cause of the tissue-damaging inflammatory lesions, with macrophages as main producers of proinflammatory cytokines. Macrophages are considered the cause of cartilage and bone destruction by inducing inflammation and regulating osteoclast activity, e.g., by inducing RANKL production (27–30). The number of infiltrated macrophages seems to negatively correlate with response to therapy and the degree of joint erosion (31, 32) and patients with highly active RA show a greater amount of M1-type macrophages in the synovial fluid compared to those with lower disease scores (33). Targeting the cytokines produced by macrophages [e.g., tumor necrosis factor α (TNFα)] has been proven to be a very successful treatment (34).

When circulating monocytes from RA patients were analyzed, gene expression of several proinflammatory cytokines was increased (35, 36). $CD14^+$ monocytes showed an increased expression of CD11b, and when *ex vivo* stimulated, increased production of IL-1β and IL-6 is observed (37). Interestingly, PI3K/mTOR and MAPK signaling pathways are also activated in RA monocytes (36, 38), and inhibiting mTOR reduced synovial osteoclast formation and protected against local bone erosions and cartilage loss (39, 40). In addition, epigenetic changes have been suggested to play a role, although no genome wide epigenetic analyses in monocytes/macrophages have been performed. In RA synovial tissue the HAT/HDAC balance is moved into the direction of histone acetylation (41). HDAC1 and HDAC2 activity has been specifically analyzed in synovial fibroblasts (not in synovial macrophages), but no difference was found (42). Interestingly, etanercept and adalimumab downregulate trimetylation of H3K4, H3K27, H3K36, and H3K79, as well as acetylation of histone 3 and 4 at the promoter site of CCL2 (MCP-1) in monocytes which correlated with RA disease activity (43). In contrast, a recent study did not identify an increase in H3K4me3 at *TNFA* and *IL6* genes of circulating monocytes in RA patients (44). In addition, the metabolic changes that occur in trained immunity also occur in macrophages from RA patients: upon stimulation with LPS higher levels of ATP are present in the

patient-derived macrophages (45). Glycolysis is also upregulated, as are rate-limiting enzymes (e.g., PKM2, PFKFB3, and HK2) and the glucose transporters GLUT1 and GLUT3 (46). Functionally, glucose uptake and oxygen consumption are increased (46), whereas accumulation of glutamate, succinate, and fumarate are present as signs of a highly metabolic active state of an RA proinflammatory macrophage (47, 48), similar to a trained immunity phenotype (12, 14).

Hence, multiple similarities exist between tissue macrophages or circulating monocytes in RA and trained monocytes or macrophages. Interestingly, in RA patients an increased risk for atherosclerotic disease is seen (49), which corresponds with the hypothesis that trained macrophages contribute to the development of atherosclerotic lesions (50). How the training in RA is induced remains unknown, although several danger-associated molecular patterns (DAMPs), that could be released by local sterile inflammation and tissue damage in the joint have been proposed to induce trained immunity (51), just as the increased production of IL-32 (52). Future studies to investigate these mechanisms are warranted.

SYSTEMIC LUPUS ERYTHEMATOSUS (SLE)

In SLE several immunological abnormalities are present. The production of a number of antinuclear antibodies is the most prominent and well-known process, and they are used for diagnostic purposes. However, monocytes and macrophages also play a prominent role in the disease activity, which increasingly becomes a topic of research (53–55). In SLE patients, macrophages are characterized by a proinflammatory status and show an increased production of proinflammatory cytokines, such as IFNα, TNFα, and IL-6 (56–58). $CD16^+$ monocytes express more CD80, CD86, HLA-DR, and CX3CR1 (59) and also expression data of $CD14^+$ and non-classical monocytes demonstrate a proinflammatory phenotype (60–64). Inflammasome and interferon-regulated genes that were regulated by IRF1 (65), with IFNα as one of the main mediators (66–70), are induced in SLE monocytes. Moreover, monocytes show an improved antigen presentation capacity and are easily activated (71). It is therefore suggested that monocytes and macrophages are better capable of presenting self-antigens to autoreactive T cells and therefore inducing or maintaining disease activity (56). Interestingly, a SNP in the *IL1B* gene that was associated with lower IL-1β production upon LPS stimulation was protective for SLE (72).

Epigenetic modulation in monocytes clearly plays a role in SLE. Histones around the *TNFA* genomic region are highly acetylated in SLE monoyctes resembling high accessibility for transcription (73). Also whole-genome assessment of histone H4 of monocytes reveals hyperacetylation (74–76) and also at enhancers of monocytes SLE-specific alterations for H3K4me3 and H3K27me3 could be determined (77). Whole-genome epigenetic analysis of H3K4me3 of primary monocytes of SLE patients reveals a strong association with inflammation and immune responses related genes (78, 79). When H3K4me3 modulations were related to gene promoter site, and these were compared with the major epigenetically modulated promoter sites in *in vitro* β-glucan-trained monocytes (10), the M2 and M3 clusters (defined in β-glucan training) were also significantly modulated in SLE monocytes (**Table 1**). In another article in which monocytes from six SLE patients were compared with six controls, 136,573 DNase hypersensitivity sites (DHS) were defined. Of these DHS, 4,583 showed SLE-specific changes for H3K4me3 and 1,714 for H3K27me3 at promoter sites. At enhancer site theses numbers were 12,109 and 3,046, respectively (55). Transcription factor binding motifs analysis revealed PU.1 and CEBPB as main transcription factors related to the H3K4me3 induced genomic areas, just as seen for β-glucan-induced training (10). Also BLIMP1 and interferon-related transcription factors as STAT1/6, and IRF1/4/8 were defined (55).

In trained immunity induced by β-glucan and also by BCG, it has been shown that important changes in cellular metabolism are induced, and that changing concentrations of metabolites play a role in the modulation of epigenetic rewiring (10, 12–14).

In immune cells from SLE patients, metabolic changes are present and might influence the epigenetic landscape as well (80). SAMs are cofactors in DNA and histone methyltranferase reactions and in T cells in SLE SAMs have been shown to be modulated and influence the epigenetic landscape, both at DNA (81, 82) and histone methylation level (83, 84). Histone demethylases need α-ketogluterate and Fe^{2+} as cofactors, which were shown to be modulated in T cells of SLE patients (84). Acetyl CoA functions as an acetyl donor for histone acetyl transferases. Histone acetylation is defective in SLE, and when in mice in an SLE model HDACs were inhibited, this showed a positive effect on disease activity and nephritis (85–87).

Finally, also activation of the mTOR pathway is a marker of disease and of onset of disease in SLE. The mTOR pathway is activated in many immune cells, among others also in monocytes (88–90). Inhibition of mTOR with rapamycin has shown beneficial effects on several outcome measures, but monocytes/

TABLE 1 | Comparison of H3K4me3-related GO-terms in β-trained monocytes and monocytes of SLE patients.

	Go-term	β-Glucan-induced trained immunity	SLE
		p-Value	*p*-Value
M1	Sugar binding	3.9E−2	0.72
M2	Carboxylic acid metabolic process	7.9E−5	4.5E−2
	Cellular ketone metabolic process	1.3E−4	0.32
	Oxidoreductase	1.4E−3	4.3E−2
	Lipid metabolic process	5.4E−6	3.2E−3
M3	Signal transducer activity	2.4E−3	3.7E−2
	Receptor activity	2.1E−2	1.2E−2
M4	Cofactor binding	3.5E−3	0.16
M5	Immune response	3.00E−19	3.7E−2
	Response to wounding	5.00E−17	1.3E−2
	Chemotaxis	5.2E−7	0.79
	Cytokine activity	8.00E−12	5.3E−2
	Chemokine activity	3.7E−9	9.3E−2

H3K4me3 modulations were related to gene promoter site. Related GO-terms of the major epigenetically modulated promoter sites in in vitro β-glucan-trained monocytes, defined as M clusters (10), were compared with the same GO-terms in monocytes of SLE patients (78) and adjusted p-values are shown.

macrophages were unfortunately not part of the analysis [reviewed in Ref. (88)].

The modulation of monocytes from the peripheral blood could be due to changes induced in the bone marrow. Gene expression analysis of mononuclear bone marrow cells from SLE patients reveals that ERK, JNK, and p38 MAP kinases and STAT3 are significantly upregulated (91). As anti-dsDNA antibodies can bind to TLR4 and activate the NLRP3 inflammasome, it is tempting to speculate whether they might be the factor inducing trained immunity in SLE patients (92, 93).

SJÖGREN'S SYNDROME (SS)

Sjögren's syndrome is a chronic autoimmune disease characterized by salivary and lacrimal gland dysfunction (94). Also in the case of SS, clues can be found in literature to suggest that a trained immunity profile may characterize its myeloid cells. Immune cell infiltrates of the salivary glands in SS mainly contain macrophages and DCs with increased IL-12 and IL-18 expression and depletion of macrophages in the gland tissue improved disease symptoms in a mouse model (95–97). When peripheral $CD14^+$ monocytes were stimulated with apoptotic cells, they showed an increased production of TNFα or IL-1β and a decreased production of IL-10, thus displaying a proinflammatory profile (98, 99). Also when monocyte-derived dendritic cells were stimulated with LPS a clear proinflammatory profile was seen, with among others higher levels of TNFα, MIG, IFNα, IL-6, IL-12, MIP1α/β, MCP1 compared to healthy volunteers (100). In non-stimulated circulating monocytes, type I IFN-related genes were higher expressed compared to control monocytes, which correlated with the induction of B-cell activating factor (BAFF) (101–103). When monocytes were stimulated with IFNγ, increased IL-6 and BAFF production was seen as well (104). However, others have reported different effects, with decreased cytokine production upon PPD stimulation of PBMCs isolated from SS patients (105). Furthermore, NFκB activation is promoted by reduced IκBα expression in Sjögren monocytes (106). Increased STAT1 is seen in SS monocytes (107), similar to constitutive STAT5 activation (108).

No epigenetic assessment of monocytes from SS patients has been performed, apart from increased expression of miRNA 146a and 181a in PBMCs (109–113), and miR-34b-3p, miR-4701-5p, miR-609, miR-300, miR-3162-3p, and miR-877-3p upregulation in monocytes. These miRNAs collectively suppress TGFβ signaling, as opposed to proinflammatory interleukin-12 and Toll-like receptor/NFκB pathways (114). Analysis of cellular metabolic processes and induction of mTOR activation in monocytes/macrophages in SS has not been performed, but treatment with a rapamycin nanoparticle reduced destruction of lacrimal glands in a mouse model (115).

BEHÇET'S DISEASE (BD)

Behçet's disease is an inflammatory disorder that is characterized by oral en genital lesions, arthritis, and uveitis. The exact cause of BD is unknown (116). Myeloid cells play an important role in Behçet's disease activity, as granulocyte and monocyte adsorption apheresis reduced disease symptoms in two patients (117). Furthermore, peripheral monocytes of BD patients are activated and produce more proinflammatory cytokines, which might be a first clue for the presence of a trained immunity phenotype in monocytes of BD patients (118–122). The P2X7 receptor, involved in the activation of IL-1β production, has an increased expression on monocytes in BD, which is regulated by TNFα (123), while the expression of TLR2 and TLR4 is also upregulated (124, 125). The response of $CD14^+$ monocytes from BD patients to IFNγ showed increased production of CXCL9 and CXCL10; however, the CXCL10 production might be increased due to dysregulated posttranslational regulation (126). A whole-genome DNA methylation profiling of monocytes revealed 383 CpG sites to be differently regulated compared to healthy controls (and only 123 were found in $CD4^+$ T cells), with cytoskeleton modulation as one of the main regulated pathways (127).

SYSTEMIC SCLEROSIS (SSc)

Systemic sclerosis is a complex autoimmune disease with extensive fibrosis, vascular alterations and immune activation among its principal features (128). Also in SSc the monocyte compartment appears to play an important role. $CD14^+$ monocytes levels are increased in peripheral blood and in skin infiltrates (129, 130). An increased type I IFN signature was observed in early and definite SSc patient monocytes, which correlated with increased BAFF mRNA expression. Production of other cytokines, chemokines and their receptors (among others IL6, TNFα, and TGFβ) is upregulated as well (131–145). Monocytes of SSc patients produce more reactive oxygen species (146, 147), whereas nitric oxide production was decreased (148). SSc PBMCs produce more IL-8 and CCL18 when stimulated with IgG (149). In the vascular alterations present in SSc patients, monocytes appear to play a role as they can differentiate into fibroblast-like cells and produce extracellular matrix (modulating) proteins, resulting in a proangiogenic but impaired vasculogenic environment (132, 150–156). The macrophage activation markers CD163 and CD204 are more expressed in SSc (129, 132), which by some authors has been linked to a M2 macrophage phenotype with anti-inflammatory and profibrotic features (157). The alveolar macrophages in SSc patients with pulmonary fibrosis have a strong M2 phenotype with expression of CCL17, CCL18, and CCL22 and increased activation of STAT 3 (158). Increased TNFα production by these cells was also reported (159).

On the level of epigenetic profiles, hardly any data are available in monocytes or macrophages from SSc patients. The only data available in monocytes show that histone demethylation plays a role in the production of tissue inhibitor of metalloproteinases 1 in the presence of TLR8 stimulation (160). However, given the broad amount of data present in the literature, an epigenetic analysis on circulating monocytes in SSc would be a logical next step.

WEGENER'S GRANULOMATOSIS (WG)

Wegener's granulomatosis is a systemic inflammatory disorder characterized by vasculitis of the small- and medium-size vessels

in many organs. The exact cause remains unknown, but monocytes have been suggested to play a role in disease activity (161).

Monocytes of WG patients are activated, as shown by increased CD11b and CD64 expression, and increased concentrations of neopterin and IL-6 are found in the serum (162). The expression of adhesion molecules is increased on monocytes from WG patients (163). Interestingly, anti-PR3 induces cytokine production by monocytes and it was shown that when monocytes are primed with ANCA or PR3 antibodies, their responses to LPS and LTA stimulation increase, with more TNFα, IL-6 and IL-8 production (164) and increased expression of CD14, CD18, and several PRRs (165, 166). Monocytes of WG patients that did not respond to methotrexate showed increased intracellular levels of IL-12 and TNFα (but no IL-8) that normalized after cyclophosphamide treatment (167). Also IL-8, IL-12, and MCP-1 production was increased in WG monocytes (166, 168–170). In contrast, other studies have shown that monocytes from WG patients are shown to produce less reactive oxygen species and have impaired phagocytosis (171) and in one report, monocytes of WG patients were stimulated with LPS, they produced less TNFα compared to healthy controls (172). No studies on epigenetic modulation of cellular metabolism of monocytes in WG are available. In order to assess whether a trained immunity phenotype is indeed responsible for the functional changes observed, such studies should be performed.

SARCOIDOSIS

Sarcoidosis is a complex systemic granulomatous disorder of unknown etiology. Circulating monocytes op sarcoidosis patients produce less IL-10 (173), express more $CD16^+$ (174, 175), BAFF (166), TLR2 and TLR4 (176), IL-2R (177), adhesion molecules (178), produce more proinflammatory cytokines (176, 179–181) and oxygen radicals (182), and have increased phagocytic activity (183), thus showing an increased activated phenotype (184). Moreover, monocytes of sarcoidosis patients are more likely to form giant cells (185). Fibrin, which is newly formed in granulomas, is able to induce IL-1β production and might therefore serve as an inductor of trained immunity (186).

RNA-sequencing analysis of monocytes of sarcoidosis patients revealed several differentially expressed genes, with enrichment of ribosome, phagocytosis, lysosome, proteasome, oxidative phosphorylation, and metabolic pathways are the main pathways (187). No epigenetic analysis of monocytes in sarcoidosis has been done so far (188).

TYPE 1 DIABETES MELLITUS (T1DM)

Type 1 diabetes mellitus is an important autoimmune disease resulting in profound defects in glucose metabolism. The exact underlying mechanism is unknown, but autoimmune destruction of β-cells of the pancreas is the cause of insulin deficiency (189). Monocytes and macrophages are thought to play a key role in the development of T1DM (190, 191). When peripheral blood monocytes from recent-onset T1DM patients were assessed, more $CD14^+CD16^+$ monocytes were found, which was negatively correlated with insulin and C-peptide serum levels. Furthermore, these monocytes showed higher expression of HLA-DR and CD86, and showed an activated proinflammatory phenotype (192–196). In recent-onset T1DM patients, plasma TNFα levels were higher which correlated with CD14 expression (197). However, another study showed decreased total number of monocytes in T1DM (198). Serum levels of MIF and MCP-1 are also increased (199). Prior to development of T1DM, children show an IFN transcriptional signature in PBMCs, which might be a result of a recent upper respiratory infection. Increased expression of SIGLEC-1 on $CD14^+$ monocytes was also found (200). Furthermore, it was shown that IL-1β plays a central role in the inflammation seen in T1DM (201) and that during the development of T1DM TLR-induced IL-1β and IL-6 production from monocytes is enhanced (202). Importantly, inhibiting IL-1β production or IL-1β signaling can improve T1DM outcome (203–206). In contrast, monocyte-derived DCs did not appear to be affected in recent-onset T1DM (191).

Epigenetics has been proposed to play a role in T1DM as well (207). Assessment of DNA methylation profiles of 32 T1DM patients versus 31 healthy individuals revealed 153 hypomethylated and 225 hypermethylated loci in whole blood, and, respectively, 155 and 247 in monocytes. However, whether these are causative to the disease or a consequence of the pathological process remains unclear (208). In another study methylation variable positions were assessed in monocytes prior to development of T1DM: 132 positions were identified and associated with a gene, with important immunology-related genes as HLA-DQB1, HLA-DRB1, NFKB1A, and TNF as major examples (209). Also important histone modifications were seen in H3K9ac in monocytes, but also these were more likely to be induced after development of the disease (210). However, in one study, H3K9ac at HLA-DRB1 and HLA-DQB1 of monocytes was shown to correlate with T1DM susceptibility prior to disease (211). Differences in H3K9me3 in inflammatory and autoimmune-related pathways were found in lymphocytes of T1DM patients, but no differences were found in monocytes (212).

Cellular metabolism of monocytes in T1DM prior to disease onset is still poorly known. Only one study revealed changes in the transcriptional signature of cell metabolism, cell survival, and oxidative stress in monocytes of recent-onset DM1. Interestingly, one of the main induced genes was HIF1A (213), although mTOR does not appear among the significantly differently regulated genes.

Lastly, as BCG is able to induce trained immunity, it could be expected that BCG-vaccinated children are at higher risk to develop T1DM. However, in an observational trial no such correlation has been found (214, 215). Interestingly, in a randomized controlled trial, BCG was suggested to have a beneficial effect on insulin production, as induction of TNF production resulted in reduced autoimmune phenotype of innate immune cells and induction of Tregs (216, 217).

AUTOINFLAMMATORY DISORDERS

Autoinflammatory disorders or periodic fever syndromes consist of a set of diseases that are characterized by periodic episodes of fever and inflammation. Common symptoms

are joint pain, rash, abdominal pain, and long-term disease can result in amyloidosis. These diseases are not induced by autoantibodies or autoreactive T-cells but are the result of a hyperfunctional innate immune system, which is due to genetic defects. The familial autoinflammatory syndromes are generally rare, and the pathogenesis is not well understood for some of them (218). Here, we argue that trained immunity could be a likely contributor in these diseases.

Tumor necrosis factor receptor-associated periodic syndrome (TRAPS) is a multisystemic autoinflammatory condition associated with heterozygous TNFRSF1A mutations, presenting with a variety of clinical symptoms, many of which still unexplained. TRAPS monocytes shown an inflammatory baseline state, with enhanced IL1B and IL1R1 gene expression, also in non-active disease, whereas IFN and TGFβ are downregulated (219, 220). Also CD16 expression is upregulated (221) and MAPK can be spontaneously activated (220). Interestingly, a TRAPS patient with a monocytic fasciitis has been successfully treated with tacrolimus (an mTOR inhibitor) (222).

Cryopyrin-associated periodic syndromes (CAPS) are caused by a mutation in NLRP3 inflammasome, resulting in increased IL-1β and IL-18 production, but impaired production of the anti-inflammatory IL-6 and IL-1RA cytokines (223, 224). Interestingly, although the genetic defect is the main cause of these abnormalities, epigenetic analysis of CAPS monocytes revealed that DNA methylation was also affected, resulting at increased expression of inflammasome-related genes. When CAPS patients were treated with IL-1 neutralizing therapies, their methylation profile reversed toward that of healthy controls (225).

In familial Mediterranean fever (FMF), *ex vivo* LPS-stimulated PBMCs and monocytes produce more IL-1α and β, IL-6, IL-8, IL-12, IL-18, and TNFα, and in non-stimulated PBMCs higher production of IL-6 and TNFα was found (226–230), and also expression of CD11b was increased (231).

Hyper-IgD syndrome (HIDS) is an autoinflammatory disorder caused by a mutation in mevalonate kinase (232, 233), in which patients experience periodic attacks of sterile inflammation with symptoms such as fever, skin lesions, lymphadenopathy, and arthralgia (234). Interestingly, PBMCs of HIDS patients produce more cytokines in unstimulated as well as stimulated state and the IgD itself was able to induce cytokine production (235–238). In a whole-blood transcriptome analysis several glycolysis-related genes were higher expressed in HIDS patients, which decreased after canakinumab treatment (239). In addition, we recently have shown broad genome-wide changes in the H3K27Ac marker in monocytes of HIDS patients, which are due to mevalonate accumulation and are believed to express a trained immunity profile (Bekkering et al., 2018 Cell in press).

The common factor in these autoinflammatory syndromes is overproduction of IL-1β, which is one of the reasons why anti-IL-1 therapeutic approaches are successful (240). As IL-1β is considered as a causal factor and plausibly plays a role in maintaining disease, accumulating evidence suggests that IL-1β is an important inducer of trained immunity. Interestingly, old studies have shown that injection of IL-1β in mice prevented death from subsequent bacterial and fungal infections (241, 242). It is tempting to hypothesize that IL-1β induces trained immunity and prevent from the subsequent infections, by epigenetically modifying monocytes and macrophages resulting in more proinflammatory immune cells. To further substantiate this hypothesis, we have recently performed experiments in which human monocytes are *ex vivo* trained with IL-1β. This indeed resulted in trained monocytes that produced more IL-6 and TNFα upon restimulation with LPS, and also increased H3K4me3 occupancy at the promoters of *IL6* and *TNFA* was observed (Arts et al., Cell Host Microbe 2018, in press). While IL-1 can induce beneficial effects in infections through induction of trained immunity, a negative consequence could be induction of overinflammation, which might result in an autoinflammatory disease. This thus opens a potential new field of research, where trained immunity in these autoinflammatory diseases should be further evaluated.

CHRONIC GRANULOMATOUS DISEASE (CGD)

Chronic granulomatous disease is an inherited immunological disorder, in which intracellular superoxide radical production is deficient. Although CGD is an immunodeficiency, it also has autoinflammatory characteristics, which is why it is discussed here as well. Normally CGD presents in the first years of life with severe recurrent bacterial and fungal infections, but it can also present later in life (243). CGD phagocytes are impaired in destroying phagocytozed microorganisms, rendering the patients susceptible to bacterial and fungal infections. Besides this immunodeficiency, CGD patients suffer from various auto inflammatory symptoms, such as granuloma formation and Crohn-like colitis (244). Also monocytes from CGD patients display a proinflammatory phenotype with increased secretion of inflammasome-mediated cytokines (IL-1β, IL-18) possibly due the inflammasome triggering effect of ROS, but also increases of other cytokines and chemokines, and NKκB and ERK expression upon stimulation (245–247). Circulating monocytes display an inflammatory phenotype with more $CD16^+$ expression and more intracellular IL-1β and TNFα (247). However, others have shown lower TNFα production by CGD monocytes (248). Incubation of CGD monocytes with rapamycin (an mTOR inhibitor) counterbalanced the preactivation state of monocytes *ex vivo* (247), hence implicating a role for mTOR. IL-1 inhibition reduced inflammation in humans and reduced disease activity of, e.g., CGD-associated colitis, possibly also by restoring autophagy (249, 250). Interestingly, injection of fungal β-glucan results in hyperinflammation and necrosis in CGD mice associated with increased IL-1β, IL-6, and TNFα production (251–253).

Metabolically also clear differences were found in CGD monocytes. Several metabolites of the tryptophan pathway accumulate and indoleamine 2,3-dioxygenase is activated (254), just as seen in monocytes stimulated with LPS or IFNγ (255). CGD monocytes have been shown to higher acidification (256), which might be the result of increased lactate production.

TABLE 2 | Overview of trained immunity-related patterns in autoimmune and autoinflammatory diseases.

	Cytokines and chemokines	Metabolism of immune cells	Epigenetic marks	mTOR signaling	Others
Rheumatoid arthritis	Circulating monocytes have increased expression of proinflammatory cytokines (35, 36) *Ex vivo*-stimulated monocytes produce more IL-1β and IL-6 (37)	Higher ATP levels upon LPS stimulation of macrophages (45) Upregulated glycolysis (46) Increased oxygen consumption (46) Accumulation of succinate in macrophages (47) Accumulation of succinate, fumarate, glutamate in synovial fluid (48)	H3K4me3 at *TNFA* and *IL6* is not induced in monocytes (44)	PI3K/mTOR signaling pathway and MAPK are activated in RA monocytes (36, 38)	Increased CD11b expression on CD14 circulating monocytes (37)
SLE	Cirulating monocytes produce more proinflammatory cytokines (56–58) SNP in the *IL1B* gene was protective for SLE (72).	No studies specific on monocytes	Histones around *TNFA* are highly acetylated in monoyctes (73) histone H4 of monocytes is hyperacetylated (74–76) H3K4me3 of SLE monocytes are associated with inflammation and immune response-related genes (78, 79) SLE-specific H3K4me3 and H3K27me3 (enhancer) modifications (55, 77)	Activated mTOR pathway in monocytes/macorphages (88–90) Rapamycin inhibition improves outcome (88)	$CD16^+$ monocytes express more CD80, CD86, HLA-DR and CX3CR1 (59) $CD14^+$ and non-classical monocytes display a proinflammatory phenotype (60–64) Inflammasome and interferon-regulated genes are induced in moncytes (65–70) monocytes show an improved antigen presentation capacity (71) ERK, JNK, and p38 MAP kinases and STAT3 are significantly upregulated in mononuclear bone marrow cells (91).
Sjögren	$CD14^+$ monocytes stimulated with apoptotic cells show increased TNFα and IL-1β, and decreased IL-10 production (98, 99). Monocyte-derived DCs produce more proinflammatory cytokines (100) Higher expression of IFN I-related genes, which correlated with BAFF (101–103) IFNγ-stimulated monocytes produce more IL-6 and BAFF (104)	?	Several miRNAs are upregulated in monocytes (114)	?	NFκB activation is promoted by reduced IκBα expression in monocytes (106) Increased STAT1 activation (107) Constitutive STAT5 activation (108)
Behçet's disease	Peripheral monocytes are activated and produce more proinflammatory cytokines (118–122) Increased production of CXCL9 and 10 upon IFNγ stimulation (126).	?	DNA methylation profiling of monocytes revealed 383 CpG sites to be differently regulated in monocytes (127)	?	Increased P2X7 receptor (123), and TLR2 and 4 expression (124, 125)
Systemic	Monocytes display an increased IFN type I signature, but also other cytokines, chemokines and their receptors are upregulated (131–145) A SNP in TLR2, which results in increased production of TNFα and IL-6 of monocytes, was associated with SSc (257)	?	?	?	Monocytes produce more ROS (146, 147), whereas NO production is decreased (148) Increased expression of CD163 and CD204 (129, 132)

(*Continued*)

TABLE 2 | Continued

	Cytokines and chemokines	Metabolism of immune cells	Epigenetic marks	mTOR signaling	Others
Wegener's granulomatosis	Increased IL-6 expression (162) Increased production of several proinflammatory cytokines (164, 166, 168–170)	?	?	?	Increased CD11b and CD64 expression (162) and CD14, CD18, and several PRRs (165, 166) Increased expression of adhesion molecules (163)
Sarcoidosis	Higher production of proinflammatory cytokines (176, 179–181)	RNA-sequencing of monocytes shows enrichment of oxidative phosphorylation and metabolic pathways (187)	?	?	Higher expression of $CD14^+CD16^+$ (174, 175), BAFF (166), TLR2 and 4 (176), IL-2R (177), adhesion molecules (178) Higher production of oxygen radicals (182) and increased phagocytic activity (183) More likely to form giant cells (185)
T1DM	Higher plasma levels of TNF, MCP-1, and MIF (197, 199), and TLR-induced IL-1β and IL-6 production by monocytes is increased (200–202). IL-1β inhibition improves T1DM outcome (203–206)	Gene expression of recent-onset T1DM monocytes shows signature with cellular metabolism and oxidative stress as main pathways, and with HIF1A among the induced genes (213)	Several DNA hypo and hypermethylated loci were defined in T1DM monocytes (208, 209). H3K9ac marks are correlated with T1DM (210, 211)	?	More CD14 + CD16 + monocytes in recent-onset T1DM patients, with higher HLA-DR and CD86 expression and proinflammatory phenotype (192–196).
TRAPS	Enhanced IL1B and IL1R1, and decreased IFN and TGFB expression (219, 220)	?	?	Monocytic fasciitis successfully treated with tacrolimus (222)	Upregulated CD16 expression (221) Spontaneous MAKP activation (220)
CAPS	Increased IL-1β and IL-18 production, Production of Il-6 and IL-1RA appears to be impaired (223, 224)	DNA methylation was affected, resulting at increased expression of inflammasome-related genes (225)	?	?	?
FMF	LPS-stimulated PBMCs and monocytes produce more IL-1α and β and non-stimulated PBMCs produce more of IL-6 and TNFα (226–228)	?	?	?	Higher expression of CD11b (231)
HIDS	PBMCs produce more cytokines in unstimulated or stimulated state (235–238)	?	?	?	?
CGD	Monocytes display a proinflammatory phenotype with increased secretion of IL-1β and IL-18, but also other cytokines and chemokines (245–247) More IL-1β and TNFα expression (247)	Metabolites of the tryptophan pathway accumulate and indoleamine 2,3-dioxygenase (IDO) is activated (254) Monocytes show higher acidification (256)	?	Incubation of monocytes with rapamycin counterbalanced the preactivation state (247)	Increased NK-κB and ERK expression upon stimulation (246, 247) More $CD16^+$ expression (247)

CONCLUSION

In this review, we present an overview of the data supporting the concept that monocytes from patients with several autoimmune and autoinflammatory diseases display features consistent with a trained immunity phenotype. The phenotype of a trained monocyte has been defined with characteristics as (1) increased cytokine production, (2) changes in cellular metabolism (mainly increased glycolysis and lactate production), and (3) epigenetic rewiring (**Table 2**). Trained immunity could serve a role in the initiation of the disease and in the maintenance or aggravation of the symptoms. In the case of disease initiation, a genetic or environmental factor (or combinations of both) would induce trained monocytes/macrophages that initiate the disease. In the case of disease progression, monocytes/macrophages become trained and are therefore easier activated, which would result in the maintenance or deterioration of disease symptoms. This is an important distinction to take into account, as different experimental approaches would apply.

By providing a molecular mechanism in the described diseases in terms of trained immunity, we inherently describe potential novel therapies. For certain components of the metabolic pathways and epigenetic pathways described to be important for trained immunity, specific and non-specific inhibitors are already available and new ones are being developed. We have shown before that by inhibiting specific metabolic pathways or by specifically inhibiting certain epigenetic modulating enzymes, the induction of trained immunity can be counteracted (12–15). Hence, by identifying the specific trained immunity pathways that play a role in the induction and progression of disease activity in these autoinflammatory and autoimmune diseases, it is hoped that novel targeted immunotherapies will be developed.

However, all data presented here are circumstantial and do not prove a causal relation between the disease symptoms and monocyte function. Therefore, specifically applied experiments on the role of trained immunity in these diseases are essential to further unravel the role of trained immunity. By elucidating the potential role of trained immunity in these (but supposedly also other) diseases, new steps can be made in better understanding the pathophysiology of these diseases. Even more importantly, this could potentially lead to new approaches for therapeutic intervention in these diseases.

AUTHOR CONTRIBUTIONS

RA wrote the first draft and LJ and MN made revisions.

FUNDING

MN was supported by an ERC Consolidator Grant (#310372) and a Spinoza Grant of the Netherlands Organization for Scientific Research. LJ was supported by a Competitiveness Operational Programme grant of the Romanian Ministry of European Funds (HINT, ID P_37_762; MySMIS 103587).

REFERENCES

1. Netea MG, Quintin J, van der Meer JW. Trained immunity: a memory for innate host defense. *Cell Host Microbe* (2011) 9(5):355–61. doi:10.1016/j.chom.2011.04.006
2. Milutinovic B, Kurtz J. Immune memory in invertebrates. *Semin Immunol* (2016) 28(4):328–42. doi:10.1016/j.smim.2016.05.004
3. Kleinnijenhuis J, Quintin J, Preijers F, Joosten LA, Jacobs C, Xavier RJ, et al. BCG-induced trained immunity in NK cells: role for non-specific protection to infection. *Clin Immunol* (2014) 155(2):213–9. doi:10.1016/j.clim.2014.10.005
4. O'Sullivan TE, Sun JC, Lanier LL. Natural killer cell memory. *Immunity* (2015) 43(4):634–45. doi:10.1016/j.immuni.2015.09.013
5. Quintin J, Saeed S, Martens JH, Giamarellos-Bourboulis EJ, Ifrim DC, Logie C, et al. *Candida albicans* infection affords protection against reinfection via functional reprogramming of monocytes. *Cell Host Microbe* (2012) 12(2):223–32. doi:10.1016/j.chom.2012.06.006
6. Kleinnijenhuis J, Quintin J, Preijers F, Joosten LA, Ifrim DC, Saeed S, et al. Bacille Calmette-Guerin induces NOD2-dependent nonspecific protection from reinfection via epigenetic reprogramming of monocytes. *Proc Natl Acad Sci U S A* (2012) 109(43):17537–42. doi:10.1073/pnas.1202870109
7. Aaby P, Kollmann TR, Benn CS. Nonspecific effects of neonatal and infant vaccination: public-health, immunological and conceptual challenges. *Nat Immunol* (2014) 15(10):895–9. doi:10.1038/ni.2961
8. Aaby P, Roth A, Ravn H, Napirna BM, Rodrigues A, Lisse IM, et al. Randomized trial of BCG vaccination at birth to low-birth-weight children: beneficial nonspecific effects in the neonatal period? *J Infect Dis* (2011) 204(2):245–52. doi:10.1093/infdis/jir240
9. Arts RJW, Moorlag S, Novakovic B, Li Y, Wang SY, Oosting M, et al. BCG vaccination protects against experimental viral infection in humans through the induction of cytokines associated with trained immunity. *Cell Host Microbe* (2018) 23(1):89–100e5. doi:10.1016/j.chom.2017.12.010
10. Saeed S, Quintin J, Kerstens HH, Rao NA, Aghajanirefah A, Matarese F, et al. Epigenetic programming of monocyte-to-macrophage differentiation and trained innate immunity. *Science* (2014) 345(6204):1251086. doi:10.1126/science.1251086
11. Netea MG, Joosten LA, Latz E, Mills KH, Natoli G, Stunnenberg HG, et al. Trained immunity: a program of innate immune memory in health and disease. *Science* (2016) 352(6284):aaf1098. doi:10.1126/science.aaf1098
12. Cheng SC, Quintin J, Cramer RA, Shepardson KM, Saeed S, Kumar V, et al. mTOR- and HIF-1alpha-mediated aerobic glycolysis as metabolic basis for trained immunity. *Science* (2014) 345(6204):1250684. doi:10.1126/science.1250684
13. Arts RJ, Carvalho A, La Rocca C, Palma C, Rodrigues F, Silvestre R, et al. Immunometabolic pathways in BCG-induced trained immunity. *Cell Rep* (2016) 17(10):2562–71. doi:10.1016/j.celrep.2016.11.011
14. Arts RJ, Novakovic B, Ter Horst R, Carvalho A, Bekkering S, Lachmandas E, et al. Glutaminolysis and fumarate accumulation integrate immunometabolic and epigenetic programs in trained immunity. *Cell Metab* (2016) 24(6):807–19. doi:10.1016/j.cmet.2016.10.008
15. Arts RJ, Joosten LA, Netea MG. Immunometabolic circuits in trained immunity. *Semin Immunol* (2016) 28(5):425–30. doi:10.1016/j.smim.2016.09.002
16. Donohoe DR, Bultman SJ. Metaboloepigenetics: interrelationships between energy metabolism and epigenetic control of gene expression. *J Cell Physiol* (2012) 227(9):3169–77. doi:10.1002/jcp.24054
17. Bekkering S, Arts RJW, Novakovic B, Kourtzelis I, van der Heijden C, Li Y, et al. Metabolic induction of trained immunity through the mevalonate pathway. *Cell* (2018) 172(1–2):135–46e9. doi:10.1016/j.cell.2017.11.025
18. Novakovic B, Habibi E, Wang SY, Arts RJ, Davar R, Megchelenbrink W, et al. beta-Glucan reverses the epigenetic state of LPS-induced immunological tolerance. *Cell* (2016) 167(5):1354–68e14.
19. Catrina AI, Joshua V, Klareskog L, Malmstrom V. Mechanisms involved in triggering rheumatoid arthritis. *Immunol Rev* (2016) 269(1):162–74. doi:10.1111/imr.12379
20. Moulton VR, Tsokos GC. T cell signaling abnormalities contribute to aberrant immune cell function and autoimmunity. *J Clin Invest* (2015) 125(6):2220–7. doi:10.1172/JCI78087

21. Bordignon C, Canu A, Dyczko A, Leone S, Monti P. T-cell metabolism as a target to control autoreactive T cells in beta-cell autoimmunity. *Curr Diab Rep* (2017) 17(5):24. doi:10.1007/s11892-017-0848-5
22. McInnes IB, Schett G. The pathogenesis of rheumatoid arthritis. *N Engl J Med* (2011) 365(23):2205–19. doi:10.1056/NEJMra1004965
23. Lee DM, Weinblatt ME. Rheumatoid arthritis. *Lancet* (2001) 358(9285): 903–11. doi:10.1016/S0140-6736(01)06075-5
24. Theofilopoulos AN, Gonzalez-Quintial R, Lawson BR, Koh YT, Stern ME, Kono DH, et al. Sensors of the innate immune system: their link to rheumatic diseases. *Nat Rev Rheumatol* (2010) 6(3):146–56. doi:10.1038/nrrheum.2009.278
25. Waldner H. The role of innate immune responses in autoimmune disease development. *Autoimmun Rev* (2009) 8(5):400–4. doi:10.1016/j.autrev.2008.12.019
26. Takai T. Roles of Fc receptors in autoimmunity. *Nat Rev Immunol* (2002) 2(8):580–92. doi:10.1038/nri856
27. Toh ML, Bonnefoy JY, Accart N, Cochin S, Pohle S, Haegel H, et al. Bone- and cartilage-protective effects of a monoclonal antibody against colony-stimulating factor 1 receptor in experimental arthritis. *Arthritis Rheumatol* (2014) 66(11):2989–3000. doi:10.1002/art.38624
28. Horwood NJ, Elliott J, Martin TJ, Gillespie MT. IL-12 alone and in synergy with IL-18 inhibits osteoclast formation in vitro. *J Immunol* (2001) 166(8):4915–21. doi:10.4049/jimmunol.166.8.4915
29. Horwood NJ. Macrophage polarization and bone formation: a review. *Clin Rev Allergy Immunol* (2016) 51(1):79–86. doi:10.1007/s12016-015-8519-2
30. Walsh MC, Choi Y. Biology of the RANKL-RANK-OPG system in immunity, bone, and beyond. *Front Immunol* (2014) 5:511. doi:10.3389/fimmu.2014.00511
31. Gerlag DM, Tak PP. Novel approaches for the treatment of rheumatoid arthritis: lessons from the evaluation of synovial biomarkers in clinical trials. *Best Pract Res Clin Rheumatol* (2008) 22(2):311–23. doi:10.1016/j.berh.2008.02.002
32. Mulherin D, Fitzgerald O, Bresnihan B. Synovial tissue macrophage populations and articular damage in rheumatoid arthritis. *Arthritis Rheum* (1996) 39(1):115–24. doi:10.1002/art.1780390116
33. Hamilton JA, Tak PP. The dynamics of macrophage lineage populations in inflammatory and autoimmune diseases. *Arthritis Rheum* (2009) 60(5):1210–21. doi:10.1002/art.24505
34. Onuora S. Rheumatoid arthritis: anti-TNF agents go head-to-head. *Nat Rev Rheumatol* (2017) 13(1):2. doi:10.1038/nrrheum.2016.206
35. Stuhlmuller B, Ungethum U, Scholze S, Martinez L, Backhaus M, Kraetsch HG, et al. Identification of known and novel genes in activated monocytes from patients with rheumatoid arthritis. *Arthritis Rheum* (2000) 43(4):775–90. doi:10.1002/1529-0131(200004)43:4<775::AID-ANR8>3.0.CO;2-7
36. Haupl T, Ostensen M, Grutzkau A, Radbruch A, Burmester GR, Villiger PM. Reactivation of rheumatoid arthritis after pregnancy: increased phagocyte and recurring lymphocyte gene activity. *Arthritis Rheum* (2008) 58(10):2981–92. doi:10.1002/art.23907
37. Liote F, Boval-Boizard B, Weill D, Kuntz D, Wautier JL. Blood monocyte activation in rheumatoid arthritis: increased monocyte adhesiveness, integrin expression, and cytokine release. *Clin Exp Immunol* (1996) 106(1):13–9. doi:10.1046/j.1365-2249.1996.d01-820.x
38. Malemud CJ. The PI3K/Akt/PTEN/mTOR pathway: a fruitful target for inducing cell death in rheumatoid arthritis? *Future Med Chem* (2015) 7(9):1137–47. doi:10.4155/fmc.15.55
39. Cejka D, Hayer S, Niederreiter B, Sieghart W, Fuereder T, Zwerina J, et al. Mammalian target of rapamycin signaling is crucial for joint destruction in experimental arthritis and is activated in osteoclasts from patients with rheumatoid arthritis. *Arthritis Rheum* (2010) 62(8):2294–302. doi:10.1002/art.27504
40. Lu Y, Parker N, Kleindl PJ, Cross VA, Wollak K, Westrick E, et al. Anti-inflammatory activity of a novel folic acid targeted conjugate of the mTOR inhibitor everolimus. *Mol Med* (2015) 21:584–96. doi:10.2119/molmed.2015.00040
41. Huber LC, Brock M, Hemmatazad H, Giger OT, Moritz F, Trenkmann M, et al. Histone deacetylase/acetylase activity in total synovial tissue derived from rheumatoid arthritis and osteoarthritis patients. *Arthritis Rheum* (2007) 56(4):1087–93. doi:10.1002/art.22512
42. Maciejewska Rodrigues H, Jungel A, Gay RE, Gay S. Innate immunity, epigenetics and autoimmunity in rheumatoid arthritis. *Mol Immunol* (2009) 47(1):12–8. doi:10.1016/j.molimm.2009.01.010
43. Lin YC, Lin YC, Huang MY, Kuo PL, Wu CC, Lee MS, et al. Tumor necrosis factor-alpha inhibitors suppress CCL2 chemokine in monocytes via epigenetic modification. *Mol Immunol* (2017) 83:82–91. doi:10.1016/j.molimm.2017.01.009
44. Messemaker TC, Mikkers HMM, Huizinga TW, Toes REM, van der Helm-van Mil AHM, Kurreeman F. Inflammatory genes TNFalpha and IL6 display no signs of increased H3K4me3 in circulating monocytes from untreated rheumatoid arthritis patients. *Genes Immun* (2017).
45. Weyand CM, Zeisbrich M, Goronzy JJ. Metabolic signatures of T-cells and macrophages in rheumatoid arthritis. *Curr Opin Immunol* (2017) 46:112–20. doi:10.1016/j.coi.2017.04.010
46. Shirai T, Nazarewicz RR, Wallis BB, Yanes RE, Watanabe R, Hilhorst M, et al. The glycolytic enzyme PKM2 bridges metabolic and inflammatory dysfunction in coronary artery disease. *J Exp Med* (2016) 213(3):337–54. doi:10.1084/jem.20150900
47. Littlewood-Evans A, Sarret S, Apfel V, Loesle P, Dawson J, Zhang J, et al. GPR91 senses extracellular succinate released from inflammatory macrophages and exacerbates rheumatoid arthritis. *J Exp Med* (2016) 213(9): 1655–62. doi:10.1084/jem.20160061
48. Kim S, Hwang J, Xuan J, Jung YH, Cha HS, Kim KH. Global metabolite profiling of synovial fluid for the specific diagnosis of rheumatoid arthritis from other inflammatory arthritis. *PLoS One* (2014) 9(6):e97501. doi:10.1371/journal.pone.0097501
49. Fransen J, Kazemi-Bajestani SM, Bredie SJ, Popa CD. Rheumatoid arthritis disadvantages younger patients for cardiovascular diseases: a meta-analysis. *PLoS One* (2016) 11(6):e0157360. doi:10.1371/journal.pone.0157360
50. Christ A, Bekkering S, Latz E, Riksen NP. Long-term activation of the innate immune system in atherosclerosis. *Semin Immunol* (2016) 28(4):384–93. doi:10.1016/j.smim.2016.04.004
51. Crisan TO, Netea MG, Joosten LA. Innate immune memory: implications for host responses to damage-associated molecular patterns. *Eur J Immunol* (2016) 46(4):817–28. doi:10.1002/eji.201545497
52. Heinhuis B, Koenders MI, van Riel PL, van de Loo FA, Dinarello CA, Netea MG, et al. Tumour necrosis factor alpha-driven IL-32 expression in rheumatoid arthritis synovial tissue amplifies an inflammatory cascade. *Ann Rheum Dis* (2011) 70(4):660–7. doi:10.1136/ard.2010.139196
53. Pisetsky DS. The role of innate immunity in the induction of autoimmunity. *Autoimmun Rev* (2008) 8(1):69–72. doi:10.1016/j.autrev.2008.07.028
54. Morell M, Varela N, Maranon C. Myeloid populations in systemic autoimmune diseases. *Clin Rev Allergy Immunol* (2017) 53(2):198–218. doi:10.1007/s12016-017-8606-7
55. Liu L, Yin X, Wen L, Yang C, Sheng Y, Lin Y, et al. Several critical cell types, tissues, and pathways are implicated in genome-wide association studies for systemic lupus erythematosus. *G3 (Bethesda)* (2016) 6(6):1503–11. doi:10.1534/g3.116.027326
56. Kavai M, Szegedi G. Immune complex clearance by monocytes and macrophages in systemic lupus erythematosus. *Autoimmun Rev* (2007) 6(7):497–502. doi:10.1016/j.autrev.2007.01.017
57. Sestak AL, Furnrohr BG, Harley JB, Merrill JT, Namjou B. The genetics of systemic lupus erythematosus and implications for targeted therapy. *Ann Rheum Dis* (2011) 70(Suppl 1):i37–43. doi:10.1136/ard.2010.138057
58. Steinbach F, Henke F, Krause B, Thiele B, Burmester GR, Hiepe F. Monocytes from systemic lupus erythematous patients are severely altered in phenotype and lineage flexibility. *Ann Rheum Dis* (2000) 59(4):283–8. doi:10.1136/ard.59.4.283
59. Zhu H, Hu F, Sun X, Zhang X, Zhu L, Liu X, et al. CD16+ Monocyte subset was enriched and functionally exacerbated in driving T-cell activation and B-cell response in systemic lupus erythematosus. *Front Immunol* (2016) 7:512. doi:10.3389/fimmu.2016.00512
60. Lyons PA, McKinney EF, Rayner TF, Hatton A, Woffendin HB, Koukoulaki M, et al. Novel expression signatures identified by transcriptional analysis of separated leucocyte subsets in systemic lupus erythematosus and vasculitis. *Ann Rheum Dis* (2010) 69(6):1208–13. doi:10.1136/ard.2009.108043
61. Dozmorov MG, Dominguez N, Bean K, Macwana SR, Roberts V, Glass E, et al. B-cell and monocyte contribution to systemic lupus erythematosus

identified by cell-type-specific differential expression analysis in RNA-seq data. *Bioinform Biol Insights* (2015) 9(Suppl 3):11–9. doi:10.4137/BBI.S29470
62. Mukherjee R, Kanti Barman P, Kumar Thatoi P, Tripathy R, Kumar Das B, Ravindran B. Non-Classical monocytes display inflammatory features: validation in sepsis and systemic lupus erythematous. *Sci Rep* (2015) 5:13886. doi:10.1038/srep13886
63. O'Gorman WE, Hsieh EW, Savig ES, Gherardini PF, Hernandez JD, Hansmann L, et al. Single-cell systems-level analysis of human toll-like receptor activation defines a chemokine signature in patients with systemic lupus erythematosus. *J Allergy Clin Immunol* (2015) 136(5):1326–36. doi:10.1016/j.jaci.2015.04.008
64. Shi L, Zhang Z, Yu AM, Wang W, Wei Z, Akhter E, et al. The SLE transcriptome exhibits evidence of chronic endotoxin exposure and has widespread dysregulation of non-coding and coding RNAs. *PLoS One* (2014) 9(5):e93846. doi:10.1371/journal.pone.0093846
65. Liu J, Berthier CC, Kahlenberg JM. Enhanced inflammasome activity in systemic lupus erythematosus is mediated via type I interferon upregulation of interferon regulatory factor 1. *Arthritis Rheumatol* (2017) 69(9):1840–9. doi:10.1002/art.40166
66. Lopez P, Rodriguez-Carrio J, Caminal-Montero L, Mozo L, Suarez A. A pathogenic IFNalpha, BLyS and IL-17 axis in systemic lupus erythematosus patients. *Sci Rep* (2016) 6:20651. doi:10.1038/srep20651
67. Eloranta ML, Ronnblom L. Cause and consequences of the activated type I interferon system in SLE. *J Mol Med (Berl)* (2016) 94(10):1103–10. doi:10.1007/s00109-016-1421-4
68. Baechler EC, Batliwalla FM, Karypis G, Gaffney PM, Ortmann WA, Espe KJ, et al. Interferon-inducible gene expression signature in peripheral blood cells of patients with severe lupus. *Proc Natl Acad Sci U S A* (2003) 100(5):2610–5. doi:10.1073/pnas.0337679100
69. Bennett L, Palucka AK, Arce E, Cantrell V, Borvak J, Banchereau J, et al. Interferon and granulopoiesis signatures in systemic lupus erythematosus blood. *J Exp Med* (2003) 197(6):711–23. doi:10.1084/jem.20021553
70. Kirou KA, Lee C, George S, Louca K, Papagiannis IG, Peterson MG, et al. Coordinate overexpression of interferon-alpha-induced genes in systemic lupus erythematosus. *Arthritis Rheum* (2004) 50(12):3958–67. doi:10.1002/art.20798
71. Byrne JC, Ni Gabhann J, Lazzari E, Mahony R, Smith S, Stacey K, et al. Genetics of SLE: functional relevance for monocytes/macrophages in disease. *Clin Dev Immunol* (2012) 2012:582352. doi:10.1155/2012/582352
72. Camargo JF, Correa PA, Castiblanco J, Anaya JM. Interleukin-1beta polymorphisms in Colombian patients with autoimmune rheumatic diseases. *Genes Immun* (2004) 5(8):609–14. doi:10.1038/sj.gene.6364133
73. Sullivan KE, Suriano A, Dietzmann K, Lin J, Goldman D, Petri MA. The TNFalpha locus is altered in monocytes from patients with systemic lupus erythematosus. *Clin Immunol* (2007) 123(1):74–81. doi:10.1016/j.clim.2006.12.008
74. Zhang Z, Song L, Maurer K, Petri MA, Sullivan KE. Global H4 acetylation analysis by ChIP-chip in systemic lupus erythematosus monocytes. *Genes Immun* (2010) 11(2):124–33. doi:10.1038/gene.2009.66
75. Leung YT, Shi L, Maurer K, Song L, Zhang Z, Petri M, et al. Interferon regulatory factor 1 and histone H4 acetylation in systemic lupus erythematosus. *Epigenetics* (2015) 10(3):191–9. doi:10.1080/15592294.2015.1009764
76. Zhang Z, Maurer K, Perin JC, Song L, Sullivan KE. Cytokine-induced monocyte characteristics in SLE. *J Biomed Biotechnol* (2010) 2010:507475. doi:10.1155/2010/507475
77. Shi L, Zhang Z, Song L, Leung YT, Petri MA, Sullivan KE. Monocyte enhancers are highly altered in systemic lupus erythematosus. *Epigenomics* (2015) 7(6):921–35. doi:10.2217/epi.15.47
78. Zhang Z, Shi L, Dawany N, Kelsen J, Petri MA, Sullivan KE. H3K4 trimethylation breadth at transcription start sites impacts the transcriptome of systemic lupus erythematosus. *Clin Epigenetics* (2016) 8:14. doi:10.1186/s13148-016-0179-4
79. Dai Y, Zhang L, Hu C, Zhang Y. Genome-wide analysis of histone H3 lysine 4 trimethylation by ChIP-chip in peripheral blood mononuclear cells of systemic lupus erythematosus patients. *Clin Exp Rheumatol* (2010) 28(2):158–68.
80. Oaks Z, Perl A. Metabolic control of the epigenome in systemic lupus erythematosus. *Autoimmunity* (2014) 47(4):256–64. doi:10.3109/08916934.2013.834495
81. Richardson B, Scheinbart L, Strahler J, Gross L, Hanash S, Johnson M. Evidence for impaired T cell DNA methylation in systemic lupus erythematosus and rheumatoid arthritis. *Arthritis Rheum* (1990) 33(11):1665–73. doi:10.1002/art.1780331109
82. Deng C, Kaplan MJ, Yang J, Ray D, Zhang Z, McCune WJ, et al. Decreased ras-mitogen-activated protein kinase signaling may cause DNA hypomethylation in T lymphocytes from lupus patients. *Arthritis Rheum* (2001) 44(2):397–407. doi:10.1002/1529-0131(200102)44:2<397::AID-ANR59>3.0.CO;2-N
83. Rauen T, Grammatikos AP, Hedrich CM, Floege J, Tenbrock K, Ohl K, et al. cAMP-responsive element modulator alpha (CREMalpha) contributes to decreased Notch-1 expression in T cells from patients with active systemic lupus erythematosus (SLE). *J Biol Chem* (2012) 287(51):42525–32. doi:10.1074/jbc.M112.425371
84. Zhang Q, Long H, Liao J, Zhao M, Liang G, Wu X, et al. Inhibited expression of hematopoietic progenitor kinase 1 associated with loss of jumonji domain containing 3 promoter binding contributes to autoimmunity in systemic lupus erythematosus. *J Autoimmun* (2011) 37(3):180–9. doi:10.1016/j.jaut.2011.09.006
85. Forster N, Gallinat S, Jablonska J, Weiss S, Elsasser HP, Lutz W. p300 Protein acetyltransferase activity suppresses systemic lupus erythematosus-like autoimmune disease in mice. *J Immunol* (2007) 178(11):6941–8. doi:10.4049/jimmunol.178.11.6941
86. Hu N, Long H, Zhao M, Yin H, Lu Q. Aberrant expression pattern of histone acetylation modifiers and mitigation of lupus by SIRT1-siRNA in MRL/lpr mice. *Scand J Rheumatol* (2009) 38(6):464–71. doi:10.3109/03009740902895750
87. Mishra N, Reilly CM, Brown DR, Ruiz P, Gilkeson GS. Histone deacetylase inhibitors modulate renal disease in the MRL-lpr/lpr mouse. *J Clin Invest* (2003) 111(4):539–52. doi:10.1172/JCI16153
88. Oaks Z, Winans T, Huang N, Banki K, Perl A. Activation of the mechanistic target of rapamycin in SLE: explosion of evidence in the last five years. *Curr Rheumatol Rep* (2016) 18(12):73. doi:10.1007/s11926-016-0622-8
89. Canaud G, Bienaime F, Tabarin F, Bataillon G, Seilhean D, Noel LH, et al. Inhibition of the mTORC pathway in the antiphospholipid syndrome. *N Engl J Med* (2014) 371(4):303–12. doi:10.1056/NEJMoa1312890
90. Perl A. Activation of mTOR (mechanistic target of rapamycin) in rheumatic diseases. *Nat Rev Rheumatol* (2016) 12(3):169–82. doi:10.1038/nrrheum.2015.172
91. Nakou M, Bertsias G, Stagakis I, Centola M, Tassiulas I, Hatziapostolou M, et al. Gene network analysis of bone marrow mononuclear cells reveals activation of multiple kinase pathways in human systemic lupus erythematosus. *PLoS One* (2010) 5(10):e13351. doi:10.1371/journal.pone.0013351
92. Zhang H, Fu R, Guo C, Huang Y, Wang H, Wang S, et al. Anti-dsDNA antibodies bind to TLR4 and activate NLRP3 inflammasome in lupus monocytes/macrophages. *J Transl Med* (2016) 14(1):156. doi:10.1186/s12967-016-0911-z
93. Carvalheiro T, Gomes D, Pinto LA, Ines L, Lopes A, Henriques A, et al. Sera from patients with active systemic lupus erythematosus patients enhance the toll-like receptor 4 response in monocyte subsets. *J Inflamm (Lond)* (2015) 12:38. doi:10.1186/s12950-015-0083-2
94. Fox RI. Sjogren's syndrome. *Lancet* (2005) 366(9482):321–31. doi:10.1016/S0140-6736(05)66990-5
95. Manoussakis MN, Boiu S, Korkolopoulou P, Kapsogeorgou EK, Kavantzas N, Ziakas P, et al. Rates of infiltration by macrophages and dendritic cells and expression of interleukin-18 and interleukin-12 in the chronic inflammatory lesions of Sjogren's syndrome: correlation with certain features of immune hyperactivity and factors associated with high risk of lymphoma development. *Arthritis Rheum* (2007) 56(12):3977–88. doi:10.1002/art.23073
96. Zhou D, McNamara NA. Macrophages: important players in primary Sjogren's syndrome? *Expert Rev Clin Immunol* (2014) 10(4):513–20. doi:10.1586/1744666X.2014.900441
97. Zhou D, Chen YT, Chen F, Gallup M, Vijmasi T, Bahrami AF, et al. Critical involvement of macrophage infiltration in the development of Sjogren's syndrome-associated dry eye. *Am J Pathol* (2012) 181(3):753–60. doi:10.1016/j.ajpath.2012.05.014
98. Hauk V, Fraccaroli L, Grasso E, Eimon A, Ramhorst R, Hubscher O, et al. Monocytes from Sjogren's syndrome patients display increased vasoactive intestinal peptide receptor 2 expression and impaired apoptotic cell

phagocytosis. *Clin Exp Immunol* (2014) 177(3):662–70. doi:10.1111/cei.12378
99. Enk C, Oxholm P, Tvede N, Bendtzen K. Blood mononuclear cells in patients with primary Sjogren's syndrome: production of interleukins, enumeration of interleukin-2 receptors, and DNA synthesis. *Scand J Rheumatol Suppl* (1986) 61:131–4.
100. Volchenkov R, Brun JG, Jonsson R, Appel S. In vitro suppression of immune responses using monocyte-derived tolerogenic dendritic cells from patients with primary Sjogren's syndrome. *Arthritis Res Ther* (2013) 15(5):R114. doi:10.1186/ar4294
101. Brkic Z, Maria NI, van Helden-Meeuwsen CG, van de Merwe JP, van Daele PL, Dalm VA, et al. Prevalence of interferon type I signature in CD14 monocytes of patients with Sjogren's syndrome and association with disease activity and BAFF gene expression. *Ann Rheum Dis* (2013) 72(5):728–35. doi:10.1136/annrheumdis-2012-201381
102. Wildenberg ME, van Helden-Meeuwsen CG, van de Merwe JP, Drexhage HA, Versnel MA. Systemic increase in type I interferon activity in Sjogren's syndrome: a putative role for plasmacytoid dendritic cells. *Eur J Immunol* (2008) 38(7):2024–33. doi:10.1002/eji.200738008
103. Lavie F, Miceli-Richard C, Ittah M, Sellam J, Gottenberg JE, Mariette X. Increase of B cell-activating factor of the TNF family (BAFF) after rituximab treatment: insights into a new regulating system of BAFF production. *Ann Rheum Dis* (2007) 66(5):700–3. doi:10.1136/ard.2006.060772
104. Yoshimoto K, Tanaka M, Kojima M, Setoyama Y, Kameda H, Suzuki K, et al. Regulatory mechanisms for the production of BAFF and IL-6 are impaired in monocytes of patients of primary Sjogren's syndrome. *Arthritis Res Ther* (2011) 13(5):R170. doi:10.1186/ar3493
105. Eriksson P, Andersson C, Ekerfelt C, Ernerudh J, Skogh T. Sjogren's syndrome with myalgia is associated with subnormal secretion of cytokines by peripheral blood mononuclear cells. *J Rheumatol* (2004) 31(4):729–35.
106. Lisi S, Sisto M, Lofrumento DD, D'Amore M. Altered IkappaBalpha expression promotes NF-kappaB activation in monocytes from primary Sjogren's syndrome patients. *Pathology* (2012) 44(6):557–61. doi:10.1097/PAT.0b013e3283580388
107. Pertovaara M, Silvennoinen O, Isomaki P. Cytokine-induced STAT1 activation is increased in patients with primary Sjogren's syndrome. *Clin Immunol* (2016) 165:60–7. doi:10.1016/j.clim.2016.03.010
108. Pertovaara M, Silvennoinen O, Isomaki P. STAT-5 is activated constitutively in T cells, B cells and monocytes from patients with primary Sjogren's syndrome. *Clin Exp Immunol* (2015) 181(1):29–38. doi:10.1111/cei.12614
109. Lu Q, Renaudineau Y, Cha S, Ilei G, Brooks WH, Selmi C, et al. Epigenetics in autoimmune disorders: highlights of the 10th Sjogren's syndrome symposium. *Autoimmun Rev* (2010) 9(9):627–30. doi:10.1016/j.autrev.2010.05.011
110. Le Dantec C, Varin MM, Brooks WH, Pers JO, Youinou P, Renaudineau Y. Epigenetics and Sjogren's syndrome. *Curr Pharm Biotechnol* (2012) 13(10):2046–53. doi:10.2174/138920112802273326
111. Peng L, Ma W, Yi F, Yang YJ, Lin W, Chen H, et al. MicroRNA profiling in Chinese patients with primary Sjogren syndrome reveals elevated miRNA-181a in peripheral blood mononuclear cells. *J Rheumatol* (2014) 41(11):2208–13. doi:10.3899/jrheum.131154
112. Pauley KM, Stewart CM, Gauna AE, Dupre LC, Kuklani R, Chan AL, et al. Altered miR-146a expression in Sjogren's syndrome and its functional role in innate immunity. *Eur J Immunol* (2011) 41(7):2029–39. doi:10.1002/eji.201040757
113. Zilahi E, Tarr T, Papp G, Griger Z, Sipka S, Zeher M. Increased microRNA-146a/b, TRAF6 gene and decreased IRAK1 gene expressions in the peripheral mononuclear cells of patients with Sjogren's syndrome. *Immunol Lett* (2012) 141(2):165–8. doi:10.1016/j.imlet.2011.09.006
114. Williams AE, Choi K, Chan AL, Lee YJ, Reeves WH, Bubb MR, et al. Sjogren's syndrome-associated microRNAs in CD14(+) monocytes unveils targeted TGFbeta signaling. *Arthritis Res Ther* (2016) 18(1):95. doi:10.1186/s13075-016-0987-0
115. Shah M, Edman MC, Janga SR, Shi P, Dhandhukia J, Liu S, et al. A rapamycin-binding protein polymer nanoparticle shows potent therapeutic activity in suppressing autoimmune dacryoadenitis in a mouse model of Sjogren's syndrome. *J Control Release* (2013) 171(3):269–79. doi:10.1016/j.jconrel.2013.07.016
116. Wechsler B, Davatchi F, Mizushima Y, Hamza M, Dilsen N, Kansu E, et al. Criteria for diagnosis of Behcet's disease. International study group for Behcet's disease. *Lancet* (1990) 335(8697):1078–80.
117. Kanekura T, Gushi A, Iwata M, Fukumaru S, Sakamoto R, Kawahara K, et al. Treatment of Behcet's disease with granulocyte and monocyte adsorption apheresis. *J Am Acad Dermatol* (2004) 51(2 Suppl):S83–7. doi:10.1016/j.jaad.2003.12.023
118. Slobodin G, Toukan Y, Rosner I, Rozenbaum M, Boulman N, Pavlotzky E, et al. LPS-stimulated production of TNF-alpha by peripheral blood monocytes in patients with Behcet's disease. *Clin Rheumatol* (2007) 26(5):764–7. doi:10.1007/s10067-006-0371-6
119. Sahin S, Lawrence R, Direskeneli H, Hamuryudan V, Yazici H, Akoglu T. Monocyte activity in Behcet's disease. *Br J Rheumatol* (1996) 35(5):424–9. doi:10.1093/rheumatology/35.5.424
120. Mege JL, Dilsen N, Sanguedolce V, Gul A, Bongrand P, Roux H, et al. Overproduction of monocyte derived tumor necrosis factor alpha, interleukin (IL) 6, IL-8 and increased neutrophil superoxide generation in Behcet's disease. A comparative study with familial Mediterranean fever and healthy subjects. *J Rheumatol* (1993) 20(9):1544–9.
121. Nakamura S, Sugita M, Tanaka S, Ohno S. [Enhanced production of in vitro tumor necrosis factor-alpha from monocytes in Behcet's disease]. *Nippon Ganka Gakkai Zasshi* (1992) 96(10):1282–5.
122. Morton LT, Situnayake D, Wallace GR. Genetics of Behcet's disease. *Curr Opin Rheumatol* (2016) 28(1):39–44. doi:10.1097/BOR.0000000000000234
123. Castrichini M, Lazzerini PE, Gamberucci A, Capecchi PL, Franceschini R, Natale M, et al. The purinergic P2x7 receptor is expressed on monocytes in Behcet's disease and is modulated by TNF-alpha. *Eur J Immunol* (2014) 44(1):227–38. doi:10.1002/eji.201343353
124. Neves FS, Carrasco S, Goldenstein-Schainberg C, Goncalves CR, de Mello SB. Neutrophil hyperchemotaxis in Behcet's disease: a possible role for monocytes orchestrating bacterial-induced innate immune responses. *Clin Rheumatol* (2009) 28(12):1403–10. doi:10.1007/s10067-009-1261-5
125. Do JE, Kwon SY, Park S, Lee ES. Effects of vitamin D on expression of toll-like receptors of monocytes from patients with Behcet's disease. *Rheumatology (Oxford)* (2008) 47(6):840–8. doi:10.1093/rheumatology/ken109
126. Ambrose N, Khan E, Ravindran R, Lightstone L, Abraham S, Botto M, et al. The exaggerated inflammatory response in Behcet's syndrome: identification of dysfunctional post-transcriptional regulation of the IFN-gamma/CXCL10 IP-10 pathway. *Clin Exp Immunol* (2015) 181(3):427–33. doi:10.1111/cei.12655
127. Hughes T, Ture-Ozdemir F, Alibaz-Oner F, Coit P, Direskeneli H, Sawalha AH. Epigenome-wide scan identifies a treatment-responsive pattern of altered DNA methylation among cytoskeletal remodeling genes in monocytes and CD4+ T cells from patients with Behcet's disease. *Arthritis Rheumatol* (2014) 66(6):1648–58. doi:10.1002/art.38409
128. Gabrielli A, Avvedimento EV, Krieg T. Scleroderma. *N Engl J Med* (2009) 360(19):1989–2003. doi:10.1056/NEJMra0806188
129. Higashi-Kuwata N, Jinnin M, Makino T, Fukushima S, Inoue Y, Muchemwa FC, et al. Characterization of monocyte/macrophage subsets in the skin and peripheral blood derived from patients with systemic sclerosis. *Arthritis Res Ther* (2010) 12(4):R128. doi:10.1186/ar3066
130. Kraling BM, Maul GG, Jimenez SA. Mononuclear cellular infiltrates in clinically involved skin from patients with systemic sclerosis of recent onset predominantly consist of monocytes/macrophages. *Pathobiology* (1995) 63(1):48–56. doi:10.1159/000163933
131. Brkic Z, van Bon L, Cossu M, van Helden-Meeuwsen CG, Vonk MC, Knaapen H, et al. The interferon type I signature is present in systemic sclerosis before overt fibrosis and might contribute to its pathogenesis through high BAFF gene expression and high collagen synthesis. *Ann Rheum Dis* (2016) 75(8):1567–73. doi:10.1136/annrheumdis-2015-207392
132. Mathai SK, Gulati M, Peng X, Russell TR, Shaw AC, Rubinowitz AN, et al. Circulating monocytes from systemic sclerosis patients with interstitial lung disease show an enhanced profibrotic phenotype. *Lab Invest* (2010) 90(6):812–23. doi:10.1038/labinvest.2010.73
133. Duan H, Fleming J, Pritchard DK, Amon LM, Xue J, Arnett HA, et al. Combined analysis of monocyte and lymphocyte messenger RNA expression with serum protein profiles in patients with scleroderma. *Arthritis Rheum* (2008) 58(5):1465–74. doi:10.1002/art.23451
134. York MR, Nagai T, Mangini AJ, Lemaire R, van Seventer JM, Lafyatis R. A macrophage marker, Siglec-1, is increased on circulating monocytes in

patients with systemic sclerosis and induced by type I interferons and toll-like receptor agonists. *Arthritis Rheum* (2007) 56(3):1010–20. doi:10.1002/art.22382
135. Masuda A, Yasuoka H, Satoh T, Okazaki Y, Yamaguchi Y, Kuwana M. Versican is upregulated in circulating monocytes in patients with systemic sclerosis and amplifies a CCL2-mediated pathogenic loop. *Arthritis Res Ther* (2013) 15(4):R74. doi:10.1186/ar4251
136. Varga J, Abraham D. Systemic sclerosis: a prototypic multisystem fibrotic disorder. *J Clin Invest* (2007) 117(3):557–67. doi:10.1172/JCI31139
137. Truchetet ME, Allanore Y, Montanari E, Chizzolini C, Brembilla NC. Prostaglandin I(2) analogues enhance already exuberant Th17 cell responses in systemic sclerosis. *Ann Rheum Dis* (2012) 71(12):2044–50. doi:10.1136/annrheumdis-2012-201400
138. Eloranta ML, Franck-Larsson K, Lovgren T, Kalamajski S, Ronnblom A, Rubin K, et al. Type I interferon system activation and association with disease manifestations in systemic sclerosis. *Ann Rheum Dis* (2010) 69(7):1396–402. doi:10.1136/ard.2009.121400
139. Hasegawa M, Sato S, Takehara K. Augmented production of chemokines (monocyte chemotactic protein-1 (MCP-1), macrophage inflammatory protein-1alpha (MIP-1alpha) and MIP-1beta) in patients with systemic sclerosis: MCP-1 and MIP-1alpha may be involved in the development of pulmonary fibrosis. *Clin Exp Immunol* (1999) 117(1):159–65.
140. Giacomelli R, Cipriani P, Danese C, Pizzuto F, Lattanzio R, Parzanese I, et al. Peripheral blood mononuclear cells of patients with systemic sclerosis produce increased amounts of interleukin 6, but not transforming growth factor beta 1. *J Rheumatol* (1996) 23(2):291–6.
141. Crestani B, Seta N, De Bandt M, Soler P, Rolland C, Dehoux M, et al. Interleukin 6 secretion by monocytes and alveolar macrophages in systemic sclerosis with lung involvement. *Am J Respir Crit Care Med* (1994) 149(5):1260–5. doi:10.1164/ajrccm.149.5.8173768
142. Deguchi Y. Spontaneous increase of transforming growth factor beta production by bronchoalveolar mononuclear cells of patients with systemic autoimmune diseases affecting the lung. *Ann Rheum Dis* (1992) 51(3):362–5. doi:10.1136/ard.51.3.362
143. Umehara H, Kumagai S, Murakami M, Suginoshita T, Tanaka K, Hashida S, et al. Enhanced production of interleukin-1 and tumor necrosis factor alpha by cultured peripheral blood monocytes from patients with scleroderma. *Arthritis Rheum* (1990) 33(6):893–7. doi:10.1002/art.1780330619
144. Westacott CI, Whicher JT, Hutton CW, Dieppe PA. Increased spontaneous production of interleukin-1 together with inhibitory activity in systemic sclerosis. *Clin Sci (Lond)* (1988) 75(6):561–7. doi:10.1042/cs0750561
145. Andrews BS, Friou GJ, Berman MA, Sandborg CI, Mirick GR, Cesario TC. Changes in circulating monocytes in patients with progressive systemic sclerosis. *J Rheumatol* (1987) 14(5):930–5.
146. Allanore Y, Borderie D, Perianin A, Lemarechal H, Ekindjian OG, Kahan A. Nifedipine protects against overproduction of superoxide anion by monocytes from patients with systemic sclerosis. *Arthritis Res Ther* (2005) 7(1):R93–100. doi:10.1186/ar1614
147. Sambo P, Jannino L, Candela M, Salvi A, Donini M, Dusi S, et al. Monocytes of patients with systemic sclerosis (scleroderma spontaneously release in vitro increased amounts of superoxide anion). *J Invest Dermatol* (1999) 112(1):78–84. doi:10.1046/j.1523-1747.1999.00476.x
148. Allanore Y, Borderie D, Hilliquin P, Hernvann A, Levacher M, Lemarechal H, et al. Low levels of nitric oxide (NO) in systemic sclerosis: inducible NO synthase production is decreased in cultured peripheral blood monocyte/macrophage cells. *Rheumatology (Oxford)* (2001) 40(10):1089–96. doi:10.1093/rheumatology/40.10.1089
149. Gunther J, Kill A, Becker MO, Heidecke H, Rademacher J, Siegert E, et al. Angiotensin receptor type 1 and endothelin receptor type A on immune cells mediate migration and the expression of IL-8 and CCL18 when stimulated by autoantibodies from systemic sclerosis patients. *Arthritis Res Ther* (2014) 16(2):R65. doi:10.1186/ar4503
150. Yamaguchi Y, Kuwana M. Proangiogenic hematopoietic cells of monocytic origin: roles in vascular regeneration and pathogenic processes of systemic sclerosis. *Histol Histopathol* (2013) 28(2):175–83. doi:10.14670/HH-28.175
151. Elisa T, Antonio P, Giuseppe P, Alessandro B, Giuseppe A, Federico C, et al. Endothelin receptors expressed by immune cells are involved in modulation of inflammation and in fibrosis: relevance to the pathogenesis of systemic sclerosis. *J Immunol Res* (2015) 2015:147616. doi:10.1155/2015/147616
152. Ciechomska M, Huigens CA, Hugle T, Stanly T, Gessner A, Griffiths B, et al. Toll-like receptor-mediated, enhanced production of profibrotic TIMP-1 in monocytes from patients with systemic sclerosis: role of serum factors. *Ann Rheum Dis* (2013) 72(8):1382–9. doi:10.1136/annrheumdis-2012-201958
153. Binai N, O'Reilly S, Griffiths B, van Laar JM, Hugle T. Differentiation potential of CD14+ monocytes into myofibroblasts in patients with systemic sclerosis. *PLoS One* (2012) 7(3):e33508. doi:10.1371/journal.pone.0033508
154. Yamaguchi Y, Okazaki Y, Seta N, Satoh T, Takahashi K, Ikezawa Z, et al. Enhanced angiogenic potency of monocytic endothelial progenitor cells in patients with systemic sclerosis. *Arthritis Res Ther* (2010) 12(6):R205. doi:10.1186/ar3180
155. Campioni D, Lo Monaco A, Lanza F, Moretti S, Ferrari L, Fotinidi M, et al. CXCR4 pos circulating progenitor cells coexpressing monocytic and endothelial markers correlating with fibrotic clinical features are present in the peripheral blood of patients affected by systemic sclerosis. *Haematologica* (2008) 93(8):1233–7. doi:10.3324/haematol.12526
156. Koch AE, Litvak MA, Burrows JC, Polverini PJ. Decreased monocyte-mediated angiogenesis in scleroderma. *Clin Immunol Immunopathol* (1992) 64(2):153–60. doi:10.1016/0090-1229(92)90193-R
157. Christmann RB, Lafyatis R. The cytokine language of monocytes and macrophages in systemic sclerosis. *Arthritis Res Ther* (2010) 12(5):146. doi:10.1186/ar3167
158. Pechkovsky DV, Prasse A, Kollert F, Engel KM, Dentler J, Luttmann W, et al. Alternatively activated alveolar macrophages in pulmonary fibrosis-mediator production and intracellular signal transduction. *Clin Immunol* (2010) 137(1):89–101. doi:10.1016/j.clim.2010.06.017
159. Pantelidis P, McGrath DS, Southcott AM, Black CM, du Bois RM. Tumour necrosis factor-alpha production in fibrosing alveolitis is macrophage subset specific. *Respir Res* (2001) 2(6):365–72. doi:10.1186/rr87
160. Ciechomska M, O'Reilly S, Przyborski S, Oakley F, Bogunia-Kubik K, van Laar JM. Histone Demethylation and toll-like receptor 8-dependent cross-talk in monocytes promotes transdifferentiation of fibroblasts in systemic sclerosis via Fra-2. *Arthritis Rheumatol* (2016) 68(6):1493–504. doi:10.1002/art.39602
161. Harper L, Savage CO. Pathogenesis of ANCA-associated systemic vasculitis. *J Pathol* (2000) 190(3):349–59. doi:10.1002/(SICI)1096-9896(200002)190:3<349::AID-PATH524>3.0.CO;2-A
162. Muller Kobold AC, Kallenberg CG, Tervaert JW. Monocyte activation in patients with Wegener's granulomatosis. *Ann Rheum Dis* (1999) 58(4):237–45. doi:10.1136/ard.58.4.237
163. Wikman A, Fagergren A, Gunnar OJS, Lundahl J, Jacobson SH. Monocyte activation and relationship to anti-proteinase 3 in acute vasculitis. *Nephrol Dial Transplant* (2003) 18(9):1792–9. doi:10.1093/ndt/gfg216
164. Hattar K, van Burck S, Bickenbach A, Grandel U, Maus U, Lohmeyer J, et al. Anti-proteinase 3 antibodies (c-ANCA) prime CD14-dependent leukocyte activation. *J Leukoc Biol* (2005) 78(4):992–1000. doi:10.1189/jlb.0902442
165. Nowack R, Schwalbe K, Flores-Suarez LF, Yard B, van der Woude FJ. Upregulation of CD14 and CD18 on monocytes In vitro by antineutrophil cytoplasmic autoantibodies. *J Am Soc Nephrol* (2000) 11(9):1639–46.
166. Uehara A, Sato T, Iwashiro A, Yokota S. PR3-ANCA in Wegener's granulomatosis prime human mononuclear cells for enhanced activation via TLRs and NOD1/2. *Diagn Pathol* (2009) 4:23. doi:10.1186/1746-1596-4-23
167. Lamprecht P, Kumanovics G, Mueller A, Csernok E, Komocsi A, Trabandt A, et al. Elevated monocytic IL-12 and TNF-alpha production in Wegener's granulomatosis is normalized by cyclophosphamide and corticosteroid therapy. *Clin Exp Immunol* (2002) 128(1):181–6. doi:10.1046/j.1365-2249.2002.01801.x
168. Ralston DR, Marsh CB, Lowe MP, Wewers MD. Antineutrophil cytoplasmic antibodies induce monocyte IL-8 release. Role of surface proteinase-3, alpha1-antitrypsin, and Fcgamma receptors. *J Clin Invest* (1997) 100(6):1416–24. doi:10.1172/JCI119662
169. Ludviksson BR, Sneller MC, Chua KS, Talar-Williams C, Langford CA, Ehrhardt RO, et al. Active Wegener's granulomatosis is associated with HLA-DR+ CD4+ T cells exhibiting an unbalanced Th1-type T cell cytokine pattern: reversal with IL-10. *J Immunol* (1998) 160(7):3602–9.
170. Casselman BL, Kilgore KS, Miller BF, Warren JS. Antibodies to neutrophil cytoplasmic antigens induce monocyte chemoattractant protein-1 secretion from human monocytes. *J Lab Clin Med* (1995) 126(5):495–502.

171. Johansson AC, Ohlsson S, Pettersson A, Bengtsson AA, Selga D, Hansson M, et al. Impaired phagocytosis and reactive oxygen species production in phagocytes is associated with systemic vasculitis. *Arthritis Res Ther* (2016) 18:92. doi:10.1186/s13075-016-0994-1
172. Park J, Lee EB, Song YW. Decreased tumour necrosis factor-alpha production by monocytes of granulomatosis with polyangiitis. *Scand J Rheumatol* (2014) 43(5):403–8. doi:10.3109/03009742.2014.894568
173. Crawshaw A, Kendrick YR, McMichael AJ, Ho LP. Abnormalities in iNKT cells are associated with impaired ability of monocytes to produce IL-10 and suppress T-cell proliferation in sarcoidosis. *Eur J Immunol* (2014) 44(7):2165–74. doi:10.1002/eji.201344284
174. Okamoto H, Mizuno K, Horio T. Circulating CD14+ CD16+ monocytes are expanded in sarcoidosis patients. *J Dermatol* (2003) 30(7):503–9. doi:10.1111/j.1346-8138.2003.tb00424.x
175. Homolka J, Lorenz J, Zuchold HD, Muller-Quernheim J. Evaluation of soluble CD 14 and neopterin as serum parameters of the inflammatory activity of pulmonary sarcoidosis. *Clin Investig* (1992) 70(10):909–16. doi:10.1007/BF00180437
176. Wiken M, Grunewald J, Eklund A, Wahlstrom J. Higher monocyte expression of TLR2 and TLR4, and enhanced pro-inflammatory synergy of TLR2 with NOD2 stimulation in sarcoidosis. *J Clin Immunol* (2009) 29(1):78–89. doi:10.1007/s10875-008-9225-0
177. Ina Y, Takada K, Sato T, Yamamoto M, Noda M, Morishita M. Soluble interleukin 2 receptors in patients with sarcoidosis. *Possible origin.Chest* (1992) 102(4):1128–33. doi:10.1378/chest.102.4.1128
178. Thole AA, Rodrigues CA, Milward G, Negreiros, Porto LC, Carvalho L. Ultrastructural study of expression of adhesion molecules between blood monocytes and alveolar macrophages from patients with pulmonary sarcoidosis. *J Submicrosc Cytol Pathol* (2001) 33(4):419–24.
179. Sahashi K, Ina Y, Takada K, Sato T, Yamamoto M, Morishita M. Significance of interleukin 6 in patients with sarcoidosis. *Chest* (1994) 106(1):156–60. doi:10.1378/chest.106.1.156
180. Terao I, Hashimoto S, Horie T. Effect of GM-CSF on TNF-alpha and IL-1-beta production by alveolar macrophages and peripheral blood monocytes from patients with sarcoidosis. *Int Arch Allergy Immunol* (1993) 102(3):242–8. doi:10.1159/000236532
181. Tercelj M, Stopinsek S, Ihan A, Salobir B, Simcic S, Wraber B, et al. In vitro and in vivo reactivity to fungal cell wall agents in sarcoidosis. *Clin Exp Immunol* (2011) 166(1):87–93. doi:10.1111/j.1365-2249.2011.04456.x
182. Barth J, Entzian P, Petermann W. Increased release of free oxygen radicals by phagocytosing and nonphagocytosing cells from patients with active pulmonary sarcoidosis as revealed by luminol-dependent chemiluminescence. *Klin Wochenschr* (1988) 66(7):292–7. doi:10.1007/BF01727514
183. Dubaniewicz A, Typiak M, Wybieralska M, Szadurska M, Nowakowski S, Staniewicz-Panasik A, et al. Changed phagocytic activity and pattern of Fcgamma and complement receptors on blood monocytes in sarcoidosis. *Hum Immunol* (2012) 73(8):788–94. doi:10.1016/j.humimm.2012.05.005
184. Heron M, Grutters JC, van Velzen-Blad H, Veltkamp M, Claessen AME, van den Bosch JMM. Increased expression of CD16, CD69, and very late antigen-1 on blood monocytes in active sarcoidosis. *Chest* (2008) 134(5):1001–8. doi:10.1378/chest.08-0443
185. Mizuno K, Okamoto H, Horio T. Heightened ability of monocytes from sarcoidosis patients to form multi-nucleated giant cells in vitro by supernatants of concanavalin A-stimulated mononuclear cells. *Clin Exp Immunol* (2001) 126(1):151–6. doi:10.1046/j.1365-2249.2001.01655.x
186. Perez RL, Roman J. Fibrin enhances the expression of IL-1 beta by human peripheral blood mononuclear cells. Implications in pulmonary inflammation. *J Immunol* (1995) 154(4):1879–87.
187. Talreja J, Farshi P, Alazizi A, Luca F, Pique-Regi R, Samavati L. RNA-sequencing Identifies Novel Pathways in sarcoidosis monocytes. *Sci Rep* (2017) 7(1):2720. doi:10.1038/s41598-017-02941-4
188. Liu Y, Li H, Xiao T, Lu Q. Epigenetics in immune-mediated pulmonary diseases. *Clin Rev Allergy Immunol* (2013) 45(3):314–30. doi:10.1007/s12016-013-8398-3
189. Pociot F, Lernmark A. Genetic risk factors for type 1 diabetes. *Lancet* (2016) 387(10035):2331–9. doi:10.1016/S0140-6736(16)30582-7
190. Espinoza-Jimenez A, Peon AN, Terrazas LI. Alternatively activated macrophages in types 1 and 2 diabetes. *Mediators Inflamm* (2012) 2012:815953. doi:10.1155/2012/815953
191. Zacher T, Knerr I, Rascher W, Kalden JR, Wassmuth R. Characterization of monocyte-derived dendritic cells in recent-onset diabetes mellitus type 1. *Clin Immunol* (2002) 105(1):17–24. doi:10.1006/clim.2002.5265
192. Ren X, Mou W, Su C, Chen X, Zhang H, Cao B, et al. Increase in peripheral blood intermediate monocytes is associated with the development of recent-onset type 1 diabetes mellitus in children. *Int J Biol Sci* (2017) 13(2):209–18. doi:10.7150/ijbs.15659
193. Ryba-Stanislawowska M, Mysliwska J, Juhas U, Mysliwiec M. Elevated levels of peripheral blood CD14(bright) CD16+ and CD14(dim) CD16+ monocytes may contribute to the development of retinopathy in patients with juvenile onset type 1 diabetes. *APMIS* (2015) 123(9):793–9. doi:10.1111/apm.12419
194. Brooks-Worrell BM, Iyer D, Coraza I, Hampe CS, Nalini R, Ozer K, et al. Islet-specific T-cell responses and proinflammatory monocytes define subtypes of autoantibody-negative ketosis-prone diabetes. *Diabetes Care* (2013) 36(12):4098–103. doi:10.2337/dc12-2328
195. Josefsen K, Nielsen H, Lorentzen S, Damsbo P, Buschard K. Circulating monocytes are activated in newly diagnosed type 1 diabetes mellitus patients. *Clin Exp Immunol* (1994) 98(3):489–93. doi:10.1111/j.1365-2249.1994.tb05517.x
196. Litherland SA, She JX, Schatz D, Fuller K, Hutson AD, Peng RH, et al. Aberrant monocyte prostaglandin synthase 2 (PGS2) expression in type 1 diabetes before and after disease onset. *Pediatr Diabetes* (2003) 4(1):10–8. doi:10.1034/j.1399-5448.2003.00042.x
197. Mysliwska J, Smardzewski M, Marek-Trzonkowska N, Mysliwiec M, Raczynska K. Expansion of CD14+CD16+ monocytes producing TNF-alpha in complication-free diabetes type 1 juvenile onset patients. *Cytokine* (2012) 60(1):309–17. doi:10.1016/j.cyto.2012.03.010
198. Harsunen MH, Puff R, D'Orlando O, Giannopoulou E, Lachmann L, Beyerlein A, et al. Reduced blood leukocyte and neutrophil numbers in the pathogenesis of type 1 diabetes. *Horm Metab Res* (2013) 45(6):467–70. doi:10.1055/s-0032-1331226
199. Ismail NA, Abd El Baky AN, Ragab S, Hamed M, Hashish MA, Shehata A. Monocyte chemoattractant protein 1 and macrophage migration inhibitory factor in children with type 1 diabetes. *J Pediatr Endocrinol Metab* (2016) 29(6):641–5. doi:10.1515/jpem-2015-0340
200. Ferreira RC, Guo H, Coulson RM, Smyth DJ, Pekalski ML, Burren OS, et al. A type I interferon transcriptional signature precedes autoimmunity in children genetically at risk for type 1 diabetes. *Diabetes* (2014) 63(7):2538–50. doi:10.2337/db13-1777
201. Wolter TR, Wong R, Sarkar SA, Zipris D. DNA microarray analysis for the identification of innate immune pathways implicated in virus-induced autoimmune diabetes. *Clin Immunol* (2009) 132(1):103–15. doi:10.1016/j.clim.2009.02.007
202. Alkanani AK, Rewers M, Dong F, Waugh K, Gottlieb PA, Zipris D. Dysregulated toll-like receptor-induced interleukin-1beta and interleukin-6 responses in subjects at risk for the development of type 1 diabetes. *Diabetes* (2012) 61(10):2525–33. doi:10.2337/db12-0099
203. Hara N, Alkanani AK, Dinarello CA, Zipris D. Modulation of virus-induced innate immunity and type 1 diabetes by IL-1 blockade. *Innate Immun* (2014) 20(6):574–84. doi:10.1177/1753425913502242
204. Londono P, Komura A, Hara N, Zipris D. Brief dexamethasone treatment during acute infection prevents virus-induced autoimmune diabetes. *Clin Immunol* (2010) 135(3):401–11. doi:10.1016/j.clim.2010.01.007
205. Hara N, Alkanani AK, Dinarello CA, Zipris D. Histone deacetylase inhibitor suppresses virus-induced proinflammatory responses and type 1 diabetes. *J Mol Med (Berl)* (2014) 92(1):93–102. doi:10.1007/s00109-013-1078-1
206. Gottlieb PA, Alkanani AK, Michels AW, Lewis EC, Shapiro L, Dinarello CA, et al. alpha1-Antitrypsin therapy downregulates toll-like receptor-induced IL-1beta responses in monocytes and myeloid dendritic cells and may improve islet function in recently diagnosed patients with type 1 diabetes. *J Clin Endocrinol Metab* (2014) 99(8):E1418–26. doi:10.1210/jc.2013-3864
207. Litherland SA. Immunopathogenic interaction of environmental triggers and genetic susceptibility in diabetes: is epigenetics the missing link? *Diabetes* (2008) 57(12):3184–6. doi:10.2337/db08-1275
208. Chen Z, Miao F, Paterson AD, Lachin JM, Zhang L, Schones DE, et al. Epigenomic profiling reveals an association between persistence of DNA methylation and metabolic memory in the DCCT/EDIC type 1 diabetes

cohort. *Proc Natl Acad Sci U S A* (2016) 113(21):E3002–11. doi:10.1073/pnas.1603712113
209. Rakyan VK, Beyan H, Down TA, Hawa MI, Maslau S, Aden D, et al. Identification of type 1 diabetes-associated DNA methylation variable positions that precede disease diagnosis. *PLoS Genet* (2011) 7(9):e1002300. doi:10.1371/journal.pgen.1002300
210. Miao F, Chen Z, Genuth S, Paterson A, Zhang L, Wu X, et al. Evaluating the role of epigenetic histone modifications in the metabolic memory of type 1 diabetes. *Diabetes* (2014) 63(5):1748–62. doi:10.2337/db13-1251
211. Miao F, Chen Z, Zhang L, Liu Z, Wu X, Yuan YC, et al. Profiles of epigenetic histone post-translational modifications at type 1 diabetes susceptible genes. *J Biol Chem* (2012) 287(20):16335–45. doi:10.1074/jbc.M111.330373
212. Miao F, Smith DD, Zhang L, Min A, Feng W, Natarajan R. Lymphocytes from patients with type 1 diabetes display a distinct profile of chromatin histone H3 lysine 9 dimethylation: an epigenetic study in diabetes. *Diabetes* (2008) 57(12):3189–98. doi:10.2337/db08-0645
213. Irvine KM, Gallego P, An X, Best SE, Thomas G, Wells C, et al. Peripheral blood monocyte gene expression profile clinically stratifies patients with recent-onset type 1 diabetes. *Diabetes* (2012) 61(5):1281–90. doi:10.2337/db11-1549
214. Rousseau MC, El-Zein M, Conus F, Legault L, Parent ME. Bacillus Calmette-Guerin (BCG) vaccination in infancy and risk of childhood diabetes. *Paediatr Perinat Epidemiol* (2016) 30(2):141–8. doi:10.1111/ppe.12263
215. Huppmann M, Baumgarten A, Ziegler AG, Bonifacio E. Neonatal Bacille Calmette-Guerin vaccination and type 1 diabetes. *Diabetes Care* (2005) 28(5):1204–6. doi:10.2337/diacare.28.5.1204
216. Faustman DL, Wang L, Okubo Y, Burger D, Ban L, Man G, et al. Proof-of-concept, randomized, controlled clinical trial of Bacillus-Calmette-Guerin for treatment of long-term type 1 diabetes. *PLoS One* (2012) 7(8):e41756. doi:10.1371/journal.pone.0041756
217. Faustman DL. TNF, TNF inducers, and TNFR2 agonists: a new path to type 1 diabetes treatment. *Diabetes Metab Res Rev* (2018) 34(1). doi:10.1002/dmrr.2941
218. Sag E, Bilginer Y, Ozen S. Autoinflammatory diseases with PERIODIC FEVERS. *Curr Rheumatol Rep* (2017) 19(7):41. doi:10.1007/s11926-017-0670-8
219. Borghini S, Ferrera D, Prigione I, Fiore M, Ferraris C, Mirisola V, et al. Gene expression profile in TNF receptor-associated periodic syndrome reveals constitutively enhanced pathways and new players in the underlying inflammation. *Clin Exp Rheumatol* (2016) 34(6 Suppl 102):S121–8.
220. Bachetti T, Ceccherini I. Tumor necrosis factor receptor-associated periodic syndrome as a model linking autophagy and inflammation in protein aggregation diseases. *J Mol Med (Berl)* (2014) 92(6):583–94. doi:10.1007/s00109-014-1150-5
221. Todd I, Radford PM, Ziegler-Heitbrock L, Ghaemmaghami AM, Powell RJ, Tighe PJ. Elevated CD16 expression by monocytes from patients with tumor necrosis factor receptor-associated periodic syndrome. *Arthritis Rheum* (2007) 56(12):4182–8. doi:10.1002/art.23133
222. Ida H, Aramaki T, Arima K, Origuchi T, Kawakami A, Eguchi K. Successful treatment using tacrolimus (FK506) in a patient with TNF receptor-associated periodic syndrome (TRAPS) complicated by monocytic fasciitis. *Rheumatology (Oxford)* (2006) 45(9):1171–3. doi:10.1093/rheumatology/kel178
223. Carta S, Tassi S, Delfino L, Omenetti A, Raffa S, Torrisi MR, et al. Deficient production of IL-1 receptor antagonist and IL-6 coupled to oxidative stress in cryopyrin-associated periodic syndrome monocytes. *Ann Rheum Dis* (2012) 71(9):1577–81. doi:10.1136/annrheumdis-2012-201340
224. Mortimer L, Moreau F, MacDonald JA, Chadee K. NLRP3 inflammasome inhibition is disrupted in a group of auto-inflammatory disease CAPS mutations. *Nat Immunol* (2016) 17(10):1176–86. doi:10.1038/ni.3538
225. Vento-Tormo R, Alvarez-Errico D, Garcia-Gomez A, Hernandez-Rodriguez J, Bujan S, Basagana M, et al. DNA demethylation of inflammasome-associated genes is enhanced in patients with cryopyrin-associated periodic syndromes. *J Allergy Clin Immunol* (2017) 139(1):202–11e6. doi:10.1016/j.jaci.2016.05.016
226. Ibrahim JN, Jounblat R, Delwail A, Abou-Ghoch J, Salem N, Chouery E, et al. Ex vivo PBMC cytokine profile in familial Mediterranean fever patients: Involvement of IL-1beta, IL-1alpha and Th17-associated cytokines and decrease of Th1 and Th2 cytokines. *Cytokine* (2014) 69(2):248–54. doi:10.1016/j.cyto.2014.06.012
227. Schattner A, Lachmi M, Livneh A, Pras M, Hahn T. Tumor necrosis factor in familial Mediterranean fever. *Am J Med* (1991) 90(4):434–8. doi:10.1016/0002-9343(91)90602-T
228. Davtyan TK, Hakopyan GS, Avetisyan SA, Mkrtchyan NR. Impaired endotoxin tolerance induction in patients with familial Mediterranean fever. *Pathobiology* (2006) 73(1):26–39. doi:10.1159/000093089
229. Direskeneli H, Ozdogan H, Korkmaz C, Akoglu T, Yazici H. Serum soluble intercellular adhesion molecule 1 and interleukin 8 levels in familial Mediterranean fever. *J Rheumatol* (1999) 26(9):1983–6.
230. Simsek I, Pay S, Pekel A, Dinc A, Musabak U, Erdem H, et al. Serum proinflammatory cytokines directing T helper 1 polarization in patients with familial Mediterranean fever. *Rheumatol Int* (2007) 27(9):807–11. doi:10.1007/s00296-006-0301-6
231. Davtyan TK, Harutyunyan VA, Hakobyan GS, Avetisyan SA. Heightened endotoxin susceptibility of monocytes and neutrophils during familial Mediterranean fever. *FEMS Immunol Med Microbiol* (2008) 52(3):370–8. doi:10.1111/j.1574-695X.2008.00385.x
232. Drenth JP, Cuisset L, Grateau G, Vasseur C, van de Velde-Visser SD, de Jong JG, et al. Mutations in the gene encoding mevalonate kinase cause hyper-IgD and periodic fever syndrome. International Hyper-IgD Study Group. *Nat Genet* (1999) 22(2):178–81. doi:10.1038/9696
233. Houten SM, Kuis W, Duran M, de Koning TJ, van Royen-Kerkhof A, Romeijn GJ, et al. Mutations in MVK, encoding mevalonate kinase, cause hyperimmunoglobulinaemia D and periodic fever syndrome. *Nat Genet* (1999) 22(2):175–7. doi:10.1038/9691
234. van der Meer JW, Vossen JM, Radl J, van Nieuwkoop JA, Meyer CJ, Lobatto S, et al. Hyperimmunoglobulinaemia D and periodic fever: a new syndrome. *Lancet* (1984) 1(8386):1087–90. doi:10.1016/S0140-6736(84)92505-4
235. Drenth JP, van der Meer JW, Kushner I. Unstimulated peripheral blood mononuclear cells from patients with the hyper-IgD syndrome produce cytokines capable of potent induction of C-reactive protein and serum amyloid A in Hep3B cells. *J Immunol* (1996) 157(1):400–4.
236. Stoffels M, Jongekrijg J, Remijn T, Kok N, van der Meer JW, Simon A. TLR2/TLR4-dependent exaggerated cytokine production in hyperimmunoglobulinaemia D and periodic fever syndrome. *Rheumatology (Oxford)* (2015) 54(2):363–8. doi:10.1093/rheumatology/keu341
237. Rigante D, Emmi G, Fastiggi M, Silvestri E, Cantarini L. Macrophage activation syndrome in the course of monogenic autoinflammatory disorders. *Clin Rheumatol* (2015) 34(8):1333–9. doi:10.1007/s10067-015-2923-0
238. Mulders-Manders CM, Simon A. Hyper-IgD syndrome/mevalonate kinase deficiency: what is new? *Semin Immunopathol* (2015) 37(4):371–6. doi:10.1007/s00281-015-0492-6
239. Arostegui JI, Anton J, Calvo I, Robles A, Iglesias E, Lopez-Montesinos B, et al. Open-label, phase II study to assess the efficacy and safety of canakinumab treatment in active hyperimmunoglobulinemia D with periodic fever syndrome. *Arthritis Rheumatol* (2017) 69(i):1679–88. doi:10.1002/art.40146
240. Dinarello CA, Simon A, van der Meer JW. Treating inflammation by blocking interleukin-1 in a broad spectrum of diseases. *Nat Rev Drug Discov* (2012) 11(8):633–52. doi:10.1038/nrd3800
241. van der Meer JW, Barza M, Wolff SM, Dinarello CA. A low dose of recombinant interleukin 1 protects granulocytopenic mice from lethal gram-negative infection. *Proc Natl Acad Sci U S A* (1988) 85(5):1620–3. doi:10.1073/pnas.85.5.1620
242. Van't Wout JW, Van der Meer JW, Barza M, Dinarello CA. Protection of neutropenic mice from lethal *Candida albicans* infection by recombinant interleukin 1. *Eur J Immunol* (1988) 18(7):1143–6. doi:10.1002/eji.1830180728
243. Liese JG, Jendrossek V, Jansson A, Petropoulou T, Kloos S, Gahr M, et al. Chronic granulomatous disease in adults. *Lancet* (1996) 347(8996):220–3. doi:10.1016/S0140-6736(96)90403-1
244. Rieber N, Hector A, Kuijpers T, Roos D, Hartl D. Current concepts of hyperinflammation in chronic granulomatous disease. *Clin Dev Immunol* (2012) 2012:252460. doi:10.1155/2012/252460
245. van de Veerdonk FL, Smeekens SP, Joosten LA, Kullberg BJ, Dinarello CA, van der Meer JW, et al. Reactive oxygen species-independent activation of the IL-1beta inflammasome in cells from patients with chronic granulomatous disease. *Proc Natl Acad Sci U S A* (2010) 107(7):3030–3. doi:10.1073/pnas.0914795107

246. Meissner F, Seger RA, Moshous D, Fischer A, Reichenbach J, Zychlinsky A. Inflammasome activation in NADPH oxidase defective mononuclear phagocytes from patients with chronic granulomatous disease. *Blood* (2010) 116(9):1570–3. doi:10.1182/blood-2010-01-264218
247. Gabrion A, Hmitou I, Moshous D, Neven B, Lefevre-Utile A, Diana JS, et al. Mammalian target of rapamycin inhibition counterbalances the inflammatory status of immune cells in patients with chronic granulomatous disease. *J Allergy Clin Immunol* (2017) 139(5):1641–9e6. doi:10.1016/j.jaci.2016.08.033
248. Selmeczy Z, Szelenyi J, Nemet K, Vizi ES. The inducibility of TNF-alpha production is different in the granulocytic and monocytic differentiated forms of wild type and CGD-mutant PLB-985 cells. *Immunol Cell Biol* (2003) 81(6):472–9. doi:10.1046/j.1440-1711.2003.01190.x
249. de Luca A, Smeekens SP, Casagrande A, Iannitti R, Conway KL, Gresnigt MS, et al. IL-1 receptor blockade restores autophagy and reduces inflammation in chronic granulomatous disease in mice and in humans. *Proc Natl Acad Sci U S A* (2014) 111(9):3526–31. doi:10.1073/pnas.1322831111
250. van de Veerdonk FL, Dinarello CA. Deficient autophagy unravels the ROS paradox in chronic granulomatous disease. *Autophagy* (2014) 10(6):1141–2. doi:10.4161/auto.28638
251. Schappi M, Deffert C, Fiette L, Gavazzi G, Herrmann F, Belli D, et al. Branched fungal beta-glucan causes hyperinflammation and necrosis in phagocyte NADPH oxidase-deficient mice. *J Pathol* (2008) 214(4):434–44. doi:10.1002/path.2298
252. Deffert C, Carnesecchi S, Yuan H, Rougemont AL, Kelkka T, Holmdahl R, et al. Hyperinflammation of chronic granulomatous disease is abolished by NOX2 reconstitution in macrophages and dendritic cells. *J Pathol* (2012) 228(3):341–50. doi:10.1002/path.4061
253. Brown KL, Bylund J, MacDonald KL, Song-Zhao GX, Elliott MR, Falsafi R, et al. ROS-deficient monocytes have aberrant gene expression that correlates with inflammatory disorders of chronic granulomatous disease. *Clin Immunol* (2008) 129(1):90–102. doi:10.1016/j.clim.2008.06.005
254. De Ravin SS, Zarember KA, Long-Priel D, Chan KC, Fox SD, Gallin JI, et al. Tryptophan/kynurenine metabolism in human leukocytes is independent of superoxide and is fully maintained in chronic granulomatous disease. *Blood* (2010) 116(10):1755–60. doi:10.1182/blood-2009-07-233734
255. Fujigaki H, Saito K, Fujigaki S, Takemura M, Sudo K, Ishiguro H, et al. The signal transducer and activator of transcription 1alpha and interferon regulatory factor 1 are not essential for the induction of indoleamine 2,3-dioxygenase by lipopolysaccharide: involvement of p38 mitogen-activated protein kinase and nuclear factor-kappaB pathways, and synergistic effect of several proinflammatory cytokines. *J Biochem* (2006) 139 (4):655–62. doi:10.1093/jb/mvj072
256. Bernardo J, Brennan L, Brink HF, Ortiz MF, Newburger PE, Simons ER. Chemotactic peptide-induced cytoplasmic pH changes in incubated human monocytes. *J Leukoc Biol* (1993) 53(6):673–8. doi:10.1002/jlb.53.6.673
257. Broen JC, Bossini-Castillo L, van Bon L, Vonk MC, Knaapen H, Beretta L, et al. A rare polymorphism in the gene for toll-like receptor 2 is associated with systemic sclerosis phenotype and increases the production of inflammatory mediators. *Arthritis Rheum* (2012) 64(1):264–71. doi:10.1002/art.33325

Conflict of Interest Statement: The authors declare that the research was conducted in the absence of any commercial or financial relationships that could be construed as a potential conflict of interest.

frontiers in Immunology

ORIGINAL RESEARCH
published: 26 February 2018
doi: 10.3389/fimmu.2018.00349

Sonic Hedgehog Signaling Regulates Hematopoietic Stem/Progenitor Cell Activation during the Granulopoietic Response to Systemic Bacterial Infection

*Xin Shi[1], Shengcai Wei[2], Kevin J. Simms[1], Devan N. Cumpston[1], Thomas J. Ewing[1] and Ping Zhang[1]**

[1] Department of Integrative Medical Sciences, College of Medicine, Northeast Ohio Medical University, Rootstown, OH, United States, [2] Department of Dermatology, Zhujiang Hospital, Southern Medical University, Guangzhou, China

Activation and reprogramming of hematopoietic stem/progenitor cells play a critical role in the granulopoietic response to bacterial infection. Our current study determined the significance of Sonic hedgehog (SHH) signaling in the regulation of hematopoietic precursor cell activity during the host defense response to systemic bacterial infection. Bacteremia was induced in male Balb/c mice *via* intravenous injection (i.v.) of *Escherichia coli* (5×10^7 CFUs/mouse). Control mice received i.v. saline. SHH protein level in bone marrow cell (BMC) lysates was markedly increased at both 24 and 48 h of bacteremia. By contrast, the amount of soluble SHH ligand in marrow elutes was significantly reduced. These contrasting alterations suggested that SHH ligand release from BMCs was reduced and/or binding of soluble SHH ligand to BMCs was enhanced. At both 12 and 24 h of bacteremia, SHH mRNA expression by BMCs was significantly upregulated. This upregulation of SHH mRNA expression was followed by a marked increase in SHH protein expression in BMCs. Activation of the ERK1/2–SP1 pathway was involved in mediating the upregulation of SHH gene expression. The major cell type showing the enhancement of SHH expression in the bone marrow was lineage positive cells. Gli1 positioned downstream of the SHH receptor activation serves as a key component of the hedgehog (HH) pathway. Primitive hematopoietic precursor cells exhibited the highest level of baseline Gli1 expression, suggesting that they were active cells responding to SHH ligand stimulation. Along with the increased expression of SHH in the bone marrow, expression of Gli1 by marrow cells was significantly upregulated at both mRNA and protein levels following bacteremia. This enhancement of Gli1 expression was correlated with activation of hematopoietic stem/progenitor cell proliferation. Mice with Gli1 gene deletion showed attenuation in activation of marrow hematopoietic stem/progenitor cell proliferation and inhibition of increase in blood granulocytes following bacteremia. Our results indicate that SHH signaling is critically important in the regulation of hematopoietic stem/progenitor cell activation and reprogramming during the granulopoietic response to serious bacterial infection.

Keywords: hedgehog signaling, hematopoietic stem cells, progenitor cells, the granulopoietic response, bacterial infection

OPEN ACCESS

Edited by:
Liwu Li,
Virginia Tech, United States

Reviewed by:
Sulie L. Chang,
Seton Hall University, United States
Kushagra Bansal,
Harvard Medical School, United States

****Correspondence:***
Ping Zhang
pzhang@neomed.edu

Specialty section:
This article was submitted to Molecular Innate Immunity, a section of the journal Frontiers in Immunology

Received: *30 October 2017*
Accepted: *07 February 2018*
Published: *26 February 2018*

Citation:
Shi X, Wei S, Simms KJ, Cumpston DN, Ewing TJ and Zhang P (2018) Sonic Hedgehog Signaling Regulates Hematopoietic Stem/Progenitor Cell Activation during the Granulopoietic Response to Systemic Bacterial Infection. Front. Immunol. 9:349. doi: 10.3389/fimmu.2018.00349

INTRODUCTION

Primitive hematopoietic precursor cells, specifically hematopoietic stem cells (HSCs), are rare event cells in the bone marrow. In normal circumstances, most of these upstream precursors are maintained in the quiescent state with only a small proportion of them entering into cell cycling for self-renewal and/or proliferation (1). The homeostasis of HSC quiescence, self-renewal, proliferation, and differentiation secures maintaining the appropriate pool of HSCs while giving rise to all types of blood cells in the body. Our recent studies have revealed that primitive hematopoietic precursor cells in the adult bone marrow constitute a key component of the host immune defense system (2–4). During bacterial infection, marrow primitive hematopoietic precursor cells activate rapidly. While increasing proliferation to expand their own population in the bone marrow, these cells reprogram their transcriptional polarization toward enhancing commitment to granulocyte lineage (lin) development. Evoking the granulopoietic response to bacterial infection is critically important for boosting granulocyte production in order for reinforcing the phagocytic defense against invading pathogens. Currently, knowledge about cell signaling mechanisms underlying the activation and reprograming of primitive hematopoietic precursor cells in the process of the granulopoietic response to bacterial infection remains scant.

Hedgehog (HH) signaling has been reported to regulate stem cell activity during embryogenesis (5, 6) and in adulthood (7, 8). In mammals, three HH genes, including Sonic (*shh*), Indian (*ihh*), and Desert (*dhh*) HH, have been identified (9, 10). These gene products are initially 45-kDa precursor proteins, which are cleaved and then subjected to cholesterol and palmitoyl modification to produce a 19 kDa active N-terminal fragment (11–13). Among three HH proteins, Sonic hedgehog (SHH) is the best studied ligand (14). SHH molecules are expressed on the cell surface as transmembrane proteins (8, 15–17). SHH signals can be mediated through cell-to-cell contact between adjacent cells expressing the SHH receptor patched (PTCH) 1 and 2. Alternatively, NH2-terminal cleavage of SHH can generate a soluble SHH ligand to interact with distal cells expressing PTCH receptors. Binding of SHH ligand to PTCH abolishes PTCH-exerted repression of Smoothened (SMO) allowing SMO to become active, which activates SHH target gene transcription through the glioma-associated oncogene (Gli) transcription factor family (15–17). In the Gli family, Gli2 exists in both a full-length active form and a truncated repressor form (18, 19). Activated SMO prevents cell process of full-length Gli2 transcription factor into a truncated repressor, enabling Gli2 nuclear translocation to activate the transcription of target genes, particular Gli1 (19–22). Gli1 is a key transcriptional activator for expression of genes for cell proliferation and survival. Gli1 also activates Gli1 and PTCH (1 and 2) gene expression, which serves as positive and negative feedbacks of SHH signaling, respectively (17–23). SHH has been reported to promote primitive hematopoietic precursor proliferation and myeloid differentiation in mouse models (8, 24, 25). At the present time, nevertheless, it remains elusive if SHH–Gli1 signaling participates in the regulation of primitive hematopoietic precursor cell activation and reprograming in host defense against serious bacterial infection.

In this study, we employed both *in vivo* and *in vitro* model systems with manipulations of specific genes to determine the alteration of SHH–Gli1 signal system in bone marrow hematopoietic niche environment and in primitive hematopoietic cells. Our focus was on delineating the role of SHH–Gli1 signaling in the regulation of hematopoietic precursor cell activity during the granulopoietic response to systemic bacterial infection.

MATERIALS AND METHODS

Animals

Male BALB/c mice (6–8 weeks old) were purchased from Charles River Laboratories (Wilmington, MA, USA). Male *Gli1*^{null} mice (6–8 weeks old, derived from STOCK Gli1tm2Alj/J Gli1lacZ mutant mice with 129S1/SvImJ strain background) were bred at Northeast Ohio Medical University Comparative Medicine Unit. Breeding pairs of *Gli1*^{null} (STOCK Gli1tm2Alj/J Gli1lacZ, Stock No. 008211) and the background control (129S1/SvImJ, Stock No. 002448) mouse strains were purchased from The Jackson Laboratory (Bar Harbor, ME, USA). All animals were housed in specific pathogen-free facilities with a 12 h light/dark cycle. This study was carried out in accordance with the recommendations of National Institutes of Health guidelines. The protocol was approved by the Institutional Animal Care and Use Committees of Northeast Ohio Medical University and Michigan State University prior to initiation of all experiments.

Bacteremia was induced in mice as described previously with minor modifications (4). Briefly, an intravenous (i.v. through the penile vein) injection of live *Escherichia coli* (*E. coli*, strain E11775 from the American Type Culture Collection, Rockville, MD; 5×10^7 CFUs in 100 μl of pyrogen-free saline/mouse) was given to mice under anesthesia with inhalation of isoflurane (Henry Schein Animal Health, Dublin, OH, USA). Control mice received i.v. injection of an equal volume of pyrogen-free saline. In a subset of experiments, *E. coli* (5×10^7 CFU in 50 μl pyrogen-free saline/mouse) or saline was i.v. injected into mice. Bromodeoxyuridine (5-bromo-2′-deoxyuridine or BrdU, BD Biosciences, San Diego, CA, USA; 1 mg in 100 μl of saline/mouse) was i.v. administered at the same time. Animals were sacrificed at scheduled time points as indicated in each figure legend in the Section "Results".

At the time of sacrifice, a heparinized blood sample was obtained by cardiac puncture. White blood cells (WBCs) were quantified under a light microscope with a hemocytometer. Both femurs and tibias were collected. Bone marrow cells (BMCs) were flushed out from these bones with a total volume of 2 ml RPMI-1640 medium (Life Technologies, Grand Island, NY, USA) containing 2% bovine serum albumin (BSA, HyClone Laboratories, Logan, UT) through a 23-gage needle. BMCs were filtered through a 70-μm nylon mesh (Sefar America Inc., Kansas City, MO, USA). Contaminating erythrocytes in BMC samples were lysed with RBC lysis solution (Qiagen Sciences, Germantown, MD). Nucleated BMCs were washed with RPMI-1640 medium containing 2% BSA and then quantified under a light microscope with a hemocytometer. For determination of SHH level in bone

marrow elute and nucleated BMC lysate samples, collected femurs, and tibias from each mouse were flushed with a total volume of 0.5 ml of phosphate-buffered saline (PBS, Life Technologies Co, Grand Island, NY, USA) through a 23-gage needle. Bone marrow elute samples were filtered through a 70-μm nylon mesh. After centrifugation at 500 × *g* for 5 min, bone marrow eluate (supernatant) samples were collected. Contaminating erythrocytes in the remaining BMC samples were lysed with RBC lysis solution as above. After washing twice with PBS, nucleated BMCs were collected. BMC lysate samples were prepared by lysing cells with a lysing buffer (10 mM Tris–HCl buffer containing 1% Triton X-100, 5 mM EDTA, 50 mM NaCl, 30 mM sodium pyrophosphate, 2 mM sodium orthovanadate, 1 mM PMSF, 50 mM sodium fluoride, 5 mg/ml aprotinin, 5 mg/ml pepstatin, and 5 mg/ml leupeptin, pH 7.6). After centrifugation at 10,000 × *g* for 10 min at 4°C, the supernatant of BMC lysate sample was collected. Bone marrow eluate and cell lysate samples were stored at −80°C till determination of SHH level.

Preparation of Bacteria

For each experiment, a frozen stock culture of *E. coli* was added to tryptic soy broth and incubated for 18 h at 37°C in an orbital shaker. Bacteria were collected and washed twice with PBS. Suspension of bacteria in saline at appropriate concentrations was prepared based on its optical density at 600 nm. Actual numbers of viable bacteria were verified by standard plate counts of the bacterial suspensions on MacConkey agar plates following overnight incubation at 37°C.

Culture of Primary Mouse BMCs

Isolated mouse BMCs were suspended in StemSpan serum-free medium (StemCell Technologies, Vancouver, BC, Canada) containing 20% mouse plasma and then plated into 24-well tissue culture plates with 500 μl of cell suspension (containing 5×10^6 cells) per well. Culture of cells was conducted without or with lipopolysaccharide (LPS, *E. coli* 0111:B4, 20 ng/ml, Sigma-Aldrich Co., LLC, St. Louis, MO, USA) stimulation in the absence and presence of specific mitogen-activated protein kinase kinase1/2 (MEK1/2) inhibitor PD98059 (25 μM, LC Laboratories, Woburn, MA, USA) for 18 h.

Determination of SHH Level with ELISA

Sonic hedgehog level in bone marrow elute and cell lysate samples was determined with enzyme-linked immunosorbent assay (ELISA) using the Mouse Shh-N ELISA Kit (Abcam, Cambridge, MA, USA) and the protocol provided by the manufacturer.

Determination of Protein Content with BCA Protein Assay

Protein content in biological samples was determined using the BCA Protein Assay Kit (Thermo Fisher Scientific, Rockford, IL, USA) with the protocol provided by the manufacturer.

Flourochrome Conjugation of Antibody

Flourochrome labeling of anti-human/mouse Gli1 antibody (Clone #388516, R&D Systems, Minneapolis, MN, USA) and the matched isotype control antibody (Clone # 54447, R&D Systems) was performed using DyLight 405 Microscale Antibody Labeling Kit (Thermo Fisher Scientific) with the protocol provided by the manufacturer.

Flow Cytometric Analysis and Cell Sorting

Cell phenotype, cell membrane expression of SHH, and intracellular expression of specificity protein 1 (SP1) as well as Gli1 was determined with flow cytometry as previously described (2–4). Briefly, nucleated BMCs or WBCs suspended in RPMI-1640 containing 2% BSA (1×10^6 cells in 100 μl medium) were added with a mixed panel of biotinylated anti-mouse lin markers [10 μg/ml of each antibody against CD3e (clone 145-2C11), CD45R/B220 (clone RA3-6B2), CD11b (Mac-1, clone M1/70), TER-119 (clone TER-119)] with or without granulocyte differentiation antigen-1 (Gr-1 or Ly-6G/Ly-6C, clone RB6-8C5), or isotype control antibodies (clones A19-3, R35-95, A95-1) (BD Biosciences). Following incubation for 20 min at 4°C, flourochrome-conjugated streptavidin, anti-mouse stem cell growth factor receptor (c-kit or CD117, clone 2B8) and anti-mouse stem cell antigen-1 (anti-Sca-1, Ly-6A/E, clone D7) without or with anti-Gr1 (Ly-6G, clone 1A8), or the matched isotype control antibodies (BD Biosciences) were added into the incubation system at the final concentration of 10 μg/ml for each agent. Samples were further incubated in the dark for 20 min at 4°C. Antibody-stained cells were then washed with cold PBS containing 2% BSA. For measuring cell BrdU incorporation, cells were further processed using a BD BrdU Flow Kit (BD Biosciences) with the procedure provided by the manufacturer. For measuring cell expression of SHH and SP1, cells were further processed to make both cell membrane and nuclear membrane permeable for antibody using the procedure (without the step of DNA digestion with DNase) provided by BD BrdU Flow Kit (BD Biosciences). Permeablized cells were incubated with 10 μg/ml of anti-human/mouse SHH (Clone E1, Santa Cruz Biotechnology, Inc., Dallas, TX, USA) and anti-human/mouse SP1 antibody (Clone E3, Santa Cruz Biotechnology, Inc.), respectively, in the dark for 20 min at room temperature. Each cell sample was then added with 10 μg/ml of the corresponding flourochrome-conjugated second antibody [polyclonal goat anti-mouse IgG (H + L), Life Technologies, Eugene, OR, USA and anti-mouse IgG2a, clone R-1915, BD Biosciences]. The cells were further incubated in the dark for 20 min at room temperature. The background staining control samples were incubated with the respective flourochrome-conjugated second antibody only. For determining cell expression of Gli1, permeablized cells were incubated with 10 μg/ml of flourochrome-conjugated anti-human/mouse Gli1 antibody (Clone #388516, R&D Systems) and the isotype control antibody (Clone # 54447, R&D Systems), respectively, in the dark for 20 min at room temperature. At the end of the staining procedure, cells were washed with the washing buffer provided with the BD BrdU Flow Kit (BD Biosciences) and then suspended in 0.5 ml of PBS containing 1% paraformaldehyde. Analysis of cell phenotypes, BrdU incorporation, expression of SHH, SP1, and Gli1 was performed on a FACSAria Fusion flow cytometer with FACSDiva software (Becton Dickinson, San Jose, CA, USA). Cell populations of interest were gated based on their marker or marker combinations. Depending on the cell types

being analyzed, the number of cells acquired in each sample was in the range of 5,000–300,000. In a subset of experiments, gated bone marrow lin$^-$c-kit$^+$ cells were sorted with FACSAria Fusion flow cytometer (Becton Dickinson).

Granulocyte-Macrophage Colony-Forming Unit (CFU-GM) Assays

Granulocyte-macrophage colony-forming unit assays of freshly sorted bone marrow lin$^-$c-kit$^+$ cells were performed by culturing the cells in Methocult GF M3534 medium (StemCell Technologies, Vancouver, BC, Canada) in the absence and presence of recombinant murine SHH (200 ng/ml, eBioscience/Thermo Fisher Scientific). One milliliter of Methocult GF M3534 medium containing 100 cells was plated to a 35 mm NunclonTM dish (Nunc, Rodkilde, Denmark). The cultures were conducted for seven days at 37°C in an atmosphere of 5% CO2. Colonies containing 50 or more cells were then enumerated.

Western Blot Analysis

Western blot analysis of phosphorylated extracellular signal-regulated kinase 1/2 (phospho-ERK1/2) and total ERK1/2 protein expression by cells was performed using the protocol reported previously (4, 26, 27) with minor modifications. Protein was extracted from nucleated BMCs with the lysis buffer described above. Protein concentration was determined using BCA protein assay kit (Thermo Fisher Scientific). Thirty micrograms of protein sample were resolved using the 12% SDS-PAGE ready gel (Bio-Rad Laboratories, Hercules, CA, USA) and transferred to a polyvinylidene difluoride membrane (Bio-Rad Laboratories). The membrane was blocked with 5% milk in tris-buffered saline (Bio-Rad Laboratories) containing 0.1% Tween 20 (Sigma-Aldrich Co.) (TBST buffer) and hybridized sequentially with the primary antibody against phospho-ERK1/2 (anti-mouse phospho-p44/42 MAPK Thr202/Tyr204) and the corresponding HRP-conjugated secondary antibody (Cell Signaling Technology). Determination of the bound antibody was conducted using Amersham ECL Prime Western blotting Detection System (GE Healthcare, Piscataway, NJ) and imaged using Amersham Imager 600 (GE Healthcare Biosciences AB, Uppsala, Sweden). The membrane was stripped with Re-Blot Plus Mild Antibody Stripping Solution (EMD Millipore Cop., Billerica, MA, USA) and then re-probed sequentially with rabbit anti-mouse total ERK1/2 or anti-β-actin antibody (Cell Signaling Technology) and the corresponding HRP-conjugated goat anti-rabbit IgG to determine total ERK1/2 or anti-β-actin content, respectively. Semi-quantification was performed using the ImageJ software. Data are presented as the normalized intensity ratio of the detected protein band versus the loading reference (total ERK1/2 or β-actin) band in the same sample.

Real-time RT-PCR Determination

Total RNA samples were prepared from nucleated BMCs and sorted marrow lin$^-$c-kit$^+$ cells with TRIzol reagent (Thermo Fisher Scientific) and RNeasy Plus Mini Kit (Qiagen, Valencia, CA, USA) using procedures provided by the manufacturers. Real-time RT-PCR analysis of mRNA expression by cells was performed as reported previously (28). Each RNA sample was subjected to 2-step real-time RT-PCR using iScriptTM Reverse Transcription Supermix kit and SsoFastTM EvaGreen® Supermix kit (Bio-Rad Laboratories), respectively, on the CFX96TM Real-Time System (Bio-Rad Laboratories). The amplification primer pairs were as follows:

SHH
Forward 5′-TCCAAAGCTCACATCCACTG
Reverse 5′-CGTAAGTCCTTCACCAGCTTG
Gli1
Forward 5′-TTGTGGGAGGGAAGAAACCG
Reverse 5′-AGCCAGATCCATATGCTGCC
18SrRNA
Forward 5′-ATTCGAACGTCTGCCCTATAA
Reverse 5′-GTCACCCGTGGTCACCATG

These sets of primers were designed using Primer Express software (Life Technologies Co.). The expression of SHH and Gli1mRNA was determined by normalizing the cycle threshold number of their individual mRNA with that of 18S rRNA in each sample. Changes in specific gene mRNA expression by cells from groups with different treatments are expressed as fold alterations over the baseline expression by cells from the corresponding control group.

Reporter Gene Analysis of Murine SHH Promoter Activity

HEK 293T cells (ATCC CRL-11268, American Type Culture Collection) were cultured in Opti-MEM reduced serum medium (Thermo Fisher Scientific) and transfected with pGL4.20[luc2/Puro] promoter reporter vector (Promega, Madison, WI, USA) containing murine shh promoter sequence [240 bp (from −258 to − 497) including 10 SP1 binding sites] in the absence and presence of co-transfection with SP1 expression vector (pUNO1-mSP1 vector, InvivoGen, San Diego, CA, USA). The activity of shh promoter in transfected HEK 293 T cells were determined following culture of cells for 48 h with the Dual-Luciferase® Reporter (DLR™) Assay System on a Glomax 96 Microplate Luminometer (Promega).

Statistical Analysis

Data are presented as mean ± SEM. The sample size is indicated in each figure legend. Statistical analysis was conducted using Student's *t*-test for comparison between two groups and one-way ANOVA followed by Student–Newman–Keuls test for comparison among multiple groups. Difference with statistical significance is accepted at $p < 0.05$.

RESULTS

Upregulation of SHH Expression by BMCs in Response to Bacteremia

Flow cytometric analysis showed that cells in marrow lin$^+$ and lin$^-$c-kit$^+$ subpopulations significantly increased their expression of SHH 24 and 48 h following i.v. challenge with *E. coli* (**Figure 1**). Marrow lin$^-$ cells also exhibited a significant increase

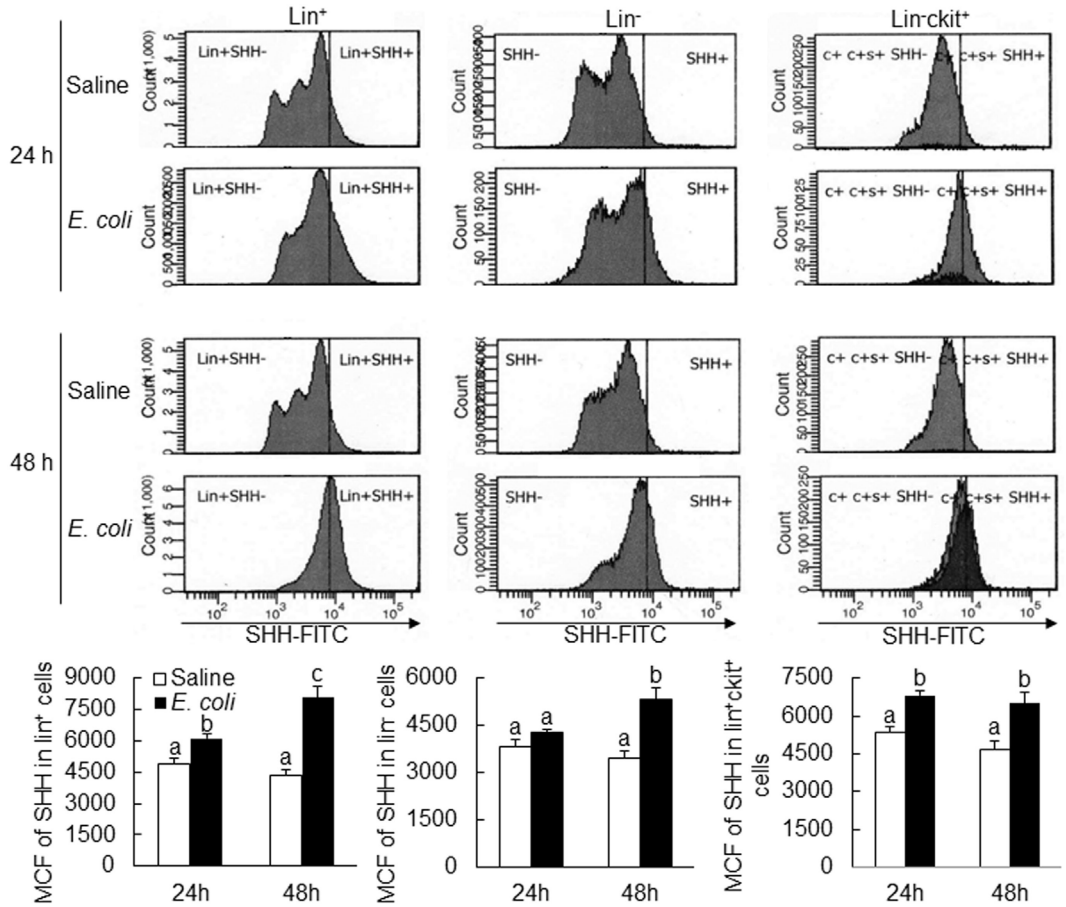

FIGURE 1 | Changes in Sonic hedgehog (SHH) expression by bone marrow cells following systemic *E. coli* infection. Saline: i.v. injection of saline; *E. coli*: i.v. injection of *E. coli*; MCF, mean channel fluorescent intensity. Data are presented as mean ± SEM. $N = 5$. Bars with different letters in each panel are statically different ($p < 0.05$).

in SHH expression 48 h following initiation of bacteremia. This increase in cell expression of SHH in response to systemic bacterial infection was validated by ELISA analysis (**Figure 2**). In association with the increase in SHH protein expression, SHH mRNA expression by BMCs was markedly upregulated 12 and 24 h following bacteremia (**Figure 3A**), indicating that the regulation at the transcriptional level was involved in the increase in SHH ligand expression by marrow cells in response to *E. coli* bacteremia. In contrast to the increase in cell-associated SHH level, the level of soluble SHH in bone marrow elute samples was markedly reduced at both 24 and 48 h post i.v. *E. coli* challenge (**Figure 2**), suggesting that either the release of SHH ligand by BMCs was reduced or cell binding of soluble SHH ligand in the hematopoietic niche environment was enhanced or possibly both following the systemic bacterial infection.

Activation of ERK1/2-SP1 Signaling in Mediating Upregulation of SHH Expression

Analysis of murine *shh* promoter sequence using the AliBaba2.1 database predicted 14 Sp1 transcription factor binding sites with the identity of sequence greater than 80%. Toll-like receptor 4 (TLR4)-ERK1/2 signaling promotes SP1 expression (29, 30). We, therefore, determined if ERK-SP1 signaling was involved in the regulation of SHH expression during the host response to bacteremia. As shown in **Figure 3B**, phospho-ERK1/2 level in BMCs was markedly increased at the early stage (8 h) of bacteremia. Flow cytometric analysis showed that SP1 expression in marrow lin^+, $lin^-c\text{-}kit^+$ and $lin^-c\text{-}kit^+Sca\text{-}1^+$ (LKS, a cell population enriched with HSCs) cells was significantly upregulated 18 h post i.v. challenge with *E. coli* (**Figures 3C,D**). In the *in vitro* culture system, stimulation with LPS caused a significant increase in SHH expression by cultured BMCs (**Figure 3E**). This LPS-stimulated increase in SHH expression was abolished by specific MEK1/2 inhibitor PD98059. Reporter gene analysis demonstrated that SP1 markedly activated murine SHH promoter-driven luciferase expression or activity in HEK 293T cells (**Figure 3F**).

Baseline Gli1 Expression by BMC Subpopulations

Activation of Gli1 expression by target cells responding to the SHH ligand stimulation is a key step in the SHH signal pathway,

which promotes expression of downstream genes for modification of cell activities. We measured the level of Gli1 expression by mouse BMC subpopulations at different stages of differentiation and observed that marrow LKS cells expressed the highest level of Gli1 (**Figure 4**). Gli1 expression reduced with the maturation of hematopoietic cells. Lin$^+$ cells expressed the lowest level of Gli1. These data suggest that primitive hematopoietic precursor cells, particularly HSCs, might be the most active cells responding to the stimulation of SHH ligand under the homeostatic circumstance.

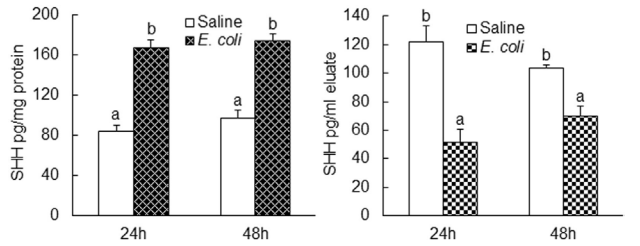

FIGURE 2 | Changes in Sonic hedgehog (SHH) protein level in bone marrow cells lysate and bone marrow elute samples following systemic *E. coli* infection. Saline: i.v. injection of saline; *E. coli*: i.v. injection of *E. coli*. Data are presented as mean ± SEM. $N = 5$. Bars with different letters in each panel are statically different ($p < 0.05$).

Increase in Gli1 Expression in BMCs following Bacteremia

Twenty-four hours following bacteremia, the percentage of Gli1$^+$ cells was significantly increased in LKS, lin$^-$c-kit$^+$ and lin$^+$ cell subpopulations (**Figures 5** and **6**). The numbers of Gli1$^+$LKS and Gli1$^+$lin$^+$ cells in BMCs were significantly increased. Whereas the number of Gli1 positive lin$^-$c-kit$^+$Sca-1$^-$ cells (LKS$^-$ cells, an enriched myeloid progenitor cell population downstream of LKS cells) in BMCs was markedly reduced (**Figure 5**). Mean channel fluorescent intensity (MCF, reflecting the level of specific antigen in the gated cell population) of Gli1 was significantly elevated in LKS and lin$^+$ cell subpopulations 24 h following bacteremia (**Figure 7**). Real-time RT-PCR determination showed that Gli1 mRNA expression was significantly upregulated in lin$^-$c-kit$^+$ cells 24 h following bacteremia (**Figure 8A**). By 48 h of bacteremia, the percentage of Gli1$^+$ cells was significantly increased in LKS, LKS$^-$, lin$^-$c-kit$^+$, lin$^-$, and lin$^+$ cell subpopulations (**Figures 5** and **6**). The numbers of Gli1$^+$LKS, Gli1$^+$lin$^-$c-kit$^+$, and Gli1$^+$lin$^+$ cells in BMCs were also significantly increased. However, the number of Gli1$^+$LKS$^-$ cells in BMCs remained significantly reduced (**Figure 5**). MCF of Gli1 was significantly elevated in LKS, LKS$^-$, lin$^-$c-kit$^+$, lin$^-$, and lin$^+$ cell subpopulations 48 h following bacteremia (**Figure 7**).

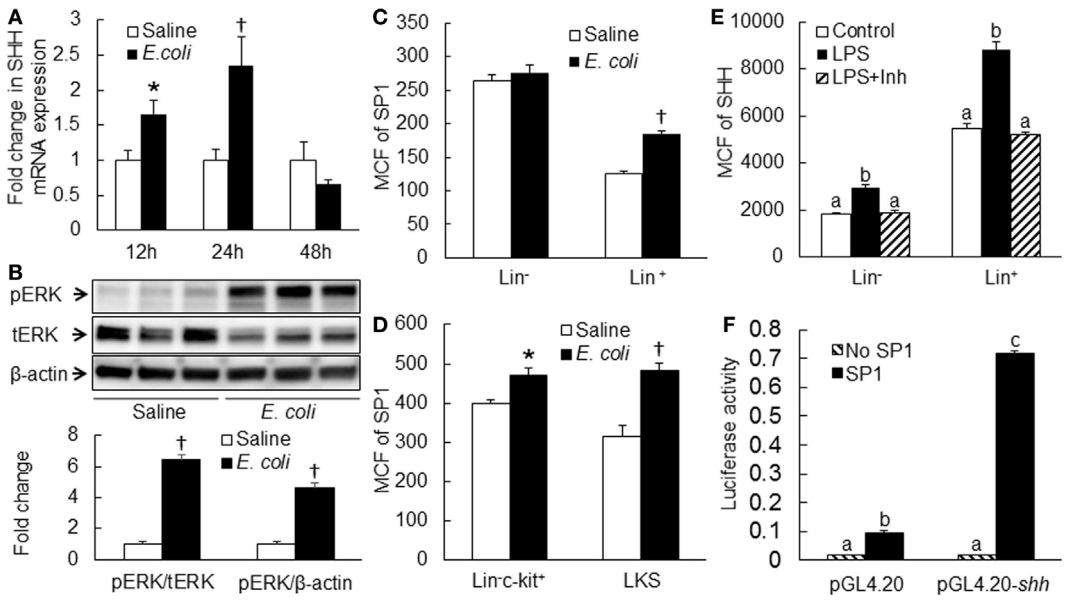

FIGURE 3 | **(A)** Changes in Sonic hedgehog (SHH) mRNA expression by bone marrow cells (BMCs) following systemic *E. coli* infection. Saline: i.v. injection of saline; *E. coli*: i.v. injection of *E. coli*. Data are mean ± SEM. $N = 4$–9. *$p < 0.05$ compared to Saline group; †$p < 0.01$ compared to Saline group. **(B)** Activation of ERK1/2 in BMCs at 8 h of systemic *E. coli* infection. Saline: i.v. injection of saline; *E. coli*: i.v. injection of *E. coli*; pERK: phospho-ERK1/2; tERK: total ERK1/2. Data in the bar figure panel are mean ± SEM. $n = 5$. † $p < 0.01$ compared to Saline group. **(C,D)** Changes in SP1 expression by BMCs at 18 h of systemic *E. coli* infection. Saline: i.v. injection of saline; *E. coli*: i.v. injection of *E. coli*; MCF: mean channel fluorescent intensity. Data are mean ± SEM. N = 5. *$p < 0.05$ compared to Saline group; †$p < 0.01$ compared to Saline group. **(E)** Block of lipopolysaccharide (LPS)-induced SHH expression by BMCs by PD0325901. Control, control cell culture; LPS, LPS stimulation; LPS + Inh, LPS stimulation in the presence of PD0325901. Data are mean ± SEM. $N = 5$. Bars with different letters in each cell subpopulation are statistically different ($p < 0.05$). **(F)** SP1-induced enhancement of *shh* promoter activity in cultured HEK293 T cells. No SP1: cell transfected with control vector; SP1: cell transfected with SP1 expression vector; pGL4.20: cells transfected with control pGL4.20 promoter reporter vector; pGL4.20-shh: cells transfected with pGL4.20 promoter reporter vector containing murine shh promoter sequence. Data are mean ± SEM. $N = 6$. *$p < 0.05$ compared to the corresponding group transfected with control vector without SP1 gene.

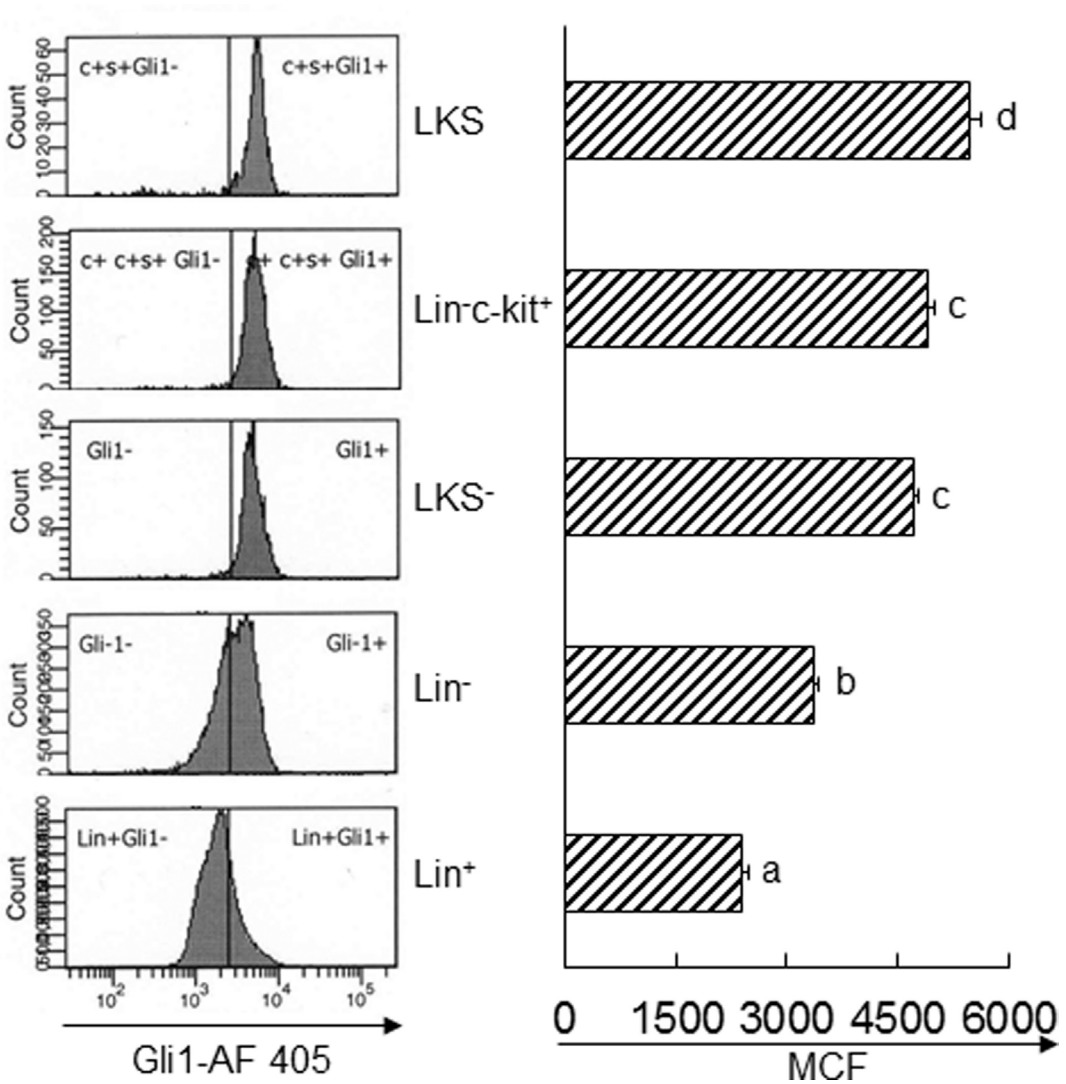

FIGURE 4 | Baseline expression of Gli1 by subtypes of bone marrow cells. Data are presented as mean ± SEM. $N = 4$. Bars with different letters are statistically different ($p < 0.05$).

SHH–Gli1 Signaling in Activation of Primitive Hematopoietic Precursor Cells

To determine the role of SHH–Gli1 signaling in the activation and reprograming of primitive hematopoietic precursor cells during the granulopoietic response to systemic bacterial infection, we conducted *in vivo* cell BrdU incorporation and *in vitro* CFU-GM forming activity experiments. As shown in **Figure 8B**, the percentage of $BrdU^+Gli1^+$ cells in LKS cell subpopulation was significantly increased 24 h following bacteremia. The interesting observation was that the increase in BrdU incorporation into LKS cells following bacteremia was essentially in those cells expressing Gli1 (**Figure 8C**). $Gli1^-$LKS did not show any increase in BrdU incorporation. These data suggest that upregulation of Gli1 expression may play a critical role in LKS activation of proliferation during the host response to bacteremia. *In vitro* culture of sorted marrow $lin^-c\text{-}kit^+$ cells in Methocult GF M3534 medium showed that stimulation with recombinant murine SHH ligand significantly increased CFU-GM forming activity of $lin^-c\text{-}kit^+$ cells (**Figure 8D**), indicating the enhancement of these hematopoietic precursor cell commitment toward myeloid differentiation and granulocyte lin development in response to SHH stimulation.

Impairment of the Granulopoietic Response to Bacteremia with Gli1 Gene Deletion

To further verify the role of SHH–Gli1 signaling in the activation of primitive hematopoietic precursor cells during the granulopoietic response to serious bacterial infection, we employed an *in vivo* model of mice with *Gli1* deletion. As shown in **Figure 9A**, the activity of BrdU incorporation into LKS cells

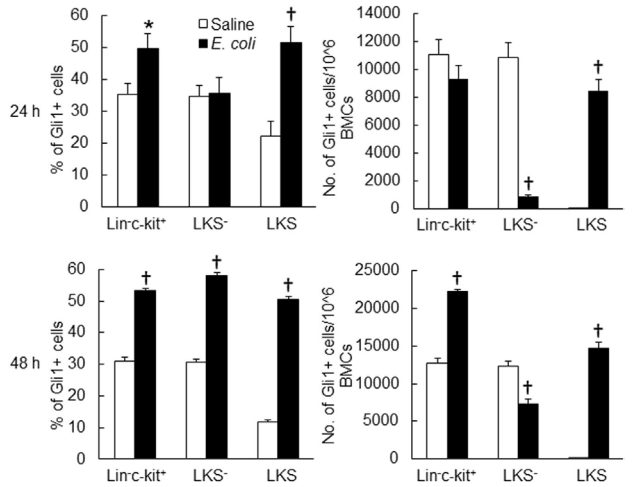

FIGURE 5 | Changes in Gli1+ cells in marrow lin−ckit+, LKS−, and LKS cell subpopulations 24 and 48 h following systemic *E. coli* infection. Saline: i.v. injection of saline; *E. coli*: i.v. injection of *E. coli*. Data are mean ± SEM. $N = 5–7$. $^*p < 0.05$; $\dagger p < 0.01$ compared to the corresponding Saline group.

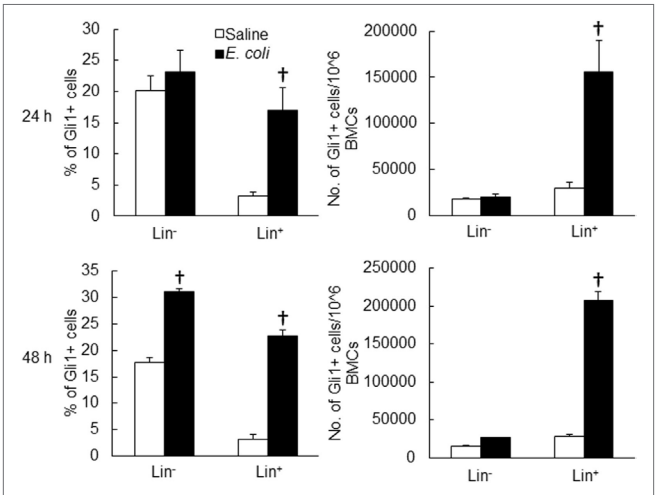

FIGURE 6 | Changes in Gli1+ cells in marrow lin− and lin+ cell subpopulations 24 and 48 h following systemic *E. coli* infection. Saline: i.v. injection of saline; *E. coli*: i.v. injection of *E. coli*. Data are mean ± SEM. $N = 5–7$. $\dagger p < 0.01$ compared to the corresponding Saline group.

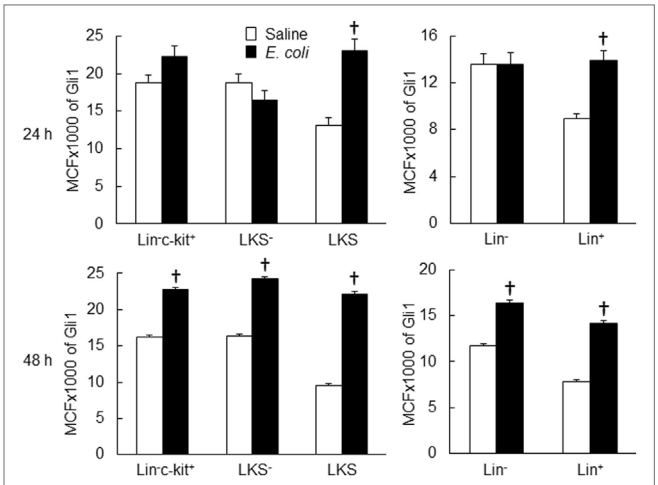

FIGURE 7 | Changes in mean channel fluorescent intensity (MCF) of Gli1 expression by marrow cell subpopulations 24 and 48 h following systemic *E. coli* infection. Saline: i.v. injection of saline; *E. coli*: i.v. injection of *E. coli*. Data are mean ± SEM. $N = 5–7$. $\dagger p < 0.01$ compared to the corresponding Saline group.

was significantly increased in wild-type mice 24 h following bacteremia. *Gli1* deletion did not affect the baseline activity of BrdU incorporation into LKS cells. However, bacteremia-induced activation of BrdU incorporation into LKS cells was significantly attenuated in mice with *Gli1* deletion. The activity of BrdU incorporation into marrow lin− cells was also tended to increase (though did not reach the static significance) in response to bacteremia in wild-type mice (**Figure 9B**). This tendency was not seen in mice with *Gli1* deletion. Furthermore, the number of granulocytes in the systemic circulation was significantly increased following bacteremia in wild-type mice (**Figure 9C**). *Gli1* gene deletion inhibited the increase in granulocytes in the blood stream following systemic *E. coli* infection.

DISCUSSION

Activation of the SHH–Gli1 signal transduction pathway initiates at the engagement of SHH ligand to its receptors (PTCH 1 and 2) on the surface of cells (31). Our current study revealed that *E. coli* bacteremia significantly upregulated SHH expression by bone marrow hematopoietic cells. Twenty-four hours post intravenous challenge with *E. coli*, SHH protein expression by arrow lin+ and lin-c-kit+ cells was significantly upregulated. Furthermore, marrow lin+, lin−, and lin-c-kit+ cells all exhibited a significant increase in SHH expression at 48 h of *E. coli* bacteremia. This increase in SHH expression by marrow hematopoietic cells may support the activation of SHH signaling in the SHH responding cells. Since lin+ cells constitute the major hematopoietic cell population in the bone marrow. They apparently serve as the predominant resource for producing SHH ligand in the bone marrow. An interesting observation was that in contrast to the significant increase in the level of cell-associated SHH, the soluble SHH level in the bone marrow reduced markedly following *E. coli* bacteremia. Therefore, the potential for soluble SHH ligand to activate the SHH signal pathway in distant cells seems to be restricted in this circumstance. Rather, the direct contact between adjacent cells expressing SHH ligand and the correspondent receptors, respectively, is likely critical for effective activation of SHH signaling in the SHH responding cells following systemic bacterial infection. Studies have shown that primitive hematopoietic precursor cells, such as HSCs and upstream progenitors, preferentially lodge in their specific niche compartment relatively separating from sites for storing more mature cells in the bone marrow (32). Even within the HSC population, those maintaining the status of dormancy are believed to reside in the unique niche structures differing from

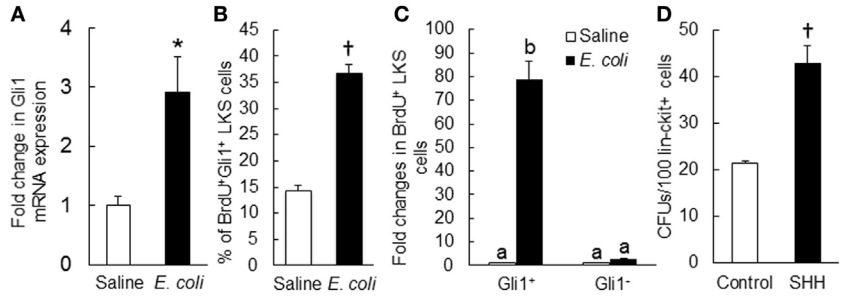

FIGURE 8 | **(A)** Change in Gli1 mRNA expression by marrow lin⁻ckit⁺ cells at 24 h of systemic *E. coli* infection. Saline: i.v. injection of saline; *E. coli*: i.v. injection of *E. coli*. Values are mean ± SEM. $N = 3$. *$p < 0.05$ compared to the Saline group. **(B)** Change in percent of BrdU⁺Gli1⁺ LKS cells in the bone marrow and **(C)** Fold changes in the number of proliferating (BrdU⁺) LKS cells with and without Gli1 expression in the bone marrow at 24 h of systemic *E. coli* infection. Saline: i.v. injection of saline; *E. coli*: i.v. injection of *E. coli*. Data are mean ± SEM. $N = 4$ in each group. †$p < 0.01$ compared to the corresponding Saline group in **(B)**; bars with different letters in **(C)** are statistically different ($p < 0.05$). **(D)** Sonic hedgehog (SHH)-stimulated increase in granulocyte-macrophage colony-forming unit (CFU-GM) formation in cultured marrow lin⁻ckit⁺ cells. Control, without SHH stimulation; SHH, with SHH stimulation. Data are mean ± SEM. $N = 4$. †$p < 0.01$ compared to the control group.

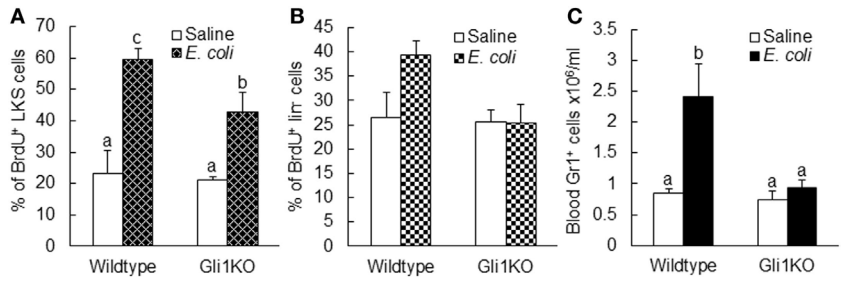

FIGURE 9 | Alteration of BrdU incorporation into marrow LKS **(A)** and lin⁻ **(B)** cells as well as the number of circulating granulocytes **(C)** 24 h after i.v. challenge with *E. coli* in mice with *Gli1* gene deletion. Data are presented as mean ± SEM. $N = 5$–6. Bars with different letters in each panel are statistically different ($p < 0.05$).

places housing their counterparts undergoing proliferation in the bone marrow (33). Take these facts into consideration, it is likely that the enhanced expression of SHH by primitive hematopoietic precursor cells may play an important role in initial activation of SHH signaling in themselves. The upregulated expression of SHH by more mature lin⁺ hematopoietic cells may provide continuing support to activation of SHH signaling in lin-committed precursor cells during the granulopoietic response to systemic *E. coli* infection. In this study, changes in SHH expression were analyzed primarily in marrow hematopoietic cells. Bone marrow niche environment contains other cell types, including osteoblast cells, stromal cells, and endothelial cells. Further investigation on the alteration of SHH expression by these niche cell types will be helpful for further elucidating their possible involvement in the regulation of SHH signaling in hematopoietic precursor cells during the host response to systemic bacterial infection.

In this study, we observed that SHH mRNA expression by nucleated BMCs was significantly upregulated during the early stage of *E. coli* bacteremia, indicating the involvement of transcriptional regulation in the enhancement of SHH expression. To delineate the underlying signaling mechanism, we analyzed murine *shh* promoter sequence using the AliBaba2.1 database. Fourteen SP1 transcription factor binding sites with the identity of sequence greater than 80% were detected. Previous studies have shown that hematopoietic cells including HSCs express full profiles of TLRs (34). Ligand (such as LPS) binding to TLR4 activates the Ras-c-Raf-mitogen-activated protein kinase ERK kinase 1/2 (MEK1/2) system which in turn activates the ERK1/2 signaling component (35, 36). Phosphorylation of ERK1/2 promotes its nuclear translocation to activate SP1 expression (29, 30). In the current study, we observed that the level of phospho-ERK1/2 in BMCs was markedly increased at 8 h of bacteremia. SP1 expression in marrow lin⁺, lin⁻c-kit⁺, and LKS cells was significantly increased 18 h following *E. coli* infection. Inhibition of ERK1/2 activation with specific MEK1/2 inhibitor PD98059 abolished LPS-stimulated increase in SHH expression by cultured BMCs. Furthermore, reporter gene analysis demonstrated that SP1 markedly activated murine SHH promoter. These results demonstrate that the TLR4–ERK1/2–SP1 signal pathway plays a key role in the regulation of SHH expression by hematopoietic cells in the bone marrow during the host response to bacteremia.

Gli1 is a key transcription factor in the SHH signal pathway, activation of which promotes expression of downstream gene products for programming cell fate and modulating cell activities (17–23). We determined the level of Gli1 expression by BMC subtypes at different stages of differentiation in control mice. Under

homeostatic circumstance, the marrow LKS cells expressed the highest level of Gli1. Gli1 expression reduced with the maturation of hematopoietic cells. The lowest level of Gli1 expression was seen in Lin^+ cells. These observations suggest that primitive hematopoietic precursor cells, particularly HSCs (LKS cells), have a strong activity of SHH signaling in normal state. Our data support the significant role of SHH signaling in the regulation of HSC and upstream progenitor cell function under homeostatic condition. Previous studies have shown that SHH promotes primitive hematopoietic precursor cell proliferation and their myeloid differentiation (8, 24, 25). With cell differentiation into the mature stage, the SHH signaling activity reduces. This observation suggests that mature hematopoietic cells might no longer heavily rely on SHH signaling for the regulation of their functional activities in the homeostatic state.

In response to systemic *E. coli* infection, marrow hematopoietic cells significantly increased Gli1 expression in our current study. In marrow lin^- hematopoietic precursor cell fraction, LKS cells were most active in increasing Gli1 expression. *E. coli* bacteremia caused a marked increase in both the number of $Gli1^+$LKS cells and the level of Gli1 protein expression by LKS cells. These data demonstrate that marrow primitive hematopoietic precursor cells possess a substantial capacity to actively respond to enhanced stimulation of SHH ligand in their niche environment during the host response to an infectious challenge. Although the percentage of $Gli1^+$ cells in the LKS^- subpopulation and the level of Gli1 protein expression by LKS^- cells increased, the total number of $Gli1^+$ LKS^- cells in BMCs significantly reduced by 48 h following bacteremia. This observation suggests that SHH signaling is also activated in LKS^- cells following systemic *E. coli* infection. The reduction in the number of $Gli1^+$ LKS^- cells in BMCs is likely caused by conversion of LKS^- cells to cells no longer belonging to the LKS^- phenotype. Our previous investigations have shown that re-expression of Sca-1 by LKS^- cells leads to phenotypic conversion of LKS^- cells to LKS cells, which play an important role in the rapid expansion of LKS cell pool in the bone marrow during the host response to serious bacterial infection (2, 3, 37). It is apparent that the phenotypic conversion of $Gli1^+$ LKS^- cells may also contribute to the marked increase in the number of $Gli1^+$ LKS cells in BMCs following bacteremia in our current study. Transcriptional activation is involved in the increase in Gli1 expression by hematopoietic precursor cells in response to *E. coli* infection. In our current study, Gli1 mRNA expression was significantly upregulated in $lin^-c\text{-}kit^+$ cells at 24 h following bacteremia. The enhancement of Gli1 expression was also detected in marrow lin^+ cells during systemic *E. coli* infection in this study. This increase in Gli1 expression in marrow lin^+ cells appears to imply that the activation of the SHH signaling may also participate in the regulation of functional activities in lin-committed hematopoietic progenitors during the granulopoietic response to the systemic bacterial infection.

The HH signal pathway is a developmentally conserved regulator for stem cell activities. Studies have shown that HH signaling is involved in the regulation of adult HSC function. Neutralization of HH ligands with specific antibodies inhibits cytokine-induced proliferation of primitive human hematopoietic cells (8). Conversely, SHH treatment induces the expansion of pluripotent human hematopoietic repopulating cells in the recipient immunodeficient mice. Downstream activation of the HH signal pathway induces expansion of primitive bone marrow hematopoietic cells under homeostatic conditions and during acute regenerative response to 5-fluorouracil-induced ablation of actively cycling cells in the hematopoietic system (7). Deletion of *Gli1* in mice causes accumulation of more quiescent HSCs as well as decrease in myeloid development (25). In the current study, we examined the role of SHH–Gli1 signaling in the activation of primitive hematopoietic precursor cells during the granulopoietic response to system bacterial infection. The results showed that the increase in proliferative activity (as reflected by cell BrdU incorporation) in LKS cells following bacteremia was essentially in those cells expressing Gli1. By contrast, $Gli1^-$LKS did not exhibit any activation of proliferation. Furthermore, *in vitro* stimulation with recombinant murine SHH ligand significantly increased CFU-GM forming activity of sorted $lin^-c\text{-}kit^+$ cells. These data indicate that the SHH–Gli1 signal pathway participates in mediating primitive hematopoietic precursor cell activation and reprograming for enhancing their commitment toward granulocyte lin development.

Employing an *in vivo* murine model with *Gli1* deletion, we further verified the role of SHH–Gli1 signaling in mediating primitive hematopoietic precursor cell activation during the granulopoietic response to systemic *E. coli* infection. Our data showed that bacteremia-induced activation of proliferation in primitive hematopoietic precursor cells was significantly attenuated in mice with *Gli1* deletion. Accompanied with the inhibition of primitive hematopoietic precursor cell activation, the increase in the number of granulocytes in the systemic circulation during the host response to *E. coli* bacteremia was also inhibited in mice with *Gli1* gene deletion. Our results from the current investigation demonstrate that activation of SHH–Gli1 signaling plays a pivotal role in mediating primitive hematopoietic precursor cell activation during the granulopoietic response to serious bacterial infection.

ETHICS STATEMENT

This study was carried out in accordance with the recommendations of National Institutes of Health guidelines. The protocol was approved by the Institutional Animal Care and Use Committees of Northeast Ohio Medical University and Michigan State University prior to initiation of all experiments.

AUTHOR CONTRIBUTIONS

XS: substantial contributions to concept, designing and conducting experiments, data acquisition, analysis, and interpretation; participating in drafting the work; final approval of the version for publication; agreement to be accountable for all aspects of the work in ensuring that questions related to the accuracy or integrity of any part of the work are appropriately investigated and resolved. SW, KS, DC, and TE: substantial contributions to conducting experiments, data acquisition and analysis; participating in drafting the work; final approval of the version for publication; agreement to be accountable for all aspects of the work

in ensuring that questions related to the accuracy or integrity of any part of the work are appropriately investigated and resolved. PZ: substantial contributions to the conception and design of the work; conducting experiments, data acquisition, analysis, and interpretation; drafting the work; final approval of the version for publication; agreement to be accountable for all aspects of the work in ensuring that questions related to the accuracy or integrity of any part of the work are appropriately investigated and resolved, financially responsible for the entire study.

FUNDING

This investigation was supported by NIH grants R01AA022816 and R01AA019676.

REFERENCES

1. Eaves CJ. Hematopoietic stem cells: concepts, definitions, and the new reality. *Blood* (2015) 125:2605–13. doi:10.1182/blood-2014-12-570200
2. Zhang P, Nelson S, Bagby GJ, Siggins R II, Shellito JE, Welsh DA. The lineage-c-Kit+Sca-1+ cell response to *Escherichia coli* bacteremia in balb/c mice. *Stem Cells* (2008) 26:1778–86. doi:10.1634/stemcells.2007-1027
3. Shi X, Siggins RW, Stanford WL, Melvan JN, Basson MD, Zhang P. Toll-like receptor 4/stem cell antigen 1 signaling promotes hematopoietic precursor cell commitment to granulocyte development during the granulopoietic response to *Escherichia coli* bacteremia. *Infect Immun* (2013) 81:2197–205. doi:10.1128/IAI.01280-12
4. Shi X, Lin YP, Gao B, Zhang P. Impairment of hematopoietic precursor cell activation during the granulopoietic response to bacteremia in mice with chronic-plus-binge alcohol administration. *Infect Immun* (2017) 85:e369–317. doi:10.1128/IAI.00369-17
5. Dyer MA, Farrington SM, Mohn D, Munday JR, Baron MH. Indian hedgehog activates hematopoiesis and vasculogenesis and can respecify prospective neurectodermal cell fate in the mouse embryo. *Development* (2001) 128: 1717–30.
6. Gering M, Patient R. Hedgehog signaling is required for adult blood stem cell formation in *zebrafish* embryos. *Dev Cell* (2005) 8:389–400. doi:10.1016/j.devcel.2005.01.010
7. Trowbridge JJ, Scott MP, Bhatia M. Hedgehog modulates cell cycle regulators in stem cells to control hematopoietic regeneration. *Proc Natl Acad Sci U S A* (2006) 103:14134–9. doi:10.1073/pnas.0604568103
8. Bhardwaj G, Murdoch B, Wu D, Baker DP, Williams KP, Chadwick K, et al. Sonic hedgehog induces the proliferation of primitive human hematopoietic cells via BMP regulation. *Nat Immunol* (2001) 2:172–80. doi:10.1038/84282
9. Perrimon N. Hedgehog and beyond. *Cell* (1995) 80:517–20. doi:10.1016/0092-8674(95)90503-0
10. Hammerschmidt M, Brook A, McMahon AP. The world according to hedgehog. *Trends Genet* (1997) 13:14–21. doi:10.1016/S0168-9525(96)10051-2
11. Porter JA, von Kessler DP, Ekker SC, Young KE, Lee JJ, Moses K, et al. The product of hedgehog autoproteolytic cleavage active in local and long-range signalling. *Nature* (1995) 374:363–6. doi:10.1038/374363a0
12. Lee JJ, Ekker SC, von Kessler DP, Porter JA, Sun BI, Beachy PA. Autoproteolysis in hedgehog protein biogenesis. *Science* (1994) 266:1528–37. doi:10.1126/science.7985023
13. Beachy PA, Cooper MK, Young KE, von Kessler DP, Park WJ, Hall TM, et al. Multiple roles of cholesterol in hedgehog protein biogenesis and signaling. *Cold Spring Harb Symp Quant Biol* (1997) 62:191–204. doi:10.1101/SQB.1997.062.01.025
14. VChoy SW, Cheng SH. Hedgehog signaling. *Vitam Horm* (2012) 88:1–23. doi:10.1016/B978-0-12-394622-5.00001-8
15. Ryan KE, Chiang C. Hedgehog secretion and signal transduction in vertebrates. *J Biol Chem* (2012) 287:17905–13. doi:10.1074/jbc.R112.356006
16. Murone M, Rosenthal A, de Sauvage FJ. Hedgehog signal transduction: from flies to vertebrates. *Exp Cell Res* (1999) 253:25–33. doi:10.1006/excr.1999.4676
17. Irvine DA, Copland M. Targeting hedgehog in hematologic malignancy. *Blood* (2012) 119:2196–204. doi:10.1182/blood-2011-10-383752
18. Sasaki H, Nishizaki Y, Hui C, Nakafuku M, Kondoh H. Regulation of Gli2 and Gli3 activities by an amino-terminal repression domain: implication of Gli2 and Gli3 as primary mediators of Shh signaling. *Development* (1999) 126:3915–24.
19. Hui CC, Angers S. Gli proteins in development and disease. *Annu Rev Cell Dev Biol* (2011) 27:513–37. doi:10.1146/annurev-cellbio-092910-154048
20. Wang C, Pan Y, Wang B. Suppressor of fused and Spop regulate the stability, processing and function of Gli2 and Gli3 full-length activators but not their repressors. *Development* (2010) 137:2001–9. doi:10.1242/dev.052126
21. Pan Y, Wang C, Wang B. Phosphorylation of Gli2 by protein kinase A is required for Gli2 processing and degradation and the sonic hedgehog-regulated mouse development. *Dev Biol* (2009) 326:177–89. doi:10.1016/j.ydbio.2008.11.009
22. Ingham PW, Nakano Y, Seger C. Mechanisms and functions of hedgehog signalling across the metazoa. *Nat Rev Genet* (2011) 12:393–406. doi:10.1038/nrg2984
23. Katoh Y, Katoh M. Hedgehog target genes: mechanisms of carcinogenesis induced by aberrant hedgehog signaling activation. *Curr Mol Med* (2009) 9:873–86. doi:10.2174/156652409789105570
24. Kiuru M, Hidaka C, Hubner RH, Solomon J, Krause A, Leopold PL, et al. Sonic hedgehog expands diaphyseal trabecular bone altering bone marrow niche and lymphocyte compartment. *Mol Ther* (2009) 17:1442–52. doi:10.1038/mt.2009.102
25. Merchant A, Joseph G, Wang Q, Brennan S, Matsui W. Gli1 regulates the proliferation and differentiation of HSCs and myeloid progenitors. *Blood* (2010) 115:2391–6. doi:10.1182/blood-2009-09-241703
26. Melvan JN, Siggins RW, Stanford WL, Porretta C, Nelson S, Bagby GJ, et al. Alcohol impairs the myeloid proliferative response to bacteremia in mice by inhibiting the stem cell antigen-1/ERK pathway. *J Immunol* (2012) 188:1961–9. doi:10.4049/jimmunol.1102395
27. Siggins RW, Melvan JN, Welsh DA, Bagby GJ, Nelson S, Zhang P. Alcohol suppresses the granulopoietic response to pulmonary *Streptococcus pneumoniae* infection with enhancement of STAT3 signaling. *J Immunol* (2011) 186:4306–13. doi:10.4049/jimmunol.1002885
28. Shi X, Chang CC, Basson MD, Upham BL, Wei LX, Zhang P. Alcohol disrupts human liver stem/progenitor cell proliferation and differentiation. *J Stem Cell Res Ther* (2014) 4(1000205):1–8. doi:10.4172/2157-7633.1000205
29. Chanteux H, Guisset AC, Pilette C, Sibille Y. LPS induces IL-10 production by human alveolar macrophages via MAPKinases- and Sp1-dependent mechanisms. *Respir Res* (2007) 8:71. doi:10.1186/1465-9921-8-71
30. Liu YW, Chen CC, Wang JM, Chang WC, Huang YC, Chung SY, et al. Role of transcriptional factors Sp1, c-Rel, and c-Jun in LPS-induced C/EBPdelta gene expression of mouse macrophages. *Cell Mol Life Sci* (2007) 64:3282–94. doi:10.1007/s00018-007-7375-5
31. Villavicencio EH, Walterhouse DO, Iannaccone PM. The sonic hedgehog-patched-gli pathway in human development and disease. *Am J Hum Genet* (2000) 67:1047–54. doi:10.1016/S0002-9297(07)62934-6
32. Heazlewood SY, Oteiza A, Cao H, Nilsson SK. Analyzing hematopoietic stem cell homing, lodgment, and engraftment to better understand the bone marrow niche. *Ann N Y Acad Sci* (2014) 1310:119–28. doi:10.1111/nyas.12329
33. Kunisaki Y, Bruns I, Scheiermann C, Ahmed J, Pinho S, Zhang D, et al. Arteriolar niches maintain haematopoietic stem cell quiescence. *Nature* (2013) 502:637–43. doi:10.1038/nature12612
34. Nagai Y, Garrett KP, Ohta S, Bahrun U, Kouro T, Akira S, et al. Toll-like receptors on hematopoietic progenitor cells stimulate innate immune system replenishment. *Immunity* (2006) 24:801–12. doi:10.1016/j.immuni.2006.04.008
35. Guha M, Mackman N. LPS induction of gene expression in human monocytes. *Cell Signal* (2001) 13:85–94. doi:10.1016/S0898-6568(00)00149-2
36. Guha M, O'Connell MA, Pawlinski R, Hollis A, McGovern P, Yan SF, et al. Lipopolysaccharide activation of the MEK-ERK1/2 pathway in human monocytic cells mediates tissue factor and tumor necrosis factor alpha expression by inducing Elk-1 phosphorylation and Egr-1 expression. *Blood* (2001) 98:1429–39. doi:10.1182/blood.V98.5.1429
37. Zhang P, Welsh DA, Siggins RW II, Bagby GJ, Raasch CE, Happel KI, et al. Acute alcohol intoxication inhibits the lineage- c-kit+ Sca-1+ cell response

to *Escherichia coli* bacteremia. *J Immunol* (2009) 182:1568–76. doi:10.4049/jimmunol.182.3.1568

Conflict of Interest Statement: The authors declare that the research was conducted in the absence of any commercial or financial relationships that could be construed as a potential conflict of interest.

frontiers in Immunology

ORIGINAL RESEARCH
published: 09 March 2018
doi: 10.3389/fimmu.2018.00419

Mitochondrial Sirtuin 4 Resolves Immune Tolerance in Monocytes by Rebalancing Glycolysis and Glucose Oxidation Homeostasis

Jie Tao[1], Jingpu Zhang[1], Yun Ling[1], Charles E. McCall[2] and Tie Fu Liu[1,2]**

[1] Scientific Research Center, Shanghai Public Health Clinical Center, Fudan University, Shanghai, China, [2] Molecular Medicine Section, Department of Internal Medicine, Wake Forest University, Winston-Salem, NC, United States*

The goal of this investigation was to define the molecular mechanism underlying physiologic conversion of immune tolerance to resolution of the acute inflammatory response, which is unknown. An example of this knowledge gap and its clinical importance is the broad-based energy deficit and immunometabolic paralysis in blood monocytes from non-survivors of human and mouse sepsis that precludes sepsis resolution. This immunometabolic dysregulation is biomarked by *ex vivo* endotoxin tolerance to increased glycolysis and TNF-α expression. To investigate how tolerance switches to resolution, we adapted our previously documented models associated with acute inflammatory, immune, and metabolic reprogramming that induces endotoxin tolerance as a model of sepsis in human monocytes. We report here that mitochondrial sirtuin 4 (SIRT4) physiologically breaks tolerance and resolves acute inflammation in human monocytes by coordinately reprogramming of metabolism and bioenergetics. We find that increased SIRT4 mRNA and protein expression during immune tolerance counters the increase in pyruvate dehydrogenase kinase 1 (PDK1) and SIRT1 that promote tolerance by switching glucose-dependent support of immune resistance to fatty acid oxidation support of immune tolerance. By decreasing PDK1, pyruvate dehydrogenase complex reactivation rebalances mitochondrial respiration, and by decreasing SIRT1, SIRT4 represses fatty acid oxidation. The precise mechanism for the mitochondrial SIRT4 nuclear feedback is unclear. Our findings are consistent with a new concept in which mitochondrial SIRT4 directs the axis that controls anabolic and catabolic energy sources.

Keywords: monocytes/macrophages, acute inflammatory resolution, glucose metabolic homeostasis, sirtuin 4, pyruvate dehydrogenase complex, pyruvate dehydrogenase kinase

OPEN ACCESS

Edited by:
Kai Fang,
University of California, Los Angeles, United States

Reviewed by:
Alessandra Durazzo,
Consiglio per la ricerca in agricoltura e l'analisi dell'economia agraria (CREA), Italy
David Dombrowicz,
Institut National de la Santé et de la Recherche Médicale (INSERM), France

***Correspondence:**
Charles E. McCall
chmccall@wakehealth.edu;
Tie Fu Liu
liutiefu@shaphc.org

Specialty section:
This article was submitted to Inflammation, a section of the journal Frontiers in Immunology

Received: *16 December 2017*
Accepted: *15 February 2018*
Published: *09 March 2018*

Citation:
Tao J, Zhang J, Ling Y, McCall CE and Liu TF (2018) Mitochondrial Sirtuin 4 Resolves Immune Tolerance in Monocytes by Rebalancing Glycolysis and Glucose Oxidation Homeostasis. Front. Immunol. 9:419. doi: 10.3389/fimmu.2018.00419

INTRODUCTION

When stressed through TLR4 and other inflammatory and innate immune receptors, monocytes sequentially reprogram their highly conserved life-protection sequence of *resistance*, *tolerance*, *and resolution* (1). Emerging data support that metabolism and bioenergetics coordinately reprogram immune resistance and tolerance during acute inflammation, and that this integrated immunometabolic network dysregulates during many acute and chronic inflammation disorders (2, 3). Different metabolic and energy needs drive functions of distinct immune cell lineages, such as monocytes, macrophages, dendritic cells, T effector, and repressor cells (4), but the energy sources are consistent: glucose and amino acids support the metabolic and anabolic biosynthetic

needs of the effector immune cells that resist inflection; fatty acid oxidation (FAO) with decreased lipogenesis support the catabolic processes associated with tolerance and immune repressor cells (5–7). Despite these gains in understanding how immunity and metabolism are integrated during resistance and tolerance, the reprogramming processes that promote inflammation resolution are unclear. The goal of this investigation was to identify the physiologic path that resolves the acute inflammatory response.

In this context, we have previously reported that epigenetic reprogramming of tolerance in human and mouse monocytes is directed by a nuclear sirtuin 1 (SIRT1) and SIRT6 axis (8) and SIRT1-RelB-SIRT3 axis (9). This NAD redox sensing checkpoint switches the glycolysis-dependent resistance phenotype to the FAO-dependent tolerance phenotype (10, 11). We also discovered that mitochondrial pyruvate dehydrogenase kinase 1 (PDK1) persistently deactivates pyruvate dehydrogenase complex (PDC), which is downstream of nuclear epigenetic reprogramming of tolerance by nuclear SIRT1 in mice and human septic monocytes. PDC is the rate-limiting step in decarboxylating pyruvate to acetyl CoA and oxidizing Krebs cycle glucose-based carbons that support oxidative phosphorylation (12). SIRT1 is a key regulator of fatty acid lipolysis and FAO (13). Glucose is known to primarily support anabolism and FAO to support catabolic processes. Dominance of catabolic energy over anabolic energy during tolerance deprives immune cells of glucose carbons needed to resist infection.

In this study of inflammation resolution, we adapted our published models of mouse and human acute inflammation that simulate sepsis, which use primary monocytes and THP-1-transformed monocytes to reprogram glucose anabolic fueling of the immune resistance phenotype to FAO fueling of the immune tolerance (10). Based on the known ability of mitochondrial sirtuin 4 (SIRT4) (14) to oppose the catabolic effects of mitochondrial SIRT3 that support fatty acid β oxidation and tolerance (15, 16), we surmised that SIRT4 might reprogram tolerance to resolution. Here, we report that SIRT4 breaks tolerance and promotes acute inflammation resolution in monocytes.

MATERIALS AND METHODS

Chemicals and Standards

Bacterial endotoxin [lipopolysaccharide endotoxin (LPS)] was purchased from Sigma (*Escherichia coli* 0111:B4); D-[5-^{3}H(N)]-glucose, D-[6-^{14}C]-glucose, 1-[^{14}C]-palmitic acid and hyamine were obtained from Perkin-Elmer; Mito stress kit was from Seahorse Bioscience; Cell-Tak was from BD company; colorimetric assay kits for pyruvate dehydrogenase (PDH), lactate dehydrogenase (LDH) activities and for pyruvate and lactate levels were from Biovision; gene-specific TaqMan primer/probe sets were from Applied Biosystems; SIRT4 gene-specific siRNA and control siRNA were from Santa Cruz Biotechnology; SIRT4 Flag (Plasmid #13815) (17), control pcDNA3.1+ without SIRT4 sequence, lentiCRISPRv2 vector, lentivirus helper plasmids psPAX2 and pND2.G were from Addgene; gene-specific antibodies were purchased from Gentex company.

Modeling the Acute Inflammatory Response in THP-1 Human Monocytes

THP-1 cells from the American Type Culture Collection were maintained in RPMI 1640 medium (Invitrogen) supplemented with 100 U/ml penicillin, 100 μg/ml streptomycin, 2 mM L-glutamine, and 10% fetal bovine serum (HyClone, Logan, UT) in a humidified incubator with 5% CO_2 at 37°C. Cells were stimulated with 1 μg/ml of bacterial endotoxin LPS (*Escherichia coli* 0111:B4, Sigma) for indicated times to generate inflammatory phases of initiation (0–8 h), endotoxin tolerance (24–48 h), and resolution (48–96 h). Endotoxin tolerance is determined after a second stimulation with LPS at 1 μg/ml for 1 h.

Modeling the Acute Inflammatory Response in Human Peripheral Blood Mononuclear Cells

Healthy human blood samples were collected according to the protocol approved by Shanghai Public Health Clinical Center Ethics Committee, Fudan University. Peripheral blood mononuclear cells were purified by ficoll-hypaque density gradient centrifugation. Cells were maintained in complete RPMI 1640 culture medium for the indicated times in the presence or absence of 100 ng/ml LPS for SIRT4 gene expression and protein assay.

Measuring Glucose and FAO

Oxidation of glucose and fatty acid was measured by radiolabeling as described previously (10). Briefly, cells were starved in triplicate in polypropylene vials for 30 min at 37°C in glucose-free Hank's buffer. The vials were then placed into glass scintillation tube. After addition to cells 1 μCi of D-[6-^{14}C]-glucose and 2.5 mM cold glucose or 1 μCi of 1-[^{14}C]-palmitic acid in 0.2% BSA-Hank's buffer, the scintillation tubes were sealed and rotated at 37°C in a water bath for 1 h. Metabolic reaction was then stopped by injecting 200 μl of 2N HCl into the central vials, and 500 μl of hyamine (Perkin-Elmer) was injected into the scintillation tube. $^{14}CO_2$ generated by the oxidation of D-[6-^{14}C]-glucose or 1-[^{14}C]-palmitic acid was collected by overnight shaking at room temperature, $^{14}CO_2$ in hyamine was counted using a β-counter. One μCi of D-[6-^{14}C]-glucose alone or 1-[^{14}C]-palmitic acid alone in the same amount of buffer was set for background counts.

Glycolysis Assays

Glycolysis was measured by the conversion of D-[5-^{3}H(N)]-glucose to tritiated water as described elsewhere (10). In brief, after starvation with glucose-free RPMI (Gibco) medium, Cells were incubated in triplicates with 1 μCi of D-[5-^{3}H(N)]-glucose (Perkin-Elmer) at 37°C for 1 h in scintillation tubes containing 1 ml of H_2O. The reaction was stopped by adding HCl (1N final) and scintillation tube was sealed. $[^{3}H]_2O$ generated by enolase activity from D-[5-^{3}H(N)]-glucose was vaporized for overnight at 50°C oven and cooled down for another overnight at 4°C. After removal of the central wells, $[^{3}H]_2O$ was counted using a β-counter for detection of glycolytic rate. One μCi of D-[5-^{3}H(N)]-glucose alone in triplicates was set for background control. One μCi of

$[^3H]_2O$ (Perkin-Elmer) alone in triplicates was set for detecting the efficiency of this water vapor exchange.

Mitochondrial Respiration Monitoring

Mitochondrial oxidative phosphorylation reactions were assessed by comparing the ratio of oxygen consumption rate (OCR) and extracellular acidification rate (ECAR) with a cell Mito stress kit using an XFe-24 Extracellular Flux Analyzer (Seahorse Bioscience) (9). XFe sensor was pre-calibrated in XFe calibrate medium for overnight at 37°C in a CO_2-free incubator. The 24-well microplate was pretreated for 20 min with Cell-Tak 3.5 μg/cm^2 surface area (BD Biosciences) in 0.1 M sodium bicarbonate (pH 8.0) buffer. Excess Cell-Tak was removed by two washes with sterile water. THP-1 cells (2×10^5/well) in bicarbonate-free and Hepes-free RPMI medium (pH 7.4, Invitrogen) supplemented with 2% FBS were set into a Cell-Tak pretreated microplate and pre-incubated for 1 h at 37°C in a CO_2-free incubator. Then 10-fold concentrated compounds (Seahorse Biosciences) of oligomycin (Complex V inhibitor), carbonyl cyanide-*p*-trifluoromethoxyphenylhydrazone (FCCP, electron transport chain uncoupler), or a mixture of rotenone (Complex I inhibitor) and antimycin A (Complex III inhibitor) were loaded into a sensor cartridge to produce final concentration of them at 1 μM, 1.5 μM, 100 nM, and 1 μM, respectively. After a 30 min calibration of the XFe sensor with the pre-incubated sensor cartridge, the cell plate was loaded into the analyzer, OCR and ECAR were analyzed under basal condition and followed by sequential injection of the complex inhibitors oligomycin, FCCP, and the mixture of rotenone and antimycin A. Data were analyzed using XFe software (Seahorse Bioscience) and normalized with protein loaded in each well. Four replicates of each sample were analyzed.

Enzyme Activity Assays

Colorimetric assay kits (Biovision) were used to biochemically assess the enzymatic activities of PDH and LDH according to the manufacture's instruction. In brief, cells (1×10^6) were lysed for 10 min in ice cold assay buffer, supernatants were collected by centrifugation and 10 μl of supernatant of each sample were loaded into 96-well plate in duplicates and adjusted the volume to 50 μl/well with assay buffer. Optic density (OD) at 450 nm was read immediately (OD-0) and 30 min (OD-30) after incubation at room temperature. Sample OD was calculated by subtracting OD-0 from OD-30. NADH standard curve was generated by adding 0, 2, 4, 6, 8, and 10 μl of 1.25 mM NADH Standard into a series of wells to generate 0, 2.5, 5.0, 7.5, 10, and 12.5 nmol/well of NADH Standard after adjusting the volume to 50 μl/well with assay buffer. Data were normalized with loaded protein.

Intracellular Pyruvate and Lactate Levels

Intracellular pyruvate and lactate were measured by colorimetric assay kits (BioAssay Systems, CA, USA) according to manufacturer's instruction. Briefly, 10 μl of samples or standards were transferred into 96-well plates in duplicates. Ninety microliters of working solution were added into each wells and incubated for 30 min at room temperature. Optical density at 570 nm was read and concentration of pyruvate or lactate was calculated from standard curve.

Real-time RT-PCR

Levels of human TNF-α, SIRT1, SIRT4, and PDK1 mRNA were measured as describe previously (8–10) by quantitative real-time RT-PCR using gene-specific TaqMan primer/probe sets in an ABI prism 7000 Sequence Detection System (Applied Biosystems). GAPDH mRNA transcription was used for internal loading control.

SIRT4 Gene-Specific Knockdown and Knockout

For SIRT4 knockdown, 60 pMol of a pool of three target-specific siRNA (Santa Cruz Biotechnology) were electronically transfected into responsive THP-1 cells for 24 h using Amaxa Nucleofector kit V and Amaxa nucleofector II device (Lonza, Inc.) and a pool of scrambled siRNAs was transfected as a negative control. The inhibition efficiency of knockdown is ~70% mRNA reduction on basal and after LPS stimulation.

For over-expression of SIRT4, THP-1 cells were electronically transfected with SIRT4 Flag (Plasmid #13815) (17) or pcDNA3.1+ without SIRT4 sequence for 24 h, cells were then processed for experiments. Basal SIRT4 mRNA level of SIRT4 plasmid transfected cells was 2.5-fold higher than that of control cells.

For SIRT4 knockout using CRISPR-Cas9 technique, the gRNA in lentiCRISPRv2 vector (Addgene, Cambridge, MA, USA) was designed as follows Oligo 1: 5′-CACCGGAGGCT CCTAGTAATGACCG-3′, Oligo 2: 3′-AAACCGGTCATTACTA GGAGCCTCC-5′. The lentiCRISPRv2 plasmid harboring the gRNA sequence and Cas9 gene, lentivirus helper plasmids psPAX2 and pND2.G (Addgene, Cambridge, MA, USA) were co-transfected into HEK-293T cells (American Type Culture Collection) using HG-trans293 (Healthgene, Canada) according to the manufacturer's protocol. Virus-containing supernatants were collected 48 h and 72 h after transfection, respectively, filtered to eliminate cells, and infect target cells in the presence of 8 μg/ml polybrene. 72 h later, infected cells were cultured with 1 μg/ml puromycin for 7 days, puromycin resistant cells were set for experiments. LentiCRISPRv2 vector without SIRT4 gRNA sequence was used as control. SIRT4 gRNA containing cells reduced more than 90% SIRT4 protein level based on immunoblotting assay.

Western Blot Analysis

Protein levels were analyzed as described previously (8). In brief, equal amounts (50 μg) of cell lysates were separated by SDS-PAGE electrophoresis and transferred to a polyvinylidene difluoride membrane (Perkin-Elmer Life Sciences). Blots were blocked with 5% milk-PBST for 1 h at room temperature and probed for overnight at 4°C using primary antibodies against SIRT4, PDK1, PDC, p-PDC E1α-S_{232} (Genetex), and GAPDH. Protein complexes were detected by incubation for 1 h at room temperature with secondary antibodies conjugated to horseradish peroxidase (Sigma) diluted at 1:2,000 in blocking buffer and then detected by Enhanced Chemiluminescence Plus (GE Healthcare). Protein

binds were scanned and densitometry analysis was performed using ImageJ software.

Statistical Analyses

Differences of immune metabolic changes between two related conditions were analyzed by Student's *t*-test using GraphPad Prism version 6 (San Diego, CA, USA). *P*-values of less than 0.05 were considered significant. For experiments with more than two groups, Prism's Two Way Analysis of Variance (ANOVA) was used with *post hoc* analysis of across multiple means. Exact *P* values are shown. Data points are Mean ± SEM of replicates.

RESULTS

Simultaneous Immune Metabolic Switches Reprogram Physiological Resolution of Acute Inflammatory Response

To understand if the physiological switch of immune suppression to inflammatory resolution also aligns with metabolic and energetic changes, we first timed the recovery of acute inflammatory response using a validated human monocyte THP-1 cell model of sepsis (8–10). THP-1 cells were stimulated with high dose (1 μg/ml) LPS for different times till 96 h. Pro-inflammatory cytokine TNF-α gene was monitored by real-time RT-PCR analysis. TNF-α mRNA of THP-1 cells was emerged peak transcription at 1 h ($P = 0.0021$), repressed at 8 h ($P = 0.0025$) and sustained at low level till 96 h after primary LPS stimulation. To determine the time of physiological recovery from immune suppression, THP-1 cells received second LPS stimulation at different time points after the first LPS stimulation. TNF-α transcription was not significantly induced at 8 h ($P = 0.1262$) and 24 h ($P = 0.2625$), indicating the generation of immune tolerance; however, TNF-α was significantly induced at 48 h after first LPS ($P = 0.0006$) and was gradually increased at 72 h ($P = 0.0003$) and 96 h ($P = 0.0006$) in response to second LPS stimulation (**Figure 1A**). This observation indicates that immune tolerant monocytes are physiologically able to resolve their immune repressor state.

As the immune tolerance in monocytes requires a switch from glucose to fatty acid metabolism (10), we reasoned the second switch from tolerance to resolution might reverse this alignment. To test this possibility, we assessed the dynamics of metabolic ratio of glucose oxidation (GO) to fatty acid oxidation (FAO) during the course of acute inflammatory response using radiolabeling analysis. Consistence with our premise, the ratio of $^{14}CO_2$ production of ^{14}C-glucose to that of ^{14}C-palmitic acid was significantly decreased at 24 h ($P = 0.0003$), but increased 48 h after LPS stimulation (resolving switch, $P = 0.0086$) and restored toward the basal level ($P = 0.1797$, **Figure 1B**).

Concordant with this metabolic shift, the ratio of mitochondrial OCR and glycolytic ECAR increased at 24 h and returned to baseline at 48 h (**Figure 1C**) as described previously (9). These findings are consistent with the notion that physiological resolution of acute inflammation restores metabolic and energy homeostasis.

Increases in SIRT4 Expression Parallel Development of Immune Tolerance Reprogramming and Precede Resolution of the Acute Inflammatory Response

Since mitochondrial SIRT4 may counter the effects of SIRT3 (14), which we reported links to SIRT1 epigenetic reprogramming of immune tolerance (8), we hypothesized that SIRT4 activity might contribute to acute inflammatory resolution by countering SIRT1 and SIRT3 effects support of catabolic immune repressor pathways. To test this possibility, we determined the dynamics of gene expression of the seven mammalian sirtuin members in THP-1 cell model of acute inflammatory response. In contrast to the moderate increases in SIRT1, SIRT3, and SIRT6 gene expression during the early phase, SIRT4 was the only gene that was dramatically induced during the tolerance

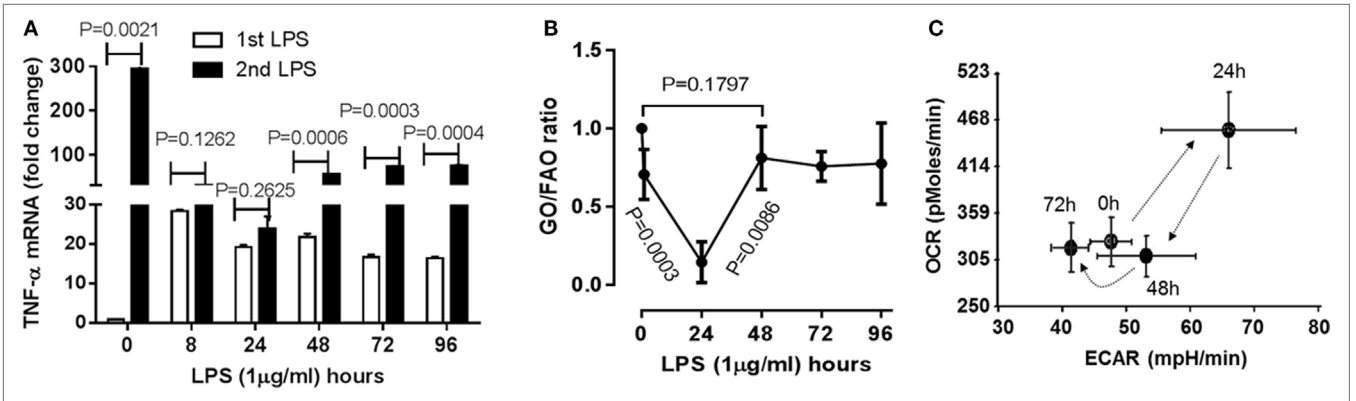

FIGURE 1 | Time-dependent immunometabolic reprogramming of the acute inflammatory response to endotoxin in THP-1 human monocytes. **(A)** THP-1 cells received a primary dose of 1 μg/ml of lipopolysaccharide endotoxin (LPS) and were monitored for 96 h. A second LPS dose was given to track development and resolution of immune tolerance, as assessed by TNF-α mRNA induction by real-time RT-PCR. **(B)** Cellular metabolic rates of glucose (GO) and fatty acid oxidation (FAO) were analyzed using D-[6-^{14}C]glucose and 1-[^{14}C]palmitic acid, and expressed as GO/FAO ratios of $^{14}CO_2$ production. **(C)** Oxygen Consumption Rate (OCR) and Extracellular Acidification Rate (ECAR) were determined using Seahorse XFe-24 Analyzer and energy index was platted as the ratio of the two. **(A)** $N = 3$, **(B)** $N = 3$, **(C)** $N = 4$. *P* values from analysis of variance and *post hoc* comparisons.

phase (**Figure 2A**). We further detailed the time course of SIRT4 expression and found that LPS stimulation did not significantly induce SIRT4 expression at 8 h ($P = 0.0666$), but its mRNA level was significantly increased at 24 h ($P = 0.0093$), reached its peak at 48 h, and then returned toward baseline ($P = 0.0006$, **Figure 2B**). Consistent with an increase in gene expression, we found elevated SIRT4 protein levels at 24 h, with peaking at 48 h (**Figure 2C**). The delay in SIRT4 induction by LPS paralleled with the time course of endotoxin tolerance emergence, suggesting SIRT4 might play a role in counteracting effects of SIRT1-RelB-SIRT3 immune tolerance axis during recovery of acute inflammatory response.

SIRT4 Regulates Glycolysis

Since glucose is a substrate for glycolysis and contributes to immune anabolic resistance mechanisms, which are repressed by the SIRT1-SIRT6 axis while increasing fatty acid as substrate for catabolic energetics (10), we tested whether SIRT4 participates in the regulation of glycolysis dynamics during inflammatory resolution. Using gene-specific RNAi technology, we assessed glycolysis dynamics by monitoring ^3H_2O production of ^{3}H-glucose in THP-1 cells. In response to LPS stimulation, ^3H_2O generation in control THP-1 cells increased at 8 h, decreased at 24 h and returned toward baseline at 48 h. In contrast, SIRT4 knockdown sustained high ^3H_2O count at 24 ($P = 0.0003$) and 48 h ($P = 0.0113$) compared with control vector effects (**Figure 3A**). Consistent with radiolabeling results, biochemical analysis showed significant increases in LDH activity (**Figure 3B**) and increased the lactate to pyruvate ratio (**Figure 3C**) in SIRT4 knockdown cells comparing to that of control THP-1 cells at 24 and 48 h after LPS stimulation. These data suggested that SIRT4 enhances glycolysis-dependent increases in pyruvate support of glucose oxidation, and a possible reversal mechanism for immune tolerance (10).

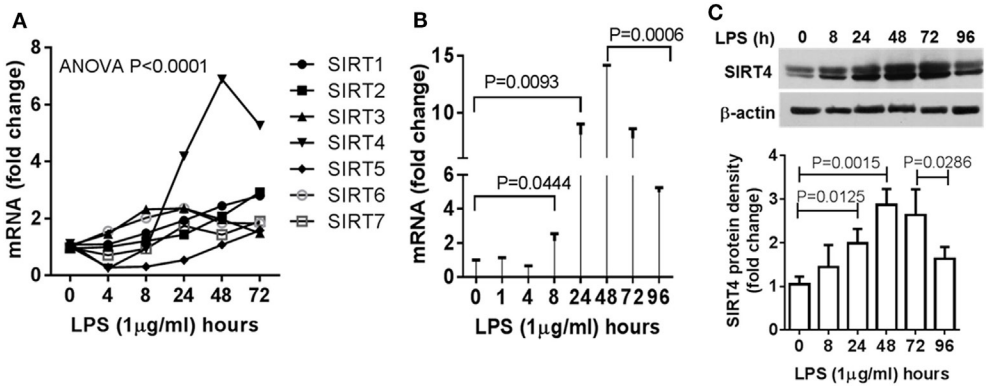

FIGURE 2 | Dynamics of sirtuin 4 (SIRT4) induction during early resolution of the acute inflammation response. THP-1 cells were stimulated with 1 μg/ml lipopolysaccharide (LPS) for indicated times. Gene expression dynamics of mammalian sirtuin family members **(A)** and SIRT4 gene transcription **(B)** were evaluated using real-time RT-PCR analysis. **(C)** Changes of SIRT4 protein level were determined by immunoblotting. Triplicate mean values ± SE of one of five independent experiments displays in bar graph **(A–C)**, $N = 3$. *P* values from analysis of variance and *post hoc* comparisons.

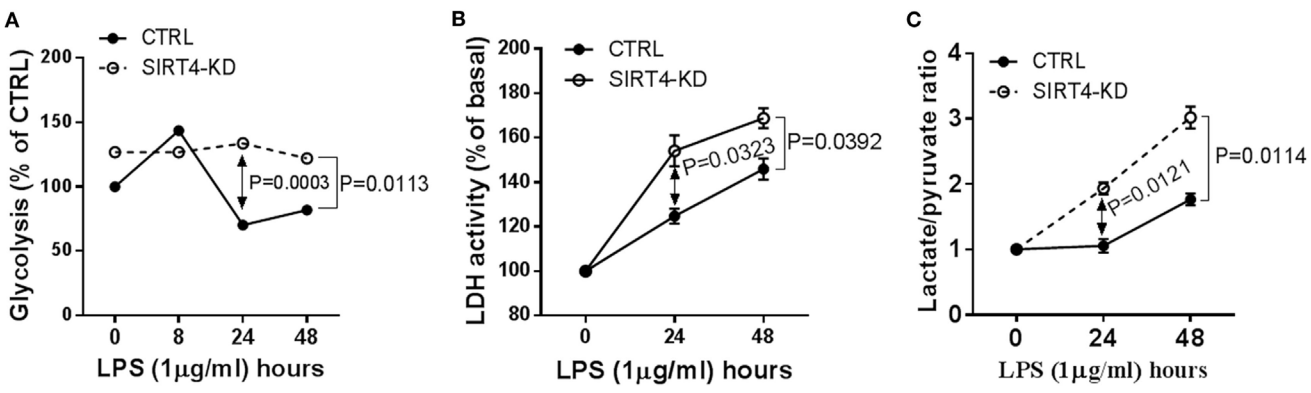

FIGURE 3 | Depleting sirtuin 4 (SIRT4) sustains glycolytic activity during physiological resolution of acute inflammatory response. Control knockdown and SIRT4 knockdown THP-1 cells were stimulated with 1 μg/ml lipopolysaccharide (LPS) for indicated times. **(A)** Cellular glycolytic activity was assessed by the conversion of D-[5-^{3}H(N)]glucose to ^3H_2O, the changes of ^3H_2O generation rate in control and SIRT4 knockdown cells were plotted. **(B)** Changes of lactate dehydrogenase (LDH) activity and **(C)** Changes of ratio of cellular lactate to pyruvate level in both control and SIRT4 knockdown cells were assayed using colorimetric assay kit. One of three independent experiments is presented as mean values ± SE of triplicates. KD, knockdown.

SIRT4 Increases PDC Activity by Repressing PDK1 Expression

The decarboxylase activity of PDC by increasing acetyl CoA levels in mitochondria directs the oxidation of glucose-based carbons by the TCA cycle and in doing so may alter the cytosol glycolysis to glucose oxidation ratio. To study the dynamics of PDC activity, we used a biochemical assay of PDC enzymatic activity in wild-type and SIRT4 knockdown THP-1 cells. In response to LPS stimulation, PDC activity significantly decreased at 24 hour in both control and SIRT4 deficient cells ($P = 0.0091$, $P = 0.0171$, respectively). PDC enzymatic activity of control cells significantly increased at 48 h ($P = 0.0004$) and restored to the basal level ($P = 0.1019$). In contrast, PDC enzymatic activity in SIRT4 knockdown cells did not change significantly at 48 h compared to 24 h ($P = 0.3488$), but was significantly lower than that of control cells ($P = 0.0064$, **Figure 4A**). These findings suggest that SIRT4 expression restores PDC enzymatic activity, the major rate-limiting step in glucose oxidation, as immune tolerance resolves and catabolic energetics switch toward glucose driven anabolic oxidative fueling.

Pyruvate dehydrogenase complex activity is primarily regulated by PDK-mediated posttranslational phosphorylation of its E1α subcomponent on specific serines (10, 18). We asked if SIRT4 expression alters PDK1 regulation of PDC during acute inflammatory resolution by comparing PDK1 gene expression in control and SIRT4 knockdown THP-1 cells in response to LPS stimulation. After stimulating for 48 h, the peak time of SIRT4 induction, control THP-1 cells decreased PDK1 mRNA levels. In contrast, SIRT4 knockdown significantly increased PDK1 mRNA level ($P = 0.00296$, **Figure 4B**).

To determine if PDK1 transcription was efficiently translated, we established SIRT4 knockout THP-1 cells using CRISPR/Cas9 strategy. Consistent with the dynamics of SIRT4 and PDK1 mRNA levels, LPS stimulation induced a time-dependent increase in SIRT4 protein levels while decreasing PDK1 protein levels in wild-type THP-1 cells. In contrast, PDK1 protein level gradually increased in SIRT4 knockout cells (**Figure 4C**).

We then tested the association of PDK1 induction with PDC E1α phosphorylation. LPS stimulation dramatically induced PDK1 phosphorylation at residue functional serine 232 (S232) on E1α at 1 h, sustained the high level at 24 h, at which time it decreased to basal level at 48 h in wild-type THP-1 cells. In contrast, SIRT4 knockout increased the basal level of phosphorylated PDC E1α-S232 and maintained high levels in response to LPS stimulation (**Figure 4D**). This paralleled low level of PDC activity in SIRT4 knockdown THP-1 cells (**Figure 4A**).

SIRT4 Alters Mitochondrial Respiration

We next asked the effect of SIRT4 on glucose oxidation by PDC activation might change mitochondrial respiration. To test this,

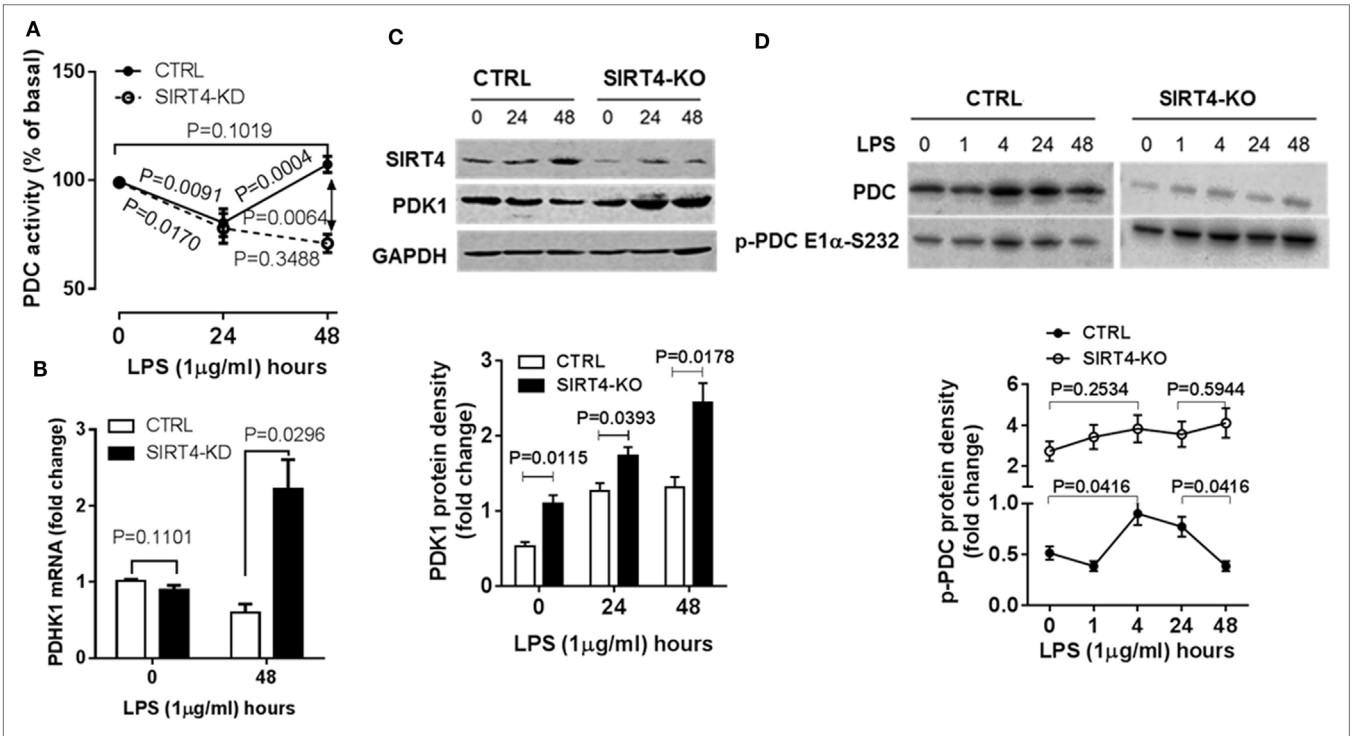

FIGURE 4 | Depleting sirtuin 4 (SIRT4) hampers recovery of PDC inhibition by increasing PDK1 expression during physiological resolution of acute inflammatory response. Control and SIRT4 knockdown or control and SIRT4 knockout THP-1 cells were stimulated with 1 μg/ml lipopolysaccharide (LPS). **(A)** PDC decarboxylase activity was evaluated by commercial colorimetric assay kit ($N = 3$). **(B)** PDK1 mRNA transcription was measured using real-time RT-PCR. PDK1 protein levels **(C)** and PDC protein levels and S232 phosphorylated PDC E1α levels **(D)** were shown by immunoblotting. Bar graphs depict mean values ± SE of $N = 3$. PDC, pyruvate dehydrogenase complex, PDK1, pyruvate dehydrogenase kinase 1, GAPDH, glyceraldehyde 3-phosphate dehydrogenase, KD, knockdown, KO, knockout.

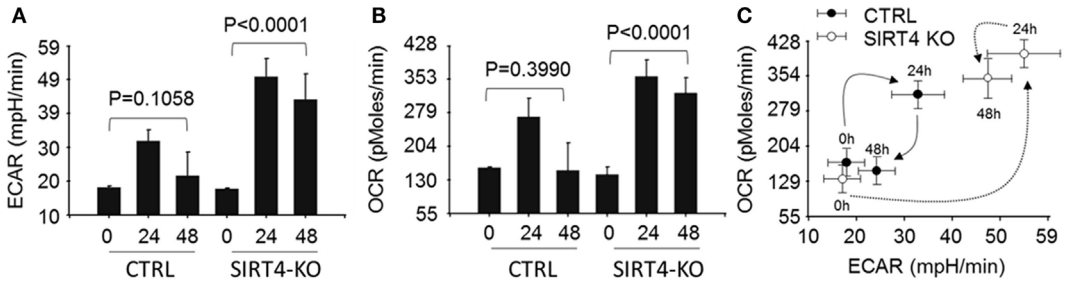

FIGURE 5 | Depleting sirtuin 4 (SIRT4) impedes restoration of energetic homeostasis during physiologic resolution of acute inflammatory response. Control knockout and SIRT4 knockout THP-1 cells were stimulated with 1 μg/ml lipopolysaccharide (LPS) for 0, 24, or 48 h, changes of energetics were examined using Seahorse XFe-24 analyzer, the difference of basal oxygen consumption rate (OCR) **(A)** and extracellular acidification rate (ECAR) **(B)** in response to LPS stimulation in the presence or absence of SIRT4 was presented as mean values ± SE of three independent experiments in **(A,B)**. OCR to ECAR ratio **(C)** is plotted as mean values ± SE of multiple reading points within 8 min measurements, $N = 3$.

wild-type and SIRT4 knockout THP-1 cells were stimulated with LPS across time points that estimate basal, resistant, and tolerant states (0, 24, and 48 h) and measured changes of OCR and ECAR using the Agilent Seahorse respiration analyzer. OCR and ECAR were significantly increased at 24 h and returned to baseline at 48 h ($P = 0.1058$) in control knockout cells stimulated with LPS. In contrast, OCR and ECAR were dramatically enhanced at 24 h and sustained high levels for 48 h in SIRT4 knockout cells following LPS stimulation (**Figures 5A,5B**; Figure S1 in Supplementary Material). We assessed the cell energy index as OCR/ECAR, and found that it returned to baseline at 48 h in control knockdown cells, but remained high in SIRT4 knockdown cells (**Figure 5C**; Figure S1 in Supplementary Material). These data suggest that SIRT4 rebalances mitochondrial bioenergetics by increasing PDC activation as immune tolerance decreases and inflammation resolves toward a homeostasis state.

SIRT4 Represses SIRT1 Expression during the Monocyte Acute Inflammatory Response

SIRT1 is master metabolic sensor and regulator and key energy rheostat during the acute inflammatory response, and drives immune resistance to immune tolerance (8). Blocking SIRT1 during the immune tolerance sepsis phenotype in mice restores immunometabolic and energy homeostasis, resolves systemic inflammation and markedly improves survival (19). It also may epigenetically regulate a set of genes that includes PDK (10). We reasoned SIRT4 might counteract SIRT1 activity to promote physiological resolution of acute immunometabolic response. To test this possibility, we assessed LPS-mediated SIRT1 gene expression in the SIRT4 knockdown or SIRT4 overexpressing cells. In response to LPS stimulation, SIRT4 knockout cells expressed significantly higher SIRT1 mRNA than that of control knockdown cells at 24 ($P = 0.0142$) and at 48 h ($P = 0.0053$, **Figure 6A**). In support of this observation, SIRT1 protein level was increased in SIRT4 knockdown cells comparing to that of control knockdown cells (**Figure 6B**). Moreover, overexpression of SIRT4 significantly suppressed SIRT1 transcription at 24 h ($P = 0.0038$) and at 48 h ($P = 0.0032$) (**Figure 6C**). Thus, SIRT4 may contribute to physiological resolution of acute inflammation by limiting SIRT1 control over specific gene sets during immune tolerance in monocytes.

SIRT4 Reprograms Immune Tolerance in Human Peripheral Blood Mononuclear Cells

To add support of concept in THP-1 cells, we used human primary blood mononuclear cells stimulated with high dose LPS (100 ng/ml), and monitored SIRT4 and PDK1 expression and mitochondrial energy indices by the Seahorse mitochondrial stress test. In principle with our observations in THP-1 cells, LPS stimulation significantly induced SIRT4 gene transcription (**Figure 7A**) and protein translation (**Figure 7B**). PDK1 protein levels decreased when SIRT4 levels increased, suggesting a bioenergy switch (**Figure 7B**). In support of this, OCR/ECAR ratio energy increased at 8 h to reflect an anabolic fueling, sustained at 24 h and returned toward baseline at 48 h (**Figure 7C**; Figure S2 in Supplementary Material). Together, these data support our THP-1 derived concept in a primary immune cell circulating population strongly stressed over time by endotoxin.

DISCUSSION

This study shows that NAD-dependent SIRT4 is a physiologic contributor to acute inflammatory resolution in human monocytes that acts by breaking immune tolerance. The first step in this reprogramming pathway is that SIRT4 expression is selectively increased over other SIRTs as immune tolerance peaks and TNF α expression capacity returns. SIRT4 increases the ratio of glucose oxidation to fatty acid oxidation, as previously reported after inhibiting SIRT1 (9). This study shows SIRT4 physiologically converts the FAO pathway for catabolic energetics to glucose oxidation. As a mechanism by which increased SIRT4 controls energy use and distribution, this study shows that SIRT4 acts by controlling the expression of PDK1 and SIRT1 (**Figure 7D**), which are master metabolic bioenergy sensors and metabolic regulators of cell energetics and metabolism, as found in tolerant

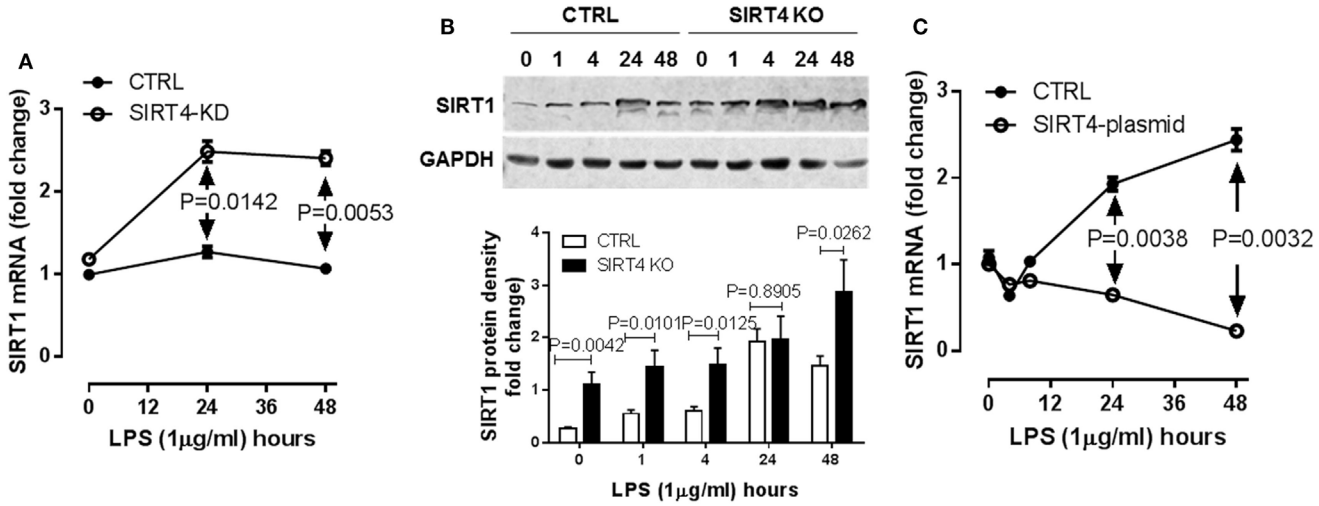

FIGURE 6 | Sirtuin 4 (SIRT4) represses SIRT1 expression in response to endotoxin. Control knockdown and SIRT4 knockdown THP-1 cells were stimulated with 1 μg/ml lipopolysaccharide endotoxin (LPS) for indicated times, **(A)** SIRT1 transcription was evaluated using real-time RT-PCR, data are shown as mean values ± SE of one of two independent experiments. **(B)** Changes of SIRT1 proteins in control and SIRT4 knockout cells were shown by immunoblotting. **(C)** THP-1 cells were electronically transfected either with SIRT4 plasmid or control plasmid for 24 h and stimulated with 1 μg/ml LPS for indicated times, SIRT1 transcription was evaluated using real-time RT-PCR, data are displayed as triplicate mean values ± SE of one of $N = 3$. Bar graphs depict mean values ± SE of $N = 3$.

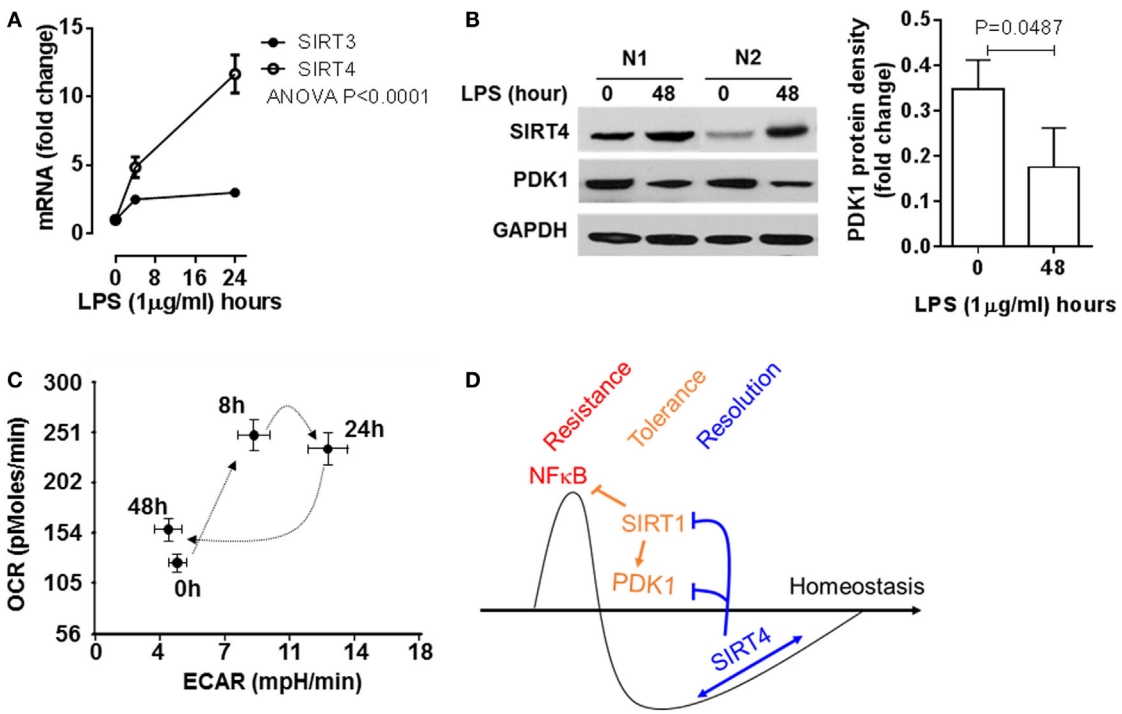

FIGURE 7 | Sirtuin 4 (SIRT4) expression and the mitochondrial bioenergy indices are reprogrammed in human primary blood mononuclear cells during an acute inflammatory response. Healthy peripheral blood mononuclear cells were stimulated with 100 ng/ml lipopolysaccharide (LPS) for indicated times, **(A)** SIRT3 and SIRT4 gene induction was assessed using real-time-RT-PCR analysis ($n = 3$). **(B)** Protein levels of SIRT4 and pyruvate dehydrogenase kinase 1 (PDK1) were detected by western blotting. **(C)** Cellular energetic changes of OCR to extracellular acidification rate (ECAR) ratio were evaluated using Seahorse XFe-24 analyzer ($N = 3$). **(D)** Schematic of mechanism of SIRT4 regulating inflammatory resolution. *P* values from analysis of variance and *post hoc* comparisons. Bar graphs depict mean values ± SE of $N = 5$.

monocytes, septic mice splenocytes, and septic human blood monocytes (10). The clinical importance of this metabolic and immune switch by SIRT1-PDC/PDK1 axis is that blocking SIRT1 in septic mice resolves immune and metabolic tolerance and improves survival in septic mice (19). This study also highlights the importance of substrate selection and bioenergetics in driving

innate immune cell fate and function (5–7). This substrate selection paradigm of glucose and amino acids for immune resistance and FAO for immune tolerance applies to innate and antigen specific cells (5–7).

In this study, mitochondrial SIRT4 appears to be indirectly promoting anabolism by increasing glucose metabolism after inhibiting expression of mitochondrial PDK1, which increases glycolysis and opens the pyruvate gate for glucose oxidative fueling. In contrast, mitochondrial SIRT3 directly supports catabolic energy by supporting the functions of TCA cycle proteins (20) and by activating glutamate dehydrogenase (21), which SIRT4 can counter (22). Mitochondrial SIRT4 further supports anabolic biosynthetic processes by repressing malonyl-CoA decarboxylase to increase lipid biosynthesis (23). In contrast, SIRT 3 promotes long-chain fatty acid β oxidation (24) as catabolic fuel during states of nutrient deficiency, which is typical of tolerance. Whether or how SIRT4 and SIRT3 directly control PDC function is unclear. SIRT4 is reported to directly inactivate rather activate PDC (25), but these effects as a lipoamidase and deacylase are controversial (26–28).

A surprising finding in this study is that SIRT4 may signal nuclear processes from its known mitochondrial site, although that SIRT4 may transfer into the nucleus is not excluded in this study. However, there are precedents for how mitochondrial SIRT4 may cross signal to the nucleus. One way is by generating reactive oxygen species and converting superoxide to H_2O_2 as a diffusible signaling molecule (29). For example, mitochondrial generated H_2O_2 activates the cytoplasmic Keap-1/Nrf2 antioxidant system (30). H_2O_2 also directly and reversibly oxidizes nuclear SIRT1 (31) and SIRT6 cysteine thiols (32) to inactivate or reactivate glycolysis and glucose transport during the acute inflammatory response in monocytes. Other mitochondrial signaling pathways could link SIRT4 mitochondrial effects with the nucleus, including levels of citrate (33), fumarate (34), succinate (35), and alpha ketoglutarate (36). Other important unanswered questions raised by this study are: what nuclear transcription and epigenetic system supports SIRT4 transcription and translation and movement to mitochondria, and how SIRT1 and PDK1 and SIRT4 are reciprocally controlled by transcriptional and epigenetic processes.

In summary, we show that SIRT4 operates at the intersection of inflammation tolerance and resolution in monocytes. It reverses fatty acid energy expenditure to glucose energetics by controlling expression and functions of the nuclear SIRT1 axis and the mitochondrial PDC/PDK1 axis. These two cross-roads restore lipid biogenesis as one pathway that retrieves the biosynthetic needs of immunometabolic homeostasis. Expanding this cell-based concept at the mechanistic level and translating it to human or animal diseases may provide clarity to understanding and treating inflammatory diseases.

ETHICS STATEMENT

The Shanghai Public Health Clinical Center Ethics Committee of Fudan University approved the human subject component of this study and the consent form.

AUTHOR CONTRIBUTIONS

Conception/design of study: TL and CM. Acquisition of data: TL, JT, JZ and YL. Analysis/interpretation of data: TL, CM, and YL. Drafting the manuscript: TL and CM. Approval of manuscript: TL and CM.

FUNDING

This study was supported by Shanghai Public Health Clinical Center development fund RCJJP24 to TL and NIH grant R01AI065791 and R01GM102497 to CM.

SUPPLEMENTARY MATERIAL

The Supplementary Material for this article can be found online at http://www.frontiersin.org/articles/10.3389/fimmu.2018.00419/full#supplementary-material.

REFERENCES

1. Brodsky IE, Medzhitov R. Targeting of immune signalling networks by bacterial pathogens. *Nat Cell Biol* (2009) 11:521–6. doi:10.1038/ncb0509-521
2. Lackey DE, Olefsky JM. Regulation of metabolism by the innate immune system. *Nat Rev Endocrinol* (2016) 12:15–28. doi:10.1038/nrendo.2015.189
3. Buck MD, Sowell RT, Kaech SM, Pearce EL. Metabolic instruction of immunity. *Cell* (2017) 169:570–86. doi:10.1016/j.cell.2017.04.004
4. Norata GD, Caligiuri G, Chavakis T, Matarese G, Netea MG, Nicoletti A, et al. The cellular and molecular basis of translational immunometabolism. *Immunity* (2015) 43:421–34. doi:10.1016/j.immuni.2015.08.023
5. Hosios AM, Hecht VC, Danai LV, Johnson MO, Rathmell JC, Steinhauser ML, et al. Amino acids rather than glucose account for the majority of cell mass in proliferating mammalian cells. *Dev Cell* (2016) 36:540–9. doi:10.1016/j.devcel.2016.02.012
6. Olenchock BA, Rathmell JC, Vander Heiden MG. Biochemical underpinnings of immune cell metabolic phenotypes. *Immunity* (2017) 46:703–13. doi:10.1016/j.immuni.2017.04.013
7. Freemerman AJ, Johnson AR, Sacks GN, Milner JJ, Kirk EL, Troester MA, et al. Metabolic reprogramming of macrophages: glucose transporter 1 (GLUT1)-mediated glucose metabolism drives a proinflammatory phenotype. *J Biol Chem* (2014) 289:7884–96. doi:10.1074/jbc.M113.522037
8. Liu TF, Yoza BK, El Gazzar M, Vachharajani VT, McCall CE. NAD+-dependent SIRT1 deacetylase participates in epigenetic reprogramming during endotoxin tolerance. *J Biol Chem* (2011) 286:9856–64. doi:10.1074/jbc.M110.196790
9. Liu TF, Vachharajani V, Millet P, Bharadwaj MS, Molina AJ, McCall CE. Sequential actions of SIRT1-RELB-SIRT3 coordinate nuclear-mitochondrial communication during immunometabolic adaptation to acute inflammation and sepsis. *J Biol Chem* (2015) 290:396–408. doi:10.1074/jbc.M114.566349
10. Liu TF, Vachharajani VT, Yoza BK, McCall CE. NAD+-dependent sirtuin 1 and 6 proteins coordinate a switch from glucose to fatty acid oxidation during the acute inflammatory response. *J Biol Chem* (2012) 287:25758–69. doi:10.1074/jbc.M112.362343
11. Singer M, De Santis V, Vitale D, Jeffcoate W. Multiorgan failure is an adaptive, endocrine-mediated, metabolic response to overwhelming systemic inflammation. *Lancet* (2014) 364:545–8. doi:10.1016/S0140-6736(04)16815-3

12. Beeckmans S, Kanarek L. Enzyme-enzyme interactions as modulators of the metabolic flux through the citric acid cycle. *Biochem Soc Symp* (1987) 54:163–72.
13. Schug TT, Li X. Sirtuin 1 in lipid metabolism and obesity. *Ann Med* (2011) 43:198–211. doi:10.3109/07853890.2010.547211
14. Osborne B, Bentley NL, Montgomery MK, Turner N. The role of mitochondrial sirtuins in health and disease. *Free Radic Biol Med* (2016) 100:164–74. doi:10.1016/j.freeradbiomed.2016.04.197
15. Baeza J, Smallegan MJ, Denu JM. Mechanisms and dynamics of protein acetylation in mitochondria. *Trends Biochem Sci* (2016) 41:231–44. doi:10.1016/j.tibs.2015.12.006
16. Ansari A, Rahman MS, Saha SK, Saikot FK, Deep A, Kim KH. Function of the SIRT3 mitochondrial deacetylase in cellular physiology, cancer, and neurodegenerative disease. *Aging Cell* (2017) 16:4–16. doi:10.1111/acel.12538
17. North BJ, Marshall BL, Borra MT, Denu JM, Verdin E. The human Sir2 ortholog, SIRT2, is an NAD+-dependent tubulin deacetylase. *Mol Cell* (2003) 11:437–44. doi:10.1016/S1097-2765(03)00038-8
18. Rardin MJ, Wiley SE, Naviaux RK, Murphy AN, Dixon JE. Monitoring phosphorylation of the pyruvate dehydrogenase complex. *Anal Biochem* (2009) 389:157–64. doi:10.1016/j.ab.2009.03.040
19. Vachharajani VT, Liu T, Brown CM, Wang X, Buechler NL, Wells JD, et al. SIRT1 inhibition during the hypoinflammatory phenotype of sepsis enhances immunity and improves outcome. *J Leukoc Biol* (2014) 96:785–96. doi:10.1189/jlb.3MA0114-034RR
20. Parihar P, Solanki I, Mansuri ML, Parihar MS. Mitochondrial sirtuins: emerging roles in metabolic regulations, energy homeostasis and diseases. *Exp Gerontol* (2015) 61:130–41. doi:10.1016/j.exger.2014.12.004
21. Pacella-Ince L, Zander-Fox DL, Lan M. Mitochondrial SIRT3 and its target glutamate dehydrogenase are altered in follicular cells of women with reduced ovarian reserve or advanced maternal age. *Hum Reprod* (2014) 29:1490–9. doi:10.1093/humrep/deu071
22. Haigis MC, Mostoslavsky R, Haigis KM, Fahie K, Christodoulou DC, Murphy AJ, et al. SIRT4 inhibits glutamate dehydrogenase and opposes the effects of calorie restriction in pancreatic beta cells. *Cell* (2006) 126:941–54. doi:10.1016/j.cell.2006.06.057
23. Laurent G, German NJ, Saha AK, de Boer VC, Davies M, Koves TR, et al. SIRT4 coordinates the balance between lipid synthesis and catabolism by repressing malonyl CoA decarboxylase. *Mol Cell* (2013) 50:686–98. doi:10.1016/j.molcel.2013.05.012
24. Bharathi SS, Zhang Y, Mohsen AW, Uppala R, Balasubramani M, Schreiber E, et al. Sirtuin 3 (SIRT3) protein regulates long-chain acyl-CoA dehydrogenase by deacetylating conserved lysines near the active site. *J Biol Chem* (2013) 288:33837–47. doi:10.1074/jbc.M113.510354
25. Mathias RA, Greco TM, Oberstein A, Budayeva HG, Chakrabarti R, Rowland EA, et al. Sirtuin 4 is a lipoamidase regulating pyruvate dehydrogenase complex activity. *Cell* (2014) 159:1615–25. doi:10.1016/j.cell.2014.11.046
26. Du J, Jiang H, Lin H. Investigating the ADP-ribosyltransferase activity of sirtuins with NAD analogues and 32P-NAD. *Biochemistry* (2009) 48:2878–90. doi:10.1021/bi802093g
27. Feldman JL, Baeza J, Denu JM. Activation of the protein deacetylase SIRT6 by long-chain fatty acids and widespread deacylation by mammalian sirtuins. *J Biol Chem* (2013) 288:31350–6. doi:10.1074/jbc.C113.511261
28. Tan M, Peng C, Anderson KA, Chhoy P, Xie Z, Dai L, et al. Lysine glutarylation is a protein posttranslational modification regulated by SIRT5. *Cell Metab* (2014) 19:605–17. doi:10.1016/j.cmet.2014.03.014
29. Schieber M, Chandel NS. ROS function in redox signaling and oxidative stress. *Curr Biol* (2014) 24:R453–62. doi:10.1016/j.cub.2014.03.034
30. Itoh K, Wakabayashi N, Katoh Y, Ishii T, Igarashi K, Engel JD, et al. Keap1 represses nuclear activation of antioxidant responsive elements by Nrf2 through binding to the amino-terminal Neh2 domain. *Genes Dev* (1999) 13:76–86. doi:10.1101/gad.13.1.76
31. Kornberg MD, Sen N, Hara MR, Juluri KR, Nguyen JV, Snowman AM, et al. GAPDH mediates nitrosylation of nuclear proteins. *Nat Cell Biol* (2010) 12:1094–100. doi:10.1038/ncb2114
32. Long D, Wu H, Tsang AW, Poole LB, Yoza BK, Wang X, et al. The oxidative state of cysteine thiol 144 regulates the SIRT6 glucose homeostat. *Sci Rep* (2017) 7:11005. doi:10.1038/s41598-017-11388-6
33. O'Neill LA. A critical role for citrate metabolism in LPS signaling. *Biochem J* (2011) 438:e5–6. doi:10.1042/BJ20111386
34. Arts RJ, Novakovic B, Ter Horst R, Carvalho A, Bekkering S, Lachmandas E, et al. Glutaminolysis and fumarate accumulation integrate immunometabolic and epigenetic programs in trained immunity. *Cell Metab* (2016) 24:807–19. doi:10.1016/j.cmet.2016.10.008
35. Mills E, O'Neill LA. Succinate: a metabolic signal in inflammation. *Trends Cell Biol* (2014) 24:313–20. doi:10.1016/j.tcb.2013.11.008
36. McLain AL, Szweda PA, Szweda L. α-Ketoglutarate dehydrogenase: a mitochondrial redox sensor. *Free Radic Res* (2010) 45:29–36. doi:10.3109/10715762.2010.534163

Conflict of Interest Statement: The authors declare that the research was conducted in the absence of any commercial or financial relationships that could be construed as a potential conflict of interest.

frontiers in Immunology

ORIGINAL RESEARCH
published: 17 April 2018
doi: 10.3389/fimmu.2018.00795

A Reappraisal on the Potential Ability of Human Neutrophils to Express and Produce IL-17 Family Members *In Vitro*: Failure to Reproducibly Detect It

*Nicola Tamassia[1†], Fabio Arruda-Silva[1,2†], Federica Calzetti[1], Silvia Lonardi[3], Sara Gasperini[1], Elisa Gardiman[1], Francisco Bianchetto-Aguilera[1], Luisa Benerini Gatta[3], Giampiero Girolomoni[4], Alberto Mantovani[5,6,7], William Vermi[3] and Marco A. Cassatella[1]**

[1] Department of Medicine, Section of General Pathology, University of Verona, Verona, Italy, [2] CAPES Foundation, Ministry of Education of Brazil, Brasilia, Brazil, [3] Department of Molecular and Translational Medicine, Section of Pathology, University of Brescia, Brescia, Italy, [4] Department of Medicine, Section of Dermatology and Venereology, University of Verona, Verona, Italy, [5] Humanitas Clinical and Research Center, Rozzano, Italy, [6] Humanitas University, Pieve Emanuele, Italy, [7] The William Harvey Research Institute, Queen Mary University of London, London, United Kingdom

OPEN ACCESS

Edited by:
Liwu Li,
Virginia Tech, United States

Reviewed by:
Min Wu,
University of North Dakota, United States
Petya Dimitrova,
Institute of Microbiology, Sofia, Bulgaria

***Correspondence:**
Marco A. Cassatella
marco.cassatella@univr.it

[†]These authors have contributed equally to this work.

Specialty section:
This article was submitted to Molecular Innate Immunity, a section of the journal Frontiers in Immunology

Received: 14 February 2018
Accepted: 03 April 2018
Published: 17 April 2018

Citation:
Tamassia N, Arruda-Silva F, Calzetti F, Lonardi S, Gasperini S, Gardiman E, Bianchetto-Aguilera F, Gatta LB, Girolomoni G, Mantovani A, Vermi W and Cassatella MA (2018) A Reappraisal on the Potential Ability of Human Neutrophils to Express and Produce IL-17 Family Members In Vitro: Failure to Reproducibly Detect It. Front. Immunol. 9:795. doi: 10.3389/fimmu.2018.00795

Neutrophils are known to perform a series of effector functions that are crucial for the innate and adaptive responses, including the synthesis and secretion of a variety of cytokines. In light of the controversial data in the literature, the main objective of this study was to more in-depth reevaluate the capacity of human neutrophils to express and produce cytokines of the IL-17 family *in vitro*. By reverse transcription quantitative real-time PCR, protein measurement *via* commercial ELISA, immunohistochemistry (IHC) and immunofluorescence (IF), flow cytometry, immunoblotting, chromatin immunoprecipitation (ChIP), and ChIP-seq experiments, we found that highly pure (>99.7%) populations of human neutrophils do not express/produce IL-17A, IL-17F, IL-17AF, or IL-17B mRNA/protein upon incubation with a variety of agonists. Similar findings were observed by analyzing neutrophils isolated from active psoriatic patients. In contrast with published studies, IL-17A and IL-17F mRNA expression/production was not even found when neutrophils were incubated with extremely high concentrations of IL-6 plus IL-23, regardless of their combination with inactivated hyphae or conidia from *Aspergillus fumigatus*. Consistently, no deposition of histone marks for active (H3K27Ac) and poised (H3K4me1) genomic regulatory elements was detected at the IL-17A and IL-17F locus of resting and IL-6 plus IL-23-stimulated neutrophils, indicating a closed chromatin conformation. Concurrent experiments revealed that some commercial anti-IL-17A and anti-IL-17B antibodies (Abs), although staining neutrophils either spotted on cytospin slides or present in inflamed tissue samples by IHC/IF, do not recognize intracellular protein having the molecular weight corresponding to IL-17A or IL-17B, respectively, in immunoblotting experiments of whole neutrophil lysates. By contrast, the same Abs were found to more specifically recognize other intracellular proteins of neutrophils, suggesting that their ability to positively stain neutrophils in cytospin preparations and, eventually, tissue samples derives from IL-17A- or IL-17B-independent detections. In

sum, our data confirm and extend, also at epigenetic level, previous findings on the inability of highly purified populations of human neutrophils to express/produce IL-17A, IL-17B, and IL-17F mRNAs/proteins *in vitro*, at least under the experimental conditions herein tested. Data also provide a number of justifications explaining, in part, why it is possible to false positively detect IL-17A$^+$-neutrophils.

Keywords: neutrophils, IL-17 members, IL-17A, IL-17B, IL-17F

INTRODUCTION

The IL-17 family of cytokines consists of six members, namely IL-17A (usually referred to as IL-17), IL-17B, IL-17C, IL-17D, IL-17E (also known as IL-25), and IL-17F (1). After the discovery of a subtype of CD4$^+$ T helper, expressing IL-17A and IL-17F (currently known as Th17 cells), plenty of studies have been published correlating Th17 cells with a wide range of physiological and pathological processes. IL-17A and IL-17F are not only the most studied but also the most closely related, since they share 50% of amino acid sequence identity, adjacent gene localization (2) and binding to the same IL-17R, in this case composed by the IL-17RA and IL-17RC subunits (1). The IL-17R group comprises, in fact, five receptor subunits, IL-17RA, IL-17RB, IL-17RC, IL-17RD, and IL-17RE (3). IL-17RA was the first to be described, is ubiquitously expressed (particularly in hematopoietic cells), and functions as a common receptor subunit used by at least four ligands, namely IL-17A, IL-17C, IL-17E, and IL-17F (3). IL-17F is often coproduced with IL-17A, so that together they can also form an IL-17F/IL-17A heterodimer (4) binding to the IL-17RA/IL17RC complex as either homodimers or heterodimers (3). IL-17A and IL-17F are proinflammatory cytokines that play key regulatory roles in host defense and inflammatory diseases. They mainly mediate immune regulatory functions by promoting the generation of proinflammatory cytokines/growth factors (including G-CSF, GM-CSF, and IL-6) and chemokines (such as CXCL8, CXCL6, and CXCL1) by epithelial and other stromal cells, which ultimately lead to the attraction and activation of neutrophils and macrophages into the inflammatory site (5), as well as to granulopoeisis (6). Although crucial in protecting the host from invasion by many types of pathogens, including bacteria and fungi (7), dysregulated IL-17A and IL-17F production can lead to the development of autoimmune diseases, such as psoriasis, multiple sclerosis, and rheumatoid arthritis (RA), as well as cancer progression (5, 8). The latter observations hence make IL-17A/F as a very important target for the development of new therapies (1, 8).

As mentioned, Th17 cells are considered the main sources of IL-17A and IL-17F. However, other innate immune cells produce these cytokines, including γδ T cells, natural killer T cells, invariant natural killer cells, Paneth cells, TCRβ$^+$ natural Th17 cells, lymphoid-tissue inducer-like cells, IL-17-expressing type 3 innate lymphoid cells, and mast cells (8, 9). By contrast, it is still questionable whether human polymorphonuclear neutrophils represent sources of IL-17A or IL-17F. It is currently well established that neutrophils are crucial players in innate immune responses, not only for their capacity to perform defensive functions (10) but also for their ability to produce a large variety of cytokines (11). Concerning IL-17A and/or IL-17F, in 2010, we reported that highly purified populations of human neutrophils (>99.7%), incubated for up to 20 h with IFNγ and/or LPS *in vitro*, do not produce IL-17A (12). While a few papers substantially confirm our findings (13–17), the majority of the subsequent studies report that human neutrophils may represent sources of IL-17A (18–53). Experimental evidence proving that human neutrophils express IL-17A mostly, but not only, derives by immunohistochemistry (IHC) and/or immunofluorescence (IF) studies documenting IL-17A$^+$-neutrophils in tissue specimens from a variety of pathological conditions (18, 19, 21, 22, 25, 27, 28, 30–32, 34, 36–39, 41–43, 45, 47–49, 51, 53). Interestingly, many of these studies focus on psoriasis (20, 25, 30, 32, 35, 49), a disease characterized by an early accumulation of neutrophils in skin lesions in which neutrophil-derived mediators (such as reactive oxygen species, granule proteins, and cytokines) may alter the homeostatic state of keratinocytes and endothelial cells (54). At the end of 2014, however, Tamarozzi et al. (13) not only reported the absence of IL-17A mRNA expression and production by highly pure (99.9%) populations of resting or activated neutrophils but also demonstrated that some of the commercial polyclonal anti-IL-17A antibodies (Abs) stain neutrophils for their non-specific recognition of various intracellular proteins different from antigenic IL-17A. Nevertheless, reports describing either IL-17A-positive neutrophils in tissue samples from diseases or *in vitro*-stimulated neutrophils as sources of IL-17A, continue to be published (20, 23, 24, 26, 29, 33, 35, 40, 44, 46, 50, 52). Based on these premises, we decided to more accurately analyze the issue of whether human neutrophils produce IL-17A, as well as other IL-17 members *in vitro*.

MATERIALS AND METHODS

Cell Purification and Culture

Neutrophils were isolated from buffy coats of healthy donors (HDs) and manipulated under endotoxin-free conditions (12). In selected experiments, neutrophils were also isolated from peripheral blood of patients with severe psoriasis, as defined by either >10% body surface area involved, or Psoriasis Area and Severity Index score >10, or Dermatology Life Quality Index score >10 (55). After Ficoll-Paque gradient centrifugation of buffy coats or peripheral blood, followed by dextran sedimentation of granulocytes and hypotonic lysis of erythrocytes, neutrophils were isolated to reach 99.7 ± 0.2% purity by positively removing all contaminating cells using the EasySep neutrophil enrichment kit (StemCell Technologies, Vancouver, BC, Canada) (56). Neutrophils were then suspended at 5 × 10^6/ml in RPMI 1640

medium supplemented with 10% low (<0.5 EU/ml) endotoxin FBS (BioWhittaker-Lonza, Basel, Switzerland), incubated with or without 5 μM R848, 500 μg/ml particulate β-glucan (Invivogen, San Diego, CA, USA), 100 ng/ml ultrapure LPS (from *E. coli* 0111:B4 strain, Alexis, Enzo Life Sciences, Farmingdale, NY, USA), 1 μg/ml Pam3CSK4 (Invivogen), 50 μg/ml poly(I:C) (Invivogen), 1,000 U/ml G-CSF (Myelostim, Italfarmaco Spa, Milano, Italy), 100 U/ml IFNγ (R&D Systems, Minneapolis, MN, USA), 10 ng/ml GM-CSF (Miltenyi Biotec), 5 ng/ml TNFα (Peprotech, Rocky Hill, NJ, USA), 2–20 μg/ml IL-6 (R&D Systems), 0.2–2 μg/ml IL-23 (R&D Systems), 100–500 ng/ml IL-17A (R&D Systems), 10 μg/ml anti-IL-17A neutralizing Abs (secukinumab, Novartis, Basel, Switzerland), 100 nM fMLF, 500 μg/ml curdlan (Sigma, Saint Louis, MO, USA), 20 ng/ml phorbol mysistate acetate (PMA) (Sigma), 1 μg/ml Ionomycin (Sigma), 100 μg/ml CpG oligodeoxynucleotides (ODN) (Invivogen), and 1,000 U/ml PEGylated IFNα-2a (Pegasys, Roche, Basel, Switzerland). Inactivated conidia and hyphae from *Aspergillus fumigatus* were kindly provided by prof. Luigina Romani (University of Perugia, Italy), and used at a neutrophil-fungi ratio of 1:5 for *A. fumigatus* conidia and 1:1 for *A. fumigatus* hyphae, as previously described (57). Neutrophils were plated either in 6/24-well tissue culture plates or in polystyrene flasks (from Greiner Bio-One, Kremsmünster, Austria) for culture at 37°C, 5% CO_2 atmosphere. After the desired incubation period, neutrophils were either processed for chromatin immunoprecipitation (ChIP) experiments or collected and spun at 300 × *g* for 5 min for other types of assays. In the latter case, cell-free supernatants were immediately frozen in liquid nitrogen and stored at −80°C, while the corresponding cell pellets were either extracted for total RNA or lysed for protein analysis. Th1 and Th17 clones (58) were kindly provided by prof. Francesco Annunziato (University of Firenze). $CD4^+$ T cells were isolated by $CD4^+$ T Cell Isolation Kit (Miltenyi Biotec) and stimulated for up 72 h with anti-CD3 and anti-CD28 mAbs (5 μg/ml, BD Biosciences).

Flow Cytometry Experiments

For flow cytometry, 10^5 neutrophils were harvested after the desired treatment, centrifuged, and suspended in 100 μl PBS containing 10% complement-inactivated human serum for FcγR blocking. Neutrophils were then stained for 15 min at T room with: APC anti-human IL-17RA/CD217 (clone 424LTS) and APC mouse IgG1κ, as isotype control (clone P3.6.2.8.1) from eBioscience (San Diego, CA, USA); PE anti-human IL-17RC (clone 309822) and mouse PE IgG2B isotype control from R&D systems; PE-vio770 anti-human CD11b (clone ICRF44), FITC anti-human CD66b (clone G10F5), and PerCP-Cy5.6 anti-human CD16 (clone 3G8) from BioLegend (San Diego, CA, USA); APC anti-human CD62L (clone 145/15 Miltenyi Biotec), all at working dilutions specified in the corresponding datasheets. Sample fluorescence was then measured by MACSQuant Analyzer (Miltenyi Biotec), while data analysis performed using FlowJo software version 10 from Tree Star (Ashland, OR, USA) (59). For neutrophils of psoriatic patients, 100 μl whole blood were stained with APC anti-human IL-17RA and PE anti-human IL-17RC Abs in combination with the following mAbs: VioBlue anti-human CD14 (clone TÜK4), PE anti-human CD56 (clone AF12-7H3), PE-Vio770 anti-human CD3 (clone BW264/56), APC anti-human CD19 (clone LT19) from Miltenyi; Brilliant Violet anti-human CD45 (clone 2D1), PerCP-Cy5.5 anti-human CD16 (clone 3G8), and APC-Cy7 anti-human HLA-DR (clone L243) from BioLegend. After red cells lysis by the ammonium chloride buffer, sample fluorescence was immediately measured as previously described.

Superoxide Anion Measurement

After isolation, neutrophils were suspended at the concentration of 2×10^6 cells/ml in HBSS buffer containing 0.5 mM $CaCl_2$ and 1 mg/ml glucose. Neutrophils (100 μl/well) were then distributed in a 96-well plate and incubated for 10 min at 37°C prior to the addition of 80 μM cytochrome *c*, 2 mM NaN_3 (Sigma) and the indicated stimuli, including 20 ng/ml PMA as control. Plates were then incubated at 37°C in an automated ELx808IU microplate reader (BioTek Instruments, Inc., Winooski, VT, USA) to record cytochrome *c* reduction (*via* absorbance at 550 and 468 nm, at intervals of 5 min for 90 min). O_2^- production was finally calculated using an extinction coefficient of 24.5 mM (60).

Immunocitochemistry, IHC and IF

Cytospin preparations of neutrophils (61) previously cultured with the indicated stimuli were stained by ematoxylin and eosin for morphological evaluation. After coverslip removal, specimens were rehydrated through a scale of alcohols, with endogenous peroxidase activity blocked by treatment with 0.3% H_2O_2 in methanol for 20 min. Anti-human IL-17A (AF-317-NA), IL-17B (AF1248), and CXCL8 (AF-208) goat IgG pAbs from R&D Systems were 1:50 diluted, added to specimens for 60 min and then revealed using the goat-on-Rodent HRP-polymer (Biocare Medical, Pacheco, CA, USA) followed by diaminobenzidine. Omission of the primary antibody, as well as isotype control staining, was also performed as negative controls. For IL-17A and IL-17B tissue immunostaining, 4-μm tissue sections from two FFPE cases of pustular psoriasis were deparaffinized and rehydrated through a scale of alcohols. Endogenous peroxidase activity was then blocked by treatment with 0.3% H_2O_2 in methanol for 20 min. Epitope retrieval was performed using a microwave oven in 1.0 mM EDTA buffer (pH 8.0), for 3 cycles of 5 min at 750 W. IL-17A and IL-17B were diluted 1:50 and revealed using the goat HRP-polymer (IHC) or the horse anti-goat IgG biotinylated (Vector Laboratories, Peterborough, UK) followed by streptavidin-FITC (Southern Biotech, Birmingham, AL, USA). DAPI was used for counterstaining. For double IHC, anti-IL-17A and IL-17B Abs were diluted 1:500, and after revelation (as detailed above), anti-CD66b Abs (diluted 1:80 from BioLegend) were added to the sections. Mach4 AP polymer was used as secondary antibody followed by Ferangi Blue as chromogen. Ematoxylin was used for counterstaining.

Cytokine Production

Cytokine concentrations in cell-free supernatants and cell lysates were measured by commercial enzyme-linked immunosorbent (ELISA) kits, specific for: IL-17A (DY317 from R&D systems and 88-7176 from eBioscience), IL-17A/F (88-7117, eBioscience), IL-17B [ABKA2223 from Abnova (Taipei, Taiwan) and ab171344 from Abcam (Cambridge, United Kingdom)], IL-17F (887478, eBioscience), and CXCL8 (Mabtech, Nacka Strand, Sweden). ELISA detection limits were 4 pg/ml (eBioscience) and

15.6 pg/ml (R&D) for IL-17A, 30 pg/ml for IL-17A/F, 24 pg/ml (Abnova) and 10 pg/ml (Abcam) for IL-17B, 16 pg/ml for IL-17F, and 8 pg/ml for CXCL8.

Reverse Transcription Quantitative Real-Time PCR (RT-qPCR)

Total RNA was extracted from neutrophils by the RNeasy Mini Kit (Qiagen, Venlo, Limburg, Netherlands), as previously detailed (62). To completely remove any possible contaminating DNA, an on-column DNase digestion with the RNase-free DNase set (Qiagen) was performed during total RNA isolation. Total RNA was then reverse-transcribed into cDNA using Superscript III (Life Technologies, Carlsbad, CA, USA) and random hexamer primers (Life Technologies), while qPCR was carried out using Fast SYBR® Green Master Mix (Life Technologies). Sequences of gene-specific primer pairs (Life Technologies) are listed in Table S1 in Supplementary Material. Data were calculated by Q-Gene software[1] and expressed as mean normalized expression units after GAPDH normalization (63).

Immunoblotting Experiments

Total neutrophil proteins were recovered from protein-rich flow-through solutions after the first centrifugation step of the RNeasy mini kit (Qiagen) procedure used for total RNA extraction, as previously described (62). Protein-rich flow-through from neutrophils were then immunoblotted by standard procedures using the anti-human IL-17A (AF-317-NA) and IL-17B (AF1248) goat IgG pAbs from R&D Systems; anti-human phospho-STAT3 (Tyr705) rabbit pAbs (#9131, Cell Signaling, Beverly, MA, USA); anti-human STAT3 rabbit pAbs (sc-482, Santa Cruz Biotechnology, Dallas, TX, USA), and anti-human β-actin mAbs (A5060 from Sigma). Blotted proteins were detected by using the Odyssey infrared imaging system (LI-COR Biosciences, Lincoln, NE, USA) (62).

ChIP Assays

Chromatin immunoprecipitation experiments were performed exactly as previously described (62). Briefly, nuclear extracts from 2×10^6 neutrophils or Th17 cell lines were immunoprecipitated using 1 µl anti-H3K4me1 (ab8895) and anti-H3K27Ac (ab4729) pAbs (both from Abcam, Cambridge, United Kingdom). Coimmunoprecipitated material was subjected to qPCR analysis using the specific promoter primers (purchased from Life Technologies) listed in Table S2 in Supplementary Material. Data from qPCR were expressed as percentage over input DNA and are displayed as mean ± SEM.

ChIP-seq

Purified DNA from H3K27Ac and H3K4me1 ChIP assays (performed as described in the previous paragraph) was adapter-ligated and PCR-amplified for sequencing on HiSeq2000 platform (Illumina, Cambridge, UK) using TruSeq DNA Library Prep Kit (Illumina). After sequencing, reads were quality-filtered according to the Illumina pipeline. Single end (51 bp) reads were then mapped to the human genome (Genome Reference Consortium GRCh37, Feb/2009) using BOWTIE v1.0.0 (64). Only reads with no more than two mismatches (when compared to the reference genome) were converted to tag directories using HOMER's module known as "makeTagDirectory," and then converted to BedGraph format using HOMER's module known as "makeUCSCfile," to be finally normalized to 10^7 total tag counts. ChIP-seq signals were visualized using Integrative Genomics Viewer. For H3K4me1 and H3K27Ac ChIP-seqs of Th17 cells, 36 bp reads, already filtered and mapped, were downloaded from database of the "roadmap epigenomics project"[2] (NIH Epigenomics Roadmap Initiative). Aligned reads were then converted to BedGraph format and normalized to 10^7 total tag counts.

Gene Expression Data Set of Normal Hematopoietic Stem and Progenitor Cells

Gene expression profiles of cells from normal bone marrow at different stages of human granulopoiesis were downloaded from Gene Expression Omnibus Database (GEO number: GSE42519) (65). Gene expression means and SEs were calculated from the values of the biological replicates present in the GEO database.

Statistical Analysis

Data are expressed as mean ± SEM or mean ± SD. Statistical evaluation was performed by using, depending on the experiment type, Student's *t*-test or two-way ANOVA followed by Bonferroni's *post hoc* test. P values <0.05 were considered as statistically significant.

Study Approval

Human samples were obtained following informed written consent by both HDs and psoriatic patients. This study was carried out in accordance with the recommendations of Ethic Committee of the Azienda Ospedaliera Universitaria Integrata di Verona (Italy). All the experimental protocols were approved by the Ethic Committee and all subjects gave written informed consent in accordance with the Declaration of Helsinki.

RESULTS

Human Neutrophils Incubated With a Variety of Agonists *In Vitro* Do Not Express IL-17 Members at Both mRNA and Protein Levels

We have previously shown that human neutrophils (>99.7% purity), incubated with 100 U/ml IFNγ and/or 100 ng/ml ultrapure LPS for up to 20 h *in vitro*, do not produce IL-17A protein (12). Additional RT-qPCR experiments not only confirmed our previous data (**Figure 1A**) but also revealed that other agonists, including 5 µM R848 and/or 1,000 U/ml IFNα (**Figure 1B**), 10 ng/ml GM-CSF, 100 nM fMLF (**Figure 1C**),

[1] http://www.gene-quantification.de/download.html (Accessed: February 10, 2018).

[2] http://egg2.wustl.edu/roadmap/web_portal/processed_data.html (Accessed: February 10, 2018)

1,000 U/ml G-CSF, and 5 ng/ml TNFα (**Figure 1D**), similarly fail to induce an accumulation of transcripts encoding IL-17A (**Figures 1A–D**, left panels), IL-17F (**Figures 1A–D**, middle panels), IL-17B, IL-17C, IL-17D, and IL-17E (data not shown) in neutrophils. LPS and/or IFNγ, R848 and/or IFNα, GM-CSF or fMLF, however, were found to modulate the expression of CXCL8 mRNA (**Figures 1A–C**, right panels), while G-CSF or TNFα modulated that of IL-1ra mRNA (**Figure 1D**, right panel), as expected (62, 66, 67). Consistent with the gene expression data, neither IL-17A, IL-17F (**Table 1**) nor IL-17A/F and IL-17B (data not shown) proteins could be detected in supernatants harvested from neutrophils incubated for 20 h with the stimuli used for the experiments shown in **Figure 1**, as well as with 500 μg/ml β-glucan, 500 μg/ml curdlan, 1 μg/ml Pam3CSK4,

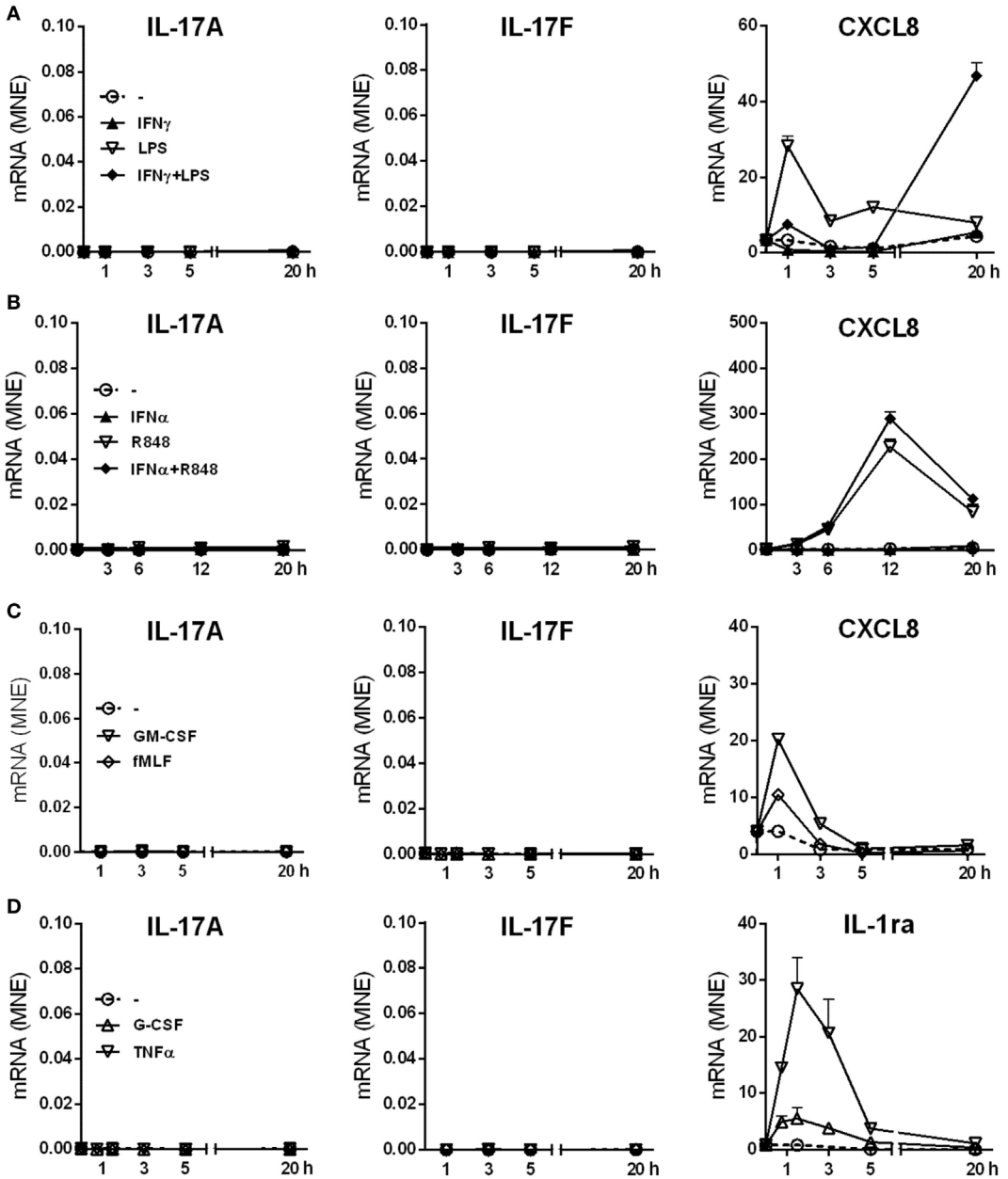

FIGURE 1 | IL-17A, IL-17F, CXCL8, and IL-1ra mRNA expression levels in human neutrophils activated by a variety of stimuli. Human neutrophils were cultured at 5 × 10^6/ml for up to 20 h with **(A)** 100 U/ml IFNγ and/or 100 ng/ml LPS; **(B)** 1,000 U/ml IFNα and/or 5 μM R848; **(C)** 10 ng/ml GM-CSF or 100 nM fMLF; **(D)** 1,000 U/ml G-CSF or 5 ng/ml TNFα. IL-17A, IL-17F, CXCL8, and IL-1ra mRNA expression was evaluated by reverse transcription quantitative real-time PCR (RT-qPCR) and data depicted as mean normalized expression (MNE) units after GAPDH mRNA normalization. The experiments depicted in each panels **(A–D)** are representative of at least three ones with similar results. Error bars stand for SEs calculated from triplicate qPCR reactions.

50 μg/ml poly(IC), and 100 μg/ml CpG ODN. Noteworthy, we used ELISA kits from two different commercial sources (see Materials and Methods) for either IL-17A or IL-17B, in both cases giving equivalent information. On the other hand, stimulus-dependent levels of CXCL8 could be measured in supernatants from our stimulated neutrophils, indicating that agonists were effective and cells fully responsive (**Table 1**). In any case, validity of both IL-17 primers and ELISA kits was demonstrated by the detection of either IL-17A, IL-17D, IL-17E, and IL-17F transcripts in human Th17, but not Th1, cell lines (Figure S1 in Supplementary Material), or IL-17A and IL-17F proteins in supernatants from $CD4^+$ T cells activated with anti-CD3/anti-CD28 mAbs (**Table 1**). We could also detect intracellular IL-17B in lysates of human cerebral cortex (data not shown), as expected (68).

In other experiments, neutrophils were incubated for 3 h with 20 μg/ml IL-6 plus 2 μg/ml IL-23, in the presence or the absence of inactivated conidia, or hyphae, from *A. fumigatus*. These experiments were done with the purpose to mimic, as much as possible, recently described experimental conditions shown to induce not only IL-17A and IL-17F but also IL-17RC, mRNA expression (23, 24, 29, 39, 40, 44). Neutrophils were also incubated with 100–500 ng/ml IL-17A to reinvestigate (12) whether they respond to IL-17A or not. As shown in **Figure 2**, neutrophils treated with either IL-17A or IL-6 plus IL-23 (in the presence or the absence of inactivated *A. fumigatus* conidia/hyphae), showed neither induction of IL-17A (**Figure 2A**), IL-17F (**Figure 2B**), and IL-17RC (**Figure 2C**) mRNAs nor upregulation of the constitutively expressed IL-17RA transcript levels (**Figure 2D**). Similar results were obtained when incubation was prolonged up to 6 h (data not shown), or when neutrophils were stimulated with PMA/ionomycin after pretreatment for 1 h with IL-6 plus IL-23 (Figure S2 in Supplementary Material). Elevated levels of IL-17RC mRNAs were, however, detected in HBECs (data not shown), used as control cells (12), thus confirming that our primers were correctly designed. Importantly, the capacity of IL-6 plus IL-23 to stimulate neutrophils was evidenced by their ability to time-dependently promote STAT3 phosphorylation (**Figure 2E**), as well as to upregulate SOCS3 mRNA expression (**Figure 2F**), such an effect being potentiated by inactivated *A. fumigatus* conidia/hyphae (**Figure 2F**). By contrast, IL-17A-treatment influenced neither SOCS3 (**Figure 2F**) nor CXCL8 (data not shown) mRNA levels in neutrophils. Furthermore, no IL-17A (**Figure 3A**), IL-17F, or IL-17AF (data not shown) proteins were detected by ELISA either intracellularly or in supernatants harvested from neutrophils incubated with IL-6 plus IL-23, in the presence or the absence of inactivated *A. fumigatus* conidia/hyphae. Under the same experimental conditions, CXCL8 protein was newly synthesized and released by neutrophils incubated with IL-6 plus IL-23 in the presence of inactivated *A. fumigatus* conidia/hyphae, but not in their absence (**Figure 3B**). Finally, no IL-17A was detected in IL-6 plus IL-23-stimulated neutrophils by intracellular staining experiments (data not shown), using the anti-human IL-17A eBio64DEC17 mouse IgG1 (from eBioscience) previously shown to function under identical experimental conditions by Taylor et al. (39). We have no clues explaining why we did not reproduce the positive effects on IL-17 expression by IL-6 plus IL-23 (23, 24, 29, 39, 40), with or without inactivated *A. fumigatus* conidia/hyphae. One possibility is that the hyphal extracts from *A. fumigatus* used by Taylor and colleagues (39), but not our inactivated conidia/hyphae, contain some undefined PAMP(s) that effectively promote(s) IL-17A production/IL-17RC expression by human neutrophils.

Taken together, our data extend previous findings on the inability of human neutrophils to express IL-17 members at the mRNA and protein levels under various activating conditions (13–16). Data also confirm and extend our previous findings (12) on the inability of IL-17A to directly modify IL-17A, IL-17F, IL-17RA, IL-17RC, SOCS3, and CXCL8 gene expression in human neutrophils.

TABLE 1 | Lack of IL-17A and IL-17F production by activated human neutrophils.

Stimuli	IL-17A (pg/ml)	IL-17F (pg/ml)	CXCL8 (ng/ml)
Neutrophils			
–	nd	nd	0.07 ± 0.05
500 μg/ml β-glucan	nd	nd	0.41 ± 0.16*
500 μg/ml curdlan	nd	nd	0.49 ± 0.02***
10 ng/ml GM-CSF	nd	nd	0.30 ± 0.13*
100 nM fMLF	nd	nd	0.33 ± 0.12*
5 ng/ml TNFα	nd	nd	1.22 ± 0.90
1 μg/ml Pam3CyS	nd	nd	10.31 ± 3.85**
50 μg/ml poly(I:C)	nd	nd	0.02 ± 0.02
100 ng/ml LPS	nd	nd	0.89 ± 0.22**
5 μM R848	nd	nd	9.47 ± 3.35**
100 μg/ml CpG ODN	nd	nd	5.57 ± 1.1***
100 U/ml IFNγ	nd	nd	0.10 ± 0.04
100 U/ml IFNγ + 100 ng/ml LPS	nd	nd	2.51 ± 1.1**
$CD4^+$ T cells			
–	nd	nd	2.51 ± 1.1
5 μg/ml anti-CD3/CD28	739.6 ± 56.6***	948.9 ± 95.4***	172.6 ± 25.1***

Human neutrophils (5 × 10^6/ml) were cultured for 20 h with the indicated stimuli. $CD4^+$ T cells were stimulated for up to 72 h with anti-CD3 and anti-CD28 mAbs. Cell-free supernatants were then harvested and IL-17A, IL-17F, and CXCL8 content measured by specific ELISA. Values represent the mean ± SD (n = 3).

*Asterisks stand for significant increases as compared to untreated cells: *P < 0.05, **P < 0.01, ***P < 0.001, by Student's t-test.*

nd, not detected; ODN, oligodeoxynucleotides.

Human Neutrophils Incubated With IL-6 Plus IL-23, in the Presence or the Absence of Inactivated *A. fumigatus* Hyphae/Conidia, Do Not Express IL-17RC

Flow cyometry experiments confirmed (12) that neutrophils, either freshly isolated, or incubated for 3 h in the absence, or the presence of IFNγ plus LPS (**Figure 4A**), display only surface IL-17RA, but not IL-17RC. No IL-17RC surface levels were also observed in neutrophils incubated with either R848 (**Figure 4A**), or IL-6 plus IL-23, in the latter case in the absence, or in the presence of either inactivated *A. fumigatus* conidia/hyphae, or IL-17A (**Figure 4B**). IL-17RA surface levels were downregulated in neutrophils treated with IFNγ plus LPS, R848 (**Figure 4A**) and IL-6 plus IL-23 with IL-17A (**Figure 4B**). In these experiments, HBEC were, again, used as positive control

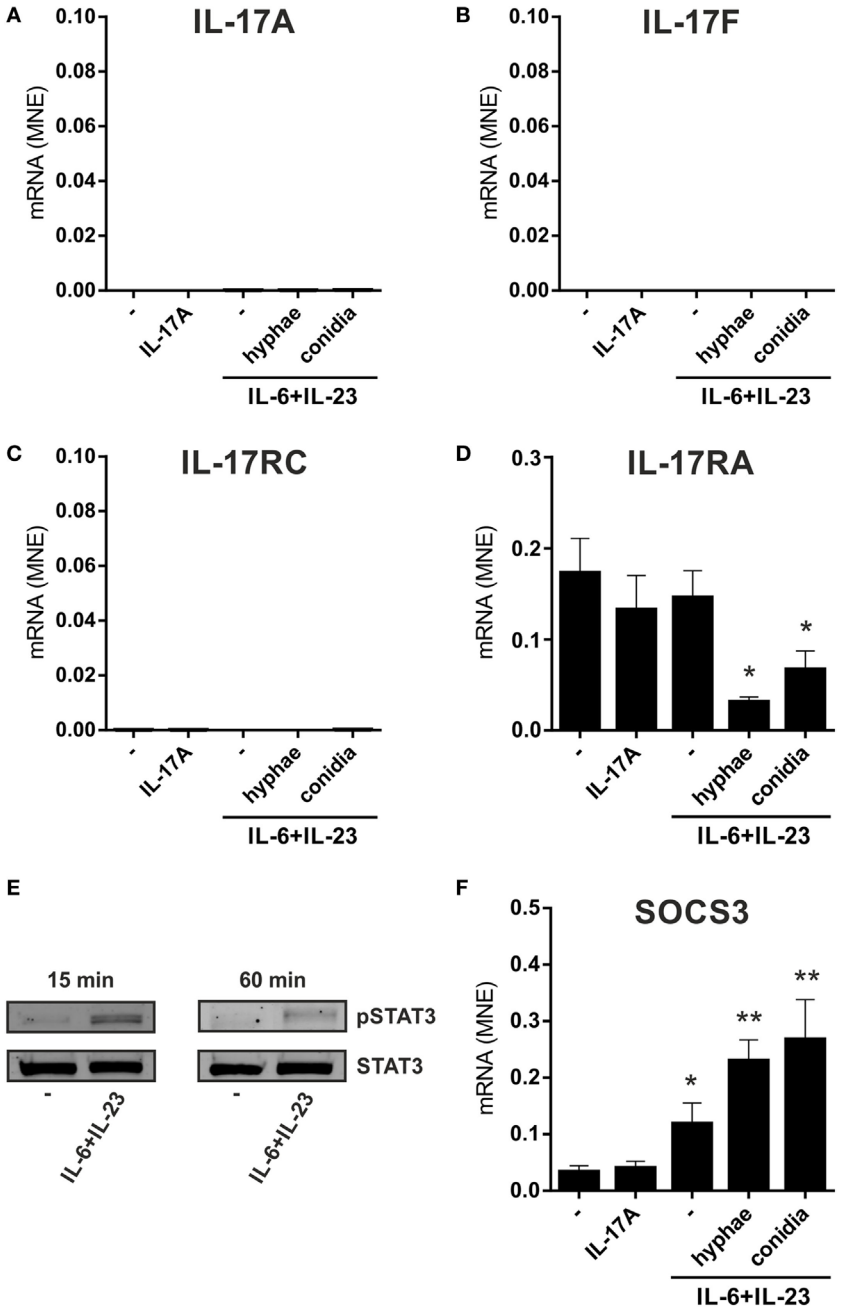

FIGURE 2 | No induction of IL-17A, IL-17F, and IL-17RC mRNA expression in neutrophils incubated with IL-6 plus IL-23, in combination with inactivated *Aspergillus fumigatus* hyphae or conidia. Neutrophils (5×10^6/ml) were incubated either with 100 ng/ml rIL-17A for 2 h or with or without 20 μg/ml IL-6 plus 2 μg/ml IL-23 for 1 h, prior to adding, or not, inactivated *A. fumigatus* conidia (1:5 neutrophils/conidia ratio) and hyphae (1:1 neutrophils/hyphae ratio) for additional 1 h. Neutrophils were then harvested for RNA extraction to evaluate IL-17A **(A)**, IL-17F **(B)**, IL-17RC **(C)**, IL-17RA **(D)**, and SOCS3 **(F)** mRNA expression by reverse transcription quantitative real-time PCR. Gene expression data are depicted as mean normalized expression (MNE) units after GAPDH mRNA normalization (mean ± SEM, $n = 4$). Asterisks stand for significant differences as compared to untreated cells: $^*P < 0.05$, $^{**}P < 0.01$, by Student's *t*-test. **(E)** Immunoblot displaying STAT3 tyrosine phosphorylation in neutrophils, either untreated or cultured for 15 or 60 min with 20 μg/ml IL-6 plus 2 μg/ml IL-23 (representative experiment, $n = 2$).

for both IL-17RA and IL-17RC surface expression (data not shown) (12). It should be pointed out that, for the investigation of surface IL-17RC, we have been using the same anti-IL-17RC, directly PE-conjugated, Abs used in Taylor et al.'s study (39), other than the anti-IL-17RC biotin-conjugated Abs that necessitate PE-conjugated streptavidin for detection (12), without noticing any difference between them. By the way, IFNγ plus LPS and R848 (Figure S3A in Supplementary Material), as well as IL-6 plus IL-23 in the presence of inactivated *A. fumigatus* conidia/hyphae (Figure S3B in Supplementary Material),

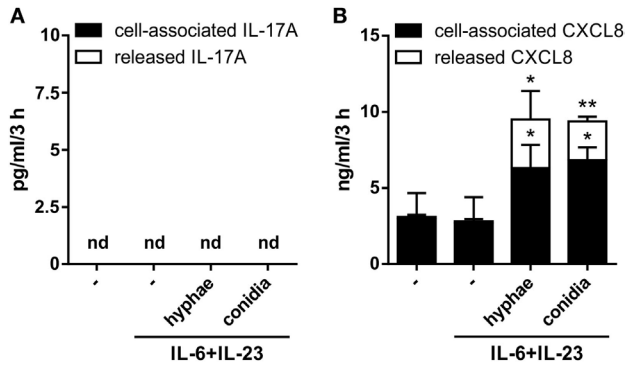

FIGURE 3 | Lack of IL-17A and IL-17F production by human neutrophils activated by IL-6 plus IL-23 in combination with inactivated *Aspergillus fumigatus* hyphae or conidia. Neutrophils (5×10^6/ml) were incubated with or without 20 μg/ml IL-6 plus 2 μg/ml IL-23 and then cultured for three more hours in the presence or not of inactivated *A. fumigatus* conidia and hyphae (used at 1:5 and 1:1, respectively). After incubation, IL-17A **(A)** and CXCL8 **(B)** levels were determined in cell-free supernatants and in corresponding cell pellets by specific ELISA. Values are depicted as the mean ± SD or as not detected (nd) when values were under the detection limit ($n = 3$). Asterisks stand for significant differences as compared to untreated cells: $^*P < 0.05$, $^{**}P < 0.01$, by Student's *t*-test.

variably modulated both CD11b and CD62L expression. All in all, data illustrate that IL-6 plus IL-23, regardless of their combination with inactivated *A. fumigatus* conidia/hyphae, and despite their capacity to upregulate SOCS3 mRNA expression (**Figure 2F**), do not induce the expression of IL-17RC in our hands, contradicting some studies (39, 44).

O_2^- Production by Neutrophils Stimulated With Inactivated *A. fumigatus* Hyphae After Preincubation With IL-6 plus IL-23 Is Not Modified by Either Exogenous IL-17A or IL-17A Inhibitors

We then measured the capacity to release O_2^- by neutrophils preincubated with or without IL-6 plus IL-23 for 1 h, and then treated for one additional hour with inactivated *A. fumigatus* hyphae, in the presence or the absence of either IL-17A or anti-IL-17A neutralizing Abs (Figure S4 in Supplementary Material). As control, neutrophils were also stimulated with either inactivated *A. fumigatus* hyphae alone or 20 ng/ml PMA. As shown in Figure S4 in Supplementary Material, inactivated *A. fumigatus* hyphae were found to trigger a remarkable O_2^- production by neutrophils, even though lower than PMA. However, *A. fumigatus* hyphae-stimulated O_2^- release was not potentiated by the preincubation of neutrophils with IL-6 plus IL-23 (which, by themselves, did not trigger any O_2^- production) (Figure S4 in Supplementary Material). Under the latter experimental conditions, addition of either IL-17A or anti-IL-17A neutralizing Abs (αIL-17A Abs) did not influence the effect of inactivated *A. fumigatus* hyphae on neutrophil-derived O_2^- (Figure S4 in Supplementary Material), supporting the lack of induction of surface IL-17RC expression and endogenous IL-17A, respectively.

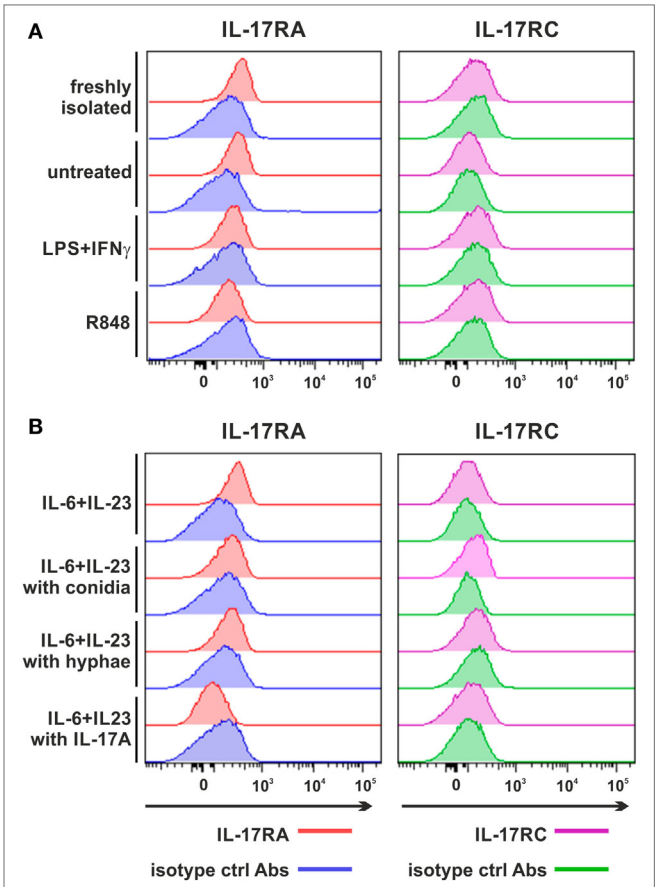

FIGURE 4 | Expression of surface IL-17RA and IL-17RC in neutrophils activated under various experimental conditions. Expression of surface IL-17RA (left panel) and IL-17RC (right panel) was evaluated by flow cytometry in neutrophils either freshly isolated or cultured for 3 h without or with 100 U/ml IFNγ plus 100 ng/ml LPS, 5 μM R848 **(A)**, 20 μg/ml IL-6 plus 2 μg/ml IL-23 alone or in the presence of inactivated *Aspergillus fumigatus* conidia, hyphae or 500 ng/ml rIL-17A **(B)**. Graphs depict a representative experiment out of three independent ones with similar results. Histograms show staining by specific and isotype control Abs, respectively, for each stimulatory condition.

Chromatin Organization at the IL-17A and IL-17F Genomic Loci of Human Neutrophils

Signatures of histone posttranslational modifications at a specific gene locus provide indicative elements to predict whether such a gene can be transcribed or not (69, 70). Therefore, we evaluated the presence of histone marks associated to active (e.g., H3K27Ac) and poised (e.g., H3K4me1) genomic regulatory elements (71) at the *IL17A* and *IL17F* loci of human neutrophils. Genome-wide ChIP-seq assays demonstrated that, in freshly isolated neutrophils, the entire genomic region containing *IL17A* and *IL17F* loci is completely devoid of H3K27Ac and H3K4me1 (**Figure 5**). By contrast, based on data available from the NIH Epigenomics Roadmap Initiative (72), multiple H3K4me1 peaks are present in the same genomic regions of PMA/ionomcyin-stimulated Th17 cells, while H3K27Ac peaks

localize at the *IL17A* locus only (**Figure 5**). To validate the previous data, we performed H3K27Ac and H3K4me1 qPCR ChIPs using neutrophils incubated for 1 h either with or without 20 μg/ml IL-6 plus 2 μg/ml IL-23, as well as Th17 cell lines (in which IL-17A and IL-17F mRNA is constitutively transcribed), used as positive controls (**Figure 6**). Based on the H3K4me1 peaks from the ChIP-seqs of Th17 cell lines (72) (**Figure 5**), we designed specific primers amplifying potential regulatory regions at the *IL17A* and *IL17F* genomic loci, namely IL-17A#1 and IL-17F#1 for enhancers, and IL-17A#2, IL-17A#3, and IL-17F#2 for promoters (**Figures 6A,B**). As expected, Th17 cell lines displayed constitutively bound H3K4me1 at their IL-17A and IL-17F promoters and enhancers (**Figures 6A,B**, left panels). We also detected high levels of H3K27Ac at the IL-17A and IL-17F promoters and enhancers of Th17 cell lines (**Figures 6A,B**, right panels), in line with their constitutive expression of both IL-17A and IL-17F mRNA (data not shown). By contrast, we did not observe any H3K4me1 or H3K27Ac at the *IL17A* and *IL17F* loci of neutrophils, either under resting conditions (thus confirming the ChIP-seq data shown in **Figure 5**) or after incubation with IL-6 plus IL-23 (**Figures 6A,B**). In fact, the H3K4me1 and H3K27Ac levels at the IL-17A and IL-17F enhancers in neutrophils were similar to those ones present at the PRL promoter, a genomic region with a closed chromatin conformation in myeloid cells, herein used to determine the signal background (**Figures 6A,B**). Notably, measurable amounts of H3K4me1 and H3K27Ac were found at the SOCS3 promoter of neutrophils under resting conditions, as well as in Th17 cell lines (**Figure 6C**). Interestingly, H3K27Ac levels tended to increase in neutrophils incubated with IL-6 plus IL-23 (**Figure 6C**), in accordance with a supposed STAT3-dependent induction of SOCS3 mRNA (73). Taken together, data indicate that the organization of the *IL17A* and *IL17F* loci in human neutrophils is characterized by the absence of poised chromatin marks, unlike that of IL-17A- and IL-17F-producing Th17 cell lines. Data also indicate that human neutrophils do not reorganize the chromatin of the *IL17A* and *IL17F* loci in response to IL-6 plus IL-23, consistent with their inability to *de novo* accumulate IL-17A and IL-17F mRNA.

Human Neutrophils From Patients With Psoriasis Do Not Express IL-17A and/or IL-17F mRNA

We subsequently investigated whether neutrophils isolated from patients with active psoriasis could express/produce IL-17A, IL-17F, and/or IL-17RC mRNA, either constitutively or upon incubation for 20 h with IFNγ plus LPS, R848, or IL-17A. As shown in **Figure 7A**, the latter was not the case, as psoriatic neutrophils behaved similarly to neutrophils from HDs. Psoriatic neutrophils did not also respond to IL-17A (**Figure 7A**), due to their lack of surface IL-17RC expression (**Figure 7B**). Nonetheless, psoriatic neutrophils fully responded to either R848 or IFNγ plus LPS, as they accumulated CXCL8, TNFα, and SOCS3 transcripts at levels comparable to those in HD neutrophils (**Figure 7A**).

Commercial Anti-IL-17A Abs (AF-317-NA) Positively Stain Cytospins of Resting and Activated Neutrophils due to Their Non-Specific Recognition of Neutrophil Intracellular Proteins Different From IL-17A

In additional experiments, cytospin slides of resting and R848-stimulated neutrophils were incubated with goat anti-human IL-17A AF-317-NA Abs, previously shown to stain neutrophils in pathological tissues (18–22, 25, 27, 28, 30–33, 35, 36, 41–43, 45, 47–50), as also confirmed by our IHC/IF staining of inflamed psoriatic tissue (**Figure 8A**). Consistently, neutrophil cytospin slides became strongly positive upon incubation with AF-317-NA, yet with no difference between resting or R848-activated neutrophils (**Figure 8B**). By contrast, immunostaining of the same cytospins slides with anti-human CXCL8 Abs showed a strong positivity only in R848-treated neutrophils (**Figure 8B**), thus excluding methodological artifacts. Not surprisingly, neutrophils from the same experiments were found totally negative for both IL-17A mRNA expression and IL-17A production once processed for RT-qPCR analysis and ELISA. The detection of IL-17A-positive neutrophils by IHC, in the absence of IL-17A mRNA, could

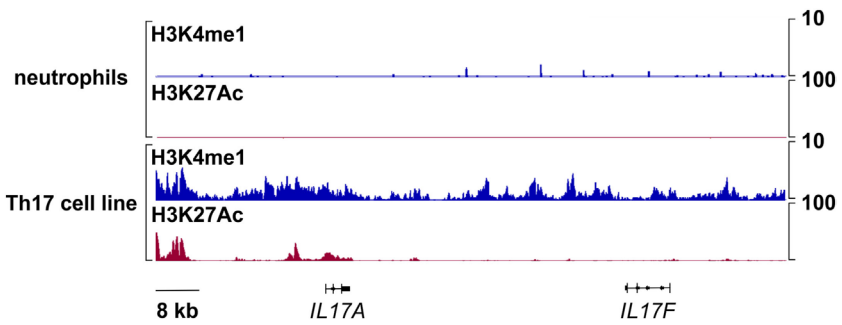

FIGURE 5 | Chromatin immunoprecipitation (ChIP)-Seq profiles of H3K4me1 and H3K27Ac at the *IL17A* and *IL17F* loci in human neutrophils and Th17 cell lines. Representative snapshots depicting H3K4me1 and H3K27Ac ChIP-seqs at the *IL17A* and *IL17F* genomic loci in freshly isolated human neutrophils or, as retrieved from NIH Epigenomics Roadmap Initiative (72), in phorbol mysistate acetate/ionomycin-stimulated Th17 cell lines.

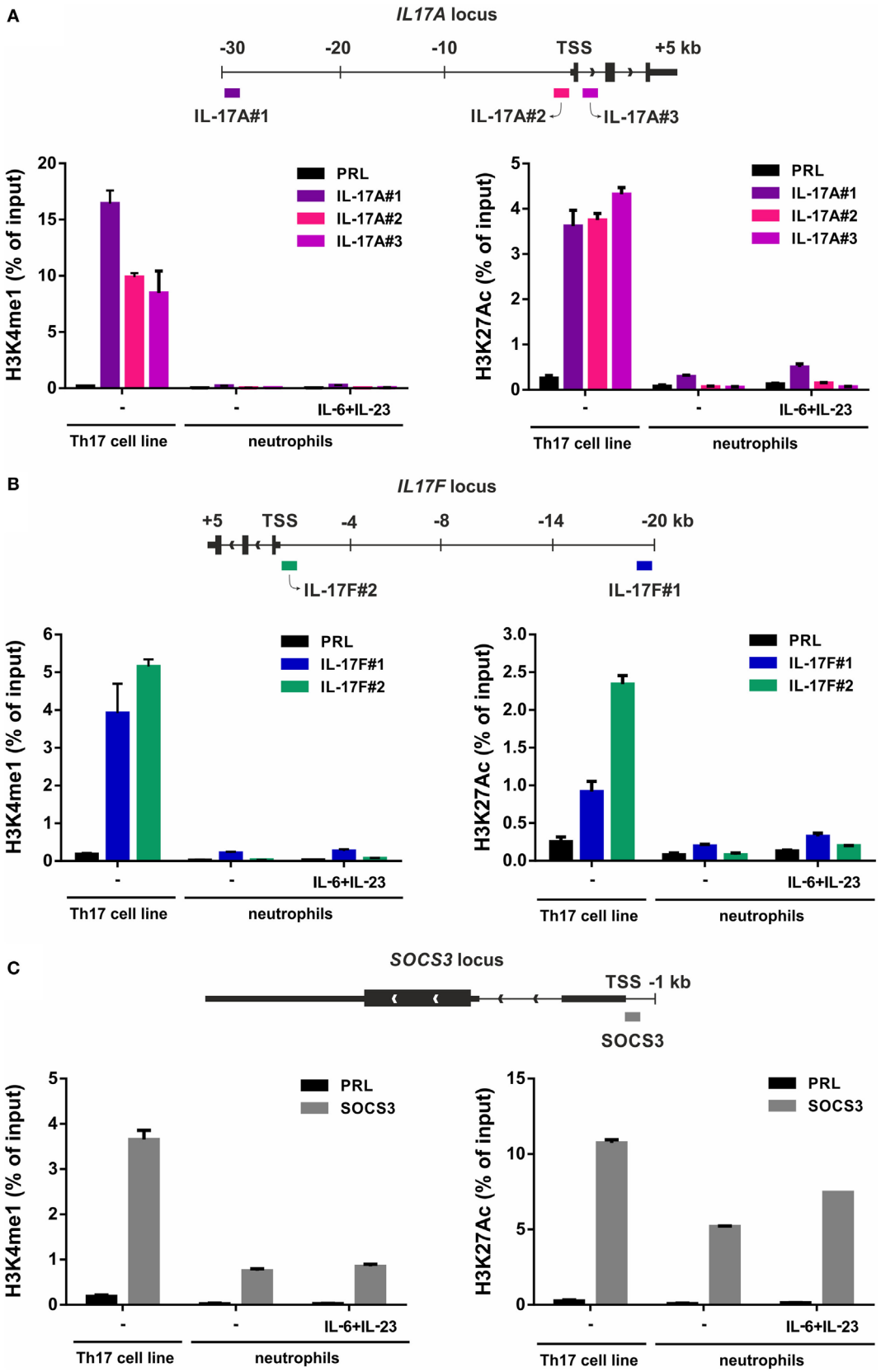

FIGURE 6 | Continued

FIGURE 6 | H3K4me1 or H3K27Ac levels at the IL-17A, IL-17F, and SOCS3 genomic loci of Th17 cell lines and resting/IL-6 plus IL-23-activated neutrophils. Enrichment levels of H3K4me1 (left panels) and H3K27Ac (right panels) at the IL-17A **(A)**, IL-17F **(B)**, and SOCS3 **(C)** genomic loci by chromatin immunoprecipitation (ChIP) analysis in human Th17 cell lines and neutrophils incubated for 1 h with or without 20 μg/ml IL-6 plus 2 μg/ml IL-23. **(A–C)** Schemes illustrating the positions of the designed primer pairs amplifying promoter and potential enhancer regions of IL-17A, IL-17F, and SOCS3 for ChIP analysis are depicted at the top of each panel. Coimmunoprecipitated DNA samples were expressed as percent of the total input. Panels in **(A–C)** depict a representative experiment out of two independent ones with similar results. Error bars represent SEs calculated from triplicate qPCR reactions.

be explained by the fact that the cytokine may be synthesized in bone marrow neutrophil precursors, at stages during which granule proteins, such as myeloperoxidase (MPO), elastase, and azurocidin 1, are formed (74). However, in transcriptomes made by Rapin et al., generated from cells isolated at different stages during granulopoiesis (65), we did not identify any IL-17A mRNA accumulation (**Figure 9**). In the same database, we not even detected IL-17RC and IL-10 mRNA (**Figure 9**), consistent with the inability of mature neutrophils to express them (12, 70). By contrast, we did find MPO, elastase, and azurocidin 1 mRNA expression only in transcriptomes of neutrophil precursors, as expected (74), thus validating the reliability of the database (65) (**Figure 9**). In any case, consistent with the absence of intracellular IL-17 (**Figure 3A**), immunoblots performed with AF-317-NA revealed that whole neutrophil lysates did not show any positive signal in correspondence of recombinant human IL-17A (rhIL-17A) molecular weight (MW) (**Figure 8C**). In these experiments, neutrophils were either freshly isolated (D1 and D2 in **Figure 8C**), or cultured for 3 h with or without R848, 2 μg/ml IL-6 plus 0.2 μg/ml IL-23 (low IL-6 plus IL-23 in **Figure 8C**), or 20 μg/ml IL-6 plus 2 μg/ml IL-23 (high IL-6 plus IL-23 in **Figure 8C**). By contrast, AF-317-NA strongly reacted in correspondence of neutrophil proteins displaying higher MW than that of rIL-17A, with no difference in signals among freshly isolated, stimulated, or untreated neutrophils (**Figure 8C**). While these data confirm the observations reported by Tamarozzi et al. (13), who also used mouse anti-IL-17A mAbs (#41802, from R&D) in addition to AF-317-NA, they are in contrast with Lin et al.'s findings (30) illustrating a constitutive IL-17A (but not IL-17F) expression in neutrophil lysates, as revealed by immunoblotting with #41802. Halwani et al. (23) too found constitutive IL-17A amounts in lysates of neutrophils from asthmatic patients, even increasing upon cell incubation with IL-21 and/or IL-23 for 18 h, as revealed by immunoblotting with unspecified Abs from R&D. However, since only portions of the immunoblots are shown in Halwani et al. (23) and Lin et al. (30) paper, it is not known whether additional proteins were recognized by Abs used. Whatever the case is, our experiments suggest that the positive staining of neutrophils detected by IHC and IF using AF-317-NA on cytospins and, possibly, tissue slides, stands for an IL-17A-unrelated binding(s) to neutrophils.

Human Neutrophils Do Not Express/Produce IL-17B

In a separate set of experiments, we also tested goat anti-IL-17B (AF1248) Abs that, in recent publications, have been shown to positively stain, by IHC and IF, neutrophils present in tissue samples from RA (75) and colon carcinoma (CCR) (76) patients. Consistently, we found that also neutrophils present in inflamed psoriatic tissue were strongly detectable by IHC and IF stainings with AF1248 (**Figure 10A**). On cytospin slides, AF1248 stained neutrophils isolated from the blood of HDs and incubated for 3 h with or without 5 μM R848 in an equivalent manner (**Figure 10B**). However, by immunoblotting of whole lysates prepared from neutrophils treated with R848 or IL-6 plus IL-23, AF1248 did not recognize any protein corresponding to the rhIL-17B MW (**Figure 10C**). These negative observations were also confirmed by measurement of intracellular, as well as, released IL-17B by two commercial ELISA (see Materials and Methods). Accordingly, no antigenic IL-17B could be measured in supernatants and whole lysates from neutrophils incubated with 5 μM R848 with or without 1,000 U/ml IFNα, 100 μg/ml LPS with or without 100 U/ml IFNγ, 2/20 μg/ml IL-6 plus 2 μg/ml IL-23 (data not shown), in agreement with the lack of IL-17B mRNA induction. Detectable IL-17B levels were, however, measured in lysates of human cerebral cortex (68), demonstrating that our two IL-17B ELISA kits were sensitive enough. Altogether, our data indicate that, similarly to the case of AF-317-NA, the positive stainings of neutrophils in cytospin slides and, possibly, tissue samples by AF1248, likely stand for an IL-17B-unrelated, non-specific, recognition occurring in human neutrophils.

DISCUSSION

In this study, we have reinvestigated in-depth whether human neutrophils produce IL-17A, IL-17B, IL-17F, and IL-17A/F *in vitro*. According to the literature, in fact, information on such an issue appears discordant, as the majority of papers sustain that human neutrophils do express/produce IL-17A (18–53), while a minority fail to detect it (12–17). This issue is even more critical if one takes into account that also the capacity of murine neutrophils to produce IL-17A, shown in a variety of mouse models of infectious and autoimmune inflammation (24, 39, 40, 77–81), has been recently questioned (82, 83). Preclinical models evidencing neutrophil-derived IL-17 as pathogenic in diseases might be, in fact, prematurely taken as proof-of-concept for immediate translational applications in humans.

Herein, by using multiple methodological approaches (RT-qPCR, ChIP, ChIP-seq, ELISA, intracellular staining, and immunoblotting), we confirm and greatly extend our previous findings (12) showing that highly purified (>99.7%) populations of human neutrophils, either resting or activated by a variety of stimulatory conditions, including TLR and dectin ligands, fungal PAMPs and cytokines, used singly or in combinations, neither express IL-17A, IL-17F, IL-17B, IL-17C, IL-17D, and IL-17E mRNA nor produce IL-17A, IL-17F, IL-17A/F, and IL-17B *in vitro*. Similarly, we show that also neutrophils isolated from

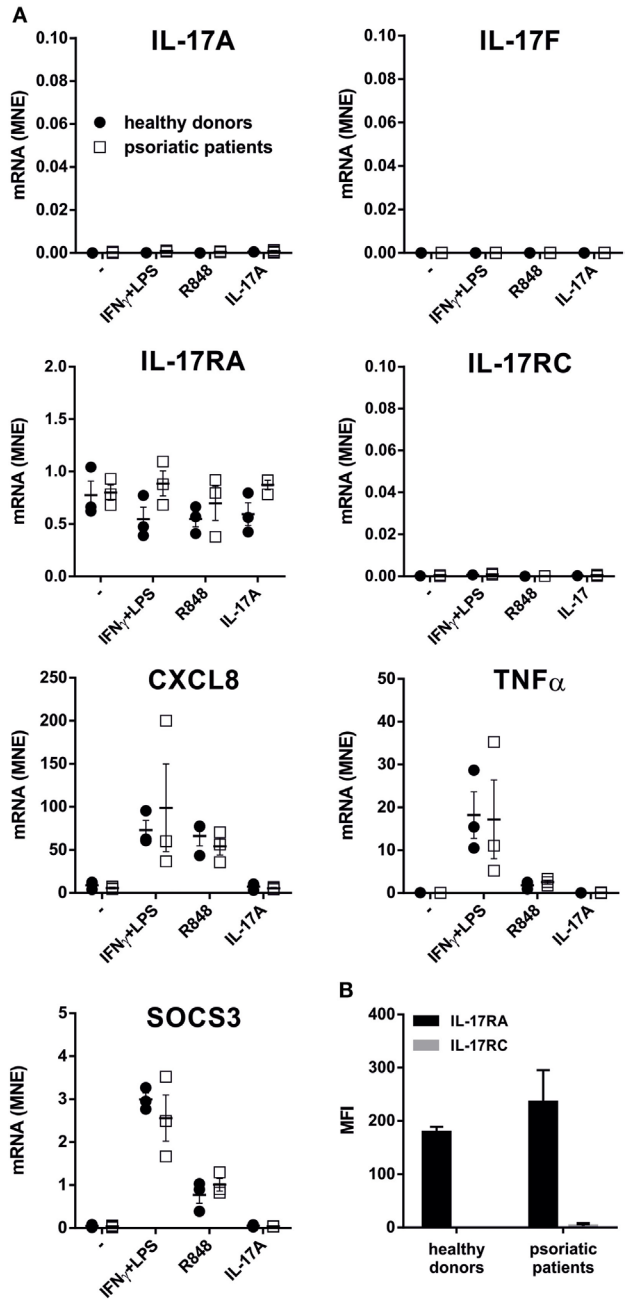

FIGURE 7 | IL-17A, IL-17F, IL-17RA, IL-17RC, CXCL8, TNFα, and SOCS3 mRNA expression, as well as IL-17R surface expression, in neutrophils from patients with psoriasis. **(A)** Neutrophils isolated from healthy donors (HDs) ($n = 3$) or psoriatic patients ($n = 3$) were cultured for 20 h with 100 U/ml IFNγ plus 100 ng/ml LPS, 5 μM R848, or 500 ng/ml IL-17A to evaluate IL-17A, IL-17F, IL-17RA, IL-17RC, CXCL8, TNFα, and SOCS3 mRNA expression by reverse transcription quantitative real-time PCR. Gene expression data are depicted as mean normalized expression (MNE) units after GAPDH mRNA normalization. **(B)** Surface IL-17RA and IL-17RC expression evaluated by flow cytometry in human neutrophils from HDs or psoriatic patients. Values represent the mean ± SEM ($n = 3$). For the data of panels **(A,B)** no significant differences between HDs or psoriatic patients were observed by two-way ANOVA followed by Bonferroni's post-test.

patients with active psoriasis do not express IL-17F, IL-17B, IL-17C, IL-17D, and IL-17E as well as IL-17RC mRNA when activated by R848, IFNγ plus LPS, and IL-17A *in vitro*. In such regard, RNA-Seq experiments made by Tamarozzi et al. (13), using neutrophils isolated by negative-selection (>99.9% pure) from HDs or RA patients (as we do), then treated for 1 h with a range of inflammatory cytokines (TNFα, GM-CSF, G-CSF, IL-6, IL-1β, CXCL8, IFNα, and IFNγ), also failed to detect any of the mRNA for IL-17 cytokine family. By contrast, Yamanaka et al. (15) have been recently reported the presence of constitutive IL-17A transcripts in neutrophils from HDs and psoriasis patients isolated by density gradient cell separation (92% purity). However, when the same cell populations were further purified by magnetic sorting (reaching a 99% purity), they were found totally devoid of IL-17A mRNA (15), indicating that contaminating monocytes/lymphocytes were actually responsible for the IL-17A mRNA expression in unsorted "neutrophils." Needless to say that Yamanaka et al.'s observations (15) are example of a notion that we have been always recommending in our studies (56, 59, 84), namely the requirement of using highly purified cell populations if one wants to obtain correct results when examining neutrophil gene expression or neutrophil-derived cytokines.

Interestingly, other studies confirm that human neutrophils do not constitutively contain IL-17A transcripts (13, 24, 29, 30, 35, 39, 40, 44), including those ultimately showing a concurrent positivity for IL-17A protein, as revealed by intracellular flow cytometry (24, 39, 40), ELISA (24, 39), confocal microscopy (39), or IHC (29). Some authors (30, 35) speculated that the absence of IL-17A mRNA in mature neutrophils indicates that the cytokine is synthesized in bone marrow neutrophil precursors, at the stages when granule proteins are formed (74). However, we would exclude such a hypothesis, as our analysis of transcriptomes generated from all types of bone marrow cell populations (65) failed to identify an IL-17A mRNA accumulation at any stage of neutrophil maturation.

We were unable to detect IL-17A and IL-17F mRNA/production/release even by human neutrophils incubated with IL-6 plus IL-23, in contrast to what repeatedly found (23, 24, 29, 39, 40). In our experiments, neutrophils did, however, respond to IL-6 plus IL-23 in terms of STAT3 phosphorylation and SOCS3 mRNA induction, indicating that the two cytokines are effectively stimulatory for neutrophils. It is intriguing that, apart from Halwani et al. (23), who found that either 20 ng/ml IL-6 or 20 ng/ml IL-23, singly used, directly induced IL-17A mRNA and protein in a fraction of neutrophils from asthmatic patients, other groups highlighted the necessity to use at least 20 μg/ml IL-6 plus 2 μg/ml IL-23 (29, 39, 40) (as we did). In this context, the paper by Hu et al. (24), based on the use of neutralizing Abs and pharmacological inhibitors, identified endogenous IL-6 and IL-23 as indirect inducers of IL-17A expression in a fraction of neutrophils either infected with *Mycobacterium tuberculosis* (MTB), or stimulated with LPS or Pam3CSK4. In this latter study, however, IL-6 and IL-23 levels corresponded to 1 ng/ml at the best. Herein, we failed to detect IL-17A mRNA expression and production in neutrophils incubated with either LPS

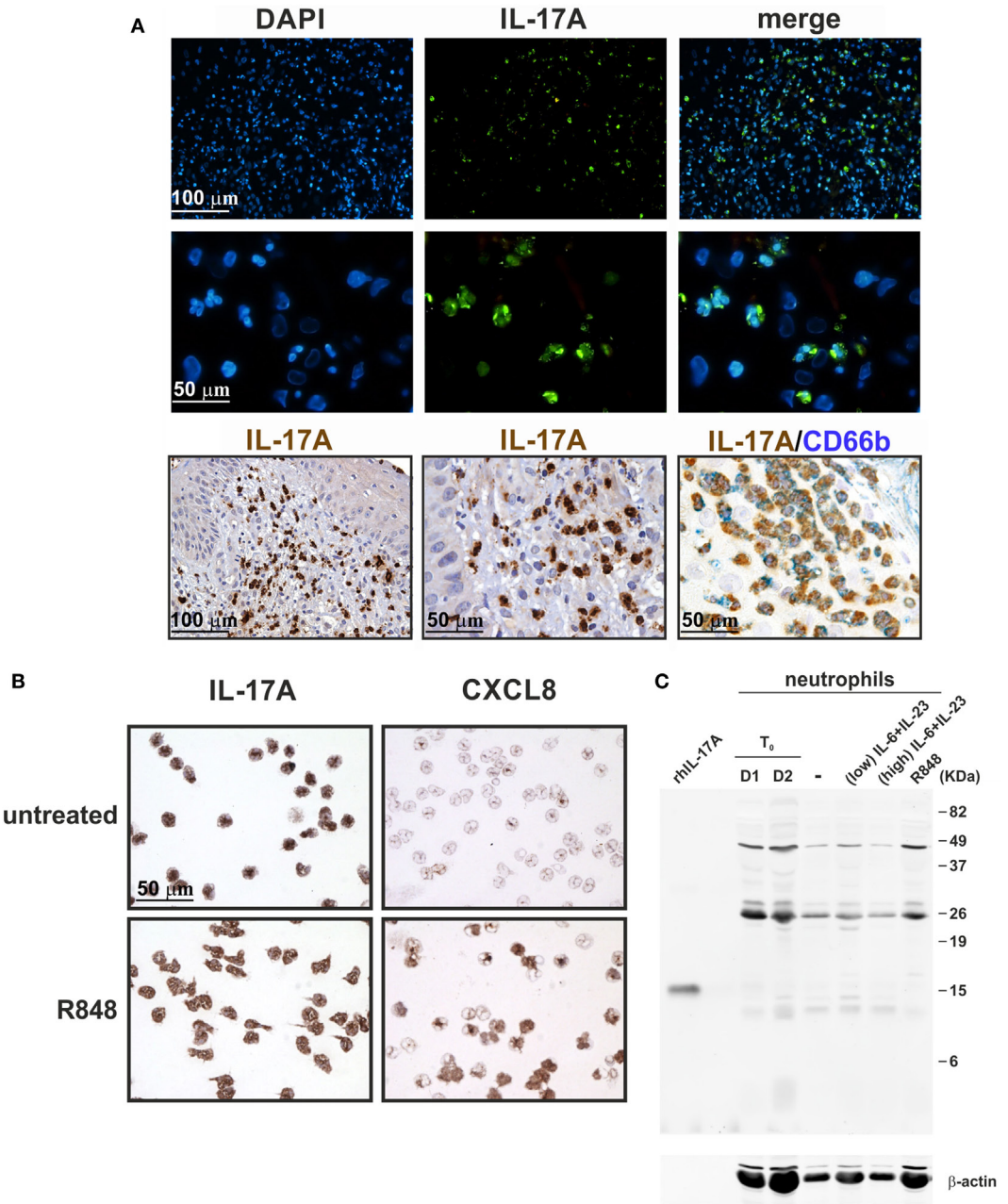

FIGURE 8 | Staining human neutrophils by anti-IL-17A (AF-317-NA) polyclonal antibodies (Abs). **(A)** Immunofluorescence (top panels) and immunohistochemistry (lower panels) stainings of two FFPE cases of human pustular psoriasis using anti-IL-17A (AF-317-NA) and anti-CD66b Abs (as labeled). Top panels show DAPI, FITC channel, and merge to recognize neutrophil shape; lower panels show different magnification of IHC and double IHC to characterize IL-17A$^+$ cells with the neutrophil marker CD66b. **(B)** Cytospins of neutrophils, either untreated (top panels) or treated with 5 μM R848 (bottom panels) for 3 h, were stained with anti-IL-17A (AF-317-NA, left panels) and anti-CXCL8 (right panels) Abs. Original magnification 200× [first row in **(A)** and left image in third row, scale bar 100 μm] and 400× [second row in **(A)**, center/right images in third row in **(A)**, as well as in **(B)**, scale bar 50 μm]. Images of the second row in **(A)** represent magnifications of images in first row. **(C)** AF-317-NA immunoblot of lysates from neutrophils either freshly isolated (T_0, from two donors) or incubated for 3 h with or without 2 μg/ml IL-6 plus 0.2 μg/ml IL-23 (low), 20 μg/ml IL-6 plus 2 μg/ml IL-23 (high), or 5 μM R848. Recombinant human IL-17A (rhIL-17A) was used as positive control. Panels **(B,C)** display representative experiments out of two independent ones with similar results.

or Pam3CSK4, even if it is true that they produce IL-6 (62) and IL-23 (our unpublished observations). Whether stimulation of neutrophils with MTB effectively promotes IL-17A expression *via* endogenous IL-6 and IL-23 remains to be verified. However, no IL-17A, IL-17B, IL-17C, or IFNγ secretion from *Mycobacterium bovis* Bacille-Calmette Guerin (BCG)-stimulated neutrophils was recently reported (14). It should be also remarked that the purity of neutrophils in studies showing an IL-17 production in

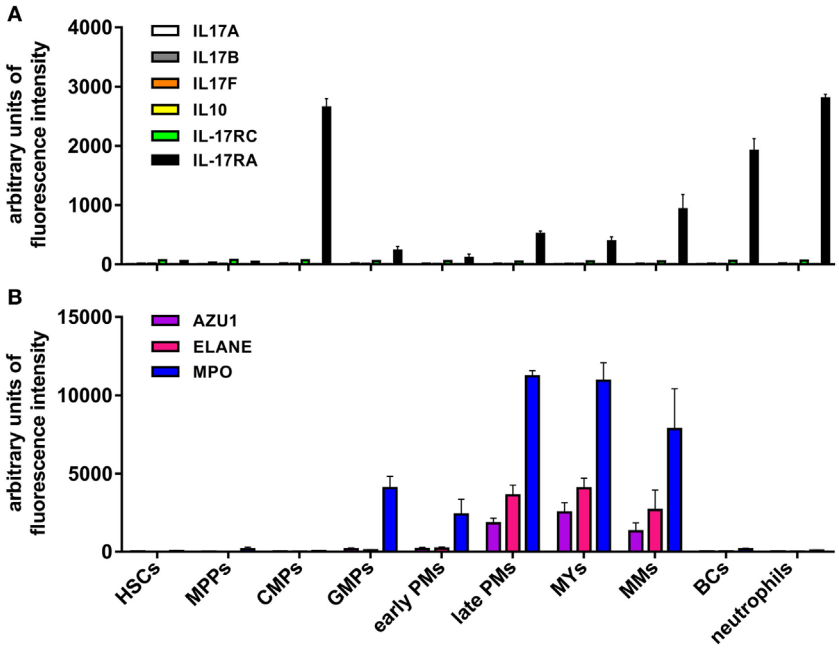

FIGURE 9 | Levels of IL-17A, IL-17B, IL-17F, IL-10, IL-17RC, IL-17RA, azurocidin, neutrophil elastase, and myeloperoxidase (MPO) mRNA expression in neutrophils at different stages of maturation. mRNA expression data derive from Gene Expression Omnibus database (accession number GSE42519) (65). **(A)** IL-17A, IL-17B, IL-17F, IL-10, IL-17RC, and IL-17RA or **(B)** azurocidin (AZU1), neutrophil elastase (ELANE), and MPO mRNA expression levels were measured in the following cell types: hematopoietic stem cells (HSCs), multipotent progenitors (MPPs), common myeloid progenitors (CMPs), granulocyte-macrophage progenitors (GMPs), early and late promyelocytes (PMs), myelocytes (MYs), metamyelocytes (MMs), band cells (BCs), and bone marrow polymorphonuclear neutrophil granulocytes. Values represent the mean ± SEM as calculated from data of the biological replicates present in the database.

response to IL-6 plus IL-23 (23, 29, 39, 40), reported to be >96% at the best (29), does not sufficiently secure fully genuine results at least in our opinion.

Nevertheless, we investigated potential mechanisms helping to clarify whether human neutrophils respond to IL-6 plus IL-23 in terms of IL-17A expression or not. ChIP assays revealed that, in resting, as well as in IL-6 plus IL-23-stimulated, neutrophils, but not in Th17 cell lines, the *IL17A* locus does not contain any H3K4me1 and H3K27Ac, which are two histone marks that are usually present in those genomic regions that act as active enhancers (85). On the other hand, the levels of H3K27Ac were found increased at the SOCS3 promoter of neutrophils incubated with IL-6 plus IL-23, consistent with the potentially inducible SOCS3 mRNA transcription. Notably, the complete absence of H3K4me1 at the *IL17A* locus of neutrophils is particularly informative, since such a histone modification is known to precede very early, but time-consuming (86), events necessary for the assembly of the transcriptional machinery, including nucleosomal depletion, H3K27Ac deposition, and enhancer activation (85). Based on our data, it appears that the chromatin at the *IL17A* locus of human neutrophils likely displays a closed conformation, inaccessible to transcription factors and, consequently, RNA polymerase, ultimately preventing IL-17A mRNA transcription in resting as well as stimulated neutrophils. It is thus very unlikely that H3K4me1 modification could be induced within 1 h, e.g., the time-point at which IL-17 mRNA expression in IL-6 plus IL23-stimulated neutrophils has been observed (29, 39, 40). Obviously, this does not exclude that there could exist some stimulatory conditions able to modify the chromatin at the *IL17A* or *IL17F* loci of human neutrophils.

A variety of studies report the presence of IL-17A$^+$-neutrophils in sample tissues from many diseases, including psoriasis (20, 25, 30, 32, 35, 49), skin inflammation (27), bullous pemphigoid (28), hidradenitis suppurativa (50), fungal keratitis (26), RA (31, 75), ankylosing spondylitis (18), systemic lupus erythematosus (41, 52), human ANCA-associated glomerulonephritis (47), cystic fibrosis (19, 36, 44), nasal polyps (53), chronic obstructive pulmonary disease (22), lung tissues during bacterial pneumonia (46), alcoholic liver diseases (48), acute renal allograft rejection (42), atherosclerotic plaques (21), cutaneous T cell lymphoma lesions (45), gastric cancer (29), cervical cancer (33), and prostate cancer (51), as revealed by IHC, IF, or intracellular flow cytometry using various commercial anti-IL-17A Abs. Not surprisingly, results occasionally appear discordant. For example, while Moran et al. (31) reported IL-17A-positive synovial tissue neutrophils using the AF-317-NA, van Baarsen et al. (16) show that synovial tissue neutrophils from arthritis patients are not stained by another antibody, namely #41802. By IHC experiments using AF-317-NA, we too detected IL-17A$^+$-neutrophils not only in skin sections of psoriasis patients but also in cytospin slides of neutrophils isolated from HDs and incubated for 3 h with or without R848, at similar levels. By contrast, we found that whole lysates of the same neutrophil populations displayed major signals at levels of proteins having MW not corresponding to that of IL-17A when

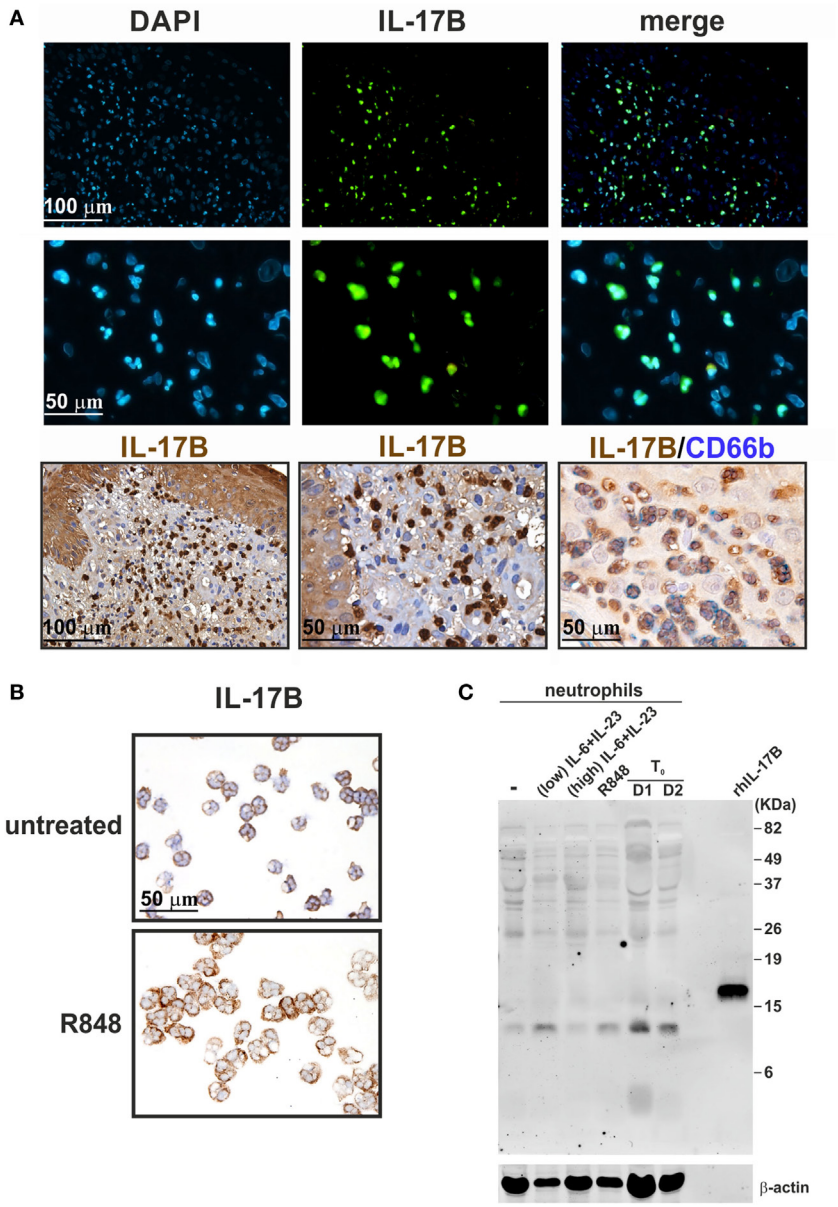

FIGURE 10 | Staining human neutrophils by anti-IL-17B (AF1248) antibodies (Abs). **(A)** Immunofluorescence (top panels) and immunohistochemistry (lower panels) staining of two FFPE cases of human pustular psoriasis using anti-IL-17B (AF1248) and CD66b Abs (as labeled). Top panels show DAPI, FITC channel, and merge to recognize neutrophil shape; lower panels show different magnification of IHC and double IHC to characterize IL-17A$^+$ cells with the neutrophil marker CD66b. **(B)** Cytospins of neutrophils incubated without (top panel) or with 5 μM R848 (bottom panel) for 3 h. Original magnification 200× [first row in **(A)** and left image in third row, scale bar 100 μm] and 400× [second row in **(A)**, center/right images in third row in **(A)**, as well as in **(B)**, scale bar 50 μm]. Images of the second row in **(A)** represent magnifications of images in first row. **(C)** AF1248 immunoblot of lysates from neutrophils either freshly isolated (T_0, from two donors) or incubated for 3 h with or without 2 μg/ml IL-6 plus 0.2 μg/ml IL-23 (low), 20 μg/ml IL-6 plus 2 μg/ml IL-23 (high), or 5 μM R848. Recombinant human IL-17B (rhIL-17B) was used as positive control. Panels **(B,C)** display representative experiments out of two independent ones with similar results.

immunoblotted with AF-317-NA. Our findings substantially confirm the observations previously made by Tamarozzi et al. (13) who also did not detect any IL-17A expression in highly pure populations of neutrophils (99.9%) by using a variety of assays including RT-qPCR, RNA-seq, western blot and ELISA, despite of finding IL-17A$^+$-neutrophils in *Wolbachia Onchocerca volvulus*-positive nodules by IHC using AF-317-NA. Notably, by immunoprecipitation experiments followed by mass spectrometry, Tamarozzi et al. (13) also uncovered that both AF-317-NA and #41802 bind to several proteins expressed in granules (including MPO, lactoferroxin, and lysozyme C) and cytoskeleton (such as keratin and profilin) of neutrophils, while other anti-human IL-17A Abs (sc-6077 from Santa Cruz, and PRS4877 from Sigma) were found to recognize multiple non-specific bands

in neutrophil immunoblots (13). All in all, data suggest that the IL-17A-positivity of human neutrophils detected by AF-317-NA and #41802 is, at least *in vitro*, likely an artifact. Whether these or other anti-IL-17A Abs, including sc-7927 (from Santa Cruz) (33, 43), ab9565 (from Abcam) (37), ab136668 (from Abcam) (46), 500-P07 and 500-P07G (from Peprotech) (43), and eBio64Dec17 (from eBioscience) (20, 26, 43), are instead reliable in specifically detecting IL-17A$^+$-neutrophils in tissue samples should be more convincingly established. For instance, in models of skin inflammation resembling psoriasis (27), accumulated neutrophils stained by AF-317-NA were shown to express IL-17 mRNA transcripts. In other studies, tissue neutrophil staining by AF-317-NA was blocked after antibody pre-adsorption with rIL-17A (18, 47), or confirmed by costaining of the same section by eBio64DEC17 (47). It is worth recalling that neutrophils express high levels of IL-17RA (12) that could in theory bind exogenously derived IL-17A, consequently leading to a positive signal in IHC or IF experiments without actual intracellular IL-17 production (87), as observed in the case of mast cells (88). Whatever the case is, we would recommend to always validate by multiple investigation methods an eventual detection of IL-17A-positive neutrophils exclusively by IHC, or IF or intracellular flow cytometry (18, 19, 21, 22, 28, 32–34, 36–38, 42, 43, 48–52).

Similar concerns can be made for the, to date, reported IL-17B expression by human neutrophils. Accordingly, IL-17B has been detected in neutrophils infiltrating the synovial membrane of RA patients (75) and the stroma of CCR cancer (76) by IHC/IF, as well as in freshly isolated neutrophils by immunoblotting (75), in all cases using #AF1248 Abs. We also detected IL-17B-positive neutrophils in psoriasis plaques and cytospin slides of freshly isolated neutrophils by IHC using #AF1248. However, we could not measure any IL-17B in lysates of freshly isolated/activated neutrophils either by using two different commercial ELISA or by #AF1248 immunoblotting. In the latter experiments, many proteins with MW different from that of rIL-17B were recognized by #AF1248, thus invalidating at least the cytospin results. Intriguingly, Kouri et al. (75) did detect IL-17B protein in lysates of neutrophils (95% pure), by both ELISA and immunoblotting using #AF1248. However, these authors showed only a portion of the western blot (75), thus rendering impossible to know whether additional major proteins were recognized by #AF1248. Curiously, we, Tamarozzi et al. (13) and Kouri et al. (75), all found that human neutrophils do not transcribe IL-17B mRNA under resting or activating condition. Furthermore, no IL-17B secretion from BCG-stimulated neutrophils was recently shown (14). In such regard, Koury et al. (75) suggested that IL-17B is synthesized only at the promyelocyte and myelocyte stage in the bone marrow, disappearing in mature neutrophils. However, our analysis of transcriptomes generated from all types of bone marrow cell populations (65) revealed that, similarly to IL-17A, also IL-17B is never transcribed during the different stages of neutrophil maturation. Altogether, data suggest that human neutrophils do not express IL-17B *in vitro*. They also suggest that the positive staining of neutrophils by IHC using AF1248 is likely due to a non-specific, IL-17B independent, binding of these Abs.

In conclusion, data shown in this study are consistent with the notion that human neutrophils are unable to express and produce IL-17A, IL-17B, or IL-17F *in vitro*.

ETHICS STATEMENT

This study was carried out in accordance with the recommendations of Ethic Committee of the Azienda Ospedaliera Universitaria Integrata di Verona (Italy). All the experimental protocols were approved by the Ethic Committee and all subjects gave written informed consent in accordance with the Declaration of Helsinki.

AUTHOR CONTRIBUTIONS

All authors were involved in discussing and drafting the article, approved the final version to be published, and had full access to all data, taking responsibility for their integrity and analysis accuracy. In particular, NT, FA-S, SG, EG, SL, LG, and FC performed the experiments; FA-S, FB-A, NT, SL, WV, and MC analyzed the results; GG provided patients; and FS, NT, AM, WV, and MC conceived the experiments and wrote the paper.

ACKNOWLEDGMENTS

We thank Luigina Romani (University of Perugia, Perugia, Italy) for inactivated *Aspergillus Fumigatus* hyphae and conidia, Alessio Mazzoni and Francesco Annunziato (University of Firenze, Firenze, Italy) for Th17 clones, Alessia Farinazzo and Bruno Bonetti (University of Verona, Verona, Italy) for protein lysate of human cerebral cortex and Gioacchino Natoli (Humanitas University, Rozzano, Milan, Italy) for his support and discussion on ChIP-seq experiments.

FUNDING

This work was supported by grants from Associazione Italiana per la Ricerca sul Cancro (AIRC, IG-20339) and Ministero dell'Istruzione, dell'Università e della Ricerca (PRIN 2015YYKPNN) to MC, and from Novartis Farma SpA (Origgio, Italia) to AM. FA-S is supported by Brazilian fellowship from Coordenação de Aperfeiçoamento de Pessoal de Nível Superior (CAPES, no Processo: 99999.013628/2013-05).

SUPPLEMENTARY MATERIAL

The Supplementary Material for this article can be found online at https://www.frontiersin.org/articles/10.3389/fimmu.2018.00795/full#supplementary-material.

REFERENCES

1. Amatya N, Garg AV, Gaffen SL. IL-17 signaling: the Yin and the Yang. *Trends Immunol* (2017) 38(5):310–22. doi:10.1016/j.it.2017.01.006

2. Hymowitz SG, Filvaroff EH, Yin JP, Lee J, Cai L, Risser P, et al. IL-17s adopt a cystine knot fold: structure and activity of a novel cytokine, IL-17F, and implications for receptor binding. *EMBO J* (2001) 20(19):5332–41. doi:10.1093/emboj/20.19.5332

3. Gaffen SL, Jain R, Garg AV, Cua DJ. The IL-23-IL-17 immune axis: from mechanisms to therapeutic testing. *Nat Rev Immunol* (2014) 14(9):585–600. doi:10.1038/nri3707
4. Wright JF, Guo Y, Quazi A, Luxenberg DP, Bennett F, Ross JF, et al. Identification of an interleukin 17F/17A heterodimer in activated human CD4+ T cells. *J Biol Chem* (2007) 282(18):13447–55. doi:10.1074/jbc.M700499200
5. Veldhoen M. Interleukin 17 is a chief orchestrator of immunity. *Nat Immunol* (2017) 18(6):612–21. doi:10.1038/ni.3742
6. Schwarzenberger P, La Russa V, Miller A, Ye P, Huang W, Zieske A, et al. IL-17 stimulates granulopoiesis in mice: use of an alternate, novel gene therapy-derived method for in vivo evaluation of cytokines. *J Immunol* (1998) 161(11):6383–9.
7. McAleer JP, Kolls JK. Mechanisms controlling Th17 cytokine expression and host defense. *J Leukoc Biol* (2011) 90(2):263–70. doi:10.1189/jlb.0211099
8. Miossec P, Kolls JK. Targeting IL-17 and TH17 cells in chronic inflammation. *Nat Rev Drug Discov* (2012) 11(10):763–76. doi:10.1038/nrd3794
9. Cua DJ, Tato CM. Innate IL-17-producing cells: the sentinels of the immune system. *Nat Rev Immunol* (2010) 10(7):479–89. doi:10.1038/nri2800
10. Scapini P, Tamassia N, Pucillo C, Cassatella MA. Granulocytes and mast cells. 7th ed. In: Paul WE, editor. *Fundamental Immunology*. Philadelphia, PA: Wolters Kluwer Health/Lippincott Williams & Wilkins (2013). p. 468–86.
11. Tecchio C, Scapini P, Pizzolo G, Cassatella MA. On the cytokines produced by human neutrophils in tumors. *Semin Cancer Biol* (2013) 23(3):159–70. doi:10.1016/j.semcancer.2013.02.004
12. Pelletier M, Maggi L, Micheletti A, Lazzeri E, Tamassia N, Costantini C, et al. Evidence for a cross-talk between human neutrophils and Th17 cells. *Blood* (2010) 115(2):335–43. doi:10.1182/blood-2009-04-216085
13. Tamarozzi F, Wright HL, Thomas HB, Edwards SW, Taylor MJ. A lack of confirmation with alternative assays questions the validity of IL-17A expression in human neutrophils using immunohistochemistry. *Immunol Lett* (2014) 162(2 Pt B):194–8. doi:10.1016/j.imlet.2014.10.025
14. Tenland E, Hakansson G, Alaridah N, Lutay N, Ronnholm A, Hallgren O, et al. Innate immune responses after airway epithelial stimulation with *Mycobacterium bovis* bacille-Calmette Guerin. *PLoS One* (2016) 11(10): e0164431. doi:10.1371/journal.pone.0164431
15. Yamanaka K, Yamagiwa A, Akeda T, Kondo M, Kakeda M, Habe K, et al. Neutrophils are not the dominant interleukin-17 producer in psoriasis. *J Dermatol* (2017) 44(7):e170–1. doi:10.1111/1346-8138.13807
16. van Baarsen LGM, Lebre MC, van der Coelen D, Aarrass S, Tang MW, Ramwadhdoebe TH, et al. Heterogeneous expression pattern of interleukin 17A (IL-17A), IL-17F and their receptors in synovium of rheumatoid arthritis, psoriatic arthritis and osteoarthritis: possible explanation for nonresponse to anti-IL-17 therapy? *Arthritis Res Ther* (2014) 16(4):426. doi:10.1186/s13075-014-0426-z
17. Nadkarni S, Smith J, Sferruzzi-Perri AN, Ledwozyw A, Kishore M, Haas R, et al. Neutrophils induce proangiogenic T cells with a regulatory phenotype in pregnancy. *Proc Natl Acad Sci U S A* (2016) 113(52):E8415–24. doi:10.1073/pnas.1611944114
18. Appel H, Maier R, Wu P, Scheer R, Hempfing A, Kayser R, et al. Analysis of IL-17(+) cells in facet joints of patients with spondyloarthritis suggests that the innate immune pathway might be of greater relevance than the Th17-mediated adaptive immune response. *Arthritis Res Ther* (2011) 13(3):R95. doi:10.1186/ar3370
19. Brodlie M, McKean MC, Johnson GE, Anderson AE, Hilkens CM, Fisher AJ, et al. Raised interleukin-17 is immunolocalised to neutrophils in cystic fibrosis lung disease. *Eur Respir J* (2011) 37(6):1378–85. doi:10.1183/09031936.00067110
20. Dyring-Andersen B, Honore TV, Madelung A, Bzorek M, Simonsen S, Clemmensen SN, et al. Interleukin (IL)-17A and IL-22-producing neutrophils in psoriatic skin. *Br J Dermatol* (2017) 177(6):e321–2. doi:10.1111/bjd.15533
21. de Boer OJ, van der Meer JJ, Teeling P, van der Loos CM, Idu MM, van Maldegem F, et al. Differential expression of interleukin-17 family cytokines in intact and complicated human atherosclerotic plaques. *J Pathol* (2010) 220(4):499–508. doi:10.1002/path.2667
22. Eustace A, Smyth LJC, Mitchell L, Williamson K, Plumb J, Singh D. Identification of cells expressing IL-17A and IL-17F in the lungs of patients with COPD. *Chest* (2011) 139(5):1089–100. doi:10.1378/chest.10-0779
23. Halwani R, Sultana A, Vazquez-Tello A, Jamhawi A, Al-Masri AA, Al-Muhsen S. Th-17 regulatory cytokines IL-21, IL-23, and IL-6 enhance neutrophil production of IL-17 cytokines during asthma. *J Asthma* (2017) 54(9):893–904. doi:10.1080/02770903.2017.1283696
24. Hu S, He W, Du X, Yang J, Wen Q, Zhong XP, et al. IL-17 production of neutrophils enhances antibacteria ability but promotes arthritis development during *Mycobacterium tuberculosis* infection. *EBioMed* (2017) 23:88–99. doi:10.1016/j.ebiom.2017.08.001
25. Kakeda M, Schlapbach C, Danelon G, Tang MM, Cecchinato V, Yawalkar N, et al. Innate immune cells express IL-17A/F in acute generalized exanthematous pustulosis and generalized pustular psoriasis. *Arch Dermatol Res* (2014) 306(10):933–8. doi:10.1007/s00403-014-1488-0
26. Karthikeyan RS, Vareechon C, Prajna NV, Dharmalingam K, Pearlman E, Lalitha P. Interleukin 17 expression in peripheral blood neutrophils from fungal keratitis patients and healthy cohorts in southern India. *J Infect Dis* (2015) 211(1):130–4. doi:10.1093/infdis/jiu381
27. Keijsers R, Hendriks AGM, van Erp PEJ, van Cranenbroek B, van de Kerkhof PCM, Koenen H, et al. In vivo induction of cutaneous inflammation results in the accumulation of extracellular trap-forming neutrophils expressing RORgammat and IL-17. *J Invest Dermatol* (2014) 134(5):1276–84. doi:10.1038/jid.2013.526
28. Le Jan S, Plee J, Vallerand D, Dupont A, Delanez E, Durlach A, et al. Innate immune cell-produced IL-17 sustains inflammation in bullous pemphigoid. *J Invest Dermatol* (2014) 134(12):2908–17. doi:10.1038/jid.2014.263
29. Li TJ, Jiang YM, Hu YF, Huang L, Yu J, Zhao LY, et al. Interleukin-17-producing neutrophils link inflammatory stimuli to disease progression by promoting angiogenesis in gastric cancer. *Clin Cancer Res* (2017) 23(6):1575–85. doi:10.1158/1078-0432.ccr-16-0617
30. Lin AM, Rubin CJ, Khandpur R, Wang JY, Riblett M, Yalavarthi S, et al. Mast cells and neutrophils release IL-17 through extracellular trap formation in psoriasis. *J Immunol* (2011) 187(1):490–500. doi:10.4049/jimmunol.1100123
31. Moran EM, Heydrich R, Ng CT, Saber TP, McCormick J, Sieper J, et al. IL-17A expression is localised to both mononuclear and polymorphonuclear synovial cell infiltrates. *PLoS One* (2011) 6(8):e24048. doi:10.1371/journal.pone.0024048
32. Patel DD, Lee DM, Kolbinger F, Antoni C. Effect of IL-17A blockade with secukinumab in autoimmune diseases. *Ann Rheum Dis* (2013) 72(Suppl 2):ii116–23. doi:10.1136/annrheumdis-2012-202371
33. Punt S, Fleuren GJ, Kritikou E, Lubberts E, Trimbos JB, Jordanova ES, et al. Angels and demons: Th17 cells represent a beneficial response, while neutrophil IL-17 is associated with poor prognosis in squamous cervical cancer. *Oncoimmunology* (2015) 4(1):e984539. doi:10.4161/2162402x.2014.984539
34. Ramirez-Velazquez C, Castillo EC, Guido-Bayardo L, Ortiz-Navarrete V. IL-17-producing peripheral blood CD177+ neutrophils increase in allergic asthmatic subjects. *Allergy Asthma Clin Immunol* (2013) 9(1):23. doi:10.1186/1710-1492-9-23
35. Reich K, Papp KA, Matheson RT, Tu JH, Bissonnette R, Bourcier M, et al. Evidence that a neutrophil-keratinocyte crosstalk is an early target of IL-17A inhibition in psoriasis. *Exp Dermatol* (2015) 24(7):529–35. doi:10.1111/exd.12710
36. Tan HL, Regamey N, Brown S, Bush A, Lloyd CM, Davies JC. The Th17 pathway in cystic fibrosis lung disease. *Am J Respir Crit Care Med* (2011) 184(2):252–8. doi:10.1164/rccm.201102-0236OC
37. Rodrigues-Diez R, Aroeira LS, Orejudo M, Bajo MA, Heffernan JJ, Rodrigues-Diez RR, et al. IL-17A is a novel player in dialysis-induced peritoneal damage. *Kidney Int* (2014) 86(2):303–15. doi:10.1038/ki.2014.33
38. Tan Z, Jiang R, Wang X, Wang Y, Lu L, Liu Q, et al. RORgammat+IL-17+ neutrophils play a critical role in hepatic ischemia-reperfusion injury. *J Mol Cell Biol* (2013) 5(2):143–6. doi:10.1093/jmcb/mjs065
39. Taylor PR, Roy S, Leal SM Jr, Sun Y, Howell SJ, Cobb BA, et al. Activation of neutrophils by autocrine IL-17A-IL-17RC interactions during fungal infection is regulated by IL-6, IL-23, RORgammat and dectin-2. *Nat Immunol* (2014) 15(2):143–51. doi:10.1038/ni.2797
40. Taylor PR, Roy S, Meszaros EC, Sun Y, Howell SJ, Malemud CJ, et al. JAK/STAT regulation of *Aspergillus fumigatus* corneal infections and IL-6/23-stimulated neutrophil, IL-17, elastase, and MMP9 activity. *J Leukoc Biol* (2016) 100(1):213–22. doi:10.1189/jlb.4A1015-483R
41. Villanueva E, Yalavarthi S, Berthier CC, Hodgin JB, Khandpur R, Lin AM, et al. Netting neutrophils induce endothelial damage, infiltrate tissues, and

expose immunostimulatory molecules in systemic lupus erythematosus. *J Immunol* (2011) 187(1):538–52. doi:10.4049/jimmunol.1100450
42. Yapici U, Kers J, Bemelman FJ, Roelofs JJ, Groothoff JW, van der Loos CM, et al. Interleukin-17 positive cells accumulate in renal allografts during acute rejection and are independent predictors of worse graft outcome. *Transpl Int* (2011) 24(10):1008–17. doi:10.1111/j.1432-2277.2011.01302.x
43. Yapici U, Roelofs JJ, Florquin S. The importance of testing anti-IL-17 antibodies from different suppliers. *Am J Transplant* (2012) 12(2):504–5. doi:10.1111/j.1600-6143.2011.03867.x
44. Taylor PR, Bonfield TL, Chmiel JF, Pearlman E. Neutrophils from F508del cystic fibrosis patients produce IL-17A and express IL-23-dependent IL-17RC. *Clin Immunol* (2016) 170:53–60. doi:10.1016/j.clim.2016.03.016
45. Fontao L, Brembilla NC, Masouye I, Kaya G, Prins C, Dupin N, et al. Interleukin-17 expression in neutrophils and Th17 cells in cutaneous T-cell lymphoma associated with neutrophilic infiltrate of the skin. *Br J Dermatol* (2012) 166(3):687–9. doi:10.1111/j.1365-2133.2011.10647.x
46. Cai S, Batra S, Langohr I, Iwakura Y, Jeyaseelan S. IFN-gamma induction by neutrophil-derived IL-17A homodimer augments pulmonary antibacterial defense. *Mucosal Immunol* (2016) 9(3):718–29. doi:10.1038/mi.2015.95
47. Velden J, Paust HJ, Hoxha E, Turner JE, Steinmetz OM, Wolf G, et al. Renal IL-17 expression in human ANCA-associated glomerulonephritis. *Am J Physiol Renal Physiol* (2012) 302(12):F1663–73. doi:10.1152/ajprenal.00683.2011
48. Lemmers A, Moreno C, Gustot T, Marechal R, Degre D, Demetter P, et al. The interleukin-17 pathway is involved in human alcoholic liver disease. *Hepatology* (2009) 49(2):646–57. doi:10.1002/hep.22680
49. Res PC, Piskin G, de Boer OJ, van der Loos CM, Teeling P, Bos JD, et al. Overrepresentation of IL-17A and IL-22 producing CD8 T cells in lesional skin suggests their involvement in the pathogenesis of psoriasis. *PLoS One* (2010) 5(11):e14108. doi:10.1371/journal.pone.0014108
50. Lima AL, Karl I, Giner T, Poppe H, Schmidt M, Presser D, et al. Keratinocytes and neutrophils are important sources of proinflammatory molecules in hidradenitis suppurativa. *Br J Dermatol* (2016) 174(3):514–21. doi:10.1111/bjd.14214
51. Vykhovanets EV, Maclennan GT, Vykhovanets OV, Gupta S. IL-17 expression by macrophages is associated with proliferative inflammatory atrophy lesions in prostate cancer patients. *Int J Clin Exp Pathol* (2011) 4(6):552–65.
52. Lopez P, Rodriguez-Carrio J, Caminal-Montero L, Mozo L, Suarez A. A pathogenic IFNalpha, BLyS and IL-17 axis in systemic lupus erythematosus patients. *Sci Rep* (2016) 6:20651. doi:10.1038/srep20651
53. Derycke L, Zhang N, Holtappels G, Dutre T, Bachert C. IL-17A as a regulator of neutrophil survival in nasal polyp disease of patients with and without cystic fibrosis. *J Cyst Fibros* (2012) 11(3):193–200. doi:10.1016/j.jcf.2011.11.007
54. Schon MP, Broekaert SM, Erpenbeck L. Sexy again: the renaissance of neutrophils in psoriasis. *Exp Dermatol* (2017) 26(4):305–11. doi:10.1111/exd.13067
55. Finlay AY. Current severe psoriasis and the rule of tens. *Br J Dermatol* (2005) 152(5):861–7. doi:10.1111/j.1365-2133.2005.06502.x
56. Calzetti F, Tamassia N, Arruda-Silva F, Gasperini S, Cassatella MA. The importance of being "pure" neutrophils. *J Allergy Clin Immunol* (2017) 139(1):352–5.e6. doi:10.1016/j.jaci.2016.06.025
57. Bozza S, Gaziano R, Spreca A, Bacci A, Montagnoli C, di Francesco P, et al. Dendritic cells transport conidia and hyphae of Aspergillus fumigatus from the airways to the draining lymph nodes and initiate disparate Th responses to the fungus. *J Immunol* (2002) 168(3):1362–71. doi:10.4049/jimmunol.168.3.1362
58. Annunziato F, Cosmi L, Santarlasci V, Maggi L, Liotta F, Mazzinghi B, et al. Phenotypic and functional features of human Th17 cells. *J Exp Med* (2007) 204(8):1849–61. doi:10.1084/jem.20070663
59. Scapini P, Calzetti F, Cassatella MA. On the detection of neutrophil-derived vascular endothelial growth factor (VEGF). *J Immunol Methods* (1999) 232(1–2):121–9. doi:10.1016/S0022-1759(99)00170-2
60. Cassatella MA, Guasparri I, Ceska M, Bazzoni F, Rossi F. Interferon-gamma inhibits interleukin-8 production by human polymorphonuclear leucocytes. *Immunology* (1993) 78(2):177–84.
61. Scapini P, Nardelli B, Nadali G, Calzetti F, Pizzolo G, Montecucco C, et al. G-CSF-stimulated neutrophils are a prominent source of functional BLyS. *J Exp Med* (2003) 197(3):297–302. doi:10.1084/jem.20021343
62. Zimmermann M, Aguilera FB, Castellucci M, Rossato M, Costa S, Lunardi C, et al. Chromatin remodelling and autocrine TNFalpha are required for optimal interleukin-6 expression in activated human neutrophils. *Nat Commun* (2015) 6:6061. doi:10.1038/ncomms7061
63. Muller PY, Janovjak H, Miserez AR, Dobbie Z. Processing of gene expression data generated by quantitative real-time RT-PCR. *Biotechniques* (2002) 32(6):1372–4.
64. Langmead B, Trapnell C, Pop M, Salzberg SL. Ultrafast and memory-efficient alignment of short DNA sequences to the human genome. *Genome Biol* (2009) 10(3):R25. doi:10.1186/gb-2009-10-3-r25
65. Rapin N, Bagger FO, Jendholm J, Mora-Jensen H, Krogh A, Kohlmann A, et al. Comparing cancer vs normal gene expression profiles identifies new disease entities and common transcriptional programs in AML patients. *Blood* (2014) 123(6):894–904. doi:10.1182/blood-2013-02-485771
66. Zimmermann M, Arruda-Silva F, Bianchetto-Aguilera F, Finotti G, Calzetti F, Scapini P, et al. IFNalpha enhances the production of IL-6 by human neutrophils activated via TLR8. *Sci Rep* (2016) 6:19674. doi:10.1038/srep19674
67. Crepaldi L, Silveri L, Calzetti F, Pinardi C, Cassatella MA. Molecular basis of the synergistic production of IL-1 receptor antagonist by human neutrophils stimulated with IL-4 and IL-10. *Int Immunol* (2002) 14(10):1145–53. doi:10.1093/intimm/dxf079
68. Moore EE, Presnell S, Garrigues U, Guilbot A, LeGuern E, Smith D, et al. Expression of IL-17B in neurons and evaluation of its possible role in the chromosome 5q-linked form of Charcot-Marie-tooth disease. *Neuromuscul Disord* (2002) 12(2):141–50. doi:10.1016/S0960-8966(01)00250-4
69. Heintzman ND, Stuart RK, Hon G, Fu Y, Ching CW, Hawkins RD, et al. Distinct and predictive chromatin signatures of transcriptional promoters and enhancers in the human genome. *Nat Genet* (2007) 39(3):311–8. doi:10.1038/ng1966
70. Tamassia N, Zimmermann M, Castellucci M, Ostuni R, Bruderek K, Schilling B, et al. Cutting edge: an inactive chromatin configuration at the IL-10 locus in human neutrophils. *J Immunol* (2013) 190(5):1921–5. doi:10.4049/jimmunol.1203022
71. Northrup DL, Zhao K. Application of ChIP-Seq and related techniques to the study of immune function. *Immunity* (2011) 34(6):830–42. doi:10.1016/j.immuni.2011.06.002
72. Bernstein BE, Stamatoyannopoulos JA, Costello JF, Ren B, Milosavljevic A, Meissner A, et al. The NIH roadmap epigenomics mapping consortium. *Nat Biotechnol* (2010) 28(10):1045–8. doi:10.1038/nbt1010-1045
73. Zhang L, Badgwell DB, Bevers JJ III, Schlessinger K, Murray PJ, Levy DE, et al. IL-6 signaling via the STAT3/SOCS3 pathway: functional analysis of the conserved STAT3 N-domain. *Mol Cell Biochem* (2006) 288(1–2):179–89. doi:10.1007/s11010-006-9137-3
74. Theilgaard-Monch K, Jacobsen LC, Borup R, Rasmussen T, Bjerregaard MD, Nielsen FC, et al. The transcriptional program of terminal granulocytic differentiation. *Blood* (2005) 105(4):1785–96. doi:10.1182/blood-2004-08-3346
75. Kouri VP, Olkkonen J, Ainola M, Li TF, Bjorkman L, Konttinen YT, et al. Neutrophils produce interleukin-17B in rheumatoid synovial tissue. *Rheumatology (Oxford)* (2014) 53(1):39–47. doi:10.1093/rheumatology/ket309
76. Al-Samadi A, Moossavi S, Salem A, Sotoudeh M, Tuovinen SM, Konttinen YT, et al. Distinctive expression pattern of interleukin-17 cytokine family members in colorectal cancer. *Tumour Biol* (2016) 37(2):1609–15. doi:10.1007/s13277-015-3941-x
77. Ferretti S, Bonneau O, Dubois GR, Jones CE, Trifilieff A. IL-17, produced by lymphocytes and neutrophils, is necessary for lipopolysaccharide-induced airway neutrophilia: IL-15 as a possible trigger. *J Immunol* (2003) 170(4):2106–12. doi:10.4049/jimmunol.170.4.2106
78. Werner JL, Gessner MA, Lilly LM, Nelson MP, Metz AE, Horn D, et al. Neutrophils produce interleukin 17A (IL-17A) in a dectin-1- and IL-23-dependent manner during invasive fungal infection. *Infect Immun* (2011) 79(10):3966–77. doi:10.1128/IAI.05493-11
79. Katayama M, Ohmura K, Yukawa N, Terao C, Hashimoto M, Yoshifuji H, et al. Neutrophils are essential as a source of IL-17 in the effector phase of arthritis. *PLoS One* (2013) 8(5):e62231. doi:10.1371/journal.pone.0062231
80. Li L, Huang L, Vergis AL, Ye H, Bajwa A, Narayan V, et al. IL-17 produced by neutrophils regulates IFN-gamma-mediated neutrophil migration in mouse kidney ischemia-reperfusion injury. *J Clin Invest* (2010) 120(1):331–42. doi:10.1172/jci38702
81. Hoshino A, Nagao T, Nagi-Miura N, Ohno N, Yasuhara M, Yamamoto K, et al. MPO-ANCA induces IL-17 production by activated neutrophils in vitro via classical complement pathway-dependent manner. *J Autoimmun* (2008) 31(1):79–89. doi:10.1016/j.jaut.2008.03.006

82. Huppler AR, Verma AH, Conti HR, Gaffen SL. Neutrophils do not express IL-17A in the context of acute oropharyngeal candidiasis. *Pathogens* (2015) 4(3):559–72. doi:10.3390/pathogens4030559
83. Price AE, Reinhardt RL, Liang HE, Locksley RM. Marking and quantifying IL-17A-producing cells in vivo. *PLoS One* (2012) 7(6):e39750. doi:10.1371/journal.pone.0039750
84. Davey MS, Tamassia N, Rossato M, Bazzoni F, Calzetti F, Bruderek K, et al. Failure to detect production of IL-10 by activated human neutrophils. *Nat Immunol* (2011) 12(11):1017–8. doi:10.1038/ni.2111
85. Calo E, Wysocka J. Modification of enhancer chromatin: what, how, and why? *Mol Cell* (2013) 49(5):825–37. doi:10.1016/j.molcel.2013.01.038
86. Ostuni R, Piccolo V, Barozzi I, Polletti S, Termanini A, Bonifacio S, et al. Latent enhancers activated by stimulation in differentiated cells. *Cell* (2013) 152(1–2):157–71. doi:10.1016/j.cell.2012.12.018
87. Huppler AR, Gaffen SL. Editorial: fake it 'til you make it: mast cells acquire IL-17 exogenously. *J Leukoc Biol* (2016) 100(3):445–6. doi:10.1189/jlb.3CE0216-071R
88. Noordenbos T, Blijdorp I, Chen S, Stap J, Mul E, Canete JD, et al. Human mast cells capture, store, and release bioactive, exogenous IL-17A. *J Leukoc Biol* (2016) 100(3):453–62. doi:10.1189/jlb.3HI1215-542R

Conflict of Interest Statement: The authors declare that the research was conducted in the absence of any commercial or financial relationships that could be construed as a potential conflict of interest.

frontiers in Immunology

ORIGINAL RESEARCH
published: 30 April 2018
doi: 10.3389/fimmu.2018.00869

Bacillus Calmette–Guérin-Induced Trained Immunity Is Not Protective for Experimental Influenza A/Anhui/1/2013 (H7N9) Infection in Mice

L. Charlotte J. de Bree[1,2,3,4], Renoud J. Marijnissen[5], Junda M. Kel[5], Sietske K. Rosendahl Huber[5], Peter Aaby[3], Christine Stabell Benn[3,4], Marcel V. W. Wijnands[5], Dimitri A. Diavatopoulos[2,6], Reinout van Crevel[1,2], Leo A. B. Joosten[1,2], Mihai G. Netea[1,2,7] and John Dulos[8]*

[1] Department of Internal Medicine, Radboud University Medical Center, Nijmegen, Netherlands, [2] Radboud Centre for Infectious Diseases (RCI), Radboud University Medical Center, Nijmegen, Netherlands, [3] Research Center for Vitamins and Vaccines, Bandim Health Project, Statens Serum Institut, Copenhagen, Denmark, [4] Odense Patient Data Explorative Network, University of Southern Denmark, Odense University Hospital, Odense, Denmark, [5] Department of Immunology, Triskelion B.V., Zeist, Netherlands, [6] Laboratory of Pediatric Infectious Diseases, Radboud Institute for Molecular Life Sciences, Radboud University Medical Center, Nijmegen, Netherlands, [7] Department for Genomics and Immunoregulation, Life and Medical Sciences Institute (LIMES), University of Bonn, Bonn, Germany, [8] Aduro Biotech Europe, Oss, Netherlands

OPEN ACCESS

Edited by:
Liwu Li,
Virginia Tech, United States

Reviewed by:
Suraj Sable,
Centers for Disease Control and Prevention, United States
Christopher Brian Lawrence,
Virginia Tech,
United States

***Correspondence:**
Renoud J. Marijnissen
rjmarijnissen@gmail.com

Specialty section:
This article was submitted to Molecular Innate Immunity, a section of the journal Frontiers in Immunology

Received: *22 January 2018*
Accepted: *09 April 2018*
Published: *30 April 2018*

Citation:
de Bree LCJ, Marijnissen RJ, Kel JM, Rosendahl Huber SK, Aaby P, Benn CS, Wijnands MVW, Diavatopoulos DA, van Crevel R, Joosten LAB, Netea MG and Dulos J (2018) Bacillus Calmette–Guérin-Induced Trained Immunity Is Not Protective for Experimental Influenza A/Anhui/1/2013 (H7N9) Infection in Mice. Front. Immunol. 9:869. doi: 10.3389/fimmu.2018.00869

Avian influenza A of the subtype H7N9 has been responsible for almost 1,600 confirmed human infections and more than 600 deaths since its first outbreak in 2013. Although sustained human-to-human transmission has not been reported yet, further adaptations to humans in the viral genome could potentially lead to an influenza pandemic, which may have severe consequences due to the absence of pre-existent immunity to this strain at population level. Currently there is no influenza A (H7N9) vaccine available. Therefore, in case of a pandemic outbreak, alternative preventive approaches are needed, ideally even independent of the type of influenza virus outbreak. Bacillus Calmette–Guérin (BCG) is known to induce strong heterologous immunological effects, and it has been shown that BCG protects against non-related infection challenges in several mouse models. BCG immunization of mice as well as human induces trained innate immune responses, resulting in increased cytokine responses upon subsequent *ex vivo* peripheral blood mononuclear cell restimulation. We investigated whether BCG (Statens Serum Institut-Denmark)-induced trained immunity may protect against a lethal avian influenza A/Anhui/1/2013 (H7N9) challenge. Here, we show that isolated splenocytes as well as peritoneal macrophages of BCG-immunized BALB/c mice displayed a trained immunity phenotype resulting in increased innate cytokine responses upon *ex vivo* restimulation. However, after H7N9 infection, no significant differences were found between the BCG immunized and the vehicle control group at the level of survival, weight loss, pulmonary influenza A nucleoprotein staining, or histopathology. In conclusion, BCG-induced trained immunity did not result in protection in an oseltamivir-sensitive influenza A/Anhui/1/2013 (H7N9) challenge mouse model.

Keywords: avian influenza A/Anhui/1/2013 (H7N9), bacillus Calmette–Guérin, trained immunity, innate immune memory, oseltamivir

INTRODUCTION

Since its first outbreak in China in 2013 until December 2017, avian influenza A (H7N9) has been responsible for 1,565 confirmed human cases, including 612 deaths (1). Infections are characterized by a high incidence of pneumonia, respiratory failure, and acute respiratory distress syndrome. Avian influenza A (H7N9) is transmitted after contact with live poultry or exposure to contaminated environments. Apart from some small reported clusters, sustained human-to-human transmission is rare (2). Nevertheless, because immunity to this strain at population level is negligible, public authorities fear that possible additional mutations and reassortment with circulating other human-adapted influenza viruses may enable human–human transmission and infection, which could potentially lead to a severe H7N9 influenza pandemic (3).

Vaccine development is part of pandemic preparedness strategies. Although numerous inactivated and live attenuated H7 vaccines are being developed, the immunogenicity of non-adjuvanted or aluminum hydroxide-adjuvanted candidate H7 vaccines is low (4, 5). Therefore, novel approaches for protection against influenza A (H7N9) are needed. Adjuvanted (MF59 or AS03) vaccines have shown to elicit enhanced immunogenicity against H7N9 (6–8). An alternative approach is to make use of non-specific beneficial effects of already existing vaccines, *via* the induction of the newly described process of trained immunity. Bacillus Calmette–Guérin (BCG) immunization confers broad heterologous protection after vaccination. Thereby, BCG could potentially offer directly available protection in case of an outbreak, independent of the type of influenza virus outbreak.

Bacillus Calmette–Guérin, the widely used live attenuated vaccine against tuberculosis, has long been known for its immune modulatory effects. Upon its introduction in Sweden in 1932, the Swedish physician Carl Näslund observed a strong decrease in childhood mortality in the first year of life in the provinces in which BCG was introduced (9). This improvement could not be explained by prevention of tuberculosis alone. Similar observations were made several times upon introduction of BCG vaccination in other countries and were validated in randomized controlled trials (10, 11). Non-specific beneficial effects after BCG immunization have been demonstrated in several mouse studies, such as *Plasmodium* (12–14), *Schistosoma* (15), and disseminated *Candida* infection models (16). Moreover, it has been shown that BCG administration improves the outcome of a lethal challenge with the seasonal influenza A/Puerto Rico/8/34 (H1N1) in an experimental mouse model (17). The heterologous protective effects of BCG vaccination are at least partially explained by the induction of trained immunity: monocytes of BCG-vaccinated individuals display increased immune responsiveness, such as enhanced cytokine production upon restimulation with unrelated pathogens and toll-like receptor (TLR) ligands, a process which is dependent on epigenetic and metabolic rewiring of myeloid cells (16, 18). In epidemiological studies, the non-specific effects of BCG vaccination are most pronounced in the first year of life, suggesting that trained immunity is most strongly activated during this first year (10, 19). This is in line with the study by Kleinnijenhuis et al. showing 1-year duration for trained immunity (20). Moreover, BCG vaccination resulted in heterologous T-helper cell 1 (Th1) and T-helper cell 17 (Th17) immune responses and enhanced immunogenicity after subsequent influenza vaccination in healthy volunteers (20, 21). Recently, we have shown that BCG vaccination resulted in reduced peak viremia after subsequent yellow fever vaccination of healthy volunteers, a process depending on the induction on monocyte responses, rather than T-cell heterologous immunity (22).

We therefore hypothesized that BCG vaccination may induce non-specific protection against influenza A (H7N9) infection, a strategy that may offer important public health benefits. In this study, we assessed the effects of BCG immunization in an experimental lethal avian influenza A/Anhui/1/2013 (H7N9) infection in BALB/c mice.

Abbreviations: BCG, bacillus Calmette–Guérin; DMEM, Dulbecco's Modified Eagle Medium; ELISA, enzyme-linked immunosorbent assay; IL-6, interleukin-6; IL-10, interleukin-10; IFN, interferon; LPS, lipopolysaccharide; MLD, mouse lethal dose; NP, nucleoprotein; PBMC, peripheral blood mononuclear cell; PHA, phytohemagglutin; RPMI, Roswell Park Memorial Institute; TCID, tissue culture infective dose; Th1, T-helper cell 1; Th17, T-helper cell 17; TLR, toll-like receptor; TNF-α, tumor necrosis factor-alpha.

MATERIALS AND METHODS

H7N9 Influenza Virus Stock Preparation and $TCID_{50}$ Determination

A/Anhui/1/2013 (H7N9) seed virus was obtained from the National Institute for Biological Standards and Control (UK). A new influenza A/Anhui/1/2013 (H7N9) virus stock was obtained after propagation in 11-day-old embryonic chicken eggs for 32 h at 37°C. Aliquots were stored at <−70°C and were confirmed to be negative for endotoxin and mycoplasma. No novel mutations were introduced in the hemagglutinin and neuraminidase segments. The homology compared to the reference amino acid sequence (GenBank) was >99%. For the 50% tissue culture infectious dose ($TCID_{50}$) assay, Madin–Darby Canine Kidney (MDCK) cells (ATCC CCL-34) were cultured in Dulbecco's Modified Eagle Medium (DMEM) (Gibco, Life technologies) with Glutamax (Gibco, Life technologies), 10% fetal calf serum (FCS) (Lonza, Switzerland), supplemented with 100 U/ml penicillin, 100 µg/ml streptomycin (Gibco, Life technologies), and 1× non-essential amino acids (Gibco, Life technologies) at 5% CO_2 and 37°C. One day prior to the start of the assay, 30,000 cells per well were seeded in 96-well flat-bottom plates (Corning) and incubated overnight (37°C, 5% CO_2). The cells were washed and incubated with serial dilutions of the influenza virus in culture medium (DMEM + glutamax, supplemented with 100 U/ml penicillin, 100 µg/ml streptomycin, 0.0004% trypsin-EDTA). After 7 days of incubation at 34°C, wells were scored for the cytopathic effect (CPE). The $TCID_{50}$ titer was calculated using the Reed–Muench method (23).

Animal Ethics Statement

Animals experiments were performed in accordance with the guidelines of the European Communities (Directive 2010/63/EU)

and Dutch legislation (The experiments on Animals Act, 1997). The animal experimental protocols were approved by an independent Animal Ethics Committee (TNO, Zeist, the Netherlands) under project license 3387 and performed in the AAALAC accredited animal facility of Triskelion. All animals were housed in a temperature and light-cycle controlled facility with unlimited access to food and water. All procedures involving live H7N9 viruses, including the animal experiments, were carried out in a biosafety level 3 (BSL-3) containment facility at Triskelion. The animals were monitored for clinical signs of influenza disease twice daily with intervals of at least 5 h. All observations, including behavioral aspects were recorded. If lethargy was observed longer than 48 h, the animal was euthanized (humane endpoint).

Influenza Challenge Model

Female BALB/cAnNCrl (BALB/c) mice were obtained (Charles River, Germany) and maintained under SPF conditions. At commencement of the experiments, animals were 6–8 weeks old. All experiments were performed with 8–10 mice per group. On day 0, mice were challenged intranasally (i.n.) with influenza A/Anhui/1/2013 (H7N9) diluted in 50 µl phosphate buffered saline (PBS) under anesthesia with ketamine/xylazine (50 and 5 mg/kg, respectively). To determine the 50% mouse lethal dose (MLD_{50}), six groups of eight animals were challenged with 7.31, 6.17, 5.02, 3.87, 2.73, or 1.58 $\log_{10}$ $TCID_{50}$ per mouse and monitored until they succumbed to infection or until scheduled sacrifice 14 days post-infection. The MLD_{50} was calculated using the Spearman–Kärber method. Throughout the experiment, clinical signs were monitored twice daily and body weight was recorded once daily until death or scheduled sacrifice.

As a reference control for the lethal challenge model, two additional groups received the neuraminidase inhibitor oseltamivir phosphate (Tamiflu®; Roche, Switzerland) dissolved in sterile water (Fresenius Kabi, the Netherlands) and stored at 2–10°C until use. One group of animals was treated with 100 mg/kg twice daily *per os* (p.o.) starting 1 h prior to the challenge on day 0 continuing until day 4, while another group received oseltamivir on days 1–5. The control group was treated with vehicle PBS (Gibco, Life technologies) p.o. on days 0–4. For evaluation of the effect of BCG, animals received either 750 µg BCG (Danish strain 1331; Statens Serum Institut, Denmark) dissolved in 200 µl PBS intravenously (i.v.), containing 2–8 × 10^6 colony-forming units, or PBS i.v. on day −7. To demonstrate induction of trained innate immune responses after BCG vaccination, five animals per group were sacrificed prior to the influenza challenge on day 0, after which splenocytes and peritoneal macrophages were isolated for *ex vivo* restimulation experiments. On day 0, the animals were challenged with a $4MLD_{50}$ dose influenza A/Anhui/1/2013 (H7N9) and monitored until they succumbed to infection or until scheduled sacrifice at 21 days post-infection. Three days after viral challenge, eight animals per group were sacrificed, and lungs were collected and prepared for histopathological analysis.

Ex Vivo Stimulations of Splenocytes and Peritoneal Macrophages

Spleen cells were isolated by gently squeezing spleens in a sterile 200 µM filter chamber. After washing with sterile PBS (1,200 rpm, 5 min, 4°C), cells were resuspended in 4 ml Roswell Park Memorial Institute (RPMI) 1640 culture medium (RPMI medium; Invitrogen, CA, USA) supplemented with 10% FCS. Cells were counted and concentrations were adjusted to 1 × 10^7 cells/ml. Cells were cultured in 24-well plates (Greiner, the Netherlands) at 5 × 10^6 cells/well, in a final volume of 1,000 µl and stimulated in duplo with RPMI, *Escherichia coli* lipopolysaccharide (LPS) (10 ng/ml, Sigma-Aldrich), phytohemagglutin (PHA) (10 µg/ml from *Phaseolus vulgaris*, Sigma-Aldrich). Poly I:C (50 µg/ml, Invivogen), heat-killed *Candida albicans* (1 × 10^6 microorganisms/ml, strain UC820), heat-killed *Salmonella typhi* (1 × 10^7 microorganisms/ml), or heat-killed *Staphylococcus aureus* (1 × 10^7 microorganisms/ml). After 2 days of incubation, 500 µl supernatant was collected and the plates were incubated for another 3 days before the remaining supernatants were harvested. The supernatants were stored at −80°C until levels of tumor necrosis factor-alpha (TNF-α), interferon (IFN)-α, IFN-γ, interleukin (IL)-17, and IL-22 were determined.

Peritoneal macrophages were isolated by injecting 5 ml of ice-cold sterile PBS in the peritoneal cavity. After centrifugation and washing, cells were resuspended in RPMI supplemented with 10 µg/ml gentamicin, 10 mM Glutamax, and 10 mM pyruvate. Cells were counted using a Z1 Coulter Particle Counter (Beckman Coulter, the Netherlands) and adjusted to 1 × 10^6 cells/ml. Cells were cultured in 96-well round-bottom microtiter plates (Costar, Corning, the Netherlands) at 1 × 10^5 cells/well, in a final volume of 200 µl. After 24 h of incubation with abovementioned stimuli in duplo {plus Pam3Cys [10 µg/ml, EMC microcollections (L2000)] instead of PHA} at 37°C in air and 5% CO_2, the plates were centrifuged at 1,400 × *g* for 8 min, and the supernatants were collected and stored at −20°C until levels of TNF-α, IL-1α, IL-1β, IL-6, and IL-10 were determined.

Quantification of Cytokine Concentrations

Cytokine concentrations were determined in supernatants using commercial enzyme-linked immunosorbent assay (ELISA) kits according to instructions of the manufacturer. TNF-α (R&D systems, MN, USA), IL-1α, IL-1β, IL-6, IL-10, IFN-α, and IFN-γ (Sanquin, the Netherlands) were determined in supernatants harvested after 2 days of culture. IL-17 and IL-22 (R&D systems) were determined in supernatants after 5 days of incubation.

Histopathology and Immunohistochemistry

For histopathological examination, the lungs of both BCG and PBS treated animal groups were isolated 3 days post-challenge. Formalin fixed lung tissues were embedded in paraffin wax, sectioned at 4 µm, and stained with hematoxylin and eosin. Per animal, three consecutive HE-stained lung sections were semi-quantitatively scored for the presence of signs of inflammation, epithelial damage, and repair. Influenza nucleoprotein (NP) was visualized by immunohistochemistry using anti-influenza A NP antibody (Millipore, clone H16-L10-4R5, mouse IgG2a) as a measure for the amount of virus present in cells in the lung according to the protocol described in Rimmelzwaan et al. (24). NP-stained sections were semi-quantitatively scored for the presence of viral

protein. All parameters were scored as absent (0), minimal (1), moderate (2), or marked (3).

Statistical Analysis

Data were analyzed using Graphpad Prism 5.0 (La Jolla, CA, USA). *p-Value < 0.05, **p-value < 0.01. Cytokine data are shown as mean ± SEM. The survival proportion at day 21 after treatment was compared to the vehicle control group using a Fisher exact two-sided test, corrected for multiple comparisons. Survival times after viral challenge of the groups were compared using a log-rank test. Change in body weight was summarized as area under the curve (AUC) in which the last observed body weight was carried forward if a mouse died/was euthanized during the study. Briefly, the weight per mouse at day 0 was used as baseline and weight change was determined relative to baseline. The AUCs for each group were summarized as mean, SD, and adjusted p-value for comparison to the vehicle control group.

RESULTS

Determination of Tissue Culture Infective Dose (TCID) and 50% MLD

Based on the CPE observed in the MDCK cells incubated with the dose formulation of A/Anhui/1/2013 (H7N9), a $TCID_{50}$ of 6.11 $\log_{10}$ $TCID_{50}$/ml was calculated (data not shown). To assess the potency of BCG vaccination *in vivo*, we established a lethal A/Anhui/1/2013 (H7N9) influenza challenge model in female BALB/c mice, by inoculating groups of mice i.n. with a dose of 7.31, 6.17, 5.02, 3.87, 2.73, or 1.58 $\log_{10}$ $TCID_{50}$/mouse. During the subsequent MLD experiment, progress of infection the body weights correlated with an increase in the number and severity of the clinical signs. Recovery of the animals was demonstrated by an increase in body weight and a decrease in clinical signs. Intranasal administration of influenza A/Anhui/1/2013 (H7N9) was lethal to female (BALB/c) mice, which has been shown previously (25). The MLD_{50} determined for the A/Anhui/1/2013 (H7N9) influenza was calculated at 4.45 $\log_{10}$ $TCID_{50}$. The infectious dose for the subsequent experimental challenge infection study was set at $4MLD_{50}$, a dose where 0–10% of the animals were expected to survive the intranasal challenge with the virus (**Figures 1A,B**).

Assessment of Oseltamivir Sensitivity of A/Anhui/1/2013 (H7N9) Challenge Model

To determine the sensitivity of the challenge model, we tested the efficacy of the most widely used anti-influenza virus drug, the neuraminidase inhibitor oseltamivir phosphate, as a reference control. Animals were challenged with an intranasal dose of $4MLD_{50}$ influenza A/Anhui/1/2013 (H7N9). The control group ($n = 10$) was treated with PBS twice daily p.o. for 5 days, starting from day 0. Eight animals were treated twice daily with 100 mg/kg oseltamivir p.o. for 5 days, starting 1 h before challenge at day 0. Another eight mice started on day 1 with 100 mg/kg oseltamivir treatment twice daily for the duration of 5 days. **Figure 2A** presents the Kaplan–Meier survival curve. In the animals of the vehicle control group, 10% survival was observed after influenza A/Anhui/1/2013 (H7N9) challenge. Treatment with 100 mg/kg oseltamivir twice daily p.o. from day 0 to day 4 resulted in 100% survival, which was significantly improved compared to the vehicle control group (p-value < 0.01) (Table S1 in Supplementary Material). Although treatment with 100 mg/kg oseltamivir twice daily p.o. from day 1 to day 5 also resulted in an increased survival proportion of 25%, this was not statistically different from the control group (Table S2 in Supplementary Material). Nevertheless, survival time was significantly increased in both oseltamivir treated groups (treatment day 0–4 p-value < 0.01, treatment day 1–5 p-value < 0.05) (Table S2 in Supplementary Material). Oseltamivir treatment starting from day 0 showed a significantly reduced body weight loss compared to the control group (p-value < 0.001), while initiating oseltamivir treatment 1 day post-challenge, did not reduce the body weight loss compared to the control group (**Figure 2B**; Table S3 in Supplementary Material).

BCG Vaccination Prior to H7N9 Infection Challenge

To test the effect of BCG against lethal influenza challenge, a total of 13 mice were BCG immunized and 13 mice were injected with PBS 1 week prior to A/Anhui/1/2013 (H7N9) challenge.

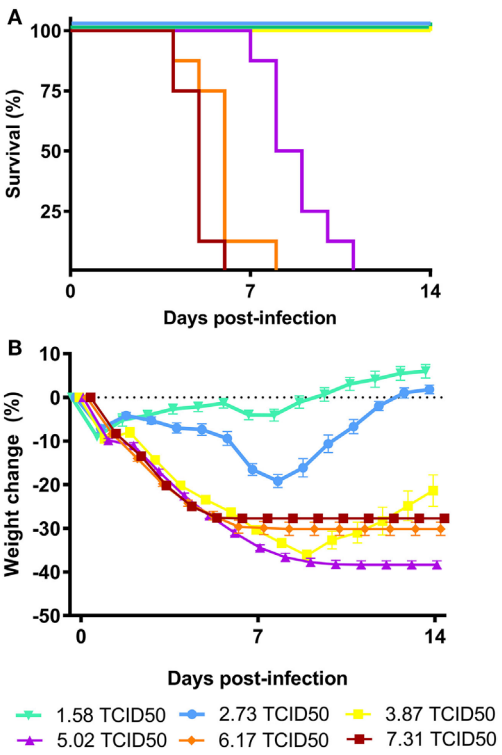

FIGURE 1 | Virulence of influenza A/Anhui/1/2013 (H7N9) in BALB/c mice. Female BALB/c mice ($n = 8$ per group) were intranasally inoculated with serial dilutions of the A/Anhui/1/2013 (H7N9) influenza virus on day 0 and survival was monitored for 14 days. Kaplan–Meyer survival curve **(A)** and mean body weight change is depicted **(B)**. The MLD_{50} was calculated using the Reed–Muench method.

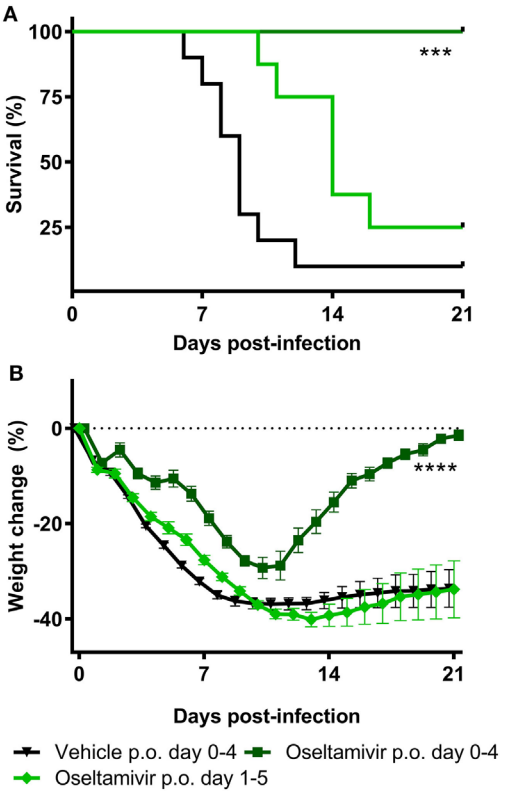

FIGURE 2 | Efficacy of oseltamivir in a lethal BALB/c mouse model. Female BALB/c mice were challenged with a dose of $4MLD_{50}$ influenza A/Anhui/1/2013 (H7N9) on day 0. Mice received 100 mg/kg twice daily p.o. Oseltamivir treatment from days 0–4 or 1–5 ($n = 8$ per group) or the vehicle control ($n = 10$) from days 0–4. Kaplan–Meyer survival curve **(A)** and mean body weight change **(B)** are depicted. Survival proportion in the oseltamivir treated groups was analyzed using a Fisher's exact two-sided test with Bonferroni correction for multiple comparisons. The effect of oseltamivir treatment on body weight was analyzed by comparing the area under curve of treatment groups with vehicle and was analyzed using a two-way ANOVA with Bonferroni correction. Error bars depict SEM. ****$p < 0.001$, ****$p < 0.0001$.

Cytokine Responses After *Ex Vivo* Splenocyte and Peritoneal Macrophage Restimulation

To assess the systemic trained immunity responses, splenocytes as well as peritoneal macrophages (5 mice per group) were isolated 7 days after BCG immunization. Both cell suspensions were restimulated with several TLR-ligands and pathogens. Cytokines were determined by ELISA in collected supernatants. TNF-α production was significantly increased in the BCG-vaccinated group after restimulation of splenocytes with all stimuli except RPMI medium control (p-value < 0.01 for all stimuli) (**Figure 3A**). Splenocyte-derived IFN-γ responses were significantly upregulated after LPS (p-value < 0.01), *C. albicans* (p-value < 0.05), and *S. typhi* (p-value < 0.05) restimulation (**Figure 3B**). No significant differences were found on splenocyte-derived IL-17 and IL-22 responses (**Figures 3C,E**). IFN-α was only determined in supernatants of splenocytes restimulated with RPMI and poly I:C. Restimulation with poly I:C resulted in a small but statistically significantly higher IFN-α response in the BCG-vaccinated group (p-value < 0.05) (**Figure 3D**). Significantly higher TNF-α production in the BCG-immunized mice was found when peritoneal macrophages were restimulated with *S. typhi* (p-value < 0.05) and *S. aureus* (p-value < 0.05) (**Figure 3F**). Although a consistent trend in increased IL-6 production was observed when peritoneal macrophages of the BCG-vaccinated group were restimulated with all pathogens and TLR ligands, only stimulation with *C. albicans* resulted in a statistically significant increase in comparison to the control group (p-value < 0.05) (**Figure 3G**). IL-1α, IL-1β, and IL-10 responses (**Figures 3H–J**) did not differ between groups.

BCG Vaccination Does Not Protect Mice During H7N9 Influenza Infection

No survival (0%) was observed in the animals of vehicle control group 11 days after A/Anhui/1/2013 (H7N9) challenge. Despite the heterologous induction of trained immunity responses, as reported above, vaccination with BCG did not result in a statistically significant improvement in survival proportion compared to the vehicle control group (12.5% survival in BCG treated group) (Table S1 in Supplementary Material). Furthermore, BCG vaccination did not result in a statistically significant improvement in survival time compared to the vehicle control group (p-value $= 0.82$) (**Figure 4A**; Table S2 in Supplementary Material). The percentage body weight change per animal was determined relative to day 0. Similar to the vehicle control group, all animals in the BCG-vaccinated displayed a steep reduction in bodyweight starting from day 1 until day 11. The single surviving animal in the BCG-treated group started to recover after day 11. BCG vaccination did not result in a significant difference in body weight loss compared to the vehicle control group (p-value $= 0.15$) (**Figure 4B**; Table S3 in Supplementary Material). From day 0 onward, the severity of influenza infection was graded as a clinical score based on the observation of one or multiple clinical signs typical for influenza infection. The mean clinical scores did not differ between the vehicle control group and BCG-immunized group (Figure S1 in Supplementary Material).

BCG Vaccination Does Not Reduce Histopathological Damage, Inflammation, or Viral Replication

Three days after challenge infection, histopathological lung examination was performed in a subgroup of both vehicle control and BCG-vaccinated mice. The pathological changes observed in the lungs isolated from these mice corresponded with acute lung injury, characterized by epithelial necrosis and infiltration of macrophages, lymphocytes, and granulocytes (**Figures 5A,B**). In addition, squamous metaplasia was observed. No differences in pathological changes between the lungs of the BCG vaccinated and vehicle control mice were observed at day 3 after challenge infection (**Figures 5C,D**). Histological scores for the amount of granulocytes, macrophages, and lymphocytes were similar between the BCG immunized and control group (**Figure 5E**). Although BCG did not have an effect on pulmonary tissue inflammation or immune cell composition, we wanted to determine

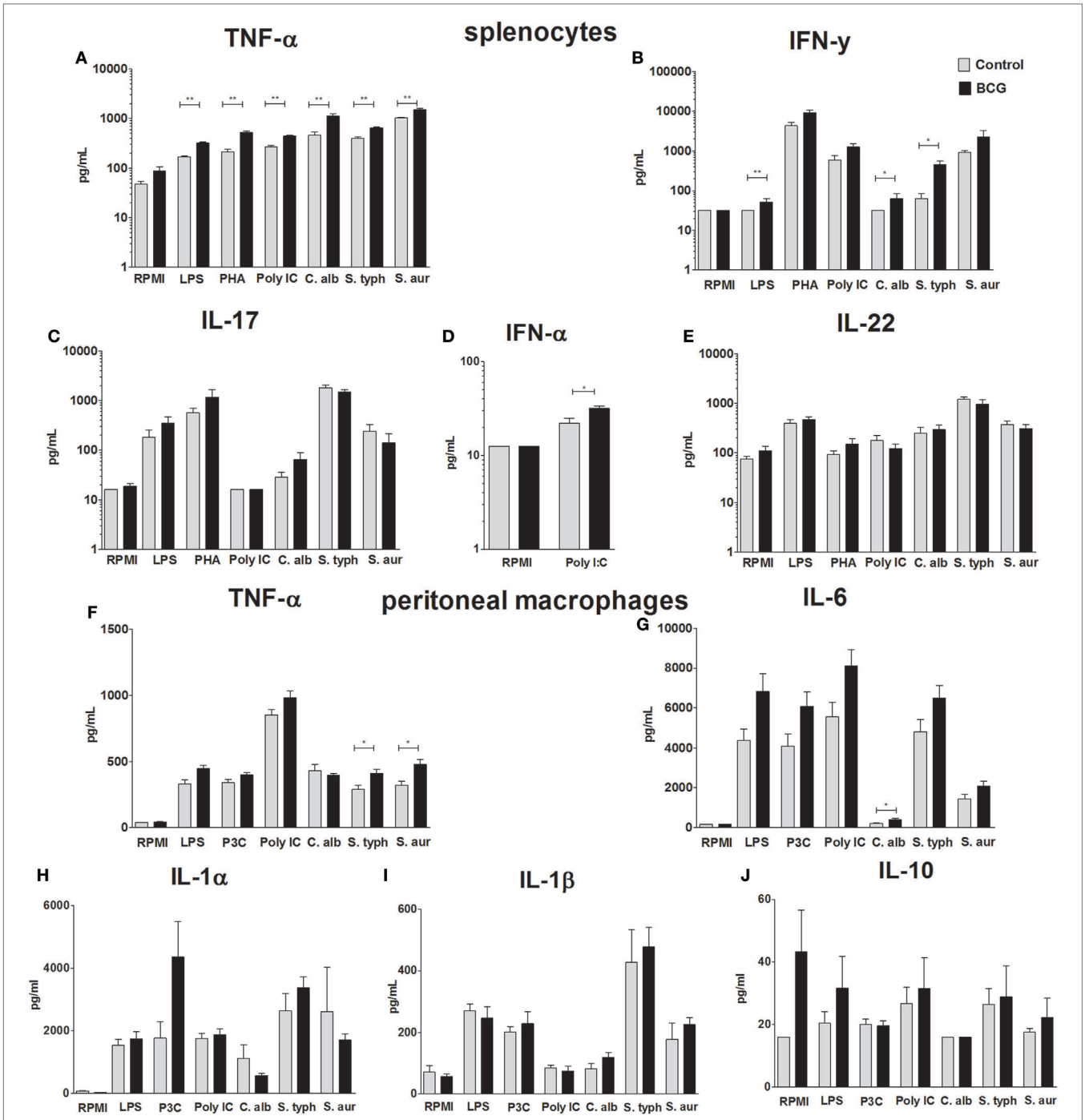

FIGURE 3 | Bacillus Calmette–Guérin (BCG)-induced trained immunity cytokine responses. To demonstrate increased innate immune response after BCG vaccination, spleen cells and peritoneal macrophages were isolated 7 days after administration of either BCG or phosphate buffered saline. Concentrations of tumor necrosis factor-alpha (TNF-α), interferon (IFN)-α, IFN-γ, interleukin (IL)-17, and IL-22 determined by enzyme-linked immunosorbent assay (ELISA) in supernatants of restimulated splenocytes with Roswell Park Memorial Institute (RPMI), lipopolysaccharide (LPS), phytohemagglutin (PHA), poly I:C, *Candida albicans*, *Salmonella typhi*, and *Staphylococcus aureus* are shown **(A–E)**. Concentrations of IL-1α, IL-1β, IL-6, IL-10, and TNF-α determined by ELISA in supernatants of restimulated peritoneal macrophages with RPMI, LPS, poly I:C, *C. albicans*, *S. typhi*, and *S. aureus* are shown **(F–J)**. Data are shown as mean ± SEM, $n = 5$ per group, $^{*}p < 0.05$, $^{**}p < 0.01$ Mann–Whitney *U* (two-sided).

the effect of BCG immunization on local influenza infection and replication (by scoring of influenza infected cells). Lung tissue sections slides were stained with influenza NP to determine the quantity of influenza virions (**Figures 6A,B**). The scores of NP stained small bronchi, large bronchi, or alveoli did not differ between groups (**Figure 6C**). This indicates that intravenous BCG

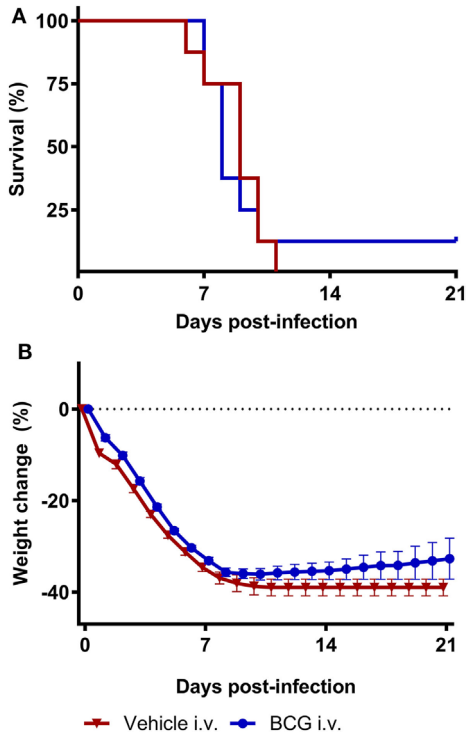

FIGURE 4 | Bacillus Calmette–Guérin (BCG) vaccination does not protect mice during H7N9 influenza infection. Female BALB/c mice were challenged with a dose of 4MLD$_{50}$ influenza A/Anhui/1/2013 (H7N9) on day 0. Mice received 750 µg BCG or the vehicle control (phosphate buffered saline) i.v. on day −7. Kaplan–Meyer survival curve **(A)** and mean body weight change **(B)** are depicted. Survival proportion in the BCG treated group was statistically analyzed using a Fisher's exact two-sided test. Survival time was statistically analyzed using a Mantel and Cox log-rank test. The effect of BCG treatment on body weight was analyzed by comparing the area under curve of treatment groups with vehicle and was statistically analyzed using a two-way ANOVA with Bonferroni correction. Data are shown as mean ± SEM, $n = 8$ per group.

administration did not reduce influenza A (H7N9) infection or replication in mice.

DISCUSSION

The avian influenza A (H7N9) virus appears to have become more virulent during recent epidemics in China, underlining the risk of a global human pandemic in the absence of specific immunity. In case of an outbreak in the absence of available specific vaccines, BCG might contribute to control of avian influenza through its non-specific protective effects, which are probably related to its capacity to induce trained immunity in monocytes. In this study, we tested the effect of intravenous BCG against a lethal influenza A/Anhui/1/2013 (H7N9) infection in mice.

We were able to reproduce previous findings regarding induction of systemic trained immunity after BCG administration in mice (16). Intravenous BCG immunization resulted in significantly increased cytokine responses upon *ex vivo* restimulation with unrelated TLR-ligands and pathogens, both in splenocytes (TNF-α, IFN-α, and IFN-γ) and peritoneal macrophage (TNF-α and IL-6). However, increased *ex vivo* cytokine production was not associated with differences in experimental avian influenza A/Anhui/1/2013 (H7N9) infection in terms of survival, clinical scores, or pulmonary inflammation.

A recent study demonstrated that low dose BCG (TICE strain) administration protects against mouse-adapted influenza virus A/Puerto Rico/8/34 (PR8) (H1N1) strain by increased efferocytosis of alveolar phagocytes, but only after i.n. and not after subcutaneously administration of BCG (26). Similar observations were reported previously; i.n. BCG (strain unspecified) immunized mice showed enhanced protection against influenza A (H1N1) PR8 challenge compared to intraperitoneally immunized mice (17). This suggests the route of BCG administration might be important in case of protection against influenza. In the study of Mukherjee et al. (26), mice were inoculated with a lower dose of BCG compared to the administered dose in our study, pointing out that not only the route of administration but maybe also the dose and inherent dose-dependent kinetics might be crucial for heterologous protection. For several TLR-ligands, it has been shown that the dose during initial priming determines if monocytes will either become trained or tolerized during the *in vitro* trained immunity model (27). One could hypothesize that induction of either training or tolerance may be different per cell and tissue type as well. Although *in vivo* dose response studies of BCG priming in the context of trained immunity have not been performed yet, these *in vitro* data indicate the initial dose might be discriminative between being protective or not. That being said, a similar dose, route of administration as well as BCG strain were nevertheless protective against a lethal *C. albicans* challenge infection in severe combined immunodeficient mice, resulting in enhanced survival, decreased kidney yeast burden, and *ex vivo* trained immunity responses (16). This may suggest that the beneficial effects of BCG vaccination have specificity, and thus induce protection against some, but not all, infections.

As reviewed by Kuiken et al. (28), the innate immune system plays an important role in the first line defense against influenza infections. Influenza recognition by TLR and RIG-1 signaling leads to production of pro-inflammatory cytokines and type I IFNs. Especially type I IFNs are known to exert antiviral activity. Nevertheless, an imbalanced cytokine response or so-called cytokine storm could be detrimental for the host. Compared to seasonal strains, severe infections with highly pathogenic H5N1 and 1918 H1N1 are more frequently associated with a dysregulated cytokine response (29, 30). Likewise, severe cases of H7N9 infections are complicated by hypercytokinemia (3, 31, 32). In the study of Mukherjee et al., intranasal BCG inoculation resulted in decreased TNF-α mRNA and increased IL-10 mRNA expression in alveolar macrophages 2 days post PR8 (H1N1) infection (26). We did not study the local pulmonary mucosal cytokine responses after intravenous administration of BCG, but our findings regarding cytokine responses of *ex vivo* restimulated splenocytes and peritoneal macrophages are pointing toward priming in a different direction, with potentiation of cytokine responses. Future studies should focus on the role of alternative cell types like alveolar macrophages.

One unavoidable limitation for the conclusions of this study is that it investigated the effect of BCG vaccination in mice.

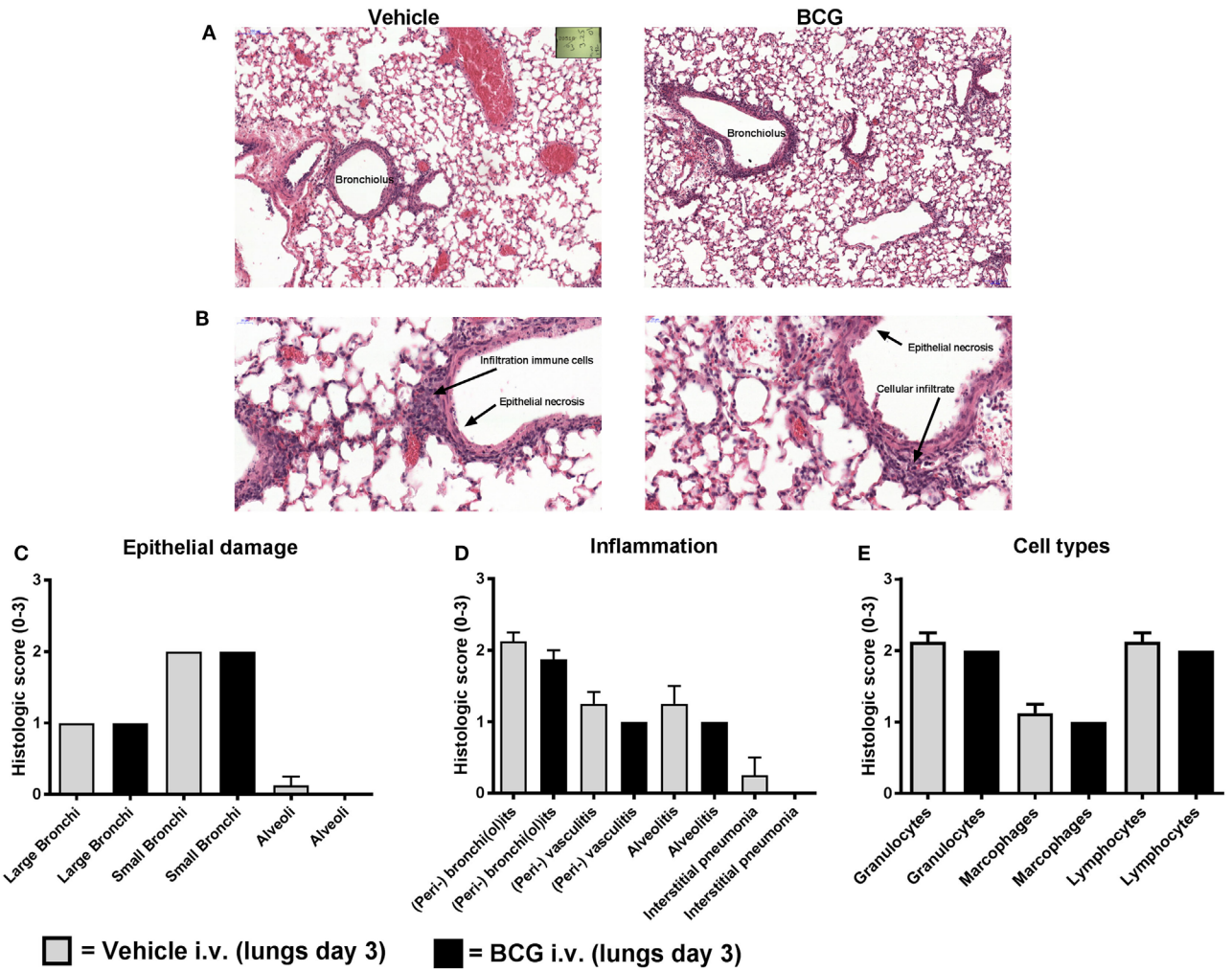

FIGURE 5 | Bacillus Calmette–Guérin (BCG) vaccination does not lead to reduction of histopathological damage and inflammation. Female BALB/c mice were challenged with a dose of 4MLD$_{50}$ influenza A/Anhui/1/2013 (H7N9) on day 0. Mice received 750 μg BCG or vehicle control (phosphate buffered saline) i.v. on day −7 (n = 8 per group). Three days after viral challenge, lungs were fixed in formalin. Paraffin-embedded tissue sections were then stained for hematoxylin and eosin. Representative histopathological image of vehicle versus BCG-treated mice are depicted **(A,B)**. Lung sections were scored from absent to marked: score "0" (absent), score "1" (minimal), score "2" (moderate), and score "3" (marked) for epithelial necrosis (damage) **(C)**, inflammation markers **(D)**, and inflammatory cell types **(E)**. Results were statistically analyzed using the Cochran–Mantel–Haenszel test. Data are shown as mean ± SEM.

Anti-mycobacterial as well as anti-influenza responses are different in mice and humans, and it is conceivable to hypothesize that BCG vaccination may exert stronger beneficial effects in humans, including against influenza infection. Recently, we have shown that BCG vaccination in healthy human volunteers protects against experimental yellow fever vaccine viremia, while the protective serological response retains intact (22). The absence of IL-1β upregulation after BCG vaccination by splenocytes and peritoneal macrophages in the current study can be explained by the differences between the human and murine immunological responses. Humans have an increased IL-1β response compared to mice and mice lack important regulators of the IL-1 pathway such as IL-37 (33).

Another limitation of the study is represented by the particularities of the BCG vaccination in mice, compared to humans. Earlier studies done in mice have shown that systemic trained immunity by BCG is induced after intravenous administration, rather than intradermal administration (34). In line with this, an earlier study by Spencer et al. showed protection against influenza A (H1N1) infection after intraperitoneal vaccination with BCG, indicating that systemic administration of BCG was protective against influenza (17). Furthermore, the administered dose of BCG the animals received and the timing of 7 days before the experimental avian influenza A/Anhui/1/2013 (H7N9) infection were equivalent to our previous intravenous BCG vaccination experimental protocols and comparable to the intraperitoneal BCG vaccination of mice (16–18). We hypothesized that in BCG-vaccinated mice, the infiltration of trained immune cells in the lungs during the experimental avian influenza A/Anhui/1/2013 (H7N9) infection would result in increased clearance of the

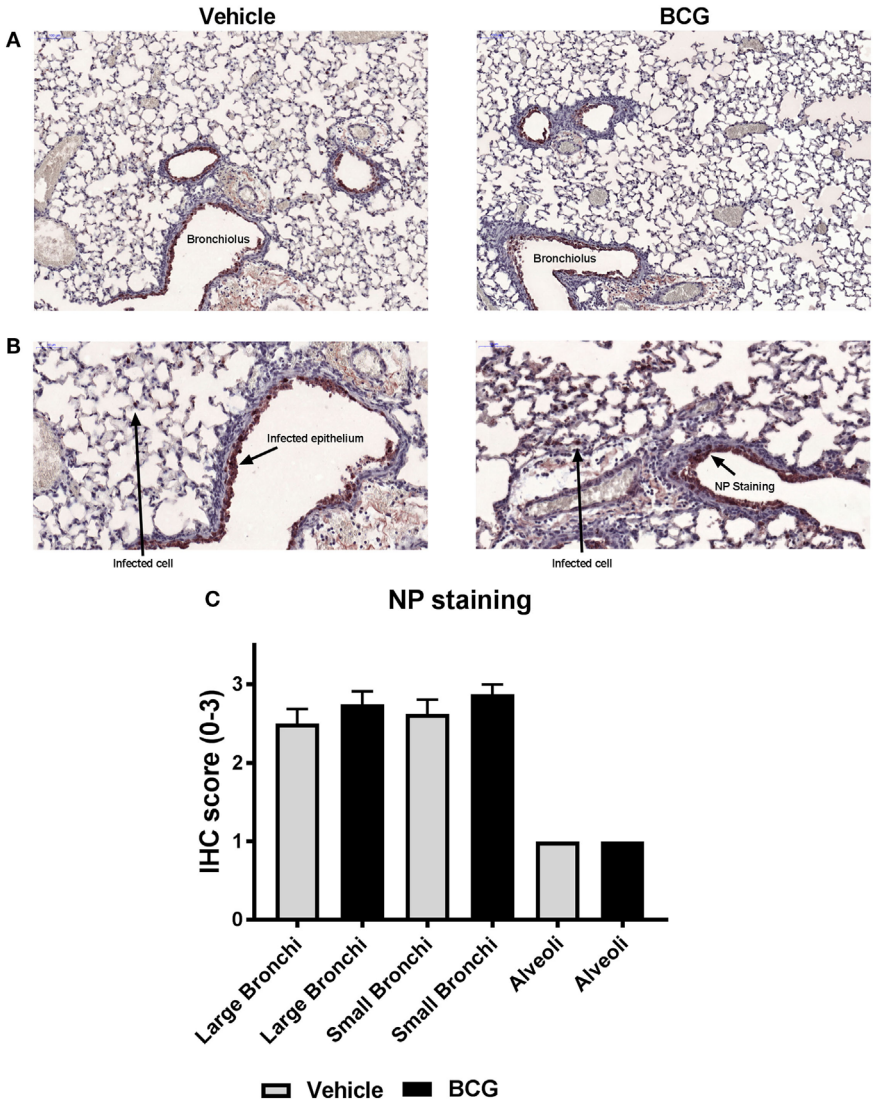

FIGURE 6 | Nucleoprotein (NP) staining of bronchi and alveoli indicates that bacillus Calmette–Guérin (BCG) does not reduce influenza virus replication. Female BALB/c mice were challenged with a dose of $4MLD_{50}$ influenza A/Anhui/1/2013 (H7N9) on day 0. Mice received 750 μg BCG or the vehicle control (phosphate buffered saline) i.v. on day −7 ($n = 8$ per group). Three days after viral challenge, lungs were fixed in formalin. Paraffin-embedded tissue sections were then stained for influenza NP. Representative images of influenza A NP-stained lungs of mice treated with vehicle versus BCG-treated mice are depicted **(A,B)**. NP-staining was scored from absent to 3: score "0" (absent), score "1" (minimal), score "2" (moderate), and score "3" (marked) **(C)**. Results were statistically analyzed using the Cochran–Mantel–Haenszel test. Data are shown as mean ± SEM.

influenza infection. While our data clearly demonstrate that this BCG vaccination model does not protect against H7N9 influenza infection, we cannot exclude that the different route of BCG administration in humans may have an effect.

Partial protection of BCG vaccination has been observed in a human-controlled malaria infection model as well, in which decreased parasitemia correlated with accelerated immune activation and trained immunity *in vivo* upon blood stage parasitemia (Walk, de Bree et al., submitted). A previous randomized controlled trial has shown BCG vaccination prior to trivalent influenza vaccination resulted in enhanced immunogenicity of the influenza vaccine, resulting in increased antibody response and seroconversion against the 2009 pandemic influenza A (H1N1) strain (21). Future studies should explore if BCG could function as an adjuvant to avian influenza vaccines as well.

In conclusion, intravenous administration of BCG enabled the induction of trained immunity, but this was not protective in a lethal influenza A/Anhui/1/2013 (H7N9) challenge infection in BALB/c mice. Future studies are needed to evaluate the anti-influenza effects of BCG vaccination in humans.

ETHICS STATEMENT

Animals experiments were performed in accordance with the guidelines of the European Communities (Directive 2010/63/EU) and Dutch legislation (The experiments on Animals Act, 1997).

The animal experimental protocols were approved by an independent Animal Ethics Committee (TNO, Zeist, the Netherlands) under project license 3387 and performed in the AAALAC accredited animal facility of Triskelion. All animals were housed in a temperature and light-cycle controlled facility with unlimited access to food and water. All procedures involving live H7N9 viruses, including the animal experiments, were carried out in a BSL-3 containment facility at Triskelion. The animals were monitored for clinical signs of influenza disease twice daily with intervals of at least 5 h. All observations, including behavioral aspects were recorded. If lethargy was observed longer than 48 h, the animal was euthanized (humane endpoint).

AUTHOR CONTRIBUTIONS

Participated in research design: RM, JD, MN, and LJ. Conducted experiments: RM and JK. Performed data analysis: RM, SH, MW, and LdB. Wrote the manuscript: LdB and RM. Critically read the manuscript: PA, RC, CSB, DD, JD, MW, MN, LJ, SH, and JK.

ACKNOWLEDGMENTS

MN was supported by an ERC Consolidator Grant (#310372) and a Spinoza Grant of the Netherlands Organization for Scientific Research. CSB and PA were supported by the Danish National Research Foundation (DNRF108).

SUPPLEMENTARY MATERIAL

The Supplementary Material for this article can be found online at https://www.frontiersin.org/articles/10.3389/fimmu.2018.00869/full#supplementary-material.

REFERENCES

1. WHO. Influenza at the Human-Animal Interface. (2017). Summary and assessment, 30 October to 7 December 2017. Available from: http://www.who.int/influenza/human_animal_interface/Influenza_Summary_IRA_HA_interface_12_07_2017.pdf
2. Wang X, Jiang H, Wu P, Uyeki TM, Feng L, Lai S, et al. Epidemiology of avian influenza A H7N9 virus in human beings across five epidemics in mainland China, 2013-17: an epidemiological study of laboratory-confirmed case series. *Lancet Infect Dis* (2017) 17(8):822–32. doi:10.1016/S1473-3099(17)30323-7
3. Chen Y, Liang W, Yang S, Wu N, Gao H, Sheng J, et al. Human infections with the emerging avian influenza A H7N9 virus from wet market poultry: clinical analysis and characterisation of viral genome. *Lancet* (2013) 381(9881):1916–25. doi:10.1016/S0140-6736(13)60903-4
4. Cox RJ, Madhun AS, Hauge S, Sjursen H, Major D, Kuhne M, et al. A phase I clinical trial of a PER.C6 cell grown influenza H7 virus vaccine. *Vaccine* (2009) 27(13):1889–97. doi:10.1016/j.vaccine.2009.01.116
5. Couch RB, Patel SM, Wade-Bowers CL, Nino D. A randomized clinical trial of an inactivated avian influenza A (H7N7) vaccine. *PLoS One* (2012) 7(12):e49704. doi:10.1371/journal.pone.0049704
6. Mulligan MJ, Bernstein DI, Winokur P, Rupp R, Anderson E, Rouphael N, et al. Serological responses to an avian influenza A/H7N9 vaccine mixed at the point-of-use with MF59 adjuvant: a randomized clinical trial. *JAMA* (2014) 312(14):1409–19. doi:10.1001/jama.2014.12854
7. Madan A, Segall N, Ferguson M, Frenette L, Kroll R, Friel D, et al. Immunogenicity and safety of an AS03-adjuvanted H7N9 pandemic influenza vaccine in a randomized trial in healthy adults. *J Infect Dis* (2016) 214(11):1717–27. doi:10.1093/infdis/jiw414
8. Jackson LA, Campbell JD, Frey SE, Edwards KM, Keitel WA, Kotloff KL, et al. Effect of varying doses of a monovalent H7N9 influenza vaccine with and without AS03 and MF59 adjuvants on immune response: a randomized clinical trial. *JAMA* (2015) 314(3):237–46. doi:10.1001/jama.2015.7916
9. Näslund C. Resultats des experiences de vaccination par le BCG poursuivies dans le Norrbotten (Suède) (Septembre 1927–Décembre 1931). Vaccination Preventative de Tuberculose, Rapports et Documents. Paris: Institut Pasteur (1932).
10. Aaby P, Roth A, Ravn H, Napirna BM, Rodrigues A, Lisse IM, et al. Randomized trial of BCG vaccination at birth to low-birth-weight children: beneficial nonspecific effects in the neonatal period? *J Infect Dis* (2011) 204(2):245–52. doi:10.1093/infdis/jir240
11. Biering-Sorensen S, Aaby P, Napirna BM, Roth A, Ravn H, Rodrigues A, et al. Small randomized trial among low-birth-weight children receiving bacillus Calmette-Guerin vaccination at first health center contact. *Pediatr Infect Dis J* (2012) 31(3):306–8. doi:10.1097/INF.0b013e3182458289
12. Parra M, Liu X, Derrick SC, Yang A, Tian J, Kolibab K, et al. Molecular analysis of non-specific protection against murine malaria induced by BCG vaccination. *PLoS One* (2013) 8(7):e66115. doi:10.1371/journal.pone.0066115
13. Matsumoto S, Yukitake H, Kanbara H, Yamada H, Kitamura A, Yamada T. *Mycobacterium bovis* bacillus Calmette-Guerin induces protective immunity against infection by *Plasmodium yoelii* at blood-stage depending on shifting immunity toward Th1 type and inducing protective IgG2a after the parasite infection. *Vaccine* (2000) 19(7–8):779–87. doi:10.1016/S0264-410X(00)00257-7
14. Clark IA, Allison AC, Cox FE. Protection of mice against *Babesia* and *Plasmodium* with BCG. *Nature* (1976) 259(5541):309–11. doi:10.1038/259309a0
15. Tribouley J, Tribouley-Duret J, Appriou M. [Effect of bacillus Callmette Guerin (BCG) on the receptivity of nude mice to *Schistosoma mansoni*]. *C R Seances Soc Biol Fil* (1978) 172(5):902–4.
16. Kleinnijenhuis J, Quintin J, Preijers F, Joosten LA, Ifrim DC, Saeed S, et al. Bacille Calmette-Guerin induces NOD2-dependent nonspecific protection from reinfection via epigenetic reprogramming of monocytes. *Proc Natl Acad Sci U S A* (2012) 109(43):17537–42. doi:10.1073/pnas.1202870109
17. Spencer JC, Ganguly R, Waldman RH. Nonspecific protection of mice against influenza virus infection by local or systemic immunization with bacille Calmette-Guerin. *J Infect Dis* (1977) 136(2):171–5. doi:10.1093/infdis/136.2.171
18. Arts RJ, Carvalho A, La Rocca C, Palma C, Rodrigues F, Silvestre R, et al. Immunometabolic pathways in BCG-induced trained immunity. *Cell Rep* (2016) 17(10):2562–71. doi:10.1016/j.celrep.2016.11.011
19. Benn CS, Netea MG, Selin LK, Aaby P. A small jab – a big effect: nonspecific immunomodulation by vaccines. *Trends Immunol* (2013) 34(9):431–9. doi:10.1016/j.it.2013.04.004
20. Kleinnijenhuis J, Quintin J, Preijers F, Benn CS, Joosten LA, Jacobs C, et al. Long-lasting effects of BCG vaccination on both heterologous Th1/Th17 responses and innate trained immunity. *J Innate Immun* (2014) 6(2):152–8. doi:10.1159/000355628
21. Leentjens J, Kox M, Stokman R, Gerretsen J, Diavatopoulos DA, van Crevel R, et al. BCG vaccination enhances the immunogenicity of subsequent influenza vaccination in healthy volunteers: a randomized, Placebo-Controlled Pilot Study. *J Infect Dis* (2015) 212(12):1930–8. doi:10.1093/infdis/jiv332
22. Arts RJW, Moorlag S, Novakovic B, Li Y, Wang SY, Oosting M, et al. BCG vaccination protects against experimental viral infection in humans through the induction of cytokines associated with trained immunity. *Cell Host Microbe* (2018) 23(1):89.e–100.e. doi:10.1016/j.chom.2017.12.010
23. Reed LJ, Muench H. A simple method of estimating fifty percent endpoints. *Am J Trop Med Hyg* (1938) 27(20):493–7.
24. Rimmelzwaan GF, Kuiken T, van Amerongen G, Bestebroer TM, Fouchier RA, Osterhaus AD. Pathogenesis of influenza A (H5N1) virus infection in a primate model. *J Virol* (2001) 75(14):6687–91. doi:10.1128/JVI.75.14.6687-6691.2001

25. Belser JA, Gustin KM, Pearce MB, Maines TR, Zeng H, Pappas C, et al. Pathogenesis and transmission of avian influenza A (H7N9) virus in ferrets and mice. *Nature* (2013) 501(7468):556–9. doi:10.1038/nature12391
26. Mukherjee S, Subramaniam R, Chen H, Smith A, Keshava S, Shams H. Boosting efferocytosis in alveolar space using BCG vaccine to protect host against influenza pneumonia. *PLoS One* (2017) 12(7):e0180143. doi:10.1371/journal.pone.0180143
27. Ifrim DC, Quintin J, Joosten LA, Jacobs C, Jansen T, Jacobs L, et al. Trained immunity or tolerance: opposing functional programs induced in human monocytes after engagement of various pattern recognition receptors. *Clin Vaccine Immunol* (2014) 21(4):534–45. doi:10.1128/CVI.00688-13
28. Kuiken T, Riteau B, Fouchier RA, Rimmelzwaan GF. Pathogenesis of influenza virus infections: the good, the bad and the ugly. *Curr Opin Virol* (2012) 2(3):276–86. doi:10.1016/j.coviro.2012.02.013
29. Short KR, Veeris R, Leijten LM, van den Brand JM, Jong VL, Stittelaar K, et al. Proinflammatory cytokine responses in extra-respiratory tissues during severe influenza. *J Infect Dis* (2017) 216(7):829–33. doi:10.1093/infdis/jix281
30. de Jong MD, Simmons CP, Thanh TT, Hien VM, Smith GJ, Chau TN, et al. Fatal outcome of human influenza A (H5N1) is associated with high viral load and hypercytokinemia. *Nat Med* (2006) 12(10):1203–7. doi:10.1038/nm1477
31. Zhou J, Guo X, Fang D, Yu Y, Si L, Wang Y, et al. Avian influenza A (H7N9) viruses isolated from patients with mild and fatal infection differ in pathogenicity and induction of cytokines. *Microb Pathog* (2017) 111:402–9. doi:10.1016/j.micpath.2017.08.022
32. Wang Z, Zhang A, Wan Y, Liu X, Qiu C, Xi X, et al. Early hypercytokinemia is associated with interferon-induced transmembrane protein-3 dysfunction and predictive of fatal H7N9 infection. *Proc Natl Acad Sci U S A* (2014) 111(2):769–74. doi:10.1073/pnas.1321748111
33. Dinarello CA. Overview of the IL-1 family in innate inflammation and acquired immunity. *Immunol Rev* (2018) 281(1):8–27. doi:10.1111/imr.12621
34. Kaufmann E, Sanz J, Dunn JL, Khan N, Mendonca LE, Pacis A, et al. BCG educates hematopoietic stem cells to generate protective innate immunity against tuberculosis. *Cell* (2018) 172(1–2):176–90.e19. doi:10.1016/j.cell.2017.12.031

Conflict of Interest Statement: JD is currently employed by Aduro Biotech, but was employed by Triskelion when the studies were performed. All other authors declare no competing interests.

The reviewer CL and handling Editor declared their shared affiliation.

Advantages of publishing in Frontiers

OPEN ACCESS
Articles are free to read for greatest visibility and readership

FAST PUBLICATION
Around 90 days from submission to decision

HIGH QUALITY PEER-REVIEW
Rigorous, collaborative, and constructive peer-review

TRANSPARENT PEER-REVIEW
Editors and reviewers acknowledged by name on published articles

Frontiers
Avenue du Tribunal-Fédéral 34
1005 Lausanne | Switzerland

Visit us: www.frontiersin.org
Contact us: info@frontiersin.org | +41 21 510 17 00

REPRODUCIBILITY OF RESEARCH
Support open data and methods to enhance research reproducibility

DIGITAL PUBLISHING
Articles designed for optimal readership across devices

FOLLOW US
@frontiersin

IMPACT METRICS
Advanced article metrics track visibility across digital media

EXTENSIVE PROMOTION
Marketing and promotion of impactful research

LOOP RESEARCH NETWORK
Our network increases your article's readership